Utilising preclinical models to investigate underlying mechanisms and treatment strategies for cognitive impairment associated with schizophrenia

A thesis submitted to the University of Manchester for the degree of Doctor of Philosophy in the Faculty of Biology, Medicine and Health

2023

Jennifer A Fletcher

School of Health Sciences

Division of Pharmacy and Optometry

Contents

WORD COUNT: 74,709

LIST OF FIGURES

Chapter 1: Introduction

Chapter 2: Methods

Chapter 3: Characterisation of the subchronic phencyclidine model

Chapter 4: Effects of apocynin and minocycline in the scPCP model

Chapter 5: Effects of exercise in the scPCP model

Chapter 6: Characterisation of the poly (I:C) model

Chapter 7: Final discussion

Chapter 8: Supplementary material

LIST OF TABLES

Chapter 1: Introduction

Chapter 2: Methods

Chapter 3: Characterisation of the subchronic phencyclidine model

Chapter 4: Effects of apocynin and minocycline in the scPCP model

Chapter 5: Effects of exercise in the scPCP model

Chapter 6: Characterisation of the poly (I:C) model

Chapter 8: Supplementary material

ABBREVIATIONS

4-PL	4 Parameter logistic
Acan	Aggrecan
ADAMTS	A disintegrin and metalloproteinase with thrombospondin motifs
ae	Acute exercise
ANOVA	Analysis of variance
Bcan	Brevican
BDNF	Brain-derived neurotrophic factor
Bral2	Brain link protein 2
BrdU	Bromodeoxyuridine
CA1	Corno ammonis 1
CA2/3	Corno ammonis 2/3
Ca^{2+}	Calcium ion
CAT	Catalase
cDNA	Complementary deoxyribonucleic acid
ce	Chronic exercise
cFC	Contextual fear conditioning
Cg1	Cingular cortex subarea 1
CGE	Caudal ganglionic eminence
ChABC	Chondroitinase ABC
CIAS	Cognitive impairment associated with schizophrenia
CNS	Central nervous system
conNOR	Continuous NOR
CSPG	Chondroitin sulphate proteoglycans
Ctrl1	Link protein 1
DG	Dentate gyrus
DI	Discrimination index
DLPFC	Dorsolateral Prefrontal Cortex
DNA	Deoxyribonucleic acid
E/I	Excitatory inhibitory imbalance
ECM	Extracellular matrix
EE	Environmental enrichment
ELISA	Enzyme-linked immunosorbent assay
Ex	Exercise
GABA	Gamma-aminobutyric acid
GAD	Glutamate decarboxylase
GAD67	Glutamic acid decarboxylase 67
Gapdh	Glyceraldehyde-3-phosphate dehydrogenase
gclm	Glutathione
GD	Gestational day
GLM	General linear model
GLMM	General linear mixed model
GPx	Glutathione peroxidase
HA	Hyaluronic acid
HAS	Hyaluronic acid synthase
HRP	Horseradish peroxidase
i.p.	Intraperitoneal
IBA1	Ionised calcium-binding adapter molecule 1
IHC	Immunohistochemistry
IL	Infralimbic
IL1β	Interleukin 1β
IQR	Interquartile range
ITI	Intertrial interval

LPS	Lipopolysaccharide
LTD	Long-term depression
LTP	Long-term potentiation
M1	Microglia subtype 1
M2	Microglia subtype 2
MATRICS	Measurement and treatment research to improve cognition in schizophrenia
MDA	Malondialdehyde
Mg^{2+}	Magnesium ion
MGE	Medial ganglionic eminence
mGLMM	General linear mixed model with maternal cytokine included
MIA	Maternal immune activation
MMP9	Matrix metalloproteinase 9
mRNA	Messenger ribonucleic acid
Na^{+}	Sodium ion
NADPH	Nicotinamide adenine dinucleotide phosphate oxidase
Ncan	Neurocan
NFκB	Nuclear factor κB
NMDA	N-methyl-D-aspar0tate
NMDAr	N-methyl-D-aspartate receptor
NOR	Novel object recognition
NOX	NADPH oxidase
NR1	NMDAr subunit 1
NR2	NMDAr subunit 2
NR2A	NMDAr subunit 2A
NR2B	NMDAr subunit 2B
OPC	Oligodendrocyte precursor cells
OS	Oxidative stress
Otx2	Orthodenticle homeobox 2
P	scPCP/PIC
p.o.	Per orum
P/A14	scPCP + scApocynin [10 mg/Kg, p.o.] + 7-day washout
P/A7	scPCP + scApocynin [10 mg/Kg, p.o.]
P/E	scPCP + exercise cohort
P/M14	scPCP + scMinocycline [40mg/Kg, p.o.] + 7-day washout
P/M7	scPCP + scMinocycline [40mg/Kg, p.o.]
P/S	scPCP + sedentary cohort
P/V7	scPCP + scVeh
PCC	Posterior cingulate cortex
PCP	Phencyclidine
PFC	Prefrontal cortex
PIC	Polyinosinic:polycytidylic acid
PNN	Perineuronal nets
Poly(I:C)	Polyinosinic:polycytidylic acid
PrL	Prelimbic cortex
PSD95	Postsynaptic density 95
PVI	Parvalbumin interneuron
qPCR	Quantitative polymerase chain reaction
raDI	Rolling average discrimination index
RFU	Relative fluorescent units

rmTBI	Repetitive mild traumatic brain injury
RNA	Ribonucleic acid
ROS	Reactive oxygen species
S1	Somatosensory cortex
SAP102	Synapse-associated protein 102
sc	Sub chronic dosing
scPCP	Subchronic phencyclidine
scVeh	Subchronic vehicle
SD	Standard deviation
Sed	Sedentary
SEM	Standard error of the mean
SNAP25	Synaptosomal-associated protein 25kDa
SOD	Superoxide dismutase
T	Trial
TBA	Thiobarbituric acid
TBARS	Thiobarbituric acid reactive substances
TIMP	Tissue inhibitors of metalloproteinases
TLR	Toll-like receptors
TMB	3,3',5,5'-Tetramethylbenzidine
TNFα	Tumour necrosis factor α
Tn-R	Tenascin-R
TRIF	TIR domain-containing adaptor-inducing IFNβ
TrkB	Tropomyosin-related kinase B
Ubc	Ubiquitin C
V	Vehicle
V/E	scVeh + exercise cohort
V/S	scVeh + sedentary cohort
V/V7	scVeh + scVeh
Vcan	Versican
VGCC	Voltage-gated calcium channels
VGlut1	Vesicular glutamate transporter 1
VH	Ventral hippocampus
WES	Simple western analysis
WFA	Wisteria floribunda
WST	Water-soluble tetrazolium
ZT	Zeitgeber time

ABSTRACT

Cognitive impairment associated with schizophrenia (CIAS) remains an unmet clinical need. A considerable challenge in studying schizophrenia is its heterogeneous nature with many causes and symptoms. However, there is increasing evidence that cognitive symptoms result from prefrontal cortex hypofunction, although the precise mechanisms remain elusive. In this thesis, we investigated markers related to synaptic, glutamatergic and GABAergic signalling in the prefrontal cortex (PFC) and dorsal hippocampus (DH) in two different in vivo models relevant to CIAS, the subchronic phencyclidine (scPCP) and maternal immune activation (MIA) with the viral mimetic polyinosinic:polycytidylic acid (poly(I:C)). Although both these models induce cognitive impairment, their construct and presentation of these deficits are distinct. We aimed to identify common pathways that might be susceptible to damage. In addition, we tested pharmacological and non-pharmacological interventions in the scPCP model.

The scPCP experiments dosed female Lister Hooded rats with PCP bidaily for seven days. In the characterisation chapter, we collected tissue for gene expression, protein and immunohistochemistry (IHC) analysis. In these tissues, we measured markers related to synaptic, glutamatergic and GABAergic signalling in the prefrontal cortex (PFC) and dorsal hippocampus (DH), as well as oxidative stress and inflammation. In the apocynin/minocycline study, we studied the effect of an antioxidant and anti-inflammatory on scPCP behaviour and pathology. In the exercise study, we studied the effect of acute and chronic exercise on behaviour and pathology. The poly(I:C) studies examined the adolescent and adult offspring of Wistar dams who underwent MIA on gestational day 15. We measured the same markers in the offspring as in the scPCP characterisation study.

scPCP induced a profound and sustained disruption to synaptic, glutamatergic and GABAergic signalling. In addition, markers related to oxidative stress and inflammation were elevated. Treatment with apocynin and minocycline showed transient attenuation of scPCP-induced novel object recognition (NOR) deficits. However, this was not sustained. Moreover, both had little effect on pathology. Acute and chronic exercise reversed scPCP pathology, although different mechanisms were explored. Finally, the offspring of the poly(I:C)-treated dams developed synaptic, glutamatergic and GABAergic impairments in adulthood. Despite different model constructs, this thesis discusses points of conversion between the two models.

DECLARATION

No portion of the work referred to in the thesis has been submitted in support of an application for another degree or qualification of this or any other university or other institute of learning.

COPYRIGHT STATEMENT

i. The author of this thesis (including any appendices and/or schedules to this thesis) owns certain copyright or related rights in it (the "Copyright") and s/he has given the University of Manchester certain rights to use such Copyright, including for administrative purposes.

ii. Copies of this thesis, either in full or in extracts and whether in hard or electronic copy, may be made only in accordance with the Copyright, Designs and Patents Act 1988 (as amended) and regulations issued under it or, where appropriate, in accordance with licensing agreements which the University has from time to time. This page must form part of any such copies made.

iii. The ownership of certain Copyright, patents, designs, trademarks and other intellectual property (the "Intellectual Property") and any reproductions of copyright works in the thesis, for example graphs and tables ("Reproductions"), which may be described in this thesis, may not be owned by the author and may be owned by third parties. Such Intellectual Property and Reproductions cannot and must not be made available for use without the prior written permission of the owner(s) of the relevant Intellectual Property and/or Reproductions.

iv. Further information on the conditions under which disclosure, publication and commercialisation of this thesis, the Copyright and any Intellectual Property and/or Reproductions described in it may take place is available in the University IP Policy (see http://documents.manchester.ac.uk/DocuInfo.aspx?DocID=24420), in any relevant Thesis restriction declarations deposited in the University Library, the University Library's regulations (see http://www.library.manchester.ac.uk/about/regulations/) and in the University's policy on Presentation of Theses.

CONTRIBUTIONS

- Chapter 3:
    - Syeda Munni, Idil Mitsadali and Cathy Jones completed the animal work from which brains were taken.
    - Brains for the IHC study were from a study carried out by Katie Landreth, and brains for this study were collected by Michael Harte.
    - Inés Jimenez Pulido completed dorsal hippocampus PCR.
- Chapter 4:
    - Animal work was carried out by b-neuro, namely Syeda Munni, Idil Mitsadali and Inés Jimenez Pulido.
    - Behavioural data were scored by Ben Grayson, Hannah Fernandes Leonard and Haneul Choi.
- Chapter 5:
    - NOR testing was assisted by Jessica Brown, Molly Gracie and Jarred Lorusso.
    - NOR tapes were double-scored by Tom Wight, Georgie Pearson and Molly Gracie.
    - Michael Harte collected acute exercise brains.
    - Tom Wight assisted with acute exercise post-mortem work.
    - Syeda Munni perfused brains.
    - The Bioimaging facility scanned slides.
    - Verina Youssef assisted with microglia staining.
    - Inés Jimenez Pulido analysed microglia density and activation states.
- Chapter 6:
    - Brains were taken from cohorts managed by Harry Potter and Rebecca Woods.
    - Rebecca Woods assisted brain preparation for WES.
    - Technical assistance for qPCR was provided by Rebecca Woods.
    - Brains for the IHC study were sectioned by Rebecca Woods.
    - The Bioimaging facility scanned slides.
    - Hannah Mellor analysed PD100 brains.
    - Jarred Lorusso provided expertise for the statistics.

ACKNOWLEDGEMENTS

I recall a student asking me during my first summer at Manchester what it takes to do a PhD. Although I was absolutely not qualified to answer, I told them that a PhD was a lot of hard work, and you really have to love what you are doing to get through it. I finished by saying that it was 80% the project and 20% the people. Well, four years down the line, I can say I have learnt two things from that conversation. First, trying to explain what a PhD is like before doing one will never age well, and two, I could not have possibly been more wrong.

It feels counterintuitive to start a document of *incredible scientific prowess* by talking about incredible luck and fortune, but how else can I explain the odds of doing my PhD with such wonderful people? I have to begin with Lauren and Jess. I don't know what hands of fate were moving to ensure that the three of us sat together, righting the world's wrongs, but I owe those hands an overwhelming debt. I will forever be grateful that Lauren didn't listen to Jess when she tried to boot her out of her seat. You are both brilliant friends and have helped me endlessly. I will forever count my blessings for going through this with you two. I already miss our times chatting away, annoying everyone else in the office with our cackles.

In our defence, the neighbouring office inhabitants were not innocent bystanders. I was fortunate to be surrounded by some absolute characters. With spins of our once creaking chairs, I could talk away with Amna, Anna, Bushra, Charlie, Cohen, Emily, Georgie, Inés, Isabella, Jess B, Laurence, Megan and Ming. All class individuals who deserve all the success. Honourable mention for Yusuf, who was always going.

When I wanted to be distracted but also feel productive, I would venture over to the Smith to see Becky and Jarred. Two of the most entertaining-meets-chaotic-meets-determined duos I have ever come across. Becky – a kindred spirit that I love to wind up. Jarred – a surprising paaaassable American who winds me up because I still get confused when he is being serious and when he is being sarcastic. Both have taught me so much and have brought me endless joy. I will continue the appreciation to the rest of the MIA group; Reinmar, Jo, Francesca and Bella. Thanks for letting me come and go as I please from that model – no guts, all glory.

Having reached the tail end of this experience, I can confidently say the most distracting person was b-neuro's very own secretary/librarian Ben Grayson. If I went to his office or heard his clippy-cloppy shoes coming into the lab, I knew it was a big chat waiting to happen. Feel like I was forever telling him what you can and can't say these days – all change from the times of rationing. In all seriousness, I cannot thank him enough for his guidance and for always listening when I occasionally had something to say. I must also thank the rest of the b-neuro team, Syeda, Idil, Katie and Cathy, Hannah and Grace for all their help.

This leads me to students – thanks to Georgie, Tom and Verina, who helped produce data for this thesis, despite my hectic supervision. I am indebted to Hannah for counting

the PD100 brains at an outrageous speed, Aleks for pioneering the microglia classification and Inés, who dragged the last of the PCR across the finish line.

Speaking of the old PhD, it would be nothing without the PNN. I am sure it was John Gigg who first suggested the idea. I am very grateful for that and his support throughout my PhD. He always has an uncanny ability to make me take a step back and revaluate things, even if it is my opinion on the Minions.

When I eventually got around to writing, it was among the company of Amna, Mona, Najla and Nuha. Thanks for opening the lights on the dark days, the unwavering understanding, and keeping the minibar stocked.

It would be a great shame not to thank Doug Steinke and Sarah Fairhurst for always giving me the best intel. Thanks to all those associated with the PGR reps and the showcase, Grace, Lauren Daniels, Aliye, Hamid, Alex, Canase, Lauren, Jess and Laurence (when he had time).

My dearest Fletcher fam – all the appreciation for being there throughout it all and never losing your faith in me. Depending on the timing and the circumstance, they've picked me up or knocked me down a peg or two, always helping me to be better. Needless to say, a doctor or no, I will forever be proudest of being a Fletcher.

A moment of silence for my calm in the storm Carrington. Thanks for dealing with my dramatic, stressy, messy self, even though, and I quote, you have no idea how stressful it is being me. Truly an unsung hero for keeping me sane, having tea with me at ungodly hours and being the one to try and wake me up in the mornings.

And so we reach the end, and what has this all been? Nothing but a ploy Michael to make you read at least one thing I have written all the way through. If you skimmed through for your name or skipped to the end, poor show, and yet in a way, predictable. I could thank you for your enthusiasm and call it a day. I could also say what a fantastic PhD supervisor you have been, but I don't want to feed the unbearable post-Prof ego. So instead, I will just say thank you for letting me do all of this. Thank you for knowing when to reality-check my crazed plans. Thank you for being encouraging and never pressuring. Thank you for all the advice and for partaking in wine-induced ego-boosting. Thank you for the karaoke mic. Thank you for being so gracious in your relegation to the third funniest person in the lab. Here's to curing everything.

If this acknowledgements section hasn't made it abundantly clear, my answer to the summer student was way off. If asked again, I would finish by saying it is 20% the project and 80% the people. Cause this PhD was a lot of 10pm bradfords, freezers failing, unexpected data and *endless* tube labelling. Still, I would go through it all again in a heartbeat if the same people were at my side… apart from writing this thesis, absolutely not doing this again.

CHAPTER 1: INTRODUCTION

1.1 Clinical overview of schizophrenia

Schizophrenia is a debilitating psychiatric disorder that affects around 1% of the global population (McGrath et al., 2008, Saha et al., 2005). Despite a relatively low prevalence rate, the disease burden, duration, and impact are high (Charlson et al., 2018). Schizophrenia is associated with an increased risk of developing chronic physical diseases (Launders et al., 2022), other mental health disorders (Tsai et al., 2013), high rates of unemployment (Dixon, 2017), reduced life expectancy (Hjorthøj et al., 2017) and devastatingly high suicide rates (Docherty et al., 2022).

1.1.1 Symptoms

Schizophrenia is characterised by positive, negative and cognitive symptoms. Positive symptoms refer to an excess of standard functions, such as delusions, hallucinations, disorganised thoughts, speech and behaviour. In contrast, negative symptoms refer to reduced normal behaviour, such as alogia, affective flattening, avolition or anhedonia (Correll et al., 2020). According to the Diagnostic and Statistical Manual of Mental Disorders, Fifth Edition (DSM-5), schizophrenia is diagnosed when an individual suffers from two recognised symptoms for over a month. The diagnostic symptoms are delusions, hallucinations, catatonia, disorganised speech, thoughts or behaviour, or one of the negative symptoms. One of the two symptoms must be delusions, hallucinations or disorganised speech. Alongside these active symptoms, there must also be a reduced function of work, relationships, or self-care (American Psychiatric, 2013). It is possible, therefore, to have two patients with a schizophrenia diagnosis but entirely different clinical presentations. As an added complication, the clinical presentation is rarely stable throughout the disease course (Tandon et al., 2013).

1.1.2 Incidence

In general, the clinical presentation follows a conserved timeline; after a prodromal phase, patients have their first psychotic episode, where an individual may hallucinate or enter a delusional state (an der Heiden et al., 2000). An estimated 30-40% of these individuals will develop schizophrenia (McGorry et al., 2008). A meta-analysis of schizophrenia diagnoses in England from 1950 to 2009 revealed an increased incidence rate in men in their early twenties, which steadily declined. Women's incidence is steadier and less prevalent, diagnosed less frequently than males until the mid-forties, where females marginally lead diagnoses (Figure 1.1) (Kirkbride et al., 2012).

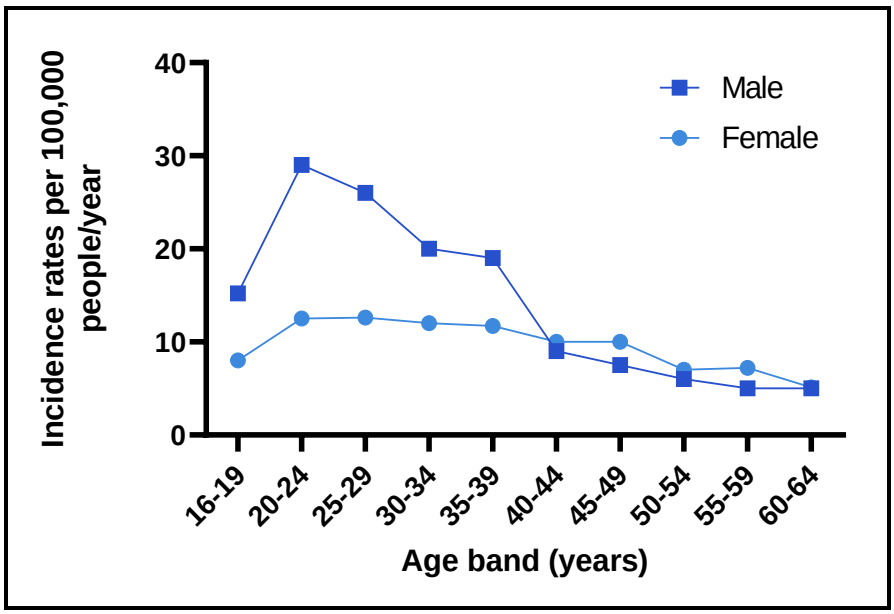

Figure 1.1: Incidence rates for schizophrenia in England from 1950-2009. (Adapted from Kirkbride et al., 2012).

1.1.3 Aetiology

The aetiology of schizophrenia is complex and heterogeneous. Early researchers of schizophrenia concluded there must be a genetic element to the disease due to the relatively high concordance rates of twins (Meehl, 1962), estimated at 44% in monozygotic twins (Avramopoulos, 2018). However, researchers also knew that compounding environmental stressors increased schizophrenia risk (Nuechterlein et al., 1984). More recently, the proposed causes of schizophrenia have been refined. The consensus is that genetic and early-life adversities alter how an individual's brain develops, resulting in a brain less resilient to stress in later life (Pruessner et al., 2017).

The advent of genomics allowed for the analysis of the whole genome in tens of thousands of patients. These studies revealed many genes that could be associated with schizophrenia risk (Schizophrenia Working Group of the Psychiatric Genomics Consortium, 2014). In addition, epidemiological data identified stressors that occurred throughout development associated with increased schizophrenia risk (Stilo et al., 2019). These environmental stressors can occur throughout neuronal development. Risk factors during pregnancy include in-utero malnutrition (Brown et al., 2008, St Clair et al., 2005), maternal infection (Estes et al., 2016, Khandaker et al., 2013) and birthing trauma (Cannon et al., 2002, Kotlicka-Antczak et al., 2014). During childhood, suffering from abuse, neglect, or adversity (Varese et al., 2012), migrating or being the child of a parent who migrated (Bourque et al., 2011), or living in a city away from green spaces

(Engemann et al., 2018) can increase risk. This genetic and environmental variation in the potential causes of schizophrenia and resulting symptom heterogeneity proves an ongoing complication in developing treatments.

1.1.4 Treatments

The goal of schizophrenia patient care is to alleviate the symptoms, prevent psychotic relapse and improve functional outcomes to encourage societal integration (Emsley et al., 2013, Patel et al., 2014). Clinicians tackle these issues with a bespoke combination of psychotherapies and antipsychotic therapies (Patel et al., 2014). Antipsychotics are a class of drugs first developed in the 1950s. In retrospect, their discovery appears serendipitous, rooted in the two World Wars, antimalarials and antihistamine drugs (Gensini et al., 2007, Krafts et al., 2012, Shen, 1999). However, since their inception, antipsychotics transformed the livelihood of patients, moving treatments from indiscriminate electroconvulsive therapy, insulin comas and lobotomies to medications that could be taken at home rather than in an institution (Remington et al., 2021, Robison et al., 2013).

1.2 Mechanisms

1.2.1 Dopamine hypothesis

The antipsychotic drugs revolutionised patient care and reframed the thinking on the underlying mechanisms of schizophrenia. The retroactive preclinical testing of the antipsychotics and studies in stimulants suggested that excessive dopamine caused positive symptoms (Bramness et al., 2016, Lieberman et al., 1987, Seeman et al., 1975), forming the basis of the dopamine hypothesis.

These ideas were refined in the early 1990s after further studies revealed dopamine levels varied in brain regions, indicating a more nuanced pathology. In addition, clozapine, which had a low affinity for the dopamine receptor, proved a highly effective drug in mitigating the positive symptoms. Building on the initial dopamine hypothesis, Davis et al. suggested that there were regional hyper- and hypo-dopaminergia. Moreover, hypo-dopaminergia in the prefrontal cortex predicted negative and cognitive symptomology (Davis et al., 1991).

The advancement of imaging studies has narrowed the dysfunction to an increased likelihood of schizophrenia patients having impaired presynaptic striatal dysfunction

resulting in increased dopamine release. This impaired signalling is thought to be a downstream consequence of many risk factors associated with schizophrenia (Howes et al., 2009).

1.2.2 Serotonin hypothesis

The antipsychotic clozapine has a low affinity for the dopamine receptor and yet has strong efficacy on symptoms. In two recent meta-analyses, clozapine was praised for alleviating positive and negative symptoms (Fabrazzo et al., 2022, Wagner et al., 2021). It transpired that clozapine had more efficacy for the serotonin 5-HT_{2A} receptor (Meltzer et al., 1989), suggesting a role of serotonin in schizophrenia pathology. Furthermore, lysergic acid diethylamide (LSD) stimulates serotonin release and can result in psychosis with a similar presentation to schizophrenia (Meltzer et al., 1989). However, the clinical data for serotonin is incredibly variable and, akin to dopamine, is considered a downstream consequence of other risk factors (Quednow et al., 2020).

1.2.3 Glutamate hypothesis

Dissociative anaesthetics that antagonise the glutamatergic N-methyl-D-aspartate receptor (NMDAr) can induce positive, negative and cognitive symptoms in healthy people, implicating the NMDAr and glutamate in schizophrenia pathophysiology (Greifenstein et al., 1958, Luby et al., 1959). These dissociative anaesthetics will be discussed in more detail in chapter three.

More broadly, the glutamate hypothesis suggests schizophrenia is due to a hypofunction of the glutamate N-methyl-D-aspartate receptor (NMDAr) (Balu, 2016). In addition to NMDAr antagonists inducing schizophrenia-like symptoms, mice that have been genetically modified to produce reduced NMDAr subunits are used to model aspects of schizophrenia behaviour and pathology (Duncan et al., 2004, Nakao et al., 2020)

Researchers have attempted to develop drugs that counteract this hypofunction with direct stimulation of NMDAr. However, this led to excitotoxicity and seizures (Witkin et al., 2021, Zeron et al., 2002). As a result, positive allosteric modulators of NMDAr and functionally linked metabotropic glutamate receptors are being developed (Dogra et al., 2022, Doreulee et al., 2009), with some showing efficacy in preclinical and early clinical trials (Geoffroy et al., 2022, Maksymetz et al., 2017, Niswender et al., 2010).

1.2.4 Neurodevelopmental hypothesis

The aetiology of schizophrenia is a combination of genetic and environmental stressors. Although schizophrenia peaks in incidence in the early twenties (Kirkbride et al., 2012), some believe that the adult onset of the disease is due to the maturation of circuitry disfigured during neurodevelopment (Pearce, 2001). Indeed, the human brain is far from its finished form at birth. Synaptogenesis, synaptic pruning, myelination and apoptosis continue throughout early life (Kolb et al., 2017, Tau et al., 2010). The prefrontal cortex is the final brain region to reach maturity at age twenty-five (Arain et al., 2013, Teffer et al., 2012).

The developmental hypothesis requires a period before symptom onset where the brain is developing atypically (Rapoport et al., 2012). Therefore, identifying individuals prior to symptom onset has been of great interest as early interventions could halt or remediate atypical development (Yung et al., 1996, Yung et al., 2011). Longitudinal studies reveal that individuals with schizophrenia showed impaired cognition thirteen or fourteen years before schizophrenia onset. Additionally, cognition continued to decline through the teenage years (Dickson et al., 2012, Jonas et al., 2022) and during the first episode of psychosis (Aas et al., 2014). After initial diagnosis, cognition declines at an expedited rate compared to healthy controls (Jonas et al., 2022).

1.3 A focus on the cognitive symptoms

Although not a prerequisite for schizophrenia diagnosis, the cognitive symptoms are highly consequential. As discussed, cognitive symptoms often predate the first episode of psychosis (Dickson et al., 2012, Jonas et al., 2022), and where other symptoms may fluctuate throughout life, cognitive symptoms remain comparatively stable (Gold, 2004). Although not every schizophrenia patient displays an impairment, it is still highly prevalent, with some 75-80% of patients suffering from cognitive symptoms (Allen et al., 2003, Leung et al., 2008).

Seven domains of cognition have been identified as affected in schizophrenia, (1) processing speed, (2) attention and concentration, (3) working memory, (4) verbal learning and memory, (5) visual learning and memory, (6) reasoning and problem-solving and, (7) social cognition (Gebreegziabhere et al., 2022). Notably, the deficits have been associated with reduced quality of life and increased need for care from relatives and professional carers (Kitchen et al., 2012, Millier et al., 2014). However, current

treatments for schizophrenia lack or have a limited impact on alleviating cognitive burdens (Stępnicki et al., 2018). Moreover, around 20% of patients report concentration and memory issues as perceived side effects of anti-psychotic treatments (McIntyre, 2009).

1.4 Pathology

Imaging is a valuable tool in understanding the brain changes in schizophrenia. Many structural irregularities, including cortical thinning, reduced hippocampal volume, and increased ventricular size, have been identified in the chronic stages of schizophrenia (van Erp et al., 2016, van Erp et al., 2018). In a longitudinal study, Ho et al. split subjects into preserved, deteriorated and compromised cognitive phenotypes and studied cortical thickness over five years. Those with preserved cognition began with scores in the tenth percentile of healthy controls and remained stable after diagnosis. Deteriorated individuals had average cognition, which then dropped below the tenth percentile post-diagnosis. Finally, the compromised group began and remained below the tenth percentile of controls. Interestingly, Ho et al. found the most pronounced change in cortical thickness in the deteriorated subtype, which correlated to the change in cognitive score (Ho et al., 2020).

The hippocampus is essential for consolidating memories from short-term storage in the hippocampus to long-term storage in the cortex (Sakaguchi et al., 2012). Hippocampal-dependent cognition includes episodic-like memory recall, spatial learning and contextual fear, as ablation of the hippocampus eradicates these abilities in rodent studies (Fanselow et al., 2010). Schizophrenia can alter hippocampal morphology. In addition to volume reductions, the hemispheres can become asymmetrical or deformed. The functionality of the hippocampus is also impaired, with increased glutamate levels, basal activity, cerebral blood flow, and hypoconnectivity of the hippocampal-prefrontal pathway (Wegrzyn et al., 2022).

The hippocampus signals directly and indirectly with the prefrontal cortex (PFC), facilitating memory acquisition, consolidation and retention (Ferraris et al., 2021, Qin et al., 2021). Beyond memory storage, the PFC is essential for working memory, response inhibition, interference control, set-shifting, planning and decision-making (Friedman et al., 2022), many of which are implicated in schizophrenia (see section 1.3). Beyond

cognitive function, outputs from the PFC to the striatum have been associated with impaired reward integration, a negative symptom (Morris et al., 2015) and in reality monitoring, associated with positive symptoms (Zmigrod et al., 2016).

Researchers can measure superficial electrical changes with electroencephalography (EEG) recordings. Gamma oscillations are the highest brain wave frequency possible and are associated with high perception and cognition (Adaikkan et al., 2020, Müller-Putz, 2020). Furthermore, in healthy individuals, gamma oscillations increase proportionately with task complexity (Basar-Eroglu et al., 2007, Cho et al., 2006, Howard et al., 2003). Alterations to gamma oscillations were detectable in first-episode patients, with regional high gamma activity at rest in patients (Andreou et al., 2015), which was present in chronic schizophrenia patients (Venables et al., 2009), suggesting impaired regulation of appropriate neuronal activity. When patients are challenged with a cognitive task, gamma frequency firing does not adapt to the task (Basar-Eroglu et al., 2007, Cho et al., 2006, Mainy et al., 2007). Indeed, evoked entrainment of neurons to a gamma frequency revealed an inability to induce or maintain gamma frequency oscillations (Kwon et al., 1999, Light et al., 2006). A key contributor to gamma frequency oscillation induction and maintenance are the parvalbumin interneurons (PVI) (Atallah et al., 2009, Buzsáki et al., 2012, Cardin et al., 2009, Le Roux et al., 2013, Malik et al., 2017).

1.5 Parvalbumin interneurons

1.5.1 Structure

PVIs are fast-spiking GABAergic neurons that express the calcium-binding protein parvalbumin (Kretsinger et al., 1989). The eponymous parvalbumin acts as a slow-calcium buffer which binds free calcium altering synaptic plasticity and dynamics (Caillard et al., 2000, Vreugdenhil et al., 2003). The presence of a slow-calcium buffer does not equate to a slow-firing neuron. On the contrary, the PVI is highly specialised to generate rapid, potent and precise signals. The dendrites of a PVI are long, often spanning several cortical layers. The surface of the dendrites and PVI cell body are littered with predominantly excitatory synapses, allowing for broad surveillance of cortical activity. Inhibitory synapses allow regulation from other PVI (Hu et al., 2014). The PVI have a unique combination of voltage-gated channels and glutamate receptors that allow for the generation of fast and uniform signals characterised by rapid

depolarisation and repolarisation of the membrane (Geiger et al., 1997, Goldberg et al., 2003, Kondo et al., 1997, Martina et al., 2000, Rudy et al., 2001).

The axon of the PVI is sparingly myelinated (Micheva et al., 2016). The axonal initial segment is unmyelinated, with the first myelin internode a distance down the axon. From here, the myelin sheathes the axon at its thickest points, leaving the thin distal axon terminals unmyelinated (Stedehouder et al., 2019, Stedehouder et al., 2017). The myelin surrounding PVI axons is more dispersed and has a different protein composition than the myelin found around excitatory neurons (Micheva et al., 2016). Typically, myelin is associated with long-distance signalling. In PVI, myelin is found in local relay systems and assists in maintaining fast-firing signals (Benamer et al., 2020). In addition, the myelin surrounding PVI axons contains a protein associated with the delivery of trophic support from oligodendrocytes to the mitochondria-rich PVI axon (Micheva et al., 2018, Snaidero et al., 2017).

The peripheral axon arborises to an impressive degree, resulting in thousands, even tens of thousands of axon terminals (Karube et al., 2004, Sik et al., 1995). In the prefrontal cortex, PVIs indiscriminately project onto virtually all its local pyramidal neurons (Packer et al., 2011). Along the axon's length, sodium channel distribution becomes more frequent, allowing the action potential to continue at high speeds down this now unmyelinated, thin and frequently dividing axon (Hu et al., 2015).

At the axon terminals, GABA is synthesised by glutamic acid decarboxylases (GAD) and packed into a vesicle by vesicular GABA transporter (VGAT) (Lee et al., 2019). The descending action potential triggers the opening of the P- and Q-type calcium channels that reside proximally to the GABA release sites. On activation, they rapidly and precisely facilitate the influx of calcium ions (Zaitsev et al., 2007). The calcium ions, in turn, trigger the exocytosis of GABA from the PVI axon (Lonchamp et al., 2009).

PVI project a powerful, fast inhibitory signal onto principal excitatory neurons. The precise location depends on their morphology. The more prevalent basket cells project onto target cells' soma and proximal dendrites, whereas the chandelier cells innovate the axonal initial segment (Kawaguchi et al., 1997). Due to the location of their projections, it has been proposed that basket cells modulate target cell inputs, and chandelier cells target cell outputs (Povysheva et al., 2013).

1.5.2 Function

The structure of PVIs suggests that they can produce a powerful, rapid inhibitory signal. This structure is utilised to produce and maintain gamma-frequency brain waves. Gamma waves are the highest frequency brain oscillations operating at 30 - 100Hz. They are detected typically during cognition, learning and memory (Malik et al., 2017). The PVI utilise their high connectivity (Packer et al., 2011) to orchestrate widespread inhibition (Buzsáki et al., 2012). The evidence for the involvement of PVIs in gamma wave oscillations is as follows: (1) the direct modulation of gamma activity by optogenetic silencing and stimulation of PVI (Cardin et al., 2009). (2) Fractional changes to PVI activity proceeding changes in gamma wave oscillations (Atallah et al., 2009). (3) PVIs synchronicity during gamma oscillations (Le Roux et al., 2013).

PVIs are also involved in feedback and feedforward inhibition (Campanac et al., 2013, Klausberger et al., 2008). Beyond simple inhibition, PVI can regulate the window for temporal summation of neuronal inputs (Pouille et al., 2001), detect marginal differences in excitatory input and inhibit all but the strongest signals (de Almeida et al., 2009) and proportionately inhibit excitatory neurons dependent on their excitatory input (Xue et al., 2014). Indeed, PVIs are critical regulators of balancing excitatory and inhibitory systems (Campanac et al., 2013).

Given PVI's ubiquitous connections, fast-firing nature and persistent monitoring, they are uniquely susceptible to damage. Most pressingly, PVIs require significant energy supplies. Oxygen consumption can increase by 30% during gamma oscillations and glucose metabolism by around 50%, reaching levels comparable to those seen in seizures. The greater the gamma frequency change or duration, the more glucose is required (Kann et al., 2014). Impaired mitochondria will impair PVI function (Inan et al., 2016, Whittaker et al., 2011). Furthermore, dysfunction in mitochondrial signalling can lead to oxidative stress and inflammation (Cuenod et al., 2022). PVI are sensitive to oxidative stress (Cabungcal et al., 2013a, Steullet et al., 2017) and inflammation (Behrens et al., 2007, Behrens et al., 2008). High levels of both can reduce PVI function and inhibitory output, ultimately leading to cognitive impairments. Unfortunately, oxidative stress and inflammation can worsen mitochondrial function (Cuenod et al., 2022), indicating the potential for a vicious cycle.

1.5.3 PVI in schizophrenia

There have been several reports of reduced PVI density in the PFC (Chung et al., 2016, Enwright et al., 2016, Fung et al., 2010, Hashimoto et al., 2003, Hoftman et al., 2015, Lewis et al., 2001) and hippocampus (Zhang et al., 2002) of schizophrenia patients. Interestingly, these differences are thought to be due to reductions in the parvalbumin protein rather than loss of the neuron itself (Filice et al., 2016, Thune et al., 2001). Considering the function of the parvalbumin protein for moderating calcium dynamics, changes in protein levels may alter PVI output.

Alterations to the channels that permit the rapid signalling of the PVI would affect its functionality. Many channels associated with the fast-firing phenotype are reduced in schizophrenia (Georgiev et al., 2014, Yanagi et al., 2014). Alternatively, mutations that alter channel functions are associated with increased schizophrenia risk (Chen et al., 2022, Guardiola-Ripoll et al., 2022, Harrison et al., 2022, Schizophrenia Working Group of the Psychiatric Genomics Consortium, 2014, Xie et al., 2018).

Efficient GABAergic output from a PVI also depends on effective GABA production and release at the synapse. However, in schizophrenia, GAD67 is reduced, suggesting impaired GABA synthesis (Hashimoto et al., 2003, Hoftman et al., 2015, Sibille et al., 2011, Volk et al., 2000, Volk et al., 2016). Mutations to the GAD67 gene have been associated with early-onset schizophrenia, reduced grey matter volume and impaired frontal lobe function (Addington et al., 2005). Parvalbumin and GAD67 expression appears functionally linked (Hashimoto et al., 2003). Indeed, it is theorised that GAD67 reductions are a maladaptive response to perceived reduced glutamatergic innervation on PVI due to NMDAr hypofunction (Gonzalez-Burgos et al., 2008).

Regarding GABA transport, GAT-1 is a transporter protein proximal to PVIs' synapses (Woo et al., 1998). GAT-1 activity determines the rate of GABA removal from the synaptic cleft. Blocking GAT-1 increases the duration of evoked inhibitory postsynaptic currents in target cells (Overstreet et al., 2003). These findings are relevant to schizophrenia as unmedicated patients have a 40% reduction in reactivity to GAT-1 antibody in the PFC (Woo et al., 1998).

1.6 Perineuronal nets

Perineuronal nets (PNN) describes the extracellular matrix, which preferentially forms around PVI in the cortex and hippocampus (Härtig et al., 1992, Yamada et al., 2015a, Yamada et al., 2015b) and excitatory synapses in the CA2 region of the hippocampus (Carstens et al., 2016). The PNN can modulate the maturation, function and survivability of the PVI. As such, PNNs have been implicated in schizophrenia pathology (Brückner et al., 2003, Carulli et al., 2010, Wen et al., 2018b).

1.6.1 Components

Beginning from the membrane surface, all PNNs begin with a hyaluronic acid synthase (HAS). These enzymes are exclusively expressed in neurons. PVI express two versions, HAS2 and HAS3 (Carulli et al., 2006). The HAS synthesises a long, unbranching chain of hyaluronic acid (HA), which projects into the extracellular space. In addition to anchoring the remaining PNN to the PVI surface, these large chains form tightly intertwined loops which alter the intracellular space and the diffusion capabilities of extracellular molecules (Hascall et al., 1997). Indeed, in HAS knockout, the cell bodies of CA1 become densely packed with little extracellular space increasing seizure risk (Arranz et al., 2014).

The next components of the PNN are the link proteins, Ctrl1 and Bral2. Both proteins are exclusively expressed by PNN-positive neurons (Bekku et al., 2003, Carulli et al., 2006). Link proteins bind the HA to the N-terminal region of the chondroitin sulphate proteoglycans (CSPGs) (Carulli et al., 2006). The CSPGs are the most dynamic and diverse element of the PNN. The four CSPGs, aggrecan, brevican, versican and neurocan, have similar structures, differing in length and, therefore, the number of chondroitin sulphate chains. Versican has four isoforms, which vary in length. The longest three, V0, V1 and V2, are included in the PNN (Avram et al., 2014, Zimmermann et al., 2008). The final component of the PNN is tenascin, of which there are two variants, C and R. The tenascins ensure a dense and regular net formation (Brückner et al., 2000, Galtrey et al., 2008, Lundell et al., 2004, Suttkus et al., 2014, Weber et al., 1999) (Complete structure in Figure 1.2).

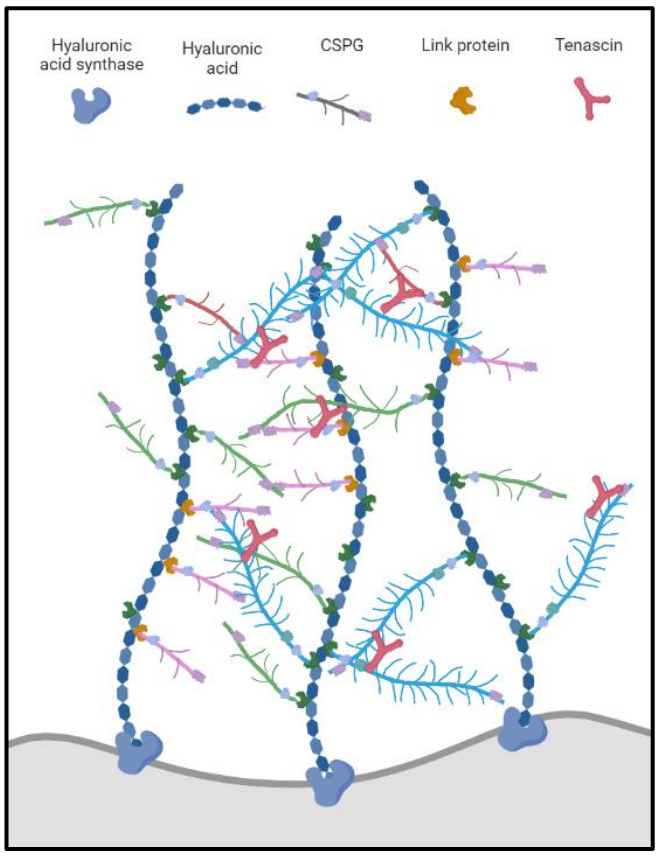

Figure 1.2: Schematic diagram of mature PNN. Hyaluronic acid synthases on the surface of the PVI produce a hyaluronic acid backbone which extends into the extracellular space. The four CSPGs, aggrecan, brevican, versican and neurocan, bind to hyaluronic acid via link proteins. Finally, tenascins attach to the terminal ends of the CSPGs.

1.6.2 Development

The PNN structure is developmentally regulated. In a seminal paper, Milev et al. measured the expression of the PNN components in the developing rat brain from gestational day (GD) 14 to eight months of age. The foetal brain expresses high levels of neurocan and V1 versican. However, these expressions rapidly decline three-fold in the first week of postnatal life. Meanwhile, the expression of aggrecan, brevican and V2 versican increase during postnatal life, then plateau in adulthood (postnatal day (PD)100+) (Milev et al., 1998).

Despite the expression of PNN components, the PNN is first detected with immunohistochemistry between the second and third postnatal week (Carulli et al., 2010, Paylor et al., 2016). In a fascinating study, Kwok et al. recreated PNN on the surface of a kidney cell. Transfecting the kidney cells with HAS3 resulted in a diffuse PNN. Adding Ctrl1- and aggrecan-expressing cells resulted in a dense PNN in cells that typically do not produce an extracellular matrix. Ctrl1- and aggrecan-expressing cells alone produced no matrix (Kwok et al., 2010). This study suggests that HAS is critical for the

initial anchoring of the PNN to the cell surface, and Crtl1 and aggrecan are necessary for dense formation.

Indeed, in the neonatal visual cortex, the PNN components, including HAS3 and aggrecan, are detectable on PD3. However, when Ctrl1 expression surges on PD14, the PNN begins to form (Carulli et al., 2010). Interestingly, dark-rearing animals reduced PNN density in the visual cortex, indicating impaired maturation (Ye et al., 2013).

1.6.3 Critical period closure

The visual cortex and dark rearing illustrate one of the functions of PNN excellently. From PD14, PNN levels in the visual cortex increase rapidly, doubling in density in the first two weeks. This growth is short-lived. By PD42, density has peaked (Ye et al., 2013). This early-life period coincides with the critical period of the visual cortex. During this time, visual inputs shape the connections and projections of the primary visual cortex and the period is associated with high plasticity, adaptability and learning (Hensch, 2005).

Monocular deprivation from birth will result in an ocular dominance shift. As the developing visual cortex receives signals from only the unaffected eye, the visual cortex adapts and only caters to the eye from which it receives signals. If the same protocol were repeated in an adult cat (monocular deprivation for three months), there would be no alteration to the visual cortex as the adult cortex was wired to receive input from both eyes and would remain that way despite intervention. The remarkable finding was that if a kitten who used both eyes for the first five weeks of life underwent monocular deprivation, there was an ocular dominance shift. In other words, the number of cells in the visual cortex responding to the unaffected eye increased, suggesting plasticity (Wiesel et al., 1963).

The juvenile visual cortex is highly plastic and adaptable to changing inputs. However, after the closure of a critical period, this plasticity ceases. At the same time, PNN density is increasing in the visual cortex. The connection between PNN maturation and critical period closure was found to be more than a correlation by Pizzorusso et al. Pizzorusso and colleagues injected chondroitinase ABC (ChABC) into the visual cortex of adult rats every two days for seven days. ChABC is a bacterially derived enzyme which breaks down the chondroitin sulphate branches of CSPGs (Suzuki et al., 2017). After the breakdown

of the PNN, monocular deprivation in adult rats resulted in an ocular dominance shift (Pizzorusso et al., 2002). This finding was replicated when aggrecan was knocked out from the visual cortex (Rowlands et al., 2018).

This ability to revert the brain to a juvenile state of plasticity was not exclusive to the visual cortex. In the basolateral amygdala, PNN density increases during early life. In adult rodents, fear conditioning produces a permanent fear response. Gogolla et al. compared fear responses in animals who started fear conditioning on PD16 and PD23. Although both showed freezing behaviour on the first and second day after training, exposure to the conditioned stimulus seven days later resulted in a fear response in the PD23 animals only. PNNs were again degraded in three-month-old rats, and re-exposure revealed the erasure of fear memories. In this case, the timing of PNN degradation was critical as fear memories were not erased if the PNN was depleted after fear conditioning (Gogolla et al., 2009a).

1.6.4 Modulation of plasticity

Given the evidence from critical period closure, PNN appears to limit the plasticity and activity of the neuron it surrounds. Further evidence comes from studies where PNN depletion improves cognition in adult rodents. For example, Romberg et al. saw improved recognition memory by deleting Ctrl1 or with ChABC administration to the perirhinal cortex (Romberg et al., 2013). In addition, working memory was enhanced when ChABC was administered to the PFC (Anderson et al., 2020) and in tenascin-R knockout mice (Morellini et al., 2010).

There are many theories as to how PNN can limit plasticity. Perhaps it is simple; the PNN forms a physical barrier that reduces the available surfaces for synapses to form. Indeed, the neuronal surface under the PNN is devoid of synaptic connections. Thus, a dense PNN would have fewer synapses (Brückner et al., 1993). Perhaps it is the polar nature of the PNN, chemically impeding the diffusion of secreted molecules (Gruskin et al., 2003). Finally, a study by Frischknect et al. suggested that the size of pores within a PNN can affect AMPAr receptor mobility and cycling. Removing the PNN removes those limits on movement, resulting in greater plasticity and paired-pulse ratios, suggesting facilitation (Frischknecht et al., 2009).

Knockout studies can give insight into the function of the individual components of the PNN. Table 1.1 summarises the outcomes of these studies. Many molecular outcomes measured in the knockout studies would typically be associated with poor cognitive outcomes, namely reduced PVI density (Favuzzi et al., 2017, Romberg et al., 2013, Rowlands et al., 2018), altered LTP dynamics (Brakebusch et al., 2002, Evers et al., 2002, Saghatelyan et al., 2001, Zhou et al., 2001) and impaired neurotransmission (Arranz et al., 2014, Favuzzi et al., 2017, Schmidt et al., 2020, Weber et al., 1999). Despite this, most demonstrated improved cognition, though limited in scope.

The work by Carulli and Kwok (discussed in section 1.6.2) suggested that Ctrl1 is imperative for PNN formation (Carulli et al., 2010, Kwok et al., 2010). In addition, the PNN of the aggrecan knockout mouse was severely reduced (see Figure 1.3), indicating that aggrecan acts as a scaffold for the remaining PNN (Rowlands et al., 2018). Perhaps the PNN will never form or mature in the Ctrl1 and aggrecan knockouts. Considering then the plasticity observed in the knockout models, these animals may maintain a prolonged state of juvenile plasticity. Given the requirement of PNN, and likely the PVI, to preserve fear memories, the cognitive enhancements seen in the knockout models may not withstand a withdrawal and retrieval period.

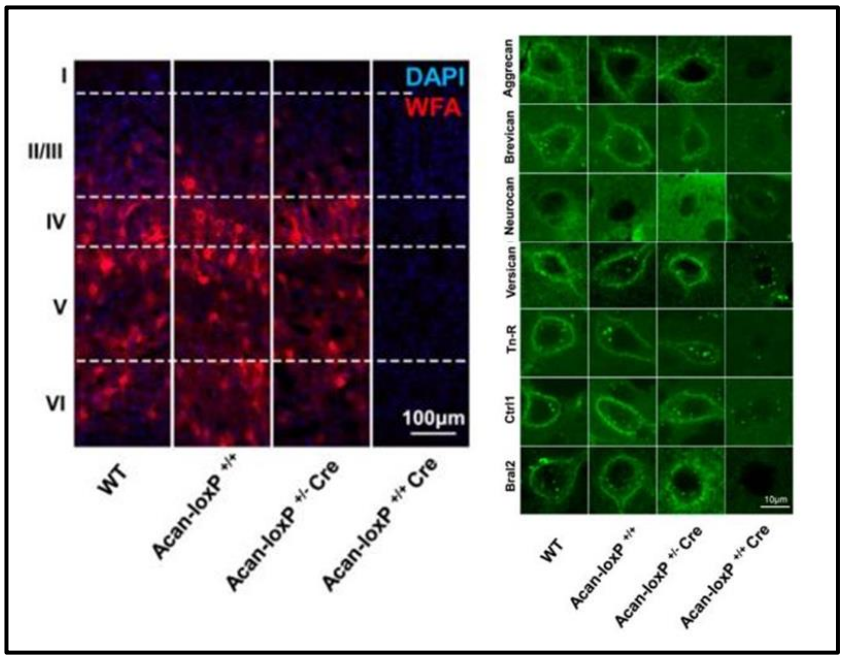

Figure 1.3: PNN staining in aggrecan knockout mouse. The left-hand image shows the layers of the barrel cortex in wildtype (WT), controls and the aggrecan knockout (Acan-loxP$^{+/+}$ Cre). The PNN stain wisteria floribunda (WFA) is absent in the knockout. The right-hand image shows representative images of each PNN component: aggrecan, brevican, neurocan, versican, tenascin-R (Tn-R), Crtl1, and brain link protein 2 (Bral2). (Taken from: Rowlands et al., 2018).

Table 1.1: Cellular origins of PNN components and knockout studies. HA(S): hyaluronic acid (synthases), Acan: aggrecan, Bcan: brevican, V2: mature versican, Ncan: neurocan, Tn: tenascin. N: neuronal, A: astrocytes, O: oligodendrocytes, NG2: oligodendrocyte progenitor cell. CA1: hippocampal region, DG: dentate gyrus, LTP: long-term potentiation, ECM: extracellular matrix, GAD: glutamic acid decarboxylase. (Cellular origins from: Carulli et al., 2006, Song et al., 2018)

Target	Cellular origin				Molecular	Behaviour	Reference
	N	A	O	NG2			
HAS2	+				↔ CA1, ↓ DG HA	-	(Arranz et al., 2014)
HAS3	+				↓ HA ↓ intracellular space, ↑ neuronal density	↑ seizure risk	
Ctrl1	++				↓ paired-pulse facilitation	↑ recognition memory	(Romberg et al., 2013)
					Diffuse/low-intensity PNN ↓ PNN around dendrites ↓ PVI density	↑ ocular plasticity	(Carulli et al., 2010)
Bral2	++				Colocalises with brevican		(Bekku et al., 2003)
Acan	++	++			↓ PNN ↓ PVI intensity	↑ ocular plasticity ↑ recognition memory	(Rowlands et al., 2018)
Bcan	+	+++			↑ neurocan Reduced LTP maintenance in adult	↔ active avoidance	(Brakebusch et al., 2002)
					↓ PVI density and activity ↓ glutamatergic synapses	↓ spatial working memory ↓ recognition memory	(Favuzzi et al., 2017)
V2	+	+	+++	++	↓ECM around nodes of Ranvier	-	(Dours-Zimmermann et al., 2009)
Ncan	+++	+			Reduced LTP maintenance in adult	-	(Zhou et al., 2001)
					↓ Aggrecan, ↑ brevican and ↑ ctrl1 protein ↓ GAD65/67 in PVI synapses	-	(Schmidt et al., 2020)
Tn-C	+	+++			↓ LTP ↓ L-type calcium channel signalling	-	(Evers et al., 2002)
Tn-R	++	+	+++	++	↑ PVI	↑ working memory	(Morellini et al., 2010)
					Diffuse PNN reduced stain for HA, Bcan and Ncan	-	(Brückner et al., 2000)
					↓ LTP, ↑ basal excitatory synapse activity	-	(Saghatelyan et al., 2001)
					↓ conduction velocity	-	(Weber et al., 1999)

A lack of PNN is consequential for PVI, as without it, they cannot mature. During development, a homeoprotein called orthodenticle homeobox 2 (Otx2) binds to the chondroitin-6-sulphates on PNN. The PNN assists the transfer of Otx2 into the PVI (Beurdeley et al., 2012), resulting in PVI maturation likely through altering gene transcription. Initially, these PNN-Otx2-PVI interactions cascade, with the maturing PVI producing more PNN that can capture more Otx2. The more Otx2, the quicker the PVI matures. Eventually, a criticality is reached where Otx2 no longer enters the PVI. This plateau could be due to the PNN becoming too dense (Beurdeley et al., 2012; Spatazza et al., 2013) or a developmental switch from chondroitin-6-sulphates to chondroitin-4-sulphates, which prevents Otx2 binding. Regardless of the precise mechanisms, the result is a stable mature PNN and PVI (Miyata et al., 2017).

Now consider the brevican (Bcan) knockout. Here the PNN appears similar to the wild type (Blosa et al., 2015, Brakebusch et al., 2002). However, the brevican knockout has impaired working and recognition memory. To understand the underlying mechanism, the function of brevican must be understood. Brevican is specifically enriched around synaptic sites (Blosa et al., 2015, Favuzzi et al., 2017). Interestingly, PVI that contain brevican in their PNN ($Bcan^{+/+}$ PVI) have two-fold the number of excitatory synapses (vesicular glutamate transporter (VGlut1) and postsynaptic density (PSD95)) compared to PVI without brevican ($Bcan^{-/-}$ PVI). Due to this, PVI associated with Bcan have different firing capabilities. Although less excitable, $Bcan^{+/+}$ PVI can fire faster and stronger than a $Bcan^{-/-}$ PVI (Favuzzi et al., 2017).

In the Bcan knockout, the PVI has reduced excitatory synapses (VGlut/PSD95) and altered firing dynamics, suggesting that Bcan is essential for synaptic development or maturation. Furthermore, isolation of the neuronal membranes and the synaptosomes showed that the AMPAr subunit GluA1 was predominately found in the membrane region rather than the synaptosome, suggesting altered GluA1 trafficking in the Bcan knockout. Indeed, analysis of the synapses revealed a 50% reduction in GluA1-VGlut/PSD95 clusters. Finally, the clusters of potassium channels integral to the fast-firing PVI phenotype were also reduced. The Bcan knockout causes profound impairment of PVI synaptic dynamics resulting in the cognitive impairments detected (Favuzzi et al., 2017).

1.6.5 Protection

Another speculated role of the PNN is to protect the neuron it surrounds. PVIs are more susceptible to oxidative stress (OS) than other interneurons (Cabungcal et al., 2013a), likely due to the high PVI energy demand required for PVI function (Kann et al., 2011). Both schizophrenia patients (Flatow et al., 2013, Kim et al., 2017b) and animal models relevant to schizophrenia suggest ongoing and prolonged OS. In a comprehensive review, Steullet et al. combined data from several diverse models and found a correlation between high oxidative stress levels and low PNN (Steullet et al., 2017).

Suttkus et al. studied the effects of oxidative stress in genetically modified mice. Wild-type mice were compared to knockout mice of brevican, Crtl1 or tenascin-R and aggrecan knockdown mice. All were treated with iron (III) chloride ($FeCl_3$). $FeCl_3$ causes the spreading of neurodegeneration and propagation of oxidative stress. In wild-type and brevican knockout mice, there was less neurodegeneration in neurons surrounded by perineuronal nets. However, in the remaining cohorts, there was no difference between those with a net and those without, indicating that the protective effect of the PNN was abolished (Suttkus et al., 2014).

1.6.6 PNN remodelling

The PNN is a dynamic structure that adapts to neuronal and system-wide changes. Selectively inhibiting a PVI can result in PNN downregulation in that PVI alone (Devienne et al., 2021). Equally, subjecting organotypic slices to non-physiological levels of potassium increases PNN expression. Subsequent blockade of calcium channels reduces PNN development (Brückner et al., 2001, Dityatev et al., 2007).

PVI and PNN are also intrinsically linked. Yamada et al. noted that parvalbumin staining intensity was increased in PVI surrounded by PNN, which they speculated was due to PNN moderating PVI maturation. Notably, the degradation of PNN with ChABC reduced PVI intensity without a loss of PVI cell number (Yamada et al., 2015b).

PNNs are broken down by two classes of enzymes. First, A disintegrin and metalloproteinase with thrombospondin motifs (ADAMTS) is a large family of enzymes. In the PNN, they cleave the proteoglycan proximal to the link protein prior to the chondroitin sulphate-rich region (Gottschall et al., 2015). Howell et al. phenotyped ADAMTS1 deficient mice. They expected that PNNs would increase in the mice; instead, they found no change to brevican or versican in the infant or juvenile mice. Infant (PD8)

female, not male, mice had increased neurocan relative to controls. This dichotomy suggests a sex-dependent difference in ADAMTS activity or flexibility to ADAMTS1 deficiency. Interestingly, adult (PD90) female mice had reduced expression of synaptic markers in the PFC compared to WT and males, but no groups saw learning or memory deficits. (Howell et al., 2012).

The matrix metalloproteinases (MMP) are a second family of enzymes that modulate PNN formation by digesting CSPGs (Ethell et al., 2007). MMP9 is the most widely studied regarding PNN. Oxidative stress-susceptible mice have upregulated MMP9. Predictably, these mice had reduced PNN expression and delayed PVI maturation. By suppressing MMP9 activity, normal PVI and PNN maturation took place despite congenital or spontaneous oxidative insult. Thus, this enzyme has intriguing prospects as a therapeutic target (Dwir et al., 2019). Fragile X is a genetic, developmental condition modelled in mice by Fmr1 gene knockout. Fmr1 null mice show altered PVI and PNN maturation, increased MMP9 expression and increased response to auditory stimuli. Wen et al. introduced an MMP9 knockdown to Fmr1 null mice and found that PVIs surrounded by PNN did not reduce in number. Moreover, MMP9 knockdown mice had a functional recovery of the auditory cortex (Wen et al., 2018a).

1.6.7 PNN in schizophrenia

There have been a handful of studies looking at PNN expression in schizophrenia. Post-mortem analyses have found reductions in PNN intensity in the PFC (Enwright et al., 2016, Mauney et al., 2013), lateral amygdala and lateral entorhinal cortex (Pantazopoulos et al., 2010). Crucially, these reductions are not global, with the visual cortex having insignificant increases in PNN (Mauney et al., 2013) and adjacent parts of the amygdala and entorhinal cortex showing no significant alterations (Pantazopoulos et al., 2010).

Reduced PNN may be due to an increased breakdown. Indeed, schizophrenia patients have increased serum MMP9 (Ali et al., 2017, Devanarayanan et al., 2016, Domenici et al., 2010, Yamamori et al., 2013). Increased MMP9 was correlated to increased markers of oxidative stress (Devanarayanan et al., 2016) and Positive and Negative Syndrome Scale (PANSS) scores (Ali et al., 2017). Whether these multi-system peripheral markers give a true insight into brain pathology remains a contention.

1.7 Chapter aims

Chapter 3: Characterisation of the subchronic phencyclidine model

1. Determine whether scPCP administration induces biomarker alterations relevant to the proposed mechanism (Figure 3.4).
2. Update the mechanism accordingly, with a focus on finding self-perpetuating interactions to speculate on how the cognitive deficits observed in the scPCP model are maintained.

Chapter 4: Effects of apocynin and minocycline in the scPCP model

1. Establish if subchronic dosing of apocynin or minocycline could attenuate the scPCP-induced NOR deficit.
2. Use central and peripheral markers of oxidative stress and inflammation to evaluate the mechanisms of drug action.
3. Measure protein targets used in the characterisation study to understand whether subchronic dosing reverses pathology.

Chapter 5: Effects of exercise in the scPCP model

1. Establish if there is evidence of altered BDNF or TrkB in scPCP-treated animals.
2. Determine the cognitive and molecular outcomes after acute and chronic exercise to understand how and when changes occur.
3. Investigate whether exercise is having any effects on the proposed scPCP mechanisms.

Chapter 6: Characterisation of the Poly (I: C) model

1. Measure markers studied in the scPCP model in the PIC model to establish if there are points of convergence and divergence.
2. Evaluate the proteins in adolescent and adult time points to understand the developmental timeline of pathology.

CHAPTER 2: METHODS

2.1 Rat husbandry

For all studies, rats were housed in double-decker cages (38×59×24 cm, GR1800, Techniplast, Italy). Each cage contained sawdust, sizzle nest bedding and a cardboard play tunnel (Datesand Group, UK). Standard rodent chow (Special Diets Services, UK) and water were available *ad libitum* unless otherwise stated. Temperature and humidity were controlled at 21^{o}C ± 2^{o}C and 55% ± 5%, respectively. Rat health was monitored through observation and weekly weighing. Unless otherwise stated, the lights were on a 12-hour light cycle with lights on at 7:00 am. All procedures carried out were under the UK Animals (Scientific Procedures) Act of 1986 and had been accepted by the University of Manchester's Animal Welfare and Ethical Review Body.

2.2 scPCP induction

Female Lister Hooded rats (239.5 ± 18.8g (mean ± standard deviation)) from Charles River were dosed using phencyclidine (2 mg/Kg, i.p.) or vehicle (0.9% saline, i.p.) bi-daily (10:00 and 16:00) for seven days. Animals then underwent a minimum of a 7-day washout, during which minimal handling occurred (Grayson et al., 2007, Neill et al., 2010).

2.3 Novel object recognition

2.3.1 Rationale

Novel object recognition (NOR) is a simple task to test recognition memory. It benefits from being a quick test with no training or adverse stimuli. The standard NOR test comprises two trials, acquisition and retention. In the first trial, animals can freely explore two identical objects. Then, animals are removed from the testing arena for an intertrial interval of variable length. In the retention phase, objects are replaced with two new objects, one familiar (i.e., the object from the acquisition trial) and a novel object. A naïve rat with intact recognition memory would spend more time exploring the novel object due to their innate preference for novelty (Grayson et al., 2015).

2.3.2 Apparatus

The NOR box is 50x50x50 cm. The walls are black plexiglass, and the white plexiglass floor is divided into nine equal squares by black lines. The objects, a drink can or a brown glass drug bottle, were placed in opposing crosshairs of the central lines (Figure 2.1). The

testing room was lit with standard lighting (8 lux), and overhead cameras recorded the animals.

Figure 2.1: NOR apparatus.

2.3.3 Habituation

Prior to behavioural testing, rats were habituated to the NOR testing arena. First, rats were allowed to explore the empty testing arena with cage mates for 15 minutes. Then, 24 hours later, rats were habituated individually in an empty arena for 15 minutes. If a rat jumped out of the testing arena during habituation, a Perspex sheet was placed over the box during testing.

2.3.4 Testing

Testing consisted of an acquisition and retention trial. Initially, the rat was placed in the corner of the arena facing the wall equidistant from both objects. The objects in the acquisition trial are identical. The rat was allowed 3 minutes to explore the objects freely. The animals were then removed and held in a holding arena adjacent to the testing arena for one minute. In the intertrial interval, the arena was wiped clean without using chemicals and the objects were replaced. Finally, in the retention phase, the rat was returned to the holding arena in the same corner. Rats were again allowed 3 minutes to explore the familiar and novel object freely. The rat was then returned to the home cage. Between rats, the arena and objects were cleaned with fragrance-free disinfectant (Phoenix, Anistel). The order and the types of objects used in each trial were

pseudorandomised to ensure the placement was not repeated for each animal across multiple NOR tests.

2.3.5 Scoring

Tapes were allocated randomised numerical codes and scored in ascending order. An animal would be considered exploring if they were actively licking, sniffing, or biting objects. Exploration time was calculated using the NOR timer (accessed: jackrrivers.com/program/). The discrimination index was calculated by finding the difference between time spent at the novel and familiar object and dividing this by total exploration time.

$$\text{Discrimination index (DI)} = \frac{\text{Time}_{\text{novel}} - \text{Time}_{\text{familiar}}}{\text{Time}_{\text{novel}} + \text{Time}_{\text{familiar}}}$$

2.3.6 Line crosses

The number of times the animal crossed the lines on the floor of the NOR chamber (Figure 2.1) was measured for both trials as a measure of locomotor activity.

2.4 Brain region classification

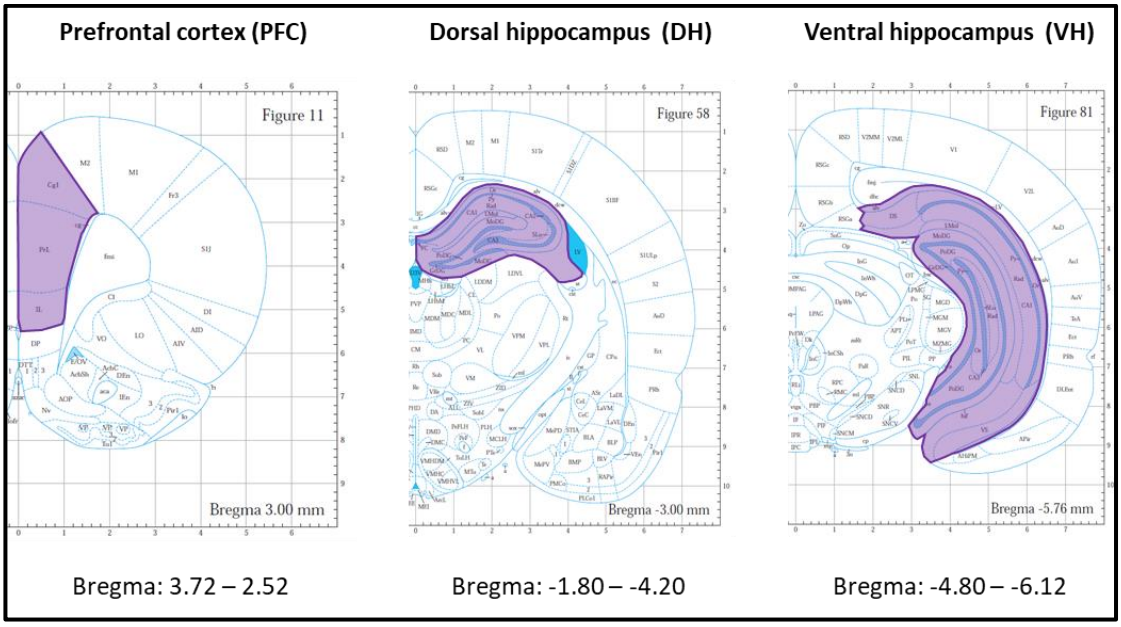

Figure 2.2: Regions of the brain used for post-mortem analysis. Bregma measurements are in millimetres (Adapted from Paxinos et al., 2007).

The definition of the ventral hippocampus used in this thesis is a misnomer. The region dissected here includes the intermediate hippocampus, which is functionally distinct from the ventral hippocampus. The ventral hippocampus would occupy the bottom third of the marked area in Figure 2.2 (Avramopoulos, 2018, Bast et al., 2009). The results using this region should be interpreted with caution.

2.5 mRNA quantification

2.5.1 Tissue collection

Rats were culled by increasing concentration of carbon dioxide, and death was confirmed by cervical dislocation. Brains were stored in RNAlater (Sigma), frozen on dry ice, and stored at -80°C.

2.5.2 Frozen brain dissection

The brains were thawed sufficiently to remove RNAlater. Dissections were completed on a plastic box covered in foil filled with dry ice to keep brains frozen to preserve RNA. The prefrontal cortex (PFC) and dorsal hippocampus (DH) were dissected and stored in RNAlater at -80°C. The following markers were used as the PFC was more difficult to isolate in tissue slices. The anterior PFC was identified in coronal sections using the earliest detection of the forceps minor of the corpus callosum. Posteriorly, the corpus callosum formation marked the PFC's termination. The PFC was isolated from these sections by cutting alongside the white matter landmarks on the lateral edges of the PFC. The rhinal fissure was used to estimate the ventral edge of the PFC. Finally, the highest point of the forceps minor of the corpus callosum was used to mark the dorsal edge of the PFC (see Figure 2.3).

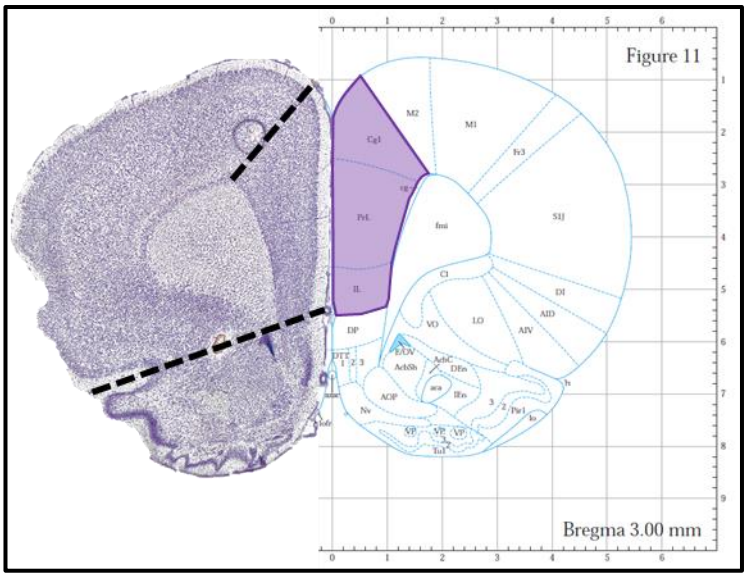

Figure 2.3: Landmarks used to dissect the prefrontal cortex in frozen sections. (Adapted from Paxinos et al., 2007).

2.5.3 RNA extraction

RNA was extracted using the innuPREP DNA/RNA Minikit (Analytik Jena). Dissected samples were sufficiently thawed on ice to remove the RNAlater solution and were

transferred into a clean 1.5 mL Eppendorf tube. Samples were manually homogenised with 450µL of the provided lysis solution RL. Tissue that had not been lysed was removed by centrifuging the samples at 14,400 rpm for one minute. Next, the supernatant was transferred into spin filter D, which was placed in a receiver tube. Spin filter D binds genomic DNA. The tube and filter were centrifuged at 12,200 rpm for 2 minutes. Next, filters were checked to ensure the solution passed through the filter. If there was still some solution above the filter, the filters and tubes were centrifuged again at 14,400 rpm for 2 minutes until all the solution had passed through. As the genomic DNA was not going to be used in this study, this filter was discarded.

The filtrate was mixed with 400µL of 70% ethanol to encourage the RNA to precipitate out of the solution. The filtrate and ethanol were mixed with a pipette and transferred into spin filter R in a clean receiver tube. This tube was centrifuged at 12,000 rpm for 2 minutes. Again, samples would be centrifuged a second time if the solution had not wholly passed through the filter. The RNA was bound to spin filter R. To remove the RNA from the filter, 500µL of washing solution HS was added to each filter and centrifuged at 12,000 rpm for 1 minute. This was repeated with 700µL of washing solution HS. The filters were span at 12,000 rpm to remove all remaining ethanol for 2 minutes. Finally, the spin filter was placed over an elution tube, and 80µL of RNase-free water was added. After a 1-minute incubation at room temperature, tubes were centrifuged at 8,000 rpm for 1 minute.

2.5.4 RNA quantification

RNA was quantified using a NanoDrop (Thermo Scientific, UK). First, 1µL of RNase-free water was applied to calibrate the NanoDrop. After calibration, 1µL of each solution was applied individually to the NanoDrop. The quantity of RNA in ng/µL, the A260/280 ratio and the A260/230 ratio were recorded for each sample. The 260/280 ratio assesses the RNA quality, a ratio that was not between 1.8 and 2.1 would be rejected and RNA extracted again. The 260/230 assesses nucleic acid purity and should be 2.0 or above. Contamination at this wavelength tends to be due to guanidine thiocyanate, commonly found in lysis buffers. Evidence suggests that high concentrations of this salt do not compromise PCR experiments (von Ahlfen et al., 2010). As such, no upper limit of 260/230 ratio was applied to samples.

2.5.5 Reverse transcription of RNA into cDNA

RNA was reverse transcribed into complementary DNA (cDNA) using the QuantiTect Reverse Transcription kit (Qiagen, UK). The kit can convert RNA quantities of up to 1µg of RNA. This value was standardised across all models and time points, with the highest possible value of 850ng being selected. Samples were diluted to 850ng of RNA with RNase-free water to produce 12µL of template RNA. Negative controls were also prepared. A no reverse transcriptase (RT) control contained RNA pooled from all samples diluted to 850ng RNA, and a no template (NT) control contained only RNase-free water. These were treated the same as samples unless otherwise stated. All samples and controls were mixed with 2µL of 7x gDNA Wipeout Buffer and incubated for 2 minutes at 42°C (Stratagene Mx3000P thermal cycler, Agilent, USA). The RT control was treated with 1µL Quantiscript Reverse Transcriptase, 4µL Quantiscript RT Buffer and 1µL RNase-free water. The remaining samples and NT control were mixed with master mix stock containing the equivalent of 1µL Quantiscript Reverse Transcriptase, 4µL Quantiscript RT Buffer and 1µL RT Primer Mix. With the addition of the template RNA, each reaction had a total volume of 20µL. Samples were mixed and incubated for 15 minutes at 42°C, then 3 minutes at 95°C in the AriaMx qPCR machine (Agilent, USA). Samples were stored at -20°C until use.

2.5.6 Reference gene selection

Three samples from each treatment, sex, strain and region were diluted to 1:50 and 1:100 for reference gene selection. The housekeeping gene panel included β-actin, β-2-microglobulin (B2m), glyceraldehyde-3-phosphate dehydrogenase (Gapdh), malate dehydrogenase 1 (Mdh1), ubiquitin C (UBC), tyrosine 3-monooxygenase/tryptophan 5-monooxygenase activation protein zeta (Ywhaz). The volumes for each reaction were 7.2µL sample, 2.8µL housekeeping primer (Thermofisher) and 10µL 2x SYBR Green PCR Master Mix (Qiagen, UK). Samples were loaded and mixed into 0.2mL microtube strips (Sarstedt, Germany). Samples underwent a thermal cycling program. After an initial PCR heat activation step, 2 minutes at 95°C, samples were amplified by cycling between denaturation steps at 95°C for 5 seconds and combined annealing and extension steps at 60°C for 10 seconds. In the final step for melting curve analysis, samples were heated to 95°C for 1 minute, cooled to 55°C for 30 seconds and finally heated to 95°C for 30 seconds. qPCR was performed on the AriaMx qPCR machine (Agilent, USA).

The quantified cycle threshold was interpreted using the GoodGeNorm workflow facilitated by KNIME software. The GoodGeNorm workflow is a prewritten piece of R code that finds the most stable housekeeping group between treatment groups using pairwise comparisons.

2.5.7 Quantitative polymerase chain reaction (qPCR)

2.5.7.a Optimisation of dilutions

A pool of cDNA from each strain, age and region was created to find the appropriate dilution of the cDNA samples. The pools were diluted to 1:50 and 1:100. These were then run, in duplicate, for each primer. For the optimisation and final qPCR plates, 8µL of diluted sample was combined with a master mix comprising 2µL of primer and 10µL of 2x SYBR Green PCR Master Mix (Qiagen, UK). Samples were loaded into 0.2mL microtube strips (Sarstedt, Germany) and mixed. Samples underwent the same thermal cycling program described in 2.5.6.

Dilutions were considered optimal if the cycle threshold (Ct) value was between 18 and 26. For Ct values of less than 18, we considered diluting the samples. For Ct values higher than 26, more concentrated samples were used.

2.5.7.b Quantification of mRNA

A 2-fold serial dilution of pooled 850ng cDNA created a standard curve, assuming complete conversion. The resulting eight standards ranged in concentration from 34-0.266ng/mL. All the standards were then further diluted with 90µL of RNase-free water. Finally, the standards, samples, RT and NT controls were combined with a master mix containing SYBR Green PCR Master Mix and the primer of interest in the same ratio described in 2.5.7.a and run in duplicate on the same thermal cycle as previously explained (section 2.5.6).

For a qPCR plate to pass, the negative controls needed no Ct value or have values ten cycles higher than the lowest Ct value of a sample. In addition, the product's melting temperature for the samples and standards needed to be within 1.5°C. Finally, the efficiency of the primer needed to be between 75-110% (details found in 8.1.1). Individual samples were excluded if Ct values were not on the standard curve or when the coefficient of variation for the duplicate was above 10%.

$$\text{Coefficient of variation (CV)\%} = \frac{\text{Standard deviation of replicate}}{\text{Average of replicate}} \times 100$$

2.5.8 Confirmation of qPCR amplicon size

To confirm that the products produced during qPCR amplification were the correct targets of the predicted amplicon size, PCR products were loaded into an agarose gel (2% in 1x TAE buffer with 0.01% gel red stain). 18µL of the qPCR product was mixed with 2µL loading buffer (1.25% (w/v) xylene cyanol FF and 30% (v/v) glycerol in water solution). 17µL of the mix was added into each well alongside 5µL a hyperladder 25bp (Bioline, UK) in the peripheral wells. The gel was separated using electrophoresis (120V) for one hour. The gel was visualised using a UV transilluminator (Gel Doc, 2000, BioRad). Representative images are provided in the supplementary materials (8.1.1).

2.5.9 RNA integrity

We checked for RNA integrity to ensure the samples were not contaminated. The RNA samples were diluted to 100ng/µL, and 2µL of 5x loading buffer (Bioline, UK) was added. The samples were added to an agarose gel (1.5% agarose and 0.01% gel red stain in 1x TAE buffer). Once loaded, the samples were separated by electrophoresis (120V). When the ribosomal RNA bands separated, gels were visualised on a UV transilluminator (Gel Doc, 2000, BioRad). Representative gels are provided in the supplementary materials (8.1.1).

2.6 Protein quantification

2.6.1 Tissue collection

Rats were culled by increasing concentration of carbon dioxide, and death was confirmed by cervical dislocation. Brains were frozen on dry ice and stored at -80°C. PFC and DH were dissected from the frozen brain and homogenised on ice in a 10-fold volume (mg:µL) of buffer (10mM Trizma base, Sigma-Aldrich; 320µM sucrose, Sigma-Aldrich; 2mM EDTA, Sigma-Aldrich; and protease- and phosphatase- inhibitor cocktails, Sigma-Aldrich) buffered to a pH of 7.4. Phenylmethylsulfonyl fluoride (PMSF) and sodium orthovanadate were added to the solution at a 1% (v/v) concentration. Samples were centrifuged at 800xg for 15 minutes at 4°C. The supernatant was collected and centrifuged at 11,700xg for 20 minutes. The resulting supernatant (S2) and pellet (P2) were collected and stored at -20°C.

2.6.2 Bradford Assay

Protein concentrations were calculated using the Bradford Assay. Samples were diluted into protein assay dye reagent concentrate (BioRad) and compared to bovine serum

albumin (Sigma) of known concentration (1.0-0.1 mg/ml protein). A standard curve was created using simple linear regression. A plate where the standard had an $R^2 < 0.9$ was rerun. Standards and samples were run in triplicate. An outlying value from a triplicate was removed if the CV value was greater than 10%.

2.6.3 Simple Western Analysis (WES)

WES is a capillary-based method of protein separation and immunodetection. It works through the same principles of a traditional western blot: sample separation, blocking, primary and secondary incubations, and visualisation. Unlike traditional western blot, these steps are automated (Harris, 2015, Lück et al., 2021).

A WES plate was prepared following the manufacturer's instructions (SM-W004, ProteinSimple). Diluted samples were mixed with dithiothreitol and fluorescent master mix in an 8:1:1 ratio. Most proteins were denatured at 95°C for five minutes, though some were denatured at 40°C for thirty minutes due to differences in subcellular location. A biotinylated ladder, the samples, antibody diluent, primary antibody, secondary antibody and luminol-peroxide mix were loaded into appropriate wells. After brief centrifugation of the plate, wash buffer was added.

The plate was placed into the WES machine. The WES machine completed the following steps. First, the load separation matrix was aspirated, and the stacking matrix was drawn up into each capillary. The ladder and samples were then loaded and lowered into the running buffer. An electrical current was applied to the samples, which were separated based on molecular weight. At the end of the separation, samples were immobilised by UV light, and the lysis buffer and non-protein components were washed out of the capillary. Then, the capillaries drew up the blocking solution, primary and secondary antibodies, flanked by wash steps. Finally, the chemiluminescent substrate was added to the capillaries, and the camera detected the chemiluminescence levels at nine different time points (1-512 seconds). The software would then calculate the peak's high dynamic range (HDR), providing the strongest signal with the lowest background. The HDR peak would be used to calculate the area under the curve, which is analogous to the quantity of protein in the sample (Figure 2.4).

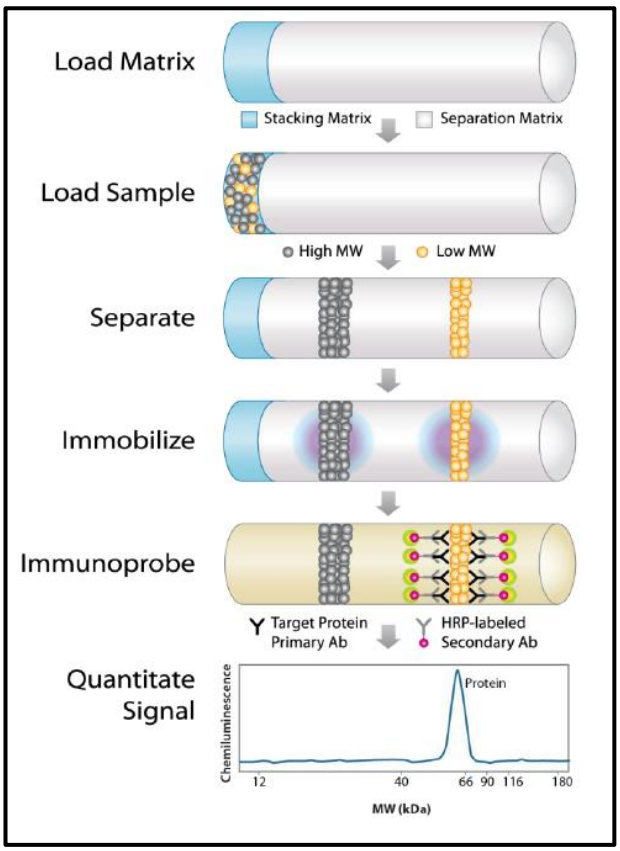

Figure 2.4: Schematic of size-based protein separation and detection on the WES machine. Taken from Protein Simple technical guide.

2.6.3.a Optimisation of novel antibodies

The ideal antibody and protein concentration was found for each study and brain region tested. The optimal antibody concentration was defined as the concentration where all the protein of interest in the sample was bound to an antibody. In addition, the optimal protein concentration was ascertained to find the most robust effect sizes between groups, if present. We tested different protein concentrations and antibody dilutions on the pooled sample to achieve this. The pooled sample was created by combining homogenate from each sample, ensuring that all treatments are equally represented.

We have found that the protein concentrations of 0.8, 0.4 and 0.2 mg/mL and antibody dilutions 1:20, 1:50, 1:100 and 1:200 work well in tissue homogenates. Twelve wells of a plate would be used to accommodate these concentrations in all iterations.

Upon completion of the assay, we would first take the peak height, or the chemiluminescence, and compare the different antibody dilutions from each protein concentration (Figure 2.5A). In theory, increasing antibody dilution in a sample with the same protein input will result in a sigmoidal relationship (Figure 2.5B). With low antibody binding at low protein concentrations (red zone), an increase in antibody

binding as concentrations increase (orange zone), then saturation of the signal (green and pink zones). Once saturated, regardless of additional antibody concentration, the peak height would not alter, as all the protein in the sample is occupied. Of the two zones in the saturation zone, we aim for the green zone, as excessive antibody concentration can result in non-specific binding or background signals. The example data in Figure 2.5BA shows saturation at 1:100 for 0.2 and 0.4mg/mL at 1:200 for 0.8mg/mL. On selecting the optimal antibody dilution (1:100 or 1:200 in our example), we next find the optimal protein concentration. Here we look at the area under the curve. Again, we expect the relationship between protein concentrations and the area under the curve to be somewhat sigmoidal, reaching a saturation when all the antibody in the reaction is utilised. Here, we aim for our samples to be in the linear portion of the theoretical graph (Figure 2.5D). In the linear portion, differences in protein levels in the treatment groups would be the most detectable. Our example data (Figure 2.4C) shows a linear relationship in the 1:100 graphs. The optimal combination here would be 0.4mg/mL protein at 1:100.

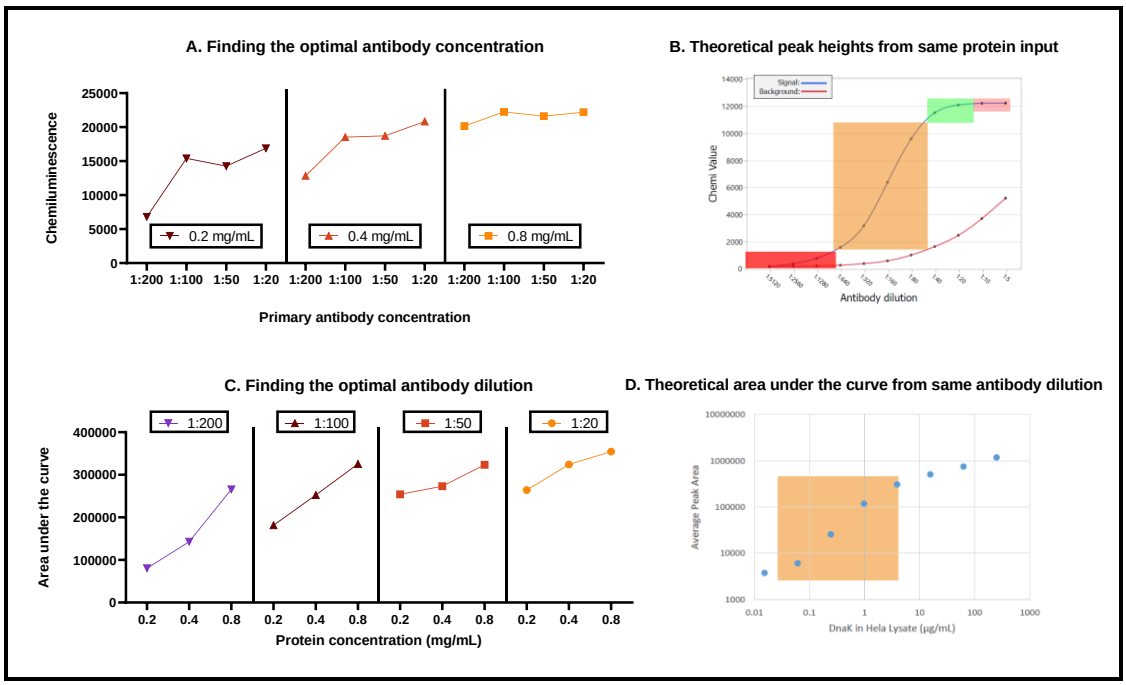

Figure 2.5: Optimisation of a novel antibody with WES.

The final step is to check the quality of the selected peak. Ideally, there should be a single peak at the approximate molecular weight. The background should be minimal, with the peak still discernible at the conclusion of the visualisation (512s). The peak height should be below 300,000 to ensure sufficient supplies of chemiluminescent substrate for the

entire detection period. The peak height should remain consistent in the first seconds after introducing the chemiluminescent substrate, with levels dropping from 8s (Figure 2.6).

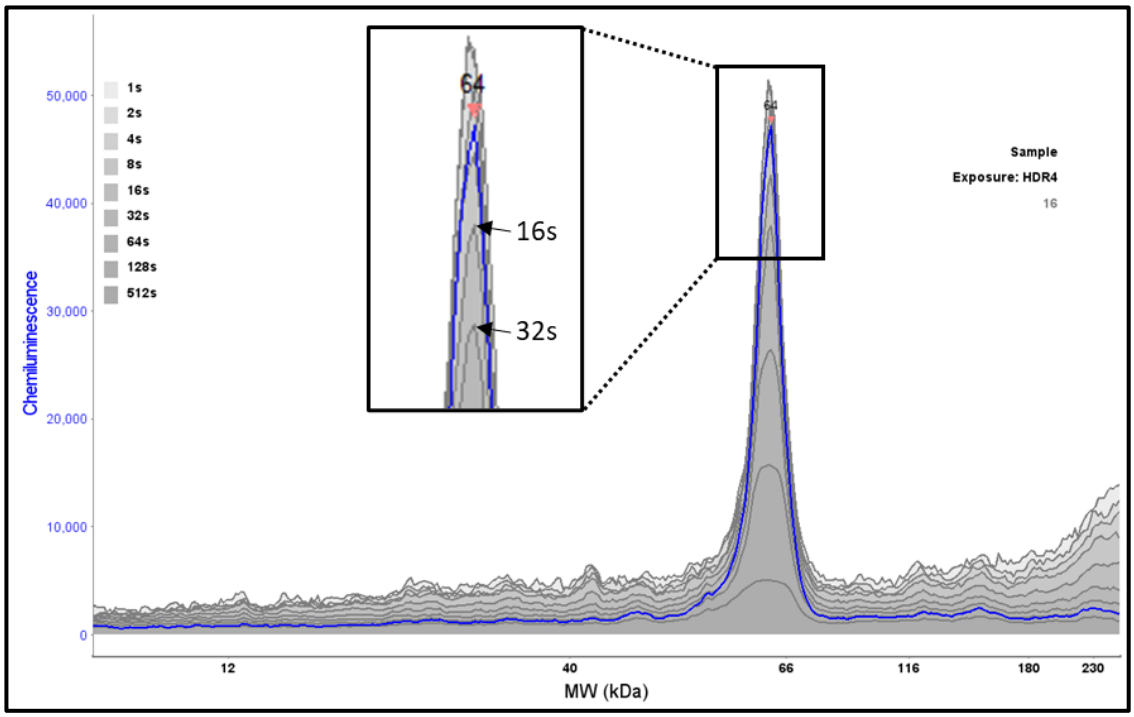

Figure 2.6: Example peak from WES.

2.6.3.b Normalisation with total protein

To normalise the protein, we used the total protein assay provided by protein simple (DM-TP01). This kit uses the same principles as a Coomassie stain, indicating the protein concentration loaded into the assay. We validated that total protein is stable across treatments and measured total protein output at different protein concentrations to ensure we were in the linear part of the graph (Figure 2.5D). Further details on the validation of total protein can be found in the supplementary material (8.1.2).

For the brain homogenate supernatant S2 samples, we ran the total protein assay at 0.2mg/mL. For the pellet (P2) samples, we used 0.1mg/mL. Once we had the total protein data for the whole cohort, we would compare the average total protein levels for each treatment to ensure that total protein was stable between treatments. The area under the curve of the protein of interest was divided by the area under the curve for the total protein to find the normalised relative protein levels.

2.6.4 ELISA optimisation

Four outcomes needed to be ascertained from the ELISA optimisation. The first was to ensure the standards produced a good curve. From this, we could conclude that the kit

and protocol worked correctly. The second was to estimate the protein concentration of samples required for the assay. Ideally, protein samples should sit in the middle of the standard curve to ensure all samples will be interpolated. The third goal was to run the experimental samples at different concentrations to ascertain the linearity of the assay. Theoretically, halving the protein input should halve the output of the protein of interest. However, this is rarely the case. Finally, we run a homogenisation buffer-only control well to ensure that none of the buffer components interact with the kit contents.

2.7 Plasma collection

Rats were culled by increasing concentration of carbon dioxide, and death was confirmed by cervical dislocation. Trunk blood was collected in EDTA tubes, then inverted ten times and stored on ice. Blood was centrifuged at 7000rpm for 5 minutes. Plasma was collected and frozen at -80°C.

2.8 Immunohistochemistry (IHC)

2.8.1 Perfusion and fixation

Rats were anaesthetised with isoflurane and perfused transcardially with 1x phosphate-buffered saline (PBS). The brains were collected and post-fixed in 4% formaldehyde for 72 hours at 4°C. Once fixed, brains were immersed in 30% sucrose for 72 hours, then flash-frozen in isopentane and stored at -80°C.

2.8.2 Sectioning

Sections were cut at 30µm using a cryostat (CM1950, Leica Biosystems). One in eight serial sections of the PFC and DH were suspended in cryoprotectant (30% ethylene glycol, 30% glycerol, 10% PBS, 30% dH_2O) for long-term storage (-20°C).

2.8.3 Staining

Sections were washed in 1x PBS three times for five minutes each. For parvalbumin and allograft inflammatory factor 1 (IBA-1) sections, sections underwent heat-induced antigen retrieval in sodium citrate buffer (0.294% (w/v) sodium citrate, 0.07% (v/v) tween-20, 500ml distilled water, pH adjusted to 6.0) for 30 minutes at 80°C. Tris-EDTA buffer was used for PNN sections (0.121% (w/v) tris-base, 0.037% (w/v) EDTA in distilled water, pH adjusted to 9.0, add $5.0x10^{-4}$% (v/v) tween-20), sections were incubated in

the buffer for 10 minutes at 80°C. Unless otherwise stated, samples were washed twice in 1x PBS between each step.

PV, PNN and IBA-1 sections were processed for light microscopy. Samples were incubated in hydrogen peroxide solution (1.5% H_2O_2, Sigma; 0.4% Triton x-100, Sigma; 10% methanol, 88.1% 1x PBS) for 30 minutes at room temperature (RT). Samples were incubated in protein block (5% normal horse serum, Vector Laboratories; 0.6% triton x-100, Sigma; 94.4% 1x PBS) for one hour. Then, without washing, incubated in biotinylated wisteria floribunda (WFA) (1:1000; 16 hours; B-1355-2, Vector Laboratories), anti-parvalbumin (1:5000; 24 hours; 235, Swant), or anti-IBA-1 (1:2000; 24 hours; ab5076, Abcam) at 4°C. On day 2, PV and IBA-1 samples were incubated with secondary antibodies (PV: horse anti-mouse; 1:200; BA-2000-15, Vector Laboratories, and IBA-1: horse anti-goat; 1:200; BA-9500-15, Vector Laboratories) for 2 hours. PV, PNN and IBA-1 sections were incubated with the VECTASTAIN Elite ABC-HRP kit (PK-4000, Vector Laboratories) for 45 minutes and visualised with a DAB substrate kit (SK-4100, Vector Laboratories). When a sufficient colour change had been observed, samples were moved into distilled water to stop the peroxidase reaction. For parvalbumin and IBA-1 sections, nickel was added to the DAB solution to produce a purple/black stain. For PNN sections, nickel was not added to produce an orange stain (see Figure 2.7). Sections were mounted onto SuperFrost slides and assigned randomised codes. Slides were then dehydrated in increasing ethanol concentrations (70%, 90% and 100%, 5 minutes each) and washed in Histoclear (National Diagnostics) for 5 minutes. Coverslips were applied with DPX mounting media (Sigma).

It should be noted that there is some contention as to the optimal methodology for identifying PNN. The most common staining method is WFA, which reportedly stains all CSPGs (Härtig et al., 1992). However, some groups recount issues with WFA staining in post-mortem samples. For example, incomplete or inconsistent staining has been described in light and confocal microscopy studies (Brückner et al., 2008, Rogers et al., 2018). The present study observed consistent PNN morphology using the stated preparation.

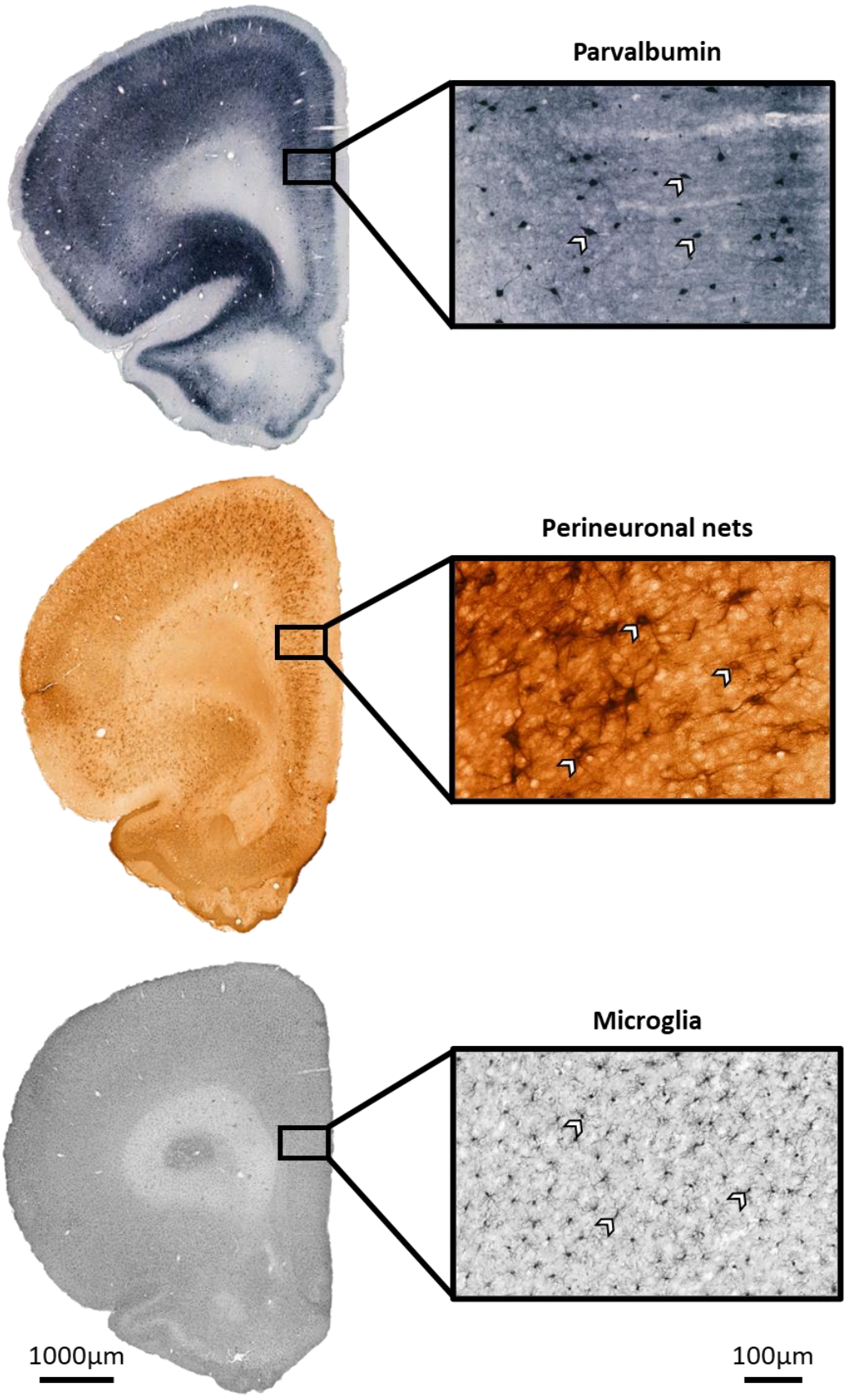

Figure 2.7: Example staining of parvalbumin, perineuronal nets and microglia in the PFC. The scale bar on the left for the x1 PFC sections. The scale bar on the right for the x20 panels. Arrows point to an example of positive cell detection.

2.8.4 Slide analysis

2.8.4.a ImagePro Plus

Images were viewed on an Olympus BX51 microscope. Sections were analysed using ImagePro Plus (version 6.3.0.512, MediaCybernetics, United States). The software captures the slide at 4x magnification, and the user delineates a region of interest from the digital version. The software then randomly selects 35 counting frames within this region. The user can define the counting frame size and magnification; in all cases, a counting frame of 120x120 µm was used at 20x magnification. The motorised stage then moves to the counting frame, and the user counts the number of neurons or nets in the region. The neuron or net number was divided by 0.0144 to give cell or net density per mm^2.

2.8.4.b Slide scanner

Images were acquired on a 3D-Histech Pannoramic-250 microscope slide-scanner using a 20x objective lens (Zeiss). Snapshots of the slide scans were taken using the Case Viewer software (3D-Histech). For PVI and PNN analysis, regions of interest were delineated, and PVI or PNNs were counted within these regions. For a PNN to be counted, the PNN needed to have formed a complete circle around a neuron. Cell or net count was divided by the area of interest to give density.

Microglia density was measured using QuPath software (0.4.2, available at https://qupath.github.io/). The prefrontal cortex was delineated, and the program automatically counted the microglia cell bodies. For each section, the threshold was modified depending on the background levels. A higher threshold would be used for sections with low backgrounds and vice versa. Density was analysed by dividing microglia cell number by the area of the region of interest.

2.9 Statistics

Statistical testing was carried out in SPSS 28.0.1.0, except for the D'Agostino and Pearson normality tests, which were done in GraphPad Prism 9.5.0. Graphs were made in GraphPad Prism 9.5.0.

2.9.1 Normality tests

The D'Agostino and Pearson ($n>7$) or Shapiro-Wilk ($n\leq7$) test was used to test for normality. Data were considered normally distributed when $p>0.05$.

2.9.2 One sample t-test

A one-sample t-test was used on normally distributed data to compare individual groups to a hypothetical mean. Data were considered significant when $p<0.05$.

2.9.3 Comparing the means of two groups

2.9.3.a Unpaired t-test

When comparing subchronic vehicle (scVeh) to subchronic PCP (scPCP) in normally distributed data, an unpaired t-test was used. In the case of unequal variance, Welch's correction was applied. The difference between groups was considered significant when $p<0.05$.

2.9.3.b Mann-Whitney U test

A Mann-Whitney U test compared scVeh and scPCP groups of not normally distributed data. The difference between groups was considered significant when $p<0.05$.

2.9.4 Comparing the mean of three or more groups

2.9.4.a One-way ANOVA

For normally distributed data, a one-way ANOVA would be used. The Brown-Forsythe test was used to assess the equality of variances. In the event of a significant ANOVA and equal variances, Tukey's post hoc test would assess the differences between groups. However, if the Brown-Forsythe test was significant ($p<0.05$), indicating unequal variances, Dunnett's T3 post hoc test would be used.

2.9.4.b Kruskal-Wallis H test

The Kruskal-Wallis H test was used in the event of not-normally distributed data. If significant, post hoc pairwise comparisons would compare the differences between each group.

2.9.5 Correlations

Pearson's correlation coefficient for normally distributed data and Spearman's correlation coefficient for not-normally distributed data were used to assess the relationship between two dependent variables. The correlation would be two-tailed for both, and a significant correlation was considered when $p<0.05$.

2.9.6 Simple linear regression

We used a simple linear regression to assess the relationship between two independent variables. In the event of a significant model, the residuals would be plotted, and the

distribution of the residuals assessed. Not normally distributed residuals will be reported.

2.9.7 General linear models

2.9.7.a Univariate general linear model

A univariate general linear model was used when we had one dependent variable and two or more independent variables. This was used on normally distributed data. A full factorial model was run, and the effects of the fixed factors and relevant interactions were used to direct post hoc testing. In the event of a significant model, we would investigate the differences between groups using pairwise comparisons of the estimated marginal means with Šidák correction.

2.9.7.b Repeated measures general linear model

A repeated measure general linear model was used for data where we had multiple outputs for a single rat, for example, the NOR object exploration times or when an animal was tested repeatedly across multiple time points. The repeated factor was classified as the within-subjects factor, and treatments, age or sex as the between-subjects factors. Mauchly's test of sphericity was conducted to determine whether a correction needed to be applied. If the test was significant and the calculated epsilon was >0.75, the Greenhouse Geisser correction would be applied. If epsilon was <0.75, the Huynh-Feldt correction would be used. If a significant within-subject effect existed, the estimated marginal means would be compared pairwise, with Šidák correction.

2.9.7.c Minimal general linear mixed model

For the maternal immune activation studies, we had to consider the dam of each offspring to establish if sibling cohorts had similar outcomes. To do this, we used a general linear mixed model (GLMM), which is generally robust to data that is not normally distributed, has unequal variances or is skewed (Schielzeth et al., 2020). To deal with data that may violate these assumptions, we applied the Satterthwaite approximation to every GLMM, which adjusted the degrees of freedom depending on the extent of the violation.

In our GLMM, the dam was used as a random subject variable. In most instances, the dam membership is a redundant parameter and will only be reported if significant. When reported, it will be reported as the parameter estimate ± the standard error.

The GLMM was run as a minimal model, which simplifies a complex multi-factorial model into a parsimonious one. A full factorial model was run initially (see Table 2.1), and then the least significant outcome was removed until no or only significant factors were left. The significant outcomes are then reported. In the case of a significant interaction, for example, age*sex, the cohort would be split into age groups, and sex ran as a main effect in the GLMM. This would be repeated in the individual sexes using age as the main effect. Analysing in this way allows the random effect of the dam to be continually assessed.

As there is evidence that the extent of the maternal immune response in the acute phase after infection can predict the extent of the offspring pathology (Potter et al., 2023), we reran the GLMM, including the maternal cytokines levels collected for each dam. In this GLMM, the maternal cytokine response would be included as a covariate, and its main effect and interactions would be assessed for each dependent variable (see Table 2.1). In the event of a significant main effect of the maternal cytokine, the relationship between the maternal immune response and the offspring-dependent variable was explored using a simple linear regression (2.9.6). In the event of a significant interaction, the data were split into the relevant cohorts (age, sex, treatment or combinations of these factors), and the main effect of the maternal cytokine was assessed.

The residuals of significant models were plotted, and the distribution was tested to ensure a GLMM was an appropriate model. In the event of non-normally distributed residuals, the data were log10 transformed, and the GLMM and residuals were reanalysed.

Table 2.1: Overview of parameters used in the GLMM.

GLMM	GLMM with maternal cytokine
Age Sex Treatment Age*Sex Age*Treatment Sex*Treatment Age*Sex*Treatment	Maternal cytokine Age*maternal cytokine Sex*maternal cytokine Treatment*maternal cytokine Age*Sex*maternal cytokine Age*Treatment*maternal cytokine Sex*Treatment*maternal cytokine Age*Sex*Treatment*maternal cytokine

CHAPTER 3: CHARACTERISATION OF THE SUBCHRONIC PHENCYCLIDINE MODEL

3.1 Introduction

3.1.1 A brief history of NMDA receptor antagonists

Phencyclidine (PCP) was developed as an anaesthetic under the trade name Sernyl by Parke-Davis in 1957. The first documented use of Serynl in human subjects was published the following year. Although the drug proved a potent anaesthetic, 5 of the 64 patients developed a manic state during the surgery. After the surgery, ten patients displayed similar side effects on emergence from anaesthesia (Greifenstein et al., 1958). Only one year after this publication, Luby et al. used the term schizophrenomimetic to describe the effects of Sernyl, stating that the observed side effects had an "impressive similarity" to schizophrenia symptoms. The side effects included delusions, disorganised thoughts, negativism, apathy and cognitive deviations (Luby et al., 1959). Inevitably, in 1967, Sernyl was withdrawn from the market (Morris et al., 2014).

Despite the clinical failure of PCP, chemists at Parke-Davis continued to search for derivatives with fewer side effects for use as an anaesthetic. In 1964, they formulated ketamine. Like PCP, ketamine is an N-methyl-D-aspartate (NMDA) receptor antagonist; however, it is less potent and has a shorter duration of action. Although the ketamine-induced schizophrenomimetic side effects remained, they quickly subsided. For example, in a study of 20 prisoners, the side effects lasted for 30 minutes for those who experienced them. Due to patients retaining consciousness during continuous administration of ketamine, Domino et al. suggested calling this class of drugs "dissociative anaesthetics" (Domino et al., 1965). Unlike PCP, ketamine is still used in the clinic as an anaesthetic (Barrett et al., 2020) and, more recently, investigated as a potential treatment for several psychiatric disorders (Peyrovian et al., 2020).

Finally, MK-801, marketed as an anti-convulsant (Clineschmidt, 1982, Hucker et al., 1983), was also found to act as an NMDA receptor (NMDAr) antagonist (Wong et al., 1986). In 1989, Olney et al. noted that MK-801, PCP and ketamine resulted in the dose-dependent development of neuronal lesions in rats. Although only an acute effect, electron microscopy revealed numerous vacuoles in layer 3 and 4 neurons. These vacuoles appeared to incorporate and break down the mitochondria, increasing in severity from 2 to 18 hours post-acute injection. After 24 hours, the neurons had normalised. MK-801 had the most detrimental effect, followed by PCP and ketamine (Olney et al., 1989). Notably, this order reflects the relative affinity of these drugs at the

NMDA receptor (Wong et al., 1986). Although there are unpublished studies that MK-801 and ketamine do not cause vacuoles in monkeys (Jansen, 2004), the neurotoxicity observed in rats by Olney et al., combined with the inconsistent efficacy and side effects observed in open-label clinical trials, halted any further clinical studies of MK-801 (Morris et al., 2014).

3.1.2 The NMDA receptor

It is evident that the NMDAr is relevant to schizophrenia symptomology, given the ability of antagonists to replicate aspects of the disease. Therefore, before discussing the antagonists further, it is essential to establish the function of the NMDAr in healthy brains. NMDA is a voltage-dependent ionotropic glutamate receptor comprising four subunits, two glycine-binding NR1 and two glutamate-binding NR2. At the resting membrane potential, the open NMDAr is blocked by a magnesium ion (Mg^{2+}), preventing the flow of other ions. However, when the ionotropic glutamate receptor α-amino-3-hydroxy-5-methyl-4-isoxazole propionic acid (AMPA) is activated, the membrane depolarises, and the Mg^{2+} block is removed, allowing sodium (Na^{+}) and calcium (Ca^{2+}) ions to flow into the post-synaptic neuron. Ca^{2+} then activates intracellular kinases, which potentiate the synapse by upregulating new AMPA receptors or increasing the efficacy of existing AMPA receptors. This process is called long-term potentiation (LTP) and is a fundamental means of learning and memory (Hayashi, 2022, Lüscher et al., 2012, Vyklicky et al., 2014).

3.1.3 Effects of acute NMDA receptor antagonism

Given that the NMDAr is critical in glutamate signalling, it would be reasonable to assume that NMDAr antagonism would lead to reduced levels of glutamate. Counterintuitively, acute exposure to NMDAr antagonists increases PFC glutamate levels in rodents (Amitai et al., 2012, Moghaddam et al., 1997, Zuo et al., 2006). Specific investigation of different neuronal subtypes revealed that acute MK-801 administration initially reduces the activity of GABAergic interneurons, which, in turn, increases glutamate neurons' activity due to reduced inhibition (Homayoun et al., 2007). It appears, therefore, that GABAergic interneurons are more susceptible to NMDAr antagonism. The composition of the NMDAr on the different neuronal subtypes may explain this difference. As stated in the previous section (3.1.2), the NMDAr comprises two NR1 and two NR2 subunits. The NR2 subunits can either be NR2A, 2B, 2C or 2D

subtypes; each has different functional properties and sensitivities. For example, 2A and 2B are less sensitive to ketamine and strongly blocked by Mg^{2+}. 2C and 2D subtypes are the opposite, with increased ketamine sensitivity and reduced potency of the Mg^{2+} block (Kotermanski et al., 2009). Glutamatergic neurons predominately express the NR2A and 2B subtypes, whereas parvalbumin and somatostatin neurons express the ketamine-sensitive NR2C and 2D (Bygrave et al., 2019). Although studies suggest that NMDAr antagonism in PVI depends on the presence of NR2A receptors (Kinney et al., 2006), the 2C and 2D are most readily blocked by NMDAr antagonists (see Figure 3.1). This selective sensitivity explains the increase in glutamate after acute treatment with PCP, MK-801 and ketamine, as it will cause disinhibition of this network (Amitai et al., 2012, Moghaddam et al., 1997, Zuo et al., 2006).

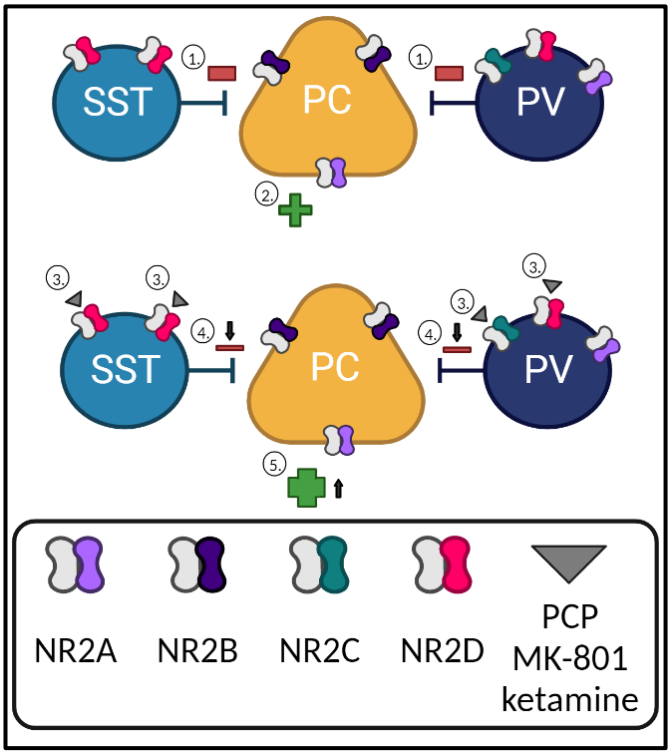

Figure 3.1: Neuronal NMDA receptor subunit distribution. Pyramidal cells (PC) express NR2A and NR2B subunits, which are less sensitive to antagonism by the dissociative anaesthetics PCP, MK-801 and ketamine. The inhibitory interneurons conversely express predominantly NR2C and NR2D, which are sensitive to antagonism. Without NMDAr antagonism, parvalbumin (PV) and somatostatin (SST) interneurons inhibit PC (1), diminishing the excitatory output (2). However, administering an NMDAr antagonist (3) reduces the inhibitory output of interneurons (4), which results in an increased excitatory drive from PC (5) and increased glutamate levels. Adapted from Bygrave et al., 2019. Image created in BioRender.com.

In keeping with increased glutamate, acute PCP increases c-fos (Castañé et al., 2015) and glucose metabolism (Gao et al., 1993) 1-3 hours after injection, which then normalises

after 48-96 hours. This activity alteration coincides with impaired social interaction behaviour (Savolainen et al., 2018) and working memory deficits (Mathews et al., 2018). It should be noted that behaviour in acute dosing models is often measured while the drug is on board. Acutely, PCP causes sedation and motor deficits (Jurado, 2013), which might interfere with behavioural measurements.

3.1.4 Subchronic dosing regimes

Many studies choose to use a subchronic dosing regimen followed by a washout due to its long-lasting effects and ability to test animals in a drug-free state (Cadinu et al., 2018). Indeed, when comparing outcomes from acute and chronic dosing regimens in both preclinical studies and recreational users of PCP, Jentsch et al. concluded that chronic exposure to PCP resulted in a more robust symptom induction, particularly those classified as negative and cognitive, compared to acute exposure (Jentsch et al., 1999).

Let us now consider the effects of repeated NMDAr blockade on GABAergic interneurons. Comparable to acute exposure, glutamate remains elevated after subchronic dosing, though reduced in magnitude (Amitai et al., 2012), indicating the persistence of reduced inhibition. In a typical brain, reduced activity of the NMDAr receptor would indicate a reduction in glutamatergic input to GABAergic interneurons. To maintain the excitatory/inhibitory (E/I) balance, the PVI would respond to reduced excitatory input with a reduced inhibitory output. A way of modulating inhibitory power is by changing the expression of parvalbumin (Collin et al., 2005) and GAD67 (Lau et al., 2012). Lisman et al. proposed that a reduction in GABAergic markers in NMDAr antagonist models is an inevitable consequence of PVI incorrectly detecting reduced glutamatergic neurotransmission due to the NMDAr dysfunction (Lisman et al., 2008). As anticipated, there are reductions in parvalbumin (Amitai et al., 2012, Behrens et al., 2008, Braun et al., 2007, Gigg et al., 2020, Jenkins et al., 2010, Landreth et al., 2020, McKibben et al., 2010) and GAD67 (Amitai et al., 2012, Behrens et al., 2008, Boczek et al., 2015, Gigg et al., 2020, Woźniak et al., 2018) after subchronic NMDAr antagonism.

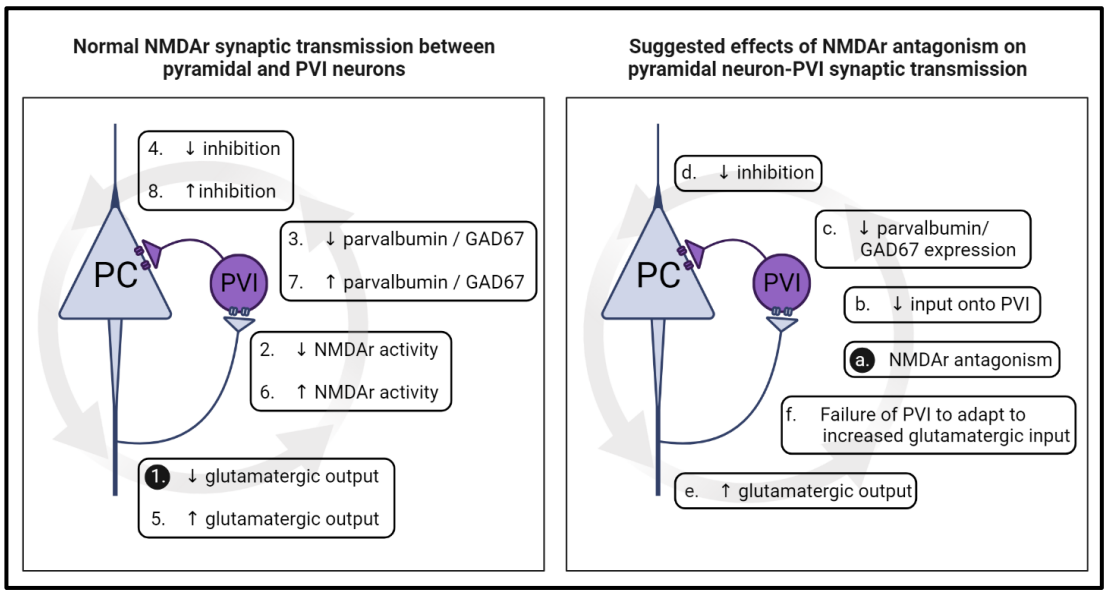

Figure 3.2: NMDAr signalling between pyramidal neurons and PVI. The left-hand panel shows normal NMDAr signalling in pyramidal cells (PC) and parvalbumin interneurons (PVI). In typical signalling, reduced glutamatergic output from PC would decrease NMDAr signalling onto the PVI (steps 1-2). It is proposed that PVI respond to reduced NMDAr activity with reduced parvalbumin and GAD67 expression to reduce the PVI inhibitory output (steps 3-4). Reduced inhibition would increase glutamatergic activity, resulting in reciprocal outcomes (steps 5-8). The right-hand panel shows the proposed outcomes when an NMDAr antagonist is administered. Blockade of NMDAr on PVI would result in reduced parvalbumin and GAD67 expression (a-c) due to reduced NMDAr activity (akin to steps 2-3). This would result in reduced inhibitory output and subsequent increased glutamatergic activity. However, as an antagonist blocks the NMDAr, the reciprocal pathway is not enacted.

3.1.5 Mechanisms

Although the data for GABAergic, particularly parvalbumin, dysfunction is convincing. It is unclear how the drug maintains its effects after washout. Thus far, the data produced a linear mechanism for parvalbumin and GAD deficits (Figure 3.3). In this model, the removal of NMDAr antagonism should recover the system, as without the pharmacological disinhibition, the inhibitory interneurons should detect the increased excitation and work to recuperate the E/I balance. Indeed, recovery is seen in acute treatment models (Castañé et al., 2015, Gao et al., 1993). It is clear there are more factors at play in the subchronic dosing regimes that explain the post-washout deficits. The final section will discuss proposed theories for sustained cognitive and pathological deficits in the absence of ongoing NMDAr antagonism.

Figure 3.3: Consequences of NMDAr antagonism for parvalbumin interneurons.

3.1.5.a Perineuronal nets

Building on the idea that changes in the PVI are corrective responses to misperceived reductions in excitatory input, what changes would be expected in PNN? A valuable study by Devienne et al. conclusively showed that inhibiting PVI using designer receptors exclusively activated by designer drugs (DREADDs) reduces PNN density (Devienne et al., 2021), showing that PNN density can reduce when PVI are less active. Furthermore, a meta-analysis of 14 papers studying PVI and PNN in genetic and environmental models relevant to schizophrenia found a strong correlation between change in PVI density and change in PVI cells surrounded by PNN (R^2 = 0.800, p<0.001, linear regression analysis). A consequence of shifting to a low PNN state, however, is that it makes the PVI more susceptible to oxidative damage, with the same studies showing a negative relationship between PV+/PNN cells and oxidative stress (R^2 = -0.036, p = 0.020) (Steullet et al., 2017).

3.1.5.b Oxidative stress

Reactive oxygen species (ROS) form when an oxygen molecule reacts with a free electron. ROS can be produced by internal processes such as cellular metabolism or respiration or in response to external stimuli such as radiation, UV or heat. Many biological processes depend on ROS, including regulating transcription proteins, hormone production, and maintaining the extracellular matrix (ECM). Critically, unmanaged ROS can damage proteins, lipids and nucleic acids. Therefore, it is crucial to moderate ROS levels in tissues. This is the function of antioxidants, which either enzymatically break down or scavenge ROS (Hunyadi, 2019).

In a comprehensive review, Yao et al. summarised several studies looking at levels of antioxidants, free radical scavenging enzymes, nitric oxide signalling, lipid peroxidation and protein modifications in the blood, urine, cerebral spinal fluid and post-mortem tissue of schizophrenia patients. Overwhelmingly, the data suggested that schizophrenia patients have decreased antioxidant levels and increased markers of ROS. Moreover, these changes were present regardless of medication status (Yao et al., 2011). The authors also highlighted research that showed a correlation between oxidative stress markers and positive, negative and cognitive symptoms (Buckman et al., 1990, Mukerjee et al., 1996, Zhang et al., 2003). More recently, studies of first-episode psychosis, treatment-responsive, and treatment-resistant patients have shown a shift from

antioxidant to oxidative stress markers in peripheral blood samples (Buosi et al., 2021, Fraguas et al., 2019). In post-mortem samples, there is also evidence of reduced glutathione, an antioxidant, in the prefrontal cortex of schizophrenia patients (Gawryluk et al., 2011, Zhang et al., 2018b), suggesting a life-long and sustained imbalance in ROS production or removal.

3.1.5.c Inflammation

Recently, a hypothetical mechanism linking oxidative stress and inflammation has been proposed to contribute to schizophrenia pathology (Bitanihirwe et al., 2020). There is some compelling evidence that chronic inflammation is involved in schizophrenia pathology. A genome-wide association study comprising of near 37,000 schizophrenia patients found a high degree of mutations were present in cells involved with the immune system (Schizophrenia Working Group of the Psychiatric Genomics Consortium, 2014). More recently, studies have shown the upregulation of inflammatory pathways in the dorsolateral prefrontal cortex (DLPFC), hippocampus and striatum of schizophrenia patients, highlighting interleukin-6 (IL6) as a significant contributor (Lanz et al., 2019, Pandey et al., 2018).

IL6 can be measured in the periphery, meaning clinicians and researchers have considered it a useful biomarker, though this work still needs validation. For example, there is evidence of increased levels of IL6 in the serum (Kristóf et al., 2022, van Kammen DP et al., 1999) and cerebral spinal fluid (Garver et al., 2003, Sasayama et al., 2013, Schwieler et al., 2015, van Kammen DP et al., 1999) of schizophrenia patients. Interestingly, increased serum IL6 is also seen in chronic ketamine users (Fan et al., 2015), further validating the link between schizophrenia pathology and altered glutamate signalling. Notably, inflated serum IL6 is detectable before disease onset and strongly predicts risk and age of onset (Upthegrove et al., 2020), again suggesting a life-long and sustained state of inflammation.

3.1.5.d An updated mechanism

Given the additional factors discussed, the revised mechanism below includes the PNN, oxidative stress and inflammation.

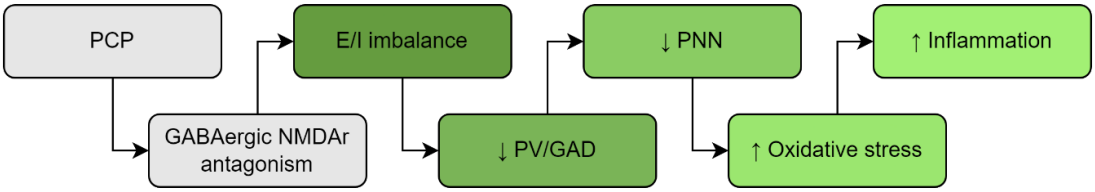

Figure 3.4: An updated mechanism for the effects of PCP dosing on PVI. Grey squares show acute effects of PCP, and green squares show potential sustained impairments after subchronic dosing.

3.1.6 Aims

This chapter aims to evaluate the following:

1. Determine whether scPCP administration induces biomarker alterations relevant to the proposed mechanism (Figure 3.4).
2. Update the mechanism accordingly, with a focus on finding self-perpetuating interactions to speculate on how the cognitive deficits observed in the scPCP model are maintained.

3.2 Methods

3.2.1 Sample collection

The samples used for the characterisation chapter were from several different cohorts of female Lister hooded rats that were housed at the University of Manchester. These animals were housed and dosed as described in 2.1 and 2.2. Rats were dosed at approximately 8-10 weeks old at the time of dosing. For all studies, the initial group size was 10. This was based on a previously conducted power analysis for the novel object recognition task using an alpha of 0.05 and a power of 0.8 (Grayson, personal communication). These studies have been summarised in the table below:

Table 3.1: Summary of different tissues used for the characterisation study. PFC: prefrontal cortex, DH: dorsal hippocampus, qPCR: quantitative polymerase chain reaction, WES: simple western analysis, PCC: protein carbonyl content, IL6: interleukin 6, ELISA: enzyme-linked immunosorbent assay, MMP: matrix metalloproteinase, IHC: immunohistochemistry.

Source	Weeks since dosing	Region	Study
b-neuro studies	22	PFC DH	qPCR
	12	PFC DH	WES PCC
	10	DH	IL6 ELISA
		DH Plasma	MMP9 ELISA
		DH	MMP2/MMP9 activity assay
(Landreth et al., 2020)	14	PFC	IHC

In all cases, the vehicle-treated animals will be referred to as scVeh and the PCP animals scPCP.

3.2.2 qPCR

Brains for this study were collected from rats culled at the end of a b-neuro study. They had a behavioural deficit in the NOR task one week after scPCP administration. Animals were dosed with vehicle or PCP 22 weeks previously. Brain tissue was collected and processed as described in section 2.4, and the resulting complementary deoxyribonucleic acid (cDNA) from the PFC and DH was used for analysis. cDNA was diluted, as detailed in Table 3.2. As all PCR samples were run on a single plate, the sample

size for this study was limited to n=7 per group per region. The rats used were randomly selected.

3.2.3 Simple western analysis

Brains were from a second b-neuro study where an NOR deficit was present. Animals were dosed with vehicle or PCP 12 weeks previously. The PFC was isolated and processed as described in sections 2.6.1 – 2.6.3.

Table 3.2: Dilutions used in the qPCR study.

Target	PFC	DH	Target	PFC	DH
Acan	1:20	1:10	IL6	1:10	1:10
Actin	-	1:100	MMP9	1:20	1:10
Bcan	1:20	1:10	Ncan	1:20	1:50
Cat1	1:200	1:200	NFκB	1:20	1:10
GAD1	1:100	1:100	PSD95	1:50	1:100
GAD2	1:100	1:100	PV	1:50	1:100
GAPDH	1:50	1:100	SNAP25	1:200	1:200
Gpx1	1:200	1:200	SOD1	1:200	1:200
Gpx4	1:200	1:200	Ubiquitin	1:50	-
Grin2A	1:100	1:100	Vcan	1:20	1:10
IL1β	1:10	1:10	VGlut1	1:50	1:200

Table 3.3: Antibody details for simple western analysis. *Samples were denatured at 40°C for 30 minutes (see 2.6.3).

Target	Product code	Supplier	Protein concentration (mg/mL)	Antibody dilution
Parvalbumin	LS-B14122	LSBio	0.8	1:50
GAD67	MAB5406	Millipore	0.8	1:100
SNAP25	Ab5666	Abcam	0.4	1:50
PSD95	Ab2723	Abcam	0.4	1:50
NR2A*	PPS012	R&D systems	0.1	1:200
NR2B*	PPS013	R&D systems	0.24	1:50

3.2.4 IL6 and MMP9 ELISAs

Brains and plasma were collected per sections 2.6.1 – 2.6.2, 2.6.4 and 2.7. These brains were from a b-neuro study where dosing had been completed 10 weeks earlier. The dorsal hippocampal regions were used for IL6 and MMP9 ELISA analysis, which were optimised using the protocol in section 2.6.4.

3.2.4.a IL6

IL6 in DH and plasma was measured using the kit HEA079Ra from Cloud-Clone Corp. No signal was detected in the plasma in the optimisations, so only tissue homogenates were used for testing. A 7-point, 2-fold serial dilution standard curve was made from a stock solution of IL6 standard (200 – 3.12 pg/mL). Wells of standard diluent and homogenisation buffer (described in section 2.6.1) were used as negative controls. 100µL of standards and samples, diluted to 2.2mg/mL protein) were pipetted into the pre-coated ELISA plate and incubated at 37°C for 1 hour. Samples were removed, and detection reagent A was added to the unwashed plate and incubated at 37°C for 1 hour. Then, the plate was washed with buffer 8 times and blotted using absorbent paper towels. This wash step is repeated between proceeding steps unless otherwise stated. Next, 100µL of detection reagent B was added and incubated for 30 minutes at 37°C. After washing, 90µL of substrate solution was added and incubated at 37°C in the dark. When the standard had fully developed, indicated by the bottom two standard points being discernible, 50µL of stop solution was added.

The plate was read at 450nm and 630nm. First, the optical density (OD) was calculated by subtracting the background reading (630) from the detection wavelength (450). Then, using the known concentrations of the standard and the calculated OD, a four-parameter logistic (4-PL) curve was created ($R^2 = 0.999$).

3.2.4.b MMP9

To measure the total MMP9 in the rat brain and plasma, we used the kit KE20006 from Proteintech. A 7-point, 2-fold serial dilution standard curve was created from a stock solution of MMP9 standard (4000 – 62.5 pg/mL). Additionally, wells of the standard diluent and the homogenisation buffer (described in section 2.6.1) were run as negative controls. Samples were prepared to a working dilution of 2.2 mg/mL protein. The plasma was at a 1:2 dilution. Then, 100µL of the standard or sample was dispensed into the 96-well precoated ELISA plate and incubated at 37°C for 2 hours.

The plates were washed with diluted wash buffer 8 times, and the remaining liquid was blotted from the wells using absorbent paper towels. This washing was repeated after the remaining steps unless otherwise stated. Next, 100µL of detection antibody was added to the wells, followed by 100µL of horse radish peroxidase (HRP)-conjugated antibody; both were incubated at 37°C for 1 hour or 40 minutes, respectively. After a

final wash, 100µL 3,3',5,5'-Tetramethylbenzidine (TMB) substrate solution was added and incubated at 37°C in the dark. When the standard curve had fully developed, indicated by a colour difference between the blank and the most dilute standard, 100µL of stop solution was added.

The plate was read at 450nm and 630nm to analyse the data. After subtracting the background (630nm) from the detection (450nm) wavelength, the OD values were used to create a 4-PL curve (R^2 = 0.998). Finally, the unknown MMP9 concentrations of the samples were interpolated from the 4-PL model.

3.2.5 MMP2/MMP9 activity assay

To measure the activity of the MMP2/MMP9 enzyme, we used theInnoZyme™ Gelatinase (MMP-2/MMP-9) Activity Assay kit (CBA003) from Merck. An 8-point, 2-fold serial dilution standard was created from stock solution (2000 – 15.6 ng/mL). Samples were diluted to 2.2 mg/mL protein. 90µL of standard or sample was added to a black 96-well plate. 10µL of MMP2/MMP9 gelatinase working solution was added to each well. The plate was incubated at 37°C for 8 hours. Fluorescence was measured at 320nm excitation and 405nm emission. The known standard concentrations and their relative fluorescent unit (RFU) were used to create a 4-PL standard curve, from which sample data was interpolated (R^2 = 0.997).

3.2.6 PCC assay

The DH from the brains used for the WES characterisation (3.2.3) study were used for the PCC assay (ab126287, Abcam). The DH was homogenised in 100µL of water. To remove the nucleic acids, we added 10µL of streptozocin and left the mix at room temperature for 15 minutes. The samples were centrifuged at 14,000xg for 5 minutes. The supernatant was removed, and the 280/260nm ratio was measured on a nanodrop to ensure no nucleic acid contamination. A further aliquot was removed for protein quantification using the Bradford assay (section 2.6.2). 100µL of 2,4-dinitrophenylhydrazine was added to each sample, which was vortexed and incubated at room temperature for 10 minutes. Then, 30µL of trichloroacetic acid was added, samples vortexed, and stored on ice for 5 minutes. Samples were centrifuged at 14,000xg for 2 minutes, and the supernatant was discarded. The pellet was washed with acetone twice, 500µL of cold acetone was added to the pellet, and the tube was sonicated for 2 minutes, stored at -20°C for 5 minutes, centrifuged for 2 minutes at

14,000xg, and finally, the acetone was removed. 200µL of guanidine solution was added and incubated for 30 minutes at 60°C. After incubation, samples were briefly centrifuged, and 100µL of the final supernatant was pipetted into a 96-well plate and read at 375 nm. The protocol recommends a dilution of 2.5 – 10 mg/mL protein. Although many samples used were at the bottom end of this range, we did not detect any samples above a water-only negative control. As samples had been homogenised in water, they could not be used for any other purpose.

3.2.7 Immunohistochemistry

The immunohistochemistry (IHC) brains were taken from a study to assess the effects of distraction and proactive interference on memory in the scPCP model (Landreth et al., 2020). Brains were collected 14 weeks after subchronic dosing. Brains were perfused, fixed and sectioned, then stained for parvalbumin and perineuronal nets (PNN) as described in section 2.8. To calculate the density of parvalbumin interneurons (PVI) and PNN, we used ImagePro Plus software (described in section 2.8.4.a).

3.2.8 Statistics

The statistical tests used in this chapter are summarised below:

Table 3.4: Summary of statistical tests used in chapter three.

Purpose	Distribution	Test	Section
Check for normality	N/A	D'Agostino and Pearson (n>7) or Shapiro-Wilk (n≤7)	2.9.1
Check for correlations	Normal Not normal	Pearson's Spearman's	2.9.5
Compare scVeh to scPCP	Normal Not normal	Unpaired t-test Mann-Whitney U	2.9.3.a 2.9.3.b

3.3 Results

3.3.1 E/I imbalance

3.3.1.a Presynaptic changes

The balance of excitation and inhibition (E/I) depends on the careful management of GABA and glutamate. Therefore, their synthesis, release, signalling, and recycling must be precisely regulated. In a glutamatergic synapse, the activated pre-synaptic neuron releases glutamate, which binds to the available receptors on the post-synaptic neuron. Then, astrocytes take up the excess glutamate, converting it into glutamine. Once converted, the astrocytes release the glutamine into the synapse, and the presynaptic neuron takes it up, ready for converting back into glutamate. Once reconstituted, the vesicle glutamate transporter (VGlut) transports glutamate into vesicles in the presynaptic terminals (Du et al., 2020). Although several proteins are involved in this system, here we will focus on VGlut1 to isolate changes to the pre-synaptic glutamatergic output.

Relative gene expression was determined using quantitative PCR. No change to the dorsal hippocampus (DH) VGlut1 gene expression was detected (scVehicle (V): 0.99 ± 0.07, scPCP (P): 0.86 ± 0.07; $t_{12} = 1.379$, $p = 0.193$) (Figure 3.5A). However, there was a significant decrease in VGlut1 expression in the PFC of scPCP-treated rats (V: 0.22 ± 0.04, P: 0.11 ± 0.02; $t_9 = 2.465$, $p = 0.036$) (Figure 3.5B). We attempted to measure protein changes in VGlut1 but could not find an antibody that produced bands at the predicted molecular weight.

In addition, E/I balance requires efficient communication between different neuronal populations. As such, we selected synaptosomal-associated protein 25kDa (SNAP25) as a general marker of synaptic function, as pre- and post-synaptic neurons terminals express SNAP25 (Antonucci et al., 2016, Tafoya et al., 2006). SNAP25 can bind to voltage-gated calcium channels in the pre-synaptic neuron, reducing the calcium $(Ca)^{2+}$ influx rate. In addition, SNAP25 moderates Ca^{2+}-mediated and slow vesicle release. Post-synaptically, SNAP25 forms a complex with postsynaptic density (PSD)95 (discussed in 3.3.1.b), allowing PSD95 to anchor to the post-synaptic space. Finally, phosphorylated SNAP25 allows the insertion of NMDAr into the post-synaptic membrane (Antonucci et al., 2016). To review, alterations to SNAP25 would change pre-synaptic Ca^{2+} concentration and vesicle release and post-synaptic NMDAr presence.

Regarding SNAP25, there was no alteration in DH (V: 1.131 ± 0.141, P: 1.084 ± 0.187; Mann-Whitney U = 22, p = 0.805) (Figure 3.5C), or PFC gene expression (V: 0.60 ± 0.09, P: 0.63 ± 0.28, t_9 = 0.200, p = 0.846) (Figure 3.5D). However, there was a notable reduction in SNAP25 protein levels in scPCP-treated rats (V: 0.69 ± 0.08, P: 0.18 ± 0.03; $t_{9.96}$ = 9.960, p<0.001 [Welch's correction applied]) (Figure 3.5E), measured using Simple Western analysis.

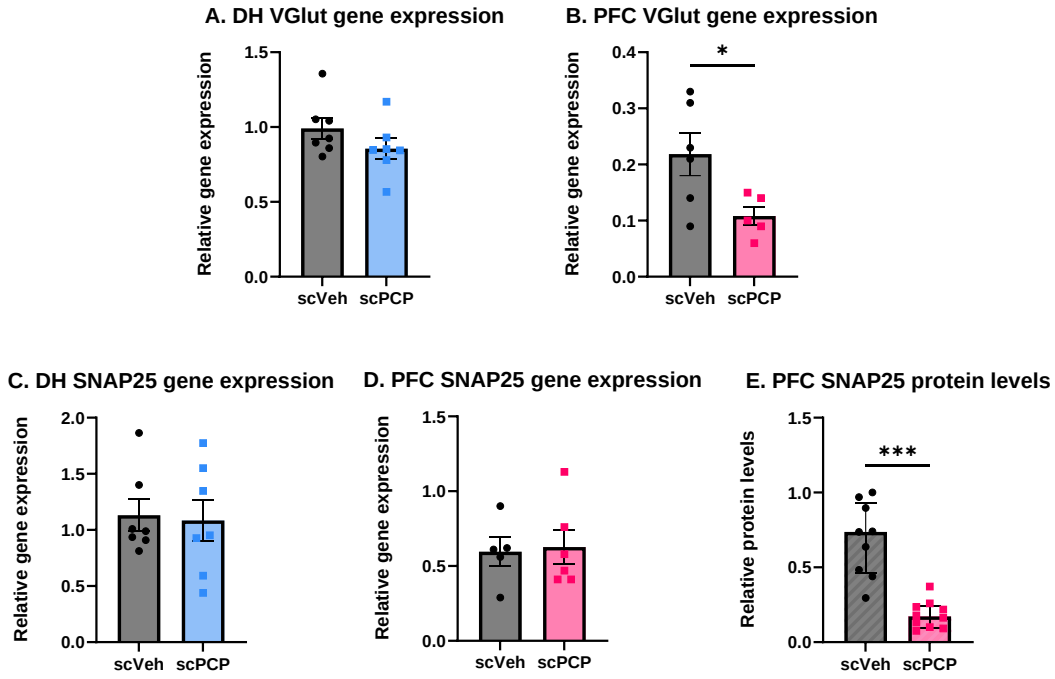

Figure 3.5: The effect of scPCP on VGlut1 and SNAP25 in the DH and PFC. Relative gene expression of VGlut1 in the **A)** DH (n=7) and **B)** PFC (n=5-6). Relative gene expression of SNAP25 in the **C)** DH (n=7) and **D)** PFC (n=6-7). **E)** Relative protein levels of SNAP25 in the PFC (n=9-10). Graphs show mean ± SEM. **D)** A Mann-Whitney test was used for gene expression of SNAP25 in the DH. Here median ± interquartile range (IQR) is shown. The remaining data were analysed with an unpaired t-test, *p<0.05, ***p<0.001.

3.3.1.b Postsynaptic changes

Once released from the presynaptic neuron, glutamate binds to glutamate receptors, including the NMDAr. As discussed in section 3.1.3, the differences in these subunits predict the differential susceptibility to PCP and its analogues. The NMDAr NR2 subunits (NR2A-D) are functionally and developmentally distinct. For example, during development, the predominant subunit is NR2B. Through experience-driven maturation, expression switches to NR2A (Yashiro et al., 2008). The NR2C and NR2D subunits are lowly expressed in the mature brain, making them difficult to measure (Vieira et al., 2020); as such, here we focused on the NR2A and NR2B subunits.

The DH showed a numerical decrease in NR2A gene expression (V: 0.30 ± 0.04, P: 0.21 ± 0.10; $t_8 = 1.547$, $p = 0.160$) (Figure 3.6A). In the PFC, there was no change to NR2A gene expression (V: 0.44 ± 0.12, P: 0.48 ± 0.14, $t_9 = 0.207$, $p = 0.841$) (Figure 3.6B)

There was no alteration to the levels of NR2A in the PFC (V: 1.86 ± 0.17, P: 1.69 ± 0.26; $t_{12} = 0.552$, $p = 0.591$) (Figure 3.6C), whereas NR2B levels had decreased in the PFC of scPCP-treated rats (V: 1.13 ± 0.16, P: 0.43 ± 0.08; $t_{12} = 3.295$, $p = 0.006$) (Figure 3.6D).

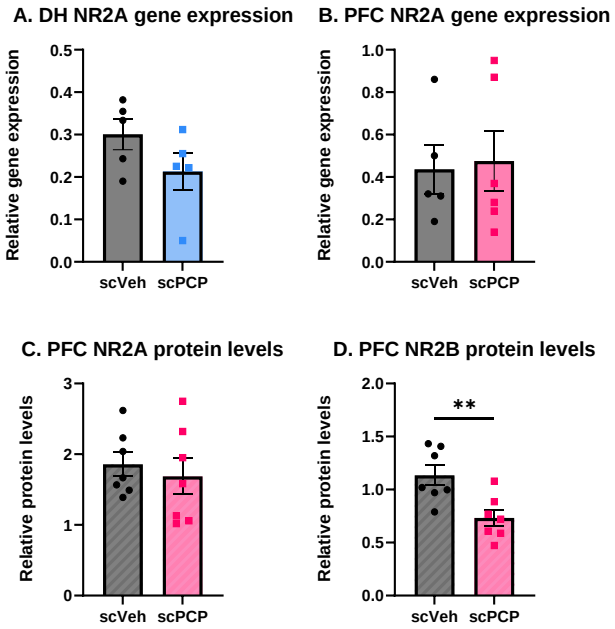

Figure 3.6: The effect of scPCP on NMDAr subunits in the DH and PFC. Relative expression of NR2A mRNA in the **A)** DH (n=5-6) and **B)** PFC (n= 5-6). Relative levels of PFC **C)** NR2A and **D)** NR2B (n=7). Graphs show mean ± SEM. Group differences were analysed with an unpaired t-test, **p<0.01.

PSD95 is a scaffolding protein found in excitatory glutamatergic synapses, which links with NMDAr directly and AMPAr indirectly. There is compelling evidence that PSD95 plays a pivotal role in AMPA/NMDA signalling. For example, increased PSD95 density provides more anchor points for AMPAr, resulting in a more rapid synapse potentiation with NMDA after long-term potentiation (LTP). Conversely, long-term depression (LTD) stimulation decreases PSD95, reducing the available scaffolding for the AMPAr. PSD95 can also directly influence the surface expression of the NMDAr and alter its response sensitivity to synaptic signalling (Keith et al., 2008). We next sought to see if there were any changes to PSD95.

Although there was no change to PSD95 gene expression in the DH (V: 0.93 ± 0.37, P: 0.86 ± 0.44; $t_9 = 0.292$, $p = 0.777$) (Figure 3.7A) or PFC (V: 0.87 ± 0.20, P: 0.80 ± 0.18; $t_{10} = 0.257$, $p = 0.803$ (Figure 3.7B), we found a significant reduction in the relative protein levels of PSD95 in the PFC (V: 0.70 ± 0.06, P: 0.56 ± 0.02; $t_{11.92} = 2.262$, $p = 0.043$ [Welch's correction applied]) (Figure 3.7C).

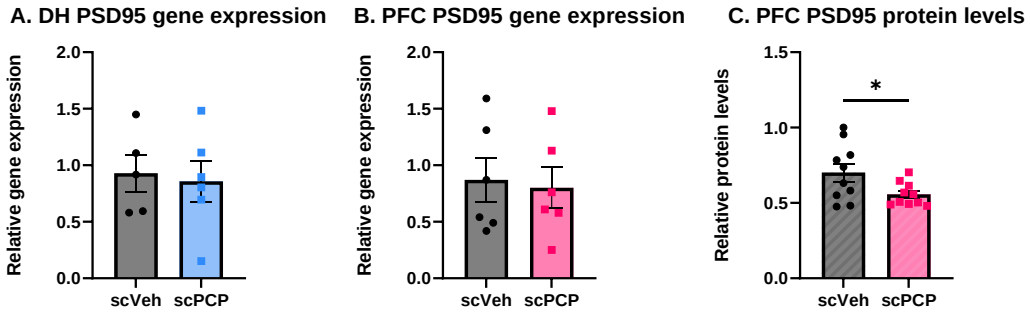

Figure 3.7: The effect of scPCP on PSD95 in the DH and PFC. A) Relative gene expression of PSD95 in the DH (n=5-6). Relative levels of PSD95 **B)** mRNA (n=6) and **C)** protein (n=10) in the PFC. Graphs show mean ± SEM. Group differences were analysed with an unpaired t-test, *p<0.05.

3.3.2 Parvalbumin

Histological evidence suggests that PVI deficits in schizophrenia are due to the lack of parvalbumin protein expression rather than the loss of neurons (Filice et al., 2016, Thune et al., 2001). Therefore, to better understand what happens to PVI after scPCP, we used qPCR, WES and IHC to measure parvalbumin.

There was no change to DH PV gene expression (V: 1.23 ± 0.10, P: 1.04 ± 0.16; $t_{12} = 0.997$, p = 0.339) (Figure 3.8A). However, the results in the PFC showed an increase in parvalbumin gene expression (V: 0.88 ± 0.07, P: 1.07 ± 0.05; $t_{12} = 2.329$, p = 0.038) (Figure 3.8B) and protein levels (V: 0.36 ± 0.03, P: 0.61 ± 0.09; $t_{10.76} = 2.652$, p = 0.023 [Welch's correction applied]) (Figure 3.8C). Despite this, the PVI cell density in the PFC decreased after scPCP dosing (V: 137.8 ± 5.36, P: 105.4 ± 3.93; $t_{17} = 4.773$, p<0.001) (Figure 3.8D).

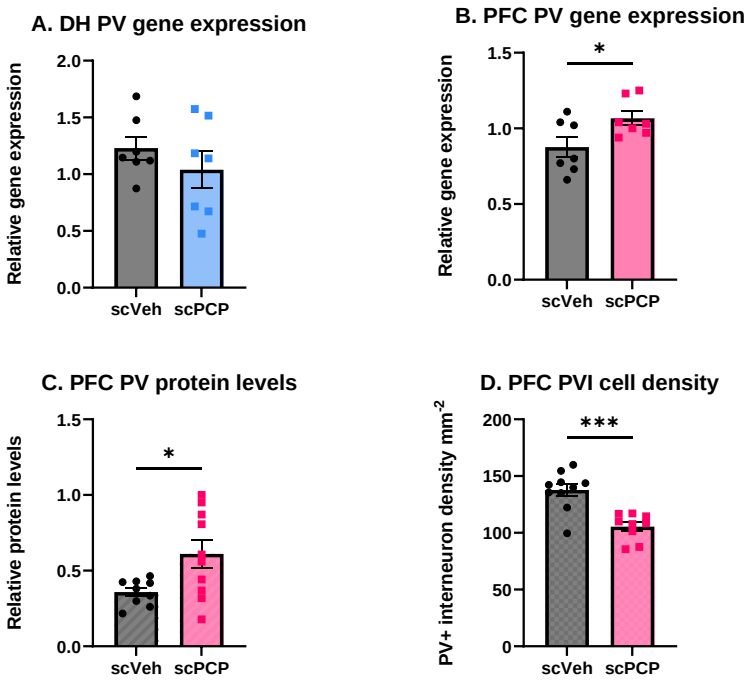

Figure 3.8: The effect of scPCP on PV in the DH and PFC. Relative gene expression of PV in the **A)** DH (n=7) and **B)** PFC (n=7). **C)** Relative PV levels in the PFC (n=9-10). **D)** PVI interneuron density in the PFC (n=9-10). Graphs show mean ± SEM. Group differences were analysed with an unpaired t-test, *p<0.05, ***p<0.001.

3.3.3 Glutamate decarboxylase

Glutamate is enzymatically converted into GABA by glutamate decarboxylase (GAD) 65 and 67. The two variants of GAD are expressed in the nerve terminals and the cell body, respectively. These spatial differences reflect functional diversity. For example, GAD65 produces GABA for neurotransmission, whereas GAD67 produces GABA used for metabolic functions, synaptogenesis and, notably, oxidation-reduction regulation (Sears et al., 2021). Here we investigated GAD1 and GAD2, the gene names for GAD67 and 65, respectively and protein levels for GAD67.

Here we saw a trend towards a decrease in GAD1 (GAD67) gene expression (V: 1.21 ± 0.08, P: 0.96 ± 0.09; t_{12} = 2.054, p = 0.063) (Figure 3.9A) and no change to GAD2 (GAD65) in the DH (V: 1.29 ± 0.20, P: 1.13 ± 0.19; t_{12} = 0.578, p = 0.574) (Figure 3.9B).

There was no change to PFC GAD1 (V: 0.55 ± 0.09, P: 0.46 ± 0.12; t_9 = 0.625, p = 0.547) (Figure 3.9C) or GAD2 expression (V: 0.79 ± 0.09, P: 0.73 ± 0.08; t_9 = 0.504, p = 0.626) (Figure 3.9D).

Finally, there was a significant reduction in the protein levels of GAD67 in the PFC of scPCP rats (V: 0.84 ± 0.04, P: 0.69 ± 0.02; t_{18} = 3.128, p = 0.006) (Figure 3.9E).

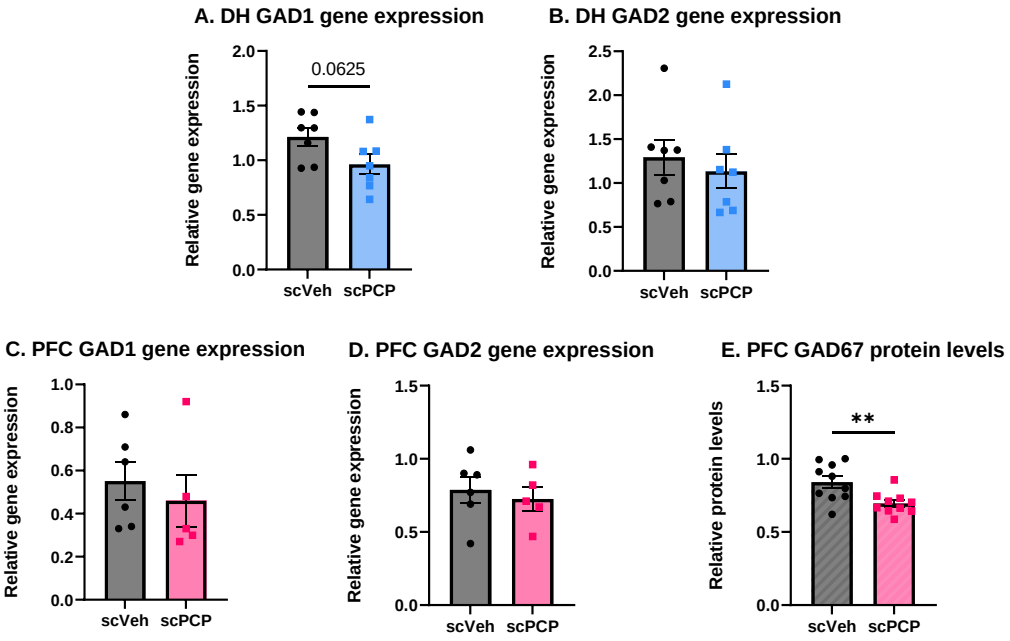

Figure 3.9: The effect of scPCP on GAD in the DH and PFC. Relative gene expression of DH **A)** GAD1 (n=7) and **B)** GAD2 (n=7). Relative gene expression of PFC **C)** GAD1 (n=5-6) and **D)** GAD2 (n=5-6). **E)** Relative protein levels of GAD67 in the PFC (n=10). Graphs show mean ± SEM. Group differences were analysed with an unpaired t-test, **p<0.01.

3.3.4 Perineuronal nets

As discussed in section 1.6, the individual components predict the function of the PNN. As such, we investigated the gene expression of each CGSP in the PFC and DH. In the PFC, WFA was used as a general stain for PNN.

In the DH, there was no change to any component gene expression, Acan (V: 9.77 ± 0.68, P: 11.30 ± 0.90; t_{10} = 1.391, p = 0.195) (Figure 3.10A), Bcan (V: 10.55 ± 1.12, P: 12.18 ± 1.28; t_{10} = 0.951, p = 0.364) (Figure 3.10B), Ncan (V: 1.86 ± 0.46, P: 1.65 ± 0.68, t_{11} = 0.665, p = 0.520) (Figure 3.10C), Vcan (V: 12.38 ± 1.62, P: 12.05 ± 2.56; t_{10} = 0.463, p = 0.654) (Figure 3.10D)

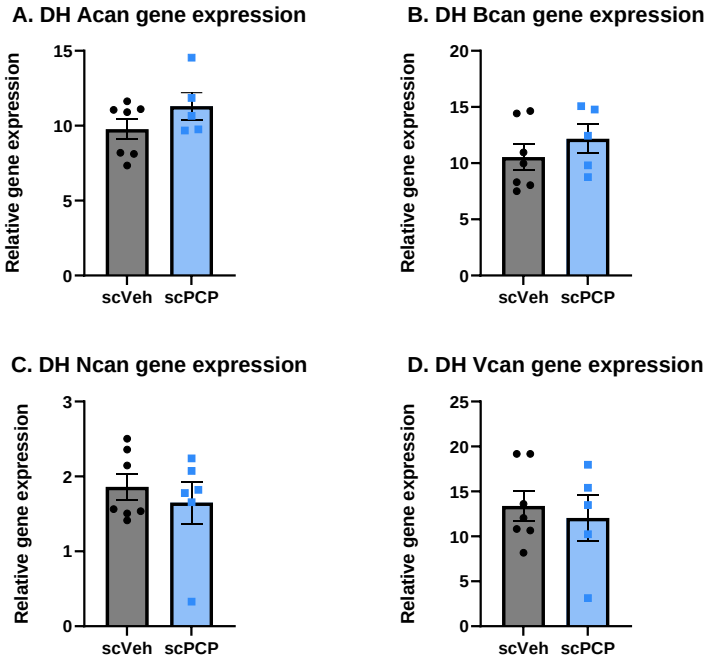

Figure 3.10: The effect of scPCP on PNN components in the DH. Relative gene expression of **A)** Acan, **B)** Bcan, **C)** Ncan and **D)** Vcan (n=5-6). Graphs show mean ± SEM. Group differences were analysed with an unpaired t-test.

In the PFC, we again saw no change to PNN component gene expression, Acan (V: 1.42 ± 0.27, P: 1.19 ± 0.19; t_{12} = 0.710, p = 0.491) (Figure 3.11A), Bcan (V: 0.17 ± 0.03, P: 0.19 ± 0.06; t_{10} = 0.224, p = 0.828) (Figure 3.11B), Ncan (V: 1.71 ± 0.21, P: 1.82 ± 0.29; t_{12} = 0.315, p = 0.758) (Figure 3.11C), Vcan (V: 3.21 ± 0.29, P: 2.85 ± 0.37; t_{12} = 0.770, p = 0.456) (Figure 3.11D). Despite this, there was a significant decrease in WFA-detected PNN in the scPCP rats (V: 106.30 ± 7.88, P: 79.36 ± 4.84; t_{18} = 2.913, p = 0.009) (Figure 3.11E).

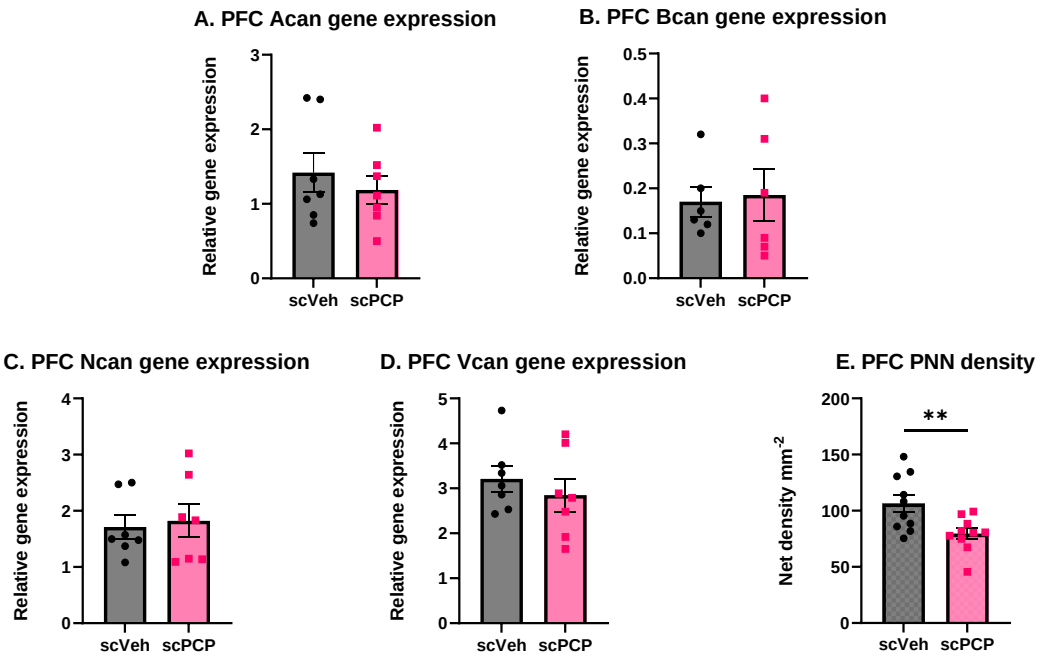

Figure 3.11: The effect of scPCP on the PNN in the PFC. Relative gene expression of **A)** Acan, **B)** Bcan, **C)** Ncan and **D)** Vcan (n=6-7). **E)** PNN density in the PFC (n=10). Graphs show mean ± SEM. Group differences were analysed with an unpaired t-test, **p<0.01.

3.3.5 MMP9

As we saw a reduction in PNN density in the absence of component mRNA changes, we next sought to determine whether this was due to increased enzymatic breakdown. There are two families of enzymes associated with PNN breakdown, a disintegrin and metalloproteinase with thrombospondin motifs (ADAMTS) (Gottschall et al., 2015) and matrix metalloproteinases (MMP) (Dwir et al., 2020). Given that MMP9 is the most widely studied in schizophrenia, we chose to investigate its prevalence and activity (Chang et al., 2011, Domenici et al., 2010, Dwir et al., 2020, Kumarasinghe et al., 2013, Yamamori et al., 2013).

There was no alteration to MMP9 expression in the DH (V: 43.74 ± 13.15, P: 42.14 ± 15.27; t_{12} = 0.0795, p = 0.938) (Figure 3.12A) or the PFC (V: 2.75 ± 0.30, P: 2.77 ± 0.21; t_{10} = 0.060, p = 0.954) (Figure 3.12B). In the dorsal hippocampus, we looked at total levels of MMP9 and the activity of the enzyme; again, we found no difference between groups (levels; V: 2081 ± 284.5, P: 2307 ± 179.3; t_{16} = 0.702, p = 0.493 (Figure 3.12C). Activity; V: 24.99 ± 3.79, P: 25.92 ± 4.86; t_{12} = 0.142, p = 0.890 (Figure 3.12D)

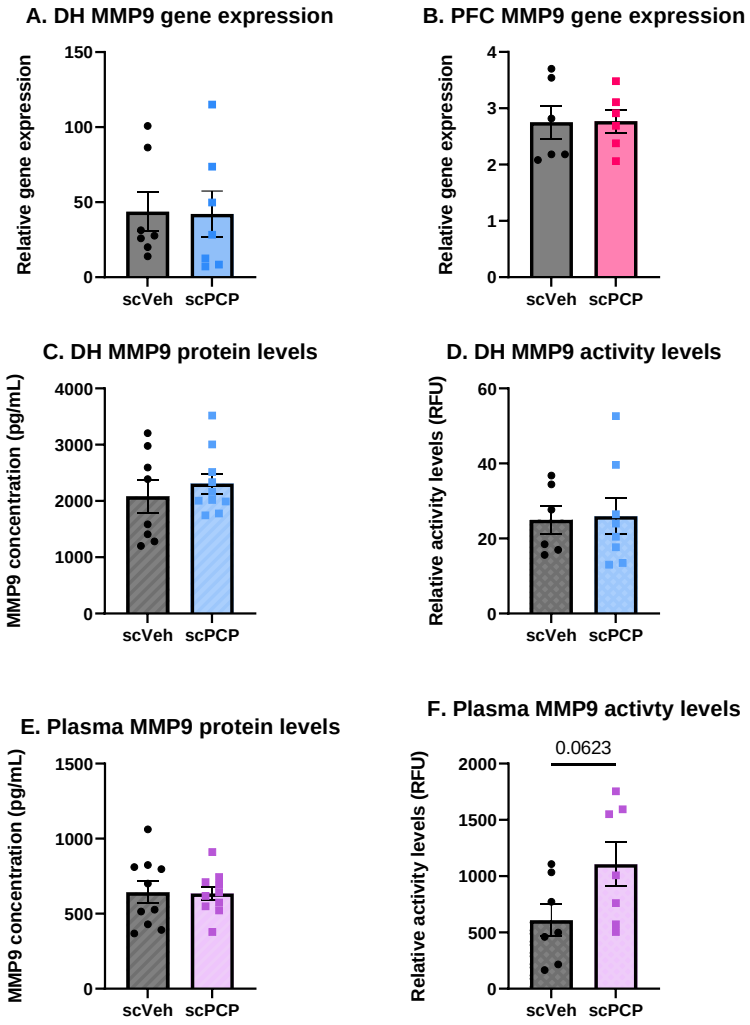

Figure 3.12: The effect of scPCP on MMP9 in the DH, PFC and plasma. Relative gene expression of MMP9 in the **A)** DH (n=7) and **B)** PFC (n=6). DH MMP9 **C)** concentration (n=8-10) and **D)** activity levels (n=6-8). Plasma MMP9 **E)** concentration (n=10) and **F)** activity levels (n=7). Graphs show mean ± SEM. Differences between groups were analysed with an unpaired t-test.

Due to the use of MMP9 as a peripheral biomarker (Yamamori et al., 2013), we were interested in measuring the levels and activity of MMP9 in the periphery and whether it correlated to brain findings. There was no difference in MMP9 levels in plasma (V: 642.4 ± 72.83, P: 634.1 ± 45.58; t_{19} = 0.096, p = 0.925) (Figure 3.12E). However, there was a

trend towards increased activity in the plasma of scPCP-treated rats (V: 607.9 ± 141.4, P = 1106.0 ± 197.1; t_{12} = 2.056, p = 0.062) (Figure 3.12F). Using Pearson's correlation coefficient, we found a negative correlation between brain and plasma activity in the cohort (r = -0.658, n= 10, p = 0.038), which did not reach significance in the individual cohorts (V: r = -0.324, n = 4, p = 0.676; P: r = -0.690, n = 6, p = 0.129).

3.3.6 Oxidative stress

Accurately measuring damaging reactive oxygen species (ROS) can be challenging due to their inherent reactivity. Consequently, it can be beneficial to measure the by-products of ROS reacting with proteins, carbohydrates and nucleic acids (Murphy et al., 2022). For example, protein carbonyls form when amino acid residues oxidise to form carbonyl groups (Hawkins et al., 2019). Here, we used a commercial kit to measure protein carbonyl content in the DH, unfortunately, the kit was not sensitive enough to detect samples above the negative control. Instead, we focused on genes relevant to the neuronal antioxidant function. For example, superoxide dismutase (SOD1) is an intracellular enzyme that facilitates the oxidation of oxygen free radicals into hydrogen peroxide (Wang et al., 2018b). Likewise, Glutathione peroxidase (GPx) and catalase (Cat) catalyse the conversion of hydrogen peroxide into oxygen and water. Here we measured the expression of SOD1, Cat and two subtypes of GPx, GPx1 and GPx4. The former is essential for protection from oxidative stress, whereas the latter is vital for preventing lipid peroxidation and cellular apoptosis (Brigelius-Flohé et al., 2013).

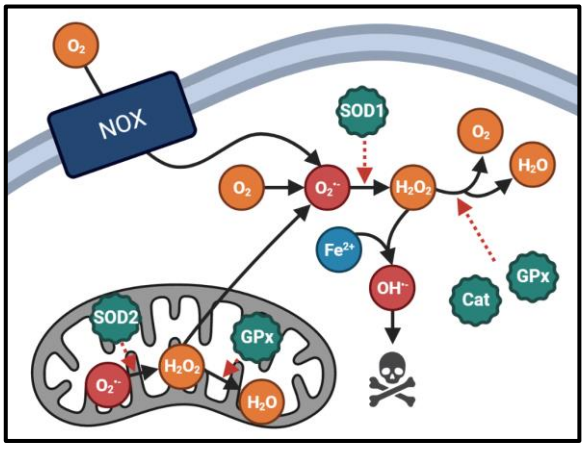

Figure 3.13: A schematic showing the subcellular action of antioxidants. ROS (red) formation in the mitochondria and cytosol and its conversion into inert compounds by antioxidants (green). Red dashed lines indicate enzymatic processes. NOX: NADPH oxidase (transmembrane protein), SOD: superoxide dismutase, Cat: catalase, GPx: glutathione peroxidase. (Adapted from: Sepasi Tehrani et al., 2018, Wang et al., 2018b). Image created in BioRender.com.

We found no change to the dorsal hippocampal expression of GPx1 (V: 1.586 ± 0.105, P: 1.732 ± 0.603; $t_{6.363}$ = 0.238, p = 0.819 [Welch's correction applied]; Figure 3.14A), GPx4 (V: 1.057 ± 0.176, P: 0.948 ± 0.268; Mann-Whitney U = 20, p = 0.620; Figure 3.14B), SOD1 (V: 0.698 ± 0.116, P: 1.035 ± 0.270; t_{11} = 1.082, p = 0.303; Figure 3.14C) and Cat1 (V: 0.670 ± 0.084, P: 0.984 ± 0.279; $t_{7.075}$ = 1.078, p = 0.317 [Welch's correction applied]; Figure 3.14D).

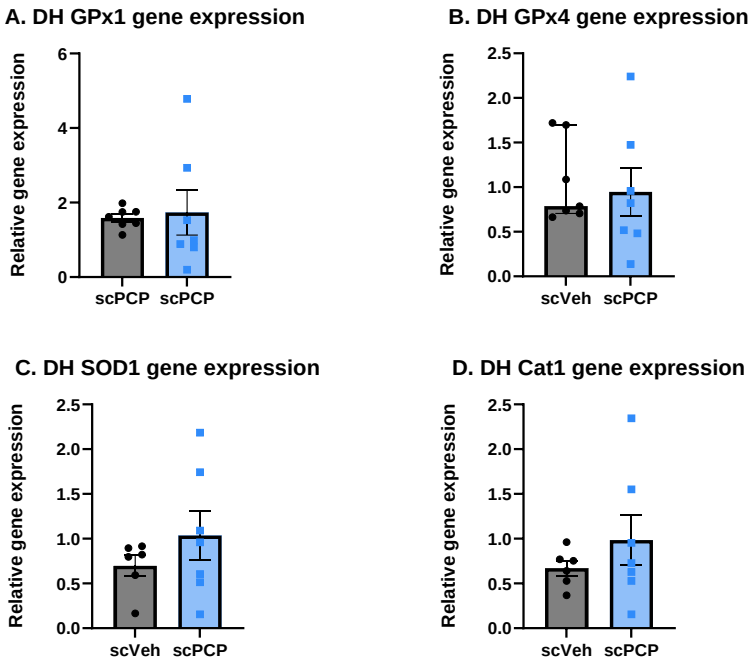

Figure 3.14: The effect of scPCP on markers related to reactive oxygen species in the DH. Relative gene expression of **A)** GPx1, **B)** GPx4, **C)** SOD1 and **D)** Cat1 in the DH (n=6-7). Graphs **A** – **C** and **D)** data were analysed with an unpaired t-test, and graphs show mean ± SEM. For **B)** group differences were analysed with a Mann-Whitney U, and graphs show median ± IQR.

We measured the same markers in the PFC. Here we found no difference in Gpx1 (V: 0.446 ± 0.034, P: 0.552 ± 0.065; Mann-Whitney U = 8, p = 0.421; Figure 3.15A), GPx4 (V: 0.463 ± 0.098, P: 0.608 ± 0.134; Mann-Whitney U = 11, p = 0.290; Figure 3.15B) or Cat1 (V: 0.708 ± 0.126, P: 0.822 ± 0.133; Mann-Whitney U = 14, p = 0.589; Figure 3.15D). However, we did find a significant increase in the gene expression of SOD1 (V: 0.266 ± 0.121, P: 0.965 ± 0.200; t_9 = 2.831, p = 0.020; Figure 3.15C).

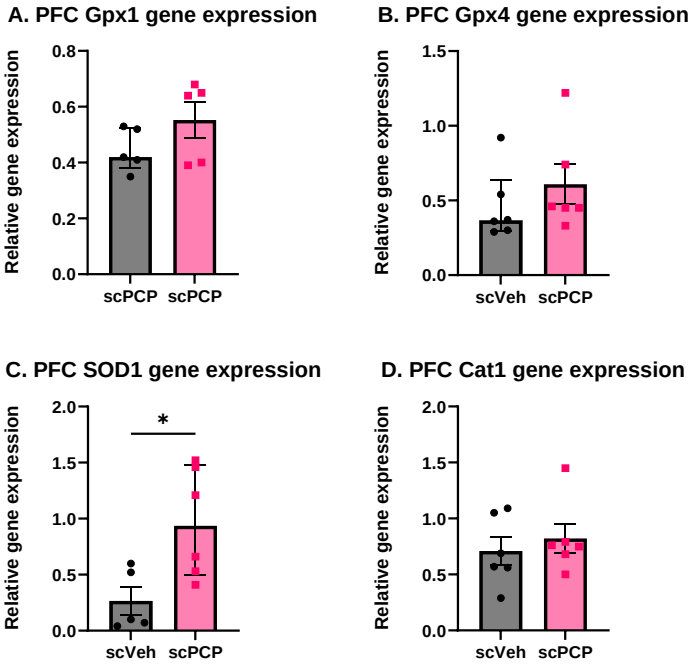

Figure 3.15: The effect of scPCP on markers related to reactive oxygen species in the PFC. Relative gene expression of **A)** GPx1 (n=5), **B)** GPx4 (n=6), **C)** SOD1 (n=5-6) and **D)** Cat1 (n=6) in the PFC. For graphs **A** – **C)** differences between groups were analysed with a Mann-Whitney U, and graphs show median ± IQR. For **D)** data were analysed with an unpaired t-test, and graphs show mean ± SEM. *p<0.05.

3.3.7 Inflammation

Acute and chronic inflammation is different in nature as well as duration. Acute inflammation involves rapid pathogen neutralisation and subsequent repair to collaterally damaged neighbouring tissue. Conversely, chronic inflammation is the persistence of low-level inflammation, often in the absence of inflamed tissue and systemic (Del Giudice et al., 2018).

Nuclear factor κB (NFκB) is a transcription factor pivotal to the induction of many pro-inflammatory cytokines, chemokines and adhesion molecules. Additionally, NFκB can regulate cell survival, proliferation and maturation. NFκB can lead to the upregulation

of interleukin 1β (IL1β) (Zhang et al., 2018a). The activation of IL1β and tumour necrosis factor α (TNFα) is also triggered by invading pathogens (Del Giudice et al., 2018). However, we could only measure NFκB and IL1β because TNFα was too lowly expressed in both scVeh and scPCP samples. In addition, there was an insufficient sample to run NFκB in the DH samples,

There was no change to NFκB in the PFC (V: 2.60 ± 0.43, P: 3.23 ± 0.45; t_9 = 1.01, p = 0.339) (Figure 3.16A). The expression of IL1β was also unchanged in the DH (V: 13.00 ± 0.67, P: 19.53 ± 5.24; $t_{4.13}$ = 1.237, p = 0.282 [Welch's correction applied]) (Figure 3.16B) and PFC (V: 2.46 ± 0.41, P: 2.07 ± 0.54; t_{10} = 0.578, p = 0.576) (Figure 3.16C).

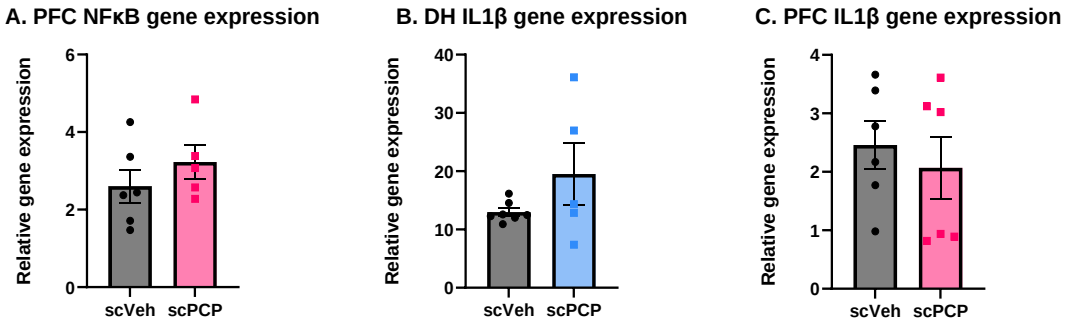

Figure 3.16: The effect of scPCP on NFκB and IL1β gene expression in the DH and PFC. Relative NFκB expression in the **A)** PFC (n=7). IL1β gene expression in the **B)** DH (n=5-7) and **C)** PFC (n=6). Graphs show mean ± SEM. Differences between groups were analysed with an unpaired t-test.

IL6 is thought to be a key mediator in the switch from acute to chronic inflammation. IL6 signals through two pathways, classic signalling and trans-signalling. Briefly, classical signalling is the binding of IL6 to receptors found on microglia, leukocytes, hepatocytes, and some epithelial cells. IL6 binding triggers intracellular signalling pathways that increase the acute immune response. The dose-response curve for classical signalling is bell-shaped; consequently, as IL6 levels continue to rise, the effectiveness of the classical signalling pathway will eventually decrease (Del Giudice et al., 2018).

The pro-inflammatory environment created by acute inflammation and classical signalling will ultimately encourage the trans-signalling pathway. Here, the IL6 receptor is cleaved from the membrane of microglia, leukocytes, hepatocytes, or epithelial cells and enters the blood circulation. As a result, the soluble IL6 receptor binds to gp130, a near-ubiquitous cell surface marker (Del Giudice et al., 2018). The binding of the soluble IL6 receptor to a neuron can cause its degeneration, whereas classical signalling

encourages neuronal regeneration, highlighting the importance of constant IL6 regulation (Rothaug et al., 2016).

Although there was no alteration to the IL6 gene expression in the DH (V: 14.24 ± 2.69, P: 16.09 ± 4.88; t_{11} = 0.345, p = 0.736) (Figure 3.17A), the protein levels were increased (V: 30.99 ± 7.66, P: 58.17 ± 7.34; t_{14} = 2.505, p = 0.025) (Figure 3.17B). Finally, scPCP increased IL6 gene expression in the PFC (V: 4.62 ± 0.42, P: 6.72 ± 0.32; t_{11} = 3.845, p = 0.003) (Figure 3.17C). Unfortunately, because of the volume and protein input required for the IL6, we could not investigate whether there was any alteration in PFC IL6 protein levels.

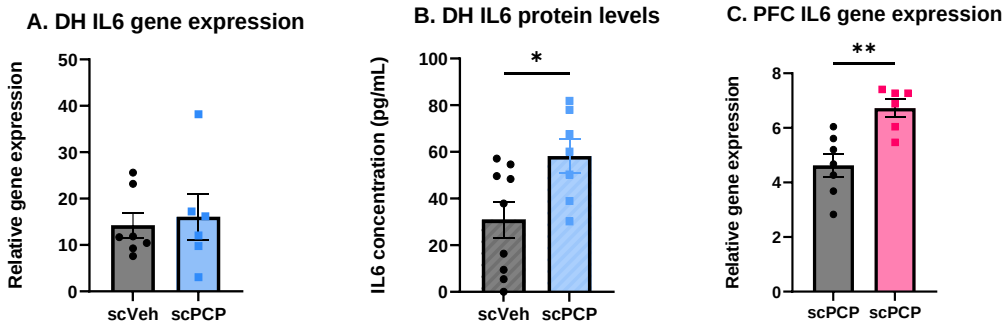

Figure 3.17: The effect of scPCP on IL6 gene expression and protein levels. DH IL6 **A)** gene expression (n=6-7) and **B)** protein levels (n=7-9). **C)** PFC IL6 gene expression (n=6-7). Graphs show mean ± SEM. Differences between groups were analysed with an unpaired t-test. *p<0.05, **p<0.01.

3.4 Discussion

3.4.1 Overview of main findings

This characterisation chapter aimed to shed light on the potential mechanisms underlying the sustained behavioural and pathological deficits observed in the scPCP model. A mechanism was proposed based on previously published data, and targets were measured from various cohorts using varied methods. The main pathological findings of scPCP dosing are summarised in Figure 3.18.

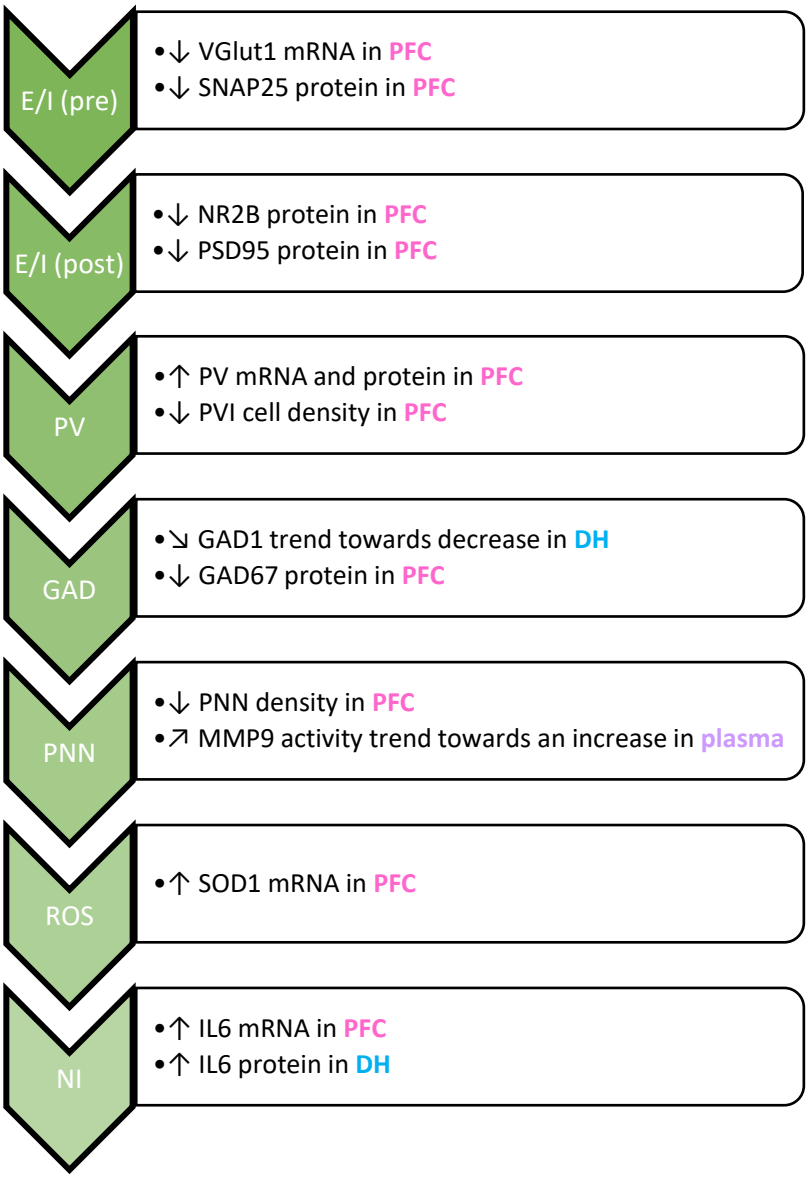

Figure 3.18: Summary of pathological consequences of scPCP dosing. Arrows show significant change from scVeh group. NMDAr: NMDA receptor, E/I: excitatory/inhibitory balance, PV: parvalbumin, GAD: glutamate decarboxylase, PNN: perineuronal nets, ROS: reactive oxygen species, NI: neuroinflammation, NR2B: NMDAr subunit 2B, PSD95: postsynaptic density 95, VGlut1: vesicle glutamate transporter, SNAP25: synaptosomal-associated protein 25kDa, PVI: parvalbumin interneuron, MMP9: matrix metalloproteinase 9, IL6: interleukin 6.

The balance between excitation and inhibition requires careful regulation for neuron-to-neuron communication and network coordination. This process is dynamically regulated through responsive changes to GABA or glutamate synthesis, release and reuptake. An imbalance between these two opposing neurotransmitters can lead to impaired cognition, motor disorder and cell death (Sears et al., 2021). In addition, mutations to genes throughout the synthesis, release and reuptake process for GABA and glutamate have been associated with increased schizophrenia risk (reviewed in: Sears et al., 2021) and all symptom domains, including cognitive deficits (Jardri et al., 2016, Liu et al., 2021b, Nakahara et al., 2022, Selten et al., 2018). Here we will review the changes we have seen after scPCP dosing and reflect on how these changes may induce E/I imbalance.

3.4.2 VGlut1

As described in 3.3.1, VGlut is a transporter of glutamate into vesicles. There are three variants of VGlut. VGlut1 is present in virtually all pyramidal and granule cells (Eastwood et al., 2005). VGlut2 is predominantly found in the thalamus, midbrain and brainstem (Moechars et al., 2006). Finally, VGlut3 is found in non-glutamatergic neurons (Seal et al., 2006). There is limited evidence of VGlut1 mutations in schizophrenia patients (Shen et al., 2009). However, several studies have found reduced VGlut1 protein or mRNA in the anterior cingulate cortex, hippocampus and dorsolateral prefrontal cortex, with no change to VGlut2 (Eastwood et al., 2005, Oni-Orisan et al., 2008, Sawada et al., 2005).

In animal studies, complete genetic knockouts of VGlut1 and VGlut2 are lethal to the developing foetus. However, heterozygous knockdowns of VGlut2 do not affect learning (Callaerts-Vegh et al., 2013), whereas VGlut1 knockdowns show impaired long-term memory, with minimal effects on short-term memory (Balschun et al., 2010, Callaerts-Vegh et al., 2013, King et al., 2014, Tordera et al., 2007). Given that VGlut1 is involved in the later stages of glutamate transmission (see section 3.3.1), it follows that early stages of glutamate signalling are not impaired. Instead, we see impairments when the pre-synaptic neuron has depleted its glutamate, the replacements of which are not being efficiently transported by VGlut1.

In the present study, we saw decreases in VGlut1 PFC mRNA (Figure 3.5B). This is in keeping with previous scPCP studies looking at VGlut1 in the PFC and hippocampus (Piyabhan et al., 2013, Piyabhan et al., 2016). A third study found that 24 hours after the

conclusion of subchronic (sc) MK-801 dosing, there was an increase in VGlut1, potentially in response to the glutamate increase seen in the acute stage of NMDAr antagonism (see 3.1.3). However, levels of VGlut1 normalised after seven days and remained comparable to vehicle animals until day 28 (Ma et al., 2020).

3.4.3 SNAP25

SNAP25 is a pre- and post-synaptic protein required for evoked synaptic signalling (Washbourne et al., 2002). Evidence shows that mutations in the SNAP25 gene increase schizophrenia risk (Fanous et al., 2010, Guan et al., 2020, Houenou et al., 2017, Wang et al., 2015).

Here, we observed a reduction of SNAP25 protein in the PFC of scPCP-treated rats (Figure 3.5E). In periods of high activity, SNAP25 becomes phosphorylated, inhibiting voltage-gated calcium channels (VGCC) (Pozzi et al., 2008). If SNAP25 is not facilitating the inhibition of VGCCs, an uncontrolled increase in presynaptic Ca^{2+} could cause mitochondrial damage, disruptions to neuronal and synaptic function, impaired learning and memory, and cell death (Calvo-Rodriguez et al., 2020, Huang et al., 2022, McDaid et al., 2020, Uryash et al., 2020).

Another presynaptic function of SNAP25 is permitting the fusion of vesicles to the pre-synaptic membrane; therefore, reduced levels of SNAP25 may alter presynaptic signalling. Post-synaptically, SNAP25 couples with PSD95 and facilitates the insertion of NMDAr into the post-synaptic membrane (Antonucci et al., 2016). These postsynaptic alterations result in decreased spine density and postsynaptic excitatory potentials (Fossati et al., 2015). SNAP25 reductions would reduce pre- and post-synaptic signalling, with post-synaptic effects predominantly impacting LTP.

3.4.4 NMDAr

PCP is an NMDAr antagonist that acutely causes NMDAr hypofunction on inhibitory interneurons (Homayoun et al., 2007). There is evidence of NMDAr dysfunction in schizophrenia patients. Mutations to the NR1 gene have been associated with schizophrenia risk and cognitive symptom severity (Qin et al., 2005, Weickert et al., 2013), and post-mortem analysis shows decreased NR1 protein and mRNA in the PFC, hippocampus and left superior frontal gyrus (Catts et al., 2015, Catts et al., 2016, Gao et al., 2000, Law et al., 2001, Sokolov, 1998). Given that the NR1 subunit is required for receptor structure and function (Traynelis et al., 2010), the reduction in NR1 would

indicate impaired NMDAr signalling in schizophrenia. Indeed, imaging studies show that patients have reduced NMDAr binding (Pilowsky et al., 2006). Although not measured here, other studies show that replicating NR1 hypofunction in mice induces working memory and social interaction deficits. Post-mortem analysis reveals PVI cell density reductions analogous to schizophrenia observations (Belforte et al., 2010, Gandal et al., 2012, Korotkova et al., 2010). Isolating the NR1 knockout to PVI results in working and recognition memory deficits and altered theta and gamma frequency oscillations (Carlén et al., 2012, Korotkova et al., 2010).

In the present study, we saw decreases in NR2B protein in the PFC and no change to NR2A mRNA or protein in the DH and the PFC (Figure 3.6). Both subunits have documented mutations that can increase schizophrenia risk (Hu et al., 2016, Iwayama-Shigeno et al., 2005, Li et al., 2007, Myers et al., 2019, Qin et al., 2005, Tarabeux et al., 2011). Although NR2A is required for the initial response to NMDAr antagonists (Picard et al., 2019), the long-term effects on NR2B observed here are in keeping with previous studies, which found reductions to NR2B density or gene methylation changes after scPCP dosing, but no change to NR2A (Lindahl et al., 2004, Loureiro et al., 2022).

In the healthy adult brain, the ratio of the NR2A and NR2B receptors can indicate the levels of LTP activity. In periods of low cortical activity, the NR2B subunit dominates; however, after high cortical activity, NR2A expression increases, and NR2B decreases (Bear et al., 2020). This activity-dependent switch is essential for the NR2B-dependent detection of early LTP and the NR2A-dependent stability of the potentiated synapse. Furthermore, the NR2B subunit is more permissible to Ca^{2+} ions and is required for initial memory acquisition (Bear et al., 2020, Rodrigues et al., 2001).

During LTP, NR2B migrates away from the potentiating dendritic spine. If this diffusion is blocked, hippocampal LTP is blocked (Dupuis et al., 2014). Indeed, the NR2B subunit is 250-fold more mobile than NR2A (Groc et al., 2006). When a small region of the dendritic surface is blocked with MK-801, NMDAr rapidly mobilises, allowing for a swift recovery of function (Tovar et al., 2002).

Finally, a dendritic spine is considered mature when it has a higher relative density of NR2A to NR2B subunits. In this state, LTP induction requires a more substantial stimulus, stabilising the synapse (Yashiro et al., 2008).

In transgenic mice that overexpress NR2B, NMDAr signalling is increased. Consequently, learning and memory are significantly improved compared to wildtype (Tang et al., 1999). In scPCP-treated mice, there is evidence of reduced NR2B in the cerebellum (Bullock et al., 2009). In addition, LTP in the hippocampus (Nomura et al., 2016) and PFC (Tanqueiro et al., 2021) is diminished, suggesting NR2B pathology. As a reminder, the present study found reduced NR2B levels in the PFC. However, we did not measure NR2B in the hippocampus.

It is noteworthy that NR2B-specific antagonists have neuroprotective effects in diseases associated with excessive glutamate, such as pain, Parkinson's disease, stroke and brain injury (Chazot, 2004, Nikam et al., 2002, Wang et al., 2005). Perhaps the downregulation of NR2B observed in scPCP animals may be a neuroprotective attempt to address E/I imbalance.

3.4.5 PSD95

The scaffolding proteins in the postsynaptic density anchor the postsynaptic proteins and organise signalling molecules. Therefore, they are vital moderators of synaptic strength (Frank et al., 2016).

Of the proteins in the postsynaptic density, PSD95 is the most abundant (Cheng et al., 2006). Abnormalities in PSD95 protein have been associated with increased schizophrenia risk (Funk et al., 2017, Hu et al., 2022, Ohnuma et al., 2000). PSD95 anchors NR2B (Frank et al., 2016) and traffics AMPAr to the postsynaptic density (Elias et al., 2007). Given that PSD95 does not directly interact with NR2A, it is somewhat counterintuitive that overexpression of PSD95 results in increased NR2A and reduced NR2B expression (Losi et al., 2003), as is seen in synapse maturation (Bear et al., 2020). However, the increased AMPAr trafficking likely results in efficient LTP generation (Elias et al., 2007).

On the other hand, the acute knockdown of scaffolding proteins PSD95, PSD93, and synapse-associated protein (SAP) 102 increased the number of silent synapses. A silent synapse has NMDAr without AMPAr (Chen et al., 2015). In comparison, silencing only PSD95 produces a synapse that can still induce LTP. However, the long-term maintenance and stability of the potentiated synapse are affected in the hippocampus (Ehrlich et al., 2007). PSD95 is important for glutamatergic postsynaptic signalling. In our

study, we found reduced levels of PSD95 in the PFC alongside NR2B deficits, indicating impaired LTP.

3.4.6 Parvalbumin

As discussed, parvalbumin interneurons (PVI) are indispensable regulators of E/I balance, which are impaired in schizophrenia. Here, we found conflicting data in the PFC. Parvalbumin mRNA (brains taken 22 weeks post-scPCP) and protein (12 weeks post-scPCP) increased. Whereas PVI density decreased (14 weeks post-scPCP) (Figure 3.8). However, reviewing published studies that have measured parvalbumin after scPCP reveals a robust reduction in PVI cell density DH and PFC that is both rapid and sustained (Table 3.5). Given these published findings and the data presented in this thesis, scPCP-treatment likely reduces PVI cell density in Lister Hooded rats.

Limiting the conclusion to Lister Hooded rats is intentional. Studies comparing behavioural and post-mortem outcomes after NMDAr antagonism in different rat strains find differing results. For example, MK-801 dosing in male Long Evans rats can produce anxiogenic behaviour and cognitive impairments, whereas Wistars in the same paradigm have no measured deficits (Uttl et al., 2018). A second study compared behavioural and pharmacokinetics after acute PCP dosing. Although the PCP concentration in the blood and the brain was comparable, Lister Hooded rats consistently performed worse in a visual discrimination task than Long Evans rats (Mohler et al., 2015).

Despite the homogeneity in the IHC analysis, there are opposing outcomes in the WES data. Gigg et al. measured parvalbumin protein from tissue homogenate in mouse DH and found a reduction, contradicting our results (Gigg et al., 2020). The different species and brain regions may explain these differences; however, other researchers in the lab have measured parvalbumin protein in Lister hooded rats, and the same inconsistencies have been noted. Indeed, parvalbumin levels after scPCP treatment can increase, decrease and remain unchanged, with no apparent effect of time since scPCP treatment, region, sex, or experimental site (Rimmer and Taylor, unpublished findings).

Table 3.5: Summary of scPCP studies that measured parvalbumin in post-mortem tissue. Time since scPCP, d: days, w: week, ♂: male, ♀: female, LH: Lister hooded, SD: Sprague Dawley, IHC: immunohistochemistry, ISH: in situ hybridisation, PFC: prefrontal cortex, DH: dorsal hippocampus, CA1: CA1 area of the hippocampus, CA2/3: CA2/3 area of the hippocampus, DG: dentate gyrus, PrL: prelimbic region of the PFC, Arrows show the direction of significant changes.

Time since scPCP	Dose (mg/Kg)	Number of dosing days	Animal	Technique	Region	Findings	Reference
1d	2	2	♂ Wistar	IHC	PFC	↓	(Amitai et al., 2012)
1d	10	10	♂ C57Bl6	ISH	PFC	↔	(Thomsen et al., 2010)
1d	10	10	♂ ICR	IHC	PFC DH	↓ ↓ CA1	(Shirai et al., 2015)
1d	2	7 on, 10 off	♂ Wistar	IHC	PFC	↓	(Amitai et al., 2012)
9d	5	bidaily, 7	♂ LH	IHC	PFC	↓	(Redrobe et al., 2012)
10d	2	2	♂ Wistar	IHC	PFC	↓	(Amitai et al., 2012)
2w	2	bidaily, 7	♀ SD	IHC	PFC DH	↔ ↔	(Riordan et al., 2018)
6w	2	bidaily, 7	♂ LH	IHC	PFC	↓ PrL	(McKibben et al., 2010)
6w	2	bidaily, 7	♀ LH	IHC	DH	↓ CA2/3 ↓ DG	(Abdul-Monim et al., 2007)
6w	2 or 5	bidaily, 7	♂ LH	IHC	DH	↓ CA1 ↓ CA2/3	(Jenkins et al., 2010)
6w	2	bidaily, 7	♂ LH	IHC	DH	↓ CA1 ↓ DG	(Jenkins et al., 2008)
7w	2	bidaily, 7	♂ Wistar	IHC	PFC	↓	(Piyabhan et al., 2019)
14w	2	bidaily, 7	♀ LH	IHC	PFC	↓	(Landreth et al., 2020)
15w	10	10	♀ C57Bl6	WES	DH	↓	(Gigg et al., 2020)

Although the inconsistent findings may be due to sampling error rather than an actual treatment effect, endogenous parvalbumin levels can change transiently, perhaps contributing to the observed irregularities.

Evidence of circadian modulation of parvalbumin interneurons in the visual cortex suggests that evoked experience can influence parvalbumin interneuron activity (Zong et al., 2022). In the PFC, both PVI and PNN density alters throughout the day (Table 3.6). Harkness et al. suggested that the increase in PNN+/PV+ compensated for the increased activity levels during the rodent active dark phase. To validate this, Harkness compared markers involved in glutamatergic and GABAergic signalling across the circadian cycle. They found a significant increase in VGlut1 and GAD65/67 puncta and AMPA signalling in the active phase. Given that the scPCP animals have impaired E/I signalling, could the inconsistent data measured within the lab reflect a failure to adapt in the scPCP animals? There is a 20% reduction in PVI density in the six hours after the start of the inactive period; whether this fluctuation in the density is sufficient to cause the differences recorded in our lab is unclear (Harkness et al., 2021).

Table 3.6: Intensity of PVI and PNN staining in the PFC across the diurnal cycle. Arrows show significant changes from the baseline (ZT0). ZT: zeitgeber time. Light cells: ZT0 = lights on, ZT6 = mid-inactive stage. Grey cells: ZT12: lights off, ZT18 = mid-active phase. WFA: wisteria floribunda stain for PNN, PV: parvalbumin. Adapted from Harkness et al., 2021.

Marker	ZT0	ZT6	ZT12	ZT18
WFA +	0	↔	↑	↑
WFA + / PV +	0	↔	↑	↑
PV +	0	↓	↓	↔
PV + / WFA +	0	↓	↔	↔

In addition, a study by Donato et al. showed that behavioural testing or environmental interventions alter parvalbumin expression. For example, three days of Morris Water Maze training can shift PVI into a low parvalbumin expression state when measured the following day. Conversely, a single contextual fear conditioning (cFC) session can shift PVI into a high-parvalbumin expression state, detectable twenty-two hours later. Fascinatingly, the low-parvalbumin expression state achieved after three weeks of exposure to environmental enrichment (EE) was maintained for eight weeks after return to standard housing and was resilient to cFC. The mechanisms of these switches are unclear, though GAD67 and synaptic puncta change alongside parvalbumin expression (Donato et al., 2015). Given the GAD67 and synaptic deficits detected in scPCP-treated

rats, perhaps their PVI failed to adapt to task-dependent changes to parvalbumin expression.

On a practical note, if parvalbumin expression changes throughout the day and in response to behaviour, it is critical to ensure homogeneity in the study design. Protocols must be designed carefully considering the behavioural testing order and proximity to culling.

As with many biological processes, any deviation from the normal can cause impairments. With parvalbumin protein, there is a window where altering the concentration will not alter synaptic dynamics (Eggermann et al., 2011). Typically, calcium will enter the PVI when stimulated with rapid firing. Parvalbumin will buffer and release calcium accordingly, allowing sustained neurotransmitter release (Celio, 1990, Collin et al., 2005). Depleting parvalbumin increases inhibitory postsynaptic currents, paired-pulse facilitation and gamma frequency oscillations compared to wildtype (Caillard et al., 2000, Vreugdenhil et al., 2003). Conversely, excessive parvalbumin leads to a high concentration of free parvalbumin, not bound to calcium or magnesium, which increases paired-pulse facilitation (Eggermann et al., 2011). In both conditions, facilitation is altered.

To summarise, changes to parvalbumin that dysregulate the buffer dynamics may lead to altered PVI activity and ultimately impaired E/I balance. These findings are noteworthy considering the proposal that PVI neurons are still present but lacking parvalbumin protein expression (Filice et al., 2016, Thune et al., 2001). Furthermore, if there is a reduction in PVI density, any changes to protein and mRNA would be in a reduced number of cells, potentially magnifying the alterations.

3.4.7 GAD67

Decreases in PFC and DH GAD67 are robust, with this finding observed in multiple studies and varied patient cohorts (Guidotti et al., 2000, Rocco et al., 2016, Thompson Ray et al., 2011, Volk et al., 2000), even in the absence of neuronal loss (Akbarian et al., 1995). Therefore, it is proposed that GAD67 reductions in schizophrenia result in compensatory reductions in parvalbumin protein (Gonzalez-Burgos et al., 2008).

We found no change to GAD2 (GAD65). The clinical literature for GAD65 is limited, with only a few recognised schizophrenia risk mutations (Zhao et al., 2007).

Fujihara et al. created a GAD67 knockdown and a knockout model. Both displayed behavioural deficits akin to those observed in recognised models relevant to schizophrenia. Unfortunately, their molecular work was mismatched, only looking at some measures in one genetic variant, making it challenging to form coherent conclusions. However, the highlights include increased PVI stain intensity in the knockout model and a reduced cell number in the heterozygous animals. It is disappointing not to have a cell count for the knockout, as confirmation of a reduced cell count in the presence of increased activity would have given further credence to our proposal of a reduced number of dysfunctional PVI (Fujihara et al., 2015).

In the current study, we found reductions to GAD67 protein in the PFC and a trend towards a decrease in GAD1 mRNA in the DH (Figure 3.9). A reduction in GAD67 in NMDAr antagonist models is, like the human studies, a robust finding (Behrens et al., 2007, Behrens et al., 2008, Bullock et al., 2009, Pollard et al., 2012, Riordan et al., 2018), with only one study showing no change in the frontal cortex, dorsal or ventral hippocampus in a mouse scPCP model (Gigg et al., 2020).

3.4.8 Perineuronal nets

Perineuronal nets describe the extracellular matrix which preferentially enwraps the parvalbumin interneurons (Wen et al., 2018b). Given the different functional roles of the components, we were interested to see if any were differentially expressed after scPCP dosing. We observed no changes to PNN components (Acan, Bcan, Ncan or Vcan) in the DH (Figure 3.10) or PFC (Figure 3.11). However, IHC analysis showed that PNN density was decreased in the PFC (Figure 3.11).

ChABC is a bacterially derived enzyme that can digest the chondroitin sulphate proteoglycans (CSPG), degrading the PNN (Bertolotto et al., 1995). It is a valuable tool for assessing the effect of PNN loss in isolation. Researchers have found that ChABC can lead to cognitive impairments and alterations to fast-firing frequencies indicating a PVI deficit (Paylor et al., 2018, Sultana et al., 2021). In addition, Paylor et al. also found a marginal increase in cFOS expression in PVI, indicating altered activity levels in the PVI when PNN is removed (Paylor et al., 2018).

Previous studies looking at NMDAr antagonists find reduced PNN levels in the PFC and the CA1 region of the hippocampus, although the latter was seen with an aggrecan-

specific stain (Fujikawa et al., 2021, Kaushik et al., 2021, Matuszko et al., 2017). The study by Kaushik et al. was of particular interest as they used high-magnification microscopy to look at the architecture of a single PNN. After scKetamine dosing, the net intensity, pore shape and area changed. The net was diffuse, and the pores were smaller and irregular in shape (Kaushik et al., 2021). Considering that the PNN pore can act as a barrier to moderate lateral diffusion of AMPA receptors (Frischknecht et al., 2009), alteration of the architecture may impair AMPA signalling. Indeed, after NMDAr antagonism, Yamada et al. found reduced colocalization of PVI with VGlut1 and GAD, suggesting that PNN decreases when there is reduced synaptic input (Yamada et al., 2017). To further validate this idea that PNN levels are driven by PVI activity, Devienne found that PNN would reduce after PVI or local excitatory inputs were inhibited. Interestingly, this reduction could be isolated to a single PNN if the inhibition was isolated to a single PVI. The data also suggested that inhibiting a single PVI reduced the PNN intensity around that PNN alone, indicating that PVI can regulate their extracellular matrix. Moreover, transcriptomic data analysis reveals that PVI can uniquely express all PNN components and several proteases that break down PNN (Devienne et al., 2021).

Interestingly, Devienne found that excitation of the local network or the PVI did not change PNN levels, suggesting that PNN is only regulated by inhibition (Devienne et al., 2021). This finding is particularly noteworthy when considering the work of Donato et al., who suggested there are two classes of PVI, early-born and late-born. The early-born PVI develop in rodents between gestational day (GD)9.5 and 11.5 and late-born between GD13.5 and 15.5. These two classes of PVI are functionally distinct. The highlights of these differences are summarised in Table 3.7.

Table 3.7: Differences between early- and late-born PVI. cFC = contextual fear conditioning, EE = environmental enrichment, MWM = Morris water maze, E = excitatory, I = inhibitory. Adapted from Donato et al., 2015.

Measure	Early-born	Late-born
PV/GAD67 intensity	↑	↓
Excitatory puncta	↑	↓
Inhibitory puncta	↓	↑
Effect of cFC / late MWM	↑ PV, ↑ E synapses	↔
Effect of EE / early MWM	↔	↓PV, ↑ I synapses
Plasticity regulated by	Excitation	Inhibition
Sensitive to ChABC	No	Yes

When the early-born PVI receive an excitatory input, parvalbumin expression and excitatory synapses increase. Conversely, the late-born PVIs reduce parvalbumin and increase inhibitory synapse density when inhibited. These alterations will further increase the inhibitory tone in early-born neurons or reduce the tone in late-born (Donato et al., 2015).

Note that the late-born PVI are sensitive to ChABC digestion (Table 3.7). Reflecting on the finding that PNN was decreased only on inhibition to the PVI (Devienne et al., 2021), this fits in with the late-born, Chondroitinase ABC (ChABC)-sensitive PVI. Could this mean that only the late-born PVI use PNN to moderate plasticity? Moreover, when early- and late-born neurons are treated with an NMDAr antagonist, Donato et al. recorded a shift towards the increased distribution of low PV-intensity, late-born PVI. Future studies could investigate this by co-staining PVI with markers for excitatory (Bassoon) and inhibitory (Gephyrin) puncta.

3.4.9 MMP9

We were specifically interested in MMP9 due to its multifaceted involvement in many cellular processes thought to be dysregulated in schizophrenia, including cognition and neuroinflammation (Vafadari et al., 2016). Presently, evidence for altered MMP9 is limited to mutations affecting MMP9 function or expression being associated with schizophrenia risk (Gao et al., 2019, Gao et al., 2018, Lepeta et al., 2017, Pan et al., 2022) and upregulation to the levels or activity of MMP9 in the plasma of schizophrenia patients (Chang et al., 2011, Domenici et al., 2010, Kumarasinghe et al., 2013, Yamamori et al., 2013).

Working with MMP enzymes raises two challenges. First, the 20 members of the MMP have a similar structure, making it challenging to design specific antibodies or assays for individual members of the MMP family. Second, the MMP enzyme family have many enzymatic targets. I*n situ*, this promiscuity is managed through local and short-lived expression. However, measuring whole regions at a snap-shot in time may not show specific pathology. (Vafadari et al., 2016). MMP9, for example, regulates NMDAr-dependent late-stage LTP (Nagy et al., 2006, Wiera et al., 2017), increases NR1-NMDAr surface trafficking (Michaluk et al., 2009) and moderates PNN degradation (Wen et al., 2018b). Therefore, MMP9 can be pro- or anti-cognition, depending on its target.

With this in mind, we saw no change to MMP9 levels in the plasma. Instead, we saw a trend towards increasing MMP9 activity in the scPCP animals (Figure 3.12). As we had collected matched brain data for these animals, we were able to investigate whether there was any correlation between plasma and brain measures. Here we found a negative correlation between brain and plasma activity, although there were no differences in brain activity between treatments.

Recently, a model has been suggested by Bitanihirwe and Woo that links MMP9 to schizophrenia. The authors propose that schizophrenia pathology is characterised by elevated inflammation, oxidative stress and MMP9, where each can potentiate the other. Of relevance to this model, Bitanihirwe notes that MMP9 can reduce orthodenticle homeobox2 (Otx2) expression, reducing Otx2-mediated, PNN-directed maturation of PVI into cortical networks (Bitanihirwe et al., 2020). Indeed, in a model with reduced MMP9, mice have a novel object location deficit (Vafadari et al., 2019), although the effect on PVI was not measured.

3.4.10 Oxidative stress

Low levels of ROS are required for normal plasticity. In the healthy brain, NMDAr activation results in Ca^{2+} influx into the post-synaptic neuron. The intracellular calcium activates membrane-bound NADPH-oxidase (NOX) enzymes (Figure 3.13), which produce superoxide required to activate intracellular signalling cascades that facilitate LTP. However, in the event of excessive intracellular calcium, the concentration of synthesised superoxide will surpass a threshold, resulting in the downregulation of the LTP-facilitating signalling cascades, reducing NMDAr signalling (Girouard et al., 2009, Wang et al., 2013b). The NMDAr-NOX relationship is not the only mechanism to regulate ROS levels. The NMDAr in isolation can reduce the flow of Ca^{2+} as it contains cysteine residues that form a disulphide bond in the presence of high ROS (Lipton et al., 2002). Finally, there is an NMDAr-antioxidant relationship. During periods of high activity, the NMDAr can facilitate the synthesis of antioxidants (Papadia et al., 2008). Equally, antioxidants can affect NMDAr activity; depleting the antioxidant glutathione from *ex vivo* slices reduced NMDA-dependent LTP (Steullet et al., 2006). Taken together, typical ROS-mediated LTP depends on a precariously balanced reciprocal relationship.

There is evidence that NMDAr antagonism can disrupt the production of antioxidants (Cartágenes et al., 2022, da Silva Araújo et al., 2017, de Araújo et al., 2021, Wesseling et

al., 2015) and increase the levels of ROS by-products (da Silva Araújo et al., 2017, He et al., 2018, Shirai et al., 2015). In our model, we saw a significant increase in the expression of SOD1 and no change to Gpx1, Gpx4 or Cat1. Previous studies looking at the effect of subchronic NMDAr antagonism models find a robust reduction in SOD activity in both the brain and plasma (Ben-Azu et al., 2018a, Ben-Azu et al., 2018b, de Oliveira et al., 2009, Eneni et al., 2023, Hou et al., 2013, Liang et al., 2022, Omeiza et al., 2023, Tadmor et al., 2018, Zugno et al., 2016). Moreover, this deficit appears to be immediate and long-term, with reduced activity present one day (Ben-Azu et al., 2016) and one month after the end of dosing (Liang et al., 2022).

In addition to SOD, NMDAr antagonism also reduced the activity of Cat1 and GPx (no isotype specified), suggesting a profound reduction in global antioxidant activity (Ben-Azu et al., 2018a, Ben-Azu et al., 2016, Ben-Azu et al., 2018b, Eneni et al., 2023, Tadmor et al., 2018, Valvassori et al., 2021, Zugno et al., 2016).

A research group has extensively used a mouse model that lacks the antioxidant glutathione (gclm) and given a good insight into the relationship between PVI, PNN and ROS. Using this model, they found that immature animals have normal levels of PVI but increased ROS (Cabungcal et al., 2013b). To investigate why immature animals were more susceptible to ROS, they measured PNN in both the gclm and wild type. In the wild-type mice, PNN density was consistent at postnatal day (PD)20, 40 and 90. However, in the gclm mice, PNN density was reduced at PD20 and 40, indicating delayed maturation. Furthermore, when an additional oxidative insult was given to mice in the ten days preceding tissue collection on PD20, 40 or 90, only the PD20 gclm mice (with immature PNN) showed a reduction in PVI density. Despite all ages and genotypes showing increased ROS markers, it was evident that immature PNN is less competent at protecting the PVI from ROS (Cabungcal et al., 2013a).

Cabungcal et al. also used ChABC elegantly to highlight the complexity of PNN modulation. In adult gclm mice, they observed increased PNN, with no change to PVI. Electrophysiological recordings showed beta and gamma power reductions compared to the wild type. They used ChABC to reduce the PNN and saw the beta and gamma power increase. Finally, they ran the same experiment in gclm mice pre-treated with an oxidative insult before ChABC; in this cohort, the beta and gamma powers were reduced (Cabungcal et al., 2013b). These findings stress the consequential effects of the broader

environment. A high-ROS environment and reduced PNN are unlikely to produce optimal PVI function.

Morishita et al. isolated gclm deficiencies to PVI to understand the mechanisms at play. ROS inevitably increased in PVI. In addition, they found reduced PVI and PNN density and increased CD68, a marker for active microglia, suggesting increased inflammation (Morishita et al., 2015). Finally, Dwir et al. showed that alterations to PNN in gclm-deficient mice depend on MMP9. Impairing the activity of MMP9 prevented PNN depletions, which allowed normal maturation in the gclm mice, even after adult spontaneous ROS insult (Dwir et al., 2019).

3.4.11 Inflammation

Finally, we looked to see if there was evidence of chronic inflammation after scPCP dosing. We found no alteration to IL1β or NFκB mRNA (Figure 3.16) and an increase in IL6 protein levels in the DH and gene expression in the PFC (Figure 3.17). We chose to look at these inflammatory factors due to the evidence of upregulation in acute and chronic schizophrenia patients (Upthegrove et al., 2020, Volk et al., 2019). NFκB is a transcription factor with many targets, including innate response immune cells like microglia, proinflammatory cytokines like IL6 and IL1β, and adhesion molecules like MMP (Liu et al., 2017). IL6 and IL1β are both involved with the pro-inflammatory response and have a role in general somatic maintenance and function (Del Giudice et al., 2018, Mendiola et al., 2018).

Here, we only saw an increase in IL6, a pro- and anti-inflammatory cytokine (Hunter et al., 2015). During the early, innate immune response, IL6 is produced by macrophages, like microglia, in response to an active infection. Its expression triggers the migration of immune cells to the point of infection. However, IL6 can also limit the inflammatory response by regulating NFκB, immune cell migration and macrophage activation, among other functions (Borovcanin et al., 2017).

Other studies in NMDAr antagonist models have found increased IL6 in treated animals' brains (Behrens et al., 2008, da Silva Araújo et al., 2017, de Araújo et al., 2021, Xiao et al., 2019, Yu et al., 2023). Behrens et al. found that IL6 was critical for the induction of scKetamine pathology as IL6 gene knockout ameliorated superoxide increases and reductions of PVI and GAD67 seen in the scKetamine animals (Behrens et al., 2008).

Returning to the chronically elevated IL6, in isolation, it is impossible to assess whether the IL6 is pro- or anti-inflammatory. Even considering the marked increase in neurotoxicity, microglia activation and other pro-inflammatory cytokines observed in NMDAr antagonist models (Milosević et al., 2000, Xiao et al., 2019, Yu et al., 2023), the IL6 response could be potentiating or alleviating these changes.

In a healthy brain, IL6 is required for neuronal development, synaptic signalling, and numerous hypothalamic functions, including temperature, food intake, sleep-wake behaviour, learning and memory (Erta et al., 2012). Indeed, there is an increase in IL6 during LTP, which inhibits NMDAr Ca^{2+} influx (Liu et al., 2013). Blocking IL6 expression, allowing unmoderated NMDAr activation, increases the strength and duration of LTP (Balschun et al., 2004). Therefore, in a system with increased IL6, there could be sustained NMDAr hypofunction. Indeed, LPS-stimulated immune activation results in reduced PVI and PNN density (Crapser et al., 2020). It is clear that IL6 is another important mediator of LTP and, more broadly, E/I balance.

3.4.12 An updated mechanism

Throughout the discussion, evidence of a more complicated mechanism than first proposed has been provided. Rather than a straight line, the effects of E/I imbalance, PVI dysregulation, oxidative stress and inflammation appear interconnected and bidirectional.

Section 3.4.10 described the relationship between NMDAr signalling, oxidative stress and antioxidants. NMDAr signalling increases antioxidant production (Papadia et al., 2008), whereas NMDAr antagonism can reduce antioxidant activity (Cartágenes et al., 2022, da Silva Araújo et al., 2017, de Araújo et al., 2021, Wesseling et al., 2015). A similar relationship was described in section 3.4.11, where NMDAr antagonism increased IL6 levels (Behrens et al., 2008), and increased IL6 can lead to NMDAr hypofunction (Liu et al., 2013). The evidence suggests oxidative stress, inflammation and NMDAr hypofunction may potentiate one another. This relationship was discussed in a seminal review by Steullet et al., who suggested that dysregulation of these systems in development due to gene and environmental risk factors associated with schizophrenia may culminate in PVI impairments in the disease state (Steullet et al., 2016).

In section 3.4.8, the inextricable link between PVI and PNN was described, with reduced PVI activity resulting in the downregulation of PNN components (Devienne et al., 2021). Destruction of the PNN using ChABC, on the other hand, can lead to reduced parvalbumin density (Yamada et al., 2015b).

Finally, the research by Suttkus and Steullet shows how PNN density and oxidative stress are positively correlated, with increased PNN protecting the neuron it surrounds from oxidative damage (Steullet et al., 2017, Suttkus et al., 2014). In addition, PNN density predicted the rate of AMPAr cycling (Frischknecht et al., 2009), which is critical for NMDAr signalling (Bear et al., 2020).

Figure 3.19 attempts to connect these proposed mechanisms while providing hypothetical routes for potentiation and propagation of pathology.

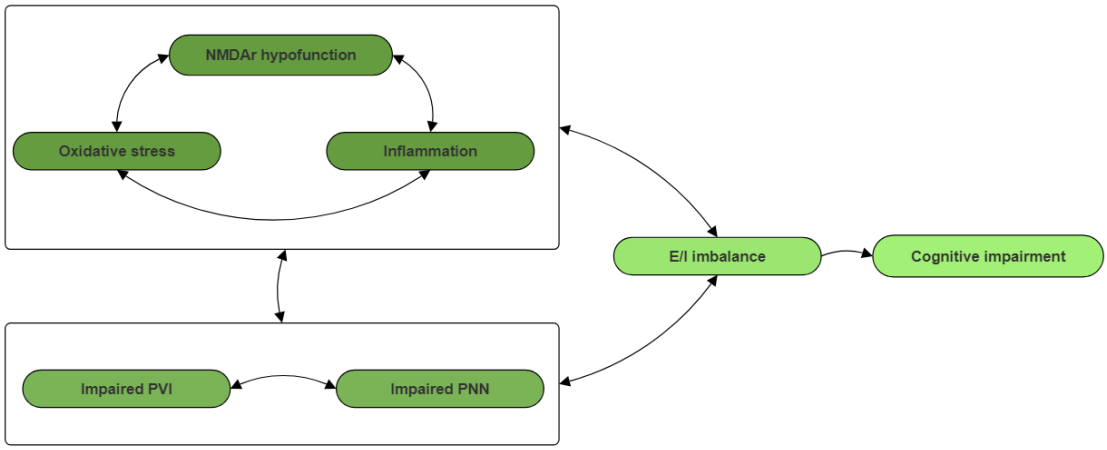

Figure 3.19: An updated mechanism based on pathology observed in the scPCP model.

3.4.13 Limitations

The primary outcome for the animal cohorts used was not molecular work. As such, there are discrepancies between the time since scPCP-dosing and the behavioural tests undertaken. In addition, some received vehicle drug treatments. Given the importance of consistency in protocol design, the studies should be interpreted in isolation and cautiously.

In our studies, the time since scPCP dosing ranged from 10 to 22 weeks. Although we saw preserved pathology, it is essential to comment on the duration of preserved deficits as it varies. For example, some observe deficits eight months after scPCP dosing (Cadinu et al., 2018), while others see deficits in scPCP-treated animals four weeks after dosing but not seven (Pyndt Jørgensen et al., 2015). Although this is an undeniable

discrepancy, the four-week defects are still in a drug-free rat (Glaxo Smith Klein, unpublished data), indicating long-term, though not permanent, pathology.

Our data for the regions is limited due to practical constraints on tissue. Ideally, we would have matched PFC and DH samples for each study. In addition, the work for the DH is limited to mRNA work, which gives limited insight into the levels in the tissue.

3.5 Chapter summary

We aimed to characterise scPCP pathology, focusing on the mechanism proposed below:

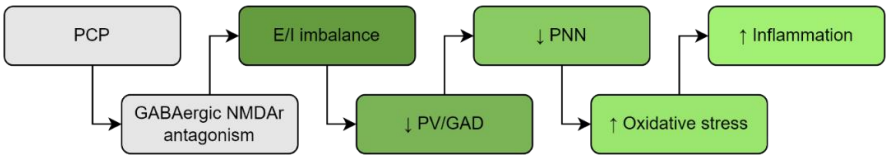

We report changes in many proteins involved in E/I balance. These findings suggest an impairment in both glutamatergic and GABAergic signalling.

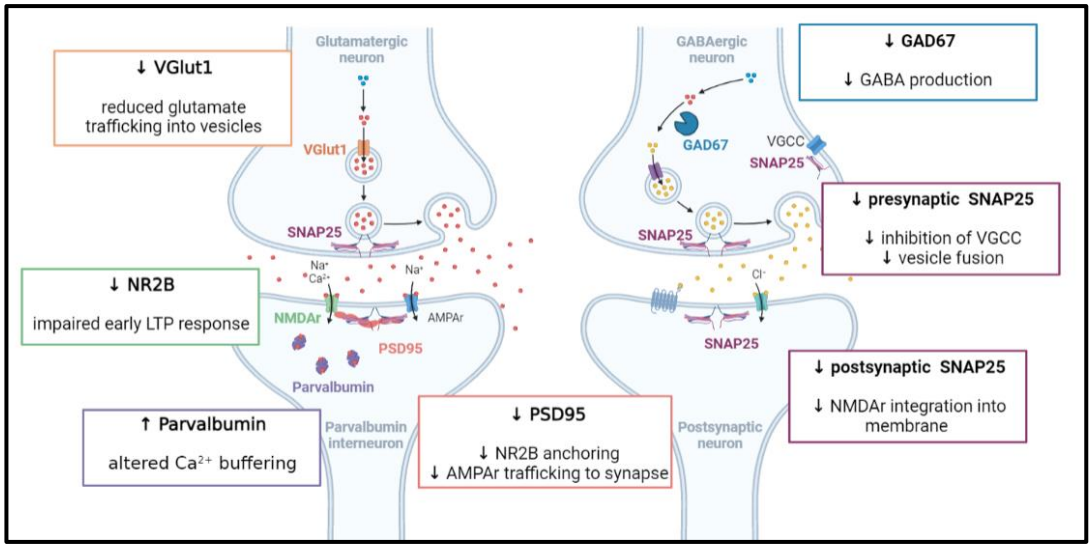

Figure 3.20: Consequences of scPCP on glutamatergic and GABAergic synapses. A summary of the significant changes detected in the scPCP model and potential consequences. All changes were detected in the PFC. As the reported data is from tissue homogenates, we cannot be sure of the cellular locations of these changes. Image created in BioRender.com.

In addition, we found reductions in PVI and PNN density and an increase in markers relevant to oxidative stress and inflammation.

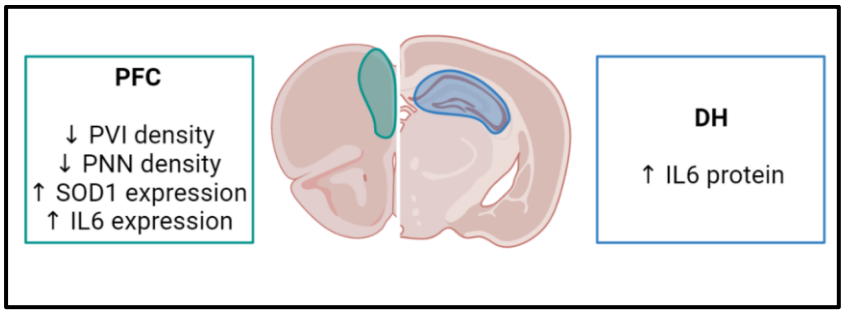

Figure 3.21: Regional consequences of scPCP administration. Image created in BioRender.com.

Given that we can moderate inflammation and oxidative stress with drugs, what would their consequence be on the scPCP model?

CHAPTER 4: EFFECTS OF APOCYNIN AND MINOCYCLINE IN THE SCPCP MODEL

4.1 Introduction

The previous chapter discussed evidence of chronic oxidative stress and inflammation in schizophrenia and the scPCP model. This chapter will examine the behavioural and molecular consequences of subchronic dosing with apocynin or minocycline.

4.1.1 Oxidative stress

4.1.1.a Clinical basis

There is considerable interest in the role of reactive oxygen species (ROS) in schizophrenia pathology. ROS levels are elevated in the serum, cerebral spinal fluid and post-mortem tissue of schizophrenia patients (Bilecki et al., 2023, Do, 2023, Ermakov et al., 2021, Więdłocha et al., 2023). Alterations to antioxidant capacity, activity or markers of ROS are observed in young people who are at ultra-high risk for psychosis (Zeni-Graiff et al., 2019), first-episode patients (MacKinley et al., 2022, Micó et al., 2011, Sarandol et al., 2015), and in chronic schizophrenia patients (Das et al., 2019, Mitra et al., 2017). Moreover, high ROS has been linked to poorer patient outcomes (Fraguas et al., 2017).

The natural adversary of ROS is antioxidants. These compounds, often derived from plants, regulate ROS. Antioxidants prevent dangerous quantities of ROS by inhibiting their creation or scavenging the excess electrons. Without effective antioxidants, the ROS will damage tissue indiscriminately, affecting lipids, proteins and DNA. Given the toxic status of ROS, it is understandable to question their presence in a healthy cell. However, biological processes, particularly metabolism, produce and require ROS (Mucha et al., 2021).

Several antioxidant compounds have been used in clinical trials to assess their effect on symptoms of schizophrenia. Table 4.1 summarises clinical trials that assessed cognitive outcomes. These studies suggest that antioxidants can benefit some cognitive domains, mainly working memory, executive function and processing speed.

Table 4.1: Efficacy of antioxidants on cognitive symptoms in schizophrenia patients. Arrows show direction of change; yellow cells/*: significant change also observed in the placebo group; green cells: cognitive improvement in the treatment group only. BACS: Brief Assessment of Cognition in Schizophrenia; CSoP: cognitive subscale of the positive and negative syndrome scale; MATRICS: Measurement and Treatment Research to Improve Cognition in Schizophrenia; ScCORS: schizophrenia cognitive rating scale; SCIP: screen for cognitive impairments in schizophrenia; SD: standard deviation; T-R: treatment-resistant.

Treatment	**Allopurinol**	**Alpha lipoic**	**Ginkgo biloba**	**L-carnosine**		**N-acetyl cysteine**					
Study	**(Weiser et al., 2012)**	**(Mishra et al., 2022)**	**(Zhang et al., 2011)**	**(Chengappa et al., 2012)**	**(Breier et al., 2018)**	**(Neill et al., 2022)**	**(Banazadeh et al., 2022)**	**(Conus et al., 2018)**	**(Rapado-Castro et al., 2017)**	**(Sepehrmanesh et al., 2018)**	**(Yang et al., 2019)**
Sample size (treatment / placebo)	123/125	10/10	78/79	33/37	14/18	42/43	27/27	32/31	27/31	42/42	13/13
Age, mean (SD) (treatment / placebo)	43.5(10.4)/ 41.8(9.6)	37.4(12.8)/ 334.6(7.9)	45.2(6.7)/ 45.4(7.3)	46.6(8.5)/ 46.5(9.0)	22.2(4.2)/ 25.0(5.2)	39.8(9.2)/ 39.7(9.4)	44.7(9.2)/ 45.4(11.4)	26.1(6.1)/ 24.7(5.9)	38.6(12.2)/ 41.0(12.4)	39.4(14.0)/ 38.8(12.5)	47.7(8.3)/ 50.4(12.5)
Daily dose	600	300	240	500 start, 2000 end	600 start, 3600 end	2000	3000	2700	2000	1200	2400
Duration of dosing (weeks)	8	8	12	4	52	16	4	26	24	12	8
Illness stage	Chronic	Chronic, T-R	Chronic	Stable chronic	Early <3 years	Chronic, T-R	Chronic	Early <1 year	Chronic	Chronic	Chronic
Attention/ vigilance	↔		↔	↔		↔		↔	↔	↑	↔
CSoP						↑					
Executive function	↑*			↑					↔	↑	
Problem-solving					↔		↔				↔
Processing speed			↔			↔		↑		↑	↔
Psychomotor speed	↑*			↔							
Social cognition						↔					
Verbal fluency	↑*							↑	↔		↔
Verbal learning	↑*					↔		↔			↔
Visual learning						↔		↔			↔
Working memory	↑			↔		↔		↔	↑	↑	↔
BACS composite	↑*				↔						
MATRICS composite						↔					
ScCoRS composite		↔									
SCIP composite							↑				

4.1.1.b Apocynin

Although not studied in clinical trials, here we used the compound apocynin. Apocynin is an NADPH oxidase (NOX)2 inhibitor. It prevents the formation of NOX2 on cellular membranes and inhibits a significant source of cellular ROS (Savla et al., 2021). In addition, inhibiting NOX2 formation has several indirect effects. For example, it may result in the upregulation of anti-inflammatory microglia. Activated microglia are categorised into pro-inflammatory (M1) or anti-inflammatory (M2) subtypes. In M1 microglia, the NOX2 is upregulated compared to resting and M2 microglia. Notably, some postulate that the presence or absence of NOX2 determines the inflammatory status of microglia (Ansari et al., 2011, Liao et al., 2012, Nayernia et al., 2014). Indeed, blocking NOX2 during a neuroinflammatory insult switched microglia to an anti-inflammatory state (Choi et al., 2012).

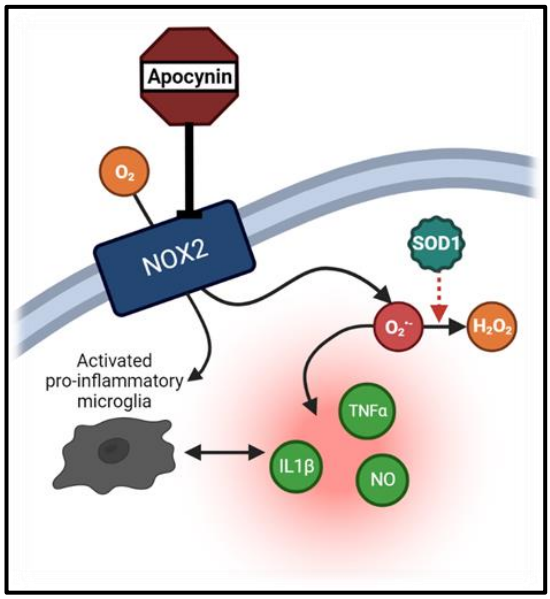

Figure 4.1: A schematic showing the effects of NOX2. Apocynin blocks the formation of NOX2. Inhibiting several functions, including the formation of ROS and the differentiation of activated microglia into pro-inflammatory subtypes NOX2: NADPH oxidase (transmembrane protein), SOD: superoxide dismutase, Cat: catalase, GPx: glutathione peroxidase. Adapted from (Savla et al., 2021, Sepasi Tehrani et al., 2018, Wang et al., 2018b). Image created in BioRender.com.

The effects of apocynin in the subchronic phencyclidine (scPCP) model were of particular interest due to the work of Behrens et al., who showed that the adverse effects of subchronic (sc) Ketamine dosing were prevented when animals were pre-treated with apocynin, demonstrating its involvement in the induction of NMDAr-antagonist pathology (Behrens et al., 2008). Although Behrens did not investigate whether the NOX2 pathway is involved in the maintenance of deficits, we measured the increased expression of SOD1 in the PFC (3.3.6).

4.1.2 Inflammation

As many anti-inflammatory drugs are available on the market, several studies have examined their effects in clinical settings. For example, a meta-analysis of 56 studies found that aspirin, oestrogens, minocycline and N-acetyl cysteine improved schizophrenia symptoms. Minocycline was the most prolifically used compound and, although limited, showed efficacy in improving some cognitive domains (Çakici et al., 2019). The data suggest that minocycline is most beneficial to patients in the early stage of schizophrenia and benefits executive function, fine locomotor speed, processing speed, visuospatial memory and working memory (Table 4.2).

Minocycline is a broad-spectrum antibiotic with numerous non-antibiotic properties, including anti-apoptosis, anti-oxidant, anti-inflammation, enzyme activity moderation (including MMPs), immunomodulation and neuroprotection (Garrido-Mesa et al., 2013). In addition, there is extensive literature testing the neuroprotective effects of minocycline in several disease models of the brain and the periphery, including Parkinson's disease (Cankaya et al., 2019), traumatic brain injury (Meythaler et al., 2019) and chronic pain (Zhou et al., 2018).

Table 4.2: The effect of minocycline on cognitive symptoms of schizophrenia patients. Arrows show significant change from baseline; yellow cells/*: significant change also observed in the placebo group; green cells highlight a cognitive improvement in minocycline-treated patients. SD: standard deviation. Zhang et al. used two doses of minocycline that had the same outcomes. Adapted from Çakici et al, 2019.

Study	(Chaudhry et al., 2012)	(Deakin et al., 2019)	(Kelly et al., 2015)	(Levkovitz et al., 2010)	(Liu et al., 2014)	(Weiser et al., 2019)	(Zhang et al., 2019)
Sample size (treatment / placebo)	69/71	64/65	29/23	36/18	39/40	100/100	25/25
Age, mean (SD) (treatment / placebo)	25.9(7.1)/ 26.6(8.3)	25.5(5.2)/ 25.7(5.1)	42.9(14.2)/ 42.3(11.0)	24.8(4.0)/ 25.5(4.06)	27.1(5.8)/ 27.7(7.3)	43.4(10.5)/ 43.5(9.7)	33.0(7.8)/ 33.7(6.2)
Daily dose (mg)	50 start, 200 end	200 start, 100 end	100	200	200	200	100 + 200
Duration of dosing (weeks)	8	52	10	22	16	16	13
Illness stage	Early (<5 years)	Early (<5 years)	Chronic	Early (<5 years)	Early (<2 years)	Chronic	Chronic
Attention / vigilance	↔		↔	↑*	↑*	↔	↑*
Executive functions	↔			↑	↑	↔	
Fine locomotor speed					↑		
IQ		↔					
Motor speed						↔	
Problem-solving			↔		↑*		↑*
Processing speed		↔	↔		↓		↓*
Psychomotor speed	↔			↔			
Social cognition			↔				
Verbal fluency					↑	↔	↑*
Verbal learning			↔		↑*		↑*
Verbal memory						↔	↑*
Visual learning			↔		↑*		↑*
Visuospatial memory	↔			↑			↑*
Working memory			↑		↑	↔	↑*

4.1.3 Aims

4. Establish if subchronic dosing of apocynin or minocycline could attenuate the scPCP-induced NOR deficit.

5. Use central and peripheral markers of oxidative stress and inflammation to evaluate the mechanisms of drug action.

6. Measure protein targets used in the characterisation study to understand whether subchronic dosing reverses pathology.

4.2 Methods

4.2.1 Study design

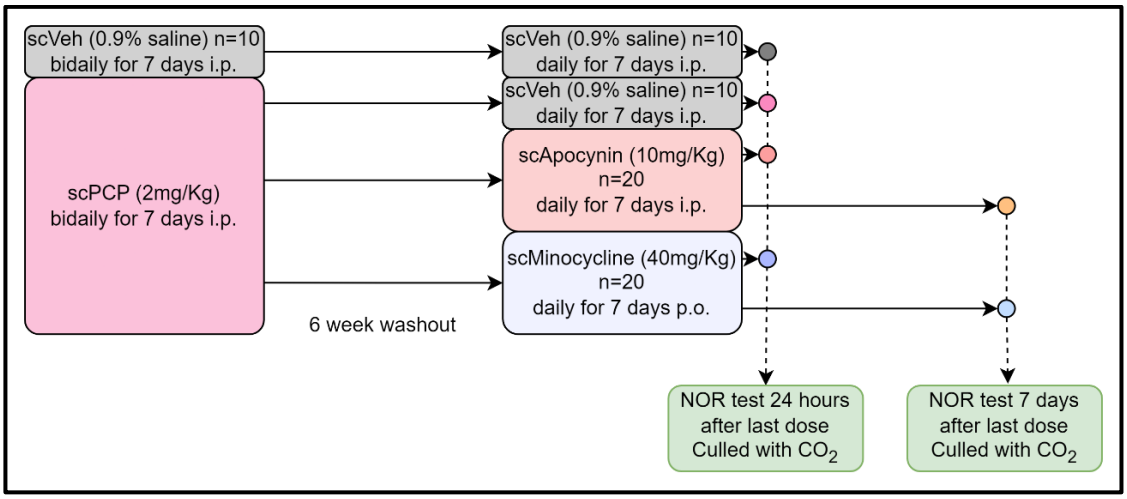

Figure 4.2: Study design of apocynin/minocycline study.

4.2.2 Dosing

Sixty female Lister hooded rats (259.7g ± 17.7, mean ± standard deviation) were acclimatised and dosed as described in sections 2.1 and 2.2. Briefly, cages of rats were randomly assigned to receive subchronic vehicle (n=10) or subchronic PCP (n=50). After a six-week washout, the ten scVeh were assigned to receive vehicle (0.9% saline, i.p., n=10). The remaining ten cages of scPCP animals (n=50) were subdivided into vehicle (0.9% saline, i.p., n=10), apocynin (10mg/Kg, 1mL/Kg, i.p., n=20), and minocycline (40mg/kg, 2ml/Kg, p.o., n=20) groups. The five rats in each cage were assigned to a different treatment group (see Table 4.3), and the order was altered sequentially for each cage. This secondary treatment was given daily for seven days. Details on dose selection for this study are provided in the supplemental material (8.2.1). During the study, two minocycline and one apocynin-treated rats were culled prematurely due to health issues.

Table 4.3: Group identifiers for apocynin and minocycline study.

Treatment	Shorthand
scVeh + scVeh	V/V7
scPCP + scVeh	P/V7
scPCP + scApocynin [10 mg/Kg, p.o.]	P/A7
scPCP + scApocynin [10 mg/Kg, p.o.] + 7-day washout	P/A14
scPCP + scMinocycline [40mg/Kg, p.o.]	P/M7
scPCP + scMinocycline [40mg/Kg, p.o.] + 7-day washout	P/M14

4.2.3 NOR

Animals were habituated to the NOR arena as described in 2.3. Habituation occurred during the intervention week. One day after the end of the second dosing week, 40 rats were tested in the NOR paradigm (section 2.3). Immediately after completion of the NOR, brains and blood were taken. The remaining 20 rats, ten treated with apocynin and ten treated with minocycline, underwent a week washout. Seven days after dosing, these animals completed the NOR test, and immediately after, plasma and brains were taken, as described in sections 2.7 and 2.6.1, respectively. NOR data was scored and analysed as described in 2.3. Two scPCP vehicle animals were excluded from the analysis because an object fell during the retention trial.

4.2.4 Tissue processing

Tissue was prepared as described in section 2.6. The resulting PFC homogenate was used for simple western analysis, whereas the DH was used for the MDA assay, SOD activity assay, IL6 ELISA and simple western analysis. Due to the high protein requirements for these assays, dilute samples were not used for all assays. Homogenates were used to achieve the greatest sample size across all four analyses.

4.2.5 MDA assay

We used an MDA assay kit from Abcam (ab118970) to measure lipid peroxidation. A 7-point, 2-fold dilution standard curve was created from the provided stock of MDA standard (0.5 – 10 µM). Distilled water and homogenisation buffer (described in section 2.6.1) were negative controls. TBA was added to standards, negative controls and samples at a 3:1 ratio. Samples were diluted to a concentration of 4mg/mL. The largest sample size of an equal number that could be achieved for this assay was 7 per group. Samples were incubated at 95°C for 60 minutes, then cooled to room temperature in an ice bath for 10 minutes. 200µL of the standard, negatives and samples were loaded into a black 96-well plate, and fluorescence was read at 532 nm excitation and 553 nm emission. A standard curve was produced using the standard RFU, and a 4-PL model was used (R^2 = 1.000). Sample MDA concentration was interpolated from the standard curve.

4.2.6 SOD activity assay

SOD activity in DH and plasma was measured using ab65354 from Abcam. The samples were diluted to 1.6 mg/mL, then prepared alongside three blanks as summarised in the below table:

Table 4.4: Composition and purpose of each component in the SOD activity assay. Quantities are given in µL. WST = water-soluble tetrazolium salt, WS = working solution.

Component	Sample	ddH_2O	WST WS	Enzyme WS	Dilution buffer	Purpose
Sample (µL)	20	0	200	20	0	Measure SOD activity in the sample
Blank 1 (µL)	0	20	200	20	0	Upper limit of the assay, all SOD in WS will be converted
Blank 2 (µL)	20	0	200	0	20	Check sample cannot react without enzyme present
Blank 3 (µL)	0	20	200	0	20	The buffers and working solution are not reactive

Prepared samples and blanks were incubated at 37°C for 20 minutes. Then 200µL of each sample and blank was pipetted into a 96-well plate and read at 450nm. As the kit contained sufficient reagent for 100 reactions, the largest sample size achievable after optimisations was 7 per group. Brain and blood samples were matched. To calculate the activity, the following equation was used:

$$\text{SOD activity (inhibition rate \%)} = \frac{(A_{blank1}-A_{blank3})-(A_{sample}-A_{blank2})}{(A_{blank1}-A_{blank3})} \times 100$$

4.2.7 IL6 ELISA

The IL6 ELISA from R&D systems (R6000B) was used to quantify DH and plasma IL6 levels. DH samples were diluted to 3.2 mg/mL protein. Three samples were too dilute to be included in the experiment (P/A7, P/M7, P/M14). A 7-point, 2-fold dilution standard was created from provided IL6 stock solution (31.25 - 2000 pg/mL). Plasma samples were diluted 2-fold in calibrator diluent. 50µL assay diluent was added to each well of the precoated ELISA plate alongside 50µL of standards, samples and negatives, then incubated for 2 hours at room temperature. The liquid was removed, and the plate was washed 8 times with diluted wash buffer. The plate was blotted with absorbent paper towels. IL6 conjugate was added and incubated for 2 hours at room temperature. Then, the plate was washed as described above again. The substrate solution was added, and the plate was incubated in the dark until the standard developed. The stop solution was

added to each well when there was a colour difference between the bottom and negative standards.

The plate was read at 450 nm and 570 nm. The readings of the corrective wavelength (570 nm) were subtracted from the reading at 450 nm. The optical density of the standards was used to produce a standard curve using a 4-PL fit (R^2 = 1.000).

4.2.8 Simple western analysis

PFC and DH were prepared, and protein targets were measured using simple western analysis as described in 2.6.3.

Table 4.5: Experimental details for WES studies in the apocynin/minocycline chapter.

Target	Product code	Supplier	Region	Protein concentration (mg/mL)	Antibody concentration
Parvalbumin	AF5058	R&D Systems	PFC	0.2	1:50
			DH	0.2	1:50
GAD67	Ab26116	Abcam	PFC	0.2	1:50
			DH	0.4	1:50
SNAP25	Ab5666	Abcam	PFC	0.4	1:50
			DH	0.4	1:50
PSD95	Ab2723	Abcam	PFC	0.4	1:50
			DH	0.2	1:100

4.2.9 Statistics

Table 4.6: Summary of statistical tests used in the apocynin/minocycline chapter.

Purpose	Distribution	Test	Section
Check for normality	N/A	D'Agostino and Pearson (n>7) or Shapiro-Wilk (n≤7)	2.9.1
Check for correlations	Normal Not normal	Pearson's Spearman's	2.9.5
Compare exploration times	Normal	Repeated measures general linear model	2.9.7.b
Compare DI to a hypothetical mean of 0	Normal	One sample t-test	2.9.2
Compare all groups	Normal Not normal	One way ANOVA Kruskal-Wallis H	2.9.4.a 2.9.4.b

In chapter five, we use repeated measure general linear models to include region as a within-subjects factor. However, due to the high protein and volume input, inconsistent animals were used throughout the postmortem analysis, limiting the power of within-subject analysis.

4.3 Results

4.3.1 Behavioural outcomes

Given that there is evidence of sustained oxidative stress and inflammation in the brains of rats treated with scPCP up to 22 weeks after dosing (Figure 3.17B and Figure 3.17C), we were interested in the effects of anti-inflammatory and antioxidant drugs on behaviour and selected pathology. For the antioxidant, we chose apocynin. Although it has not been used in a clinical trial for schizophrenia (Table 4.1), there is evidence of apocynin improving parvalbumin interneuron dysfunctions in pre-clinical studies (Behrens et al., 2007, Ji et al., 2015, Liang et al., 2016, Liu et al., 2016, Schiavone et al., 2009, Yuan et al., 2015, Zhang et al., 2016b). For an anti-inflammatory, we chose minocycline because there is clinical evidence of it having a cognitive effect in schizophrenia patients (Table 4.2). In addition, pro-cognitive doses were known in female Lister hooded rats, as acute minocycline was used to reverse scPCP-induced reversal learning deficits (Grayson, unpublished data).

4.3.1.a Acquisition trial

After the washout from scVeh or scPCP dosing, animals were dosed subchronically with vehicle, apocynin or minocycline. Twenty-four hours after the last dose of the vehicle or intervention compound, forty animals were tested with the novel object recognition (NOR) test. The remaining animals were tested one week later to assess whether the drug had lasting effects. In the acquisition trial, there was no significant within-subject effect of the item ($F_{1, 46}$ = 0.019, p = 0.891) nor the object*group interaction ($F_{5, 46}$ = 0.457, p = 0.806) (Figure 4.3A).

4.3.1.b Retention trial

There was a significant within-subject effect of the object ($F_{1, 46}$ = 33.502, p<0.001) and treatment*object ($F_{1, 46}$ = 2.819, p = 0.027). These findings indicate a difference between the time spent with familiar and novel objects in some treatment groups. We used the estimated marginal means to perform pairwise comparisons with Šidák's correction to find individual group differences. There was a significant difference between objects for V/V7 (familiar (F): 10.00 ± 1.67, novel (N): 17.80 ± 2.22, p = 0.004), P/A7 (F: 7.53 ± 1.77, N: 18.89 ± 2.36, p<0.001), and P/M7 (F: 9.62 ± 1.69, N: 19.37 ± 2.08, p <0.001). There was no difference in the scPCP-treated animals nor the animals that had undergone a further washout (P/V, P/A14, P/M14, p>0.05), indicating a cognitive deficit (Figure 4.3B).

4.3.1.c Discrimination index

We used a one-sample t-test comparing the discrimination index (DI) to a hypothetical mean of 0 or random chance, reflecting that a naïve animal in a retention trial would, due to no familiarity with either object, spend, in theory, equal times at both objects. Like the exploration times, the DI data indicated that V/V7 (t_8 = 3.718, p = 0.006), P/A7 (t_6 = 6.425, p = 0.001), and PM/7 (t_8 = 3.508, p = 0.008) were performing better than random chance. Additionally, the P/M14 group's average DI differed significantly from 0 (t_8 = 2.396, p = 0.043). Finally, there was no difference in P/V7 and P/A14 and the hypothetical mean.

In addition, we used a one-way ANOVA to assess whether there was a significant difference between treatment groups. The initial ANOVA revealed a significant effect of the treatment group on DI ($F_{5, 46}$ = 3.972, p = 0.005). Post hoc testing showed that by this metric, there was no scPCP-induced deficit (V/V7 and P/V7, p = 0.467). However, treatment with apocynin (P/A7) was able to significantly increase the DI compared to scPCP (P/V7) (p = 0.036). Despite the initial improvements after apocynin, a seven-day washout (P/A14) resulted in a significant reduction in DI compared to P/A7 (p = 0.013). However, minocycline treatment (P/M7) was not different to scPCP DI (p = 0.150). Notably, P/M7 and P/A14 were trending towards being significantly different (p = 0.069) (Figure 4.3C).

4.3.1.d Locomotion

As both apocynin and minocycline were novel compounds for testing in NOR, it is essential to assess whether these compounds alter locomotor activity. The number of line crosses on the arena floor was measured as a crude measure of locomotion. A one-way ANOVA of total line crosses found no difference between the groups ($F_{5, 46}$ = 0.399, p = 0.847). We also looked at the total exploration across acquisition and retention trials and found no difference in exploration for any treatment group ($F_{5, 47}$ = 0.417, p = 0.835) (Figure 4.3D).

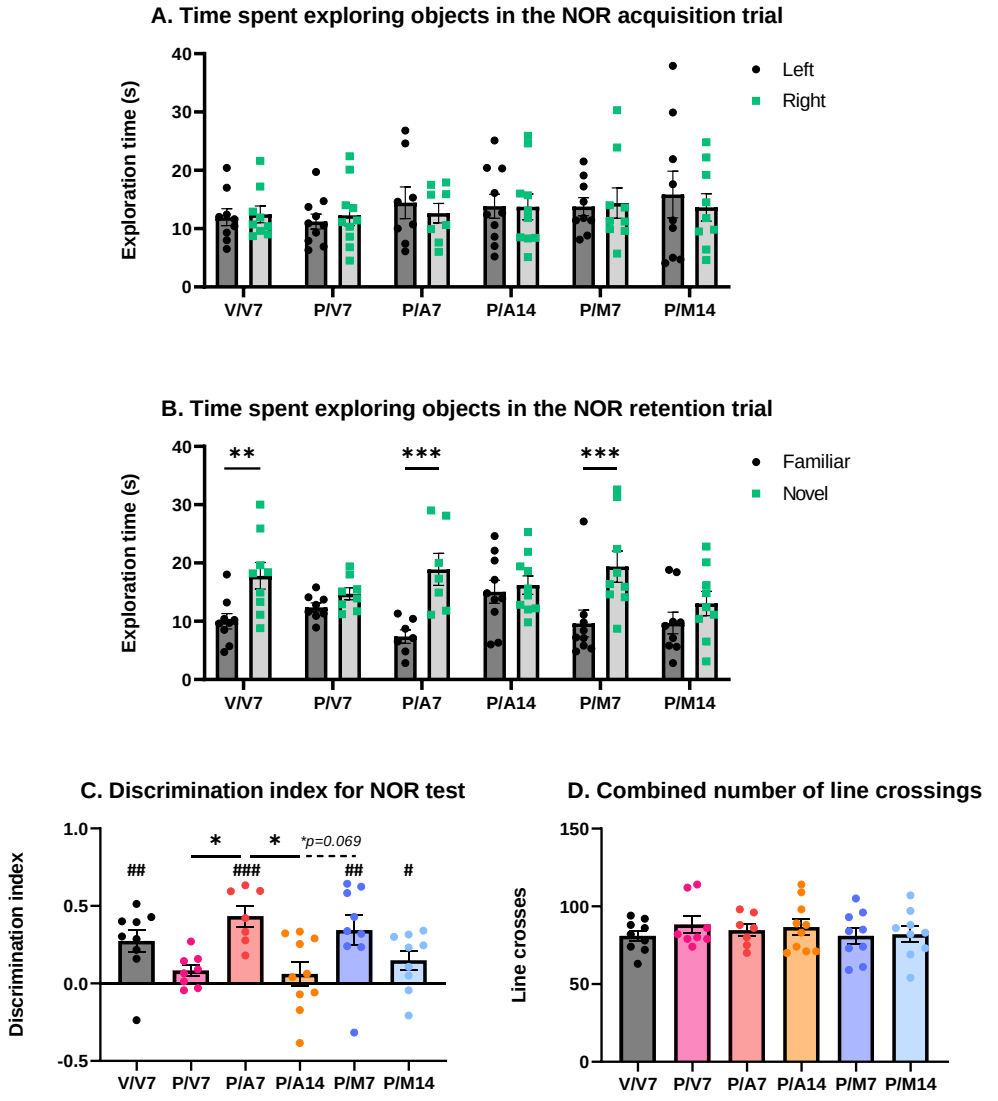

Figure 4.3: The effects of apocynin/minocycline on the scPCP-induced NOR deficit. **A)** Time spent exploring two identical objects in the acquisition trial of the NOR task following treatment with scVeh + scVeh (V/V7), scPCP + scVeh (P/V7), scPCP + scApocynin [10 mg/Kg, p.o.] (P/A7), P/A7 + 7-day washout (P/A14), scPCP + scMinocycline [40mg/Kg, p.o.] (P/M7), P/M7 + 7-day washout (P/M14). **B)** Time spent exploring the familiar and novel object in the retention trial of the NOR task. **C)** The discrimination index for each of the treatment groups. **D)** Number of line crossings during the acquisition and retention trial. For **A)** and **B)**, differences between objects were assessed with a repeated measures general linear model (GLM). The difference between the estimated marginal means for each object was analysed using a pairwise comparison with Šidák's correction. **C)** a one-sample t-test was used to compare the mean DI for each group to a hypothetical mean of 0, and a one-way ANOVA with Tukey's post hoc test was used to compare the mean DI. Finally, for **D)**, a one-way ANOVA was used to compare the differences between groups. (n=7-10). Graphs show mean ± SEM. *=difference between objects or treatment group, *p<0.05, **p<0.01, ***p<0.001. $^{\#}$=difference from a hypothetical mean of 0, $^{\#}$p<0.05, $^{\#\#}$p<0.01, $^{\#\#\#}$p<0.001.

4.3.2 Oxidative stress

Directly measuring ROS can be challenging. As such, the downstream by-products are often quantified instead. For example, polyunsaturated fats are oxidised for benign cellular processes or in radical quantities. Malondialdehyde (MDA) is a minor product of lipid peroxidation, which reacts with thiobarbituric acid (TBA) to form a detectible product (Murphy et al., 2022).

In addition to measuring the consequences of ROS, we also investigated the activity of superoxide dismutase (SOD), an enzyme that converts superoxide to hydrogen peroxide and water. When active, SOD decreases the levels of ROS (Wang et al., 2018b). We were interested in the activity of this enzyme due to it being downstream of NADPH oxidase (NOX) (Figure 3.13), which is blocked by apocynin (Bedard et al., 2007, Stolk et al., 1994).

There was a trend towards a difference between group dorsal hippocampal (DH) MDA concentration ($F_{5, 36}$ = 2.150, p = 0.082). Exploratory post hoc tests revealed a trend towards an increase in MDA concentration in the scPCP-treated animals compared to scVeh controls (P/V7 and V/V7, p = 0.086). Moreover, one week of apocynin treatment reduced these levels (P/A7 and P/V7, p = 0.016) (Figure 4.4A).

We measured the activity of SOD in DH and plasma samples. This assay adds the same quantity of superoxide to each sample. The SOD in each reacts with the superoxide to produce non-reactive products. Without SOD, the superoxide will react with the water-soluble tetrazolium salt (WST), producing a yellow formazan dye. A sample with a lot of SOD activity will inhibit this reaction, lowering the dye formation and resulting in a high inhibition rate (%). We did not find a significant effect of the treatment group on DH SOD activity ($F_{5, 42}$ = 1.704, p = 0.158) (Figure 4.4B). We analysed the SOD plasma data using a Kruskal-Wallis test, which neared statistical significance ($X^2_{(5)}$ = 10.955, p = 0.052). Exploratory post hoc testing revealed this was predominately due to increased inhibition in the P/A7 cohort (Figure 4.4C). We investigated whether levels of inhibition in the brain reflected levels in the plasma, and we found that levels were positively correlated (Spearman's rho = 0.354, p = 0.020, n = 43) (Figure 4.4D).

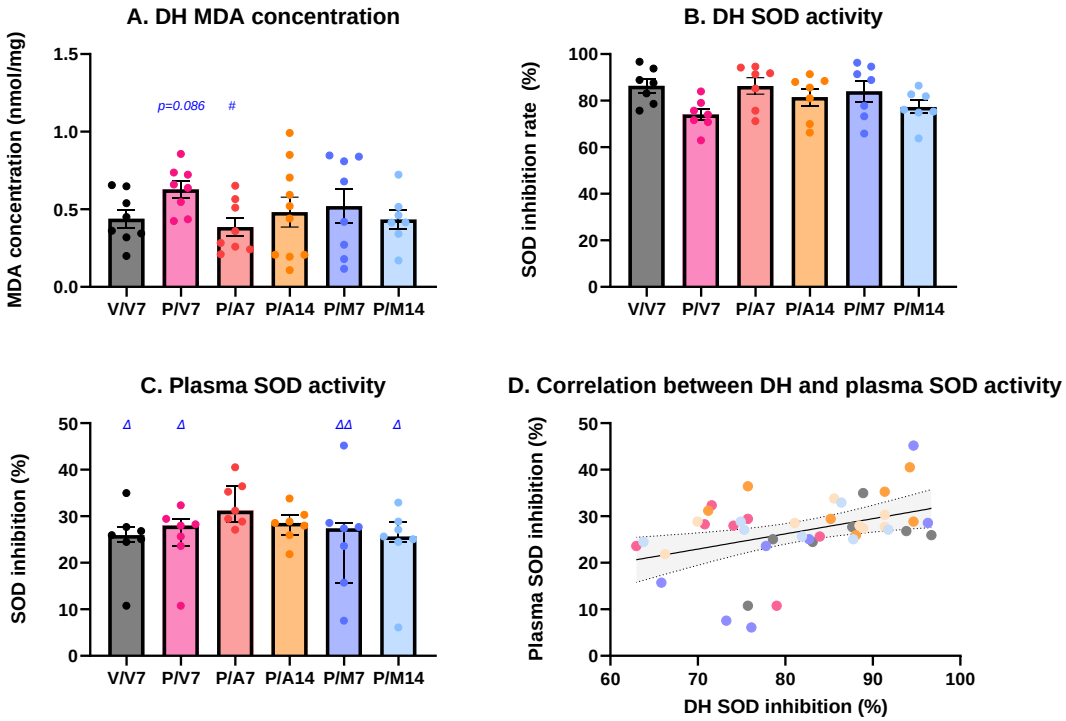

Figure 4.4: The effects of apocynin/minocycline on redox markers. **A)** Concentration of MDA in the DH of scVeh + scVeh (V/V7), scPCP + scVeh (P/V7), scPCP + scApocynin [10 mg/Kg, p.o.] (P/A7), P/A7 + 7-day washout (P/A14), scPCP + scMinocycline [40mg/Kg, p.o.] (P/M7) or P/M7 + 7-day washout (P/M14)-treated rats (n=7). SOD activity in the **B)** DH and **C)** plasma (n = 7)**. D)** The relationship between DH and plasma SOD inhibition rate (%) (n=7). **A** and **B)** were analysed with a one-way ANOVA, and graphs show mean ± SEM. For **A)** Dunnett's T3 post hoc test was used. **C)** was analysed with a Kruskal-Wallis test, and the graphs show median ± IQR. For **D)**, the graph shows data points for individual rats, and the line shows the simple linear regression with 95% confidence intervals. The colours of the data points are consistent with A–C). *=significantly different from V/V7, *p<0.05, **p<0.01, p<0.001. $^{\#}$= significantly different from P/V7, $^{\#}$p<0.05. $^{\Delta}$= significantly different from P/A7, $^{\Delta}$p<0.05, $^{\Delta\Delta}$p<0.01. Blue text indicates comparisons generated from a non-significant ANOVA or Kruskal-Wallis test.

4.3.3 Inflammation

There is evidence that minocycline downregulates proteins required for IL6 signalling (Ataie-Kachoie et al., 2013). Given that we have shown that scPCP can chronically increase IL6 (Figure 3.17), we tested what effect minocycline would have on its levels in plasma and DH.

There was a significant effect of the treatment group on DH IL6 levels ($F_{5, 56}$ = 2.872, p = 0.023), although further analysis revealed this was due to an increase in IL6 levels in the P/V7 group compared to the control (p = 0.021) confirming ongoing inflammation in the scPCP animals. Only treatment with minocycline reversed this change (p = 0.036), though this was not sustained after washout (Figure 4.5A). Next, we looked at the plasma IL6 concentration. Although there was no significant treatment effect in the initial Kruskal-Wallis test ($X^2_{(5)}$ = 9.250, p = 0.100), there were significant post hoc comparisons when comparing groups to P/V7 (V/V7: p = 0.090, P/A7: p = 0.003, P/A14: p = 0.040, P/M7: p = 0.053, P/M14: p = 0.083) (Figure 4.5B). We were interested in whether the concentrations of IL6 in the brain and plasma were correlated, particularly given that many clinical studies are being stratified based on plasma biomarkers (Boerrigter et al., 2017, Fillman et al., 2016, Sæther et al., 2023, Wu et al., 2019). However, a comparison of the whole cohort found no correlation (Pearson correlation = 0.107, p = 0.428, n = 57).

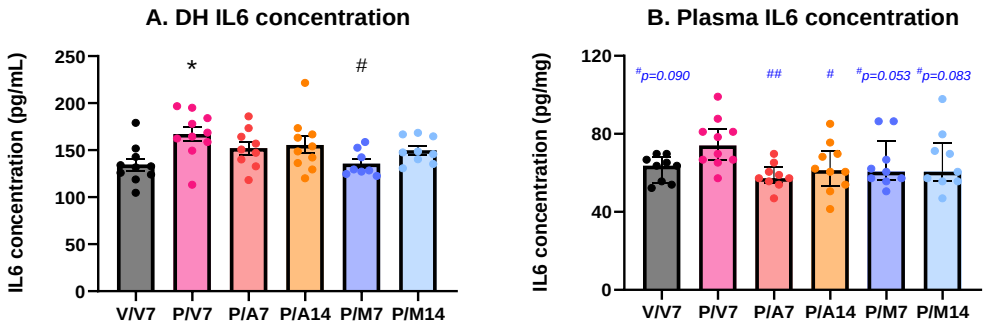

Figure 4.5: The effects of apocynin/minocycline on IL6 levels in the DH and plasma. Concentration of IL6 in the **A)** DH or the **B)** plasma of scVeh + scVeh (V/V7), scPCP + scVeh (P/V7), scPCP + scApocynin [10 mg/Kg, p.o.] (P/A7), P/A7 + 7-day washout (P/A14), scPCP + scMinocycline [40mg/Kg, p.o.] (P/M7) or P/M7 + 7-day washout (P/M14)-treated rats (n=9-10). **A)** was analysed with a one-way ANOVA with the Tukey post hoc test. The graph shows mean ± SEM. **B)** was analysed with a Kruskal-Wallis test. The graph shows median ± IQR. *=significantly different from V/V7, *p<0.05, **p<0.01, p<0.001. #= significantly different from P/V7, #p<0.05. Blue text indicates comparisons generated from a non-significant ANOVA or Kruskal-Wallis test.

4.3.4 Protein data

We chose to look at protein data in the DH and PFC, measuring a selection of the proteins studied in the characterisation chapter.

4.3.4.a Dorsal hippocampus

The group significantly affected DH PV levels ($F_{5, 47}$ = 4.206, p = 0.003). Using Tukey's post hoc test, we found there was a trend towards a decrease between V/V7 and P/V7 (p = 0.089), whereas there was a significant decrease in P/A7 (p = 0.045), and P/M14 (p = 0.001) compared to V/V7 (Figure 4.6A).

The group significantly affected DH GAD67 levels ($F_{5, 47}$ = 7.059, p<0.001). Using Tukey's post hoc, we found there was a significant reduction in all scPCP-treated rats compared to vehicle (P/V7: p = 0.020, P/A7: p<0.001, PA/17: p = 0.021, P/M7: p = 0.001, P/M14: p<0.001) (Figure 4.6B).

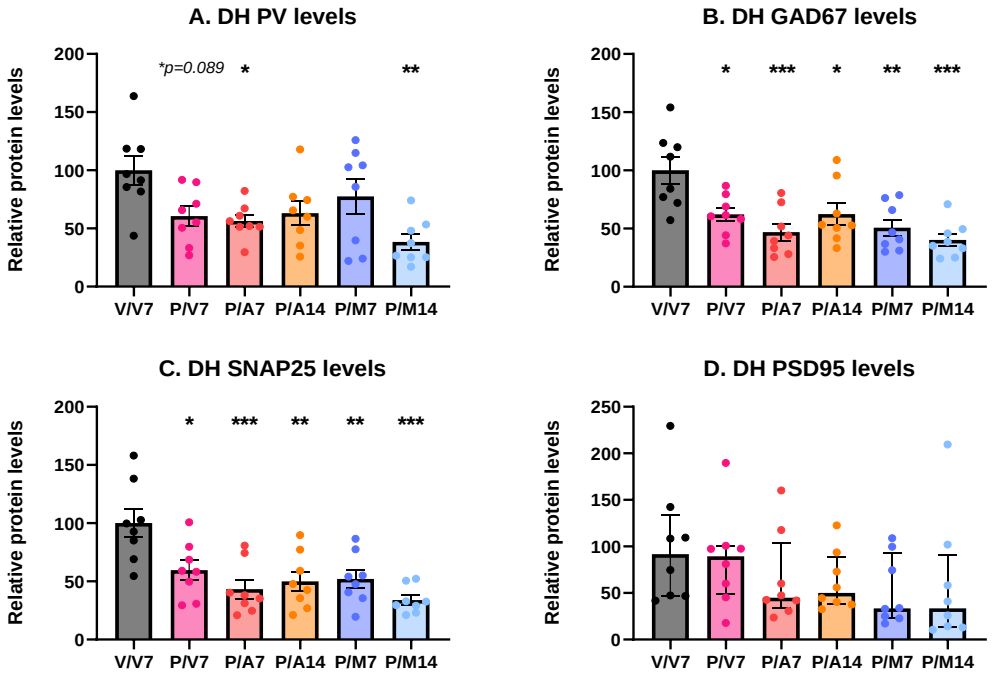

Figure 4.6: The effects of subchronic apocynin/minocycline on selected proteins in the DH. Levels of **A)** PV, **B)** GAD67, **C)** SNAP25, and **D)** PSD95 in the DH of scVeh + scVeh (V/V7), scPCP + scVeh (P/V7), scPCP + scApocynin [10 mg/Kg, p.o.] (P/A7), P/A7 + 7-day washout (P/A14), scPCP + scMinocycline [40mg/Kg, p.o.] (P/M7) or P/M7 + 7-day washout (P/M14)-treated rats (n=8). For **A–C),** data were analysed with a one-way ANOVA with Tukey's post hoc, and graphs show mean ± SEM. **D)** data were analysed with a Kruskal-Wallis H test, and the graph shows median ± IQR. *= significant difference from V/V7, *p<0.05, **p<0.01, ***p<0.001.

Treatment group significantly affected DH SNAP25 levels ($F_{5, 47}$ = 7.447, p<0.001). Like GAD67, there was a profound decrease in SNAP25 in scPCP-treated animals that was not rescued after intervention (P/V7: p = 0.018, P/A7: p<0.001, P/A14: p = 0.002, P/M7: p = 0.003, P/M14: p<0.001) (Figure 4.6C).

Finally, PSD95 was analysed with a Kruskal-Wallis H test, which found that there was no difference between the groups ($X^2_{(5)}$ = 7.557, p = 0.185) (Figure 4.6D).

4.3.4.b Prefrontal cortex

Parvalbumin levels were assessed with a Kruskal-Wallis H test, which found a significant difference between treatment groups ($X^2_{(5)}$ = 14.457, p = 0.013). Here we found a significant reduction in the level of PV after scPCP administration relative to V/V7 (p = 0.002). Interestingly, P/A7 (p = 0.006) and P/M7 (p = 0.046) could rescue parvalbumin levels compared to P/V7. However, in the apocynin washout group, parvalbumin levels significantly decrease after the further 7-day washout, with levels significantly different from V/V7 (p = 0.012) and P/A7 (p = 0.028). The remaining comparisons were insignificant (p>0.05) (Figure 4.7A).

We noted the similarity in the PFC parvalbumin data and the NOR discrimination index graph. To investigate this further, we used Spearman's rho to assess the correlation between these two parameters and found a trend towards a significant model fit where increased parvalbumin predicted good NOR performance (rho = 0.294, p = 0.052, n = 44). We explored whether this correlation remained intact when split into treatment and found it only did so in the P/M14 cohort performance (rho = 0.762, p = 0.037, n = 8).

The group significantly affected PFC GAD67 levels ($F_{5, 42}$ = 5.708, p<0.001). Post hoc analysis showed that P/V7 (p = 0.001), P/A7 (p = 0.027), P/A14 (p = 0.001), and P/M14 (p<0.001) had significantly reduced GAD67 compared to control. Although there was a strong trend to a decrease in P/M7, it was not significant (p = 0.057) (Figure 4.7B).

One-way ANOVA showed a significant effect of the treatment group on SNAP25 levels ($F_{5, 42}$ = 5.002, p = 0.001). Post hoc testing revealed that all scPCP-treated groups had decreased SNAP25 levels compared to vehicle control (P/V7: p = 0.003, P/A7: p = 0.004, P/A14: p = 0.001, P/M7: p = 0.035, P/M14: p = 0.042). The remaining comparisons were insignificant (p>0.05) (Figure 4.7C).

PSD95 levels were assessed with a Kruskal-Wallis H test, which found a significant difference between treatment groups ($X^2_{(5)}$ = 13.274, p = 0.021). In addition, pairwise comparison testing revealed that P/V7 (p = 0.009), P/A7 (p = 0.004), and P/A14 (p = 0.003) were significantly different from the V/V7 control group. There were no significant differences between the remaining groups (p>0.05) (Figure 4.7D).

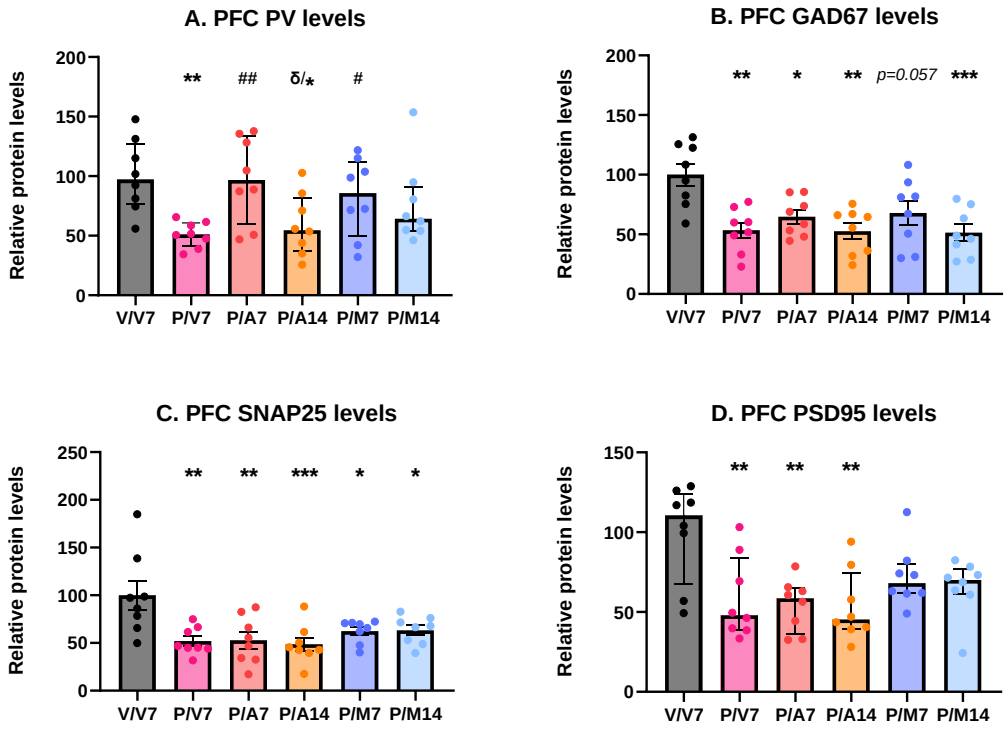

Figure 4.7: The effects of subchronic apocynin/minocycline on selected proteins in the PFC. Levels of **A)** PV, **B)** GAD67, **C)** SNAP25, and **D)** PSD95 in the PFC of scVeh + scVeh (V/V7), scPCP + scVeh (P/V7), scPCP + scApocynin [10 mg/Kg, p.o.] (P/A7), P/A7 + 7-day washout (P/A14), scPCP + scMinocycline [40mg/Kg, p.o.] (P/M7) or P/M7 + 7-day washout (P/M14)-treated rats (n=8). A and D) data were analysed with a Kruskal-Wallis H test and graphs showing median ± IQR. For **B** and **C)** data were analysed with a one-way ANOVA with Tukey's post hoc, and graphs show mean ± SEM. *= significant difference from V/V7, *p<0.05, **p<0.01, ***p<0.001; $^{\#}$= significant difference from P/V7, $^{\#}$p<0.05, $^{\#\#}$p<0.01; $^{\delta}$= significant difference between washout times within treatments, $^{\delta}$p<0.05.

4.4 Discussion

4.4.1 Overview of main findings

We investigated the effects of apocynin, an antioxidant, and minocycline, an anti-inflammatory, on behaviour and pathology to understand further what drives the scPCP deficits. In this cohort, we saw scPCP induced a cognitive deficit in the NOR test that was reversed by subchronic dosing of apocynin and minocycline. Additionally, ten animals from each intervention group were left for a further 1-week, revealing a resurfacing of the scPCP cognitive deficit. Only PFC parvalbumin significantly increased in treated animals from scPCP-only levels, mirroring the behavioural improvements. However, the lack of long-term brain changes may explain the transient behavioural improvements. For a summary, see Table 4.7.

Table 4.7: Consequences of apocynin and minocycline treatment after scPCP dosing. **Behavioural data:** FvN: familiar compared to novel, ticks show where the group spent more time at the novel object than the familiar. DI: discrimination index, ticks show where there was a significant difference between the group DI and 0. Green highlighted squares show groups performing the same as scVeh (V/V7). **Pathology data:** DH, PFC and plasma levels of markers of interest. Arrows show the direction of a significant difference from scVeh group (V/V7). Diagonal arrows show trends. Green highlighted cells show a difference from scPCP treated group (P/V7), # denotes the significance of this difference #p<0.05, ##p<0.01. Yellow cells highlight data that is not significantly different from scVeh (V/V7), nor scPCP (P/V7). Blue text indicates data from exploratory post hoc testing. δ= significant difference between washout times within treatments, δp<0.05.

Treatment		**scPCP**	**----- Apocynin -----**		**----- Minocycline -----**	
Cull day		*7*	*7*	*14*	*7*	*14*
Behaviour						
FvN		×	✓	×	✓	×
DI		×	✓	×	✓	✓
Pathology						
DH	**MDA**	↗	↔	↔	↔	↔
	SOD	↔	↔	↔	↔	↔
	IL6	↑	↔	↔	↓#	↔
	PV	↘	↓	↔	↔	↓
	GAD67	↓	↓	↓	↓	↓
	SNAP25	↓	↓	↓	↓	↓
	PSD95	↔	↔	↔	↔	↔
PFC	**PV**	↓	↔##	↓δ	↔#	↔
	GAD67	↓	↓	↓	↘	↓
	SNAP25	↓	↓	↓	↓	↓
	PSD95	↓	↓	↓	↔	↔
Plasma	**SOD**	↔	↑	↔	↔	↔
	IL6	↗	↔	↔	↔	↔

4.4.2 Behaviour

The NOR test confirmed that scPCP induces a robust cognitive deficit, with animals unable to discriminate novel from the familiar object, as previously described (Gigg et al., 2020, Landreth et al., 2020, Loureiro et al., 2022, Neugebauer et al., 2018). The cognitive deficits are attenuated in the initial intervention groups (P/A7 and P/M7) twenty-four hours after the last dose. Previous studies in rodents suggest that levels of both drugs in the brain should be minimal (Colovic et al., 2003, Okamura et al., 2018, Tarazi et al., 2019, Wang et al., 2013a), although none of this data is in female Lister Hooded rats. It would be relevant to know whether the drug is washed out of the system, as this could indicate reversals of pathology. Indeed, we included the delayed washout groups to understand if the treatments had a long-term beneficial effect (P/A14 and P/M14). However, we found neither group spent more time with the novel object, indicating that the scPCP deficits had returned. Although, when comparing DI to a hypothetical mean of zero or random chance, we found that P/M14 were significantly different, a slight group effect that suggests minocycline could have marginal effects after a one-week washout (Figure 4.3).

4.4.2.a Apocynin

Regarding NMDAr antagonist models, the literature for behaviour is limited to a study using a Ppp1r2-positive interneuron-specific NMDAr knockout model. These interneurons are predominantly cortical and hippocampal PVI. Therefore, this somewhat PVI-specific NMDAr dysfunction could reflect the hypofunction we see after scPCP dosing. The knockout was induced from the second week of age. Concurrently, apocynin was added to the drinking water of the intervention group. Of note, from three weeks of age, the mice were singly housed. Regarding behaviour, the loss of NMDAr in PVI predictably reduced performance in the y-maze task, which was exacerbated by social isolation stress. However, apocynin rescued behavioural deficits of the mutation and the social isolation stress (Jiang et al., 2013).

Due to the lack of literature on this topic, the effect of apocynin in other cognitively impaired models was investigated. The literature showed that apocynin is effective when dosed before (Hui-guo et al., 2010, Jiang et al., 2013, Schiavone et al., 2009) or after (Ji et al., 2015, Kumar et al., 2022, Qiu et al., 2016, Xianchu et al., 2021) the experimental insult. Like our study, most dosing protocols were seven days long (Kumar

et al., 2022, Liu et al., 2016, Qiu et al., 2016) and were equally beneficial as prolonged dosing.

Of these studies, two gave interesting insights into the timing of recovery. First, a single prolonged stress (SPS) model found that the delay after insult strongly predicted cognitive outcomes. Rats were isolated post-weaning. Schiavone et al. administered apocynin from week four to week seven after SPS in the early-intervention group. In the late-intervention group, rats were treated with apocynin from weeks seven to ten. Intriguingly, only the early intervention group showed cognitive improvement (Schiavone et al., 2012). In the second study modelling post-operative decline in aged mice, researchers gave apocynin in the first or second week after acute stress. All animals were killed at the end of the second week. Again, only the early intervention group showed cognitive improvement (Liu et al., 2016).

The literature suggests that apocynin has efficacy in prevention and early intervention studies. In addition, due to the broad model types reviewed here, it has efficacy in systemic inflammation, stress, diabetes, hypoxia and models relevant to NMDAr hypofunction.

4.4.2.b Minocycline

scMinocycline dosing has been used with NMDAr antagonists previously, showing an excellent ability to reverse cognitive deficits caused by the model. As in our study, minocycline was administered post-NMDAr antagonism dosing and behaviour was assessed twenty-four hours after the last drug treatment. Levkovitz et al. were the first to show efficacy in acute MK-801-treated rats in the Morris water maze test. Here only three days of pre-treatment with minocycline were sufficient to reverse the acute MK-801-induced cognitive deficit (Levkovitz et al., 2007). In the study by Fujita et al., they gave minocycline for fourteen days after scPCP dosing and tested cognition using a NOR test (Fujita et al., 2008). Whereas in the Monte study, they used a prevention (seven days minocycline followed by seven days minocycline and ketamine) and a reversal (seven days ketamine, seven days ketamine and minocycline) paradigm and a y-maze test (Monte et al., 2013). In all iterations, minocycline could alleviate cognitive symptoms.

Animal models that induce cognitive impairments reveal that scMinocycline is equally capable of rescuing cognitive impairments after the insult (Liu et al., 2007, Sharifi et al.,

2021, Zhu et al., 2014a), as it is preventing (Gholami Mahmoudian et al., 2022, Hiskens et al., 2021, Ji et al., 2020, Liu et al., 2021a, Yau et al., 2018).

In our study, we tested for cognition twenty-four hours and seven days after the last treatment dose. Initially, minocycline showed a robust attenuation of the NOR deficits. However, after one week, this effect was less pronounced. Therefore, studies that had seen an improvement after a washout period were investigated to ascertain whether minocycline had the potential to cause long-term benefits. Most published data tested their animals immediately after dosing ended, with only one study recording cognitive improvements after a substantial delay. In that study, mice were given minocycline for fourteen days before and during a recurrent, mild traumatic brain injury (rmTBI) model. Over twenty-three days, treated animals endured rmTBI on a schedule of three days of treatment and two days rest. Animals were tested using the Morris water maze 90 days later. Here, there was a significant reduction in the latency to find the platform on the final day of testing in mice treated with minocycline (Hiskens et al., 2021).

Others do not observe this long-term benefit. For example, Sharifi et al. found that scMinocycline on days 0-3 post-carotid artery occlusion (CAO) did not improve cognitive outcomes on day 32. However, scMinocycline dosing on days 21-32 after CAO improved performance in the radial arm maze (Sharifi et al., 2021). Taking these results together, we suggest the pro-cognitive effects and duration may depend on the nature of the insult, duration of minocycline and proximity to the insult. Indeed, most protocols have prolonged minocycline interventions, with studies ranging from three days to three months, and these occur at many time points relative to the insult. More beneficial effects may be seen with an altered experimental design.

4.4.3 Oxidative stress

Apocynin inhibits the formation of NOX2, a significant contributor to somatic ROS. Due to this mechanism of action, we looked at SOD activity as this is the first enzyme downstream of NOX2 (Figure 4.1). Then we chose to look at MDA as a marker of lipid peroxidation, which is a downstream effect of excessive ROS.

These markers were also tested in the minocycline-treated cohort. Minocycline targets a broad spectrum of systems despite its classification as an antibiotic. In typical conditions, nitric oxide (NO) regulates retrograde neurotransmission, cerebral blood

flow, intracellular signalling, metabolic status and dendritic spine development. However, in the ageing and the diseased brain, NO can interact with superoxides to create peroxynitrite, which damages proteins, lipids and nucleic acids (Picón-Pagès et al., 2019). The neutralisation of peroxynitrite is catalysed by the SOD enzymes (Wang et al., 2018b). Relevant to our current study, minocycline can block NO-induced cell death in neuronal cultures (Wilkins et al., 2004).

4.4.3.a SOD

Here we measured SOD activity in the brain and plasma. As a reminder, we found increased expression of the SOD gene in the PFC, but not the DH, in the characterisation chapter. Exploratory post hoc testing revealed increased SOD activity in the apocynin cohort plasma. Although we found no alteration to SOD activity in the DH, the inhibition in the DH and plasma were correlated. This is noteworthy as the SOD1 enzymes are ubiquitous in the body, suggesting systemic effects (Wang et al., 2018b).

Although there is no evidence in the literature on the effect of apocynin and minocycline on SOD in NMDAr antagonist models, it has been used in various others. In general, the insult causes a reduction in SOD activity, which is partially rescued with scApocynin or scMinocycline (Amirahmadi et al., 2022, Depciuch et al., 2022, Hui-guo et al., 2010, Motaghinejad et al., 2021, Qaid et al., 2022, Xianchu et al., 2021).

Noteworthy studies include Parvardeh et al., who treated rats with minocycline in the seven days prior to transient occlusion of the common carotid arteries and treated another cohort in the seven days after the surgery. Here they found that the recovery to regular SOD activity was only present in the rescue group and not in the prevention (Parvardeh et al., 2022). Given that prevention treatments can improve cognition (4.4.2.b), perhaps this suggests that it does so despite the persistence of reduced antioxidant activity. There was only one study that measured an increase in SOD activity. This observation was in a zinc-injection model used to generate neurodegeneration. However, minocycline reduced SOD activity to control levels, suggesting that minocycline can normalise activity regardless of direction (Kumar et al., 2016).

When looking at other antioxidants activity, namely CAT and GPx, the ability of apocynin or minocycline to increase activity is robust (Cruz-Álvarez et al., 2017, Kumar et al., 2016, Motaghinejad et al., 2021, Motaghinejad et al., 2022, Sun et al., 2014).

In this section, many animal models have been discussed, including traumatic brain injury, ischaemia, infections and drugs of abuse like PCP, ketamine, and methamphetamine. Although diverse in construct and duration, all caused increased oxidative damage and reduced antioxidant activity. Given that high NMDAr signalling leads to increased antioxidant activity (3.4.10), literature investigating NMDAr hypofunction in these models was evaluated. Like the PCP model, the models were also subject to acute increases in glutamate (Guerriero et al., 2015, Huang et al., 2008, Nishizawa, 2001, Parsegian et al., 2014) and impaired PVI (Crapser et al., 2020, Nichols et al., 2018, Park et al., 2021, Veerasakul et al., 2016), suggesting a potential common pathway.

Here we measured SOD activity. It is essential to consider what altered enzymatic activity means. A less active enzyme cannot catalyse its respective reaction at the expected rate (Prenzler et al., 2021). The regulation of catalytic kinetics is complex and multifactorial. Physical factors like temperature, pH and substrate concentrations can limit activity. It can also be limited by feedback loops, competitive inhibition, allosteric regulation, phosphorylation, or the presence or absence of co-factors (Dominiczak et al., 2019). One or many of these may be altered in the insulted brain. Investigations into the nature of these changes are beyond the scope of the data we have collected here. However, it can be assumed that if the antioxidant systems have reduced activity, there would likely be increased ROS-related damage, such as lipid peroxidation.

4.4.3.b MDA

The present study did not see a significant ANOVA model when examining the MDA concentration. However, exploratory post hoc testing revealed a trend towards an increase in MDA concentration in the P/V7 group compared to V/V7. This non-significant increase in the scPCP-treated animals was significantly reduced in the P/A7 group. Many previous studies looking at NMDAr antagonist models found an increase in MDA in the PFC, hippocampus or whole brain. Where the culling date was specified, most brains were taken at the end of the dosing week, or the latest was taken two weeks later (Ben-Azu et al., 2016, de Oliveira et al., 2009, Eneni et al., 2023, Okubo Eneni et al., 2020, Omeiza et al., 2023, Tadmor et al., 2018, Zugno et al., 2016).

There was only one study where they found no change in MDA levels after one week of dosing. In said study, they dosed mice with 100mg/Kg of ketamine for seven days and

then took the brains 30 minutes after the last injection (Hou et al., 2013). This lack of increase may be due to the dose being too high, as Oliveria et al. found a dose-dependent effect of ketamine in their rat model. Their study found that 4mg/Kg and 10mg/Kg of scKetamine would increase MDA in the PFC. However, MDA only increased in the hippocampus after 4mg/Kg, not 10mg/Kg (de Oliveira et al., 2009). Perhaps NMDAr antagonism must be in a Goldilocks zone for oxidative damage, producing sufficient NMDAr antagonism on PVI to produce glutamatergic excitotoxicity. On the other hand, an excessive dose may block all NR2 subtypes and, therefore, not cause the same increases in glutamate. Indeed, high-dose infusions of ketamine can be used to alleviate seizures in some epileptic patients (Golub et al., 2018).

One study compared the use of minocycline in prevention (seven days minocycline followed by seven days minocycline and ketamine) and reversal (seven days ketamine, seven days ketamine and minocycline) dosing schedules. In both cases, they found a significant increase of MDA in the hippocampus of scKetamine-treated mice compared to the control (132% in the prevention study and 127% in the reversal study). Our study found a more substantial increase in MDA levels (160%). However, our studies have acutely different levels of variation. Monte et al. used specific homogenisation methods for each marker they measured, which might have preserved MDA. Indeed, they had sufficient concentration to use a colourimetric detection method, whereas we used the more sensitive fluorometric approach. The high variation in our MDA concentrations may also explain why Monte saw a significant decrease where we did not. In the high-dose minocycline group, there was a 38% reduction in the prevention study and a 30% reduction in the reversal treatment. We saw a 28% reduction in P/M7 and a 34% reduction in P/M14. Therefore, our protocol has a comparable group effect. However, our tissues produce a comparatively low MDA concentration and high variation (Monte et al., 2013). A common complaint about using MDA assays is that the TBA chromogen can produce products with many other compounds. Future studies should consider bespoke tissue collection (Murphy et al., 2022).

Summarising the data from other models, apocynin and minocycline can reverse increases in MDA concentration. These reductions in MDA concentration occurred in prevention (Abdo Qaid et al., 2022, Monte et al., 2013, Qaid et al., 2022), coadministration (Abdo Qaid et al., 2022, Amirahmadi et al., 2022, Hui-guo et al., 2010,

Monte et al., 2013, Motaghinejad et al., 2022, Qaid et al., 2022) and reversal studies (Abdo Qaid et al., 2022, Depciuch et al., 2022, Ghavimi et al., 2022, Ji et al., 2015, Lu et al., 2014, Monte et al., 2013, Naderi et al., 2017, Qaid et al., 2022, Xianchu et al., 2021).

4.4.4 Inflammation

Regarding inflammation, IL6 levels were of interest due to the robust increase of brain IL6 after scNMDAr antagonist dosing (Bae et al., 2023, Ben-Azu et al., 2022, da Silva Araújo et al., 2017, de Araújo et al., 2021, Eneni et al., 2023, Tadmor et al., 2018, Wei et al., 2022, Xiao et al., 2019). A secondary reason is the effect of minocycline on IL6, which we will discuss in full later in this section.

4.4.4.a Apocynin

Although apocynin does not directly act on inflammatory cytokines, it reduces ROS and inflammation. In addition, apocynin favours activated microglia developing into the anti-inflammatory M2 phenotype (discussed in 4.1.1.b). In our study, we saw an increase in the levels of IL6 in the DH after scPCP-dosing compared to vehicle control. Apocynin did not significantly reduce IL6 levels, though it was not significantly higher than controls. The protein levels used in the assay may not have been sufficient to see the group differences effectively. Collating studies that measured changes in TNFα, IL1β and IL6, cytokines secreted by M1 microglia (Tang et al., 2016), revealed that apocynin can attenuate prolonged inflammation. The data for acute attenuation (<24 hours) is limited to a single paper; however, in this case, apocynin was not able to reduce sepsis-induced increases to IL6 (Table 4.8).

In the plasma, apocynin reduced IL6 levels in both washout conditions. This was confirmed in other studies. The first showed that three days of apocynin treatment was sufficient to subdue the increase in IL6 plasma after acute exercise (Henríquez-Olguín et al., 2016). The same result was seen in a rat model of hypertension. Simplicio et al. added apocynin to ethanol-laced drinking water for six weeks in this study. In isolation, ethanol increased IL6; however, apocynin reversed the increase (Simplicio et al., 2017).

Table 4.8: Summary of studies on the effect of apocynin on proinflammatory cytokines. Each insult described was administered acutely, and apocynin was given after the insult. Protein levels of cytokines were measured using western blot. Insult delay describes when the animal has been culled post-acute insult (~ = animals were culled post-behavioural testing, so time has been estimated). Arrows show the change in cytokine levels from insult-only control. The downward arrow indicates cytokine has returned to vehicle-control levels, and the diagonal arrow shows a significant reduction without a complete reversal. TBI: traumatic brain injury, SPS: single prolonged stress, STZ: streptozotocin-induced diabetic model, ♂: male, ♀: female, SD: Sprague Dawley rats, i.p.: intraperitoneal, sc.: sub cutaneous, p.o.: oral, D: day after insult, Hippo: hippocampus, PFC: prefrontal cortex, [a] = all time points, [1] = day 1 only.

	(Feng et al., 2017)	(Ji et al., 2015)		(Liu et al., 2016)	(Xianchu et al., 2021)
Model	TBI	Sepsis		SPS	STZ
Strain	♂ SD	♂ C57BL6		♂ SD	♂ SD
Apocynin	50mg/mL i.p.	5mg/kg i.p.		5mg/Kg sc.	16mg/Kg p.o.
Schedule	immediately	D: 0-11		D: 0-7	D: 1-112
Insult delay	12, 24 or 48 hours	1, 3, 14 and 30 days		~15 days	~118 days
Region	Hippo	PFC	Hippo	Hippo	Hippo
IL6		↔	↘[1]	↓	↓
TNFα	↘[a]	↔	↔	↔	↘
IL1β	↘[a]	↘[1]	↘[1]	↔	↓

4.4.4.b Minocycline

Minocycline inhibits proinflammatory microglia (M1) (Kobayashi et al., 2013), IL6 transcription (Scholz et al., 2015), nitric oxide synthesis (see 4.1.2) (Zhu et al., 2002), metalloproteinases (Popovic et al., 2002), and protects from NMDA-mediated excitotoxicity (Tikka et al., 2001). As such, it has many functions that would alleviate pathology, which may be sustaining scPCP-induced deficits. Initially, minocycline was able to reduce IL6 levels in the DH; however, this was not sustained after the washout.

Published studies show that minocycline can be used before, during and after the insult, with high doses (30-50 mg/Kg), showing a consistent relief to increased inflammatory markers (Table 4.9). Moreover, the studies by Zhu et al. and Hiskens et al. show a prolonged anti-inflammatory effect of minocycline, which cannot be concluded from the current data set (Hiskens et al., 2021, Zhu et al., 2014b).

Table 4.9: Summary of minocycline studies in different disease models. Duration describes the number of days the insult was applied over. Route of administration is given for minocycline. The schedule describes the time relative to the insult minocycline that was given, with negative numbers indicating pre-treatment. In the poly(I:C) study, gestational day (GD) and postnatal day (PD) are used instead. Cull day describes the day since the insult started the animal was culled (~ = animals were culled post-behavioural testing, so time has been estimated). Data includes protein and mRNA data. Arrows show the change in measurement from insult-only control. The downward arrow indicates cytokine has returned to vehicle-control levels, and the diagonal arrow shows a significant reduction without a complete reversal. scoAD: scopolamine Alzheimer's disease, rmTBI: repeated mild traumatic brain injury, LPS: lipopolysaccharide infection model, MPH: methylphenidate neurodegeneration model, I/R: ischemia/reperfusion injury, PIC: poly(I:C), ♂: male, ♀: female, SD: Sprague Dawley rats, i.p.: intraperitoneal, sc.: sub cutaneous, p.o.: oral, D: day after insult, Hippo: hippocampus, Ctx: cortex, VH: ventral hippo.

	(Amirahmadi et al., 2022)			(Hiskens et al., 2021)		(Ji et al., 2020)	(Motaghinejad et al., 2021)				(Motaghinejad et al., 2022)				(Naderi et al., 2017)	(Zhu et al., 2014a)		(Zhu et al., 2014b)	
Model	scoAD			rmTBI		LPS	Alcoholism				MPH				I/R	LPS		PIC (GD9)	
Duration	21 days			23 days		3 days	21 days				21 days				Acute	Acute		Acute	
Strain	♂ Wistar			♂ C57Bl/6J		♂ SD	♂ Wistar				♂ Wistar				♂ Wistar	♂ SD		♂ ♀ C57Bl/6	
Route	p.o.			sc.		i.p.	p.o.				i.p.				i.p.	p.o.		i.p.	
Schedule	D: 0-20			D: -14 - 23		D: 0-2	D: 0-20				D: 0-20				D: 0-6	D: 35-49		PD 10-24	
Cull day	~28			90		6	21				26				12 days	58		PD62	
Region	Hippo			Hippo	Ctx	PFC	Hippo				Hippo				Hippo	Ctx	VH	Ctx	VH
Dose (mg/Kg)	10	15	30	50	50	40	10	20	30	40	10	20	30	40	40	40	40	40	40
IL6	↔	↘	↓			↓													
TNFα	↔	↘	↓	↓	↓	↔	↔	↔	↘	↘	↘	↘	↘	↘	↘				
IL1β	↔	↔	↘				↔	↔	↓	↓	↘	↘	↘	↘	↓				
IBA1 density						↓									↓	↘	↘	↓	↓

4.4.5 Brain markers

The present study showed significant prefrontal reductions in parvalbumin, GAD67, SNAP25 and PSD95 after scPCP treatment. In the dorsal hippocampus, the changes were less significant, with a trend towards decreased parvalbumin and reductions in GAD67 and SNAP25. In terms of reversal after apocynin or minocycline, the improvements were predominantly found in the PFC. There was a significant increase in parvalbumin levels in the PFC in early intervention groups (P/A7 and P/M7), and P/M14 were neither different from V/V7 nor P/V7, mirroring the behavioural data. This data pattern was also seen in GAD67 levels, though only P/M7 was not significantly different from V/V7. The early and delayed culled minocycline-treated animals did not significantly differ from V/V7 in the PSD95 data. Although limited, minocycline appears to be the more potent treatment in this respect.

4.4.5.a Parvalbumin

Several studies have looked at the effect of apocynin on PVI in various models, likely stemming from the seminal work of Behrens et al., who showed that ketamine-induced PVI loss depends on NOX2. Mice genetically modified not to express NOX2 or wild-type mice treated with apocynin prevented PVI and GAD67 loss (Behrens et al., 2007). From then, this relationship between NOX2 and PVI was validated using apocynin in a host of other models, including social stress (Jiang et al., 2013, Schiavone et al., 2009), hypoxia (Liang et al., 2016, Yuan et al., 2015, Zhang et al., 2016b), sepsis-induced cognitive impairments (Ji et al., 2015), post-traumatic stress disorder (Liu et al., 2016), postoperative cognitive decline (Qiu et al., 2016), epilepsy (Kim et al., 2017a) and replicated in ketamine studies (Zhang et al., 2016a, Zhou et al., 2015). Consistently, these studies showed a significant increase in parvalbumin after apocynin.

In our study, we initially saw an improvement in PFC parvalbumin. Notably, parvalbumin levels predicted NOR performance, potentially indicating increased signalling in these animals compared to scPCP control. However, after a week of washout, levels had returned to P/V7 levels. Other studies delayed tissue collection after apocynin treatment for seven (Liu et al., 2016), thirty-five (Liang et al., 2016), or fifty-eight days (Zhang et al., 2016a). Despite apocynin washout, parvalbumin levels were recovered in all three compared to the insult-only control. A final study had a sixteen-day delay. However, the insult was no longer causing a behavioural or pathological deficit, so it

cannot be compared (Ji et al., 2015). Therefore, it appears apocynin can have a long-lasting effect.

Next, studies that reflected our insult washout (a delay between the insult and the apocynin intervention) were examined. After all, timings were highly consequential in the study by Schiavone et al., which noted that early intervention with apocynin could recover cognitive impairments, but delaying treatment three weeks renders apocynin obsolete (Schiavone et al., 2012). However, all studies administered the insult and intervention in proximity. Perhaps replicating this study without delay would result in a more substantial parvalbumin recovery. However, if this is the case, it suggests that apocynin would not be a good treatment for established schizophrenia, as the window for treatment is narrow. This contrasts clinical trials for other antioxidants, which had some efficacy in chronic patients (Table 4.1).

Studies involving parvalbumin and the anti-inflammatory minocycline are limited to infection models. The majority are short-term studies with proximity between the infection and treatment. In each case, parvalbumin was interpreted with immunofluorescent intensity. Pre-treatment (Gao et al., 2017), coadministration (Ji et al., 2020), and post-treatment (Mao et al., 2021) all recovered reduced parvalbumin intensity in the PFC or the CA1 and CA3 field of the hippocampus back to control levels. The final study was in a maternal infection model, where polyinosinic:polycytidylic acid (poly(I:C)) was given on gestational day (GD)12, minocycline was given to juvenile mice from postnatal day (PD)21-35, and brains were taken approximately three weeks later. Although these timings more closely reflect our study, the results did not. Poly(I:C) induced reductions in parvalbumin protein measured with western blot, and immunohistochemistry revealed a reduced cell count in the DG; both were rescued with minocycline (Xia et al., 2020). Critically, these brains were undergoing development; therefore, it is difficult to compare these studies.

4.4.5.b GAD67

For both apocynin and minocycline, there was no effect of dosing on the scPCP-induced deficits, with all groups in both regions being significantly different from scVehicle, save PFC GAD67 for P/M7 where there was a strong trend towards a difference ($p=0.057$).

GAD67 was also characterised in the Behrens study, concluding that reductions depended on ketamine activation of NOX2. Blocking NOX2 formation with apocynin

prevents ketamine-induced GAD67 deficits, with Zhou and Zhang replicating these findings (Behrens et al., 2007, Zhang et al., 2016a, Zhou et al., 2015). To further understand the mechanisms, we looked at the effect of other antioxidants in NMDAr antagonist models. Many of these compounds also have anti-inflammatory properties, hence the joint discussion. In several experiments from the same research group, a preventative (antioxidant for seven days prior to, then co-administered with one week of ketamine dosing) and a reversal (antioxidant administered for the second week of a 14-day scKetamine dosing regimen) protocol was compared using two antioxidants, morin and rutin. Morin could reverse GAD67 deficits in both protocols. However, rutin only improved in the preventative (Ben-Azu et al., 2018a, Ben-Azu et al., 2020, Oshodi et al., 2021). This study highlights a frequent roadblock in antioxidant drug development, poor absorption and low bioavailability (Ayvaz et al., 2022, Owczarek-Januszkiewicz et al., 2022), simply some antioxidants can have more rapid or more sustained effects. Indeed, apocynin has a bioavailability of 2.8% (Wang et al., 2013a), despite rapid absorption after oral administration (Zahiruddin et al., 2017). Reflecting on the characterisation chapter, which hypothesised that the reduction in GAD67 was a response to reduced NMDAr function, perhaps the lack of GAD67 recovery suggests ongoing pathology.

4.4.5.c SNAP25

We observed a significant reduction in SNAP in all scPCP-treated groups with no recovery after apocynin or minocycline. Beginning with minocycline, one study injected rats with an insecticide that induced dopaminergic neurodegeneration. They studied SNAP25 protein in the substantia nigra, where they saw progressive and sustained SNAP25 loss after four, eight and twelve weeks of dosing. However, when minocycline was co-administered, SNAP25 levels did not reduce across all 12 weeks (Singh et al., 2011). This is an interesting finding as it suggests that minocycline can quell ongoing and increasing damage. There were two further studies from the same lab studying the effect of botulinum toxin on SNAP25, though it should be noted that botulinum toxin cleaves SNAP25, so the effect of minocycline may be due to neutralisation of the toxin rather than network alterations. Here they found a significant reduction in astroglial SNAP25, which was reversed by adding minocycline to the culture (Piotrowska et al., 2017).

To our knowledge, no studies have looked at apocynin and SNAP25; however, there was a study looking at the effect of the antioxidant melatonin on middle cerebral artery occlusion (MCAO). This study was interested in the effect on AMPAr and NMDAr signalling, focusing on NR2A-PSD95 coupling. The study design was simple, a single dose of melatonin or vehicle before MCAO surgery. Brains were collected 24 hours later. MCAO resulted in reduced NR2A, SNAP25 and PSD95 protein, and using immunohistochemistry, they showed a reduction in NR2A and PSD95 co-localisation. All deficits were reversed by melatonin (Shah et al., 2019). In the visual cortex, De Pasquale showed that LTP required NOX2 activation. Indeed, blocking in vitro slices with apocynin inhibits LTP. They found that young NOX2 deficient mice (PD9-12) had comparable LTP to WT, indicating that neonatal mice may induce LTP in a NOX2-independent manner. However, by PD20-24, the time of much neuronal maturation, there was a significant drop in LTP in NOX2 deficient slices (De Pasquale et al., 2014). Unfortunately, we did not have time to look at NR2A and NR2B in these animals. However, perhaps our intervention did not recover this fundamental mechanism of LTP due to a sustained decrease in SNAP25 and PSD95. As discussed, both are fundamental for AMPAr and NMDAr trafficking (3.3.1).

4.4.5.d PSD95

Studies in minocycline using immunohistochemistry adds a fascinating layer to the NR2A-PSD95 story. In these studies, minocycline reduced PSD95 and microglia co-staining (Campos et al., 2022, Lan et al., 2022). An elegant study by Han et al. showed that after chronic social defeat stress, active microglia increase in density in the dentate gyrus (DG) of the hippocampus and then engulf rather than digest PSD95. Treatment with minocycline attenuated microglia activation and reduced aberrant synaptic confiscation (Han et al., 2022a). Indeed, western blot and qPCR lack the spatial information obtained from immunohistochemistry, and often this information is crucial for function. Although a final study used western blot to study the effects of apocynin and another antioxidant thought to inhibit NOX2 called ginsenoside Rg1. They found flanking cerebral ischemia/reperfusion injury with antioxidant treatment rescued PSD95 levels (Han et al., 2022b).

4.4.6 Limitations

Besides the limitations mentioned in the discussion, this study was limited by the lack of vehicle-treatment groups. This meant that we could not assess the effects of these compounds in vehicle animals, and it restricted the statistical models we could use. However, we sought to test scPCP-treatment initially as a proof of concept.

In addition, some of the plasma lysates were haemolysed, which can affect cytokine analysis (Karsten et al., 2018), though we did not find any effect of haemolysis when this was added into a univariate general linear model as a factor alongside treatment groups.

4.5 Chapter summary

Although apocynin and minocycline temporarily improved performance in the NOR test, there were no long-lasting effects. Nevertheless, focusing on the genuinely significant changes produced in this study reveals a limited yet insightful outcome.

Table 4.10: Consequences of subchronic apocynin and minocycline on the scPCP model. Arrows show the direction of change from the P/V7 cohort. [1]significantly different from P/V7, [2]different from neither V/V7 nor P/V7. PFC: prefrontal cortex, PV: parvalbumin, SOD: superoxide dismutase.

Treatment	----- Apocynin -----		----- Minocycline -----	
Delay	**7**	**14**	**7**	**14**
PFC	↑ PV[1]		↑ PV[1]	↗ PV[2]
DH			↓ IL6[1]	
Plasma	↓ SOD[1]			

PFC parvalbumin is the only protein marker to change in response to apocynin and minocycline treatment. Moreover, we find correlations between NOR performance and parvalbumin levels in the PFC.

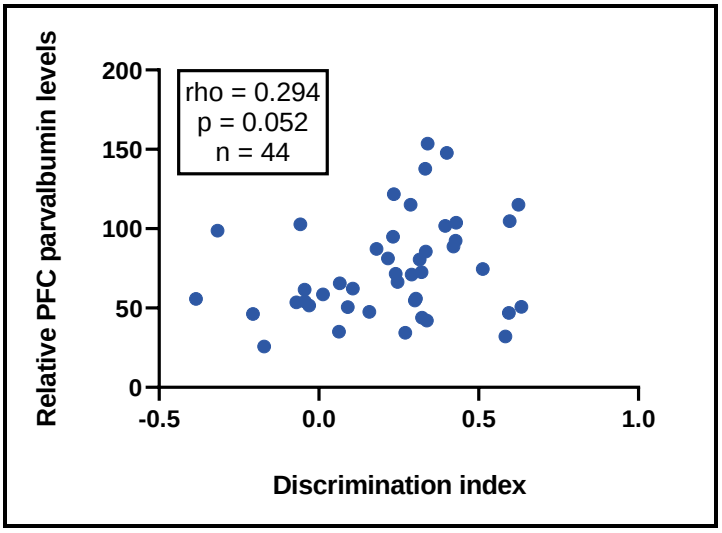

Figure 4.8: Correlation between PFC parvalbumin and NOR performance

We know that parvalbumin expression can change in the short term due to behavioural testing (Donato et al., 2015). Does the relationship between parvalbumin and the discrimination index detect in this study suggest the drugs have permitted PVI to adapt expression in response to the NOR task? Or is NOR habituation and testing insufficient to induce this change? Notably, neither treatment improved the synaptic pathology suggesting superficial improvements.

CHAPTER 5: EFFECTS OF EXERCISE IN THE SCPCP MODEL

5.1 Introduction

In the previous chapters, we have suggested ongoing excitatory/inhibitory imbalance, low-grade inflammation and changes to antioxidant activity in the subchronic phencyclidine model (scPCP). We have shown that one week of dosing with a general anti-inflammatory and antioxidant can temporarily alleviate cognitive symptoms in the scPCP-treated animal. However, there are few immediate and sustained brain changes. Indeed, the scPCP-induced cognitive deficits return after a week without dosing. This chapter focuses on exercise as a pro-cognitive intervention for cognitive impairment associated with schizophrenia (CIAS).

5.1.1 Exercise and schizophrenia

The effects of exercise on cognition for CIAS have been studied extensively in clinical trials, meta-analyses and review articles. Despite differences in patient profiles, data collection and exercise protocols, exercise appears to affect cognition positively. The specific domains that improve vary between meta-analyses; however, attention, vigilance and working memory are regularly among the significant findings (Firth et al., 2017, Girdler et al., 2019, Shimada et al., 2022, Smith et al., 2010).

Alongside the pro-cognitive effects, exercise can alleviate positive and negative symptoms (Falkai et al., 2017), as well as broader comorbidities associated with schizophrenia, such as obesity, hypertension, poor cardiovascular health and metabolic syndrome (Bueno-Antequera et al., 2020, Schmitt et al., 2018). Moreover, low physical activity strongly predicts schizophrenia risk (Bueno-Antequera et al., 2020), suggesting a bidirectional link between physical and mental well-being.

The exercise interventions which generated the most substantial improvements were protocols that offered prolonged, frequent exercise sessions (Bueno-Antequera et al., 2020, Firth et al., 2017, Shimada et al., 2022). In addition, Firth et al. identified that instructor-led training sessions led to lower attrition rates and more significant improvements (Firth et al., 2017).

A caveat to exercise interventions is that participants must comply and complete most of the program to see benefits. However, attrition rates are, on average, 22% in group interventions and 43% in solitary interventions, despite financial incentives (Firth et al., 2015). Reflecting on the motivational issues interwoven with the negative symptoms of

schizophrenia (Galderisi et al., 2018) and the increased likelihood of developing metabolic syndrome while taking second-generation antipsychotics (Muench et al., 2010), it is understandable why committing to an active lifestyle will be more challenging in schizophrenia patients than it is for the general population. Nevertheless, considering exercise's benefits and practical challenges, insight into the underlying mechanisms may highlight targets for future therapies.

5.1.2 Exercise in rodents

Rodent models are valuable tools when trying to understand the mechanisms of exercise. Broadly, there are two ways to establish an exercise model: voluntary or forced; both have merits and drawbacks. In a forced exercise paradigm, the quantity of exercise can be precisely controlled and standardised across the cohort. However, it can induce inflammation and endocrine responses associated with chronic stress (Moraska et al., 2000). On the other hand, voluntary exercise allows rodents to exercise within their means. However, it will inherently introduce a high degree of variation into the model.

Table 5.1 summarises a selection of studies examining voluntary exercise's effect on behavioural outcomes. Exercise can rapidly improve cognitive outcomes after only ten days of running wheel access (Hajisoltani et al., 2011). Notably, Hopkins et al. showed that adolescent rats retain behavioural improvements longer than adults, with adolescent animals able to discriminate between novel and familiar objects in the NOR task after four weeks of inactivity (Hopkins et al., 2011). On the other hand, in adult animals, the positive effects of exercise fade after two to three weeks of inactivity (Berchtold et al., 2010, Hopkins et al., 2011).

Table 5.2 summarises forced exercise studies. Here, we see similar improvements in cognition after exercise. As in the voluntary protocols, a period of inactivity will irradicate the enhanced cognition (Acevedo-Triana et al., 2017, Kim et al., 2013), and adolescent animals are more liable to improvements (Jin et al., 2017).

Different mechanisms have been proposed to contribute to cognitive improvement after exercise. One area of interest involves brain-derived neurotrophic factor (BDNF) and neurogenesis, which can be measured in the brain after exercise (Table 5.1 and Table 5.2).

Table 5.1: Summary of voluntary exercise study outcomes in healthy rodents. Free access: running wheel in the home cage. ♂: male, ♀: female, SD: Sprague Dawley, LE: Long Evans, RLC: reverse light cycle, MWM: Morris water maze, (PR-)NOR: (pattern recognition)-novel object recognition, ITI: intertrial interval, ASST: attentional set-shifting test, RAWM: radial arm water maze, PSD95: postsynaptic density 95, PFC: prefrontal cortex, HIPP: hippocampus, BDNF: brain derived neurotrophic factor. ↑ = improvement compared to control animals, ↑↑ = improvement compared to a different exercise cohort, ↔ = no change compared to control.

Duration	Access	Wheel resistance	Model	Housing	Behaviour	Delay?	Effect	Brain changes	Effect	Reference
10 days	Free	100g	♂ Wistar	Individual	MWM	-	↑	-	-	(Hajisoltani et al., 2011)
12 days	Free	-	♂ SD	RLC	Object in place	-	↑	Synaptophysin and PSD95 in PFC and HIPP	↑	(Brockett et al., 2015)
					NOR 5 min ITI	-	↔			
					ASST	-	↑			
3 weeks	Free	-	♂ C57BL/6	Individual	RAWM	-	↑↑	BDNF in HIPP	↑	(Berchtold et al., 2010)
						1 week	↑↑		↑	
						2 weeks	↑		↑	
						3 weeks	-		↔	
3 weeks	Free	-	♀ C57BL/6	-	PR-NOR 1.5 hour ITI	-	↔	Neurogenesis in DG	↑	(Bolz et al., 2015)
					PR-NOR 24 hour ITI	-	↑			
4 weeks	Every other day	-	♂ LE	-	NOR 24 hour ITI	-	↑	-	-	(Hopkins et al., 2010)
						2 weeks	↔			
4 weeks	Every other day	-	Adult ♂ LE	-	NOR 24 hour ITI	-	↑	-	-	(Hopkins et al., 2011)
						2 weeks	↔			
			Adolescent ♂ LE	-	NOR 24 hour ITI	-	↑			
						2 weeks	↑			
						4 weeks	↑			
6 weeks	Free	100g	♂ Wistar	-	RAWM	-	↑	BDNF in HIPP	↑	(Alomari et al., 2013)
6 weeks	Free	-	♂ and ♀ Wistar	Individual	MWM	-	↑	BDNF in HIPP	↑	(Uysal et al., 2015)

Table 5.2: Summary of forced exercise study outcomes in healthy rodents. m/min: meters/minute, ♂: male, ♀: female, SD: Sprague Dawley, RLC: reverse light cycle, RAWM: radial arm water maze, MWM: Morris water maze, BrdU: Bromodeoxyuridine, HIPP: hippocampus, BDNF: brain derived neurotrophic factor, TrkB: Tropomyosin receptor kinase B. ↑ = improvement compared to control animals, ↔ = no change compared to control.

Type	Duration	Frequency	Intensity	Model	Housing	Behaviour	Delay?	Effect	Brain changes	Effect	Ref
Automated running wheel	5 days	30 min/day	7m/min	♂ Wistar	-	T-maze	6 weeks	↔	BrdU on run days	↔	(Acevedo-Triana et al., 2017)
Swimming	4 weeks	6 days/week	60 minutes	♂ ICR	-	RAWM	4 weeks	↔	BrdU for 8 weeks	↔	(Kim et al., 2013)
									BDNF in HIPP	↔	
Treadmill	6 weeks	Daily	30 minutes 8m/min	Adolescent ♂ SD	-	RAWM	-	↑	BrdU on run days	↑	(Jin et al., 2017)
									BDNF and TrkB in HIPP	↑	
				Adult ♂ SD	-	RAWM	-	↔	BrdU on run days	↑	
									BDNF and TrkB in HIPP	↑	
Treadmill	6 weeks	5 days/week	30 minutes 8m/min	♂ and ♀ Wistar	Individual	MWM	-	↑	BDNF in HIPP	↑	(Uysal et al., 2015)
Swimming	6 weeks	5 days/week	60 minutes (5 swim/5 rest)	♂ Wistar	-	RAWM	-	↑	BDNF in HIPP	↑	(Alomari et al., 2013)
Swimming	8 weeks	6 days/week	60 minutes	♂ ICR	-	RAWM	-	↑	BrdU for 8 weeks	↑	(Kim et al., 2013)
									BDNF in HIPP	↑	
Group treadmill	24 weeks	3 days/week	60 minutes 4m/min	♂ Wistar	RLC	RAWM	-	↑	-	-	(Pietrelli et al., 2012)

5.1.3 A focus on adult neurogenesis and BDNF

Given the finding that forced and voluntary exercise can increase BDNF and markers of neurogenesis (predominantly bromodeoxyuridine (BrdU)) in the hippocampus, the consequences of neurogenesis will be discussed in more detail.

Neurogenesis in the adult rodent hippocampus occurs in the subgranular zone of the dentate gyrus (Seri et al., 2001). Once generated, the neurons migrate and differentiate into granule cells of the hippocampal granule cell layer, which incorporate into existing networks (Gonçalves et al., 2016). Initially, these neurons are synaptically silent, expressing N-methyl-D-aspartate receptor (NMDAr) without α-amino-3-hydroxy-5-methyl-4-isoxazolepropionic acid receptor (AMPAr). Then, slow γ-Aminobutyric acid (GABA) synapses form in the second week after neurogenesis. In the fourth week, glutamatergic synapses facilitate the maturation of the newly formed granule cell excitatory signals. Finally, the month-old neuron responds to fast GABAergic input (Espósito et al., 2005). Slice recordings show that PVIs are recruited by mature granule cells, which signal onto immature granule cells, integrating the neuron into the network (Alvarez et al., 2016) (see Figure 5.1).

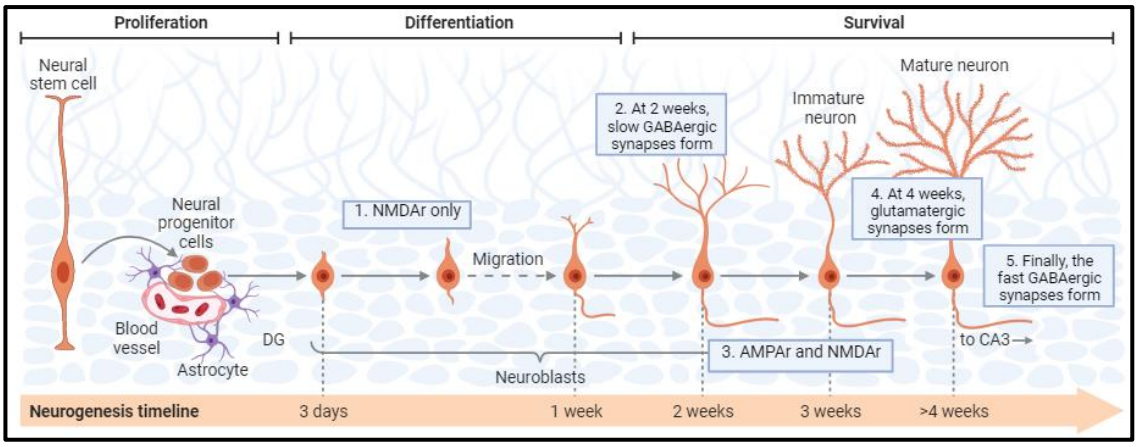

Figure 5.1: Diagram showing adult neurogenesis in the hippocampal subventricular zone. A neural stem cell proliferates in the subventricular zone and then migrates from the dentate gyrus (DG) to the CA3. During this time, the neuroblast matures in response to GABAergic and glutamatergic input. Diagram derived from a biorender.com template (Adapted from Chancey et al., 2013, Espósito et al., 2005, Ge et al., 2007).

In the first four to six weeks of life, the newly formed adult cells have unique electrophysiological properties, with enhanced long-term potentiation (LTP) facilitated by a reduced induction threshold, which is predominantly mediated by NMDAr subunit 2B (NR2B) (Ge et al., 2007). Interestingly, environmental enrichment independent of

wheel running increases the number of newly born neurons and the speed of silent synapses becoming active (Chancey et al., 2013).

The regulation of adult neurogenesis is multifaceted. Neurotransmitters, cytokines, growth factors, and epigenetic regulators can all alter neurogenesis rates (Fares et al., 2019). One such mediator is the neurotrophin BDNF. BDNF is synthesised as proBDNF, which can regulate long-term depression (LTD) by facilitating the NMDAr-induced endocytosis of AMPAr (Mizui et al., 2015). Once mature, BDNF binds to soluble tropomyosin-related kinase B (TrkB) receptors, which triggers homodimerization and phosphorylation of the complex. This complex binds to the cellular membrane, initiating a host of intracellular mechanisms that regulate neuronal and glial cell development, protection and survival. BDNF can also moderate synaptic plasticity, protein synthesis, dendritic growth, NMDAr-dependent synaptic modulation and LTP (Di Carlo et al., 2019, Kowiański et al., 2018, Leal et al., 2014). It has been speculated that a lack of proBDNF to mature BDNF conversion may contribute to schizophrenia pathology (Wang et al., 2021).

There is evidence of BDNF impairment in schizophrenia. The Val66Met mutation, which reduces BDNF secretion (Rogaeva et al., 2016), is associated with increased schizophrenia risk. Individuals with this mutation can have poor disease presentation, reduced age of onset, altered drug response and more significant cognitive impairments. Indeed, the mutation can cause cognitive impairment in healthy individuals (Beste et al., 2011, Richter-Schmidinger et al., 2011). However, the exact effect of schizophrenia on BDNF levels is controversial. For example, some studies show decreases in BDNF messenger ribose nucleic acid (mRNA) and protein (Issa et al., 2010, Thompson Ray et al., 2011, Weickert et al., 2003), whereas others find increases in BDNF mRNA in the hippocampus (Takahashi et al., 2000) or BDNF staining intensity in the CA2-4 regions of the hippocampus (Iritani et al., 2003).

Tables 5.1 and 5.2 show that exercise can increase BDNF levels in the hippocampus in animal studies. Interestingly, a comparative study by Uysal et al. found increased levels of BDNF in the hippocampus of voluntarily exercised rats compared to forced animals (Uysal et al., 2015). Perhaps the increased stress response during forced exercise (Moraska et al., 2000) downregulated BDNF expression (Notaras et al., 2020), suggesting a delicate balance is required. Finally, although limited to plasma data, clinical studies

indicate that BDNF is very responsive to changes in activity level, with immediate increases in BDNF after high-intensity exercise (Azevedo et al., 2022, Tsai et al., 2021, Walsh, 2018), which rapidly normalises 30 minutes after exercise conclusion (Reycraft et al., 2020).

5.1.4 Aims

4. Establish if there is evidence of altered BDNF or TrkB in scPCP-treated animals.
5. Determine the cognitive and molecular outcomes after acute and chronic exercise to understand how and when changes occur.
6. Investigate whether exercise is having any effects on the proposed scPCP mechanisms.

5.2 Methods

5.2.1 qPCR

The animals used for the study were the same animals used for qPCR analysis in the characterisation chapter. See section 3.2.2 for information on tissue processing. In brief, animals were taken twenty-two weeks after scPCP dosing in behaviourally assessed animals. In addition to previously discussed targets, we measured BDNF and its receptor TrkB in the prefrontal cortex (PFC) and dorsal hippocampus (DH) samples. Samples were diluted to 1:50 in the PFC and 1:100 in the DH.

5.2.2 Animal cohorts for the exercise study

Eighty female Lister hooded rats were housed and dosed as described in section 2.1. After one week of acclimatisation, cages were randomly assigned to receive sub-chronic vehicle dosing or phencyclidine for one week, as described in section 2.2. Rats then underwent a one-week washout, during which minimal handling occurred.

5.2.3 Novel object recognition

After the washout week, rats were habituated and tested in the novel object recognition (NOR) test described in section 2.3. The novel object and its location were randomised across groups in NOR tests.

5.2.4 Wheel running

5.2.4.a Apparatus

The interior floor of the double-decker cages was removed to accommodate the 30cm plastic running wheel (Pets at Home, UK). The distance travelled was measured using an odometer (Decathlon, UK). During the wheel running, rats had access to food and water.

5.2.4.b Wheel running and habituation

The protocol for the exercise has been previously published (Gonzalez et al., 2017, Mitsadali et al., 2020). Cages of animals were randomly assigned to either exercise or sedentary groups. The exercise group were allowed free access to the running wheel for one hour daily. The sedentary group were placed in the same cages, although the wheels were locked. As there is evidence that the time of day can affect the effects exercise has (Holmes et al., 2004), we ran the habituation and wheel running protocol at the same time for habituation and testing. Due to the number of wheels, cages were split into three cohorts, and these cohorts were rotated.

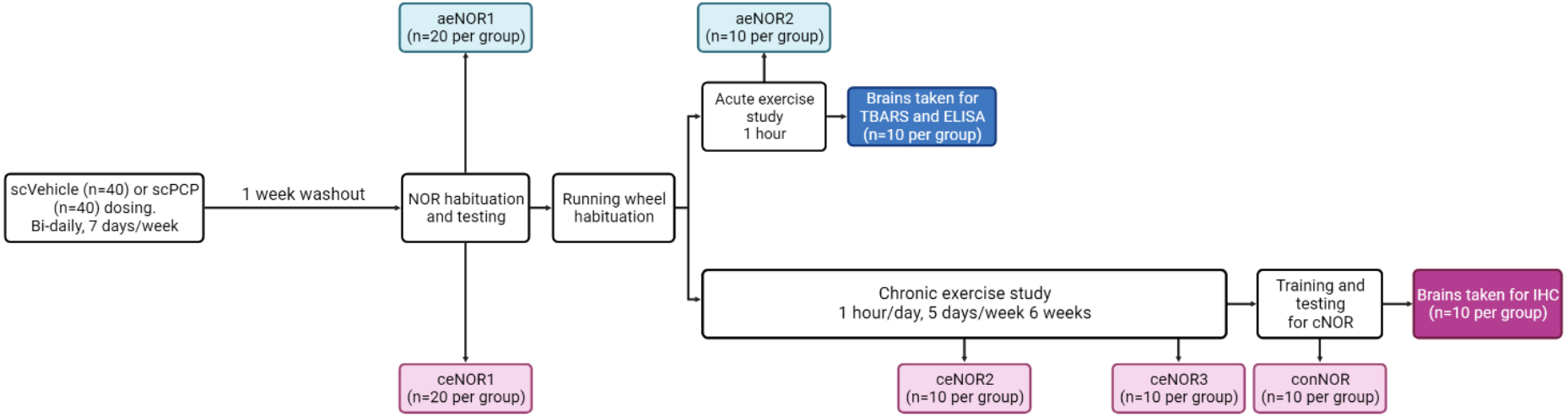

Figure 5.2: Study design for acute and chronic exercise protocols. Animals were dosed with scVehicle or scPCP twice daily for seven days, then underwent a one-week washout. Animals were habituated and tested using the novel object recognition (NOR) test. Exercised animals were habituated to the running wheels. For acute exercise animals, animals were allowed free access to a running wheel for one hour and tested in the NOR test immediately after exercise exposure, and then brains were taken. In the chronic exercise study, exercised animals were allowed access to the running wheels one hour/day, five days/week for six weeks. The sedentary animals were placed in the same cages with locked wheels. At the midpoint of exercise and the conclusion, rats were tested for cognition using the NOR test. This was done 24 hours after the final exercise bout. Animals were then habituated to the continuous NOR test (conNOR). The brains were perfused for immunohistochemistry. ae = acute exercise, ce = chronic exercise, ELISA = enzyme-linked immunosorbent assay, NOR = novel object recognition, TBARS = Thiobarbituric acid reactive substances, IHC = immunohistochemistry.

In both acute and chronic exercise studies, the experimental cohorts are identified by the following acronyms: scVeh + exercise cohort (V/E), scVeh + sedentary cohort (V/S), scPCP + exercise cohort (P/E) and scPCP + sedentary cohort (V/S).

5.2.5 Acute exercise study design

Forty female Lister hooded rats (222.4 ± 23.4 g, mean ± SD at the start of dosing) were used for this study (weight changes are detailed in the supplementary material 8.3.1). The rats underwent testing after the initial NOR test and wheel running habituation. Testing for sedentary and running animals was held on two consecutive days, with the sedentary cohort tested and culled first (day six after washout week) and the running cohort tested and culled on the subsequent day (day seven post washout week). Splitting the days into sedentary and running was a practical choice, as switching between locked and unlocked wheels would introduce varied delays.

On the day of testing, rats were moved into cages with either a locked or unlocked running wheel for one hour. After this hour, rats were transferred into the NOR testing room. Rats were culled fifteen minutes after removal from the wheel cage by carbon dioxide asphyxiation. Brains were harvested and stored on dry ice until long-term storage at -80°C. For a full experimental timeline, see Figure 5.2.

5.2.5.a Molecular analysis

Brains were collected, and the prefrontal cortex (PFC), dorsal hippocampus (DH) and ventral hippocampus (VH) were dissected. The regions were homogenised and prepared (2.6.1 and 2.6.2).

a. i) BDNF ELISA

The ELISA was optimised as described in 2.6.4 using EKU02787 from Biomatik. Samples were diluted to 2.5 mg/mL protein. Due to constrained well numbers, only nine samples from the ventral hippocampus were selected from each group. An 8-point, 2-fold standard curve was created (31.25 – 1000 pg/mL), including a diluent-only control. The standards and samples were pipetted into the pre-coated 96-well plate and incubated for 1 hour at 37°C. The samples were removed from each well without washing. Next, detection reagent A was pipetted into the plate and incubated for one hour at 37°C. The samples were washed eight times with wash buffer, and the remaining wash solution was removed from the plate by inverting the plate onto absorbent paper. Then, detection reagent B was added and incubated for 30 minutes at 37°C. The wash step

was repeated. Finally, the substrate solution was added and developed in the dark. Once the stop solution was added, the plate was read on a microplate reader at 450 nm. The standard curve was calculated using a 4-PL model (p = 0.997). One sample from the V/S group could not be interpolated from the standard curve as the absorbance was greater than the top standard.

a. ii) TBARS assay

We used the thiobarbituric acid reactive substances (TBARS) assay (DTBA-100, BioAssaySystems, USA) to measure lipid peroxidation. A 6-point standard curve was created (1.5, 0.9, 0.45, 0.2, 0.1, 0µM malondialdehyde (MDA)). Given the required input volume and protein concentration, we could only test the VH. Samples were diluted to 4 mg/mL. Thiobarbituric acid (TBA) reagent was added to samples at a 1:1 dilution, briefly vortexed, and then incubated at 100°C for 60 minutes. Samples were cooled on ice for 10 minutes, vortexed and briefly centrifuged. Samples were loaded into a black flat-bottom 96-well plate. The plate was read at 530nm excitation and 550nm emission. A standard curve was calculated using linear regression (R^2 = 0.998, y = 158966x + 424.7)

The concentration of MDA was calculated using the following equation where F is the fluorescent readout for the sample or the blank (0µM):

$$\text{TBARS} = \frac{F_{sample} - F_{blank}}{\text{the slope of the standard curve}}$$

5.2.6 Chronic exercise study design

Forty female Lister hooded rats (236.4 ± 20.5g (mean ± standard deviation)) were housed and dosed as described in sections 2.1 and 2.2 (weight changes are detailed in the supplementary material 8.4.1). During the middle third of the active or dark cycle, rats are the most active, and exercise-induced adult neurogenesis peaks (Boakes et al., 2021, Burghardt et al., 2004, Holmes et al., 2004). As such, we chose to reverse the animals' light cycle, with lights off at 07:00 (12:12 light cycle).

After initial NOR testing and wheel habituation (habituation distance ran provided in the supplementary material 8.4.2), exercised animals were given free access to the running wheel for one hour per day, five days per week, for six weeks. Sedentary animals were placed in the same cages but with locked wheels. For the complete experimental timeline, see Figure 5.2.

Cognition in the animals was reassessed at the midpoint and conclusion of the exercise protocol. The NOR test was carried out twenty-four hours after the last exercise bout. We tested the animals in the middle third of the dark cycle. Animals were transported to the testing arena on trolleys covered by a light-safe blanket and remained covered until the testing time to minimise time spent in the erroneous light stage.

5.2.6.a Continuous NOR

a. i) Rationale

The working memory capacity is limited by inhibitory control, which is the ability to ignore irrelevant stimuli (Tiego et al., 2018). During the standard NOR, the animal is removed from the testing arena. However, when the animal is left undisturbed, and the objects are swapped while the animal is in the box, scPCP-treated rats can differentiate between familiar and novel objects (Grayson et al., 2014). This finding indicates that scPCP does not impair memory formation but may limit inhibitory control. In this case, removal from the box is sufficiently distracting to overload the working memory capacity. To test this, we used a continuous NOR paradigm. Here the rats are trained to shuttle between the testing and holding arena, minimising and standardising the distraction levels between multiple NOR trials.

a. ii) Apparatus

The dimensions and walls of the conNOR testing arena are identical to the standard NOR arena (50x50x50cm). However, in the conNOR arena, the floor is a metal grate. Additionally, a clear Perspex lid is fixed to the box. An automated door connects the holding arena (23x36x50cm) to the testing arena. The objects were placed in the back corners of the testing arena, 10 cm away from each wall. Both arenas contained a pellet dispenser (see Figure 5.3). ABET II software controlled the gate, dispensers and overhead camera (Campden Instruments Ltd, UK).

a. iii) Study design

Due to the observation that the pro-cognitive effects of exercise decline as early as two weeks after exercise cessation (Acevedo-Triana et al., 2017, Berchtold et al., 2010, Hopkins et al., 2010, Hopkins et al., 2011, Kim et al., 2013), we habituated and tested all animals for the continuous NOR in the 15 days after exercise cessation. We were limited to one conNOR box, so we could not test all animals in the middle third of the light cycle. conNOR testing was held from 9:00 – 14:30, and animals were culled from 14:30 – 17:00, in the same running order as the conNOR testing. Due to practical limitations, one cage

of sedentary scPCP-treated animals was culled the day after conNOR testing. Details on the testing and cull days since exercise are found in the supplementary material (8.4.3).

a. iv) Habituation

For 72 hours before training and during habituation and testing, rats were food-restricted (12g/rat/day) and maintained >90% free-feeding weight. For habituation and testing, care was taken to only move the rat in or out of the holding arena cage. Habituation comprised four stages; each was 20 minutes in duration. Rats were habituated to the arena in groups, then individually in the first and second stages. The connecting gate was raised during both habituation stages allowing free movement between the holding and testing arena. Additionally, the dispensers released pellets every 60 seconds. Animals proceeded to the next habituation stage when they actively explored the testing and holding chambers.

Animals were then trained to shuttle between the arenas. Rats were placed in the holding arena, and on taking a food pellet, the gate would open, and a food pellet would be dispensed in the testing arena. The gate would close when the rat travelled through and only reopen when the food pellet was taken from the experimental arena. After a delay, the gate would reopen, and a pellet would dispense in the holding arena. This would continue until the termination of the timer. Rats would proceed to the final habituation stage when they shuttled quickly between the chambers at least eighteen times during the 20-minute habituation.

In the final habituation stage, rats were placed in the holding arena, and the gate opened once they had taken a pellet. They were then allowed to explore two identical objects for five minutes in the experimental arena. At the conclusion, the gate reopened, and a pellet was dispensed in the holding chamber. Next, the rat entered the holding chamber, triggering the gate to close for a 1-minute intertrial interval (ITI). During this time, the objects were replaced with identical novel objects, and the gate opened at the ITI. Rats would then explore these objects for 5 minutes. If the rat failed to enter the testing chamber within 3 minutes at the start or after the ITI or did not explore the objects for more than 20 seconds, they returned to the third habituation phase.

a. v) Testing

Animals were placed into the holding arena; on taking the food pellet, a 1-minute ITI commenced. Only the consumption of this first pellet was required for advancement to

the next stage; subsequent timings depended on the rat shuttling between the arenas. The gate opened at the end of the ITI and would close as the rat shuttled through the gate, starting the 3-minute exploration timer. The experimental chamber contained two identical objects. Rats were allowed to explore these objects freely. At the end of the 3 minutes, the gate would reopen, and on shuttling through, the gate closed, and the 1-minute ITI timer commenced. The objects would be exchanged for a novel and familiar object. This process continued for twelve retention trials. Two running orders of the object were selected; the objects were of similar size but varied in shape, material, and colour; the running orders aimed to distribute these differences throughout the test.

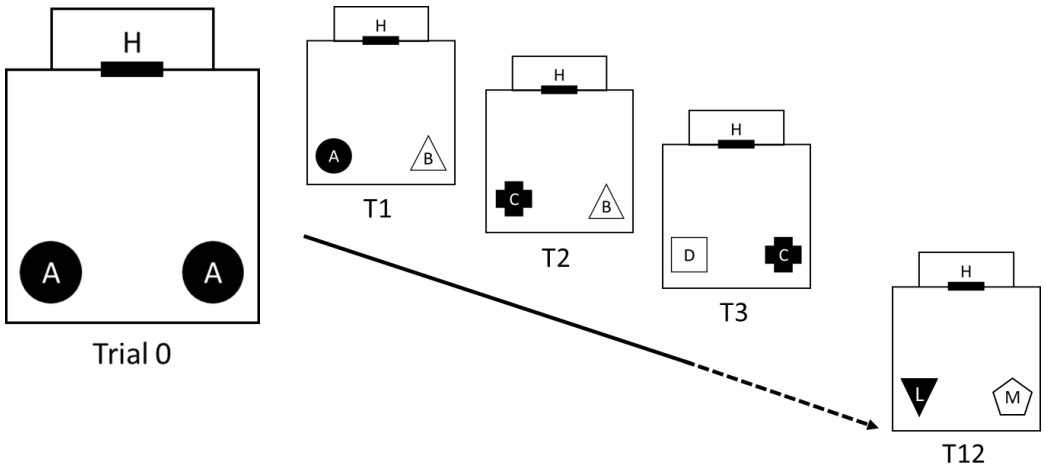

Figure 5.3: conNOR testing arena and experimental design. The trial 0 box shows the testing arena with two identical objects. An automated door connects the holding (H) arena to the testing arena. The remaining trials (T) show the progression of the novel objects.

a. vi) Scoring

Each trial was saved as a separate file. Files were given randomised numerical codes and scored in ascending order. Exploration time was calculated using the NOR timer (accessed: jackrrivers.com/program/). Finally, a rolling average of DI was calculated by averaging the DI for the trial and the four previous trials.

$$\text{Rolling average}_{(Tn)} = \frac{DI_{(Tn-4)} + DI_{(Tn-3)} + DI_{(Tn-2)} + DI_{(Tn-1)} + DI_{(Tn)}}{5}$$

Due to the novelty of this test, we found that some objects or object pairings were not optimal and resulted in minimal or excessive exploration. Therefore, together with other users, we developed an exclusion criterion for object pairings that was retroactively applied to our data set. These included trials where the exploration of both objects was

less than 5 seconds combined. In addition, objects were excluded when the DI in all treatment groups for a particular object pairing was less than zero, indicating a treatment- and intervention-independent object preference.

5.2.6.b Immunohistochemistry

Brains were processed and stained for parvalbumin, perineuronal nets and microglia, as described in section 2.8.

For the parvalbumin staining of the DH, we counted parvalbumin in sections taken from bregma -2.64 to -4.68mm. The DH was split into regions, CA1, CA2/3 and the dentate gyrus (DG) (Figure 5.4). Due to poor tissue quality, n=7 was the largest sample size of an equal number that could be achieved with the DH samples.

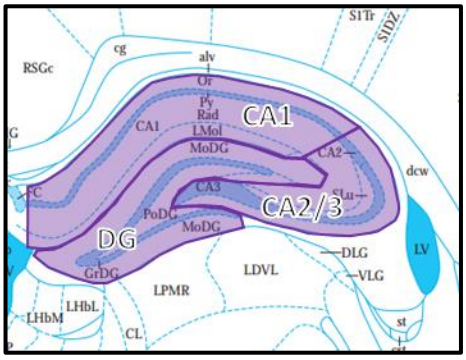

Figure 5.4: Regions of the dorsal hippocampus. CA1, CA2/3 and the hippocampus's dentate gyrus (DG) regions (Adapted from Paxinos et al., 2007).

In addition to calculating density, microglia were classified into different activation states based on their morphology. We based our classification on the work by Cotel et al. (Figure 5.5). Here, we characterised microglia as resting when they had processes originating from several locations around the cell body, and the processes were more than three times the length of the cell body. In periods of inflammation, microglia become activated, and their morphology changes in addition to their secreted factors and membrane-bound proteins (Kierdorf et al., 2013). Figure 5.5B shows the intermediate microglia, characterised by processes originating from a single peninsular. The processes are shorter and thicker, around one to three times the length of the cell body. Finally, there are ameboid microglia, with a distinct, enlarged cell body and minimal processes that were generally shorter than one length of the cell body.

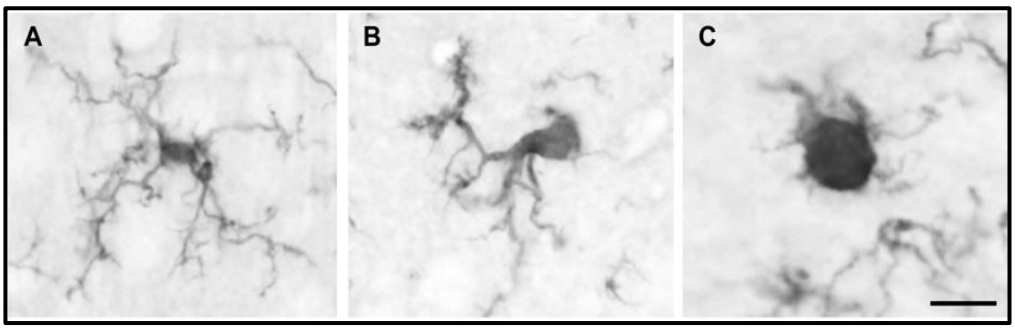

Figure 5.5: Representative image of microglia morphologies. A) resting, **B)** intermediate and **C)** ameboid microglia (taken from Cotel et al., 2015)

We attempted to stain for BDNF (28205-1-AP, Proteintech) and TrkB (Ab187041, Abcam, sc-377218, Santa Cruz, 13129-1-AP, Proteintech) in these tissues. However, we did not achieve a stain that could be analysed confidently.

5.2.7 Statistics

Purpose	Distribution	Test	Section
Check for normality	N/A	D'Agostino and Pearson (n>7) or Shapiro-Wilk (n≤7)	2.9.1
Check for correlations	Normal Not normal	Pearson's Spearman's	2.9.5
Compare several measures from one individual	Normal	Repeated-measures general linear model	2.9.7.b
Compare DI to a hypothetical mean of 0	Normal	One sample t-test	2.9.2
Compare two groups	Normal Not normal	Unpaired t-test Mann-Whitney U	2.9.3.a 2.9.3.b
Compare all groups	Normal Not normal	One way ANOVA Kruskal-Wallis H	2.9.4.a 2.9.4.b

5.3 Results

5.3.1 BDNF

We first wanted to establish if there was a change in BDNF in the scPCP-treated animals. Therefore, we measured BDNF and its receptor TrkB mRNA in the PFC and DH in the same brains used in the characterisation chapter. As a reminder, these animals were dosed with vehicle or scPCP 22 weeks before testing.

Here we found that there was a reduction in the BDNF mRNA in the PFC (Mann-Whitney U = 4.000, scVeh (V) = 7.520, scPCP (P) = 2.860, p = 0.007) (Figure 5.6A) and no change to PFC TrkB (t_{12} = 0.617, p = 0.549) (Figure 5.6B), DH BDNF (t_{12} = 1.472, p = 0.167) (Figure 5.6C) and DH TrkB (t_{12} = 1.190, p = 0.257) (Figure 5.6D).

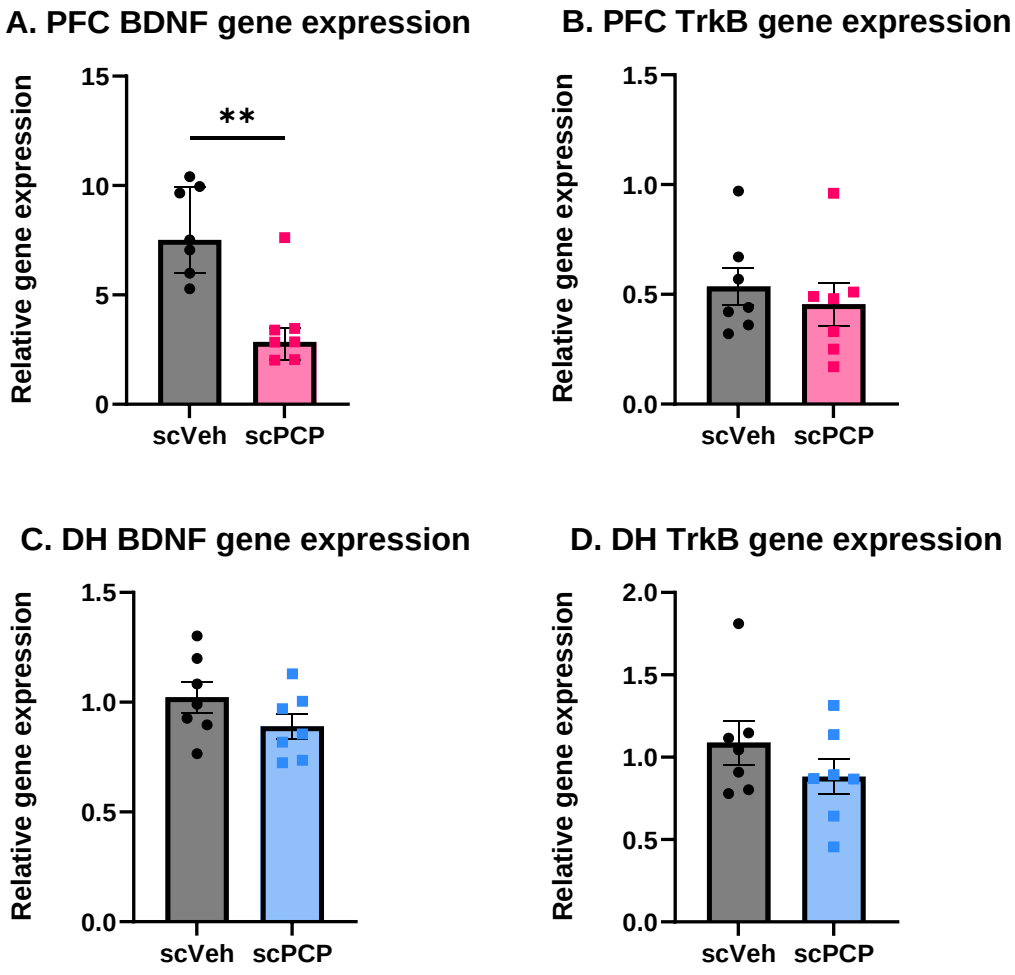

Figure 5.6: The effect of scPCP on BDNF and TrkB in the PFC and DH. Relative expression of PFC **A)** BDNF and **B)** TrkB and DH **C)** BDNF and **D)** TrkB, (n=7). Differences between groups in **A)** were analysed with a Mann-Whitney U test. The graph shows mean ± IQR. **B-D)** were analysed with an unpaired t-test, and graphs show mean ± SEM. **p<0.01.

5.3.2 Acute exercise study

5.3.2.a Baseline NOR

Before acute exercise intervention, we wished to confirm that scPCP dosing induced a cognitive deficit.

a. i) Acquisition trial

After the washout week from scVeh or scPCP dosing, animals were habituated and tested using the NOR task. In the acquisition trial, there were no significant within-subject effects of the object ($F_{1, 38} = 0.451$, $p = 0.504$) nor object*group interaction ($F_{1, 38} = 0.154$, $p = 0.696$), indicating that regardless of treatment group, there was no difference between time spent at left and right object (Figure 5.7A).

a. ii) Retention trial

In the retention trial, there was a significant within-subject effect of the object ($F_{1, 38} = 12.532$, $p = 0.001$). However, the treatment*object interaction was not significant ($F_{1, 38} = 1.242$, $p = 0.272$). These findings indicate that both scVeh- and scPCP-treated rats were spending more time at the novel object (Figure 5.7A).

a. iii) Discrimination index

We used the one-sample t-test to compare discrimination index (DI) values to a hypothetical value of 0. This analysis confirmed that scVeh animals were able to discriminate the novel from the familiar object ($t_{19} = 5.069$, $p<0.001$), whereas the scPCP groups were impaired in the NOR task ($t_{19} = 1.742$, $p = 0.098$).

In addition, we used an unpaired t-test to estimate the difference between groups. This analysis showed that scVeh animals had a significantly higher DI than scPCP-treated animals ($t_{38} = 2.121$, $p = 0.041$) (Figure 5.7B).

5.3.2.b Acute exercise

After running wheel habituation, exercise animals were given free access to a running wheel for one hour. There was considerable variation in the running distance on the habituation and testing days. To ensure the treatment did not significantly affect running distance, we performed a repeated-measures general linear model (GLM), where time was the within-subjects factor and treatment was the between-subjects factor. Mauchly's test indicated sphericity ($\chi^2(5) = 19.224$, $p = 0.002$. As the estimated epsilon value was less than 0.75 ($\varepsilon = 0.589$), we used the Greenhouse-Geisser correction to mitigate the effect of unequal variances.

The experimental day had a significant within-subjects effect on the distance travelled ($F_{3, 1.766} = 4.269$, $p = 0.027$), whereas the day*treatment interaction was insignificant ($F_{3, 1.215} = 1.215$, $p = 0.306$). There was no effect of the between-subjects effect of treatment ($F_{1, 18} = 0.612$, $p = 0.444$). These results show that although there was a significant difference between the distance run across the habituation and testing days, there was no difference between scVeh and scPCP running distance (Figure 5.7C).

5.3.2.c Effects of acute exercise on NOR

Immediately after the conclusion of exercise or sedentary protocols, rats were tested again using the NOR test to assess if acute exercise had improved cognition in the scVeh or scPCP groups.

c. i) Acquisition trial

For the acquisition trial, there were no within-subject effects of the object ($F_{1, 36} = 0.103$, $p = 0.750$), object*treatment ($F_{1, 36} = 0.010$, $p = 0.921$), object*exercise ($F_{1, 36} = 0.365$, $p = 0.549$), and object*treatment*exercises ($F_{1, 36} = 0.000$, $p = 0.993$) interactions. However, treatment significantly affected exploration time in the acquisition trial ($F_{1, 36} = 4.337$, $p = 0.044$). This was due to a significant increase in the time scPCP animals spent exploring the identical objects (scVeh (V): 12.69 ± 0.88, scPCP (P): 15.28 ± 0.88, $p = 0.044$) (Figure 5.7D).

c. ii) Retention trial

There was a significant effect of the object in the retention trial ($F_{1, 36} = 54.870$, $p<0.001$) and the object*treatment interaction ($F_{1, 36} = 6.832$, $p = 0.013$). The remaining object interactions, object*exercise ($F_{1, 36} = 1.874$, $p = 0.180$) and object*treatment*exercise ($F_{1, 36} = 1.291$, $p = 0.264$) were insignificant. These data suggest a significant difference between the time spent between the objects in the scVeh or the scPCP group, but no effect of exercise. Regarding the significant object*treatment interaction, we used post hoc comparisons to explore the simple main effect of treatment. This analysis showed that both treatments were able to discriminate between familiar and novel objects (V/familiar (F): 7.93 ± 2.99, V/novel (N): 15.68 ± 5.70, $p<0.001$; P/F: 10.62 ± 4.56, P/N: 14.23 ± 5.40, $p = 0.002$) (Figure 5.7D).

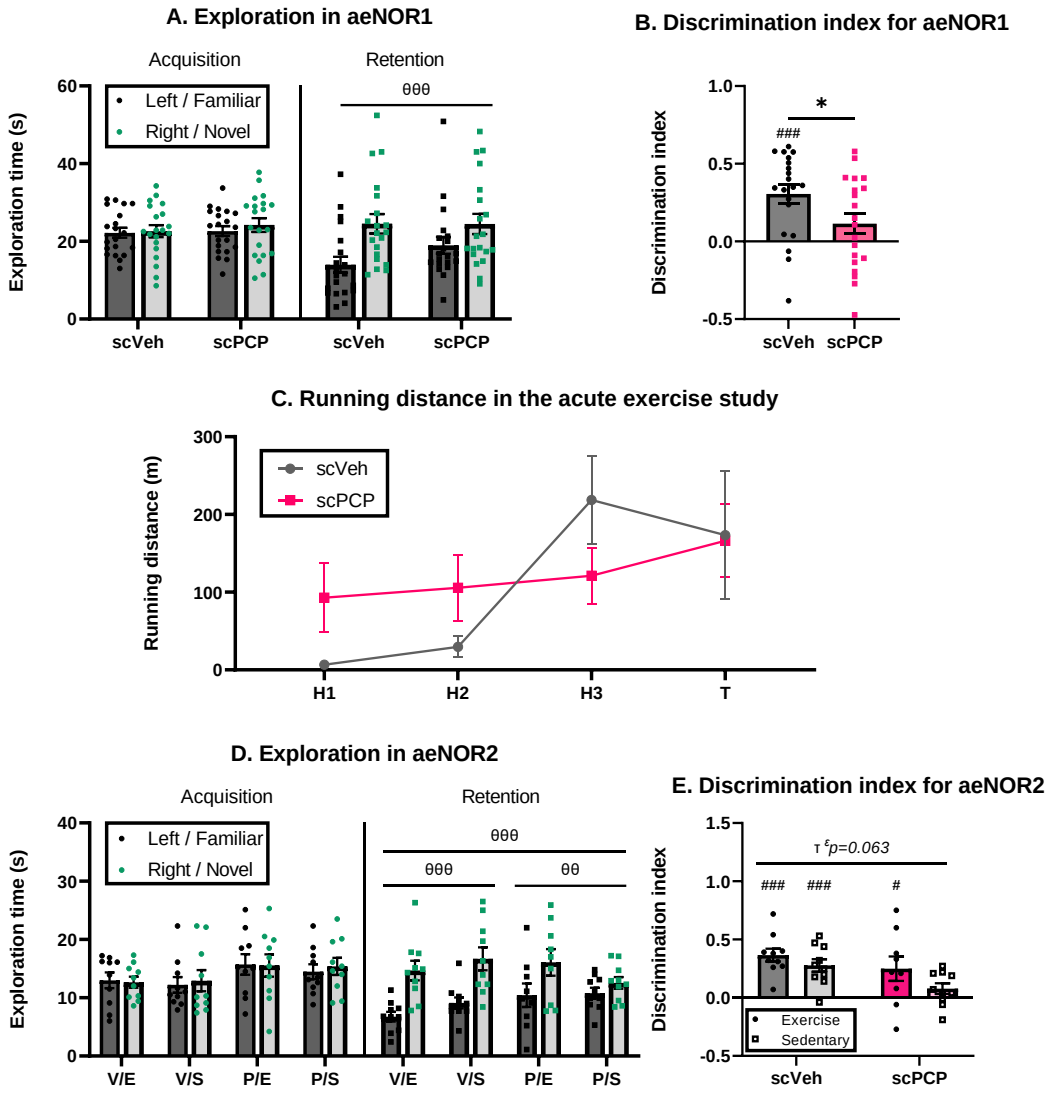

Figure 5.7: Acute exercise behavioural data. Time spent exploring two identical objects in the acquisition trial and familiar and novel objects in the retention trial of the NOR task following **A)** treatment with scVeh or scPCP or **D)** acute exercise (V/E: scVeh + exercise, V/S: scVeh + sedentary, P/E: scPCP + exercise, P/S: scPCP + sedentary). Object differences were analysed with a repeated-measures general linear model (GLM). The difference between the estimated marginal means for each object was analysed using a pairwise comparison with Šidák's correction. $^{\theta}$=difference between objects, $^{\theta\theta}$p<0.01, $^{\theta\theta\theta}$p<0.001. The discrimination index for scVeh- and scPCP-treated animals **B)** before and **E)** after acute exercise. A one-sample t-test was used to compare the mean DI for each group to a hypothetical mean of 0. $^{\#}$=difference from a hypothetical mean of 0, $^{\#}$p<0.05, $^{\#\#\#}$p<0.001. For **B)**, an unpaired t-test was used to compare treatment groups. *=difference between groups, *p<0.05. Finally, **C)** Average running distance in the acute exercise study. H: habituation days (1 – 3). T: testing day. Data were analysed with a repeated-measures GLM. All graphs show mean ± SEM. **A + B)** n = 20, **C - E)** n = 10.

c. iii) Discrimination index

Using a one-sample t-test revealed there was a significant difference between V/E (p<0.001), V/S (p<0.001), P/E (p = 0.047) and a hypothetical mean of zero, indicating that

all these groups performed significantly better than random chance. However, in the P/S group, there was no difference, indicating a cognitive deficit (p = 0.108).

Comparing the DI means for each group using a univariate GLM revealed a significant effect of treatment ($F_{1, 38}$ = 5.630, p = 0.023) and a near-significant effect of exercise ($F_{1, 38}$ = 3.700, p = 0.063). A greater DI drove the treatment effect in the scVeh cohort (V: 0.323 ± 0.173, P: 0.160 ± 0.251, p = 0.023). Although insignificant, the trend towards an effect of exercise was driven by a greater DI of the exercise cohort (E: 0.312 ± 0.252, S: 0.180 ± 0.185). (Figure 5.7E).

5.3.2.d Post-mortem analysis

d. i) BDNF ELISA

To investigate the concentration of BDNF in the brain homogenates, we used an ELISA. We measured changes in the PFC, DH and VH regions. We used a repeated-measures GLM, where the region was used as the repeated measure and treatment and exercise were between-measures factors. Mauchly's test indicated there was a difference in variation ($\chi^2(2)$ = 16.044, p<0.001, as the estimated epsilon value was greater than 0.75 (ε = 0.815), we used the Huynh-Feldt correction.

There was a significant difference between the BDNF concentrations in each region ($F_{1.63, 57.05}$ = 62.529, p<0.001). Interestingly, a significant region*treatment interaction (F1.63, 57.05 = 14.339, p<0.001) indicated a significant treatment effect in select regions. Simple main effect analysis revealed this difference was in the DH (V: 320.8 ± 32.6, P: 140.1 ± 31.7; p<0.001) and VH (V: 63.6 ± 11.7, P: 97.4 ± 11.4; p = 0.045), with no change in the PFC (p = 0.756).

Finally, there was a trend towards a significant region*treatment*exercise interaction ($F_{1.63, 57.05}$ = 3.161, p = 0.060). Exploratory post hoc testing revealed significant differences in BDNF levels in the DH, with exercise increasing BDNF concentration in the scPCP-treated animals between V/S and P/S (p<0.001) and P/E and P/S (p = 0.041). There were significant increases in BDNF concentration in the VH in the P/E group compared to the V/E group (p = 0.015).

For the between-subject effects, there was a significant effect of treatment ($F_{1, 35}$ = 5.781, p = 0.022) and treatment*exercise ($F_{1, 35}$ = 5.858, p = 0.021), whereas there was no effect of exercise alone ($F_{1, 35}$ = 0.259, p = 0.614). Indeed, looking at the mean BDNF

levels across all three regions measured revealed a significant reduction in scPCP-treated animals (V: 234.2 ± 13.8, P: 188.0 ± 13.4; p = 0.022). Regarding the significant interaction between treatment and exercise, there was only a significant treatment effect when analysing the sedentary animals (V/S: 252.6 ± 20.0, P/S: 159.8 ± 19.0; p = 0.002). Additionally, exercise increased the average BDNF concentration across the three regions in the scPCP-treated animals only (P/E: 216.2 ± 19.0, P/S: 159.8 ± 19.0; p = 0.043) (Figure 5.8A).

We were interested if there was any correlation between our behavioural and pathological outcomes. We found a correlation between post-exercise (aeNOR2) DI and BDNF in the DH (Spearman's correlation coefficient: 0.386, p = 0.014). We performed a linear regression on the complete data cohort and plotted the line to view the visual trend (R^2 = 0.118, p = 0.032) (Figure 5.8B).

d. ii) TBARS assay

Next, we looked if exercise altered oxidative stress markers in these animals. We chose to look at the TBARS assay. Unfortunately, we could only test the VH due to the high protein and volume input.

The results were promising; however, the data was highly variable, as in the MDA assay used in chapter 4. Indeed, we found that Levene's test of variances was significant ($L_{3, 36}$ = 4.211, p = 0.012). However, univariate GLMs are relatively robust to alterations in variance, particularly when group sizes are equal (Ananda et al., 1997). Exercise significantly affected MDA concentration ($F_{3, 36}$ = 5.390, p = 0.026), reducing concentration compared to sedentary controls (Ex: 1.018 ± 0.214, Sed: 1.906 ± 0.674). The remaining between-subject effects of treatment ($F_{1, 39}$ = 0.912, p = 0.346) and the treatment*exercise interaction ($F_{1, 39}$ = 1.450, p = 0.236) were insignificant (Figure 5.8C).

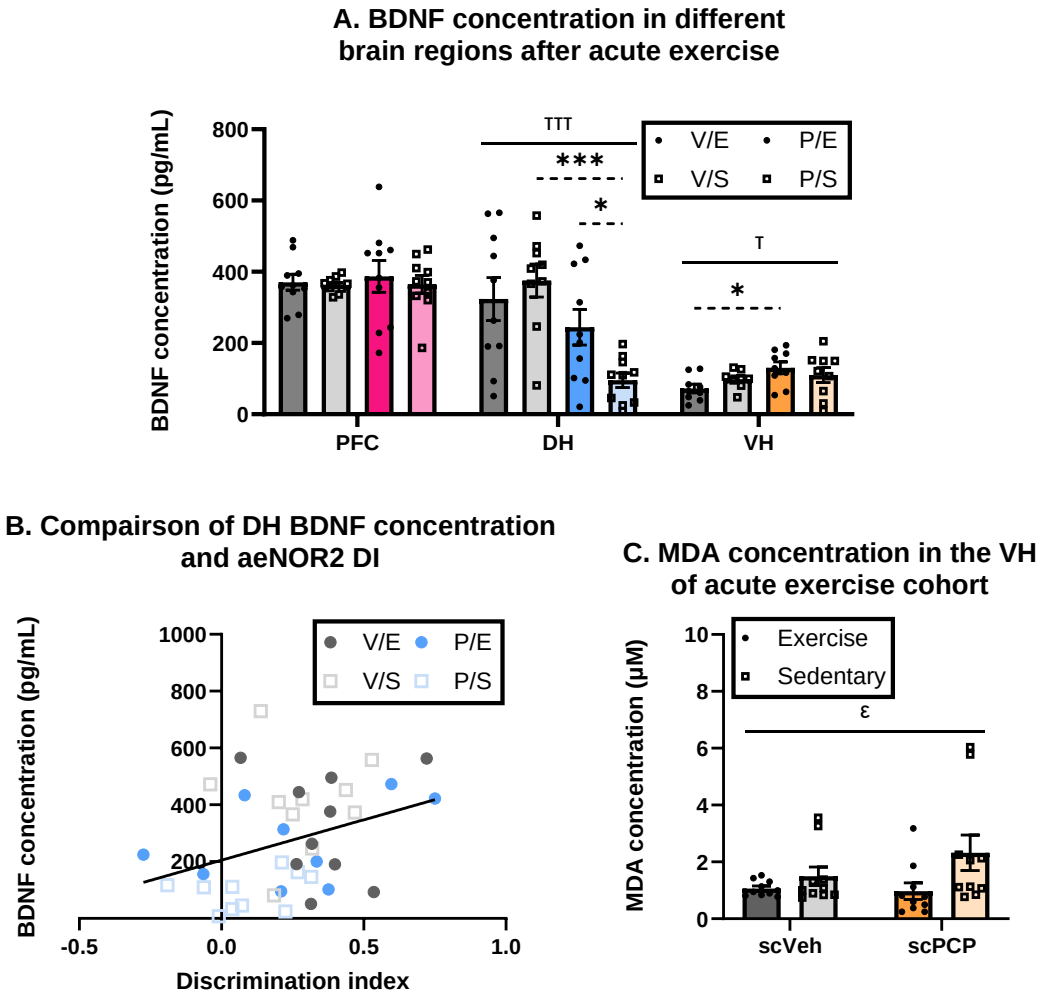

Figure 5.8: BDNF and MDA concentration in acute study rats. **A)** BDDF concentration of V/E, V/S, P/E and P/S groups in the PFC, DH and VH. Dashed comparison lines indicate pairwise testing from a trending interaction of a repeated-measures GLM. The difference between the estimated marginal means for each object was analysed using a pairwise comparison with Šidák's correction. ^{T}=effect of treatment, ^{T}p<0.05, ^{TTT}p<0.001. *=difference between groups, *p<0.05, ***p<0.001 (n=9-10). **B)** Correlation analysis of DH BDNF concentration and the NOR data from aeNOR2. The line is the linear regression of all DH data combined (y = 284.0x + 205.1) (n=8-10). **C)** MDA concentration was calculated with the TBARS assay (n=10). Differences between groups were assessed with a univariate GLM. The difference between the estimated marginal means for each object was analysed using a pairwise comparison with Šidák's correction. $^{\varepsilon}$=effect of exercise, $^{\varepsilon}$p<0.05. Graphs show mean ± SEM.

5.3.3 Chronic exercise study

5.3.3.a Standard NOR

a. i) ceNOR1

Before the exercise intervention, the chronic exercise cohort underwent NOR testing to assess cognition in the scVeh and the scPCP-treated animals. Although the animals are naïve to exercise, we will include exercise in our analysis to ensure there was no difference in the cohorts used.

In the initial NOR, there was no effect of the object in the acquisition task ($F_{1, 36}$ = 0.583, p = 0.450) or any interactions with treatment ($F_{1, 36}$ = 0.803, p = 0.376), exercise ($F_{1, 36}$ = 0.819, p = 0.372), or the object*treatment*exercise interaction ($F_{1, 36}$ = 0.59, p = 0.810). The lack of object effect indicates no difference between the time spent at the left or right object (Figure 5.9A).

In the retention trial, however, there was a significant effect of the object ($F_{1, 36}$ = 21.688, p<0.001), which was maintained in the object by treatment interaction ($F_{1, 36}$ = 20.644, p<0.001). To understand which treatment led to this object effect, we ran post hoc comparisons on the mean times spent at each object. Looking at the differences between scVeh- and scPCP-treated animals, we found a significant difference between the time spent at the familiar and novel objects in the scVeh-treated animals (p<0.001). In the scPCP-treated animals, there was no difference (p = 0.937), indicating impaired cognition in the scPCP group only.

Returning to the main within-subject effects, we found no significant effect of the object in its interaction with exercise ($F_{1, 36}$ = 0.123, p = 0.728) or the object*treatment*exercise interaction ($F_{1, 36}$ = 0.261, p = 0.612) (Figure 5.9A).

a. ii) ceNOR2

The second NOR task was held twenty-four hours after the 15th exercise bout, which was the midpoint of exercise. In the acquisition trial, there was no significant overall effect of the object ($F_{1, 36}$ = 1.480, p = 0.232), object*exercise ($F_{1, 36}$ = 0.969, p = 0.331) or object*treatment*exercise interactions ($F_{1, 36}$ = 0.154, p = 0.697). However, there was a significant object*treatment interaction ($F_{1, 36}$ = 6.543, p = 0.015). Post hoc testing revealed this was due to a difference in time spent at the left object in the scPCP-treated animals (p = 0.011), specifically in the P/S cohort (p = 0.036), which could indicate a place preference. The novel object was on the left-hand side for half of the retention trials, so

the data were split accordingly. We assessed whether the object preference in the P/S group was stronger when the novel object was on the left. Here we found no significant difference in the object preference for the retention trial ($F_{1, 8}$ = 0.005, p = 0.946) or the object*novel object location interaction ($F_{1, 8}$ = 1.849, p = 0.211), indicating no difference in the time spent at the novel object when it was on the left or the right hand side (Figure 5.9B).

In the retention trial, there was a significant effect of the object ($F_{1, 36}$ = 13.280, p<0.001) and the object*treatment interaction ($F_{1, 36}$ = 5.021, p = 0.031). There was no significant interaction for exercise ($F_{1, 36}$ = 0.563, p = 0.458) or the object*treatment*exercise interaction ($F_{1, 36}$ = 0.623, p = 0.435). These findings suggest a difference in the time spent at the objects in one of the treatment groups; however, exercise is not having an effect. Post hoc testing revealed that the scVeh-treated animals spent more time at the novel object (p = 0.025). The object had no effect in the scPCP-treated animals (p = 0.740) (Figure 5.9B).

a. iii) ceNOR3

After completing the six weeks of exercise, a final NOR test was held. In the acquisition trial of the third NOR, we found that there was a significant effect of the object ($F_{1, 36}$ = 4.760, p = 0.036), with none of the remaining object interactions being significant: treatment ($F_{1, 36}$ = 0.777, p = 0.384), exercise ($F_{1, 36}$ = 2.270, p = 0.141) and treatment*exercise ($F_{1, 36}$ = 0.871, p = 0.357). As the rats explored the left object more than the right (L: 14.0 ± 0.77, R: 12.5 ± 0.71), we studied the retention trials to ensure that this place preference was not affecting the outcomes. There were no significant interactions between the object and the side of the novel object (LvR) ($F_{1, 32}$ = 1.802, p = 0.189). In addition, the object*LvR*treatment ($F_{1, 32}$ = 0.352, p = 0.002), object*LvR*exercise ($F_{1, 32}$ = 1.238, p = 0.274) and the object*LvR*treatment*exercise ($F_{1, 32}$ = 3.649, p = 0.065) interactions were not significant, indicating the place preference did not affect the retention trial (Figure 5.9C).

In the retention trial, there was a significant effect of the object ($F_{1, 36}$ = 32.740, p<0.001) and the object*exercise interaction ($F_{1, 36}$ = 9.758, p = 0.004). Here the exercised animals were spending significantly more time at the novel object (F: 9.392 ± 0.890, N: 16.394 ± 1.192; p<0.001), whereas there was a trend in the sedentary animals (F: 10.242 ± 0.819, N: 12.299 ± 1.902; p = 0.061). There was no effect of the treatment ($F_{1, 36}$ = 1.144, p =

0.292) and a trend for the object*treatment*exercise interaction ($F_{1, 36}$ = 3.270, p = 0.079). Further investigations of the trend revealed there was a significant difference between time spent at the familiar and novel object in the V/E (p<0.001), V/S (p = 0.010), and P/E (p<0.001) cohorts. However, there was no difference in the P/S group (p = 0.890), suggesting that chronic exercise had attenuated the scPCP-induced behavioural deficits (Figure 5.9C).

a. iv) Discrimination index

The discrimination index can be helpful when investigating the longitudinal changes in NOR performance in the same cohort, as it scales all performances into the same range, allowing us to see if there were changes over time. There were no significant within-subjects effects of the trial ($F_{2, 72}$ = 0.305, p = 0.738), suggesting a high degree of variability in an individual's NOR performance across repeated measures. This was true in all the interactions: trial*treatment ($F_{2, 72}$ = 2.088, p = 0.131), trial*exercise ($F_{2, 72}$ = 2.436, p = 0.095) and trial*treatment*exercise interactions ($F_{2, 72}$ = 0.650, p = 0.525) (Figure 5.9D).

We also used a one-sample t-test to assess whether there was a significant difference between the DI and a hypothetical value of zero. The findings are summarised in Table 5.3.

Table 5.3: Summary of one sample t-tests for the chronic exercise NOR tests. t: t-test value, df: degrees of freedom, p: p-value

	ceNOR1			ceNOR2			ceNOR3		
	t	*df*	*p*	*t*	*df*	*p*	*t*	*df*	*p*
V/E	4.138	9	0.003	3.600	9	0.006	7.084	9	<0.001
V/S	5.427	9	<0.001	4.805	9	<0.001	3.248	9	0.010
P/E	-0.316	9	0.759	1.849	9	0.097	5.575	9	<0.001
P/S	0.527	9	0.611	-0.140	9	0.892	0.066	9	0.949

a. v) Chronic exercise

We collected the distance each rat had travelled at the end of each exercise session. First, we wanted to ensure there were no differences between the treatment groups. We found no effect of treatment ($F_{1, 19}$ = 0.328, p = 0.574) (Figure 5.9E). As there was a cognitive improvement in the last NOR test, we wanted to confirm that this was due to prolonged exercise exposure and not increased running activity in the latter half of the running protocol. A repeated-measures GLM found no difference between the first and

last half of the exercise averages ($F_{1, 18} = 0.377$, $p = 0.547$), nor was there an interaction between the study half and the treatment group ($F_{1, 18} = 1.798$, $p = 0.197$) (Figure 5.9F).

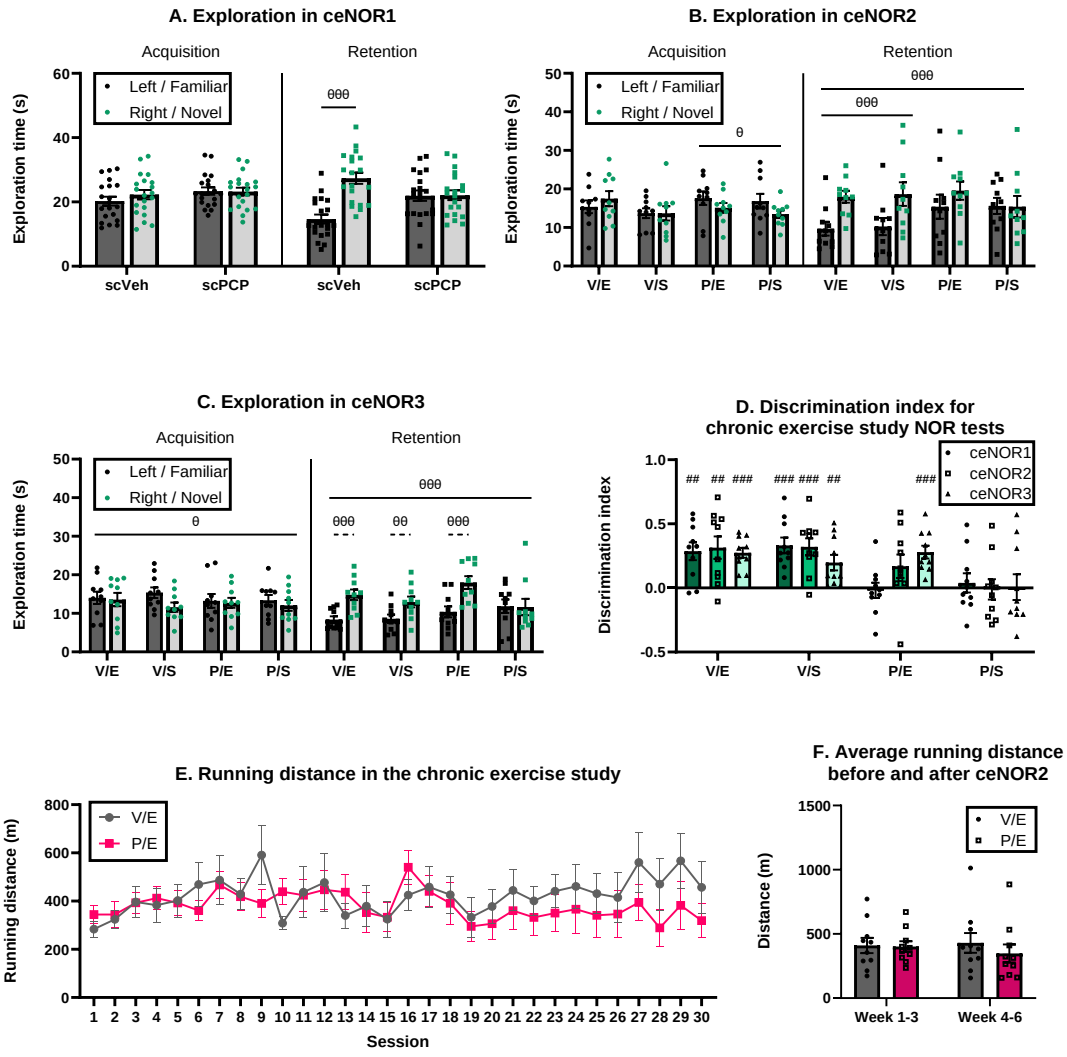

Figure 5.9: NOR data from the chronic exercise study. Exploration times in the acquisition and retention trials for **A)** ceNOR1 (n=20), **B)** ceNOR2 (n=10) and **C)** NOR3 (n=10). Differences between objects were calculated using a repeated-measures GLM. **D)** The discrimination index from the 3 NOR trials from the chronic NOR study. Differences from a hypothetical mean of 0 were calculated with a one-sample t-test (n=10). **E)** Average running distance of both treatments in the thirty exercise sessions that were one hour in duration and held for six weeks. Differences between groups were measured with a repeated-measures GLM (n=10). **F)** Average time each animal spent running in the first and last half of the exercise training. Differences were calculated using a repeated-measures GLM (n=10). Graphs show average ± SEM. $^{\theta}$= effect of object, $^{\theta}p<0.05$, $^{\theta\theta}p<0.01$, $^{\theta\theta\theta}p<0.001$. $^{\#}$= different from a hypothetical mean of zero, $^{\#\#}p<0.01$, $^{\#\#\#}p<0.001$. Dashed lines indicated post hoc analysis originating from a non-significant effect.

5.3.3.b Continuous NOR

After completing the final NOR task, animals were habituated and trained for the continuous NOR task. Unfortunately, some trials were missing videos due to initial issues with the software workflow.

b. i) First NOR trials

We were interested in the first acquisition and retention trial as we have shown in the standard NOR tasks that P/S rats cannot discriminate between familiar and novel objects (Figure 5.9). However, studies have shown that scPCP-treated animals can complete NOR when distraction is minimised (Grayson et al., 2014, Landreth et al., 2020).

In the acquisition trial, there was no effect of the object ($F_{1, 36} = 0.180$, $p = 0.674$), nor its interactions with treatment ($F_{1, 36} = 0.361$, $p = 0.552$), exercise ($F_{1, 36} = 0.452$, $p = 0.506$) or the object*treatment*exercise interaction ($F_{1, 36} = 0.156$, $p = 0.695$). Interestingly, exercise had a significant between-subject effect on the average exploration time ($F_{1, 36} = 9.391$, $p = 0.004$), with exercised animals exploring for less time (Ex: 11.65 ± 10.03, Sed: 17.92 ± 6.63) (Figure 5.10A).

In the retention trial, there was a significant effect of the object ($F_{1, 36} = 55.809$, $p<0.001$) and no effect of the interactions: treatment ($F_{1, 36} = 0.377$, $p = 0.543$), exercise ($F_{1, 36} = 0.264$, $p = 0.611$) and treatment*run ($F_{1, 36} = 0.374$, $p = 0.545$). In addition, there was no longer a between-subjects effect of exercise ($F_{1, 36} = 1.586$, $p = 0.216$). These results suggest a difference between the time spent at familiar and novel objects in all groups (Figure 5.10A).

b. ii) Discrimination index

Plotting the raw DI data for all assessed trials revealed that initially, all groups successfully discriminated between objects. However, from the fourth trial, there was a reduction in the non-exercised cohorts. We wished to assess whether there was a reduction in the DI from the initial trial to quantify the visual reduction. To do this, we used a repeated measures GLM. There were no significant within-subject effects, although the trial was nearing significance ($F_{9, 99} = 1.873$, $p = 0.065$), suggesting a trend towards DI changing across trials. Interestingly there was a significant between-subjects effect of treatment ($F_{1, 11} = 5.064$, $p = 0.046$) and exercise ($F_{1, 11} = 29.312$, $p<0.001$), though there was no significant interaction ($F_{1, 11} = 0.024$, $p = 0.880$). These between-

subject factors are the overall average for the ten trials, indicating a significant effect of both exercise and treatment on the overall average performance.

As we were interested in the long-term changes in performance from the initial trial, where every group could discriminate, we looked at post hoc comparisons for each group compared to their first trial. Here we found minimal significant data. Only P/S groups showed a significant difference from the first trial on trial nine ($p = 0.012$) and a trend on trial eight ($p = 0.068$) (Figure 5.10B).

These changes were not as profound as we expected and were likely due to the high degree of variation, partly due to the two different running orders we selected. We chose, therefore, to do a rolling average of the DI to try and reduce the data noise and give a better idea of the overall trends. We used the same repeated-measures GLM, which found there was a significant difference in the variance of the groups ($\chi^2(44) = 271.983$, $p<0.001$), as the estimated epsilon value was less than 0.75 ($\varepsilon = 0.400$), we used the Greenhouse-Geisser correction to mitigate the effect of unequal variances. We found a significant effect of the trial ($F_{3.60, 115.30} = 9.425$, $p<0.001$). There was also a significant interaction between trial*exercise ($F_{3.60, 115.30} = 6.935$, $p<0.001$). There was no effect of the trial*treatment ($F_{3.60, 115.30} = 0.336$, $p = 0.834$) and the trial*treatment*exercise interactions ($F_{3.60, 115.30} = 0.891$, $p = 0.464$).

We sought to compare the later trials with the first to assess the maintenance or loss of discrimination ability as time went on. As a significant trial*exercise interaction existed, we grouped the data into exercise and sedentary cohorts. In the exercise cohort, there were no differences between the first and the later trials ($p>0.900$). However, in the sedentary cohorts, despite early trials indicating maintained ability (trial (T) 2-4: $p=1.000$, T5: $p = 0.604$, T6: $p = 0.307$), performance rapidly declined after trial 6 (T7: $p = 0.001$, T8-10: $p<0.001$) (Figure 5.10C).

b. iii) Trial bins

We wanted to dissect the differences between the groups further, so we split the rolling average (ra)DI data set into three bins (T1-4, T5-7 and T8-10). Using a repeated measures GLM, we found a significant within-subjects interaction of the bin ($F_{2, 66} = 11.162$, $p<0.001$) and the bin*exercise interaction ($F_{2, 66} = 7.787$, $p<0.001$). There was no significant effect of bin*treatment ($F_{2, 66} = 0.127$, $p = 0.887$), nor bin*treatment*exercise interactions ($F_{2, 66} = 1.153$, 0.322). Pairwise comparisons revealed no significant

differences in the first bin of trials 1-4. In the second bin, P/E and P/S were significantly different (p = 0.001), and V/S and P/S were trending towards a difference (p = 0.082). Finally, in the last bin, there was a significant difference between the V/E and V/S groups (p<0.001) and P/E and P/S groups (p<0.001) (Figure 5.10D).

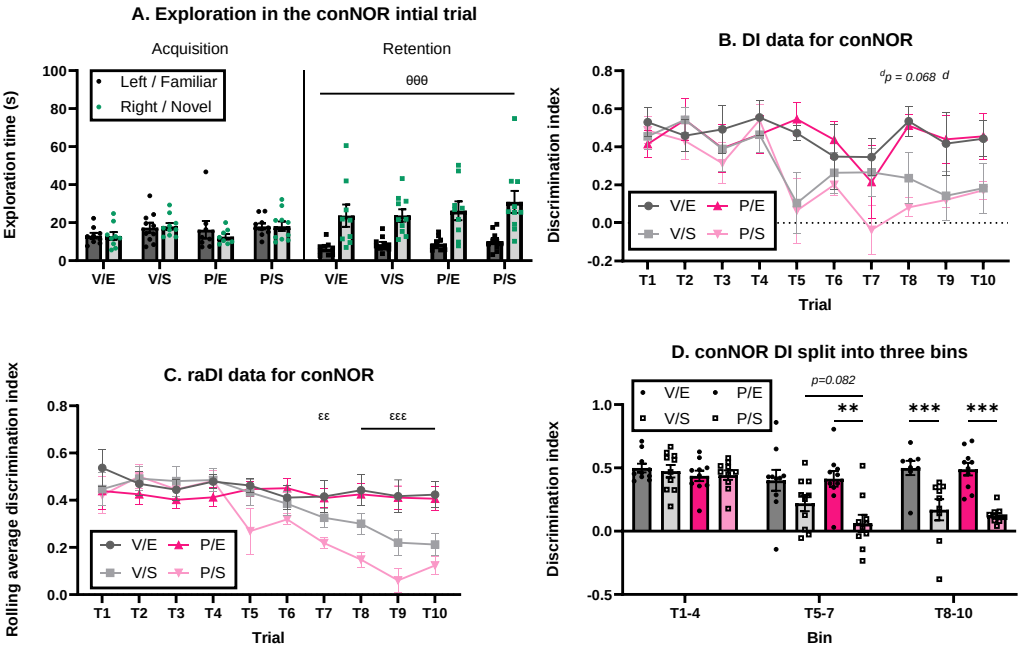

Figure 5.10: Continuous NOR data for chronic exercise study. A) Exploration times in the acquisition and first retention trial of the conNOR task, $^{\theta}$=effect of the object, $^{\theta\theta\theta}$p<0.001, (n=8-10). **B)** DI (n=6-10) for the conNOR task, b=difference between V/S T1 DI, d=difference between P/S T1 DI. **C)** Rolling average DI (n=8-10) for the continuous NOR task, $^{\varepsilon}$=effect of exercise, $^{\varepsilon\varepsilon}$p<0.01, $^{\varepsilon\varepsilon\varepsilon}$p<0.001. **D)** conNOR task split into three trial bins, *=difference between groups, n=8-10. Data were analysed with a repeated-measures GLM. Data expressed as mean ± SEM.

5.3.3.c Immunohistochemistry

c. i) Dorsal hippocampal parvalbumin density

We measured PVI density in each hippocampus region (CA1, CA2/3, DG) and analysed the data using a repeated-measures GLM. Here we found no significant within-subjects effects, suggesting that the relative distribution of PVI density across the three regions was consistent. Between subjects, there was a significant effect of treatment, with scPCP treatment reducing PVI density in the DH (scVeh: 23.00 ± 8.86, scPCP: 18.39 ± 7.89; $F_{1, 24}$ = 9.344, p = 0.005) and exercise increasing density (Ex: 23.48 ± 8.32, Sed: 17.91 ± 8.10; $F_{1, 24}$ = 13.663, p = 0.001), with no effect of the interaction ($F_{1, 24}$ = 0.000, p = 0.995) (Figure 5.11A).

c. ii) Prefrontal cortex parvalbumin density

We looked at the density of parvalbumin interneurons in the PFC. Using a univariate GLM, we found there was a significant effect of treatment, with scPCP reducing parvalbumin (scVeh: 96.99 ± 14.64, scPCP: 77.65 ± 18.72; $F_{1, 39}$ = 20.529, p<0.001). In addition, exercise increased PVI density (Ex: 97.69 ± 19.62, Sed: 76.95 ± 12.28; $F_{1, 39}$ = 23.632, p<0.001). However, the interaction had no effect ($F_{1, 39}$ = 0.094, p = 0.761) (Figure 5.11B).

c. iii) Perineuronal nets

As with the PVI, treatment had a significant effect (scVeh: 68.20 ± 17.68, scPCP: 58.00 ± 9.90; $F_{1, 39}$ = 6.532, p = 0.015). In addition, there was an effect of exercise; however, exercise reduced PNN density (Ex: 53.35 ± 3.32, Sed: 72.85 ± 11.10; $F_{1, 39}$ = 23.873, p<0.001). Finally, there was no effect of the interaction ($F_{1, 39}$ = 1.899, p = 0.177) (Figure 5.11C).

c. iv) PNN/PVI ratio

We looked at the ratio of the PNN compared to the PVI. We used a Kruskal-Wallis test because the resulting data were not normally distributed and were robust to transformation. This analysis found a significant model $\chi(3)$ = 21.645, p<0.001. Specifically, there was a significant effect of exercise both in the scVeh treated animals (p<0.001) and the scPCP-treated animals (p = 0.004) (Figure 5.11D).

c. v) Microglia

One animal was excluded due to poor tissue quality, and by identification of the poor-quality slide, the treatment group of the animal was revealed.

We stained for microglia using ionized calcium-binding adapter molecule 1 (IBA1), which is a protein found in macrophages, including microglia (Ohsawa et al., 2000). We first looked at the microglia density. The data were log10 transformed to produce a normally distributed data set and were analysed with a univariate GLM. Here we found no significant difference in the microglia density on treatment ($F_{1, 38}$ = 1.318, p = 0.259), exercise ($F_{1, 38}$ = 0.121, p = 0.730) nor the interaction ($F_{1, 38}$ = 2.487, p = 0.124) (Figure 5.11E).

We next chose to look at the activation states, where we found that scPCP treatment significantly reduced the number of resting microglia ($F_{1, 38}$ = 8.086, p = 0.007). With no effect of exercise ($F_{1, 38}$ = 2.270, p = 0141) or the interaction ($F_{1, 38}$ = 0.239, p = 0.628) on the proportion of resting microglia (Figure 5.11F).

There was also a significant effect of treatment on the intermediate population; here, scPCP-treatment increased the percentage of intermediate microglia ($F_{1, 38}$ = 7.265, p = 0.011). There was no effect of exercise ($F_{1, 38}$ = 0.736, p = 0.397), nor its interaction ($F_{1, 38}$ = 0.138, p = 0.712) (Figure 5.11F).

Finally, the activated microglia were not normally distributed, which was robust to transformation. We used a Kruskal-Wallis test, $\chi(3) = 8.194$, p = 0.042. Specifically, there was a significant effect of exercise both in the scVeh treated animals (p<0.001) and the scPCP-treated animals (p = 0.004) (Figure 5.11F).

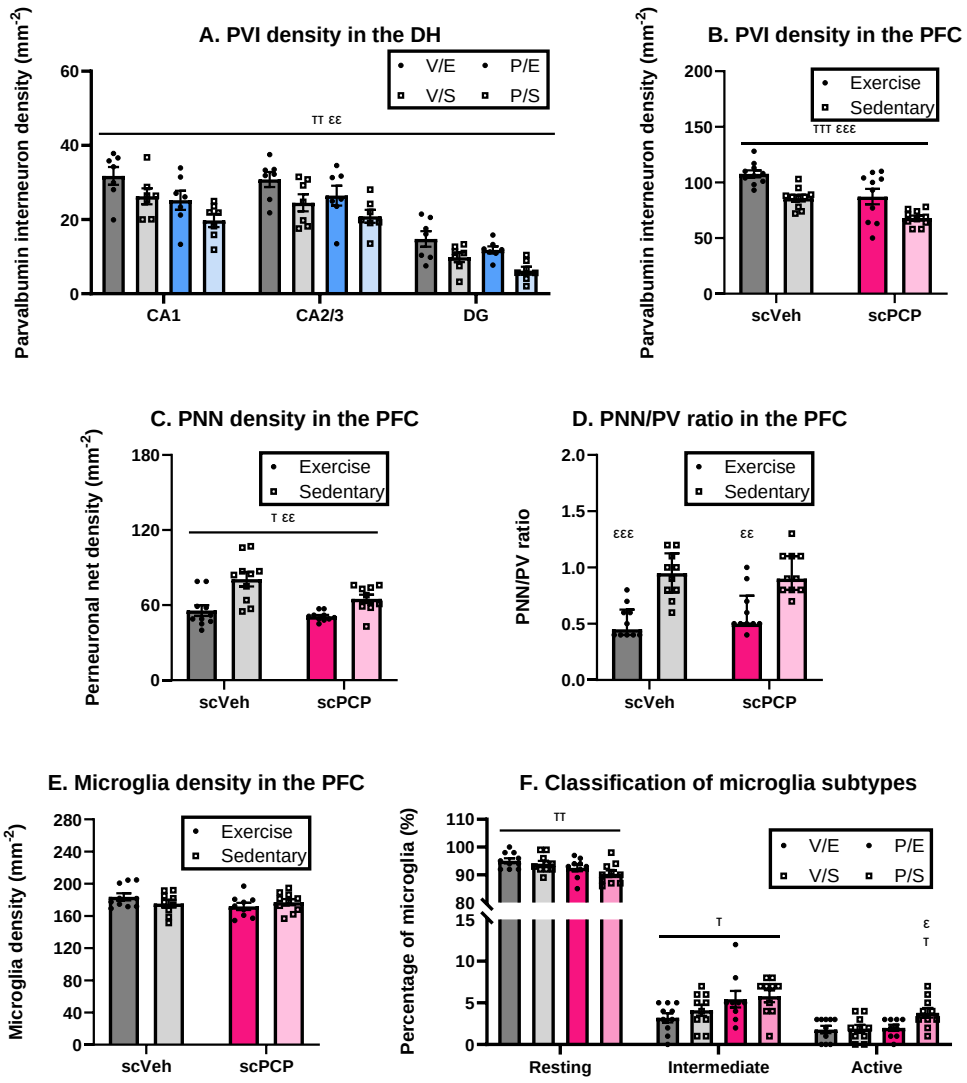

Figure 5.11: Immunohistochemistry outcomes for chronic exercise study. The density of **A)** PVI in the DH. Differences between groups tested with a repeated-measures GLM (n=7). The density of **B)** PVI and **C)** PNN in the PFC in the scPCP model after exercise intervention (n=10), differences analysed using a univariate GLM. **D)** the ratio of PNN compared to PVI in the chronic exercise study (n=10). Differences were measured using a Kruskal-Wallis test. Here, the graph shows median ± IQR. **E)** Microglia density and **F)** its activation states. Differences were analysed using a univariate GLM except for the active microglia data, which used a Kruskal Wallis (n=9-10). $^{\varepsilon}$=significant effect of exercise, $^{\varepsilon}p<0.05$ $^{\varepsilon\varepsilon}p<0.01$, and $^{\varepsilon\varepsilon\varepsilon}p<0.001$. ^{T}=significant effect of treatment, $^{T}p<0.05$, $^{TT}p<0.01$, $^{TTT}p<0.001$. Graphs show mean ± SEM.

5.3.3.d Correlation analysis

Finally, we assessed whether there was a correlation between behavioural and molecular outcomes. We found that the later trials of the conNOR test were highly correlated to the PNN/PVI ratio of the rats (Table 5.4). Graphing the PNN/PVI ratio against the average of the five significant trials revealed a negative correlation between the ratio and conNOR (Figure 5.12). Specifically, low PNN/PVI ratios were associated with superior conNOR performance.

Table 5.4: Spearman's correlation outcomes for PNN/PVI ratio and conNOR trials

conNOR trial	*T1*	*T2*	*T3*	*T4*	*T5*	*T6*	*T7*	*T8*	*T9*	*T10*
Correlation coefficient	-0.049	-0.097	-0.145	0.204	-0.334	-0.483	0.024	-0.418	-0.408	-0.499
Significance	0.774	0.561	0.372	0.206	0.038	0.002	0.884	0.009	0.011	0.002
N	37	38	40	40	39	40	38	38	38	36

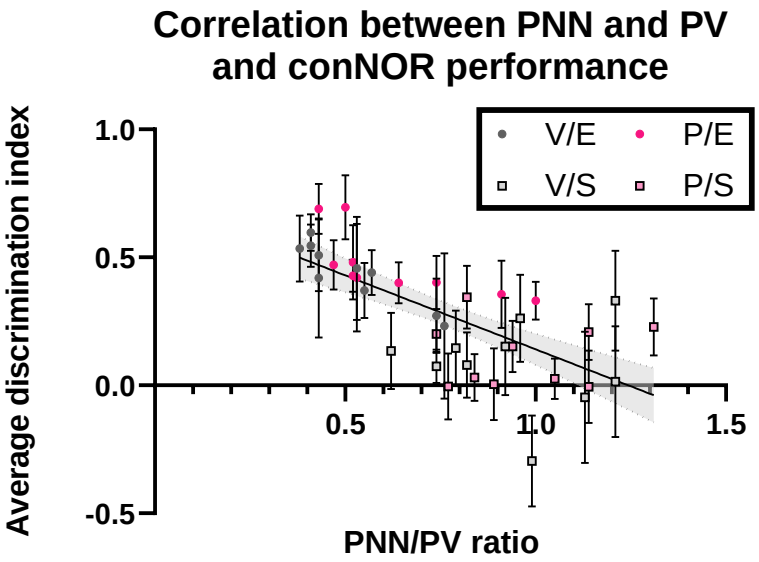

Figure 5.12: Correlation between PNN and PVI ratio continuous NOR performance. The discrimination index for the five significant trials (T5, T6 and T8 – 10) compared to the PNN/PV ratio. The graph shows the average DI ± SEM for each animal. The linear regression of these points is included (R^2 = 0.1786, p<0.001) with 95% confidence intervals.

5.4 Discussion

5.4.1 Overview of main findings

In the present chapter, we investigated the effects of acute and chronic exercise in the scPCP model. The novel findings included a long-term reduction in BDNF expression in the PFC, exercise reversing scPCP-induced cognitive deficits in a manner dependent on exercise proximity and exercise duration, and finally, exercise reversing many model-induced molecular deficits, including BDNF, PVI, PNN and activated microglia (see Table 5.5).

Table 5.5: The consequences of acute and chronic exercise in the scPCP model. In the qPCR studies, arrows show the direction of change compared to scVeh-treated animals. In exercise studies, arrows show changes from scVeh/sedentary controls (V/S). ^{E}=overall effect of exercise, ^{T}=overall effect of treatment. Green boxes highlight the positive effects of exercise. Red boxes show the adverse effects of the model. Yellow boxes show trends. PFC: prefrontal cortex, DH: dorsal hippocampus, VH: ventral hippocampus, BDNF: brain-derived neurotrophic factor, TrkB: tropomyosin receptor kinase B, TBARS: thiobarbituric acid reactive substances, (ra)DI: (rolling average) discrimination index, aeNOR: acute exercise novel object recognition, ceNOR: chronic exercise NOR, conNOR: continuous NOR, CA1-3: fields of the DH, DG: dentate gyrus, PVI: parvalbumin interneurons, PNN: perineuronal nets, V/E: scVeh/exercise, P/E: scPCP/exercise, P/S: scPCP/sedentary.

qPCR		
		scPCP
PFC BDNF		↓
DH BDNF		↔
PFC TrkB		↔
DH TrkB		↔

Acute exercise				
		P/S	**P/E**	**V/E**
aeNOR1 DI		↓		*N/A*
aeNOR2 DI		↓^{T}	↗^{E}	↔
BDNF	**PFC**	↔	↔	↔
	DH	↓	↔	↔
	VH	↑	↑	↔
TBARS		↑	↔	↔

Chronic exercise				
		P/S	**P/E**	**V/E**
ceNOR1 DI		↓		*N/A*
ceNOR2 DI		↓	↓	↔
ceNOR3 DI		↓	↔	↔
T7-T10 of conNOR raDI		↔	↑	↑
DH PVI		↓^{T}	↑^{E}	↑^{E}
PFC PVI		↓^{T}	↑^{E}	↑^{E}
PFC PNN		↓^{T}	↓^{E}	↓^{E}
PFC microglia	**Density**	↔	↔	↔
	Resting	↓^{T}	↓^{T}	↔
	Intermediate	↓^{T}	↓^{T}	↔
	Active	↑^{T}	↔^{E}	↔

5.4.2 BDNF

BDNF is considered a key mediator of the positive effects of exercise (Adlard et al., 2004a, Boehme et al., 2011, Gómez-Pinilla et al., 2002, Lee et al., 2012). As such, one of our primary aims was to establish whether there was any evidence of dysregulation of BDNF or its receptor TrkB in the scPCP-treated rats. We found reduced BDNF mRNA in the PFC twenty-two weeks after scPCP-dosing, suggesting a chronic reduction in BDNF expression in the PFC (Figure 5.6A).

5.4.2.a Role of BDNF and TrkB

Although we have not measured BDNF protein in the scPCP-treated animals, the reduction in mRNA could indicate reduced protein levels. Indeed, there is evidence of reduced BDNF protein immediately (Semba et al., 2006) and twenty-five days after scPCP dosing (Tan et al., 2020). We were interested in the role of BDNF and, by extension, TrkB in the PFC to understand the consequences of chronically reduced BDNF expression in this region. Developmentally, BDNF expression peaks during young adulthood and remains stable throughout life. Meanwhile, TrkB expression spikes before the synaptic pruning occurs in early development and stabilises (Notaras et al., 2019).

BDNF is only expressed in prefrontal excitatory neurons, while its receptor TrkB is expressed in excitatory neurons and inhibitory interneurons. Further investigations into the TrkB receptors on inhibitory interneurons found that they were predominantly expressed on PVI. When BDNF binds to PVI-TrkB, the expression of parvalbumin and GAD67 increases (Lewis et al., 2005). This relationship has, more recently, been confirmed by a TrkB knockout (Lau et al., 2022). When measuring BDNF, TrkB, parvalbumin and GAD67 in the brains of schizophrenia patients, Hashimoto et al. found reductions of all four targets in the PFC. Moreover, they found that TrkB was a stronger predictor of PV and GAD67 loss than BDNF (Hashimoto et al., 2005). Lewis et al. speculated that the early reduction of BDNF mRNA in schizophrenia patients could result in a loss of parvalbumin and GAD67, kickstarting the loss of E/I balance (Lewis et al., 2005).

We did not see any change to TrkB in our study. However, further investigations into the primer we selected revealed a limitation of our analysis. We used primers that bind to exons seven and eight, which code for the extracellular TrkB receptor. However, in the

study by Hashimoto et al., they used a primer specific for the tyrosine kinase domain (Hashimoto et al., 2005). The TrkB gene can be spliced in two locations in the intracellular coding exons, which leads to two functionally distinct isoforms. In Figure 5.13, we have illustrated the intracellular pathways involved in the truncated (left-hand side) and true (right-hand side) TrkB.

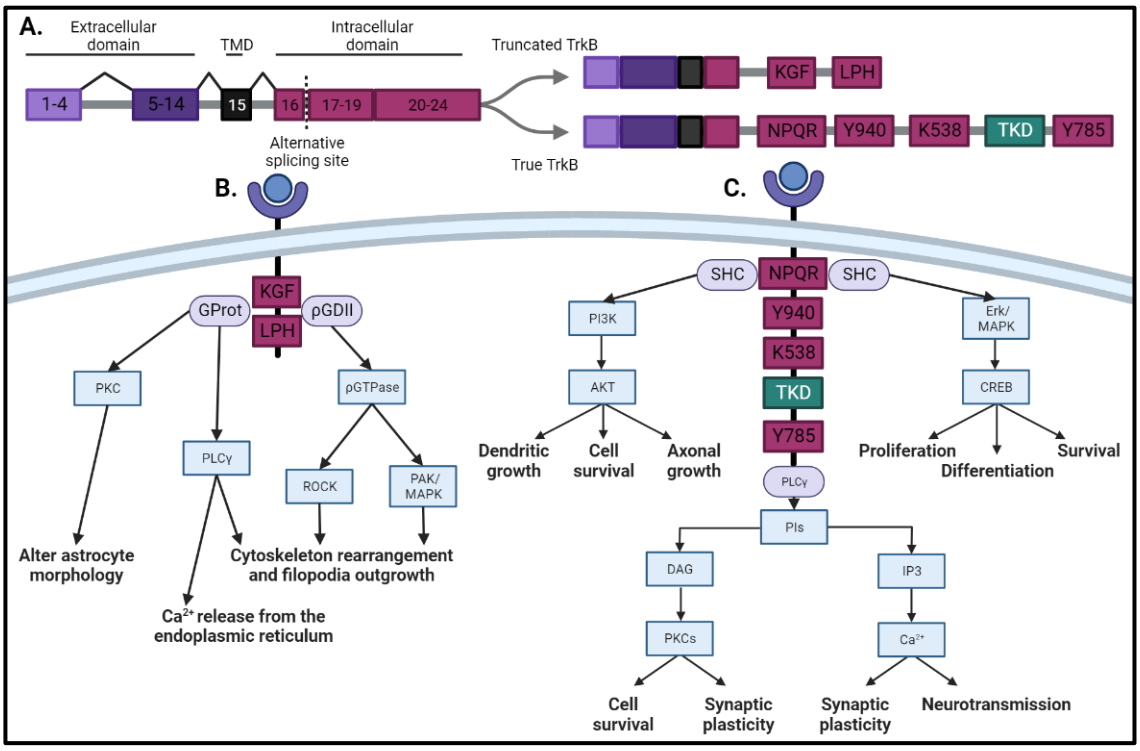

Figure 5.13: Intercellular pathways of truncated and true TrkB. A) Shows the TrkB gene with its extracellular domain exons (1-14), transmembrane domain (TMD, 15) and intracellular domain exons (16-24). Between exon 16 and 17, an alternative splicing site forms two proteins, truncated and true TrkB. **B)** shows the intracellular pathways from the truncated TrkB, and **C)** shows the pathways from true TrkB. Note the tyrosine kinase domain (TKD) in green, present only in the true TrkB isoform (adapted from Fenner, 2012).

The tyrosine kinase domain (TKD) targeted by Hashimoto is only found in the true TrkB, which results in many cellular functions associated with BDNF, including cell survival, differentiation and synaptic plasticity (Fenner, 2012). Interestingly, a study by Wong et al. found an increase in the expression of truncated TrkB in schizophrenia patients (Wong et al., 2013), which affects astrocyte morphology, the cytoskeleton and calcium release from the endoplasmic reticulum. Notably, the truncated TrkB acts as an inhibitor of true TrkB signalling (Fenner, 2012), so its overexpression in schizophrenia could indicate dysregulation of true TrkB expression and reductions of its downstream outputs (Figure 5.13). To understand the effects of scPCP on TrkB isoforms, primers specific for the distinct intracellular domains should be used.

5.4.2.b What are the consequences of chronically reduced BDNF?

Knockout or knockdown studies were explored to explore what effect this might have. Overexpressing BDNF improves cognitive performance in the Y-maze task (Modarresi et al., 2021). In knockout studies, the nature and the severity of the cognitive deficits induced depended on the location and the developmental stage of induction. Knockouts specific to the CA3 and partially the DG of the hippocampus resulted in NOR deficits, with no changes to spatial or fear memories (Ito et al., 2011); however, when Gorski et al. broadened the knockout to the forebrain, which includes the hippocampus and PFC, spatial and fear memory deficits were induced. Moreover, the most severe phenotype was produced in the early onset conditional knockout (Gorski et al., 2003). Knockdown models, which reduced BDNF levels by 60%, were insufficient to produce a discernible difference in fear learning performance compared to the wild-type control (Chourbaji et al., 2004). However, an independent study in a BDNF knockdown model found an attentional set-shifting deficit (Harb et al., 2021). Therefore, depending on the magnitude of protein level reduction the reduced PFC expression detected in this study enacts, the behaviour and GABAergic function outcomes could be consequential.

5.4.2.c Neurogenesis

BDNF functions are closely linked with neurogenesis in the hippocampus (Camuso et al., 2022). There is evidence of reduced proliferation and impaired maturation of neuronal progenitors in schizophrenia patients (Allen et al., 2016, Reif et al., 2006, Walton et al., 2012), suggesting impaired adult neurogenesis. In the current study, we did not measure hippocampal neurogenesis directly. However, the findings of other researchers will be discussed.

Subchronic NMDAr antagonist models reduce cell proliferation, indicated by reduced bromodeoxyuridine (BrdU) staining. This deficit is present regardless of the proximity of scNMDAr dosing and BrdU injection, suggesting a chronic impairment (Ding et al., 2019, Liu et al., 2006, Maeda et al., 2007, Song et al., 2016, Yu et al., 2023). Prolonging the time between BrdU injections and tissue collection allows cell survivability to be assessed. Here, the data is controversial, with some finding increased cell survival after a 2-3 week delay (Keilhoff et al., 2004), others finding no change after one week (Liu et al., 2006), and finally, reduced cell survivability was detected after a 28-day delay (Maeda et al., 2007). Though the timings of when the BrdU fluctuated, Keilhoff and Liu

co-administered BrdU and PCP, whereas Maeda administered the BrdU after PCP dosing.

In a 2014 review, Schoenfeld and Cameron speculated that reductions to adult neurogenesis would reduce tolerance to stress and may lead to mental illness. Conversely, certain medications, exercise and environmental enrichment were listed as examples that improve adult neurogenesis, which acts as a stress buffer, leading to resilience (Schoenfeld et al., 2015). Perhaps this is why exercise can prevent scPCP-induced deficits when given as a pre-treatment (Koseki et al., 2012, Mitsadali et al., 2020).

5.4.3 Acute exercise study

In the acute study, we saw an induction of a scPCP NOR deficit when analysing the discrimination index. However, the exploration time revealed that the scPCP-animals could discriminate between novel and familiar objects, suggesting a weak treatment effect. In the second NOR test, the effect of treatment was stronger, with a trend towards an effect of exercise, though the discrimination index suggested that acute exercise could reverse the scPCP-induced deficits. Despite a weak effect, this finding conflicted with the acute exercise study, where three weeks of wheel running was insufficient to reverse the NOR deficit. This indicates that different mechanisms may be at play in acute and chronic exercise protocols. As in our study, clinical data suggests that acute exercise (<60 minutes in duration) can improve cognition transiently, lasting no more than twenty-four hours (Basso et al., 2015, Etnier et al., 2014, Etnier et al., 2020, Johnson et al., 2019, Loprinzi et al., 2020, Mou et al., 2023, Sng et al., 2018).

5.4.3.a BDNF

The present study showed an increase in dorsal hippocampal BDNF in the exercised scPCP-treated animals that was noticeably absent in the exercised vehicles. In naïve animals, this lack of DH BDNF protein increase was present after short exposure to running wheels (one day with running wheel: Adlard et al., 2004b, two days with running wheel: Berchtold et al., 2005). Both studies investigated BDNF at different time points during the experiment and found that BDNF was first elevated from sedentary controls after twenty-one days of continuous access to a running wheel. Interestingly Adlard and Rasmussen looked at BDNF mRNA and found mRNA levels increased acutely after two hours of exercise (Adlard et al., 2004b, Rasmussen et al., 2009). In addition to BDNF,

acute exercise results in the upregulation of phosphorylated TrkB and CREB, which is involved in BDNF-TrkB intracellular signalling in the PFC (Baranowski et al., 2018). The rapid upregulation of BDNF and upregulation of TrkB signalling molecules could indicate a swift utilisation of translated BDNF.

This observation of increased BDNF protein in impaired animals but no change in wild type is reminiscent of cognition data in clinical studies. Yamazaki et al. found no working memory improvement after fifteen minutes of cycling. However, when they looked at individual performances, they noted the most significant improvements in those with the worst initial baseline (Yamazaki et al., 2018). A second study split the participants into high- and low-fitness cohorts. Low-fitness individuals saw benefits after moderate-intensity continuous exercise and after ten minutes of high intensity; meanwhile, the high-fitness individuals did not improve from baseline after the same exercises. Extending the high-intensity workout to twenty minutes reduced the low-fitness performance and improved the high-fitness group's performance (Mou et al., 2023). Equally, in a study of healthy young men, moderate cycling for 20 minutes increased cognitive performance, whereas cycling for 10 or 45 minutes had negligible benefits (Chang et al., 2015). It appears that exercise must occur at an appropriate intensity to see positive effects, and the nature of this is based on the individual. Indeed, with BDNF, low or moderate-intensity exercise can increase BDNF levels in rodents, whereas high intensity does not alter levels (Lou et al., 2008, Wu et al., 2020). This model is visualised in Figure 5.14.

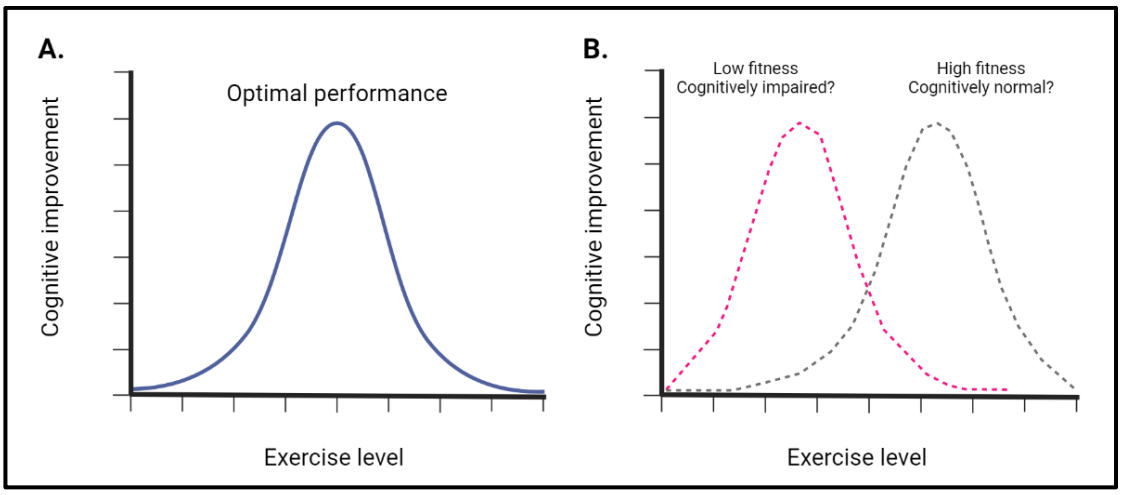

Figure 5.14: Hypothetical relationship between exercise intensity and cognition. (Adapted from the model developed by Yerkes et al., 1908, which suggests a relationship between stress and performance).

In sub- and chronic exercise studies, increased BDNF is a robust finding (Abel et al., 2013, Adlard et al., 2004b, Molteni et al., 2002). Once elevated by twenty-eight days of wheel access, BDNF protein can remain elevated in the hippocampus for seven days after exercise cessation. Interestingly, exercise appears to prime BDNF expression. Rats exercised for two weeks saw a 50% increase in BDNF protein levels. After two weeks of inactivity, BDNF levels return to baseline. After those two weeks of rest, just two days of wheel access can increase BDNF levels to 40% greater than the control, suggesting that exposure to running can create a molecular memory, increasing expression (Berchtold et al., 2005).

The BDNF response appears critical to many pro-cognitive effects of exercise. For example, when a BDNF antagonist or blocker was administered alongside exercise, the pro-cognitive behaviours induced by exercise were attenuated (Griesbach et al., 2009, Vaynman et al., 2004). On the other hand, giving BDNF to MK-801-treated mice improved performance in the fear conditioning tests and reversed some molecular alterations, notably reducing IL6 expression in the PFC (Shi et al., 2022).

5.4.3.b TBARs assay

The relationship described in Figure 5.14 parallels the effect of exercise on reactive oxygen species. In a 2015 review, Pingitore et al. commented on how short- or low-intensity exercise slightly improves performance, moderate exercise intensity or duration shows benefit to an optimal point, and finally, prolonged or strenuous exercise can have a detrimental effect. They suggested that this may be due to changes in the redox balance. Exercise causes increases in reactive oxygen species, switching the redox system towards oxidation. However, exercise will eventually lead to the upregulation of antioxidants, addressing the redox imbalance and potentially pushing the system to a reducing or net-antioxidant state. Pingitore et al. describe how this relationship between exercise nature and benefit depends on the individual's age, sex and fitness levels in addition to the intensity and duration of exercise, akin to what was described in Figure 5.14B (Pingitore et al., 2015).

A confounding factor in the literature is that many acute exercise studies are exhaustion studies, where rodents are forced to run until it is determined that they are no longer able. In these protocols, MDA concentration increases in the brains in the brains of exercised animals (Nogueira et al., 2020, Somani et al., 1996), with Liu et al. isolating the

MDA increase to the mitochondria (Liu et al., 2000). This increase in MDA is also seen in the plasma of healthy, untrained males subject to high-intensity exercise (Cho et al., 2022). Following the model of Pingitore et al., perhaps the individuals in these studies have pushed passed the positive redox effects and are in a net-ROS state, resulting in MDA increases. This is despite increased antioxidant activity after exercise (Cho et al., 2022, Somani et al., 1996).

Our study showed a decrease in MDA concentrations in the VH in the P/E group compared to the P/S. This decrease after acute exercise may be due to our moderate-intensity voluntary exercise protocol and the rats not entering a net-ROS state.

The effect of chronic exercise on redox balance is a more consistent finding, with reductions in ROS markers and increased activity of antioxidants (Cheng et al., 2014, Fazelzadeh et al., 2021). In a 2006 study, Radak et al. found that eight weeks of swimming training could improve cognition and reduce cortical ROS. Leaving these animals for eight weeks attenuated the cognitive enhancement; however, the reduction in ROS remained after eight weeks of inactivity (Radak et al., 2006).

5.4.4 Chronic exercise study

5.4.4.a Behaviour

In the current study, we saw that six weeks, not three weeks, of wheel access, was required for the scPCP-induced NOR deficit to reverse. The studies on the behavioural outcomes of exercise in NMDAr models are summarised in Table 5.6. These studies suggest that exercise, whether pre-, during or post-NMDAr antagonism, positively affects behaviour. An interesting finding is the duration of the effect of exercise. In Table 5.1 and Table 5.2, some studies documented that as early as two weeks after exercise cessation, there was no longer a pro-cognitive effect of exercise (Acevedo-Triana et al., 2017, Berchtold et al., 2010, Hopkins et al., 2010, Hopkins et al., 2011, Kim et al., 2013). However, the effect appears to be more stable in the NMDAr models, particularly in the prevention study, where the positive effects of exercise remain for three months after exercise (Mitsadali et al., 2020). In rescue studies, the scPCP-induced deficit returns after four weeks of inactivity (Heaney, 2020). Unfortunately, pathology was not completed in the study by Mitsadali or Heaney, so it cannot be ascertained whether the reason for the longevity of effects in prevention studies is due to prevention or rescue of the pathology we have described in the model in this thesis.

Table 5.6: Summary of behavioural outcomes after exercise in NMDAr models. The table is split into prevention, coadministration and rescue studies depending on whether the exercise intervention was before, alongside, or after NMDAr dosing. EE: enriched environment – these studies were only included if the EE included a running wheel. m/min: metre/minute. RLC: reverse light condition, IH: individually housed. ASST: attention set shifting, NOR: novel object, ITI: intertrial interval, MWM: Morris water maze, CFDL: contextual fear discrimination learning. Weeks post-I: number of weeks since exercise or EE ended. The NMDAr column notes the effect of NMDAr antagonism on the behaviour compared to scVeh/no-intervention control. NMDAr + intervention: effect of the intervention on NMDAr antagonist-treated group. Vehicle + intervention: the effect of the intervention on vehicle groups.

Study type	Type	Duration	Frequency	Intensity	Model	Duration	Housing	Behaviour	Weeks post-I	NMDAr	NMDAr + intervention	vehicle + intervention	Ref
Prevention	Running wheel	1 hour	5 days/week, 6 weeks	Free access	PCP	Bidaily, 7 days	RLC	ASST	8–12	↓	↑	↔	(Mitsadali et al., 2020)
								NOR 1 min ITI	2	↓	↑	↔	
									4	↓	↑	↔	
									11	↓	↑	↔	
	EE w/wheel	12 h/d	4 weeks	Free access	PCP	14 days	-	NOR 24-hour ITI	2–3	↓	↑	↔	(Koseki et al., 2012)
Coadministration	Running wheel	Free access	2 weeks	Free access	MK-801	Before each run	IH	MWM	< 2	↓	↑	↔	(Kim et al., 2014)
	Treadmill	45 – 50 minutes	5 days/week, 5 weeks	5 – 8 m/min	MK-801	Before each run	-	T-maze	1–2	↓	↑	↑	(Yi et al., 2020)
								CFDL	1–2	↓	↑	↑	
Rescue	Treadmill	30 min	5 days/4 weeks	10m/min	PCP	12 days	-	NOR 24-hour ITI	-	↓	↑	↔	(Koizumi et al., 2021)
	Running wheel	1 hour	5 days/week, 6 weeks	Free access	PCP	Bidaily, 7 days	RLC	NOR 1 min ITI	0	↓	↑	↔	(Heaney, 2020)
									2	↓	↑	↔	
									4	↓	↓	↔	
	EE w/wheel	Free access	7 days	-	MK-801	7	EE	NOR 24-hour ITI	< 2	↓	↑	↔	(Huang et al., 2021a)

Noticeably, we saw no alteration to cognition in the scVeh-treated animals, which starkly contrasts the overwhelmingly positive effect of exercise described in healthy controls in previous studies (Table 5.1 and Table 5.2). However, the collated data from NMDAr antagonist models (Table 5.6) showed that many studies did not see improvements in the control groups. Reflecting on the tasks selected, we suspect this is due to a ceiling effect in the NOR task. We do not see improvements as the vehicle animals already perform near-optimally in this task. Indeed Brockett et al. did not see any effect of exercise in a study of naïve animals tested with the NOR task with a five-minute ITI. However, exercise significantly improved performance in more complex tasks, namely object-in-place and attentional set-shifting (Brockett et al., 2015).

5.4.4.b Continuous NOR

As we had not confirmed a pro-cognitive effect in the V/E group, we chose to look at a second behavioural task. The continuous NOR task modifies the traditional one by relaying multiple retention trials. It also removes the requirement for the experimenter to remove the animal from the box. Landreth et al. compared the outcomes of animals in the standard and continuous NOR tests. They found that scPCP-treated rats had the expected standard NOR deficits. However, they showed no impairment in the initial continuous NOR trials. In the continuous NOR, as the test continued, the performance of the scPCP-treated animals declined at an expedited rate compared to scVehicle-treated controls. Landreth et al. suggested that the difference in outcomes between the standard NOR and the initial trial of the continuous NOR was due to the increased sensitivity of scPCP-treated rats to distraction (Landreth et al., 2020). This sensitivity to distraction has been observed previously, with Grayson et al. showing attenuation of the scPCP-induced NOR deficit when the rat is not removed from the testing arena (Grayson et al., 2014).

On the other hand, the expedited decline in performance was thought to be due to proactive interference (Landreth et al., 2020). First, interference should be defined. Interference is one method of forgetting information (Medina, 2018). It specifically occurs when a previous memory conflicts with current memory formation. It can happen proactively, where an old memory prevents a new one, or retroactively, where a new memory interferes with an old one (Bennett, 1975).

Like the conNOR task, clinical tests for memory interference involve memorising pairs of words or symbols for later recall. This process can be repeated several times with new words and combinations (Crawford et al., 2020). In schizophrenia patients, the extent of memory interference is controversial, with some finding strong effects and others finding none (Girard et al., 2018, Hill et al., 2004, Kaller et al., 2014, Mayer et al., 2016, O'Carroll et al., 1993, Torres et al., 2001). These studies selected patients based on schizophrenia diagnosis rather than specific cognitive symptoms. Differences may, therefore, be due to the diversity of the tested population.

The effects of exercise on memory interference are convincing. Acute exercise reduces the effect of both retroactive memory interference (Etnier et al., 2014, Etnier et al., 2020, Loprinzi et al., 2020, Wingate et al., 2018) and proactive interference (Johnson et al., 2019, Wingate et al., 2018) in healthy controls.

5.4.4.c Parvalbumin interneurons

We measured PVI density in the PFC and DH in the exercise study. However, as the causes and potential consequences of reduced PVI density have been discussed in chapter 3, the focus here will be on the effects of chronic exercise only.

Likely due to the relationship between exercise and neurogenesis, studies looking at the effect of exercise on the parvalbumin interneurons tend to focus on the hippocampus. Table 5.7 summarises studies in naïve and NMDAr antagonist-treated animals. Three studies warrant further discussion. First, Arida et al. compared the effects of voluntary and forced exercise. Although the intervention was brief, they found increased PVI density in the hilus of the DG in both protocols. In addition to PVI density, they studied the density of the dendritic fibres, where they saw increases in the density of parvalbumin-stained fibres in the voluntary exercise group compared to the forced exercise group. Arida et al. interpreted this increase in fibre density as increased synaptic connections (Arida et al., 2004). Second, Kim (2014) and Yi (2020) investigated PVI density after exercise in the scMK-801 model. They found that exercise could reverse the hippocampus's drug-induced cognitive deficits and PVI pathology. Kim (2014) measured increases in hippocampal BDNF, and Yi (2020) suggested that the reversal depended on hippocampal neurogenesis, as ablating PVI in the DG prevented exercise-induced neurogenesis and behaviour rescue (Kim et al., 2014, Yi et al., 2020).

Table 5.7: Summary of parvalbumin changes in NMDAr antagonist models after exercise. The table is split into studies in naïve animals and NMDAr models. m/min: metre/minute. WT: wild-type animals, IH: individually housed, days post-I: number of days since exercise ended. IHC: immunohistochemistry, PV in NMDAr column notes the effect of NMDAr antagonism on PV compared to scVeh/no-intervention control. NMDAr + intervention: effect of the intervention on NMDAr antagonist-treated group. Vehicle + intervention: the effect of the intervention on vehicle groups. CA1-3: fields of the hippocampus. DG: dentate gyrus. For the Arida et al. study, they split the DG into the molecular (M), granular (G) and hilus (H) of the DG. They also looked at the fibre (F) thickness in the hilus.

Type	Duration	Frequency	Intensity	Model	Duration	Housing	days post-I	Method	PV in NMDAr	NMDAr + intervention	vehicle + intervention	Ref
Wheel running	45 minutes	Daily, 10 days	Free access	--- WT ---		-	0	IHC	-	-	↔ M+G DG ↑ H DG ↑ F DG	(Arida et al., 2004)
Treadmill	45 minutes	Daily, 10 days	12 -22 m/min	--- WT ---		-	0	IHC	-	-	↔ M+G DG ↑ H DG ↔ F DG	
Treadmill	35 minutes	5 days/ 4 weeks	8 – 12 m/min	--- WT ---		-	0	IHC	-	-	↑ CA1 ↑ CA2/3 ↗ DG	(Placencia et al., 2019)
Treadmill	30 minutes	5 days/ 5 weeks	5 – 10 m/min	--- WT ---		-	> 3	IHC	-	-	↑ CA1 ↑ CA2/3 ↗ DG	(Nguyen et al., 2013)
Treadmill	5 – 60 minutes	Daily, 39 days	5 – 18 m/min	--- WT ---		-	0	WB	-	-	↑	(Gomes da Silva et al., 2010)
								IHC	-	-	↑ CA1 ↑ CA2/3 ↔ DG	
Running wheel	Free access	2 weeks	Free access	MK-801	Before each run	IH	< 2	IHC	↓ CA2/3	↑ CA2/3	↔ CA2/3	(Kim et al., 2014)
Treadmill	45 – 50 minutes	5 days/ 5 weeks	5 – 8 m/min	MK-801	Before each run	-	7–14	IHC	↓ DG	↑ DG	↑ DG	(Yi et al., 2020)

As discussed in 5.1.3, adult neurogenesis depends on GABAergic input for newly born neurons to mature (Figure 5.1). Our study shows a significant increase in PVI density in the DG of the DH after exercise in scVeh and scPCP-treated animals. Given that our study and others have shown an increase in BDNF in the DH after exercise (5.4.2) and BDNF increases GABAergic maturation in hippocampal cultures (Berghuis et al., 2004), these increases may be due to increased numbers of newly-born GABAergic cells. Indeed, environmental enrichment increases the number of newly born neurons and the speed of silent synapses becoming active (Chancey et al., 2013), suggesting increased GABAergic input. Another mechanism may be that as mature granule cells increase in number due to exercise-induced neurogenesis, they recruit proportionately more PVIs to signal onto the newly born immature granule cells (Alvarez et al., 2016). Alternatively, the increase in PVI density could be due to PVI neurons not expressing parvalbumin protein now returning to typical levels (Enwright et al., 2016, Hashimoto et al., 2003).

We also measured an increase in PFC PVI density after exercise. Examples in the literature are more limited in the PFC. Many studies use prolonged exposure to an enriched environment (EE), which includes running wheel alongside other novel housing. These studies find that EE could reverse model-induced PVI reductions in the PFC (Dwir et al., 2021, Murueta-Goyena et al., 2018, Sun et al., 2016, Zhang et al., 2016b). These studies also explored the effects of EE on mechanisms relevant to scPCP. For example, EE reduced model-induced oxidative stress (Sun et al., 2016, Zhang et al., 2016b) and GAD67 reductions (Murueta-Goyena et al., 2018, Sun et al., 2016).

5.4.4.d Perineuronal nets

As in the chapter 3, we saw a reduction in the density of PNN in response to scPCP-dosing. After exercise, PNN density counterintuitively decreases rather than rescuing the deficit. This reduction was present in both scVeh and scPCP-treated rats. This finding is replicated in the cingulate cortex and regions of the hippocampus after six weeks of free access to a running wheel in naïve animals (Smith et al., 2015) and in the prelimbic region after only one day of exposure to an enriched environment (Slaker et al., 2016).

In this case, reducing PNN density may promote plasticity (1.6.4). A handful of studies evidence increased synaptic proteins, including PSD95, and synapse number after acute and chronic exercise interventions (Belaya et al., 2020, Fahimi et al., 2017, Molteni et al., 2002, Stamenkovic et al., 2017, Tong et al., 2001, Wang et al., 2018a, Yau et al.,

2014). Moreover, exercise can increase NMDAr-dependent LTP in the DG (Dahlin et al., 2019, Farmer et al., 2004, O'Callaghan et al., 2007, van Praag et al., 1999), which may be mediated by exercise-induced changes to NMDAr subunits. NR2B upregulates in the hippocampus after 3 days of exercise and remains elevated at six weeks (Farmer et al., 2004, Molteni et al., 2002). NR2A initially increases at the three and seven-day timepoint, then normalises at the four and six-week timepoint (Farmer et al., 2004, Molteni et al., 2002). These studies indicate a robust and rapid recovery of synaptic function, which was not seen in the drug intervention study.

5.4.4.e Microglia

As discussed in chapters 3 and 4, schizophrenia is associated with low-grade inflammation, which IL6 may mediate. In addition, IL6 is a crucial cytokine when considering the physiological response to exercise, as it can be released from muscle during regular contraction (Steensberg et al., 2000). It was Pederson et al. who pioneered the early work surrounding IL6 release after exercise, naming the cytokines released from muscle myokines. Pederson noted that at rest, the muscle IL6 gene is silent. However, IL6 is transcribed and translated rapidly on sustained muscle contraction, exponentially increasing IL6 levels in plasma (Pedersen et al., 2003). Later studies confirmed that the IL6 increase after exercise is independent of other pro-inflammatory cytokines, suggesting that the increase is due to a mechanism other than a classic acute immune response (Figure 5.15). Furthermore, IL6 has a robust anti-inflammatory effect in the periphery, inhibiting tumour necrosis factor α (TNFα) and upregulating an anti-inflammatory IL10 (Petersen et al., 2005).

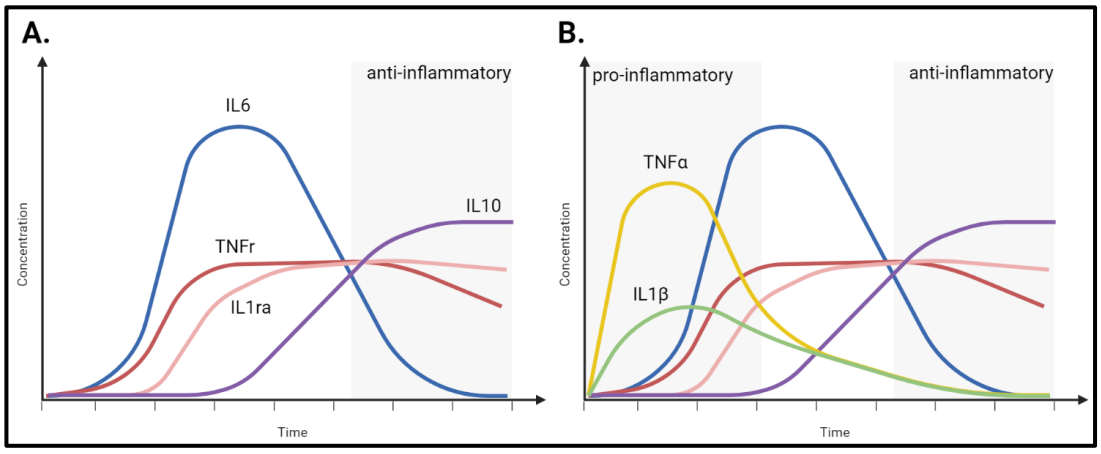

Figure 5.15: Cytokine response in exercise compared to acute immune response. Response in **A)** exercise and **B)** acute infection. Exercise results in the release of IL6 independent of pro-inflammatory TNFα and IL1β release (Adapted from Petersen et al., 2005).

Centrally, regular exercise can reduce the concentration of cytokines in disease models (Kim et al., 2021, Ko et al., 2020, Parachikova et al., 2008, Robison et al., 2019, Wang et al., 2018a). In the chronic exercise study, we had a tissue for immunohistochemistry; therefore, we chose to stain for IBA1, which stains for a protein involved in the phagocytic properties of microglia (Ohsawa et al., 2000).

We saw no change to IBA1 density in the PFC after scPCP dosing or exercise. The outcomes after NMDAr antagonism vary in the literature; some observe no change in the PFC and hippocampus (Hou et al., 2013, Wei et al., 2022). Others find increased density in the hippocampus (Xiao et al., 2019, Yu et al., 2023).

Analysing microglial density in isolation does not indicate a brain in a net pro- or anti-inflammatory state. Microglia are a dynamic cell type that can alter into different subtypes, characterised by distinct gene and protein expression, metabolites and morphology (Paolicelli et al., 2022). Here we looked at the morphology of microglia, which we broadly categorised into resting, intermediate and active. Although we classified microglia as resting, this is a misnomer as these microglia are active, surveying the environment and actively neutralising potential threats (Nimmerjahn et al., 2005).

We saw an increase in the active microglia in the scPCP-treated animals that was ameliorated in the exercised animals. Active microglia change morphology in response to inflammation and cytokines. When active, these microglia secrete proinflammatory factors (Kettenmann et al., 2013, Subramaniam et al., 2017) or anti-inflammatory factors depending on the environment (Subramaniam et al., 2017) (Figure 5.16). Here we have only looked at the morphology, so we cannot make confident assumptions about the state of the microglia. Although, we have shown evidence of ongoing, low-grade IL6 in the previous chapters, which could indicate a brain in a pro-inflammatory state. Despite the circumstantial evidence, the limitations of interpreting three-dimensional morphology from a two-dimensional plane are blatant. Recently, a multidisciplinary consortium stressed the need to use a combination of ultrastructure, morphology, metabolomics, proteomics, transcriptomics and epigenomics to confidently conclude the nature of the microglia (Paolicelli et al., 2022).

Despite the primitive nature of our morphology analysis, the increase in active microglia is corroborated by a study looking at the effect of twenty-eight days of MK-801 dosing in mice, with Gomes et al. finding a significant increase in the percentage of active microglia in the mPFC and hippocampus (Gomes et al., 2015).

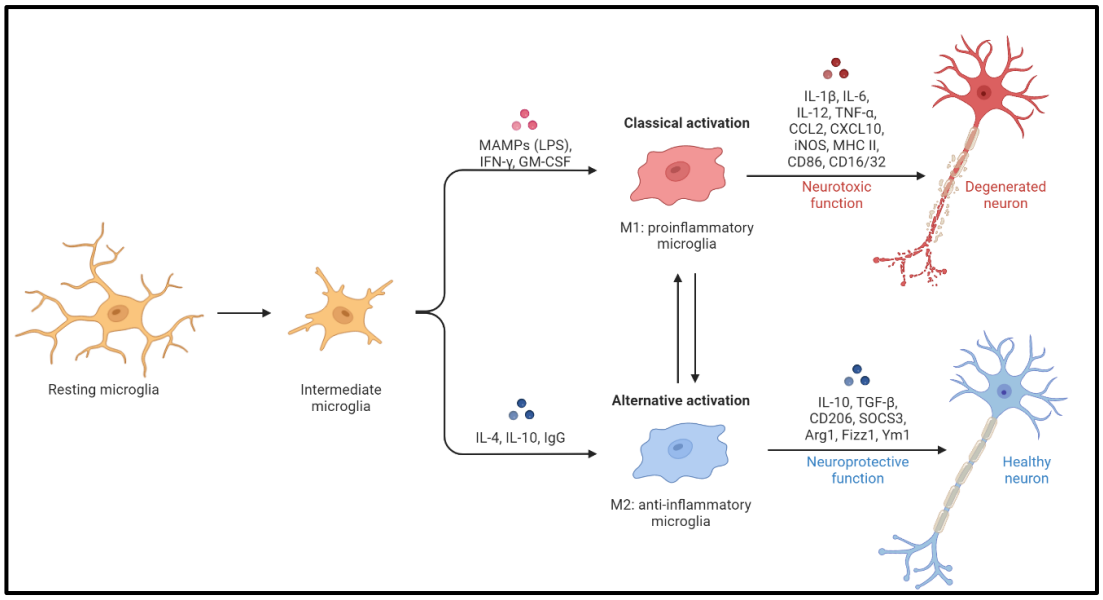

Figure 5.16: Schematic of microglia morphology and function. In low inflammatory states, "resting" microglia survey the CNS. When the resting microglia are triggered by an inflammatory mediator (MAMPs, LPS, IFN-γ, GM-CSF), microglia morphology transforms into an active ameboid shape, which secretes proinflammatory, neurotoxic cytokines and components. On the other hand, anti-inflammatory mediators (IL4, IL10, IgG) result in anti-inflammatory microglia, which secrete neuroprotective substances (adapted from a biorender.com template based on Subramaniam et al., 2017).

5.4.5 Limitations

5.4.5.a Running data

In both the acute and chronic exercise studies, we wanted to look at the running levels and see if these relate to any behavioural or pathological outcomes. Pre-clinical and clinical studies have shown correlations between exercise intensity and behavioural improvements (Firth et al., 2015, Firth et al., 2017, Mitsadali et al., 2020). We did not see any correlation between distances ran and any measured outcomes. However, we are not confident that the data collected is reliable. The detector was wired and would often become dislodged by the rat or the wheel's movement, resulting in incomplete data collection for a running session.

5.4.5.b Differences in the time of day

The acute and chronic exercise studies were conducted in the light and dark phases of the light cycle, respectively. The timing of the day can profoundly affect behavioural and

molecular outcomes. In circadian studies, the term zeitgeber time (ZT) is used, where ZT0 is the time when lights are switched on, indicating the start of the rodent rest period. ZT12 is when lights are switched off, commencing the active period. In a comparative study, Hwang et al. compared the effects of exercise at ZT0, ZT6 and ZT12. They found the most significant improvements in behaviour and DG neurogenesis when the animals ran at ZT6 and ZT12 (Hwang et al., 2016). Holmes et al. ran a similar study, exercising animals for 0, 1 or 3 hours at ZT6, ZT12 and ZT18. They saw a time-dependent increase in neurogenesis in animals exercised at ZT12 and ZT18, with the most significant increases in the 3-hour ZT18 cohort (Holmes et al., 2004). Many biological processes may be responsible for the increased adult neurogenesis during the active cycle, including body temperature, locomotor activity, feeding, and hormones regulated by the circadian cycle (Ali et al., 2022).

5.4.5.c NMDAr antagonist models

As the chapters using the scPCP model conclude, the general limitations of the model should be discussed. The model is based on the observation that PCP dosing in humans results in side effects similar to schizophrenia symptoms (Luby et al., 1959). However, the original paper reported individuals suffering out-of-body experiences (Greifenstein et al., 1958), which do not reflect schizophrenia symptoms (Blackmore, 1986). This could be due to limitations on the questions asked in the postoperative period by Greifenstein et al. More recently, Carhart-Harris et al. documented the effects of ketamine in healthy controls and found that they more closely aligned to depression rather than schizophrenia. However, the authors did stress that ketamine produced very variable and unreliable outcomes in their study (Carhart-Harris et al., 2013). Further acute studies in humans frequently report delirium, cognitive impairment, affective change and behaviour differences like aggression, repetitive movements or mutism, however, these effects are temporary (Pearlson, 1981, Pradhan, 1984). Notably, haloperidol is able to alleviate the symptoms of acute phencyclidine-induced psychosis (Giannini et al., 1987).

The effects of repeated doses of phencyclidine in humans are limited to case reports of drug users. This inherently introduces variation that makes conclusions tentative, including the frequency and dose of administration, whether PCP is taken exclusively or with other drugs and mental health background. Despite these confounds, some

noteworthy patterns emerge. First, the psychosis induced by repeated PCP use can persist longer than acute administration, generally lasting one month, though one patient had psychosis lasting 90 days (Allen et al., 1978, Fauman et al., 1976, Rainey et al., 1975). Second, antipsychotics have mixed efficacy on PCP-induced psychosis, with some patients responding gradually to haloperidol, chlorpromazine or thiothixene. However, some patients did not improve (Allen et al., 1978, Giannini et al., 1984). Finally, PCP appears to only induce psychosis in select individuals relative to the prevalence of PCP abuse, and there are limited accounts of PCP-induced psychosis (Fauman et al., 1976). The reason why these individuals are susceptible is unknown.

A further limitation of the scPCP model is its inability to replicate the genetic and developmental aspects of schizophrenia, which is a fundamental component of schizophrenia aetiology. Moreover, given the fluctuating nature of schizophrenia symptoms (Novak et al., 2022), the persistence of the positive symptoms may reflect acute psychosis rather than entrenched disease. However, construct and face validity is difficult to achieve in animal models relevant to schizophrenia. Schizophrenia has a complex aetiology, with hundreds of risk genes combined with various environmental stressors. As stated, the symptoms can fluctuate throughout the disease course. Therefore, a truly clinically relevant model would be impossible to design.

5.5 Chapter summary

Exercise proved a potent therapy in alleviating scPCP-induced cognitive deficits and pathology.

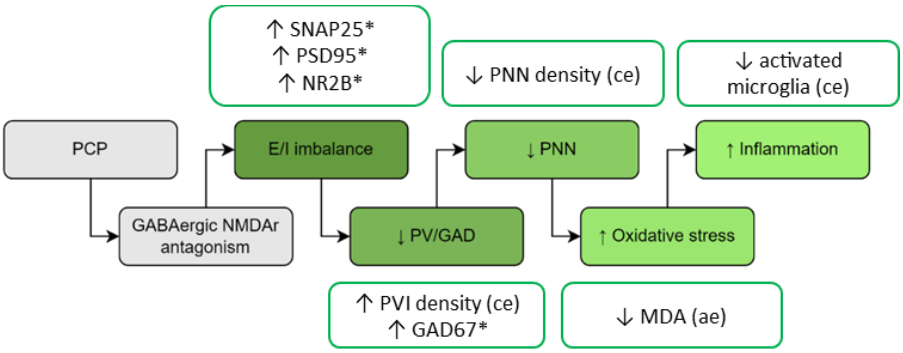

Figure 5.17: Consequences of acute and chronic exercise on scPCP pathology. *Evidence compiled from the literature.

Notably, exercise increased PVI density in the dentate gyrus of the dorsal hippocampus.

We propose three explanations for these increases.

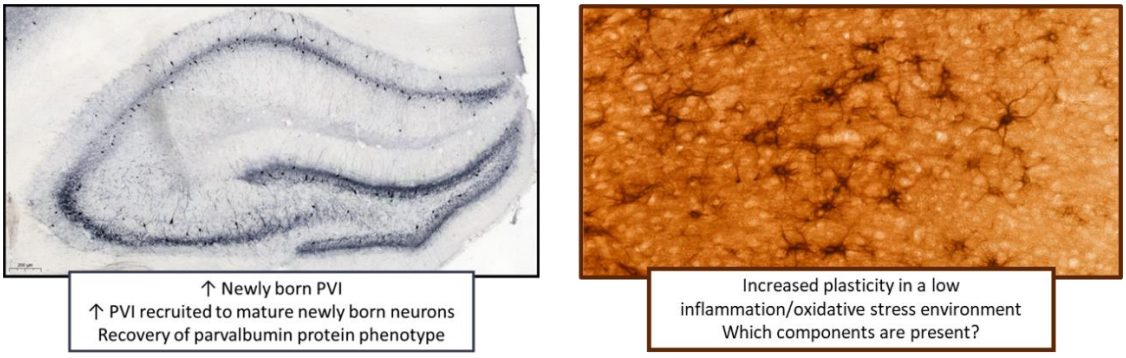

Figure 5.18: Dorsal hippocampal section stained for parvalbumin and PFC stain of PNN. 5x and 20x magnification.

Finally, we reported decreased PNN density in the PFC. We hypothesise that the reduction in PNN is to facilitate increased plasticity. Although we see improvements in cognition and PNN, deciphering the structure of the PNN in disease and rescue would add a dimension to the understanding of PNN changes.

CHAPTER 6: CHARACTERISATION OF THE POLY (I:C) MODEL

6.1 Introduction

6.1.1 Clinical rationale

The rationale for associating maternal infection with increased schizophrenia risk comes from observing heightened incidence after disease outbreaks (Byrne et al., 2007, Penner et al., 2007). Interestingly, the risk is not associated with a single pathogen, with increased schizophrenia risk attributed to bacterial (Sørensen et al., 2009), viral (influenza: Brown et al., 2004a, rubella: Brown et al., 2001, herpes simplex type 2: Buka et al., 2008, polio: Suvisaari et al., 1999) and parasitic infection (Toxoplasma gondii: Brown et al., 2005, Mortensen et al., 2007).

6.1.2 Maternal immune activation

Given the heterogeneity of pathogens, it has been speculated that maternal immune activation (MIA) increases the offspring's risk of schizophrenia diagnosis rather than a specific effect of a particular disease (Brown et al., 2004b, Buka et al., 2001). Several proinflammatory cytokines have been detected in the placenta (IL1β, TNFα and IL6), amniotic fluid (TNFα and IL6), and foetal brain (IL1β, TNFα, IL6, IL10, MCP1, VEGF, iNOS) after MIA in rodent models (reviewed in Patterson, 2009).

The relationship between MIA and offspring impairments has been further validated by studies where researchers can attenuate offspring phenotype by knocking out IL6, a cytokine essential for acute immune response, or co-administering anti-IL6 antibody alongside MIA (Choi et al., 2016, Smith et al., 2007). Equally, blocking the cytokine IL17a downstream of IL6 can also ameliorate the effects of MIA (Choi et al., 2016).

6.1.3 Animal models of MIA

The most common methods of inducing MIA in rodents are lipopolysaccharide (LPS) and polyinosinic:polycytidylic acid (often referred to as poly(I:C), however, here, we will use PIC). LPS and PIC mimic bacterial and viral infections, respectively (Chamera et al., 2020, Mueller et al., 2019, Murray et al., 2017, Wischhof et al., 2015). Both mimetics bind to toll-like receptors (TLR). LPS binds to TLR4, which triggers the MyD88 pathway (Kawai et al., 1999), resulting in the transcription of NFκB and proinflammatory cytokines. In addition, TLR4 activation triggers a second pathway, the TIR domain-containing adaptor-inducing IFNβ (TRIF) pathway, which ultimately causes the upregulation of interferon type one and NFκB (Lu et al., 2008). PIC binds to endosome-bound TLR3, which triggers

the TRIF pathway only (Komal et al., 2021). Interferons can regulate the expression of vast numbers of genes. In general, the function of interferon-stimulated genes is to increase the adaptive immune response and bolster anti-viral defences (Schoggins, 2019).

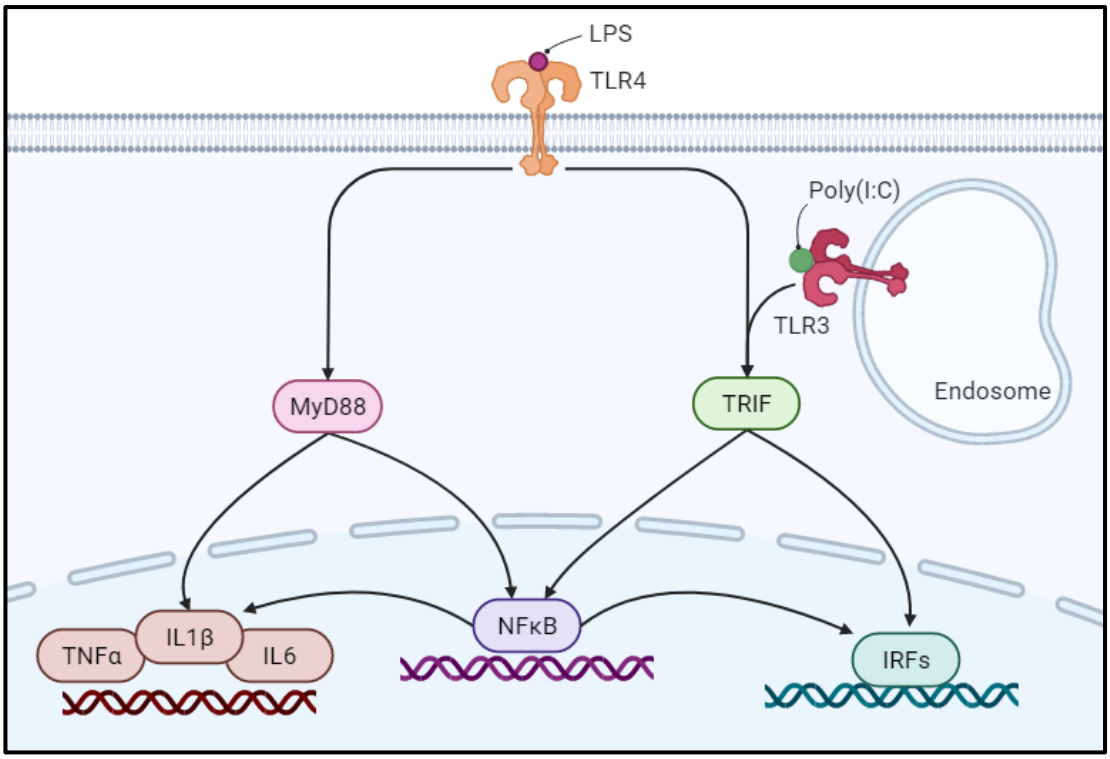

Figure 6.1: Overview of the PIC/TLR3 and LPS/TRL4 signalling pathways. PIC binding to TLR3 results in TRIF-dependent upregulation of type one interferons (IRFs) and NFκB. LPS binding to TRL4 triggers the TRIF and MyD88 pathways, upregulating NFκB and proinflammatory cytokines (Komal et al., 2021, Lu et al., 2008).

6.1.4 Timings of MIA

Several studies have investigated the effects of maternal immune activation on levels of peripheral inflammatory cytokines in the maternal plasma. In general, an acute inflammatory response is indicated by a marked increase in pro- and anti-inflammatory cytokines. After twenty-four hours, cytokine levels tend to decrease back to control levels (summarised in Table 6.1). The treated cohorts tend to have noticeably higher variation in the measured maternal cytokine response. Interestingly a recent study found that maternal cytokine levels could predict some maternal and adult behaviours (Potter et al., 2023), suggesting that the intensity of the immune response could predict pathology.

Table 6.1: Changes to maternal cytokines after maternal immune activation with PIC. Maternal cytokines were measured in serum at different time points post maternal immune activation with PIC compared to control. The gestational day indicates the day when PIC was administered. IL: interleukin, TNFα: tumour necrosis factor, INF: interferon.

Gestational day	Early (2-4 hours)	Mid (6-8 hours)	Delayed (24 hours +)	Reference
9	↑TNFα ↑IL10	↑TNFα ↑IL10		(Meyer et al., 2006a)
	↑IL6 ↑TNFα ↑IL1β ↑IL10	↑IL6 ↑IL10 ↔TNFα ↔IL1β		(Meyer et al., 2006b)
	↑IL6 ↑TNFα ↑IL10		↔IL6 ↔TNFα ↔IL10	(Giovanoli et al., 2013)
12	↑IL6 ↔TNFα ↔IL17a ↔IL10		↔IL6 ↔TNFα ↔IL17a ↔IL10	(Garcia-Valtanen et al., 2020)
			↑IL6 (24 hours) ↔IL6 (48 hours)	(Goeden et al., 2016)
12.5	↑IL6 ↑IL1β			(Smith et al., 2007)
15	↑TNFα ↑IL1β ↔IL6 ↔IL10			(Ballendine et al., 2015)
	↑IL6 ↔TNFα			(Lins et al., 2018)
	↑IL6			(Murray et al., 2019)
	↑IL6			(Kowash et al., 2019)
	↑TNFα ↔IL6			(Potter et al., 2023)
	↑IL6 ↑TNFα			(Dalton et al., 2012)
	↑IL6 ↑TNFα ↔IL1β		↔IL6 ↔TNFα ↔IL1β	(Kowash et al., 2022)
		↑TNFα ↑IL1β		(Missault et al., 2014)
16	↑TNFα	↔TNFα	↔TNFα	(Gilmore et al., 2005)
17	↑IL6 ↑TNFα ↑IL10			(Vuillermot et al., 2012)
	↑IL6 ↑TNFα ↑IL1β			(Giovanoli et al., 2015)
	↑TNFα ↑IL10	↑TNFα ↑IL10		(Meyer et al., 2006a)
	↑IL6 ↑TNFα ↑IL1β ↑IL10	↑IL6 ↑IL10 ↔TNFα ↔IL1β		(Meyer et al., 2006b)

6.1.5 Neurodevelopment

Although the cytokine data suggest that an inflammatory insult at any point during gestation can induce an immune response in the pregnant dam, consider the state of the developing brain when the insult occurs. The neural tube closes on gestational day (GD)9.5 in mice and 10.5 in rats, marking the beginning of brain development (Semple et al., 2013). On neural tube closure, the newly formed neuroepithelium begins to divide symmetrically, with some cells differentiating into radial glial cells that form the cortical plate. From GD11 onwards, immature neurons migrate along well-defined pathways radially. Numerous transcription factors tightly regulate this process of migration and maturation. By the end of gestation, the cortical layers have formed in an "inside-out" fashion, with the later-born, superficial neurons migrating over the earlier-born, deep neurons (Cadwell et al., 2019, Kepecs et al., 2014, Molyneaux et al., 2007).

The cortical layers transform throughout development before the final conformation seen in adulthood (Molyneaux et al., 2007). Therefore, the layer-specific and neuronal progenitor markers are valuable tools in monitoring the correct migration and maturation. During the early stages of neurodevelopment (GD9.5-12.5), the preplate develops, forming the superficial marginal zone, cortical plate and subplate. The cortical plate will develop into the layered cortex from GD12.5 onwards (Molyneaux et al., 2007). Therefore, insults during this time could have the most global effects. Indeed, PIC-induced MIA during this early stage of neurodevelopment results in dysregulated expression of superficial (Shin Yim et al., 2017, Soumiya et al., 2011) and deep cortical layer markers in foetal and neonatal offspring (<PD10) (Choi et al., 2016). Notably, Choi et al. prevented these alterations with a pre-treatment of IL-17a blocking antibody, directly implicating the maternal immune response (Choi et al., 2016).

Later in gestation (GD13.5-16.5), the subventricular zone sequentially creates the neurons destined for layers 5, 4, and the upper layers (Molyneaux et al., 2007). LPS-induced MIA on GD13.5 increased layer 4 and 5 neurons on PD8 (Stolp et al., 2011). While studies looking at superficial layer markers found that they were less affected at this gestational stage, with MIA at GD14.5 causing dysregulated superficial proteins in only a small percentage of offspring (13%) (Shin Yim et al., 2017). Using whole genome microarray analysis following LPS-induced MIA on GD15.5, Oskvig et al. reported the downregulation of pathways crucial for neurogenesis, neurotransmission, neuronal

migration, and neurite outgrowth. In contrast, upregulated pathways included genes for cellular stress and death (Oskvig et al., 2012). Ghiani et al. found that immature neuronal markers were reduced and differentially expressed in cortical layers two days after LPS treatment on GD15 and GD16, indicating issues with neurogenesis and migration (Ghiani et al., 2011). On GD17.5, the production and migration of neuronal progenitors cease (Molyneaux et al., 2007); fittingly, induction of MIA on GD18.5 no longer produces dysregulation in cortical layers (Shin Yim et al., 2017).

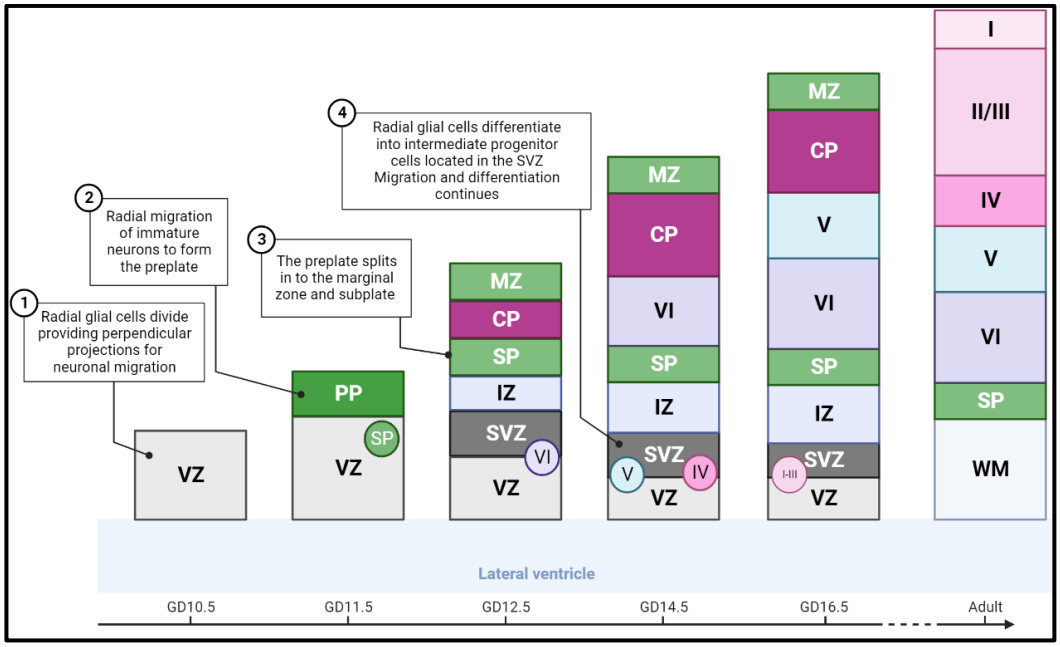

Figure 6.2: Cortical neuronal development. Neuronal cells originate from the ventricular and subventricular zones (VZ and SVZ). The circles within these zones show the earliest birth date of each neuronal cell layer. On GD12.5, the preplate (PP) splits into the marginal zone (MZ) and subplate (SP). The cortical plate (CP) forms the basis of the multi-layered cortex (I-VI) found in the adult brain. In the adult brain, white matter (WM) has formed (Adapted from Molnár et al., 2012, Molyneaux et al., 2007, Penisson et al., 2019)

6.1.6 Inhibitory neuronal development

The inhibitory neurons originate from the medial ganglionic eminence (MGE) and the caudal ganglionic eminence (CGE) of the telencephalon, which proliferate from GD9.5 and GD12.5, respectively (Miyoshi et al., 2010). MIA on GD9.5 reduced inhibitory MGE-derived precursors transiently, normalising by GD14.5. Despite the recovery, inhibitory neurons were reduced in superficial layers from GD14.5 to PD9, predominantly in the somatosensory (S1) cortex. At PD15, when the mature cortical layers have developed, the GABAergic progenitors are reduced in both superficial and deep cell layers (Vasistha et al., 2020). As the caudal ganglionic eminence (CGE) does not produce neurons until GD12.5 (Miyoshi et al., 2010), Vasistha et al. looked to see what effect MIA-induction on

GD12.5 would have on MGE- and CGE-specific markers. Predictably, they found a significant decrease in CGE-specific markers at GD14.5 and no change in MGE-specific markers (Vasistha et al., 2020). Squarzoni et al. found dysregulated expression of a GABAergic interneuron transcription factor after LPS treatment on GD13.5 in a separate study. By PD7, the deeper layers had fewer progenitors, suggesting altered migration rather than proliferation (Squarzoni et al., 2014). IL6 injections from GD12 until tissue collection on GD14 also caused altered GABAergic progenitor migration (Gumusoglu et al., 2017). LPS treatment on GD15 resulted in a transient reduction of factors related to interneuron migration, which normalised in foetal brains 24 hours after injection (Oskvig et al., 2012). Finally, Vasistha et al. found MIA-induction on GD16.5 counterintuitively increased in both MGE- and CGE-specific markers, solidifying the consequential impact of MIA-timing on neurodevelopment (Vasistha et al., 2020).

Neurodevelopment is evidently a highly regulated process with precise spatial and temporal benchmarks. Analysis of gene expression after maternal exposure to flu, PIC or IL6 in early neurodevelopment indicated a switch from genes relevant to neurogenesis to genes for neuroprotection in the acute phase of infection (Garbett et al., 2012). Indeed, there are many MIA studies with evidence of decreased neurogenesis or cell survival in foetal (Cui et al., 2009, De Miranda et al., 2010, Oskvig et al., 2012, Stolp et al., 2011), juvenile (Cui et al., 2009, Lin et al., 2014, Meyer et al., 2006b, Piontkewitz et al., 2012, Zhao et al., 2019) and adult (Cui et al., 2009, Graciarena et al., 2010, Hao et al., 2010, Lin et al., 2014, Samuelsson et al., 2006, Vallières et al., 2002, Wolf et al., 2011, Zhang et al., 2015) brains, see Table 6.2 for a summary. Markers of cell death are, interestingly, absent in animals exposed to MIA in early development (GD8-13.5) (Meyer et al., 2006b, Samuelsson et al., 2006, Stolp et al., 2011, Vasistha et al., 2020) and present in offspring exposed in late gestation (GD15-20) in both pre and postnatal tissue (De Miranda et al., 2010, Meyer et al., 2006b, Oskvig et al., 2012, Rousset et al., 2006, Samuelsson et al., 2006) (summarised in Table 6.3).

Table 6.2: Studies investigating the effect of MIA on neurogenesis and cell survival. Arrows show the change in direction, and multiple arrows show significant differences from other cohorts in the same study. LPS = Lipopolysaccharide, IL6 = interleukin 6, PIC = poly(I:C), CA1 = CA1 area of the hippocampus, CA2 = CA2 area of the hippocampus, CA3 = CA3 area of the hippocampus, DG = dentate gyrus, VZ = ventricular zone, PD = postnatal day, GD = gestational day, DCX = doublecortin, pH3 = phospho-histone H3, BrdU = Bromodeoxyuridine, GCL: granule cell layer.

Gestational day	Method of MIA	Region	Age of offspring measurement	Measure	Neurogenesis and proliferation	Cell number or survival	Reference
Transgenic overexpression of IL6	IL6	DG	PD84-112	24 hours after BrdU	↓ GCL		(Vallières et al., 2002)
			PD115-143	31 days after BrdU NeuN	↓ GCL	↓ BrdU/NeuN in GCL	
8, 10 + 12	LPS	CA1	PD84	Cell number		↓	(Hao et al., 2010)
			PD280			↓↓	
			PD560			↓↓↓	
9	PIC	DG	PD24	DCX	↓ in subGCL and outer GCL		(Meyer et al., 2006b)
10.5	LPS	DG	PD22	BrdU on PD21	↓		(Lin et al., 2014)
				DCX	↓		
			PD91	BrdU on PD90	↓		
				DCX	↓		
13.5	LPS	VZ	GD14	pH3	↓ BrdU ↓ pH3		(Stolp et al., 2011)
			GD15.5	BrdU to dam 2 hours post LPS	↔ BrdU ↔ pH3		
14, 16, 18 + 20	LPS	DG	PD67	BrdU on PDs 60-67	↓BrdU ↓DCX ↓BrdU/DCX	↓BrdU/NeuN	(Graciarena et al., 2010)
			PD97	NeuN DCX	↓BrdU	↓BrdU/NeuN	
15 + 16	LPS	DG	PD23	BrdU 4 hours after last LPS injection	↔		(Cui et al., 2009)
			PD42	BrdU on PD14		↓	

			PD60	BrdU 2 hours before cull	↔		
			PD88	BrdU on PD60		↔	
15	LPS	Cortex	GD15 (+4 hours after LPS)	mRNA /pathway analysis	↓ neurogenesis genes		(Oskvig et al., 2012)
	PIC	DG	PD196	BrdU on PD30-35		↓	(Zhang et al., 2015)
	PIC	DG	PD37	BrdU on PD 14–16		↓	(Piontkewitz et al., 2012)
			PD57	BrdU on PD 34–36		↓	
			PD72	BrdU on PD 49–51		↔	
			PD100	BrdU on PD 77–79		↔	
	PIC	DG	PD90	BrdU (PD57-59) Ki67 DCX NeuN	↓ Ki67/DCX ↓ BrdU/DCX ↓ Ki67	↓ BrdU ↓BrdU/NeuN	(Wolf et al., 2011)
16	PIC	Cortex	GD18	BrdU on GD16	↓		(De Miranda et al., 2010)
17	PIC	DG	PD24	DCX	↓ outer GCL		(Meyer et al., 2006b)
18	PIC	DG	PD28	BrdU on PD 27-28 DCX	↓ BrdU ↓BrdU/DCX ↓DCX		(Zhao et al., 2019)
18 + 19	LPS	DG	PD26	BrdU 4 hours after last LPS injection		↓	(Cui et al., 2009)
			PD14	BrdU 2 hours before cull	↔		
			PD42	BrdU on PD14		↓	
			PD60	BrdU 2 hours before cull	↔		
			PD88	BrdU on PD60		↔	

Table 6.3: Summary of studies investigating the effect of MIA on cell death. PIC = Poly(I:C), LPS = Lipopolysaccharide, S1 = somatosensory cortex, DG = dentate gyrus, M1 = motor cortex, PD = postnatal day, GD = gestational day, TUNEL = Terminal deoxynucleotidyl transferase dUTP nick end labelling, ♂: male, ♀: female.

Gestational day	Method of MIA	Region investigated	Age of offspring measurement	Measure	Change	Reference

8, 10 + 12	IL6	Hippocampus	PD28	Caspase-3	↔ ♂ ↔ ♀	(Samuelsson et al., 2006)
				Procaspase-3	↔ ♂ ↔ ♀	
			PD168	Caspase-3	↔ ♂ ↔ ♀	
9	PIC	DG	PD24	Caspase-3	↔	(Meyer et al., 2006b)
9.5	PIC	S1 / M1	GD17.5, PD3, PD6	Caspase-3	↔	(Vasistha et al., 2020)
13.5	LPS	Cortex	8 hours after LPS	TUNEL assay / Caspase -3	↔	(Stolp et al., 2011)
15	LPS	Cortex	GD15 (+4 hours after LPS)	mRNA /pathway analysis	↑ cellular stress and cell death pathways	(Oskvig et al., 2012)
16	PIC	Cortex	GD18	Caspase-3	↑	(De Miranda et al., 2010)
16, 18 + 20	IL6	Hippocampus	PD28	Caspase-3	↔ ♂	(Samuelsson et al., 2006)
					↑ ♀	
				Procaspase-3	↔ ♂	
					↑ ♀	
			PD168	Caspase-3	↑ ♂ ↑ ♀	
17	PIC	DG	PD24	Caspase-3	↑	(Meyer et al., 2006b)
19 + 20	LPS	Subventricular striatal zone	PD1	Caspase-3	↑	(Rousset et al., 2006)
		Periventricular striatum and germinative ventricular zone	PD7		↑	
		Periventricular striatum		TUNEL assay	↑	

6.1.7 Poly (I:C) maternal immune activation in mid-gestation

As MIA can induce acute maternal inflammation, which may lead to profound and long-lasting consequences for neuronal health, the next section will consider the effects that MIA may have on offspring cognition. Given the dynamic nature of neurodevelopment, the studies in Table 6.4 have focused on studies in rats where PIC was administered on GD15 to match the present study (Table 6.4a and b).

Table 6.4: Studies investigating the effect of GD15 MIA with PIC on offspring cognition. **Part A:** Green boxes: positive effect of model, red box: negative effect of model. Strain – SD: Sprague Dawley, LH: Lister hooded, LE: Long Evans. Dose in mg/Kg dam bodyweight on GD15. i.p.: intraperitoneal route, i.v.: intravenous. ♂: male, ♀: female. Offspring – sex of offspring tested ♂: male, ♀: female. Age – in postnatal days when cognition was assessed. ITI – intertrial interval between acquisition and retention trials, min: minute. DI: discrimination index, CM: cross-modal.

Strain	Dose/route	Offspring	Age	ITI	Outcome	Reference
Novel object recognition						
Wistar	10, i.p.	♂ and ♀	35	30 min	↔	(Potter et al., 2023)
SD	5, i.p.	♀ only	42-46	24 hours	↑ DI	(Su et al., 2022)
LH	10, i.p.	♂ and ♀	52-58	1 hour	↔	(Goh et al., 2020)
Wistar	4, i.v.	♂ only	58-60	2 hours	↔	(Guerrin et al., 2022)
SD	4, i.v.	♀ only	70-77	1 hour	↓ DI	(Osborne et al., 2019)
SD	4, i.v.	♂ and ♀	72	1 hour	↓ DI	(Osborne et al., 2017)
SD	5, i.p.	♂ only	84-88	24 hours	↓ DI	(Lian et al., 2022)
Wistar	4, i.v.	♂ only	88-90	2 hours	↓ DI	(Guerrin et al., 2022)
Wistar	10, i.p.	♂ and ♀	121	30 min	↔	(Potter et al., 2023)
Cross-modal object recognition						
SD	4, i.v.	♂ only	56 -112	1 hour	↔	(Lins et al., 2018)
LE	4, i.v.	♂ only	60-80	1 hour	↓ DI for CM	(Ballendine et al., 2015)
Associative object-in-place						
LE	4, i.v.	♂ only	60-80	1 hour	↓ DI	(Ballendine et al., 2015)
Novel location discrimination						
LH	10, i.p.	♂ and ♀	59-65	1 minute	↔	(Goh et al., 2020)

Table 6.4: Summary of studies investigating the effect of GD15 MIA with PIC on offspring cognition. **Part B:** Strain – SD: Sprague Dawley, LH: Lister hooded, LE: Long Evans. Dose in mg/Kg dam bodyweight on GD15. i.p.: intraperitoneal route, i.v.: intravenous. Offspring – sex of offspring tested ♂: male, ♀: female. Age – in postnatal days when cognition was assessed. ITI – intertrial interval between acquisition and retention trials, min: minute. ED: extra-dimensional shift, R3: reversal 3.

Strain	Dose and route	Offspring	Age	Outcome	Ref
Odd object exploration					
SD	4, i.v.	♂ only	56 - 112	↓ time interacting with odd object	(Lins et al., 2018)
T-maze					
SD	4, i.v.	♀ only	70-77	↔	(Osborne et al., 2019)
SD	4, i.v.	♂ and ♀	78	↓ correct entries %	(Osborne et al., 2017)
Radial arm maze					
Wistar	10, i.p.	♂ and ♀	128-137	↑ day 3 errors	(Potter et al., 2023)
Trial-unique nonmatching-to-location					
LE	4, i.v.	♂ and ♀	Adult	↓ %correct for males	(Gogos et al., 2020)
Odour span task					
LE	4, i.v.	♂ and ♀	60-90	↓ completed trials on testing days 8, 9 and 12	(Murray et al., 2017)
Fear conditioned learning					
SD	4, i.v.	♂ and ♀	71 +	↔	(Yee et al., 2012)
LH	10, i.p.	♂ and ♀	79-83	↔	(Goh et al., 2020)
Attentional set-shifting					
SD	4, i.v.	♂ only	56 - 112	↓ trials to complete ↓ number of errors	(Lins et al., 2018)
LH	10, i.p.	♂ and ♀	79-125	↔	(Goh et al., 2020)
Wistar	10, i.p.	♂ and ♀	126-134	↑ trials to complete (EDS, R3) ↑ number of errors	(Potter et al., 2023)
Strategy set shifting					
LE	4, i.v.	♂ and ♀	60 +	↑ number of trials and errors in ♂ only	(Zhang et al., 2012)
LE	4, i.v.	♂ only	80-100	↑ number of regressive errors	(Ballendine et al., 2015)
Reversal learning					
SD	4, i.v.	♂ only	56 - 112	↑ days to complete	(Lins et al., 2018)
LE	4, i.v.	♂ and ♀	60 +	↓ ♂ number of errors in regressive	(Zhang et al., 2012)
LE	4, i.v.	♂ only	80-100	↔	(Ballendine et al., 2015)
LE	4, i.v.	♂ and ♀	Adult	↔	(Gogos et al., 2020)
Visual cue discrimination					
LE	4, i.v.	♂ and ♀	60 +	↔	(Zhang et al., 2012)
LE	4, i.v.	♂ only	80-100	↑ number of errors	(Ballendine et al., 2015)

The novel object recognition task is helpful because animals can complete the test at young ages, likely due to it being a task that relies on innate, untrained preferences (Grayson et al., 2015). Here, the animals develop a NOR deficit from the age of PD70,

equivalent to approximately eighteen years old in humans (Ghasemi et al., 2021). Other tests can detect deficits earlier, though the reported testing window is often too broad to make significant conclusions. Alongside object recognition tasks showing deficits in recognition memory, PIC-treated rats also demonstrate impairments in working memory (Gogos et al., 2020, Murray et al., 2017, Osborne et al., 2017, Osborne et al., 2019, Potter et al., 2023), reasoning and problem-solving (Potter et al., 2023) and cognitive flexibility (Ballendine et al., 2015, Lins et al., 2018, Zhang et al., 2012).

6.1.8 Aims

1. Measure markers studied in the scPCP model in the PIC model to establish if there are points of convergence and divergence.

2. Evaluate the proteins in adolescent and adult time points to understand the developmental timeline of pathology.

6.2 Methods

6.2.1 Animal work

Other researchers completed the animal work (see contributions). Therefore, the animal work methods shall be discussed in brief here. Animals were housed throughout the study as described in 2.1. To induce maternal immune activation (MIA), male and female Wistar rats, sourced from Charles River, were mated in-house. Female mating weight 262 ± 1.97 (mean ± SEM). Mating pairs were housed in pairs in cages where bedding was removed, and a metal grate was placed on the floor. GD1 was assigned when a vaginal plug was observed. Females were then pair-housed until GD15. Dams were pseudorandomised to receive vehicle or PIC, and experimenters were blinded to the treatment group. On GD15, pregnant dams were injected with low molecular weight PIC (10mg/Kg bodyweight, i.p. InvivoGen) or vehicle (saline, 0.9%) (GD15 weight 313 ± 5.30g) between the hours of 9:00 and 10:00. Three hours after injection, tail vein blood was collected. Plasma was isolated by centrifuging the blood at 10,000xg for five minutes, then flash frozen on dry ice and stored at -80°C until use. Body weight was monitored throughout pregnancy to monitor dam health.

The collected plasma was used to measure IL6 and TNFα as these tend to be increased after PIC induction on PD15 (Ballendine et al., 2015, Dalton et al., 2012, Kowash et al., 2019, Kowash et al., 2022, Lins et al., 2018, Missault et al., 2014, Murray et al., 2019, Potter et al., 2023). These were measured using the commercial ELISA kits ab100784 for TNFα and ab100772 for IL6. In some cases, there was insufficient plasma to run the ELISAs.

Table 6.5: Origin of tissues used for post-mortem analysis. PIC: poly (I:C), WES: simple western analysis, qPCR: quantitative PCR, IHC: immunohistochemistry, ASST: attentional set-shifting.

Cohort	Number of dams	Study	Age of animals	Behaviourally assessed?	Deficit	Maternal cytokine
HP	Veh: 13 PIC: 16	WES	21, 35, 100	(Potter et al., 2023)	ASST at PD100	TNFα
RW	Veh: 6 PIC: 7	qPCR, IHC	35, 100	No	-	TNFα IL6

6.2.2 Tissue preparation

For both cohorts, each study (qPCR, WES, IHC) was populated with male and female offspring from each dam at each time point where possible. Offspring were assigned a code, and researchers were blinded to treatment groups.

6.2.3 qPCR

Brains were collected and dissected as described in section 2.5. The cDNA from the PFC was diluted for each target (Table 6.6).

Table 6.6: Dilutions used in the qPCR study.

Target	PFC	Target	PFC	Target	PFC
Acan	1:20	MMP9	1:20	PV	1:50
Bcan	1:20	Ncan	1:20	Ubiquitin	1:50
GAPDH	1:50	NFκB	1:20	Vcan	1:20
IL6	1:10	PSD95	1:50		

6.2.4 Simple western analysis

Brains for the simple western analysis were dissected, and protein was extracted from the PFC (section 2.6.3). For the PD35 cohort, only five brains were available for the male vehicle group. We added an additional female vehicle to balance the cohort size.

Table 6.7: Antibody details for simple western analysis. *samples were denatured at 40°C for 30 minutes (see 2.6.3).

Target	Product code	Supplier	Age	Protein concentration (mg/mL)	Antibody dilution
Parvalbumin	LS-B14122	LSBio	PD21	0.8	1:50
			PD35	0.8	1:50
			PD100	0.2	1:20
GAD67	MAB5406	Millipore	PD35	0.8	1:100
			PD100	0.2	1:50
SNAP25	Ab5666	Abcam	PD35	0.2	1:50
			PD100	0.1	1:50
PSD95	Ab2723	Abcam	PD35	0.2	1:50
			PD100	0.8	1:50
NR2A*	PPS012	R&D systems	PD21	0.035	1:100
			PD35	0.01	1:100
			PD100	0.035	1:100
NR2B*	PPS013	R&D systems	PD21	0.1	1:100
			PD35	0.07	1:100
			PD100	0.07	1:100

6.2.5 Immunohistochemistry

Brains were perfused, fixed and sectioned as described in section 2.8. Sections were stained for PVI and PNN, and the numbers of cells were counted as described.

6.2.6 Statistics

Table 6.8: Summary of statistical tests used in chapter six.

Purpose	Distribution	Test	Section
Check for normality	N/A	Shapiro-Wilk (n≤7)	2.9.1
Check for correlations	Normal Not normal	Pearson's Spearman's	2.9.5
Compare maternal cytokines	Normal	Unpaired t-test	2.9.3.a
	Not normal	Mann-Whitney U	2.9.3.b
Effects of age, sex and treatment	N/A	General linear mixed model	2.9.6.c

6.3 Results

6.3.1 Maternal immune response

We first wanted to establish that a maternal immune activation had occurred in the PIC-treated dams. Blood was taken from the tail vein three hours after PIC injection, and cytokine levels were measured in the resulting plasma. In the HP cohort, there was a significant increase in the levels of TNFα in the maternal plasma after PIC ($t_{9.327}$ = 6.263, p<0.001 [unequal variances]), the same TNFα increase was seen in the RW cohort ($t_{6.010}$ = 2.933, p = 0.026 [unequal variances]). In the RW cohort, IL6 levels were also increased ($t_{6.189}$ = 3.027, p = 0.022 [unequal variances]). We assessed whether maternal IL6 and TNFα response were linked in the RW cohort and found a cohort-wide positive correlation (Spearman's rho = 0.848, p<0.001, n=13). However, separating the dams into treatment groups revealed no significant correlation (V: rho = 0.493, p = 0.333, n=6; PIC: rho = 0.321, p = 0.498, n=7).

We were interested in the high variation in the PIC maternal cytokine response, with some dams having minimal TNFα response in both the HP and RW cohorts. Due to this variation, and previous studies showing that maternal cytokine response can predict maternal and offspring behaviour (Potter et al., 2023), we chose to include maternal cytokines as a covariate in a separate general linear mixed model (GLMM) to establish whether it significantly predicted offspring pathology.

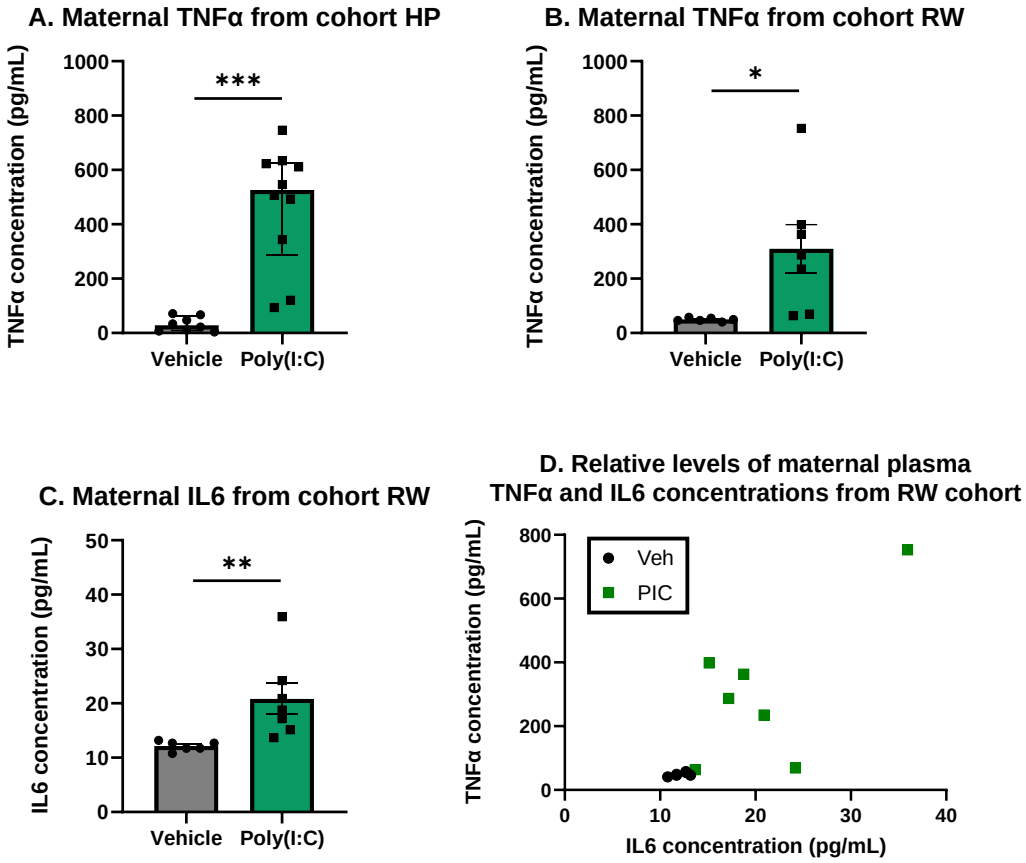

Figure 6.3: Maternal plasma cytokine levels three hours after treatment. Levels of TNFα from **A)** HP (n=13-16) and **B)** RW (n=6-7) cohort. **C)** IL6 levels in maternal plasma in the RW cohort (n=6-7). **D)** Scatter plot comparing maternal IL6 and TNFα concentrations in the RW cohort (n=6-7). Data for **A)** were analysed with Mann-Whitney U, and the graph shows median ± IQR. For graphs **B** and **C)** data were analysed with an unpaired t-test, and the graphs show mean ± SEM. **D)** was analysed with Spearman's correlation, and the graph shows the individual data points for each dam.

6.3.2 Offspring outcomes

Given the apparent induction of a maternal immune response in the PIC-exposed dams, we next investigated what outcomes this would have on the exposed offspring. We chose to investigate PD21, PD35 and PD100, though the PD21 tissue was limited to the HP cohort only. PD21, 35 and 100 are approximately equal to two, eleven and twenty-one years old in humans (Ghasemi et al., 2021). Typically, schizophrenia onset peaks in the mid-to-late twenties (Kirkbride et al., 2012), though cognitive impairments can be detected from thirteen years old (Dickson et al., 2012, Jonas et al., 2022), equivalent to PD55 in rats (Ghasemi et al., 2021). Reflecting on the cognitive behaviour data collected from rats exposed to PIC on GD15, the earliest detection of impairments was fittingly from PD56 rats (summarised in Table 6.4). Given the developmental nature of

schizophrenia and behavioural onset in the MIA model, we wished to assess markers relevant to cognition at these clinically relevant time points.

6.3.2.a VGlut1

We measured VGlut1 expression at PD35 and PD100 in the vehicle- and PIC-exposed offspring. We found that VGlut1 expression significantly decreased with age (postnatal day (PD)35: 2.708 ± 3.024, PD100: 0.619 ± 0.662; $F_{1, 30.916} = 10.955$, p = 0.002) (

Figure 6.4A). Sex and treatment were removed from the model before it reached significance, suggesting these factors did not alter offspring VGlut1 expression in the PFC.

Next, we included the maternal cytokines in the model to understand whether the prenatal environment would predict the postnatal outcomes. We investigated the cytokines independently as they were correlated (Figure 6.3). In general linear models, including highly related variables leads to multicollinearity, which can artificially inflate model estimates (Kim, 2019).

♦ *Maternal IL6*

There was an age*maternal IL6 interaction ($F_{2, 37} = 7.975$, p = 0.001), indicating maternal IL6 predicted offspring VGlut1 expression in a single age group. Indeed, analysis of the age groups in isolation revealed a near-significant effect of maternal IL6 in the PD35 cohort only ($F_{1, 14.159} = 4.177$, p = 0.060). To explore the relationship between maternal IL6 and offspring VGlut1, we performed a linear regression and found a positive relationship between the two measures ($R^2 = 0.311$, p = 0.011) (

Figure 6.4B).

♦ *Maternal TNFα*

Returning to the full cohort, we tested whether maternal TNFα predicted VGlut1 expression. Here, we found an age*maternal TNFα interaction ($F_{2, 37} = 4.717$, p = 0.015). However, analysis of the age groups did not result in any main effect of maternal TNFα.

6.3.2.b SNAP25

SNAP25 levels increased over development (PD35: 0.089 ± 0.082; PD100: 0.436 ± 0.238; $F_{1, 45} = 49.155$, p<0.001). In addition, there was a near significant effect of sex, with females having higher SNAP25 levels compared to males (males (M): 0.220 ± 0.224, females (F): 0.301 ± 0.267; $F_{1, 45} = 3.668$, p = 0.062) (

Figure 6.4C).

♦ *Maternal TNFα*

When considering the maternal cytokines, there was a significant age*treatment*maternal TNFα interaction ($F_{4, 34} = 5.339$, p = 0.002), likely driven by a trend towards a significant effect of maternal TNFα in the PD100 PIC-exposed offspring ($F_{1, 8} = 4.573$, p = 0.065). In this cohort,

increased maternal TNFα predicted a trend towards increased SNAP25 in the offspring (R^2 = 0.364, p = 0.065) (

Figure 6.4D).

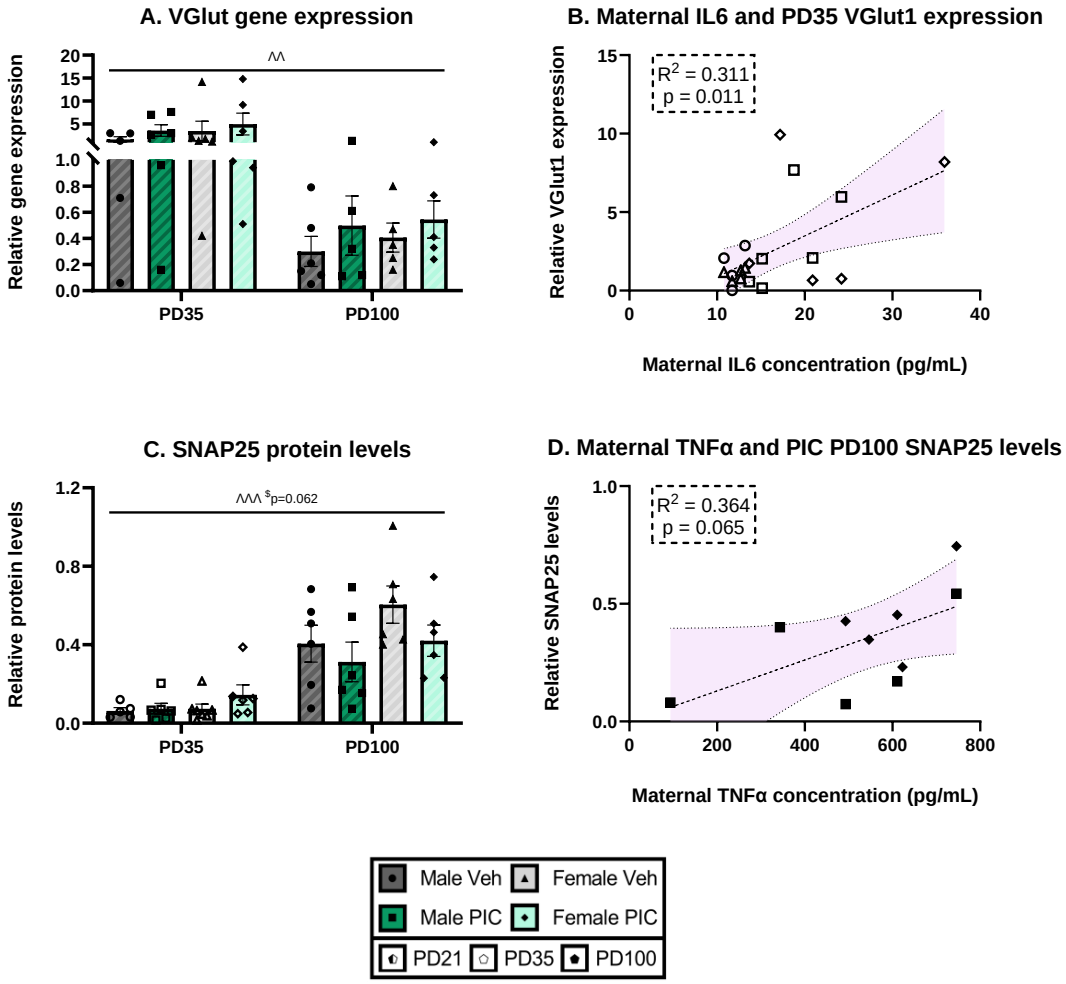

Figure 6.4: Effects of PIC on VGlut1 and SNAP25. **A)** Relative gene expression of VGlut1 in PD35 and PD100 offspring (n=5-6). **B)** Relationship between maternal IL6 plasma concentration and VGlut1 expression in PD35 offspring. **C)** Protein levels of SNAP25 in PD35 and PD100 offspring (n=5-7). **D)** Relationship between maternal TNFα plasma concentration and SNAP25 levels in the PIC-exposed PD100 offspring. For **A** and **C)** data were analysed with a GLMM. Black lines showed effects from a significant GLMM. Dashed lines show effects from a trending GLMM. ^=significant effect of age: ^p<0.05, ^^p<0.01, ^^^p<0.001. $=significant effect of sex: $p<0.05, $$p<0.01, $$$p<0.001. Ψ=significant effect of treatment: Ψp<0.05, ΨΨp<0.01, ΨΨΨp<0.001. Graphs show mean ± SEM. For **B** and **D)** graphs show data points for individual offspring, and the line shows the simple linear regression with 95% confidence intervals. A dashed line denotes a regression resulting from a trending (p<0.080) GLMM.

6.3.2.c NMDAr receptor

c. i) NR2A

Age significantly affected NR2A levels ($F_{2, 62.087} = 3.947$, $p = 0.024$), with levels increasing across the developmental timeline (PD21: 4.787 ± 1.699, PD35: 6.968 ± 4.505, PD100: 7.869 ± 4.732) (Figure 6.5A). The remaining variables and inclusion of the maternal cytokines did not produce significant models.

c. ii) NR2B

There was a significant effect of age ($F_{2, 69} = 13.846$, $p<0.001$) on NR2B levels due to levels peaking at PD35 (PD21: 1.076 ± 0.474, PD35 1.511 ± 0.722, PD100: 0.707 ± 0.307) (Figure 6.5B).

♦ *Maternal TNFα*

When we included maternal TNFα in the model, there was a significant interaction of age*sex*treatment*maternal TNFα ($F_{12, 18.631} = 2.574$, $p = 0.033$), indicating a single cohort where maternal TNFα may affect NR2B levels. However, exploring the unique groups did not reveal any that had a significant or trending main effect of maternal TNFα.

c. iii) NMDAr subunit ratio

We were interested in the ratio of the subunits as this fluctuates during development (Liu et al., 2004, Riva et al., 1994, Snell et al., 2001). As expected, there was a significant effect of age ($F_{2, 54.088} = 24.738$, $p<0.001$), with the ratio increasing in adulthood (PD21: 5.273 ± 2.765, PD35: 4.791 ± 3.060, PD100: 13.432 ± 9.547). In addition, males had an increased ratio compared to females (males (M): 9.124 ± 8.764, females (F): 6.493 ± 4.828; $F_{1, 50.048} = 5.307$, $p = 0.025$), and prenatal exposure to PIC reduced the subunit ratio (V: 9.278 ± 8.101, P: 6.271 ± 5.605; $F_{1, 17.116} = 5.348$, $p = 0.033$).

In addition to the main effects, there were interactions between age*sex ($F_{2, 56.120} = 5.610$, $p = 0.006$) and age*treatment ($F_{2, 54.266} = 3.381$, $p = 0.041$). Further investigations revealed that the effects of sex and treatment were limited to the PD100 cohort, with increased levels in the male (M: 17.730 ± 10.786, F: 9.491 ± 6.413; $F_{1, 14.927} = 6.988$, $p = 0.018$) and vehicle-exposed offspring (vehicle (V): 17.235 ± 9.678, PIC (P): 9.945 ± 8.333; $F_{1, 12.158} = 5.255$, $p = 0.040$) (Figure 6.5C).

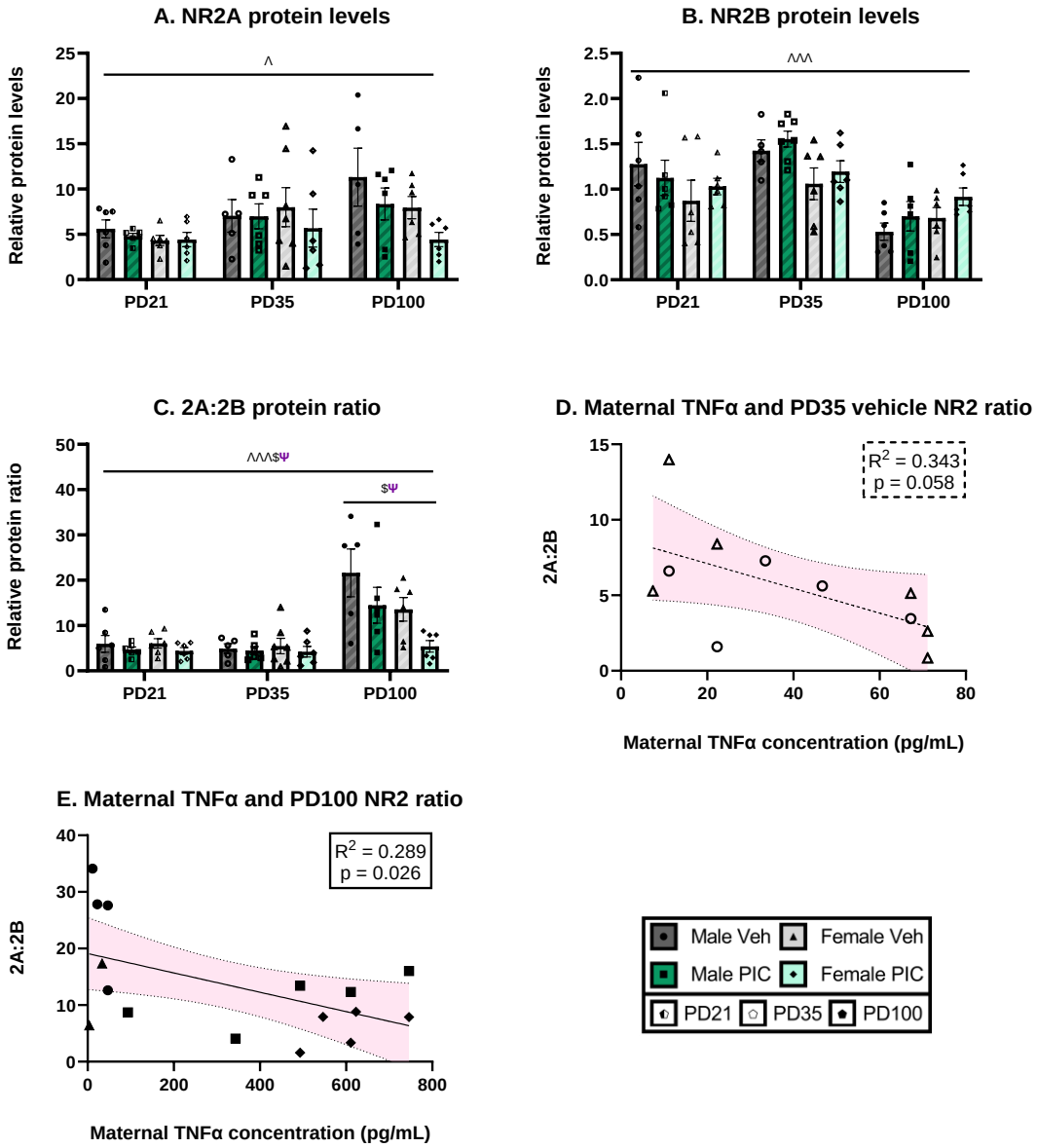

Figure 6.5: Effects of PIC on NMDAr subunit levels. Relative protein levels of **A)** NR2A and **B)** NR2B in PD21, PD35 and PD100 offspring. **C)** The ratio of NR2A and NR2B in PD21, PD35 and PD100 offspring (n=5-7). The relationship between maternal TNFα and NMDAr subunit ratio in the **D)** PD35 vehicles and **E)** PD100 offspring. For **A**–**C),** data were analysed with a GLMM. Black lines showed effects from a significant GLMM. Dashed lines show effects from a trending GLMM. ^=significant effect of age: ^p<0.05, ^^p<0.01, ^^^p<0.001. $=significant effect of sex: $p<0.05, $$p<0.01, $$$p<0.001. Ψ=significant effect of treatment: Ψp<0.05, ΨΨp<0.01, ΨΨΨp<0.001. Graphs show mean ± SEM. For **D** and **E)** graphs show data points for individual offspring, and the line shows the simple linear regression with 95% confidence intervals. A dashed line denotes a regression resulting from a trending (p<0.080) GLMM.

♦ *Maternal TNFα*

When maternal TNFα was included in the model, there was a significant interaction between age*maternal TNFα ($F_{3, 30.511}$ = 12.927, p<0.001) and age*treatment*maternal TNFα ($F_{3, 31.446}$ = 11.958, p<0.001). Regarding the latter interaction, we found a near

significant effect of maternal TNFα in the PD35 vehicle offspring ($F_{1, 9}$ = 4.708, p = 0.058), which resulted in a negative linear relationship (R^2 = 0.343, p = 0.058) (Figure 6.5D).

Regarding the significant age*maternal TNFα interaction, we found a significant main effect of maternal TNFα in the PD100 cohort ($F_{1, 15}$ = 6.094, p = 0.026), revealing a negative relationship between maternal TNFα and offspring NMDAr subunit ratio (R^2 = 0.289, p = 0.026) (Figure 6.5E).

6.3.2.d PSD95

d. i) Gene expression

Age was a significant predictor of offspring PSD95 expression with expression decreasing over development (PD35: 0.190 ± 0.110, PD100: 0.125 ± 0.071; $F_{1, 45}$ = 5.745, p = 0.021). There were no further models (Figure 6.6A).

d. ii) Protein levels

Unlike the mRNA expression, the protein levels increased over development (PD21: 0.810 ± 0.900, PD35: 1.897 ± 1.868, PD100: 1.645 ± 1.441; $F_{2, 49.903}$ = 11.293, p<0.001). In addition to the main effect of age, there were significant age*treatment ($F_{3, 39.332}$ = 4.966, p = 0.005) and age*sex*treatment interactions ($F_{7, 50.187}$ = 2.899, p = 0.013).

We first investigated the age*treatment interaction. We found a significant effect of treatment in the PD100 cohort only, with PIC exposure reducing PSD95 levels (V: 2.793 ± 0.926, F: 1.596 ± 0.667; $F_{2, 21}$ = 6.236, p = 0.007). Exploration of the age*sex*treatment interaction revealed that the treatment effect was isolated to the PD100 male offspring, where PIC exposure reduced PSD95 levels (V: 2.882 ± 1.048, P: 1.277 ± 0.534; $F_{1, 10}$ = 11.160, p = 0.007) (Figure 6.6B).

♦ *Maternal TNFα*

There were several significant interactions which included maternal TNFα, namely age ($F_{2, 37.252}$ = 8.859, p<0.001), treatment ($F_{2, 26.856}$ = 3.568, p = 0.042) age*sex ($F_{3, 36.436}$ = 3.028, p = 0.042) age*treatment ($F_{2, 37.299}$ = 8.657, p<0.001) and age*sex*treatment ($F_{3, 36.437}$ = 3.377, p = 0.029).

Beginning with the simplest interactions, we first identified PD100 as the age where there was a main effect of maternal TNFα ($F_{1, 15}$ = 4.736, p = 0.046), with increased maternal TNFα levels predicting reduced PSD95 levels in the offspring (R^2 = 0.240, p = 0.046) (Figure 6.6C).

Investigations of the remaining interactions did not produce any models with a significant main effect of maternal TNFα.

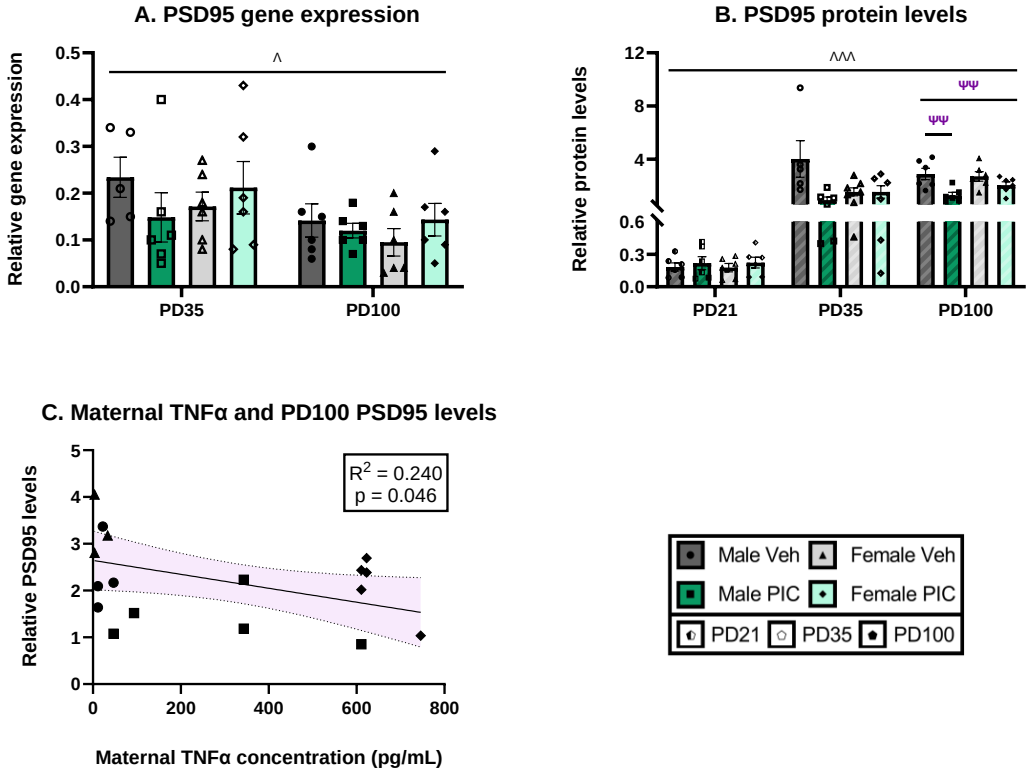

Figure 6.6: Effects of PIC on PSD95 protein expression and levels. Relative **A)** gene expression and **B)** protein levels in PD21, PD35 and PD100 offspring (n=5-7). **C)** Relationship between maternal TNFα plasma concentration and PD100 offspring PSD95 levels. For **A** and **B),** data were analysed with a GLMM. Black lines showed effects from a significant GLMM. Dashed lines show effects from a trending GLMM. $^{\wedge}$=significant effect of age: $^{\wedge}$p<0.05, $^{\wedge\wedge}$p<0.01, $^{\wedge\wedge\wedge}$p<0.001. $^{\$}$=significant effect of sex: $^{\$}$p<0.05, $^{\$\$}$p<0.01, $^{\$\$\$}$p<0.001. $^{\Psi}$=significant effect of treatment: $^{\Psi}$p<0.05, $^{\Psi\Psi}$p<0.01, $^{\Psi\Psi\Psi}$p<0.001. Graphs show mean ± SEM. For **C),** the graph shows data points for individual offspring, and the line shows the simple linear regression with 95% confidence intervals. A dashed line denotes a regression resulting from a trending (p<0.080) GLMM.

6.3.2.e GAD67

GAD67 levels increased over the developmental ages measured (PD35: 0.427 ± 0.251, PD100: 0.725 ± 0.412; $F_{1, 41.288} = 9.004$, p = 0.005). Moreover, PIC reduced GAD67 levels across all age groups (V: 0.696 ± 0.439, P: 0.456 ± 0.238; $F_{1, 17.642} = 5.606$, p = 0.030) (Figure 6.7A).

♦ *Maternal TNFα*

When maternal TNFα was included in the model, there was a significant main effect of maternal TNFα ($F_{1, 34} = 5.553$, p = 0.024). However, plotting this data did not result in a significant linear regression ($R^2 = 0.022$, p = 0.842).

In addition to its main effects, maternal TNFα interacted with treatment ($F_{1, 34} = 6.292$, p = 0.017) and sex*treatment ($F_{2, 34} = 5.121$, p = 0.011). Only the sex*treatment interaction resulted in a significant main effect of maternal TNFα. This was due to the male vehicles where increased maternal TNFα predicted increased GAD67 levels ($F_{1, 7} = 8.378$, p = 0.023; $R^2 = 0.545$, p = 0.023) (Figure 6.7B).

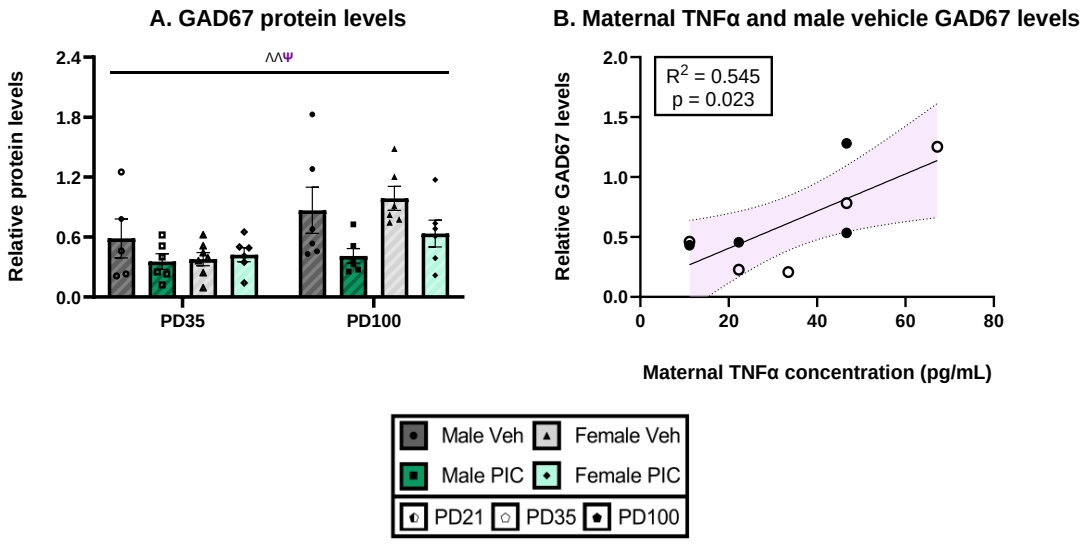

Figure 6.7: Effect of PIC on GAD67 levels. A) GAD67 protein levels in PD35 and PD100 offspring (n=5–7). **B)** Relationship between maternal TNFα plasma concentration and GAD67 levels in male vehicle offspring. For **A),** data were analysed with a GLMM. Black lines showed effects from a significant GLMM. Dashed lines show effects from a trending GLMM. ^significant effect of age: ^p<0.05, ^^p<0.01, ^^^p<0.001. $significant effect of sex: $p<0.05, $$p<0.01, $$$p<0.001. Ψsignificant effect of treatment: Ψp<0.05, ΨΨ p<0.01, ΨΨΨ p<0.001. Graphs show mean ± SEM. For **B),** the graph shows data points for individual offspring, and the line shows the simple linear regression with 95% confidence intervals. A dashed line denotes a regression resulting from a trending (p<0.080) GLMM.

6.3.2.f Parvalbumin

f. i) Gene expression

Parvalbumin expression significantly increased with age (PD35: 0.665 ± 0.667, PD100: 1.353 ± 1.123; $F_{1, 45}$ = 7.622, p = 0.008). We also observed a significantly higher expression in females (M: 0.663 ± 0.510, F: 1.355 ± 1.201; $F_{1, 45}$ = 7.734, p = 0.008) (Figure 6.8A).

♦ *Maternal IL6*

There were no models including maternal IL6.

♦ *Maternal TNFα*

By including maternal TNFα in the model, it revealed significant interactions of the cytokine with age ($F_{1, 33}$ = 6.103, p = 0.019), sex ($F_{1, 33}$ = 5.502, p = 0.025), age*treatment ($F_{1, 33}$ = 5.991, p = 0.020) and sex*treatment ($F_{1, 33}$ = 4.846, p = 0.035).

We first investigated the age*maternal TNFα interaction, here we found a significant main effect of maternal TNFα in the PD35 cohort only ($F_{1, 11.78}$ = 19.434, p<0.001), with increased maternal TNFα predicting increased parvalbumin expression (R^2 = 0.542, p<0.001) (Figure 6.8B).

Next, we looked at the sex*maternal TNFα interaction, which was likely driven by the males, who had a near significant main effect of maternal TNFα ($F_{1, 10.298}$ = 4.723, p = 0.054), producing a positive correlation (R^2 = 0.310, p = 0.011; Figure 6.8C).

The age*treatment interaction was due to a trend towards a significant main effect of maternal TNFα in the PD35 PIC-exposed offspring ($F_{1, 4.806}$ = 5.790, p = 0.063). This resulted in a positive linear relationship (R^2 = 0.518, p = 0.019), the data for which is contained in Figure 6.8B. Investigations of the sex*treatment*maternal TNFα did not result in any significant models.

f. ii) Protein levels

Age significantly affected parvalbumin protein levels, with levels peaking in PD35 (PD21: 0.22 ± 0.111, PD35: 0.775 ± 0.438, PD100: 0.579 ± 0.278; $F_{2, 67}$ = 21.624, p<0.001) (Figure 6.8D).

♦ *Maternal TNFα*

Several interactions included maternal TNFα, namely age ($F_{2, 42.483}$ = 7.891, p = 0.001), sex ($F_{1, 35.119}$ = 4.241, p = 0.047), age*treatment ($F_{2, 42.519}$ = 4.633, p = 0.015) and

sex*treatment ($F_{1, 35.145}$ = 5.070, p = 0.031). Despite these findings, further exploration of all interactions did not result in any significant main effects of maternal TNFα.

f. iii) Immunohistochemistry

There was a significant effect of sex in the PVI density, with females having increased density compared to males (M: 127.483 ± 18.734, F: 141.378 ± 26.731; $F_{1, 44}$ = 4.168, p = 0.047) (Figure 6.8C). Including the maternal cytokines in the model did not result in significant models.

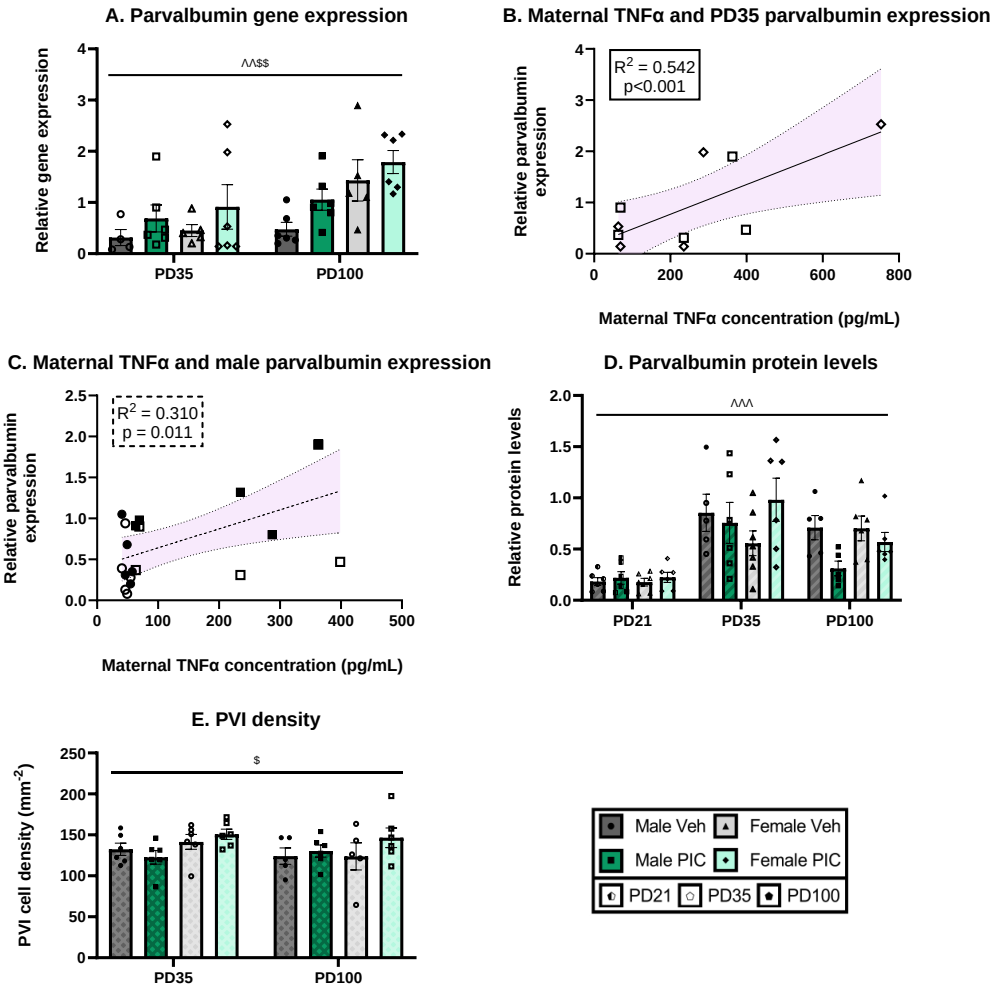

Figure 6.8: Effect of PIC on parvalbumin gene expression, protein levels and cell density. Parvalbumin **A)** gene expression, **D)** protein levels and **E)** cell density in PD21, PD35 and PD100 offspring (n=5–7). Relationship between maternal TNFα and parvalbumin expression in **B)** PD35 and **C)** male offspring. For **A**, **D** and **E)** data were analysed with a GLMM. Black lines showed effects from a significant GLMM. Dashed lines show effects from a trending GLMM. ^significant effect of age: ^p<0.05, ^^p<0.01, ^^^p<0.001. $significant effect of sex: $p<0.05, $$p<0.01, $$$p<0.001. Ψsignificant effect of treatment: Ψp<0.05, ΨΨ p<0.01, ΨΨΨ p<0.001. Graphs show mean ± SEM. For **B** and **C)** graphs show data points for individual offspring, and the line shows the simple linear regression with 95% confidence intervals. A dashed line denotes a regression resulting from a trending (p<0.080) GLMM.

6.3.2.g Perineuronal nets

g. i) Aggrecan

There were many significant effects when analysing aggrecan (Acan). First, Acan expression increases across development (PD35: 1.451 ± 1.665, PD100: 2.707 ± 2.188; $F_{1, 42}$ = 6.515, p = 0.014) in females (M: 1.234 ± 1.294, F: 2.805 ± 2.467; $F_{1, 42}$ = 9.444, p = 0.004), and in PIC treated offspring (V: 1.460 ± 1.482, P: 2.697 ± 2.327; $F_{1, 45}$ = 6.413, p = 0.015).

There was also an age*sex interaction ($F_{1, 42}$ = 4.180, p = 0.047). Further analysis of the age*sex interaction revealed it was either driven by an effect of sex in the PD100 offspring (M: 1.393 ± 0.810, F: 3.911 ± 2.382; $F_{1, 13.612}$ = 12.177, p = 0.004) or by an effect of age in the females (PD35: 1.698 ± 0.647; PD100: 3.911 ± 0.647; **$F_{1, 22}$ = 5.844, p = 0.024) (**

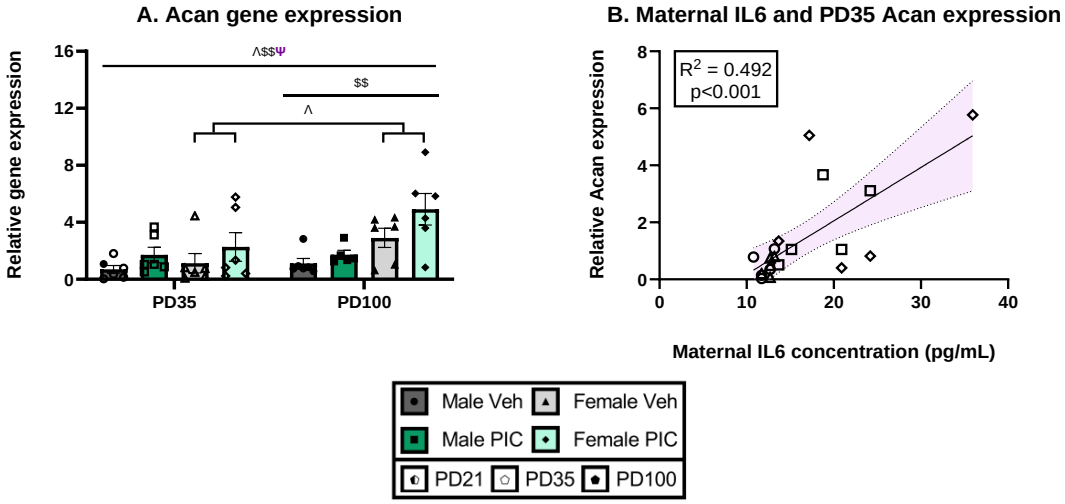

Figure 6.9A).

♦ *Maternal IL6*

Including maternal IL6 in the model revealed a significant age*maternal IL6 interaction ($F_{2, 36}$ = 6.570, p = 0.004). Investigations of the individual ages revealed that this was driven by the PD35 cohort ($F_{1, 10.975}$ = 13.906, p = 0.003). Moreover, plotting these data revealed a positive relationship between maternal IL6 and Acan expression (R^2 = 0.492,

p<0.001) (

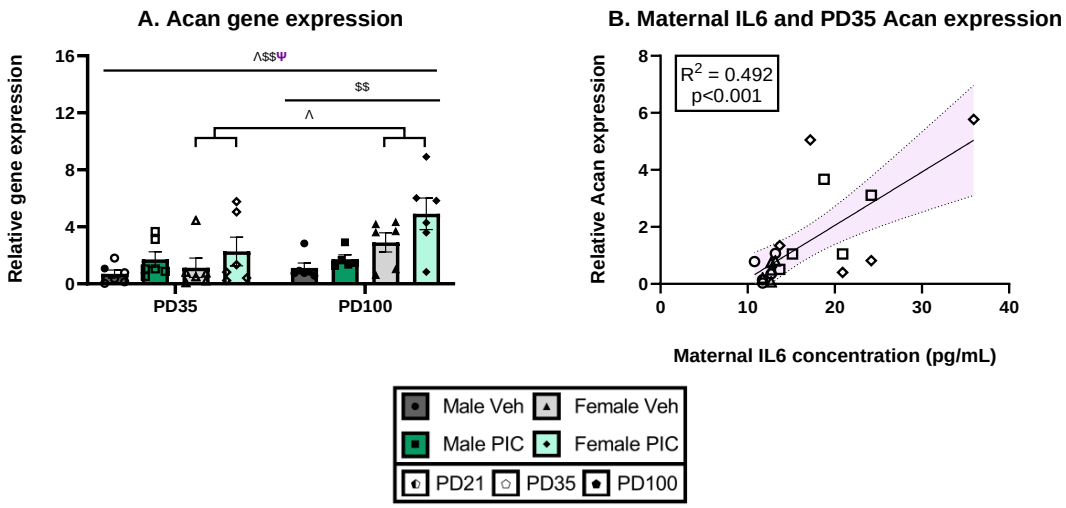

Figure 6.9B).

♦ *Maternal TNFα*

There was a significant age*treatment*TNFα interaction ($F_{4, 34}$ = 3.781, p = 0.012). However, further explorations of this interaction did not result in any significant main effects of maternal TNFα.

g. ii) Brevican

There were no significant brevican (Bcan) models when running a standard GLMM (Figure 6.10A).

♦ *Maternal IL6*

The inclusion of maternal IL6 in the model revealed a significant effect of IL6 on offspring Bcan expression ($F_{1, 35}$ = 4.215, p = 0.048). However, this did not result in a significant linear regression (R^2 = 0.023, p = 0.388).

♦ *Maternal TNFα*

There were no significant models including maternal TNFα.

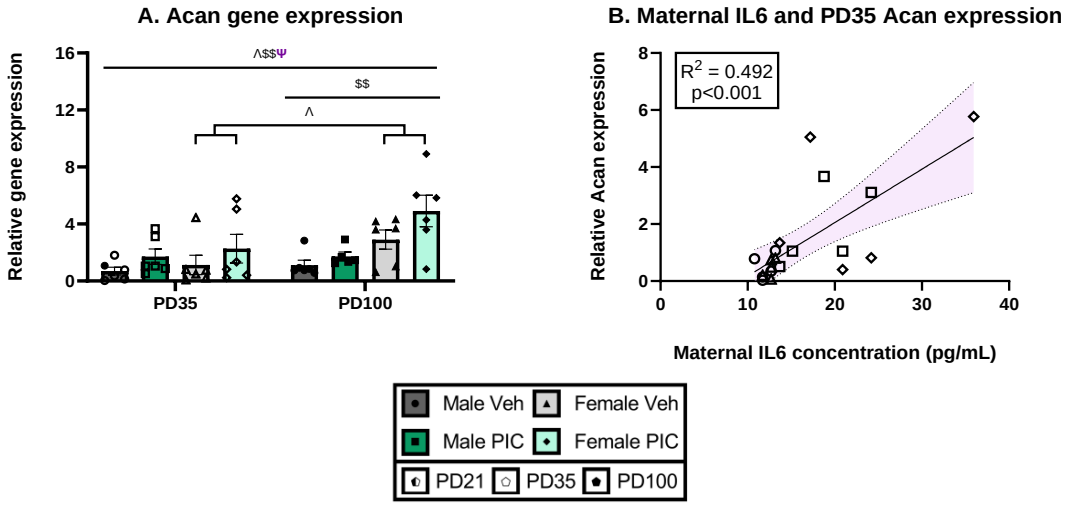

Figure 6.9: Effect of PIC on Acan expression. A) Acan expression in PD35 and PD100 offspring (n=5–6). **B)** Relationship between maternal IL6 and PD35 Acan expression. Regression of maternal IL6 plasma concentration and Acan levels in PD35 offspring. For **A),** data were analysed with a GLMM. Black lines showed effects from a significant GLMM. Dashed lines show effects from a trending GLMM. ^significant effect of age: ^p<0.05, ^^p<0.01, ^^^p<0.001. $significant effect of sex: $p<0.05, $$p<0.01, $$$p<0.001. Ψsignificant effect of treatment: Ψp<0.05, ΨΨ p<0.01, ΨΨΨ p<0.001. Graphs show mean ± SEM. For **B),** the graph shows data points for individual offspring, and the line shows the simple linear regression with 95% confidence intervals. A dashed line denotes a regression resulting from a trending (p<0.080) GLMM.

g. iii) Versican

Versican (Vcan) expression increased throughout the developmental stages we measured (PD35: 4.615 ± 4.916, PD100: 13.086 ± 9.577; $F_{1, 43} = 17.859$, p<0.001) and was increased in females (M: 5.632 ± 4.531, F: 11.758 ± 10.475; $F_{1, 43} = 9.609$, p = 0.003).

In addition, the age*sex interaction was significant ($F_{1, 43} = 5.370$, p = 0.025). This interaction was due to females having increased Vcan expression in the PD100 cohort (M: 7.574 ± 2.442; F: 18.138 ± 2.338; $F_{1, 21} = 9.767$, p = 0.005) (Figure 6.10B).

♦ *Maternal IL6*

Maternal IL6 significantly interacted with age ($F_{1, 30} = 16.561$, p<0.001), sex ($F_{1, 30} = 7.953$, p = 0.008), age*sex ($F_{1, 30} = 4.880$, p = 0.035) and age*sex*treatment ($F_{4, 30} = 3.780$, p = 0.013).

We first investigated the most straightforward interactions. In the PD35 cohort, there was a significant main effect of maternal IL6 ($F_{1, 10.808} = 6.954$, p = 0.023). Notably, the dam neared statistical significance in this model (17.904 ± 9.697 (estimate ± standard error), p = 0.064), meaning that the sibling membership predicts offspring Vcan

expression. Plotting the relationship between maternal IL6 and PD35 Vcan expression revealed a positive correlation (R^2 = 0.336, p = 0.007) (Figure 6.10C).

Next, we investigated the sex*maternal IL6 interaction, we found maternal IL6 predicted male offspring Vcan expression ($F_{1, 17}$ = 4.760, p = 0.043; R^2 = 0.219, p = 0.043) (Figure 6.10D).

The age*sex*maternal IL6 interaction further narrowed down the source of the positive relationship, with a significant effect of maternal IL6 in the PD35 males ($F_{1, 8}$ = 8.630, p = 0.019; R^2 = 0.519, p = 0.019). These data are found in Figure 6.10C and D.

Finally, although there was an age*sex*treatment*maternal IL6 interaction, individual investigations of the groups did not reveal any significant models.

♦ *Maternal TNFα*

There were several significant interactions including maternal TNFα, namely age ($F_{1, 30}$ = 15.107, p<0.001), sex ($F_{1, 30}$ = 8.236, p = 0.007), age*sex ($F_{1, 30}$ = 5.528, p = 0.025), age*treatment ($F_{1, 30}$ = 12.040, p = 0.002), sex*treatment ($F_{1, 30}$ = 7.442, p = 0.011) and age*sex*treatment ($F_{1, 30}$ = 7.192, p = 0.012).

We first sought to identify which age was predicted by maternal TNFα. There was a significant main effect of maternal TNFα in the PD35 cohort ($F_{1, 10.653}$ = 12.485, p = 0.005), resulting in a positive relationship (R^2 = 0.483, p<0.001) (Figure 6.10E).

The remaining interactions did not have a significant main effect of maternal TNFα.

Despite the significant model in the PD35 cohort, we also found significant models in the PD100 group. There was a significant sex*maternal TNFα ($F_{2, 10.029}$ = 4.891, p = 0.033) and sex*treatment*maternal TNFα interaction ($F_{2, 9.316}$ = 4.347, p = 0.046). However, there were no further significant models when exploring these interactions.

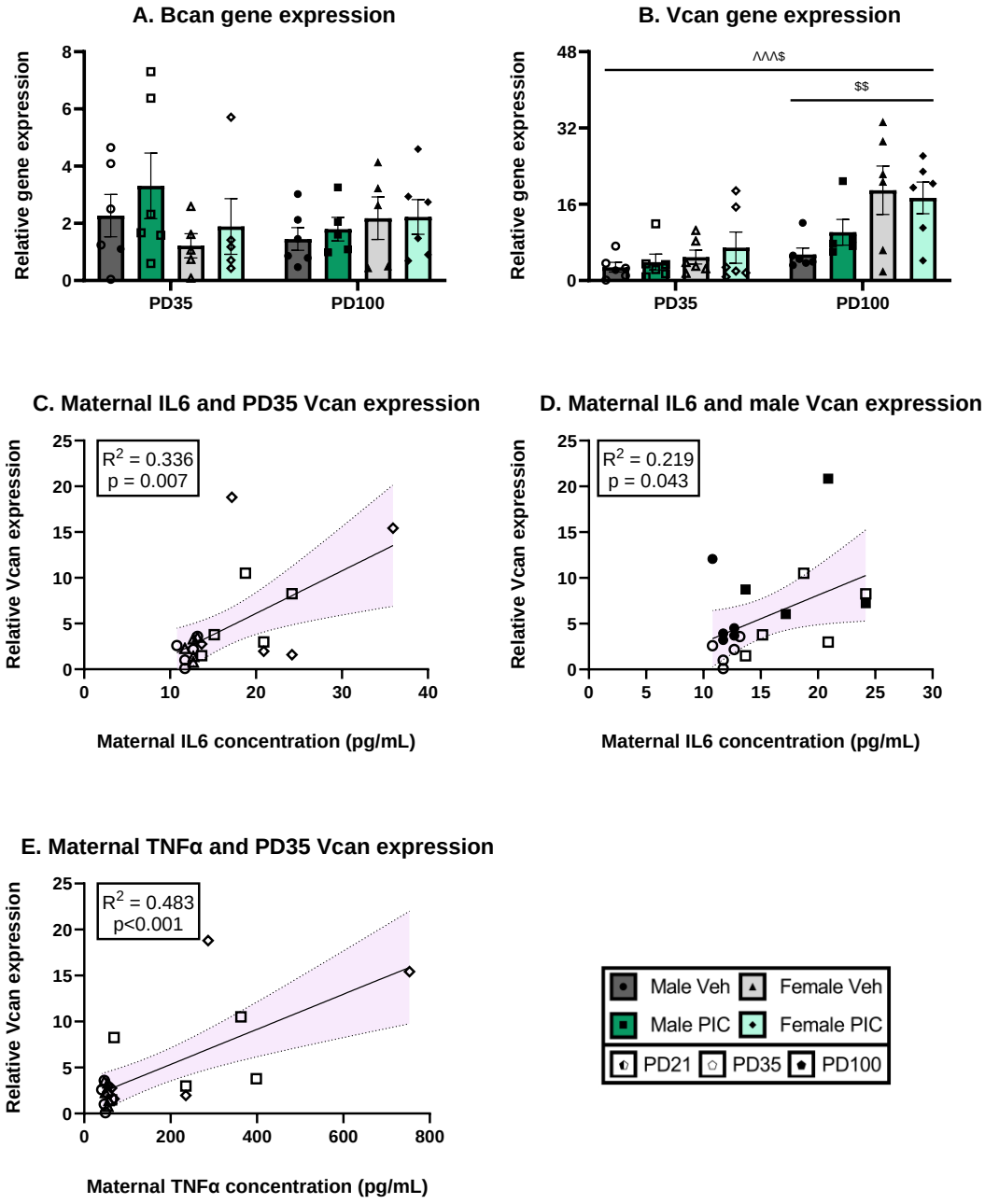

Figure 6.10: Effect of PIC on Bcan and Vcan expression. A) Bcan and **B)** Vcan expression in PD35 and PD100 offspring (n=5-6). Relationship between maternal IL6 and Vcan expression in **C)** PD35 and **D)** male offspring. **E)** Relationship between maternal TNFα and PD35 offspring Vcan expression. For **A** and **B),** data were analysed with a GLMM. Black lines showed effects from a significant GLMM. Dashed lines show effects from a trending GLMM. ^significant effect of age: ^p<0.05, ^^p<0.01, ^^^p<0.001. $significant effect of sex: $p<0.05, $$p<0.01, $$$p<0.001. Ψsignificant effect of treatment: Ψp<0.05, ΨΨ p<0.01, ΨΨΨ p<0.001. Graphs show mean ± SEM. For **C** - **E)**, graphs show data points for individual offspring, and the line shows the simple linear regression with 95% confidence intervals. A dashed line denotes a regression resulting from a trending (p<0.080) GLMM.

g. iv) Neurocan

There was a significant effect of age (PD35: 2.482 ± 2.427, PD100: 5.026 ± 3.468; $F_{1, 42}$ = 10.500, p = 0.002), treatment (V: 2.843 ± 2.973, P: 4.680 ± 3.115; $F_{1, 42}$ = 5.634, p = 0.022) and the age*sex interaction ($F_{2, 42}$ = 3.376, p = 0.044) in the neurocan (Ncan) GLMM.

To find the source of the age*sex interaction, we split the cohort into PD35 and PD100. Here we found a significant effect of sex in the PD100 cohort only (M: 3.577 ± 3.170, F: 6.476 ± 3.243; $F_{1, 9.465}$ = 5.321, p = 0.045) (Figure 6.11A).

♦ *Maternal IL6*

Including maternal IL6 in the model revealed a significant effect of the age*maternal IL6 interaction ($F_{2, 37}$ = 3.860, p = 0.030), which was driven by the PD35 cohort ($F_{1, 10.731}$ = 5.772, p = 0.038). The resulting linear regression was significant (R^2 = 0.301, p = 0.012) (Figure 6.11B).

♦ *Maternal TNFα*

There were several interactions including maternal TNFα that predicted offspring neurocan expression. There were interactions including age ($F_{1, 31}$ = 11.946, p = 0.002), sex ($F_{1, 31}$ = 6.392, p = 0.017), age*sex ($F_{1, 31}$ = 5.028, p = 0.032), age*treatment ($F_{1, 31}$ = 9.051, p = 0.005), sex*treatment ($F_{1, 31}$ = 5.028, p = 0.032) and age*sex*treatment ($F_{1, 31}$ = 7.851, p = 0.009).

Beginning with the age*maternal TNFα interaction, the maternal cytokine predicted offspring Ncan expression in the PD35 cohort only ($F_{1, 11.389}$ = 16.043, p = 0.002; R^2 = 0.513, p<0.001) (Figure 6.11C).

Investigating the sex*maternal TNFα interaction revealed a significant main effect of maternal TNFα in the males ($F_{1, 18}$ = 15.879, p<0.001; R^2 = 0.469, p<0.001) (Figure 6.11D).

Indeed, combining the PD35 and male cohorts revealed the source of the age*sex interaction ($F_{1, 8}$ = 7.100, p = 0.029; R^2 = 0.470, p = 0.029), this data are found in Figure 6.11C.

Investigations of the remaining interactions did not result in any main effects of maternal TNFα.

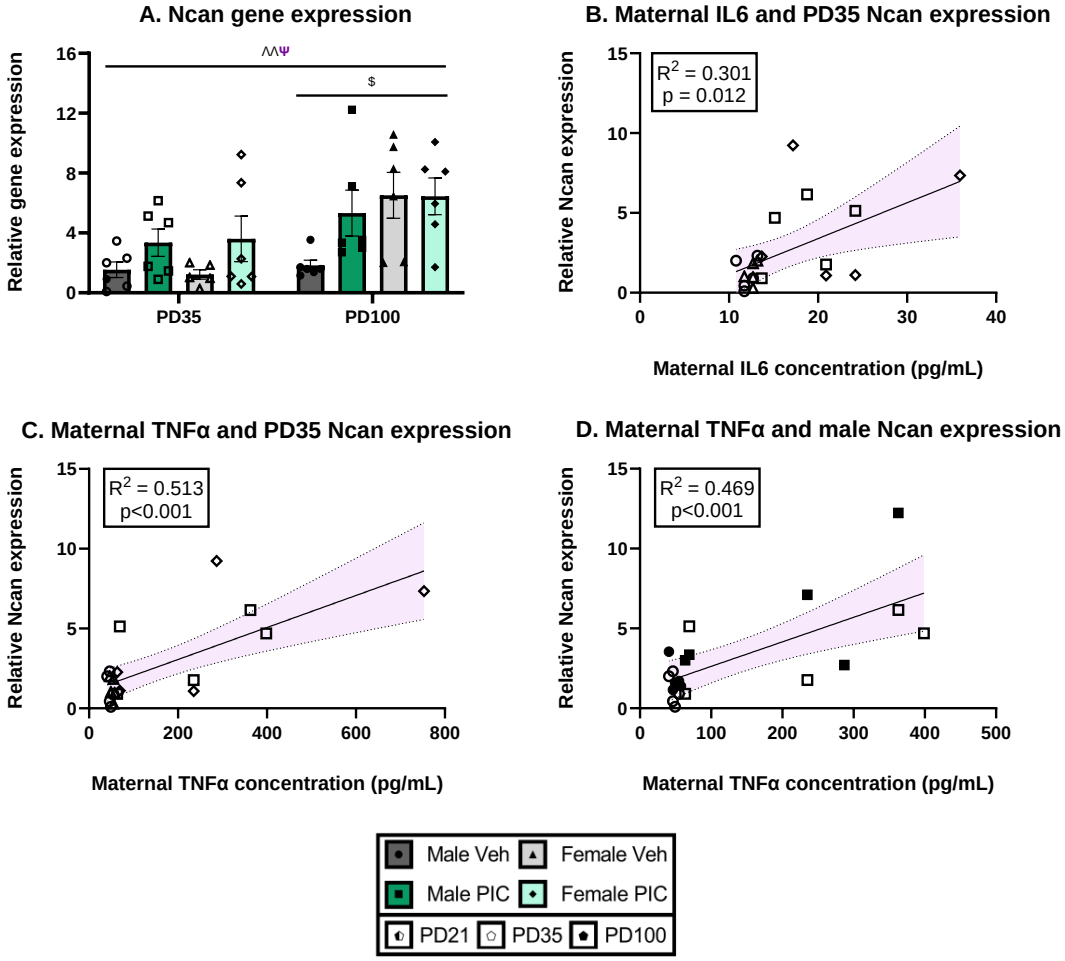

Figure 6.11: Effect of PIC on Ncan expression. A) Ncan expression in PD35 and PD100 offspring (n=5-6). **B)** Relationship between maternal IL6 and PD35 Ncan expression. Relationship between maternal TNFα and Ncan expression of **C)** PD35 and **D)** male offspring. For **A),** data were analysed with a GLMM. Black lines showed effects from a significant GLMM. Dashed lines show effects from a trending GLMM. ^significant effect of age: ^p<0.05, ^^p<0.01, ^^^p<0.001. $significant effect of sex: $p<0.05, $$p<0.01, $$$p<0.001. Ψsignificant effect of treatment: Ψp<0.05, ΨΨ p<0.01, ΨΨΨ p<0.001. Graphs show mean ± SEM. For **B** - **D)**, graphs show data points for individual offspring, and the line shows the simple linear regression with 95% confidence intervals. A dashed line denotes a regression resulting from a trending (p<0.080) GLMM.

g. v) PNN density

We analysed the PNN density using immunohistochemistry. We found a significant increase in density in the PD100 offspring compared to PD35 (PD35: 64.700 ± 10.434, PD100: 104.322 ± 13.874; $F_{1, 38.038}$ = 215.331, p<0.001) and a significant increase in the PIC-treated cohort (V: 76.561 ± 20.121, P: 91.304 ± 24.421; $F_{1, 13.943}$ = 15.591, p = 0.001) (Figure 6.12A).

♦ *Maternal IL6*

There were significant interactions including maternal IL6 and age ($F_{1, 33.096}$ = 100.472, p<0.001), treatment ($F_{1, 10.984}$ = 7.037, p = 0.023) and age*treatment ($F_{1, 33.110}$ = 4.771). Investigation of the individual ages resulted in a trend for the treatment*maternal IL6 interaction in PD100 animals ($F_{2, 8.933}$ = 3.203, p = 0.089). Further investigations of the treatment and age*treatment interactions with maternal IL6 did not result in significant models.

♦ *Maternal TNFα*

Including maternal TNFα in the model resulted in a significant age*maternal TNFα ($F_{2, 34}$ = 27.083, p<0.001) and age*treatment*maternal TNFα ($F_{2, 35}$ = 15.871, p<0.001) interactions. Investigations of the former interaction revealed a significant main effect of maternal TNFα in the PD100 cohort ($F_{1, 13.748}$ = 14.752, p = 0.002; R^2 = 0.470, p = 0.001) (Figure 6.12B). Meanwhile, analysis of the age*treatment*maternal TNFα did not result in any GLMM model.

g. vi) Relationship between PNN and PVI

Analysing the PNN/PV ratio showed a significant effect of age on the ratio, with relative PNN levels increasing in adulthood (PD35: 0.483 ± 0.945, PD100: 0.845 ± 0.114, $F_{1, 39.586}$ = 88.856, p<0.001) (Figure 6.12C).

♦ *Maternal IL6*

Including maternal IL6 resulted in its significant interaction with age ($F_{2, 31}$ = 32.046, p<0.001) and age*treatment ($F_{2, 31}$ = 11.485, p<0.001). Although explorations of the interactions did not result in any main effects of maternal IL6.

♦ *Maternal TNFα*

Like maternal IL6, TNFα produced similar outcomes. There were significant interactions of maternal TNFα with age ($F_{2, 31}$ = 23.066, p<0.001) and age*treatment ($F_{2, 31}$ = 19.056, p<0.001). Again, there were no models produced when analysing the interactions in isolation.

6.3.2.h MMP9

There was a significant effect of age (PD35: 7.506 ± 8.472, PD100: 2.628 ± 3.431; $F_{1, 33.959}$ = 9.140, p = 0.005), treatment (V: 7.283 ± 8.761, P: 2.850 ± 2.992; $F_{1, 12.101}$ = 6.167, p = 0.029) and the age*treatment interaction ($F_{1, 33.959}$ = 8.075, p = 0.008).

To investigate the age*treatment interaction, we first split the offspring into age cohorts. Here we found a significant effect of treatment in the PD35 offspring only (V: 12.017 ± 8.76, P: 2.628 ± 2.992; $F_{1, 12.849}$ = 4.994, p = 0.044). Dam neared statistical significance (33.084 ± 19.922, p = 0.097). There were no significant models when focusing on PD100s only.

Analysis of the opposing interpretation of the interaction resulted in a significant effect of age in the vehicle-exposed offspring ($F_{1, 17.970}$ = 9.884, p = 0.006), whereas there was no effect of age in the PIC-exposed offspring ($F_{1, 13.759}$ = 0.091, 0.767) (Figure 6.12D).

♦ *Maternal IL6*

There were significant interactions including maternal IL6 and age ($F_{2, 35}$ = 3.715, p = 0.034) and age*treatment ($F_{2, 35}$ = 3.603, p = 0.038). Splitting the cohort into ages and treatments did not result in significant models.

♦ *Maternal TNFα*

Significant interactions included maternal TNFα with age ($F_{2, 35}$ = 4.859, p = 0.014) and age*treatment ($F_{2, 35}$ = 4.742, p = 0.015), though dividing the cohort did not result in further models.

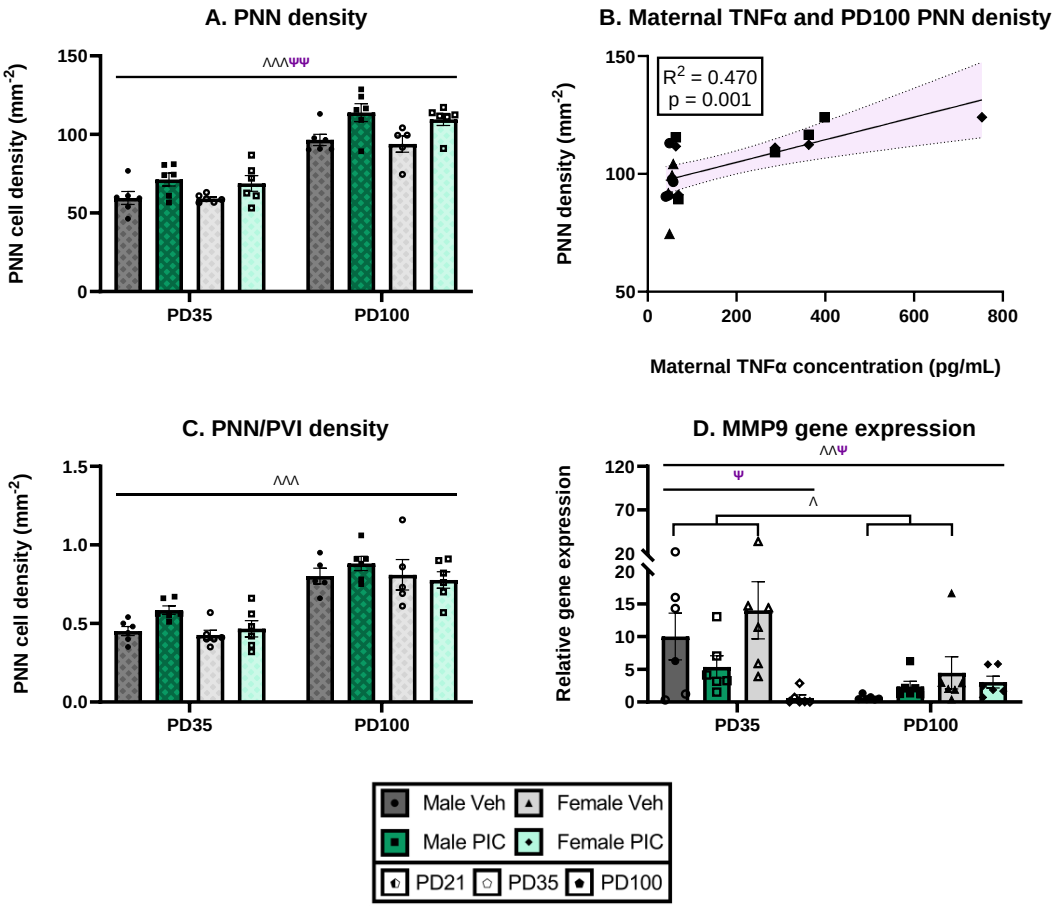

Figure 6.12: Effect of PIC on PNN, ratios of PNN and PVI and MMP9 gene expression. A) PNN density (n=5-6). **B)** Relationship between maternal TNFα and PD100 PNN density. **C)** Ratio between PNN and PVI (n=5-6). **D)** MMP9 gene expression (n=6) in PD35 and PD100 offspring. For **A**, **C** and **D)** data were analysed with a GLMM. Black lines showed effects from a significant GLMM. Dashed lines show effects from a trending GLMM. ^significant effect of age: ^p<0.05, ^^p<0.01, ^^^p<0.001. $significant effect of sex: $p<0.05, $$p<0.01, $$$p<0.001. Ψsignificant effect of treatment: Ψp<0.05, ΨΨ p<0.01, ΨΨΨ p<0.001. Graphs show mean ± SEM. For **B),** the graph shows data points for individual offspring, and the line shows the simple linear regression with 95% confidence intervals. A dashed line denotes a regression resulting from a trending (p<0.080) GLMM.

6.3.2.i Inflammation

i. i) IL1β

There was a significant effect of age with expression increasing in adulthood (PD35: 2.199 ± 2.202, PD100: 6.343 ± 4.702; $F_{1, 30.910} = 18.267$, p<0.001), sex (M: 3.108 ± 2.668, F: 5.375 ± 5.027; $F_{1, 35.180} = 5.514$, p = 0.025) and the age*sex interaction ($F_{1, 32.421} = 9.609$, p = 0.004).

Sex was a significant predictor of IL1β in the PD100 cohort ($F_{1, 21} = 9.436$, p = 0.006). Removing sex from the model revealed a significant effect of age in females only (PD35: 1.956 ± 2.030, PD100: 8.794 ± 4.818; $F_{1, 10.517} = 39.139$, p<0.001) that was not present in males (Figure 6.13A).

♦ *Maternal IL6*

Maternal IL6 interacted with age ($F_{2, 33} = 6.202$, p = 0.005) and age*sex ($F_{2, 33} = 3.561$, p = 0.040). Further analysis of these interactions revealed no main effects of maternal IL6.

♦ *Maternal TNFα*

Maternal TNFα interacted with age ($F_{2, 33} = 6.368$, p = 0.005) and age*treatment ($F_{2, 33} = 3.838$, p = 0.032). Further analysis of these interactions did not result in any significant main effects of maternal TNFα.

i. ii) NFκB

There was a significant effect of age with NFκB increasing in expression in adulthood (PD35: 5.050 ± 3.547, PD100: 7.922 ± 5.753; $F_{1, 31.622} = 5.350$, p = 0.027) and the age*sex interaction ($F_{2, 34.526} = 3.950$, p = 0.029).

The age*sex interaction may be due to the significant effect of sex found only in the PD100 cohort ($F_{1, 7.6923} = 5.627$, p = 0.047) or the effect of age found only in females ($F_{1, 10.449} = 27.023$, p<0.001). The dam neared statistical significance (16.188 ± 8.901, p = 0.069) (Figure 6.13B).

♦ *Maternal IL6*

Including maternal IL6 in the model resulted in a trend towards a significant effect of the age*maternal IL6 interaction ($F_{2, 36} = 3.048$, p = 0.060).

♦ *Maternal TNFα*

Including maternal TNFα in the model revealed it was involved in several significant interactions, including those with age ($F_{1, 33} = 5.771$, p = 0.022), sex ($F_{1, 33} = 6.793$, p = 0.014) and sex*treatment ($F_{2, 33} = 4.631$, p = 0.017).

We first explored at which age maternal TNFα predicted offspring NFκB expression. However, independent investigations revealed that segregation of the ages did not result in significant models.

Next, we analysed the sexes separately. In the males, there was a trend towards a significant effect of the treatment*TNFα interaction ($F_{2, 16}$ = 3.078, p = 0.074). There were no further models.

i. iii) IL6

IL6 expression increased with age (PD35: 1.502 ± 1.694, PD100: 13.085 ± 12.679; $F_{1, 39}$ = 33.441, p<0.001), and in females (M: 3.630 ± 3.848, F: 11.045 ± 13.776; $F_{1, 39}$ = 14.074, p <0.001). The age*sex ($F_{1, 39}$ = 12.431, p = 0.001) and age*sex*treatment interactions ($F_{4, 39}$ = 3.371, p = 0.018) were also significant.

The age*sex interaction was driven by the significant effect of sex in the PD100 cohort only (M: 3.630 ± 3.848, F: 11.045 ± 13.776; $F_{1, 20}$ = 14.355, p = 0.001). Finally, the age*sex*treatment interaction was the result of a significant effect of sex found only in the PD100 vehicles (M: 3.058 ± 0.688, F: 27.110 ± 16.741; $F_{1, 5.520}$ = 12.445, p = 0.014) and a significant treatment effect exclusive to the PD100 males (V: 3.058 ± 0.688, P: 8.467 ± 4.580; $F_{1, 9.997}$ = 8.270, p = 0.017) (Figure 6.13D).

♦ *Maternal IL6*

There were many interactions including maternal IL6, namely age ($F_{1, 30}$ = 33.211, p<0.001), sex ($F_{1, 30}$ = 16.430, p<0.001), age*sex ($F_{1, 30}$ = 13.740, p<0.001), age*treatment ($F_{1, 30}$ = 10.950, p = 0.002), sex*treatment ($F_{1, 30}$ = 13.201, p = 0.001) and age*sex*treatment ($F_{1, 30}$ = 15.065, p<0.001).

Reflecting on the age*maternal IL6 interaction, we found a significant main effect of maternal IL6 in the PD35 cohort ($F_{1, 11.081}$ = 12.060, p = 0.005), which resulted in a significant regression (R^2 = 0.464, p = 0.001) (Figure 6.13D).

Investigating the sex*maternal IL6 interaction did not result in any significant models. However, there was a significant main effect of maternal IL6 when analysing the PD35 male cohort in isolation ($F_{1, 7}$ = 6.637, p = 0.037; R^2 = 0.487, p = 0.037). Whereas in the PD35 females, there was a trend towards a significant effect of maternal IL6 on the offspring IL6 expression ($F_{1, 6.966}$ = 5.416, p = 0.053; R^2 = 0.451, p = 0.034). Data for both are found in Figure 6.13D.

Analysis of the remaining interactions did not result in any further models.

♦ *Maternal TNFα*

Maternal TNFα interacted with age ($F_{1, 30}$ = 28.873, p<0.001), sex ($F_{1, 30}$ = 18.015, p<0.001), age*sex ($F_{1, 30}$ = 16.260, p<0.001), age*treatment ($F_{1, 30}$ = 21.446, p<0.001), sex*treatment ($F_{1, 30}$ = 18.602, p<0.001) and the age*sex*treatment ($F_{1, 30}$ = 18.652, p<0.001).

Analysis of the PD35 cohort revealed a significant main effect of maternal TNFα ($F_{1, 11.554}$ = 17.322, p = 0.001), although this did not result in a significant linear regression (R^2 = 0.014, p = 0.631).

Analysis of the male cohort revealed maternal TNFα positively predicted offspring IL6 expression ($F_{1, 17}$ = 5.068, p = 0.038; R^2 = 0.230, p = 0.038) (Figure 6.13E). Moreover, exploration of the age*sex and age*sex*treatment interactions revealed it was PD100, male PIC-exposed offspring driving this relationship (age*sex: $F_{1, 8}$ = 50.231, p<0.001; R^2 = 0.438, p = 0.037. Age*sex*treatment: $F_{1, 3}$ = 11.94, p = 0.043; R^2 = 0.156, p = 0.439). Note that the latter regression is not significant (data shown in Figure 6.13E).

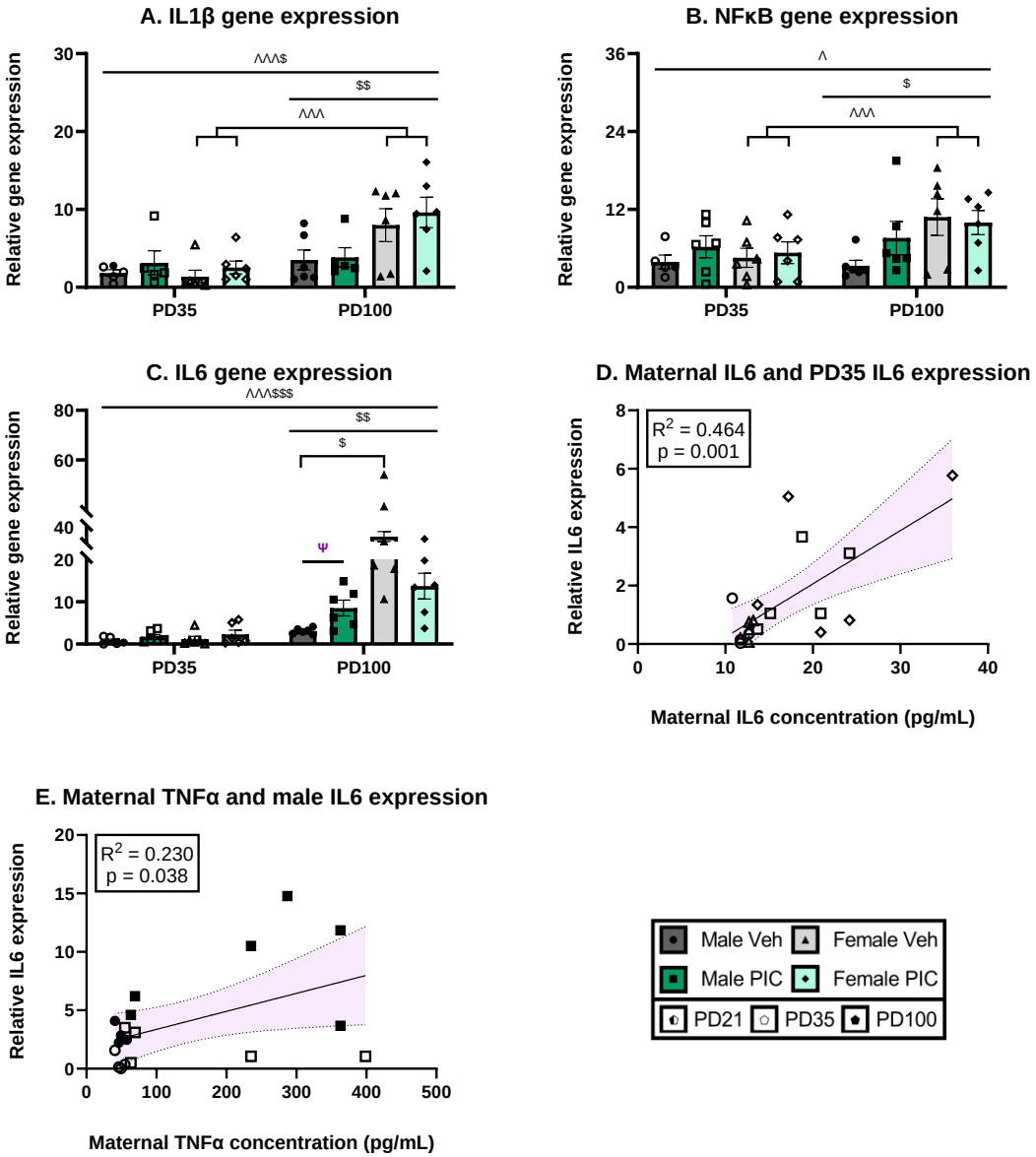

Figure 6.13: Effect of PIC on inflammatory gene expression. Gene expression of **A)** IL1β, **B)** NFκB and **C)** IL6 in PD35 and PD100 offspring (n=5-6). Relationship between **D)** maternal IL6 and PD35 IL6 expression and **E)** maternal TNFα and male offspring IL6 expression. For **A**-**C),** data were analysed with a GLMM. Black lines showed effects from a significant GLMM. Dashed lines show effects from a trending GLMM. ^significant effect of age: ^p<0.05, ^^p<0.01, ^^^p<0.001. $significant effect of sex: $p<0.05, $$p<0.01, $$$p<0.001. Ψsignificant effect of treatment: Ψp<0.05, ΨΨ p<0.01, ΨΨΨ p<0.001. Graphs show mean ± SEM. For **D** and **E),** the graphs show data points for individual offspring, and the line shows the simple linear regression with 95% confidence intervals. A dashed line denotes a regression resulting from a trending (p<0.080) GLMM.

6.3.2.j BDNF and TrkB

j. i) BDNF

There was a significant interaction between age*sex ($F_{3, 43}$ = 3.794, p = 0.017). Removing age from the model revealed a significant effect of sex in the PD100 cohort (M: 6.948 ± 4.411, F: 2.543 ± 2.301; $F_{1, 22}$ = 9.412, p = 0.006). Splitting by sex revealed a significant effect of age in the males (PD35: 2.209 ± 2.171, PD100: 6.948 ± 4.411; $F_{1, 21}$ = 10.368, p = 0.004) (Figure 6.14A).

♦ *Maternal IL6*

There were several maternal IL6 interactions: age ($F_{1, 22.560}$ = 8.112, p = 0.009), sex ($F_{1, 25.019}$ = 10.205, p = 0.004), age*sex ($F_{1, 22.825}$ = 12.476, p = 0.002), age*treatment ($F_{1, 22.561}$ = 13.312, p = 0.001), sex*treatment ($F_{1, 25.554}$ = 12.734, p = 0.001) and age*sex*treatment ($F_{1, 22.834}$= 10.045, p = 0.004). Despite the number of interactions including maternal IL6, only the age*sex*treatment interaction resulted in a significant main effect of maternal IL6. In the PD100 male vehicles ($F_{1, 30}$ = 12.038, p = 0.040; R^2 = 0.800, p = 0.041) (Figure 6.14B).

♦ *Maternal TNFα*

Like IL6, many significant interactions included maternal TNFα: age ($F_{1, 22.036}$ = 15.583, p<0.001), sex ($F_{1, 23.723}$ = 17.205, p<0.001), age*sex ($F_{1, 22.094}$ = 19.257, p<0.001) age*treatment ($F_{1, 22.002}$= 21.107, p<0.001), sex*treatment ($F_{1, 23.862}$ = 22.510, p<0.001) and age*sex*treatment ($F_{1, 22.066}$= 19.510, p<0.001). There were limited combinations with a noteworthy main effect of maternal TNFα. Namely, there was a trend in the PD100 males, with increased maternal TNFα leading to reduced BDNF expression ($F_{1, 8}$ = 4.648, p = 0.063, R^2 = 0.368, p = 0.063) (Figure 6.14C). In addition, there was a significant effect on the PD100 male vehicles. Notably, the measures had a positive relationship ($F_{1, 3}$ = 15.858, p = 0.028; R^2 = 0.841, p = 0.028) (Figure 6.14D).

j. ii) TrkB

TrkB expression decreased with age (PD35: 3.695 ± 4.223, PD100: 1.351 ± 1.400; $F_{1, 45}$ = 6.37, p = 0.013) (Figure 6.13B).

♦ *Maternal IL6*

Including maternal IL6 resulted in an age*maternal IL6 interaction ($F_{2, 37}$ = 5.137, p = 0.011), though exploration of the individual ages did not result in significant models.

♦ *Maternal TNFα*

Including maternal TNFα in the model resulted in a near significant age*sex*treatment*maternal TNFα interaction ($F_{8, 31}$ = 2.245, p = 0.051). Given this near-significant trend, we chose to do further exploratory analysis. There was a trend towards a significant effect of maternal TNFα in the PIC-exposed, male PD100 cohort ($F_{1, 3}$ = 6.276, p = 0.087).

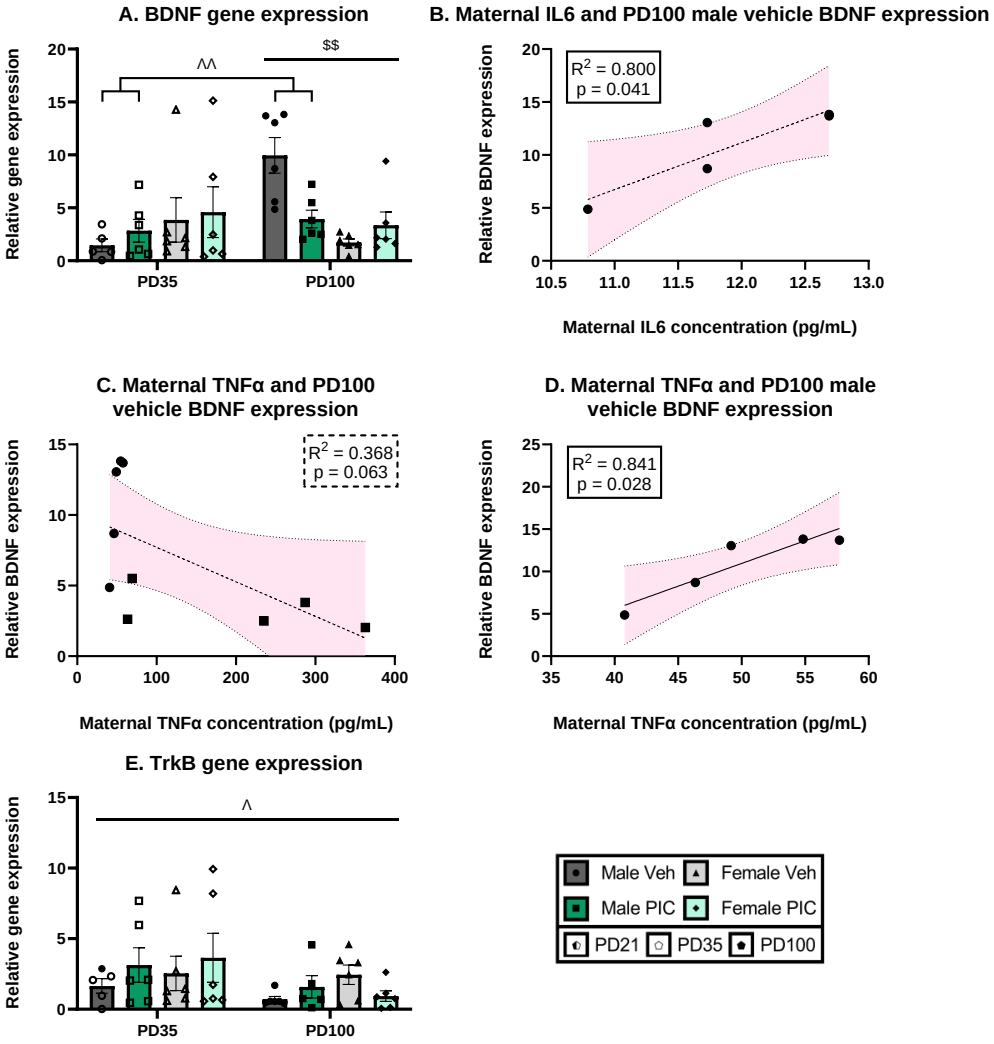

Figure 6.14: Effect of PIC on BDNF and TrkB expression. A) BDNF and **E)** TrkB expression in PD35 and PD100 offspring (n=5-6). **B)** The relationship between maternal IL6 and BDNF expression in the PD100 male vehicle offspring. The relationship between maternal TNFα and BDNF expression in the **C)** PD100 vehicle and **D)** PD100 male vehicle offspring. For **A** and **E)** data were analysed with a GLMM. Black lines showed effects from a significant GLMM. Dashed lines show effects from a trending GLMM. ^significant effect of age: ^p<0.05, ^^p<0.01, ^^^p<0.001. $^{\$}$significant effect of sex: $^{\$}$p<0.05, $^{\$\$}$p<0.01, $^{\$\$\$}$p<0.001. $^{\Psi}$significant effect of treatment: $^{\Psi}$p<0.05, $^{\Psi\Psi}$ p<0.01, $^{\Psi\Psi\Psi}$ p<0.001. Graphs show mean ± SEM. For **B**–**D),** the graphs show data points for individual offspring, and the line shows the simple linear regression with 95% confidence intervals. A dashed line denotes a regression resulting from a trending (p<0.080) GLMM.

6.4 Discussion

6.4.1 Overview of main findings

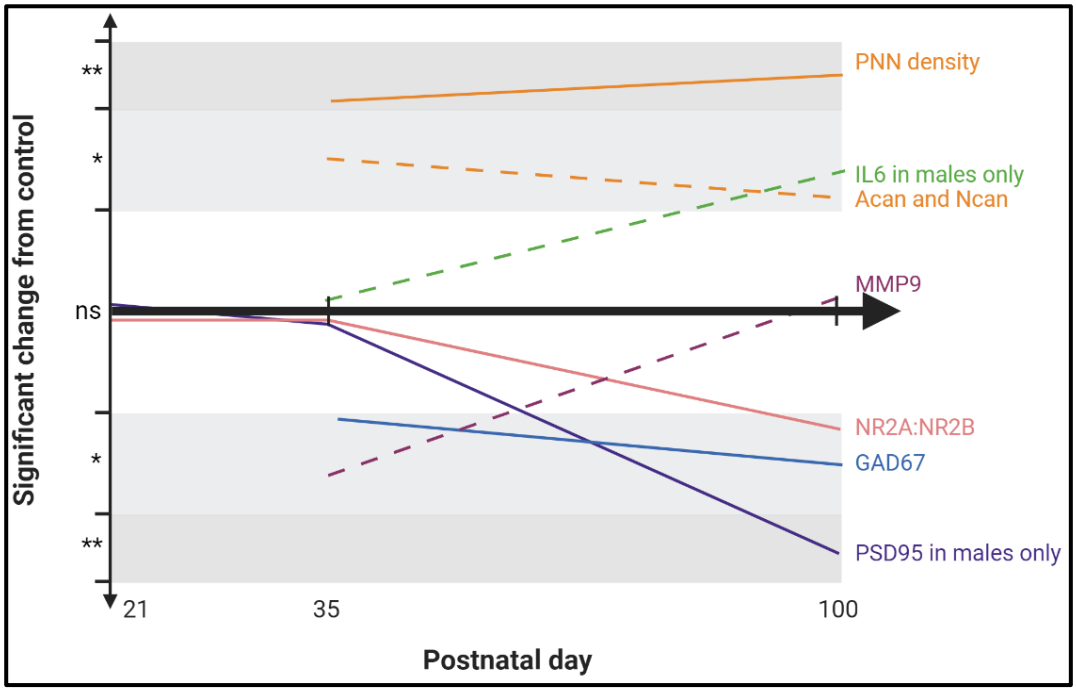

Figure 6.15: Summary of changes in PIC offspring compared to age-matched controls. Lines show an increase or decrease from age- and sex-matched controls. Only trending or significant changes are shown. $^{ns}p<0.1$, $^{*}p<0.05$, $^{**}p<0.01$. Dashed lines show mRNA data, and full lines show protein changes. $^{\#}$GAD67 only measured at PD35 and PD100.

6.4.2 The developmental onset of pathology

In this chapter, we measured markers relevant to cognition throughout development in a model of maternal immune activation. We found no alterations in the PD21 brains, though the markers we studied at this time were minimal. However, at PD35, there were alterations to GAD67 levels (Figure 6.7), Acan (Figure 6.9), Ncan (Figure 6.11A) and MMP9 expression (Figure 6.12C) and PNN density (Figure 6.12). Then at PD100, there were deficits in both sexes in NR2A:NR2B ratio (Figure 6.5). In the males, there were reductions in PSD95 (Figure 6.6) and increases in IL6 (Figure 6.13). Before discussing the implications of these changes, we will first comment on the timings of these changes.

We selected the clinically-relevant ages of PD21, 35 and 100, equating to approximately two, eleven and twenty-one years old in humans (Ghasemi et al., 2021). These ages reflect the period before peak schizophrenia diagnosis (Kirkbride et al., 2012), where cognitive impairments can be detected (Dickson et al., 2012, Jonas et al., 2022). In rodent models of MIA, cognitive impairments tend to develop from PD56 (summarised in Table 6.4). The animals we used for the WES studies were behaviourally tested. This

study found no NOR deficit at PD35; however, the animals displayed impaired attentional set-shifting when tested on PD126-134 and radial arm maze on PD128-137 (Potter et al., 2023). Therefore, these results indicate that MIA on GD15 results in behavioural impairment and pathology at clinically relevant developmental points.

6.4.3 Sex differences

A second clear pattern was the number of sex differences. There are sex differences in schizophrenia, with men often diagnosed earlier (Kirkbride et al., 2012) and more frequently (McGrath et al., 2008).

Many of the differences between our male and female cohorts were in the expression of genes, with sex differences reported in parvalbumin, Acan, Vcan, Ncan, IL1β, NFκB, IL6 and BDNF gene expression. It is recognised that there are differences in male and female gene expression throughout life and particularly during development (Berchtold et al., 2008, Shi et al., 2016). Indeed, the male and female genomes are remarkably similar, with the sex-dependent phenotypic differences achieved by differential expression of shared genes. The highly expressed genes in one sex are called sex-biased genes (Ellegren et al., 2007). In a fascinating study by Shi et al., RNA sequencing data were analysed throughout human development. They found an increased expression of male-biased genes prenatally (8-24 weeks post-conception), which then switched to female-biased genes in childhood (4 months-4 years). With levels equating during puberty (8-19 years) and adulthood (21-40 years). After establishing differing gene expression levels in development, Shi et al. assessed whether there was an overlap between the enriched genes and different brain disorders. Of the twelve disorders studied, they found the most significant enrichment of male-biased genes related to schizophrenia, with enrichment scores of around nineteen in the prenatal period, compared to a maximum score of around three in pubescent females (Shi et al., 2016).

We also saw a difference in PVI density, with females having increased density compared to males. This difference could be due to females having increased levels of oestrogen. Oestrogen has many supporting roles in the brain, including reducing oxidative stress and inflammation, increasing mitochondrial function, upregulating anti-apoptotic genes, regulating the stress response and altering dopamine activity (Brand et al., 2021). Oestrogen receptors have been identified on the presynaptic surface of PVI. Studying PVIs across the menstrual cycle shows fluctuation in PVI number and gamma frequency

oscillations that coincide with oestrogen changes (Gilfarb et al., 2022). We also see changes as oestrogen levels increase during development. Indeed, studies in rodents reveal a strong correlation between oestrogen and PVI density in the first twelve weeks of life (Wu et al., 2014). Despite the evidence of oestrogen as being neuroprotective and seemingly able to facilitate PVI maturation, an extensive review by Woodward et al. highlighted that the PVIs of females are not always more resilient to environmental stressors. The authors hypothesised that oestrogen binding to PVI increases neuronal plasticity, making them more adaptable to environmental stressors. However, adaptability does not equate to resilience (Woodward et al., 2021).

6.4.4 Dam effects

6.4.4.a Dam as a covariate

A core component of our GLMM was the inclusion of the dam as a random factor. The inclusion of a dam allows us to assess whether offspring outcomes were predicted by litter membership. If there is a dam effect, including the dam as a random variable can improve the model's fit due to some of the variation in the model being assigned to the dam (Kanters, 2022, Wang et al., 2019). Interestingly, the dam was significant, or neared significance, in many biomarkers relevant to PNN (see Table 6.9). However, this effect was only present in the PD35 brains. For Acan and Vcan, the dam was only significant when maternal cytokines were included in the model.

Table 6.9: Summary of significant and trending dam effects. All reported data are from PD35 cohorts, including both sexes and treatments. The maternal cytokines (✓/×) column shows whether the GLMM included maternal cytokines.

Measure	Maternal cytokines	Dam estimate estimate ± standard error	P value
Acan	✓	1.030 ± 0.535	p = 0.054
Vcan	✓	23.245 ± 10.714	p = 0.030
Ncan	×	4.332 ± 2.235	p = 0.053
	✓	3.185 ± 1.645	p = 0.053
PNN density	×	84.095 ± 40.573	p = 0.038
MMP9	×	11.783 ± 6.654	p = 0.077

We must provide some seemingly tangential information to explain why this interests us. The radial glial cells from which neuronal progenitors originate switch to producing oligodendrocyte precursor cells (OPC) in the last few days of rat gestation (Chen et al., 2017, Hill, 2023). Notably, these precursors are generated during GD15 in rats, aligning with PIC administration in this study. One of the mediators of the switch between OPCs and mature glial cells is IL6 (Valerio et al., 2002, Zhang et al., 2006). As PIC injection of the same dose on GD14 can lead to increased IL6 expression in the foetal brain (McColl et al., 2019), we hypothesise that this exogenous and early increase in IL6 could lead to a premature switch to gliogenesis in PIC offspring.

The tissues we used to measure PVI and PNN were also analysed for glial cells. There were reductions in oligodendrocyte precursors in adolescent and adult PIC-treated offspring brains. Later, in PD100 offspring, mature oligodendrocytes were increased while white matter astrocytes were decreased (Woods, unpublished findings), confirming altered glial cell function in the PIC-treated rats.

This glial cell dysfunction is significant due to the PNN components and MMP9 being produced partly by the glial cells. As a reminder, Acan, Bcan, Vcan, Ncan and MMP9 are all expressed by astrocytes. Oligodendrocytes produce Vcan only (Song et al., 2018). Despite the reasonably robust clinical evidence of reduced PNN in schizophrenia, our suggestion that the glial cells may be responsible for excessive PNN components is not unfounded. Glial cells stained by WFA were increased in the basolateral amygdala of schizophrenia patients by orders of magnitude (Pantazopoulos et al., 2010). In the present study, we cannot decipher the cellular origins of the PNN components. Future investigations could target single cell types to understand whether the general PNN pathology observed originates from glia.

Although the within-litter grouping for the PNN data is convincing, with sibling groups having remarkably similar density, plotting the same graph for Vcan introduces a limitation to the qPCR data analysis and the remaining significant dam effects (8.52). We only have one offspring from each dam for many PIC offspring. Reflecting on the variable often sex-dependent nature of the qPCR, perhaps the dam effect for the qPCR data is artificially inflated.

Indeed, the lack of conformity within MIA-treated litters is a recognised phenomenon. Each foetus is housed in individual amniotic sacs with independent placentas. The extent of MIA is thought to be regulated by placement in the uterine horn, placental transporters, or some other factor. Equally, the postnatal social hierarchies enacted by sibling cohorts may lead to differing postnatal stress levels, nutrient acquirement and social interaction within home cages. These natural occurrences introduce variability beyond the experimenter's control (Meyer, 2023). The study design employed in the present study inherently limits our investigation into within-litter effects. To comprehensively study this, we must study age- and sex-matched siblings.

6.4.4.b Maternal cytokines

As part of our analysis, we looked at the effect of maternal cytokines on offspring pathology. The rationale for exploring this was due to the variation observed in the PIC-treated dam cytokine response. We were interested in whether a low-responding PIC dam would result in offspring with limited pathology and vice versa. Maternal TNFα and IL6 predicted several offspring outcomes, summarised in Table 6.10. We plotted this data to understand the relationship between these two variables and found most fit a linear regression, suggesting that increased maternal cytokine response did worsen PIC-related pathology.

Table 6.10: Summary of mGLMMs with a significant effect on maternal cytokines. Arrows show the direction of the linear relationship. qPCR data is highlighted in grey, WES in blue, and IHC in green.

	PD35	PD100
NR2A:NR2B		↗ TNFα
PSD95		↘ TNFα
GAD67	Male veh: ↗ TNFα	
Acan	↗ IL6	
Vcan	↗ IL6	↗ TNFα
Ncan	↗ IL6 ↗ TNFα	
PNN density		↗ TNFα
IL6	↗ IL6	

Notably, IL6 appears to dominate the adolescent markers, with TNFα predicting adult outcomes. As maternal IL6 and TNFα are not correlated in the PIC-treated offspring (Figure 6.3), we could speculate that offspring subject to a high IL6 led to early maturation of glial cells and perineuronal nets. The offspring exposed to high TNFα have

more substantial deficits when the brain circuitry matures. Indeed, maternal TNFα predicted offspring cognitive impairment in the radial arm maze and social interaction changes in adult female offspring. Note that males were not tested (Potter et al., 2023). However, this analysis and conclusion are limited by the same design issues as the dam analysis. We are asking the model to assess the effect of maternal cytokines on one offspring of one sex and at one time point in a model plagued by inter-litter variation. In addition, maternal cytokines were measured from a plasma sample taken approximately three hours after MIA. However, slight deviations in this timing may affect cytokine levels (Arango Duque et al., 2014). Moreover, the plasma samples were assessed in a single replicate of an ELISA. Some plasma samples showed varying evidence of haemolysis, which can artificially inflate cytokine concentration (Karsten et al., 2018).

Despite these limitations, it is noteworthy that maternal cytokine analysis resulted in many significant models irrespective of dam effects. Indeed, the dam was redundant in all the GLMM models listed in Table 6.10. This finding could indicate that the variation is better predicted by a continuous variable rather than a discrete classification. This reflects the movement in clinical research to classify patients based on peripheral, mainly inflammatory, biomarkers, which may stratify patients into groups with similar pathology for targeted therapy (Boerrigter et al., 2017, Fillman et al., 2016, Sæther et al., 2023, Wu et al., 2019). Perhaps this data provides provisional backing to this.

6.4.5 Similarities to the scPCP model

Some markers were altered in the adult offspring that matched the scPCP-treated animals. Given that we have discussed the function and clinical relevance of these markers, we will discuss these markers here in brief.

6.4.5.a Synaptic dysfunction

As in the scPCP-treated animals, we saw significant reductions in adult male PSD95 protein. The data for SNAP25 was not as conclusive, with no change detected at the ages tested. The literature for synaptic changes in offspring after MIA proved equally variable. When researchers induced MIA in early gestation (GD9), synaptic signalling proteins, including synaptophysin, synaptoporin and SNARE proteins, reduced. These changes were first detected at PD52; studies looking at earlier time points (PD40) did not detect changes to these proteins (Cieślik et al., 2020, Giovanoli et al., 2016, Ibi et al., 2020). Cieślik et al. measured SNAP25 at PD52 in the cerebral cortex and did not see any

changes despite changes to other synaptic proteins (Cieślik et al., 2020). Meanwhile, Giovanoli et al. found reductions in PSD95 at PD40 and PD90 in male offspring. The authors speculated that due to the role of PSD95 in anchoring NMDAr to the postsynaptic membrane, the PSD95 deficit might contribute to the development of presynaptic deficits due to impaired glutamatergic signalling in the network (Giovanoli et al., 2016).

Although the evidence is limited, synapses in offspring exposed to MIA after GD9 appear to have delayed synaptic pathology. Where changes were detectable in GD9 offspring from GD56, later MIA-induction displayed no synaptic pathology on PD21 (Forrest et al., 2012), PD60 (Chen et al., 2020) and PD150. Synaptophysin deficits are only present in PD660 offspring (Giovanoli et al., 2015). It is essential to consider the plethora of confounding variables. Each study uses a different rodent strain, biomarker, and method of measuring said biomarkers. However, it is noteworthy that GD9.5 is the point at which microglia enter the brain. Perhaps there is a connection between this event and the earlier induction of synaptic deficits observed in GD9 MIA models, given the role of microglia in synaptic pruning (Tay et al., 2017). The IHC sections used for this study were also stained for microglia. Morphological analysis of the microglia showed an increase in ameboid microglia at PD35 (Woods, unpublished findings). Ameboid microglia are characterised by large soma size, which is observed in PFC microglia pruning synapses (Mallya et al., 2019). Although circumstantial, this theory is bolstered by the observation by Giovanoli, who measured neuronal numbers in their offspring. They found that the loss was isolated to synapses, and PIC did not affect neuronal numbers on GD9 (Giovanoli et al., 2016).

6.4.5.b GAD67

The offspring in our study had reduced GAD67 levels across both time points tested (PD35 and 100). Several studies confirm this finding with reduced levels in foetal (Nakamura et al., 2022, Oskvig et al., 2012) and adult tissue (Cassella et al., 2016, Deslauriers et al., 2013, Dickerson et al., 2014, Labouesse et al., 2015, Luoni et al., 2017, Nouel et al., 2012, Richetto et al., 2013, Richetto et al., 2014). However, some studies in younger offspring (<PD60) showed increases (Cassella et al., 2016, Fatemi et al., 2004, Harvey et al., 2012, Richetto et al., 2013). Consistent with this conflicting data for GAD, there is evidence of MIA causing increased excitation and reduced inhibition

(Bitanihirwe et al., 2010, Canetta et al., 2016, Richetto et al., 2014, Roenker et al., 2011, Soumiya et al., 2011, Thion et al., 2019, Wei et al., 2012, Zhang et al., 2015) and reduced excitation, increased inhibition (Bitanihirwe et al., 2010, Roenker et al., 2011, Thion et al., 2019). It is essential to comment on the diversity of regions used to measure these outcomes and to appreciate that excessive inhibition in one brain region may lead to increased excitation in another. The primary finding is the disruption to the E/I balance. Indeed, optogenetic manipulation of the E/I balance in the somatosensory in naïve animals can recapitulate MIA-induced behaviours. Stimulation of excitatory neurons or inhibition of the PVI induces anxiety and social deficits that reverse when light stimulation ceases (Shin Yim et al., 2017).

6.4.5.c Inflammation

Our study found increased IL6 expression in PD100 males, suggesting an ongoing inflammatory response. In an extensive review of cytokine changes in PIC-treated offspring, Hameete et al. noted that PIC exposure, particularly in mid-gestation, was associated with increased IL6. The increase was first detectible hours after PIC induction (Meyer et al., 2006b) and was maintained into adulthood (Garay et al., 2013, Tang et al., 2013, Zhao et al., 2019). Critically, for every study that shows an increase, an equal number shows no change (Giovanoli et al., 2015, Giovanoli et al., 2016, Hameete et al., 2021, Ratnayake et al., 2014, Tang et al., 2013) (for the review, see: Hameete et al., 2021). Given the cytokine levels fluctuate with stress (Petrowski et al., 2018), hormones (Piccinni et al., 2021), ageing (Huang et al., 2021b) and the circadian cycle (Lange et al., 2010), perhaps other indicators of chronic inflammation should be adopted to assess levels in the offspring.

We saw no change to NFκB and IL1β in any PIC-exposed offspring. The data regarding NFκB is limited. It is involved in the initial immune response (Figure 6.1) and is upregulated in the foetal brain four hours after LPS treatment (Ginsberg et al., 2018). However, a second study showed no change in protein levels five hours after PIC and on PD21. Although for both ages, they analysed the entire brain rather than specific regions. In addition, it is unclear whether they accounted for sex in their statistics (Khalil et al., 2013). Finally, a study which induced MIA on GD15 with PIC found an increase in an NFκB subunit (Rela) in both the hippocampus and PFC alongside IL1β, indicating ongoing inflammation in PD60 female offspring (Su et al., 2022).

Although we could not measure oxidative stress markers in these brains due to practical limitations, it is noteworthy that the data for oxidative stress is relatively consistent. MIA with LPS increases MDA and PCC in the foetal brain 24 hours after induction in conjunction with elevated SOD and CAT activity (Simões et al., 2018). Evidence of oxidative stress persists in adolescent brains, with increased MDA and reduced antioxidant capability (Cieślik et al., 2020, Romero-Miguel et al., 2021, Talukdar et al., 2020).

6.4.6 Differences to the scPCP model

It is expected that there should be differences between the scPCP model and the PIC model, given the difference in model induction method, time since the insult and the age brains were taken. It is hoped that comparing these differences can give insight into the underlying mechanisms and points of convergence.

6.4.6.a NMDAr subunits

We first want to discuss the divergent outcome for the NMDAr subunits. In the scPCP model, we saw a reduction in the NR2B subunit and discussed the potential effect this would have on the induction and maintenance of LTP. In the PIC PFC, we found a contradictory outcome. Here, the ratio of the two proteins in each animal revealed a treatment effect, with a low 2A:2B ratio across all age groups, particularly in the PD100 cohort.

The NMDAr are developmentally regulated proteins. In the developing brain, synapses are functionally silent, containing only NR2B NMDAr (Barria et al., 2002). Upon stimulation of the NMDAr, there is an activity-dependent upregulation of NR2A, and concurrently, the translation of the NR2B subunit is reduced (Yashiro et al., 2008). In the period when both NR2A and NR2B occupy the developing synapse, LTP and LTD are enhanced (Dumas, 2005).

Therefore, we expect the 2A:2B ratio to increase across development in a healthy animal. Indeed, in our vehicle animals, we see a four-fold increase in the 2A:2B ratio from PD35 to PD100. In the PIC-treated males, this increase is comparable to vehicles. However, in the PIC females, the ratio remains comparable to that seen in PD21 and PD35. Does this mean that females have not undergone the process of switching NMDAr subunit dominance?

The NMDAr switch occurs in several brain regions, including the cortex and hippocampus (Dumas, 2005). The ability to manipulate input into the visual cortex gives unparalleled insight into how this switch is moderated. Rodents that are visually deprived from birth maintain high levels of NR2B, suggesting experience-dependent maturation of NMDAr in the visual cortex. Fascinatingly, just two hours of light exposure is sufficient for the NMDAr switch and NR2A dominance. Returning animals to dark conditions for three days resulted in NR2B upregulation. Furthermore, dark rearing significantly affected NMDAr subunit composition in the visual cortex only, suggesting maturation is region-specific (Philpot et al., 2001).

The switch in the hippocampus and PFC appears to be regulated by synaptic activity, with LTP in neonatal hippocampal slices resulting in the rapid increase in NR2A (Bellone et al., 2007). Conversely, neonatal rats (PD6, 7 and 8) subjected to repeated general anaesthesia, although the precise mechanisms are unclear, have reduced NR2A when brains are studied at PD21 (Zhang et al., 2016c). Perhaps the reduced levels of NR2A in PIC-treated animals indicate reduced synaptic activity. Indeed, we have already shown reduced synaptic markers in the same tissues. Unfortunately, we do not have NR2A gene expression data, as this may have proven helpful in deciphering when gene expression changes should occur and if the PIC animals are impaired.

As a reminder, the NMDAr and PSD95 are functionally linked, anchoring and allowing the movement of NMDA subunits in the post-synaptic synapse (3.4.5). PSD95 knockout results in many functionally silent (no AMPAr) synapses and NR2B dominance. Unexpectedly, despite the complete knockout of PSD95, some synapses still had AMPAr receptors. Analysing the spine morphology, Béïque et al. found that silent synapses were located on mature spines. Moreover, there was no change to the number of spines on the CA1 neurons (Béïque et al., 2006). Could this mean that PSD95 is required to maintain mature synapses only? This was confirmed to be the case by Elias et al. During synaptogenesis, AMPAr and NMDAr are managed by synapse-associated protein 102 (SAP102), with PSD95 taking over after synaptogenesis completes. PSD95 then regulates AMPAr cycling and the NR2B to NR2A switch (Elias et al., 2008). Given this intricate relationship and the functional consequence of NMDAr location and colocalization, IHC studies should investigate whether PIC offspring, particularly females, have altered developing or matured NMDAr synapses.

The data for NMDAr subunits in MIA models are conflicting. We will give the studies in order of development. The earliest measure of NR2A and NR2B was by Hao et al., who induced MIA on GD9 with PIC. They studied mRNA and protein in the hippocampus and PFC in male offspring. They found a reduction in the mRNA and protein of both subunits at PD21. By PD35, the expression had normalised to control levels, save elevated NR2A levels in the PFC. By PD65, the overexpression had returned with NR2A and NR2B gene expression, and protein levels increased in both regions (Hao et al., 2019). Rahman also found upregulation to NR2A expression in the cortex and hippocampus (CA1 and DG) in male rats aged PD63-91. In addition, they measured binding to the NMDAr receptor, where they found increased binding NR2A specific binding, suggesting an increased 2A:2B ratio (Rahman et al., 2020). Finally, brains from PD95 found no change in mRNA expression of NR2B in the hippocampus of male offspring (Rahman et al., 2020). Notably, all the data collected are in males; our study shows the most substantial effects in females.

Refining the search for those that included female offspring revealed one study that saw increases in NR2A expression in the PFC of PD60 rats (Su et al., 2022) and another that saw reduced NMDAr binding the PFC of PD77 females, perhaps indicating a sexually dimorphic response (Osborne et al., 2019).

Indeed, future studies would need to establish whether these observed changes in NMDAr lead to electrophysiological changes. In addition, studies isolating which cells these changes are occurring on would be of great use. For example, if the NR2A reduction is on PVI, this may affect parvalbumin protein and GAD67 levels (Kinney et al., 2006) or impair PNN maturation, increasing susceptibility to oxidative insults in later life (Cardis et al., 2018).

6.4.6.b VGlut1

In this study, we saw no change to VGlut1 expression in the PFC of PIC-treated rats, though there was a slight trend to an increase. In the scPCP model, VGlut1 expression was decreased.

VGlut was investigated in two in vitro studies. The first exposed hippocampal cultures to PIC for 24 hours, then extracted and fixed the cells for staining. This direct exposure of neurons to PIC did not alter VGlut levels. However, its association with PSD95 was reduced, indicating reduced glutamatergic synapses (Sanchez-Mendoza et al., 2020).

The second study derived hippocampal neurons from embryonic mice exposed to MIA during gestation. After 14 days in vitro (DIV), PSD95 and VGlut/PSD95 co-expression increased. At 21 DIV, VGlut expression increased (Wegrzyn et al., 2021). These studies further highlight the limitation of purely looking at protein levels.

The in vivo studies found age- and region-dependent changes to VGlut. In the cortex, VGlut was downregulated in male PD24 and PD90 mice. However, VGlut was upregulated in the hippocampus at PD24 and then unchanged in PD90 (Tang et al., 2013). Kenter also saw no changes to VGlut expression in the hippocampus of PD92 male offspring (Kentner et al., 2016).

6.4.6.c Parvalbumin

Several neurodevelopmental disorders have been linked to impaired PVI function, including schizophrenia, autism and Fragile X syndrome (Cea-Del Rio et al., 2014, Dienel et al., 2019, Gao et al., 2015, Gogolla et al., 2009b, Krawczyk et al., 2016, Lewis, 2009, Nomura, 2021, Selten et al., 2018). As discussed, PVIs are critical regulators of excitatory/inhibitory (E/I) balance (see 1.5.2), which has been associated with MIA (Gao et al., 2015, Gogolla et al., 2009b, Krawczyk et al., 2016, Lewis, 2009, Nomura, 2021).

PVI may be uniquely sensitive to E/I input changes due to the two types of PVI that form during development. Donato et al. identified early- (GD9.5 or 11.5) and late- (GD13.5 or 15.5) born PVI, whose plasticity is regulated by excitatory and inhibitory inputs, respectively. Thus, in disorders with reduced excitatory input to early-born PVI, like schizophrenia, there will be reduced gamma band activity and impaired memory. In disorders with reduced inhibitory input to late-born PVI, like autism and intellectual disability, there will be impaired plasticity (Donato et al., 2015). Therefore, PVIs are potentially sensitive to MIA from GD9.5 and are affected by excitatory/inhibitory shifts in both directions.

Several studies have examined MIA's effect on PVI number or parvalbumin gene expression (summarised in Table 6.11). Looking at the outcomes of these studies, we see that early gestation MIA (PD9-12.5) can reduce PVIs in juveniles (Ducharme et al., 2012, Matsuura et al., 2018) and adult offspring (Han et al., 2016, Matsuura et al., 2018, Mueller et al., 2021, Rahman et al., 2020, Shin Yim et al., 2017). Although, two studies showed no difference in PVI density during this period (Giovanoli et al., 2014) or mRNA expression (Nakamura et al., 2022).

The data from the next developmental window (GD13-15) are more varied, with some studies showing that MIA decreases parvalbumin mRNA (Nakamura et al., 2021), others showing no effect (Nakamura et al., 2021, Thion et al., 2019), and a final study seeing an increase in PVI density in the barrel cortex of PD20 offspring (Thion et al., 2019). The variability in this period may be due to MGE-derived not actively proliferating during this period, instead altering migration (Gumusoglu et al., 2017, Oskvig et al., 2012, Squarzoni et al., 2014, Vasistha et al., 2020). Finally, several studies showed that late gestation exposure to MIA (PD15-19) resulted in decreased PVI cell density, parvalbumin protein and mRNA (Luoni et al., 2017, Piontkewitz et al., 2012, Rahman et al., 2020, Wischhof et al., 2015, Zhang et al., 2015), others saw trends towards decreases (Luoni et al., 2017, Paylor et al., 2016), or no change (Dickerson et al., 2014). The brain region and age studied throughout are inconsistent, so although a firm conclusion cannot be drawn, it is valuable to draw attention to the parallels between the apparent biphasic vulnerability and the biphasic genesis of PVI (Donato et al., 2015). Indeed, Nakamura et al. administered PIC on GD13-15, explicitly targeting the second window of PVI development. As a reminder, the PVIs born during this time express low PV/GAD67 and develop extensive inhibitory synaptic puncta in the adult brain (Donato et al., 2015). Although they found no alteration to PVI density nor intensity in the hippocampus, they did find a shift in the intensity distribution, with more PVI in a low-PV state. In addition, they measured reduced parvalbumin and GAD67 mRNA. It is unclear why MIA coinciding with the late-born PVI would result in increased late-born PVI, though the authors suggest the elevated plus maze prior to tissue collection may have resulted in transient shifts from low- to high-PV populations (Nakamura et al., 2021). In the characterisation chapter (3.4.8), we speculated whether this mechanism is impaired in scPCP animals. To confirm this, behaviourally naïve animals would need to be compared.

Our study showed no parvalbumin expression, protein levels or density change in the PFC of PIC-exposed offspring. Despite no changes, a cohort of these animals had a PFC-dependent cognitive impairment (Potter et al., 2023). This highlights the need for comprehensive and multimodal analysis of tissue. In addition, the tissue used for the mRNA, protein and IHC are not matched; it would be of great interest to know if there was a relationship between the mRNA expression and protein levels.

Table 6.11: Studies investigating the effect of MIA on postnatal parvalbumin levels. PIC = poly (I:C), LPS = Lipopolysaccharide, CA1 = CA1 area of the hippocampus, Hipp = hippocampus, mPFC = medial prefrontal cortex, S1 = sensory cortex, PrL = prelimbic cortex, NAc = nucleus accumbens EC = entorhinal cortex, DH = dorsal hippocampus, DG = dentate gyrus, FAC = frontal association cortex, PD = postnatal day, IHC = immunohistochemistry, qPCR = quantitative polymerase chain reaction, mRNA = messenger ribonucleic acid, RNAseq = next-generation RNA sequencing, ♂: males, ♀: females. *significant when combined with offspring exposed to PIC on GD10 or 19.

GD	MIA	Region investigated	Age of offspring measurement	Method of measurement	Change	Reference
9	PIC	CA1	PD21	IHC	↓	(Ducharme et al., 2012)
		Hippo	PD70	IHC	↔	(Giovanoli et al., 2014)
		Hippo	PD80	IHC	↔	(Ibi et al., 2020)
9-11	PIC	DH	PD168	qPCR	↔	(Nakamura et al., 2022)
10	PIC	Cortex, striatum and hippo	Adult	In situ hybridisation (mRNA)	↓*	(Rahman et al., 2020)
	PIC	Cingulate cortex	PD70-84	qPCR	↔	(Duchatel et al., 2019)
12	PIC	mPFC and amygdala	PD84+	RNAseq	↓ amygdala in behaviourally impaired	(Mueller et al., 2021)
12.5	PIC	S1	PD70+	IHC	↓ in layers 2+3 only	(Shin Yim et al., 2017)
12-17	PIC	mPFC, Hippo, NAc	PD78	IHC	↓ PrL and CA1 regions only	(Han et al., 2016)
		mPFC	PD36	IHC	↓	(Matsuura et al., 2018)
			PD79		↓ PrL	
13-15	PIC	Hippo	PD190	IHC	↔ cell number	(Nakamura et al., 2021)
					↓ intensity	
				qPCR	↓	
		DH	PD168	mRNA	↔	(Nakamura et al., 2022)
15	PIC	PrL	PD100	IHC	↔	(Casquero-Veiga et al., 2022)
		Basolateral amygdala			↓	
		PrL, amygdala, FAC	PD21, 35 and 90	IHC	↔	(Paylor et al., 2016)
		DH	PD84	IHC	↔	(Dickerson et al., 2014)
		DG	PD112	IHC	↓	(Zhang et al., 2015)
		Hippo	PD72 and 100	IHC	↓	(Piontkewitz et al., 2012)
15-16	LPS	mPFC, hippo, EC	PD90+	IHC	↓mPFC, CA1, lateral EC (♂) ↓mPFC (♀)	(Wischhof et al., 2015)
17	PIC	Hippo	PD133	qPCR	↔	(Luoni et al., 2017)
				WB	↓DH	
					↔ VH	
19	PIC	Cortex, striatum and hippo	Adult	mRNA	↓*	(Rahman et al., 2020)
	PIC	Cingulate cortex	PD70-84	qPCR	↔	(Duchatel et al., 2019)

6.4.6.d Perineuronal nets

To our knowledge, the first study of PNN in the PIC model was in 2016. In this study, Long-Evans rats were dosed on GD15 with high molecular weight (HMW) InvivoGen PIC at 4mg/Kg. Brains were collected on PD7, 21, 35 and 90. The authors assessed the frontal association cortex (FAc), medial prelimbic cortex (PLc: PrL and IL), amygdala (AMY) and primary auditory cortex (Pac). We were particularly interested in the PLc data as it overlaps with our PFC. Here, they found a reduction in PNN density, and co-staining confirmed that this was due to a reduction in PVI expressing PNN. PVI density did not change in this region. In the AMY, they found a reduction in PNN in the PD35 PIC animals. However, this was due to a doubling of PNN density in the vehicles, which then halved again in the PD100s. This study was done in males only (Paylor et al., 2016).

The subsequent study investigated the outcomes of GD12.5 injection of 20mg/Kg Sigma PIC in C57BL/6J mice. Here, they found a significant increase in the levels of PNN surrounding PVI in the hippocampus on PD17. Adding a second-hit stressor (hypoxia/ischemia (HI) on PD10) dramatically increased PVI and PNN density. Interestingly, in the PIC+HI condition, the authors found an invasion of Otx2-expressing monocytes in the hippocampus, which is necessary for PVI maturation (Spatazza et al., 2013). The monocytes expressed Otx2 from 4 to 14 days after HI induction. Moreover, blocking monocyte invasion through genetic knockout of a monocytic receptor that induces chemoattractant behaviour attenuates the PNN increases and reduces some anxiety-related deficits (Chen et al., 2020).

Two more recent studies have shown no change to PNN in the adult hippocampus (Nakamura et al., 2021) and prelimbic cortex (Casquero-Veiga et al., 2022). However, the final in vivo study found reductions in PNN density in the prelimbic cortex on PD85 (Zhao et al., 2021). Interestingly Zhao et al. also ran an environmental enrichment intervention including tubes and toys, but no running wheel. The dams were assigned to either enriched or standard housing. The dams stayed in their respective condition for breeding, gestation and weaning. The offspring were maintained in these housing conditions until the brains were taken on PD85. Exposure to an enriched environment reversed the PIC-induced PNN reductions (Zhao et al., 2021).

Table 6.12: Summary of in vivo studies looking at the effect of PIC on PNN levels. LE: Long Evans, C57: C57Bl/6J, W: Wistar. GD: gestational day of PIC induction. IVG: InvivoGen, HMW: high molecular weight, LMW: low molecular weight. ♂: male, ♀: female. PLc: prelimbic cortex, CA1/CA3: field of the hippocampus, DG: dentate gyrus, PrL: prelimbic region, IL: infralimbic region.

Strain	GD	PIC source	Dose (mg/Kg)	Sex	Age	Region	Change	Reference
LE	15	IVG HMW	4	♂	7	PLc	↔	(Paylor et al., 2016)
					21		↔	
					35		↔	
					90		↓	
C57	12.5	Sigma	20	♂♀	17	CA3	↑	(Chen et al., 2020)
C57	13-15	Sigma	5	♂♀	190	CA1	↔	(Nakamura et al., 2021)
						CA3	↔	
						DG	↔	
C57	12	IVG LMW	20	♂♀	85	PrL	↓	(Zhao et al., 2021)
						IL	↔	
W	15	Sigma	4	♂♀	100	PrL	↔	(Casquero-Veiga et al., 2022)

The summary table shows that most studies show no alteration to PNN density in the PFC. When there is a change in the adult tissue, PNN decreases. However, this summary highlights the animal strains, PIC suppliers and subtypes.

The rat strain affects the maternal immune response. Murray et al. assessed the acute effects of PIC administration in non-pregnant females of three different rat strains. They observed strain- and dose-dependent effects on body temperature and cytokine response three hours after injection. In this study, Wistar rats saw the most pronounced immune response (Murray et al., 2019).

The supplier of PIC can have consequential effects on the study outcome. In a comparative study, Kowash et al. characterised the differences between the two leading suppliers of PIC. Kowash et al. found that Sigma PIC induced a far greater IL6 response. However, a significant level of endotoxin contamination was detected in the Sigma PIC, which likely contributed to the immune response. In addition, the molecular weight was highly inconsistent. InvivoGen, on the other hand, had minimal contamination and highly replicable molecular weight. Although they only looked at the pregnancy outcomes, litter size and male GD21 brain weight were significantly reduced in the Sigma-treated animals compared to InvivoGen (Kowash et al., 2019). A second research group confirmed this inconsistency in Sigma PIC. Comparing multiple batches, low and high molecular weight PIC from InvivoGen resulted in a unique profile of cytokine changes in the maternal plasma, placenta and foetal brain. They found that the low

molecular weight PIC consistently had the least potent response (Mueller et al., 2019). This is likely due to high molecular weight PIC triggering cytoplasmic RNA sensors retinoic acid-inducible gene I (RIG-I) and melanoma differentiation-associated gene 5 (MDA5) receptors as well as TLR3 (Zhou et al., 2013).

In this study, we observed increased PNN density at PD35 and PD100. In addition, we saw increased expression of Acan and Vcan at both ages in the males. Finally, levels of Ncan were also upregulated in both sexes at PD35.

Increased PNN density may impair synaptic transmission. As a reminder, the degradation of PNN with Chondroitinase ABC (ChABC) can improve cognition (Anderson et al., 2020, Romberg et al., 2013). Evidence from spinal cord injury models suggests that ChABC treatment increases the density of dendritic spines, improving synaptic plasticity (Barritt et al., 2006, Massey et al., 2006), suggesting that PNN prevents spine development. There are several theories as to why the PNN limits plasticity. First, the PNN may form a physical barrier (Wang et al., 2012) or act as a buffer for the ions involved in neurotransmission (Bitanihirwe et al., 2014). Finally, if the PNN is dense with diminished pores, diffusion and cycling of AMPAr will be limited. Indeed, the removal of the PNN increases the diffusion and cycling of AMPAr receptors resulting in improved synaptic plasticity as measured by paired-pulse facilitation (Frischknecht et al., 2009). The increased levels of PNN density, above that of control, may mean the PVI cannot form synaptic connections.

We measured increased levels of Acan and Ncan. This was one of the earliest neuronal changes we detected. Although we cannot be sure that increased expression equates to the increased protein of the individual components, we saw a trend towards increasing PNN density at PD35 in males and females. This suggests that the PNN is forming at an expedited rate compared to controls. We have discussed that PIC induction on GD15 may have pushed forward gliogenesis and differentiation in section 6.4.4. Perhaps the early development of glial cells resulted in the precocious expression and development of PNN. In normal development, PNN levels around PVI increase over time, coinciding with a reduction in juvenile plasticity (Reichelt et al., 2019). Perhaps, our PVI-treated offspring did not experience a complete period of juvenile plasticity if this was the case. It would be of value to explore PNN component expression earlier in development to assess when PNN component upregulation occurs in vehicle and PIC animals.

6.4.6.e MMP9

MMP9 levels were increased in the foetal brains the day after LPS (Simões et al., 2018) and neonates (Chen et al., 2020), likely due to its role in both the pro- and anti-inflammatory immune response (Manicone et al., 2008).

Our study showed a marked reduction of PIC MMP9 at PD35 in both sexes. These reductions coincided with the increased density of the PNN. MMP9 is involved in PNN degradation, suggesting this function may be impaired in adolescent animals (Wen et al., 2018b). However, mRNA gives limited scope on the enzyme's function. A more accurate method of measuring enzymes is activity assays.

Finally, Ulbrich et al. review the consequences of central nervous system (CNS) insults on extracellular matrixes. They noted that inflammatory events could lead to the initial degradation of PNN by proteases such as MMP9. They speculate that this aims to increase network plasticity to counteract cell death. After the acute injury, MMP9 inhibitors, tissue inhibitors of metalloproteinases (TIMP), are upregulated by reactive astrocytes. In addition to releasing TIMPs, the astrocytes increase the expression and release of PNN components (Ulbrich et al., 2021). Excessive PNN components can affect OPC maturation and oligodendrocyte myelination (Yamada et al., 2022). Ulbrich et al. note that disruption of extracellular matrix synthesis and proteolysis is present in many CNS disorders (Ulbrich et al., 2021).

6.4.6.f BDNF and TrkB

In our study, we saw no change to BDNF or TrkB expression. The outcomes for BDNF in the literature were mixed. In the acute phase after MIA in the foetal brains (Gilmore et al., 2005) and in the neonatal brain (PD1-14) (Gilmore et al., 2005, Hemmerle et al., 2015), there were no changes to BDNF mRNA or protein. However, at PD60, in the whole brain, Hemmerle et al. found an increase in BDNF levels without mRNA change (Hemmerle et al., 2015). When focusing on the hippocampus only, Talukdar et al. found a reduction in BDNF mRNA in offspring aged PD60-70, indicating potential region-specificity (Talukdar et al., 2020). Finally, in adult offspring, BDNF expression was reduced in the hippocampus of 22-month-old male offspring (Giovanoli et al., 2015).

Evidence of changes in TrkB was limited. Hemmerle found a reduction in BDNF protein at PD60 but did not see any changes to TrkB at PD14, 30 and 60 in the PFC or any region of the hippocampus (Hemmerle et al., 2015). Kentner et al. found reduced TrkB

expression in the PFC of PD92 offspring, though there were no changes in the hippocampus (Kentner et al., 2016). We discussed in the exercise chapter the limitations of the primer we selected.

6.4.7 Limitations

We have mentioned several limitations throughout our discussion. The most pressing is the variability of the model. An inordinate number of alterations can be made to the MIA protocol. Different species and respective strains can be injected with different pathogens at different doses through different routes on different gestational days. The offspring are housed in various conditions, foods, cages and circadian cycles. Some remain with their litter, and others are cross-fostered. Behaviour tests are then carried out in some studies, and others are behaviourally naïve. Then brains are collected at different ages, and different sexes and markers are compared with different techniques. All of these changes can alter the outcome of the study.

We have tried to mitigate the variability in some respects. For example, using low molecular weight PIC mitigates the variability of higher molecular weight and Sigma PIC (Kowash et al., 2019). In addition, we chose to use Wistar rats, which produced the strongest and most negligible variance in immune response when compared to Lister hooded and Sprague Dawley rats (Murray et al., 2019).

Despite these efforts, the prevalence of MIA studies that combine prenatal insult with postnatal stress and detect distinct pathology indicate an adverse postnatal environment stress can alter outcomes (Lorusso et al., 2022, Monte et al., 2017, Yee et al., 2011). The cohort used for the qPCR and IHC studies were raised during the initial coronavirus lockdown, so they had altered animal husbandry. Namely, cages were not cleaned as frequently, and the rats had reduced handling compared to the protein cohort. Although this may have introduced additional stressors, the vehicle and PIC were all raised simultaneously.

6.5 Chapter summary

The PIC model induces synaptic, glutamatergic and GABAergic dysfunction in the PFC of adult offspring.

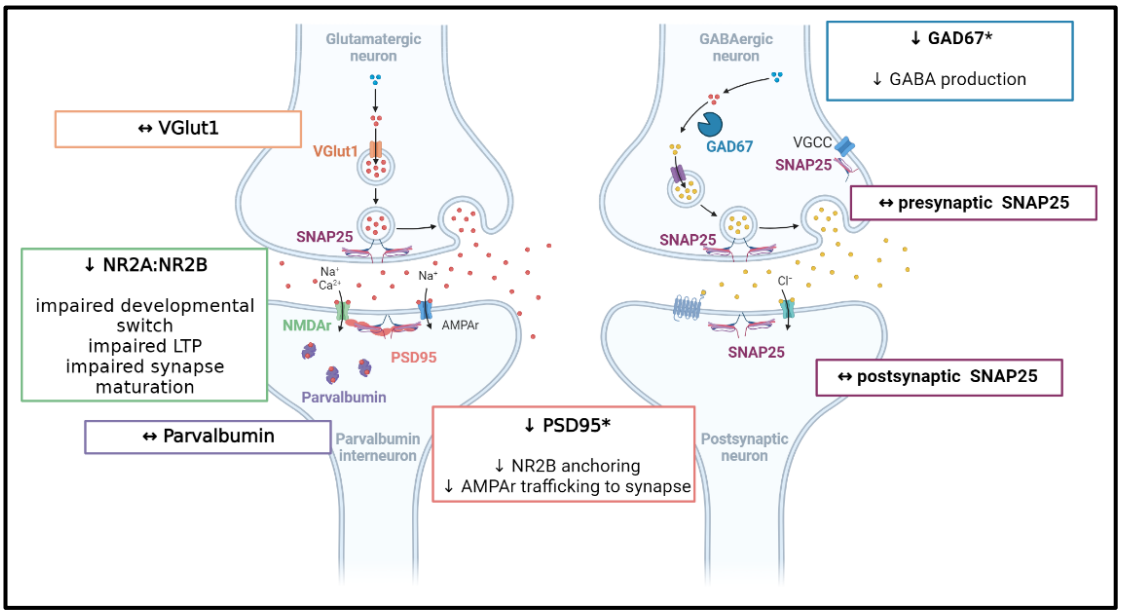

Figure 6.16: Consequences of PIC on PFC synaptic, glutamatergic and GABAergic signalling. A summary of the significant changes detected in the PIC model and potential outcomes. All changes were detected in the PFC. As the reported data is from tissue homogenates, we cannot be sure of the cellular locations of these changes. *Indicates changes that were present in the scPCP model. Image created in BioRender.com.

In the PFC, we measured an increase in perineuronal nets, which may limit the plasticity of the neuron it surrounds. In addition, we see evidence of inflammation and BDNF alterations in the male offspring.

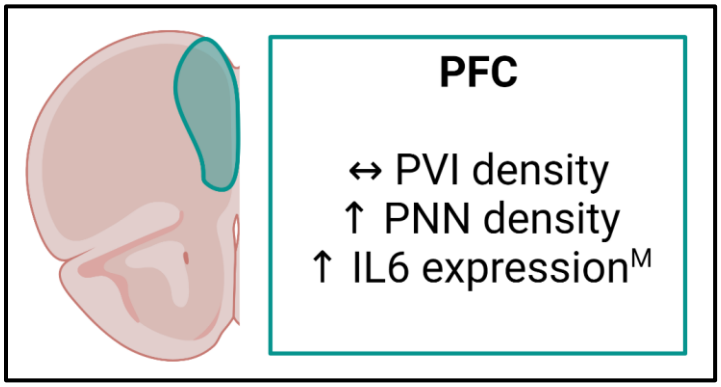

Figure 6.17: Regional consequences of PIC exposure Changes in the PFC in adult offspring. The expression changes are in males (M) only.

CHAPTER 7: FINAL DISCUSSION

7.1 The scPCP model

We described how parvalbumin interneurons (PVI) are specialised to monitor neuronal activity and adapt rapidly with intense precision. PVI can orchestrate thousands of inputs to produce rhythmic outputs (Pouille et al., 2001) PVI can compare excitatory signals from several principal neurons and silence all but the strongest (de Almeida et al., 2009). Furthermore, PVI can adapt its inhibitory output by reducing GAD67 and parvalbumin expression in response to the time of day (Harkness et al., 2021), behavioural tests (Donato et al., 2015) and hormonal cycles (Wu et al., 2014). Given its flexibility, an attempt by the PVI to adapt to NMDAr antagonism is inevitable.

In chapter three, we questioned how acute dosing of NMDAr can impair PVI function transiently (Homayoun et al., 2007), whereas bidaily dosing for one week results in sustained behavioural deficits and pathology (Cadinu et al., 2018). To investigate this, we proposed a mechanism based on the effects of acute NMDAr antagonism.

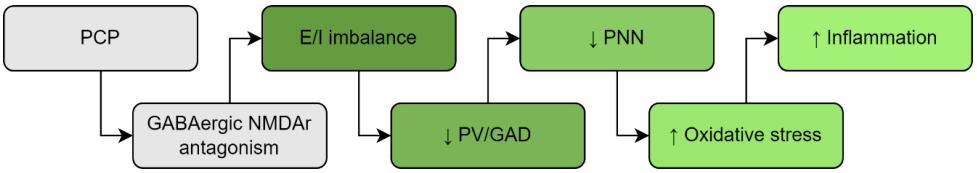

We found that the scPCP model induced profound impairments to synaptic signalling in the PFC. Presynaptically, proteins involved in neurotransmitter release in the glutamatergic (VGlut1, SNAP25) and GABAergic (GAD67, SNAP25) synapses were reduced. In addition, postsynaptic glutamatergic signalling was also impaired (NR2B, PSD95, SNAP25). The functional outlook for the scPCP model was poor, with changes indicating reduced neurotransmitter release presynaptically and impaired long-term potentiation post-synaptically, implying altered excitatory/inhibitory (E/I) balance.

In addition, we saw reductions in PFC PVI cell density and its associated PNN. In some conditions, reduced PNN can improve cognition and plasticity. However, given the presence of ongoing oxidative stress (SOD1 expression in PFC) and inflammation (IL6 mRNA in PFC, protein in DH), it is likely that without the protection of the PNN, the PVI are more susceptible to ongoing damage.

In chapter 4, we investigated whether treatment with an antioxidant or anti-inflammatory would alleviate the scPCP-induced pathology. The initial behavioural

outcomes were promising, with one week of dosing reversing NOR deficits when tested on the first drug-free day. However, these improvements were not sustained after a further washout week.

Analysis of the brains and plasma revealed marginal positive effects of treatment. The synaptic deficits were resistant to improvement. However, we did see an increase in parvalbumin levels, which correlated to cognitive improvement. As parvalbumin and behaviour are correlated, perhaps the increase is in response to increased PFC signalling during a successful NOR test. However, PVI is greater than the sum of its parts. The parvalbumin increase cannot sustain cognitive improvement after a washout without sufficient glutamatergic input (SNAP25, PSD95) and GABA synthesis (GAD67). Without these improvements, the effect is only temporary.

Reflecting on the literature, we noted that many studies do not leave a prolonged delay between the insult and treatment. Indeed, in the limited studies that did delay, treatment was not effective. Perhaps this indicates a worsening pathology in the weeks following an insult. We have not looked at mechanistic markers in brains proximal to the conclusion of scPCP. Longitudinal comparisons after scPCP may identify a self-perpetuating or worsening factor.

In chapter 5, we compared acute (1 hour) and chronic (1 hour, 5 days/week, 6 weeks) exercise protocols. There is extensive evidence of exercise improving cognition and many of our mechanistic markers. In our study, the scPCP-induced NOR deficits were reversed when the animals were tested immediately after one hour of exercise. However, in the chronic study, three weeks of exercise was insufficient to improve cognition. Instead, we saw improvements after six weeks of wheel access. Crucially, the chronic exercise study had a 24-hour delay between the last exercise bout and NOR testing, suggesting distinct mechanisms for acute and chronic exercise improvements.

In addition to the standard NOR, we tested the animals with a continuous NOR task. This showed that chronic exercise had an impressive effect on scVeh- and scPCP-treated rats. Although all groups performed well initially due to lack of distraction, the sedentary animals progressively worsened. However, the exercise animals could complete the task throughout, displaying astonishingly efficient management of memory formation and retrieval without any proactive interference.

Studying the brains and related literature evidenced that exercise has profound and multifaceted benefits that help attenuate scPCP pathology. Moreover, it gave further insight into the mechanisms. We were struck by the reduction in BDNF protein in the acute exercise study. Where other cohorts showed variability in the DH BDNF concentrations, the scPCP sedentary group was relatively consistent (Figure 5.8). Was the variation in the other groups driven by differing levels of exercise or cognitive performances? We did find that the latter was correlated to BDNF levels. Does this indicate a failure to adapt in the scPCP animals? Considering the downstream functions of BDNF (summarised in Figure 5.13), we see how the lack of these systems would contribute to scPCP pathology – reduced neurogenesis, development, survival and synaptic plasticity.

Frustratingly, we could not find a reliable marker for TrkB to see if there were any changes to the BDNF/TrkB pathway in the chronic exercise study. However, we did see increases in the density of PVI in the DG of the hippocampus. We hypothesised that this could be due to increased numbers of newly born PVI, mature PVI having been recruited to assist in granule cell maturation or recovery of the parvalbumin protein phenotype. This could be assessed with the host of cell proliferation markers or a future study incorporating BrdU injections.

We want to reiterate the work of Yi et al., who ablated the PVI in the DG. In doing so, exercise no longer rescued MK-801-induced deficits (Yi et al., 2020). Therefore, monitoring the new neurons created in exercise-induced neurogenesis would be very interesting. Would these neurons be impaired synaptically? Where do these neurons migrate? Is their maturation altered because of the network hypofunction? Is neurogenesis required for long-term positive effects?

The second key finding from the exercise study was the reduction of PNN after exercise. We want to restate briefly that the PNN function depends on its components and the environment (Avram et al., 2014, Cabungcal et al., 2013b, Favuzzi et al., 2017). In a high oxidative stress environment, low PNN does not protect the PVI (Steullet et al., 2017). However, in the event of low oxidative stress, as the evidence suggests is present in voluntary exercise protocols (Belviranlı et al., 2019, Feter et al., 2019, García-Mesa et al., 2016, Hoffman-Goetz et al., 2009), the lack of PNN can be conducive to high plasticity

states (Romberg et al., 2013, Rowlands et al., 2018). Future studies could investigate the components, the levels of oxidative stress and inflammation.

7.2 The PIC model

In the final chapter, we looked at the effects of the maternal immune activation model on our mechanistic markers. We found no pathology in the adolescent animals (PD35) in nearly all markers tested. However, there was extensive pathology in the adult offspring (PD100), reflecting clinical observations.

Core to both models is synaptic dysfunction in the PFC; indeed, hypofunction of the PFC is closely linked to cognitive impairment in schizophrenia. However, we believe the induction method is very different between models. In the PIC model, we suggested that increased IL6 levels induced the OPCs to proliferate prematurely. This could result in the increased and early expression of glial-derived PNN components. Future studies should investigate PNN markers in the earlier time points of these models. In addition, studies investigating the cellular origins would be of use.

We have summarised the changes observed and the potential consequences below:

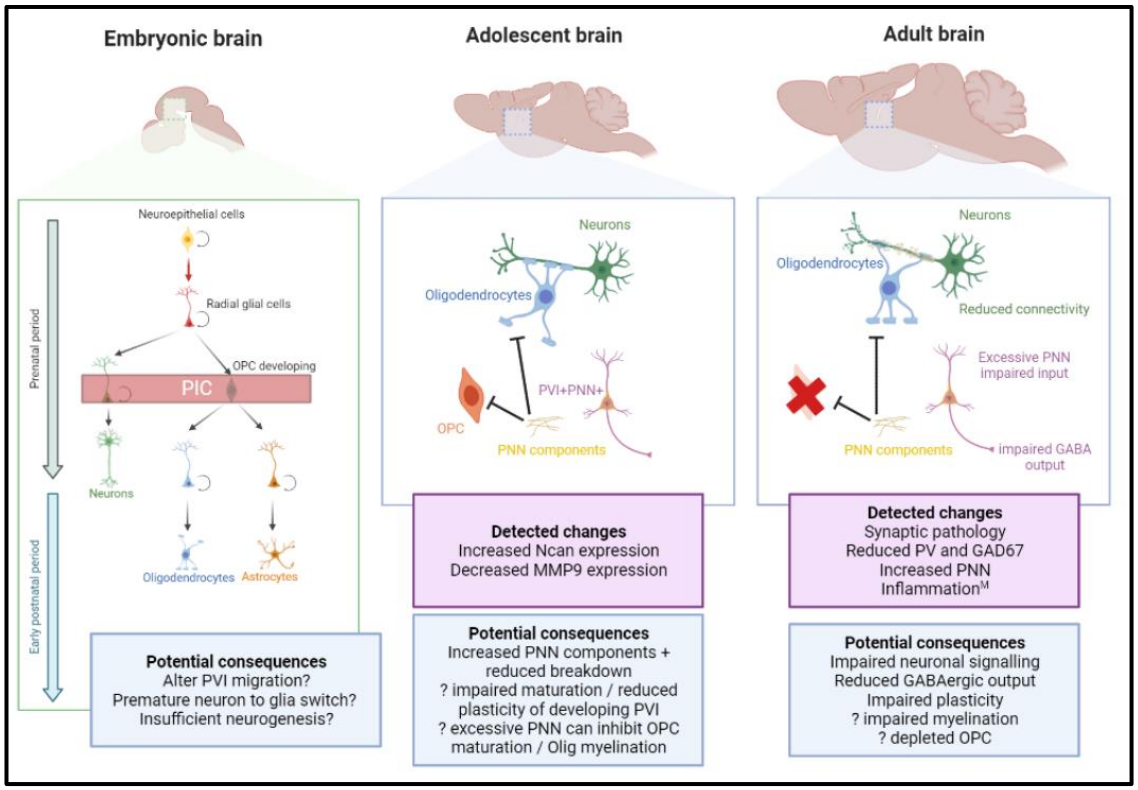

Figure 7.1: Theoretical consequences of PIC on GD15. M: change detected in males only.

7.3 Concluding remarks

Here we have presented two different models with distinct construction. Both models result in long-term brain pathology and cognitive impairment despite the differences. Notably, both have opposing outcomes for PVI and PNN. However, provisional data indicates that both combinations result in impaired PVI function. Throughout this thesis, we have discussed the unique sensitivities of the PVI to deviations in regular brain activity. These models provide the opportunity to test treatments targeting PVI function in two different scenarios.

We have also shown that synaptic dysfunction is common in both models and suggested that recovery of these connections is essential for long-term recovery. The notion that neurogenesis is required for the positive effects of exercise warrants further investigation into how these new neurons integrate into the network. Moreover, understanding the functionality and levels of damage in these adult-born neurons in both models could be of great therapeutic use.

CHAPTER 8: SUPPLEMENTARY MATERIAL

8.1 Methods

8.1.1 qPCR

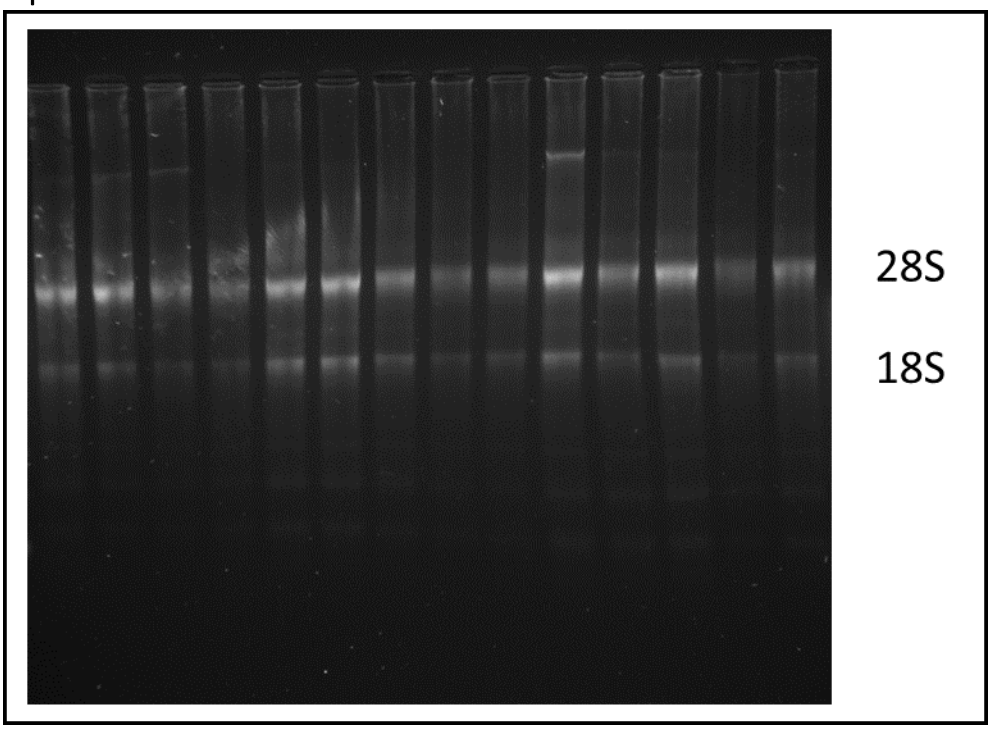

Figure 8.1: Representative image of RNA integrity. Discrete bands at 28S and 18S, with the intensity of 28S bands being approximately twice that of 18S, indicated good-quality RNA.

Table 8.1: qPCR primer information. GeneGlobe ID is a unique identifier for the QuantiTect primers from Qiagen. The table also details the exons spanned by the primer and the predicted amplicon size in base pairs (bp)

Target	GeneGlobe ID	Exons spanned	Amplicon size (bp)
Acan	QT00189518	2/3	90
Bcan	QT00176638	6/7	144
BDNF	QT00375998	-	143
Cat1	QT00182700	11/12	99
GAD1	QT00194600	11/12/13	98
GAD2	QT00190778	8/9/10	99
Gpx1	QT01799903	-	76
Gpx4	QT00174853	2/3/4	104
Grin2A	QT01588069	4/5	101
IL1β	QT00181657	3/4	91
IL6	QT00182896	1/2	128
MMP9	QT00178290	12/13	149
Ncan	QT00177240	11/12	89
NFκB	QT01577975	5/6	99
PSD95	QT00183414	6/7	63
PV	QT00176862	3/4	111
SNAP25	QT00196413	2/3	126
SOD1	QT00174888	4/5	109
TrkB	QT00181923	7/8	103
Vcan	QT01598814	10/11/12	146
VGlut	QT00176624	10/11/12	156

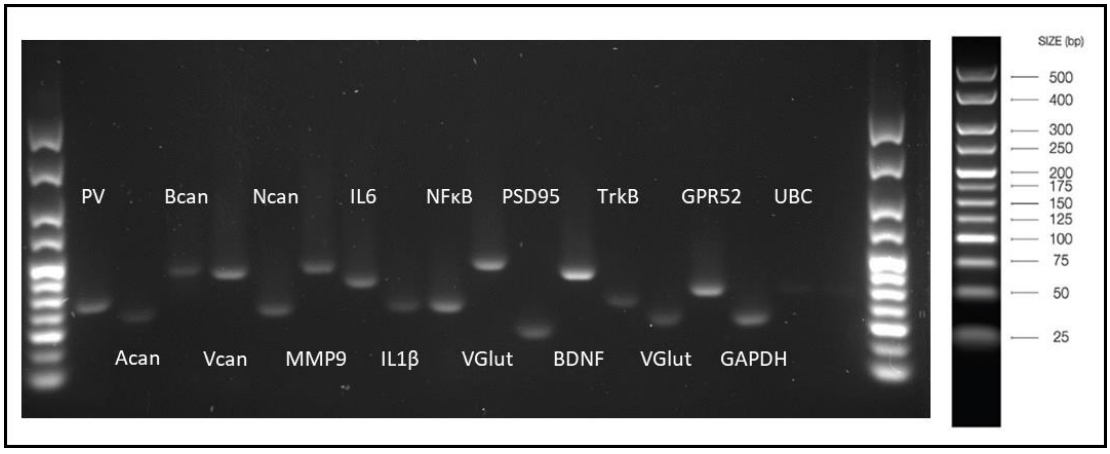

Figure 8.2: Representative image of gel to check qPCR product size.

Table 8.2: qPCR primer efficiency and standard curve R^2 data. Tm range: melt temperature range across all samples. Average cycle threshold (Ct) value across all samples. RT (no reverse transcriptase) and NTc (no template) control values. Most negatives had no Ct. y> 10 cycles indicates negatives that had a cycle threshold but was 10 cycles higher than the lowest standard.

Target	R^2 (ΔRn)	Efficiency (%)	Tm range	Avg Ct	RT	NTc
Acan	0.99	98.5	1.5	28.76	No Ct	No Ct
Actin	1.00	99.9	1	19.53	y > 10 cycles	y > 10 cycles
Bcan	0.86	79.1	0.5	27.53	No Ct	No Ct
BDNF	1.00	104.4	1.5	23.22	No Ct	No Ct
Cat1	0.99	110.9	1.5	22.18	No Ct	No Ct
GAD1	1.00	102.3	1	21.27	No Ct	No Ct
GAD2	1.00	101.5	0.5	20.70	No Ct	No Ct
GAPDH	0.99	98.1	0.5	18.97	y > 10 cycles	y > 10 cycles
GAPDH (2)	0.99	98.1	1	20.62	y > 10 cycles	y > 10 cycles
Gpx1	1.00	103.3	1	20.36	No Ct	No Ct
Gpx4	1.00	99.7	0.5	19.54	y > 10 cycles	No Ct
Grin2A	1.00	98.5	0.5	24.16	No Ct	No Ct
IL1β	0.99	104.3	1.5	30.80	No Ct	No Ct
IL6	0.97	90.5	1	30.49	No Ct	No Ct
MMP9	0.99	107.8	1	28.08	No Ct	No Ct
Ncan	1.00	90.5	0.5	21.73	No Ct	No Ct
NFκB	0.95	97.5	1.5	23.93	No Ct	No Ct
PSD95	0.96	96	1	24.47	No Ct	y > 10 cycles
PV	0.99	98.1	0.5	21.68	y > 10 cycles	No Ct
SNAP25	1.00	101.5	1	17.24	No Ct	No Ct
SOD1	0.99	106.9	1	20.15	y > 10 cycles	No Ct
TrkB	0.97	105.2	1.5	20.29	No Ct	No Ct
Ubiquitin	1.00	107.6	0.5	17.58	y > 10 cycles	y > 10 cycles
Vcan	0.99	91.6	0.5	23.95	No Ct	No Ct
VGlut	0.99	107.7	1	21.78	No Ct	No Ct

8.1.2 WES

To validate the use of total protein as a housekeeping mechanism, we loaded the two samples of each treatment group in duplicate at 0.8, 0.4 and 0.2 mg/mL of protein. We used repeated measures GLM (see 2.9.7.b) to assess whether the treatment had an effect. In all selected tissues, there were no significant effects of treatment. In addition, we found a positive correlation between protein concentration and the area under the curve, suggesting we had not saturated the assay (see 2.6.3.a).

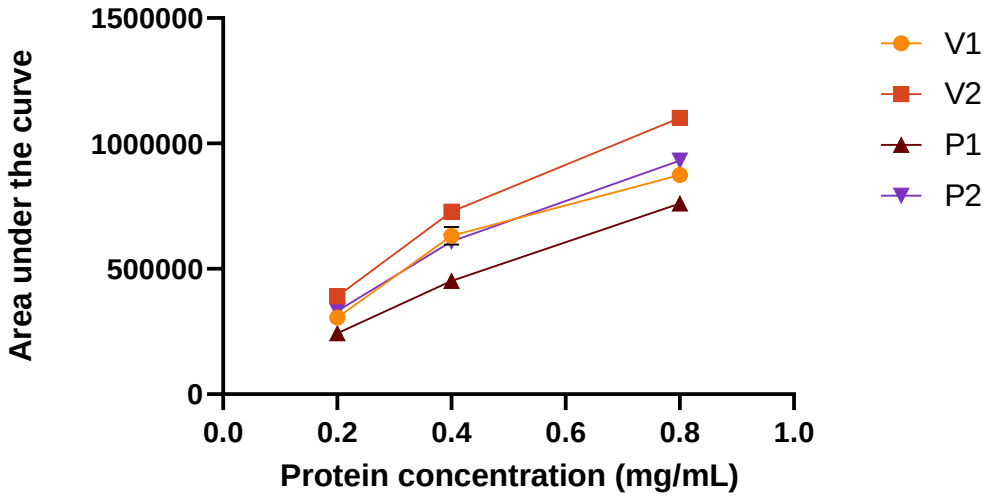

Figure 8.3: Total protein validation as a method of normalisation. The area under the curve for four samples in duplicate from two treatment groups at three different protein concentrations.

8.2 Apocynin/minocycline

8.2.1 Dose selection for apocynin/minocycline study

We completed an acute study to select an appropriate dose for the apocynin/minocycline study. 60 animals were dosed with vehicle (0.9% saline, n = 10) or scPCP (2mg/Kg, n = 50) bidaily for one week. After a one-week washout, animals were habituated to the NOR testing arena and then dosed with apocynin (0.5, 1, 5 and 10mg/Kg, i.p.; n = 10 per dose) or vehicle. Forty-five minutes later, animals were tested using the NOR test with a one-minute ITI. Using a repeated-measures GLM with the treatment group as a fixed factor and the object as a within-subjects factor, we found a significant effect of the object*treatment interaction ($F_{1, 54}$ = 34.800, p = 0.023). Using the estimated marginal means, we found this was driven by the scVeh group (p = 0.006) and the scPCP + apocynin 10mg/Kg group (p = 0.025). We ran a one-sample t-test on the DI and found there was a significant difference between the scVeh (t_9 = 4.949, p<0.001), scPCP + apocynin 0.5mg/Kg (t_9 = 1.996, p = 0.017) and scPCP + apocynin 10mg/Kg (t_9 = 2.438, p = 0.038) group DI and random chance. There was no difference in the line crossings ($F_{5, 54}$ = 1.365, p = 0.252, one-way ANOVA).

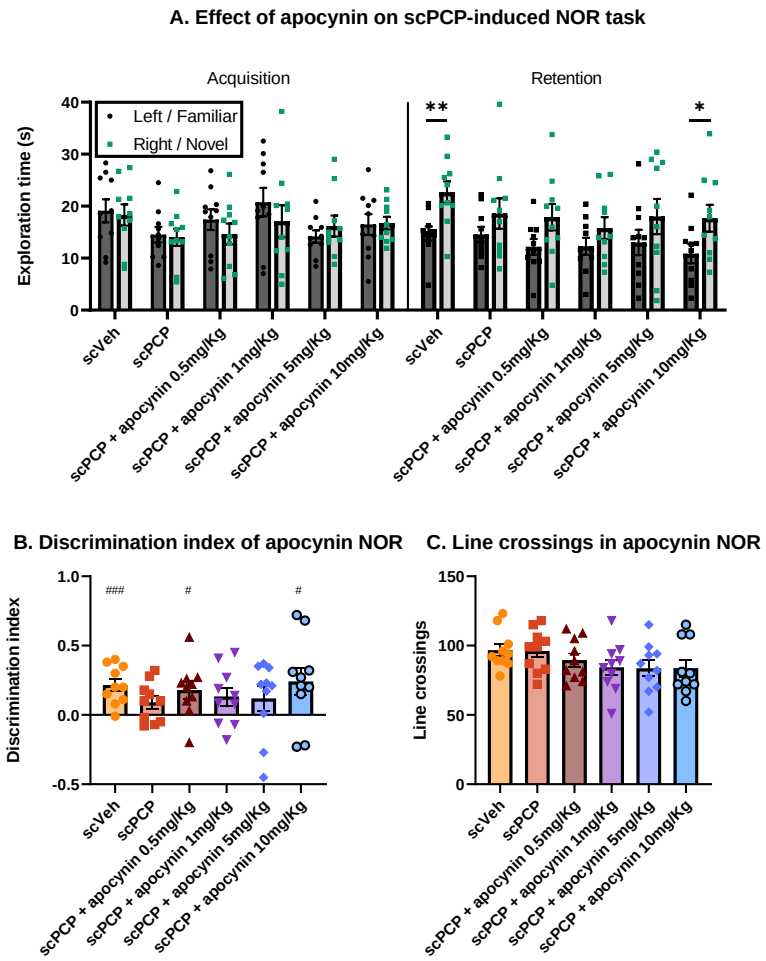

Figure 8.4: The effects of acute apocynin on the scPCP-induced NOR deficit. **A)** Time spent exploring in the acquisition and retention trials of the NOR task following treatment with scVeh + acute (a)Veh (scVeh), scPCP + aVeh (scPCP), scPCP + aApocynin i.p. at 0.5 mg/Kg, 1 mg/Kg, 5 mg/Kg, and 10 mg/Kg. **B)** The discrimination index for each of the treatment groups. **C)** Number of line crossings during the acquisition and retention trial. For **A)** differences between objects were assessed with a repeated measures general linear model (GLM). The difference between the estimated marginal means for each object was analysed using a pairwise comparison with Šidák's correction. **B)** a one-sample t-test was used to compare the mean DI for each group to a hypothetical mean of 0. Finally, for **C)**, a one-way ANOVA was used to compare the differences between groups. (n=10). Graphs show mean ± SEM. *=difference between objects, *p<0.05, **p<0.01, ***p<0.001. $^{\#}$=difference from a hypothetical mean of 0, $^{\#}$p<0.05, $^{\#\#}$p<0.01, $^{\#\#\#}$p<0.001

One week later, rats were assigned to receive minocycline (5, 10, 20, 40mg/Kg, p.o.; n = 10 per dose) or vehicle. One hundred twenty minutes later, animals were tested using the NOR task with a one-minute ITI. Data were analysed in the same way as the subchronic study (4.3.1). Repeated measures GLM revealed a significant effect of the object*treatment interaction ($F_{1\ 52}$ = 10.95, p = 0.002), which was due to effective discrimination in the scVeh (p = 0.047) and scPCP + minocycline 40mg/Kg (p = 0.016) groups. One sample t-test revealed only the scPCP + minocycline 40mg/Kg cohort was

performing above random chance (t_8 = 4.498, p = 0.002), though scVeh were trending (t_9 = 2.137, p = 0.061). Finally, there were no differences in line crossing ($F_{5, 52}$ = 1.425, p = 0.231, one-way ANOVA).

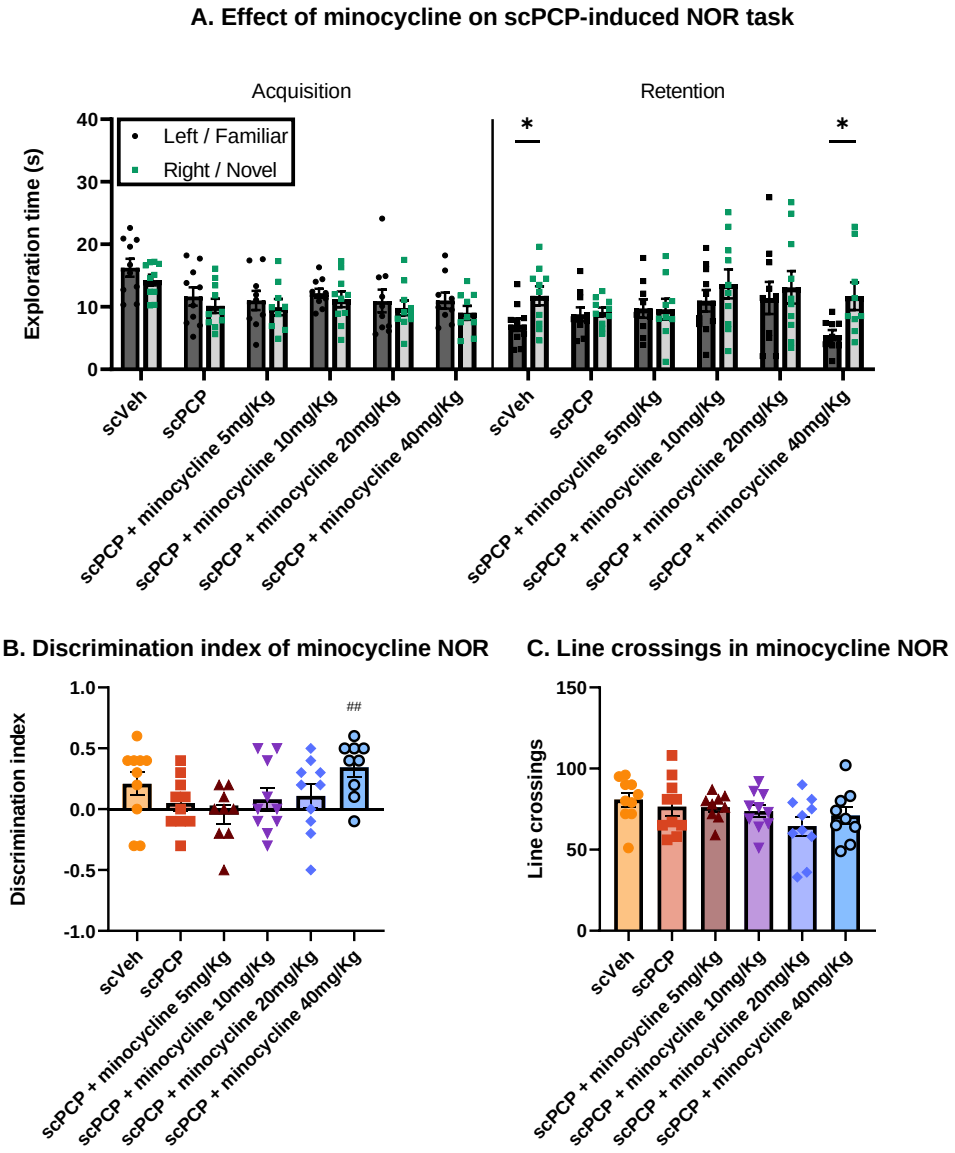

Figure 8.5: The effects of acute minocycline on the scPCP-induced NOR deficit. **A)** Time spent exploring in the acquisition and retention trials of the NOR task following treatment with scVeh + acute (a)Veh (scVeh), scPCP + aVeh (scPCP), scPCP + aMinocycline p.o. at 5 mg/Kg, 10 mg/Kg, 20 mg/Kg, and 40 mg/Kg. **B)** The discrimination index for each of the treatment groups. **C)** Number of line crossings during the acquisition and retention trial. For **A)** differences between objects were assessed with a repeated measures general linear model (GLM). The difference between the estimated marginal means for each object was analysed using a pairwise comparison with Šidák's correction. **B)** a one-sample t-test was used to compare the mean DI for each group to a hypothetical mean of 0. Finally, for **C)**, a one-way ANOVA was used to compare the differences between groups. (n=9-10). Graphs show mean ± SEM. *=difference between objects, *p<0.05, **p<0.01, ***p<0.001. $^{\#}$=difference from a hypothetical mean of 0, $^{\#}$p<0.05, $^{\#\#}$p<0.01, $^{\#\#\#}$p<0.001

8.2.2 Animal weights

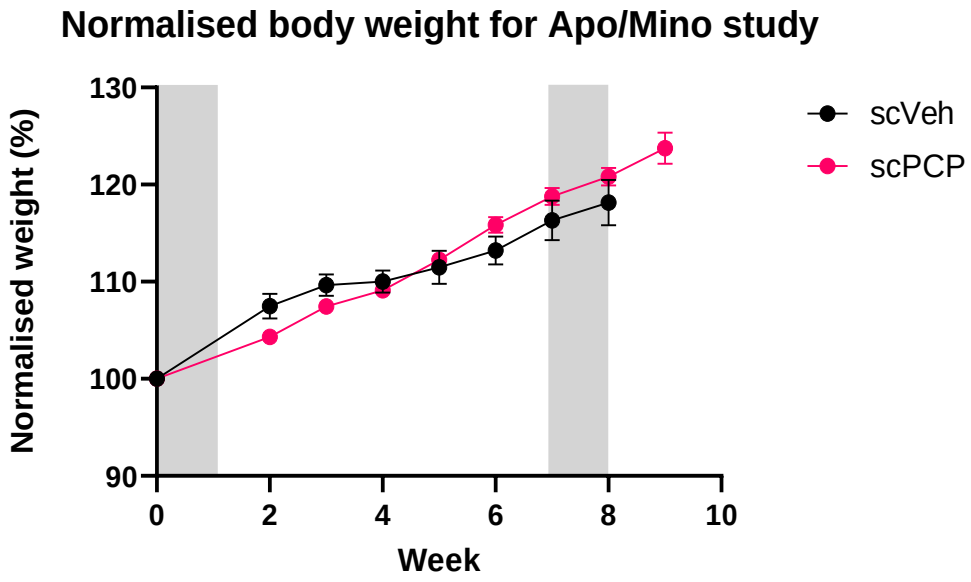

Figure 8.6: Change in animal weight compared to pre-dosing baseline. The grey box between weeks 0 and 1 indicates the scVeh or scPCP dosing week. The grey box between weeks 7 and 8 indicates the apocynin or minocycline intervention week. There were no differences between the treatment group weights ($F_{1, 58}$ = 0.0493, p = 0.825, RM GLM).

8.3 Acute exercise study

8.3.1 Animal weights

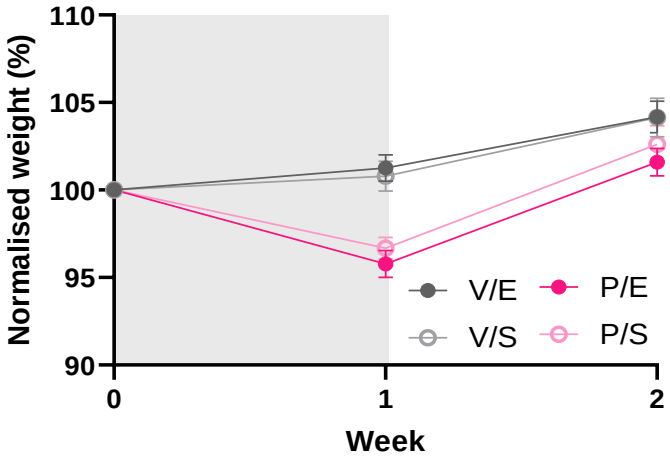

Figure 8.7: Normalised weight of animals from acute exercise study. The grey box between weeks 0 and 1 indicates the scVeh or scPCP dosing week. There was a significant difference between groups ($F_{3, 36}$ = 6.995, p<0.001, RM GLM). Specifically, there were differences in the scPCP-treated animals after the dosing week (V/E vs P/E, p<0.001 and V/S vs P/S, p = 0.007, Šidák), which normalised one week later.

8.3.2 Habituation and running data

Table 8.3: Distance ran by exercised rats in the acute exercise study. (*) faulty data collection

Cage	Rat	Distance ran (m)			
		Habituation			Acute exercise
		1	2	3	
1	1	12.6	78.5	283.8	251.3
	2	0.0	11.5	266.0	17.0
	3	0.0	0.0	0.0	2.5
	4	0.0	11.3	237.5	5.7*
	5	0.0	0.0	0.0	280.1
2	1	0.0	0.0	0.0	0.0
	2	13.6	83.8	218.9	378.9
	3	0.0	0.0	0.0	5.7
	4	20.4	16.8	67.0	791.7
	5	0.0	5.7	458.0	0.0*
7	1	0.0	0.0	0.0	0.0
	2	32.5	238.8	291.6	26.2
	3	0.0	0.0	0.0	3.7
	4	446.7	265.8	243.2	367.6
	5	0.0	0.0	0.0	141.4
8	1	89.5	0.0	124.1	352.9
	2	123.0	11.5	165.5	281.2
	3	205.3	296.9	178.5	245.6
	4	25.7	4.7	0.0	5.7
	5	5.7	237.5	209.2	237.5

8.4 Chronic exercise study

8.4.1 Animal weights

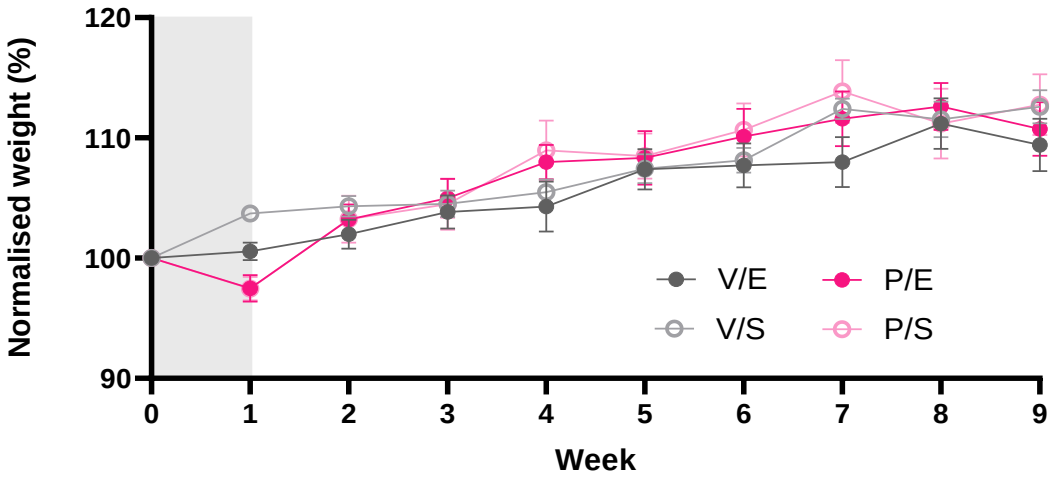

Figure 8.8: Normalised weight of animals in the chronic exercise study. The grey box between weeks 0 and 1 indicates the scVeh or scPCP dosing week. There were no differences between groups ($F_{3, 36}$ = 0.300, p = 0.825, RM GLM). Though exploratory post hoc testing revealed significant reductions in weight in the P/S group compared to V/S (p<0.001, Šidák)

8.4.2 Habituation data

Table 8.4: Distance ran during habituation for chronic exercise study.

Cage	Rat	Distance ran (m)		
		1	2	3
1	1	72.6	41.5	82.9
	2	193.8	126.4	139.9
	3	20.7	0.0	20.7
	4	0.0	10.4	0.0
	5	62.2	165.9	165.9
2	1	186.6	0.0	145.1
	2	0.0	207.3	747.8
	3	10.4	0.0	0.0
	4	103.7	72.6	0.0
	5	165.9	114.0	466.5
7	1	41.5	176.2	176.2
	2	126.4	85.0	109.8
	3	0.0	20.7	10.4
	4	10.4	93.3	165.9
	5	311.0	217.7	165.9
8	1	165.9	134.8	20.7
	2	0.0	72.6	173.1
	3	10.4	41.5	0.0
	4	622.0	829.4	0.0
	5	82.9	20.7	362.9

8.4.3 Culling days

Table 8.5: Testing and culling information for chronic exercise study. D post ex: days since last exercise session. ceNOR3: final standard NOR test. H1: group habituation, H2: individual habituation, H3: shuttle training, H4: object training of cage numbers.

D post ex	1	2	3	4	5	6	7
Testing	ceNOR3				Cage 7	Cage 1	Cage 3
Cull					Cage 7	Cage 1	Cage 3
Habituation	H1: 7, 1, 3, 5 H2: 7	H2: 1, 3 H3: 7	H2: 5 H3: 1 H4: 7	H3: 5 H4: 1	H4: 3	H4: 5	
D post ex	**8**	**9**	**10**	**11**	**12**	**13**	**14**
Testing	Cage 5				Cage 8	Cage 2	Cage 4
Cull	Cage 5				Cage 8	Cage 2	
Habituation	H1: 8, 2, 4, 6 H2: 8	H2: 2, 4 H3: 8	H2: 6 H3: 2 H4: 8	H3: 6 H4: 2	H4: 4	H4: 6	
D post ex	**15**						
Testing	Cage 6						
Cull	Cage 4 + 6						

8.5 Poly(I:C)

8.5.1 Distribution of residuals

8.5.1.a GLMM

We tested the residuals of the GLMM to see if they were normally distributed. The residuals were normally distributed for the WES and IHC data. However, several GLMMs for the qPCR data had not normally distributed residuals (Table 8.6).

Table 8.6: Normality test on GLMM residuals. The information after the underscore denotes the name of the gene target. The details of the tested cohorts are found in brackets: 35 or 100 indicate a model ran in the PD35 or PD100s, respectively. Equally, m: male, f: female, v: vehicles. Normality was analysed using the D'Agostino and Pearson test.

Residual	K^2	P value		Residual	K^2	P value	
RESID_vglut	26.04	<0.0001	****	RESID_ncan100	4.298	0.1166	ns
RESID_psd	6.225	0.0445	*	RESID_ncan(v)	5.987	0.0501	ns
RESID_pv	34.21	<0.0001	****	RESID_mmp9	26.4	<0.0001	****
RESID_pv(100)	24.11	<0.0001	****	RESID_mmp9(35)	5.623	0.0601	ns
RESID_pv(f)	17.7	0.0001	***	RESID_mmp9(35v)	1.35	0.5092	ns
RESID_pv(m100)	2.244	0.3256	ns	RESID_il1b	1.982	0.3712	ns
RESID_acan	3.525	0.1716	ns	RESID_il1b(100)	0.3307	0.8476	ns
RESID_acan(100)	4.176	0.124	ns	RESID_il1b(f)	2.134	0.344	ns
RESID_acan(f)	2.507	0.2855	ns	RESID_nfkb	3.676	0.1591	ns
RESID_acan(m)	5.349	0.0689	ns	RESID_nfkb(100)	3.419	0.1809	ns
RESID_vcan	1.434	0.4881	ns	RESID_nfkb(f)	14.88	0.0006	***
RESID_vcan(100)	0.213	0.899	ns	RESID_il6	45.07	<0.0001	****
RESID_vcan(f)	0.0489	0.9759	ns	RESID_il6(100)	18.5	<0.0001	****
RESID_vcan(m)	14.14	0.0008	***	RESID_il6(100v)	6.234	0.0443	*
RESID_ncan	5.379	0.0679	ns	RESID_il6(100m)	0.6808	0.7115	ns
RESID_ncan(35)	2.584	0.2747	ns	RESID_bdnf(100m)	1.256	0.5336	ns

The data with non-normally distributed residuals were log-transformed, and the GLMM ran in the transformed data set. We found the original GLMM results were fairly robust to transformation, with slight shifts in outcomes, summarised below:

Table 8.7: GLMM outcomes in log10 transformed data. The green text shows data that has altered in significance after transformations.

Target	Cohort grouping	Significant factor	----- Raw data -----		----- Log10 transformed -----	
VGlut	Full	Age	$F_{1, 30.916}$=10.955, p=0.002	**	$F_{1, 45}$=13.463, p<0.001	***
PSD95	Full	Age	$F_{1, 45}$=5.745, p=0.021	*	$F_{1, 45}$=5.541, p=0.023	*
PV	Full	Age	$F_{1, 45}$=7.622, p=0.008	**	$F_{1, 45}$=11.971, p=0.001	**
		Sex	$F_{1, 45}$=7.734, p=0.008	**	$F_{1, 45}$=5.709, p=0.021	*
	PD100	Sex	$F_{1, 22}$=8.792, p=0.007	**	$F_{1, 22}$=13.098, p=0.002	**
	Females	Age	$F_{1, 22}$=7.239, p=0.013	*	$F_{1, 22}$=12.881, p=0.002	**
Vcan	Males	Age	$F_{1, 20}$=5.575, p=0.028	*	$F_{1, 12.040}$=8.859, p=0.012	*
		Treatment	$F_{1, 20}$=4.146, p=0.055		$F_{1, 11.994}$=3.791, p=0.075	
MMP9	Full	Age	$F_{1, 33.959}$=9.140, p=0.005	**	ns	
		Treatment	$F_{1, 12.101}$=6.167, p=0.029	*	ns	
		Treatment*age	$F_{1, 33.959}$=8.075, p=0.008	**	$F_{3, 44}$=5.297, p=0.003	**
NFkB	Females	Age	$F_{1, 10.449}$=27.023, p<0.001	***	$F_{1, 10.428}$=27.419, p<0.001	***
IL6	Full	Age	$F_{1, 39}$=33.441, p<0.001	***	$F_{1, 12.507}$=72.731, p<0.001	***
		Sex	$F_{1, 39}$=14.074, p<0.001	***	$F_{1, 35}$=5.837, p=0.021	*
		Age*sex	$F_{1, 39}$=12.431, p=0.001	**	ns	
		Age*treatment*sex	$F_{4, 39}$=3.371, p=0.018	*	$F_{5, 30.675}$=2.999, p=0.026	*
	PD100	Sex	$F_{1, 20}$=14.355, p=0.001	**	$F_{1, 20}$=29.989, p<0.001	***
		Sex*treatment	$F_{2, 20}$=3.531, p=0.049	*	$F_{2, 20}$=6.197, p=0.008	**
	PD100 vehicles	Sex	$F_{1, 5.520}$=12.445, p=0.014	*	$F_{1, 4.996}$=64.265, p<0.001	***

For data where factors were no longer significant, we continued to analyse using the GLMM principles. Further exploration of the MMP9 outcomes revealed that the later parameters remained comparable to the raw data GLMM. In the log10 transformed GLMM, there was a significant effect of treatment in the PD35 animals ($F_{1, 22}$ = 8.881, p = 0.007) and a significant effect of sex in the adolescent PIC treated cohort ($F_{1, 3.023}$ = 526.851, p<0.001), which matched the non-transformed data outcomes. Equally, in the IL6 cohort, the effect of treatment in the adult males remained ($F_{1, 10}$ = 11.443, p = 0.007), as did the sex effect in the PD100 cohort ($F_{1, 22}$ = 20.366, p<0.001) and the adult vehicle animals ($F_{1, 4.996}$ = 64.265, p<0.001). For all transformed data GLMMs, we

retested the residuals, and all were normally distributed. Given the general conformity of outcomes, we reported the non-transformed data throughout.

8.5.1.b Linear regression of maternal cytokine GLMM outcomes

We tested the residuals of the linear regressions performed on significant maternal cytokine GLMM.

Table 8.8: Normality test on GLMM regression residuals. The information after the underscore denotes the name of the gene target. The details of the tested cohorts are found in brackets: 35 or 100 indicate a model ran in the PD35 or PD100s, respectively. Equally, m: male, f: female, v: vehicles. Normality was assessed using the D'Agostino and Pearson test.

Residual	K2	P value		Residual	K2	P value	
RESID_vglut(35m)	2.579	0.2754	ns	RESID_bcan(35f)	1.280	0.5274	ns
RESID_vglut(100m)	1.184	0.5532	ns	RESID_vcan(35m)	4.435	0.1089	ns
RESID_nr2r(100f)	0.9429	0.6241	ns	RESID_ncan(35m)	0.4942	0.7811	ns
RESID_pvi(mp)	12.53	0.0019	**	RESID_ncan(100m)	6.005	0.0497	*
RESID_gad(mv)	0.02449	0.9878	ns	RESID_nfkb(m)	7.186	0.0275	*
RESID_acan(35m)	4.804	0.0905	ns	RESID_il6(100m)	0.1926	0.9082	ns
RESID_acan(35f)	7.635	0.0220	*				

The linear regression with non-parametric residuals should be interpreted with caution.

8.5.2 Adolescent PNN density grouped into sibling cohorts

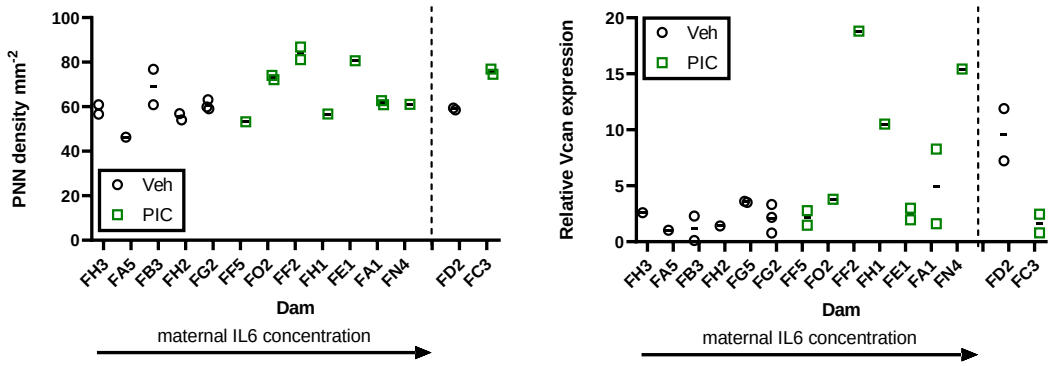

Figure 8.9: Adolescent PNN density grouped into sibling cohorts. Dams are listed in order of increasing IL6 response. IL6 data from FD2 and FC3 was not available.

CHAPTER 9: REFERENCES

AAS, M., DAZZAN, P., MONDELLI, V., MELLE, I., MURRAY, R. M. & PARIANTE, C. M. 2014. A systematic review of cognitive function in first-episode psychosis, including a discussion on childhood trauma, stress, and inflammation. *Front Psychiatry,* 4**,** 182.

ABDO QAID, E. Y., ABDULLAH, Z., ZAKARIA, R. & LONG, I. 2022. Minocycline protects against lipopolysaccharide-induced glial cells activation and oxidative stress damage in the medial prefrontal cortex (mPFC) of the rat. *Int J Neurosci***,** 1-10.

ABDUL-MONIM, Z., NEILL, J. C. & REYNOLDS, G. P. 2007. Sub-chronic psychotomimetic phencyclidine induces deficits in reversal learning and alterations in parvalbumin-immunoreactive expression in the rat. *J Psychopharmacol,* 21**,** 198-205.

ABEL, J. L. & RISSMAN, E. F. 2013. Running-induced epigenetic and gene expression changes in the adolescent brain. *Int J Dev Neurosci,* 31**,** 382-90.

ACEVEDO-TRIANA, C. A., ROJAS, M. J. & CARDENAS, P. F. 2017. Running wheel training does not change neurogenesis levels or alter working memory tasks in adult rats. *PeerJ,* 5**,** e2976.

ADAIKKAN, C. & TSAI, L. H. 2020. Gamma Entrainment: Impact on Neurocircuits, Glia, and Therapeutic Opportunities. *Trends Neurosci,* 43**,** 24-41.

ADDINGTON, A. M., GORNICK, M., DUCKWORTH, J., SPORN, A., GOGTAY, N., BOBB, A., GREENSTEIN, D., LENANE, M., GOCHMAN, P., BAKER, N., BALKISSOON, R., VAKKALANKA, R. K., WEINBERGER, D. R., RAPOPORT, J. L. & STRAUB, R. E. 2005. GAD1 (2q31.1), which encodes glutamic acid decarboxylase (GAD67), is associated with childhood-onset schizophrenia and cortical gray matter volume loss. *Mol Psychiatry,* 10**,** 581-8.

ADLARD, P. A. & COTMAN, C. W. 2004a. Voluntary exercise protects against stress-induced decreases in brain-derived neurotrophic factor protein expression. *Neuroscience,* 124**,** 985-92.

ADLARD, P. A., PERREAU, V. M., ENGESSER-CESAR, C. & COTMAN, C. W. 2004b. The timecourse of induction of brain-derived neurotrophic factor mRNA and protein in the rat hippocampus following voluntary exercise. *Neurosci Lett,* 363**,** 43-8.

AKBARIAN, S., KIM, J. J., POTKIN, S. G., HAGMAN, J. O., TAFAZZOLI, A., BUNNEY, W. E. & JONES, E. G. 1995. Gene expression for glutamic acid decarboxylase is reduced without loss of neurons in prefrontal cortex of schizophrenics. *Arch Gen Psychiatry,* 52**,** 258-66.

ALI, A. A. H. & VON GALL, C. 2022. Adult Neurogenesis under Control of the Circadian System. *Cells,* 11.

ALI, F. T., ABD EL-AZEEM, E. M., HAMED, M. A., ALI, M. A. M., ABD AL-KADER, N. M. & HASSAN, E. A. 2017. Redox dysregulation, immuno-inflammatory alterations and genetic variants of BDNF and MMP-9 in schizophrenia: Pathophysiological and phenotypic implications. *Schizophr Res,* 188**,** 98-109.

ALLEN, D. N., GOLDSTEIN, G. & WARNICK, E. 2003. A consideration of neuropsychologically normal schizophrenia. *J Int Neuropsychol Soc,* 9**,** 56-63.

ALLEN, K. M., FUNG, S. J. & WEICKERT, C. S. 2016. Cell proliferation is reduced in the hippocampus in schizophrenia. *Aust N Z J Psychiatry,* 50**,** 473-80.

ALLEN, R. M. & YOUNG, S. J. 1978. Phencyclidine-induced psychosis. *Am J Psychiatry,* 135**,** 1081-4.

ALOMARI, M. A., KHABOUR, O. F., ALZOUBI, K. H. & ALZUBI, M. A. 2013. Forced and voluntary exercises equally improve spatial learning and memory and hippocampal BDNF levels. *Behav Brain Res,* 247**,** 34-9.

ALVAREZ, D. D., GIACOMINI, D., YANG, S. M., TRINCHERO, M. F., TEMPRANA, S. G., BÜTTNER, K. A., BELTRAMONE, N. & SCHINDER, A. F. 2016. A disynaptic feedback network activated by experience promotes the integration of new granule cells. *Science,* 354**,** 459-465.

AMERICAN PSYCHIATRIC, A. 2013. *Diagnostic and Statistical Manual of Mental Disorders (DSM-5®),* Washington, UNITED STATES, American Psychiatric Publishing.

AMIRAHMADI, S., FARIMANI, F. D., AKBARIAN, M., MIRZAVI, F., ESHAGHI GHALIBAF, M. H., RAJABIAN, A. & HOSSEINI, M. 2022. Minocycline attenuates cholinergic dysfunction and neuro-inflammation-mediated cognitive impairment in scopolamine-induced Alzheimer's rat model. *Inflammopharmacology,* 30**,** 2385-2397.

AMITAI, N., KUCZENSKI, R., BEHRENS, M. M. & MARKOU, A. 2012. Repeated phencyclidine administration alters glutamate release and decreases GABA markers in the prefrontal cortex of rats. *Neuropharmacology,* 62**,** 1422-31.

AN DER HEIDEN, W. & HÄFNER, H. 2000. The epidemiology of onset and course of schizophrenia. *Eur Arch Psychiatry Clin Neurosci,* 250**,** 292-303.

ANANDA, M. M. A. & WEERAHANDI, S. TWO-WAY ANOVA WITH UNEQUAL CELL FREQUENCIES AND UNEQUAL VARIANCES. 1997.

ANDERSON, M. D., PAYLOR, J. W., SCOTT, G. A., GREBA, Q., WINSHIP, I. R. & HOWLAND, J. G. 2020. ChABC infusions into medial prefrontal cortex, but not posterior parietal cortex, improve the performance of rats tested on a novel, challenging delay in the touchscreen TUNL task. *Learn Mem,* 27**,** 222-235.

ANDREOU, C., NOLTE, G., LEICHT, G., POLOMAC, N., HANGANU-OPATZ, I. L., LAMBERT, M., ENGEL, A. K. & MULERT, C. 2015. Increased Resting-State Gamma-Band Connectivity in First-Episode Schizophrenia. *Schizophr Bull,* 41**,** 930-9.

ANSARI, M. A. & SCHEFF, S. W. 2011. NADPH-oxidase activation and cognition in Alzheimer disease progression. *Free Radic Biol Med,* 51**,** 171-8.

ANTONUCCI, F., CORRADINI, I., FOSSATI, G., TOMASONI, R., MENNA, E. & MATTEOLI, M. 2016. SNAP-25, a Known Presynaptic Protein with Emerging Postsynaptic Functions. *Front Synaptic Neurosci,* 8**,** 7.

ARAIN, M., HAQUE, M., JOHAL, L., MATHUR, P., NEL, W., RAIS, A., SANDHU, R. & SHARMA, S. 2013. Maturation of the adolescent brain. *Neuropsychiatr Dis Treat,* 9**,** 449-61.

ARANGO DUQUE, G. & DESCOTEAUX, A. 2014. Macrophage cytokines: involvement in immunity and infectious diseases. *Front Immunol,* 5**,** 491.

ARIDA, R. M., SCORZA, C. A., DA SILVA, A. V., SCORZA, F. A. & CAVALHEIRO, E. A. 2004. Differential effects of spontaneous versus forced exercise in rats on the staining of parvalbumin-positive neurons in the hippocampal formation. *Neurosci Lett,* 364**,** 135-8.

ARRANZ, A. M., PERKINS, K. L., IRIE, F., LEWIS, D. P., HRABE, J., XIAO, F., ITANO, N., KIMATA, K., HRABETOVA, S. & YAMAGUCHI, Y. 2014. Hyaluronan deficiency due to Has3 knock-out causes altered neuronal activity and seizures via reduction in brain extracellular space. *J Neurosci,* 34**,** 6164-76.

ATAIE-KACHOIE, P., MORRIS, D. L. & POURGHOLAMI, M. H. 2013. Minocycline suppresses interleukine-6, its receptor system and signaling pathways and impairs migration, invasion and adhesion capacity of ovarian cancer cells: in vitro and in vivo studies. *PLoS One,* 8**,** e60817.

ATALLAH, B. V. & SCANZIANI, M. 2009. Instantaneous modulation of gamma oscillation frequency by balancing excitation with inhibition. *Neuron,* 62**,** 566-77.

AVRAM, S., SHAPOSHNIKOV, S., BUIU, C. & MERNEA, M. 2014. Chondroitin sulfate proteoglycans: structure-function relationship with implication in neural development and brain disorders. *Biomed Res Int,* 2014**,** 642798.

AVRAMOPOULOS, D. 2018. Recent Advances in the Genetics of Schizophrenia. *Mol Neuropsychiatry,* 4**,** 35-51.

AYVAZ, H., CABAROGLU, T., AKYILDIZ, A., PALA, C. U., TEMIZKAN, R., AĞÇAM, E., AYVAZ, Z., DURAZZO, A., LUCARINI, M., DIREITO, R. & DIACONEASA, Z. 2022. Anthocyanins: Metabolic Digestion, Bioavailability, Therapeutic Effects, Current Pharmaceutical/Industrial Use, and Innovation Potential. *Antioxidants (Basel),* 12.

AZEVEDO, L. V. D. S., PEREIRA, J. R., SILVA SANTOS, R. M., ROCHA, N. P., TEIXEIRA, A. L., CHRISTO, P. P., SANTOS, V. R. & SCALZO, P. L. 2022. Acute exercise increases BDNF serum levels in patients with Parkinson's disease regardless of depression or fatigue. *Eur J Sport Sci,* 22**,** 1296-1303.

BAE, H. J., KIM, J. Y., PARK, K., YANG, X., JUNG, S. Y., PARK, S. J., KIM, D. H., SHIN, C. Y. & RYU, J. H. 2023. The effect of lansoprazole on MK-801-induced schizophrenia-like behaviors in mice. *Prog Neuropsychopharmacol Biol Psychiatry,* 120**,** 110646.

BALLENDINE, S. A., GREBA, Q., DAWICKI, W., ZHANG, X., GORDON, J. R. & HOWLAND, J. G. 2015. Behavioral alterations in rat offspring following maternal immune activation and ELR-CXC chemokine receptor antagonism during pregnancy: implications for neurodevelopmental psychiatric disorders. *Prog Neuropsychopharmacol Biol Psychiatry,* 57**,** 155-65.

BALSCHUN, D., MOECHARS, D., CALLAERTS-VEGH, Z., VERMAERCKE, B., VAN ACKER, N., ANDRIES, L. & D'HOOGE, R. 2010. Vesicular glutamate transporter VGLUT1 has a role in hippocampal long-term potentiation and spatial reversal learning. *Cereb Cortex,* 20**,** 684-93.

BALSCHUN, D., WETZEL, W., DEL REY, A., PITOSSI, F., SCHNEIDER, H., ZUSCHRATTER, W. & BESEDOVSKY, H. O. 2004. Interleukin-6: a cytokine to forget. *FASEB J,* 18**,** 1788-90.

BALU, D. T. 2016. The NMDA Receptor and Schizophrenia: From Pathophysiology to Treatment. *Adv Pharmacol,* 76**,** 351-82.

BANAZADEH, M., MEHRABANI, M., BANAZADEH, N., DABAGHZADEH, F. & SHAHABI, F. 2022. Evaluating the effect of black myrobalan on cognitive, positive, and negative symptoms in patients with chronic schizophrenia: A randomized, double-blind, placebo-controlled trial. *Phytother Res,* 36**,** 543-550.

BARANOWSKI, B. J. & MACPHERSON, R. E. K. 2018. Acute exercise induced BDNF-TrkB signalling is intact in the prefrontal cortex of obese, glucose-intolerant male mice. *Appl Physiol Nutr Metab,* 43**,** 1083-1089.

BARRETT, W., BUXHOEVEDEN, M. & DHILLON, S. 2020. Ketamine: a versatile tool for anesthesia and analgesia. *Curr Opin Anaesthesiol,* 33**,** 633-638.

BARRIA, A. & MALINOW, R. 2002. Subunit-specific NMDA receptor trafficking to synapses. *Neuron,* 35**,** 345-53.

BARRITT, A. W., DAVIES, M., MARCHAND, F., HARTLEY, R., GRIST, J., YIP, P., MCMAHON, S. B. & BRADBURY, E. J. 2006. Chondroitinase ABC promotes sprouting of intact and injured spinal systems after spinal cord injury. *J Neurosci,* 26**,** 10856-67.

BASAR-EROGLU, C., BRAND, A., HILDEBRANDT, H., KAROLINA KEDZIOR, K., MATHES, B. & SCHMIEDT, C. 2007. Working memory related gamma oscillations in schizophrenia patients. *Int J Psychophysiol,* 64**,** 39-45.

BASSO, J. C., SHANG, A., ELMAN, M., KARMOUTA, R. & SUZUKI, W. A. 2015. Acute Exercise Improves Prefrontal Cortex but not Hippocampal Function in Healthy Adults. *J Int Neuropsychol Soc,* 21**,** 791-801.

BAST, T., WILSON, I. A., WITTER, M. P. & MORRIS, R. G. 2009. From rapid place learning to behavioral performance: a key role for the intermediate hippocampus. *PLoS Biol,* 7**,** e1000089.

BEAR, M., CONNORS, B. & PARADISO, M. A. 2020. *Neuroscience : exploring the brain*.

BEDARD, K. & KRAUSE, K. H. 2007. The NOX family of ROS-generating NADPH oxidases: physiology and pathophysiology. *Physiol Rev,* 87**,** 245-313.

BEHRENS, M. M., ALI, S. S., DAO, D. N., LUCERO, J., SHEKHTMAN, G., QUICK, K. L. & DUGAN, L. L. 2007. Ketamine-induced loss of phenotype of fast-spiking interneurons is mediated by NADPH-oxidase. *Science,* 318**,** 1645-7.

BEHRENS, M. M., ALI, S. S. & DUGAN, L. L. 2008. Interleukin-6 mediates the increase in NADPH-oxidase in the ketamine model of schizophrenia. *J Neurosci,* 28**,** 13957-66.

BÉÏQUE, J. C., LIN, D. T., KANG, M. G., AIZAWA, H., TAKAMIYA, K. & HUGANIR, R. L. 2006. Synapse-specific regulation of AMPA receptor function by PSD-95. *Proc Natl Acad Sci U S A,* 103**,** 19535-40.

BEKKU, Y., SU, W. D., HIRAKAWA, S., FÄSSLER, R., OHTSUKA, A., KANG, J. S., SANDERS, J., MURAKAMI, T., NINOMIYA, Y. & OOHASHI, T. 2003. Molecular cloning of Bral2, a novel

brain-specific link protein, and immunohistochemical colocalization with brevican in perineuronal nets. *Mol Cell Neurosci,* 24**,** 148-59.

BELAYA, I., IVANOVA, M., SORVARI, A., ILICIC, M., LOPPI, S., KOIVISTO, H., VARRICCHIO, A., TIKKANEN, H., WALKER, F. R., ATALAY, M., MALM, T., GRUBMAN, A., TANILA, H. & KANNINEN, K. M. 2020. Astrocyte remodeling in the beneficial effects of long-term voluntary exercise in Alzheimer's disease. *J Neuroinflammation,* 17**,** 271.

BELFORTE, J. E., ZSIROS, V., SKLAR, E. R., JIANG, Z., YU, G., LI, Y., QUINLAN, E. M. & NAKAZAWA, K. 2010. Postnatal NMDA receptor ablation in corticolimbic interneurons confers schizophrenia-like phenotypes. *Nat Neurosci,* 13**,** 76-83.

BELLONE, C. & NICOLL, R. A. 2007. Rapid bidirectional switching of synaptic NMDA receptors. *Neuron,* 55**,** 779-85.

BELVIRANLI, M. & OKUDAN, N. 2019. Voluntary, involuntary and forced exercises almost equally reverse behavioral impairment by regulating hippocampal neurotrophic factors and oxidative stress in experimental Alzheimer's disease model. *Behav Brain Res,* 364**,** 245-255.

BEN-AZU, B., ADERIBIGBE, A. O., AJAYI, A. M., ENENI, A. O., UMUKORO, S. & IWALEWA, E. O. 2018a. Involvement of GABAergic, BDNF and Nox-2 mechanisms in the prevention and reversal of ketamine-induced schizophrenia-like behavior by morin in mice. *Brain Res Bull,* 139**,** 292-306.

BEN-AZU, B., ADERIBIGBE, A. O., AJAYI, A. M. & IWALEWA, E. O. 2016. Neuroprotective effects of the ethanol stem bark extracts of Terminalia ivorensis in ketamine-induced schizophrenia-like behaviors and oxidative damage in mice. *Pharm Biol,* 54**,** 2871-2879.

BEN-AZU, B., ADERIBIGBE, A. O., OMOGBIYA, I. A., AJAYI, A. M., OWOEYE, O., OLONODE, E. T. & IWALEWA, E. O. 2018b. Probable mechanisms involved in the antipsychotic-like activity of morin in mice. *Biomed Pharmacother,* 105**,** 1079-1090.

BEN-AZU, B., EMOKPAE, O., AJAYI, A. M., JARIKRE, T. A., ORHODE, V., ADERIBIGBE, A. O., UMUKORO, S. & IWALEWA, E. O. 2020. Repeated psychosocial stress causes glutamic acid decarboxylase isoform-67, oxidative-Nox-2 changes and neuroinflammation in mice: Prevention by treatment with a neuroactive flavonoid, morin. *Brain Res,* 1744**,** 146917.

BEN-AZU, B., URUAKA, C. I., AJAYI, A. M., JARIKRE, T. A., NWANGWA, K. E., CHILAKA, K. C., CHIJIOKE, B. S., OMONYEME, M. G., OZEGE, C. B., OFILI, E. C., WAREKOROMOR, E. B., EDIGBUE, N. L., ESIEKPE, U. V., AKAENYI, D. E. & AGU, G. O. 2022. Reversal and Preventive Pleiotropic Mechanisms Involved in the Antipsychotic-Like Effect of Taurine, an Essential β-Amino Acid in Ketamine-Induced Experimental Schizophrenia in Mice. *Neurochem Res*.

BENAMER, N., VIDAL, M., BALIA, M. & ANGULO, M. C. 2020. Myelination of parvalbumin interneurons shapes the function of cortical sensory inhibitory circuits. *Nat Commun,* 11**,** 5151.

BENNETT, R. W. 1975. Proactive interference in short-term memory: Fundamental forgetting processes. *Journal of Verbal Learning and Verbal Behavior,* 14**,** 123-144.

BERCHTOLD, N. C., CASTELLO, N. & COTMAN, C. W. 2010. Exercise and time-dependent benefits to learning and memory. *Neuroscience,* 167**,** 588-97.

BERCHTOLD, N. C., CHINN, G., CHOU, M., KESSLAK, J. P. & COTMAN, C. W. 2005. Exercise primes a molecular memory for brain-derived neurotrophic factor protein induction in the rat hippocampus. *Neuroscience,* 133**,** 853-61.

BERCHTOLD, N. C., CRIBBS, D. H., COLEMAN, P. D., ROGERS, J., HEAD, E., KIM, R., BEACH, T., MILLER, C., TRONCOSO, J., TROJANOWSKI, J. Q., ZIELKE, H. R. & COTMAN, C. W. 2008. Gene expression changes in the course of normal brain aging are sexually dimorphic. *Proc Natl Acad Sci U S A,* 105**,** 15605-10.

BERGHUIS, P., DOBSZAY, M. B., SOUSA, K. M., SCHULTE, G., MAGER, P. P., HÄRTIG, W., GÖRCS, T. J., ZILBERTER, Y., ERNFORS, P. & HARKANY, T. 2004. Brain-derived neurotrophic factor

controls functional differentiation and microcircuit formation of selectively isolated fast-spiking GABAergic interneurons. *Eur J Neurosci,* 20**,** 1290-306.

BERTOLOTTO, A., MANZARDO, E., IUDICELLO, M., LOVISETTO, C. & RICCIO, A. 1995. Disappearance of the Vicia villosa-positivity from the perineuronal net containing chondroitin proteoglycan after chondroitinase digestion. *Brain Res,* 673**,** 344-8.

BESTE, C., SCHNEIDER, D., EPPLEN, J. T. & ARNING, L. 2011. The functional BDNF Val66Met polymorphism affects functions of pre-attentive visual sensory memory processes. *Neuropharmacology,* 60**,** 467-71.

BEURDELEY, M., SPATAZZA, J., LEE, H. H., SUGIYAMA, S., BERNARD, C., DI NARDO, A. A., HENSCH, T. K. & PROCHIANTZ, A. 2012. Otx2 binding to perineuronal nets persistently regulates plasticity in the mature visual cortex. *J Neurosci,* 32**,** 9429-37.

BILECKI, W. & MAĆKOWIAK, M. 2023. Gene Expression and Epigenetic Regulation in the Prefrontal Cortex of Schizophrenia. *Genes (Basel),* 14.

BITANIHIRWE, B. K., PELEG-RAIBSTEIN, D., MOUTTET, F., FELDON, J. & MEYER, U. 2010. Late prenatal immune activation in mice leads to behavioral and neurochemical abnormalities relevant to the negative symptoms of schizophrenia. *Neuropsychopharmacology,* 35**,** 2462-78.

BITANIHIRWE, B. K. & WOO, T. U. 2014. Perineuronal nets and schizophrenia: the importance of neuronal coatings. *Neurosci Biobehav Rev,* 45**,** 85-99.

BITANIHIRWE, B. K. Y. & WOO, T. W. 2020. A conceptualized model linking matrix metalloproteinase-9 to schizophrenia pathogenesis. *Schizophr Res*.

BLACKMORE, S. 1986. Out-of-body experiences in schizophrenia. A questionnaire survey. *J Nerv Ment Dis,* 174**,** 615-9.

BLOSA, M., SONNTAG, M., JÄGER, C., WEIGEL, S., SEEGER, J., FRISCHKNECHT, R., SEIDENBECHER, C. I., MATTHEWS, R. T., ARENDT, T., RÜBSAMEN, R. & MORAWSKI, M. 2015. The extracellular matrix molecule brevican is an integral component of the machinery mediating fast synaptic transmission at the calyx of Held. *J Physiol,* 593**,** 4341-60.

BOAKES, R. A. & WU, J. 2021. Time-of-day affects the amount rats run during daily sessions in activity wheels. *Learn Behav,* 49**,** 196-203.

BOCZEK, T., LISEK, M., FERENC, B., WIKTORSKA, M., IVCHEVSKA, I. & ZYLINSKA, L. 2015. Region-specific effects of repeated ketamine administration on the presynaptic GABAergic neurochemistry in rat brain. *Neurochem Int,* 91**,** 13-25.

BOEHME, F., GIL-MOHAPEL, J., COX, A., PATTEN, A., GILES, E., BROCARDO, P. S. & CHRISTIE, B. R. 2011. Voluntary exercise induces adult hippocampal neurogenesis and BDNF expression in a rodent model of fetal alcohol spectrum disorders. *Eur J Neurosci,* 33**,** 1799-811.

BOERRIGTER, D., WEICKERT, T. W., LENROOT, R., O'DONNELL, M., GALLETLY, C., LIU, D., BURGESS, M., CADIZ, R., JACOMB, I., CATTS, V. S., FILLMAN, S. G. & WEICKERT, C. S. 2017. Using blood cytokine measures to define high inflammatory biotype of schizophrenia and schizoaffective disorder. *J Neuroinflammation,* 14**,** 188.

BOLZ, L., HEIGELE, S. & BISCHOFBERGER, J. 2015. Running Improves Pattern Separation during Novel Object Recognition. *Brain Plast,* 1**,** 129-141.

BOROVCANIN, M. M., JOVANOVIC, I., RADOSAVLJEVIC, G., PANTIC, J., MINIC JANICIJEVIC, S., ARSENIJEVIC, N. & LUKIC, M. L. 2017. Interleukin-6 in Schizophrenia-Is There a Therapeutic Relevance? *Front Psychiatry,* 8**,** 221.

BOURQUE, F., VAN DER VEN, E. & MALLA, A. 2011. A meta-analysis of the risk for psychotic disorders among first- and second-generation immigrants. *Psychol Med,* 41**,** 897-910.

BRAKEBUSCH, C., SEIDENBECHER, C. I., ASZTELY, F., RAUCH, U., MATTHIES, H., MEYER, H., KRUG, M., BÖCKERS, T. M., ZHOU, X., KREUTZ, M. R., MONTAG, D., GUNDELFINGER, E. D. & FÄSSLER, R. 2002. Brevican-deficient mice display impaired hippocampal CA1 long-term potentiation but show no obvious deficits in learning and memory. *Mol Cell Biol,* 22**,** 7417-27.

BRAMNESS, J. G. & ROGNLI, E. B. 2016. Psychosis induced by amphetamines. *Curr Opin Psychiatry,* 29**,** 236-41.

BRAND, B. A., DE BOER, J. N. & SOMMER, I. E. C. 2021. Estrogens in schizophrenia: progress, current challenges and opportunities. *Curr Opin Psychiatry,* 34**,** 228-237.

BRAUN, I., GENIUS, J., GRUNZE, H., BENDER, A., MOLLER, H. J. & RUJESCU, D. 2007. Alterations of hippocampal and prefrontal GABAergic interneurons in an animal model of psychosis induced by NMDA receptor antagonism. *Schizophr Res,* 97**,** 254-63.

BREIER, A., LIFFICK, E., HUMMER, T. A., VOHS, J. L., YANG, Z., MEHDIYOUN, N. F., VISCO, A. C., METZLER, E., ZHANG, Y. & FRANCIS, M. M. 2018. Effects of 12-month, double-blind N-acetyl cysteine on symptoms, cognition and brain morphology in early phase schizophrenia spectrum disorders. *Schizophr Res,* 199**,** 395-402.

BRIGELIUS-FLOHÉ, R. & MAIORINO, M. 2013. Glutathione peroxidases. *Biochim Biophys Acta,* 1830**,** 3289-303.

BROCKETT, A. T., LAMARCA, E. A. & GOULD, E. 2015. Physical exercise enhances cognitive flexibility as well as astrocytic and synaptic markers in the medial prefrontal cortex. *PLoS One,* 10**,** e0124859.

BROWN, A. S., BEGG, M. D., GRAVENSTEIN, S., SCHAEFER, C. A., WYATT, R. J., BRESNAHAN, M., BABULAS, V. P. & SUSSER, E. S. 2004a. Serologic evidence of prenatal influenza in the etiology of schizophrenia. *Arch Gen Psychiatry,* 61**,** 774-80.

BROWN, A. S., COHEN, P., HARKAVY-FRIEDMAN, J., BABULAS, V., MALASPINA, D., GORMAN, J. M. & SUSSER, E. S. 2001. A.E. Bennett Research Award. Prenatal rubella, premorbid abnormalities, and adult schizophrenia. *Biol Psychiatry,* 49**,** 473-86.

BROWN, A. S., HOOTON, J., SCHAEFER, C. A., ZHANG, H., PETKOVA, E., BABULAS, V., PERRIN, M., GORMAN, J. M. & SUSSER, E. S. 2004b. Elevated maternal interleukin-8 levels and risk of schizophrenia in adult offspring. *Am J Psychiatry,* 161**,** 889-95.

BROWN, A. S., SCHAEFER, C. A., QUESENBERRY, C. P., LIU, L., BABULAS, V. P. & SUSSER, E. S. 2005. Maternal exposure to toxoplasmosis and risk of schizophrenia in adult offspring. *Am J Psychiatry,* 162**,** 767-73.

BROWN, A. S. & SUSSER, E. S. 2008. Prenatal nutritional deficiency and risk of adult schizophrenia. *Schizophr Bull,* 34**,** 1054-63.

BRÜCKNER, G., BRAUER, K., HÄRTIG, W., WOLFF, J. R., RICKMANN, M. J., DEROUICHE, A., DELPECH, B., GIRARD, N., OERTEL, W. H. & REICHENBACH, A. 1993. Perineuronal nets provide a polyanionic, glia-associated form of microenvironment around certain neurons in many parts of the rat brain. *Glia,* 8**,** 183-200.

BRÜCKNER, G. & GROSCHE, J. 2001. Perineuronal nets show intrinsic patterns of extracellular matrix differentiation in organotypic slice cultures. *Exp Brain Res,* 137**,** 83-93.

BRÜCKNER, G., GROSCHE, J., HARTLAGE-RÜBSAMEN, M., SCHMIDT, S. & SCHACHNER, M. 2003. Region and lamina-specific distribution of extracellular matrix proteoglycans, hyaluronan and tenascin-R in the mouse hippocampal formation. *J Chem Neuroanat,* 26**,** 37-50.

BRÜCKNER, G., GROSCHE, J., SCHMIDT, S., HÄRTIG, W., MARGOLIS, R. U., DELPECH, B., SEIDENBECHER, C. I., CZANIERA, R. & SCHACHNER, M. 2000. Postnatal development of perineuronal nets in wild-type mice and in a mutant deficient in tenascin-R. *J Comp Neurol,* 428**,** 616-29.

BRÜCKNER, G., MORAWSKI, M. & ARENDT, T. 2008. Aggrecan-based extracellular matrix is an integral part of the human basal ganglia circuit. *Neuroscience,* 151**,** 489-504.

BUCKMAN, T. D., KLING, A., SUTPHIN, M. S., STEINBERG, A. & EIDUSON, S. 1990. Platelet glutathione peroxidase and monoamine oxidase activity in schizophrenics with CT scan abnormalities: relation to psychosocial variables. *Psychiatry Res,* 31**,** 1-14.

BUENO-ANTEQUERA, J. & MUNGUÍA-IZQUIERDO, D. 2020. Exercise and Schizophrenia. *Adv Exp Med Biol,* 1228**,** 317-332.

BUKA, S. L., CANNON, T. D., TORREY, E. F., YOLKEN, R. H. & DISORDERS, C. S. G. O. T. P. O. O. S. P. 2008. Maternal exposure to herpes simplex virus and risk of psychosis among adult offspring. *Biol Psychiatry,* 63**,** 809-15.

BUKA, S. L., TSUANG, M. T., TORREY, E. F., KLEBANOFF, M. A., WAGNER, R. L. & YOLKEN, R. H. 2001. Maternal cytokine levels during pregnancy and adult psychosis. *Brain Behav Immun,* 15**,** 411-20.

BULLOCK, W. M., BOLOGNANI, F., BOTTA, P., VALENZUELA, C. F. & PERRONE-BIZZOZERO, N. I. 2009. Schizophrenia-like GABAergic gene expression deficits in cerebellar Golgi cells from rats chronically exposed to low-dose phencyclidine. *Neurochem Int,* 55**,** 775-82.

BUOSI, P., BORGHI, F. A., LOPES, A. M., FACINCANI, I. D. S., FERNANDES-FERREIRA, R., OLIVEIRA-BRANCATI, C. I. F., DO CARMO, T. S., SOUZA, D. R. S., DA SILVA, D. G. H., DE ALMEIDA, E. A. & DE ARAÚJO FILHO, G. M. 2021. Oxidative stress biomarkers in treatment-responsive and treatment-resistant schizophrenia patients. *Trends Psychiatry Psychother,* 43**,** 278-285.

BURGHARDT, P. R., FULK, L. J., HAND, G. A. & WILSON, M. A. 2004. The effects of chronic treadmill and wheel running on behavior in rats. *Brain Res,* 1019**,** 84-96.

BUZSÁKI, G. & WANG, X. J. 2012. Mechanisms of gamma oscillations. *Annu Rev Neurosci,* 35**,** 203-25.

BYGRAVE, A. M., KILONZO, K., KULLMANN, D. M., BANNERMAN, D. M. & KÄTZEL, D. 2019. Can N-Methyl-D-Aspartate Receptor Hypofunction in Schizophrenia Be Localized to an Individual Cell Type? *Front Psychiatry,* 10**,** 835.

BYRNE, M., AGERBO, E., BENNEDSEN, B., EATON, W. W. & MORTENSEN, P. B. 2007. Obstetric conditions and risk of first admission with schizophrenia: A Danish national register based study. *Schizophrenia research.,* 97**,** 51-59.

CABUNGCAL, J. H., STEULLET, P., KRAFTSIK, R., CUENOD, M. & DO, K. Q. 2013a. Early-life insults impair parvalbumin interneurons via oxidative stress: reversal by N-acetylcysteine. *Biol Psychiatry,* 73**,** 574-82.

CABUNGCAL, J. H., STEULLET, P., MORISHITA, H., KRAFTSIK, R., CUENOD, M., HENSCH, T. K. & DO, K. Q. 2013b. Perineuronal nets protect fast-spiking interneurons against oxidative stress. *Proc Natl Acad Sci U S A,* 110**,** 9130-5.

CADINU, D., GRAYSON, B., PODDA, G., HARTE, M. K., DOOSTDAR, N. & NEILL, J. C. 2018. NMDA receptor antagonist rodent models for cognition in schizophrenia and identification of novel drug treatments, an update. *Neuropharmacology,* 142**,** 41-62.

CADWELL, C. R., BHADURI, A., MOSTAJO-RADJI, M. A., KEEFE, M. G. & NOWAKOWSKI, T. J. 2019. Development and Arealization of the Cerebral Cortex. *Neuron,* 103**,** 980-1004.

CAILLARD, O., MORENO, H., SCHWALLER, B., LLANO, I., CELIO, M. R. & MARTY, A. 2000. Role of the calcium-binding protein parvalbumin in short-term synaptic plasticity. *Proc Natl Acad Sci U S A,* 97**,** 13372-7.

ÇAKICI, N., VAN BEVEREN, N. J. M., JUDGE-HUNDAL, G., KOOLA, M. M. & SOMMER, I. E. C. 2019. An update on the efficacy of anti-inflammatory agents for patients with schizophrenia: a meta-analysis. *Psychol Med,* 49**,** 2307-2319.

CALLAERTS-VEGH, Z., MOECHARS, D., VAN ACKER, N., DANEELS, G., GORIS, I., LEO, S., NAERT, A., MEERT, T., BALSCHUN, D. & D'HOOGE, R. 2013. Haploinsufficiency of VGluT1 but not VGluT2 impairs extinction of spatial preference and response suppression. *Behav Brain Res,* 245**,** 13-21.

CALVO-RODRIGUEZ, M., HOU, S. S., SNYDER, A. C., KHARITONOVA, E. K., RUSS, A. N., DAS, S., FAN, Z., MUZIKANSKY, A., GARCIA-ALLOZA, M., SERRANO-POZO, A., HUDRY, E. & BACSKAI, B. J. 2020. Increased mitochondrial calcium levels associated with neuronal death in a mouse model of Alzheimer's disease. *Nat Commun,* 11**,** 2146.

CAMPANAC, E., GASSELIN, C., BAUDE, A., RAMA, S., ANKRI, N. & DEBANNE, D. 2013. Enhanced intrinsic excitability in basket cells maintains excitatory-inhibitory balance in hippocampal circuits. *Neuron,* 77**,** 712-22.

CAMPOS, R. M. P., BARBOSA-SILVA, M. C. & RIBEIRO-RESENDE, V. T. 2022. A period of transient synaptic density unbalancing in the motor cortex after peripheral nerve injury and the involvement of microglial cells. *Mol Cell Neurosci,* 124**,** 103791.

CAMUSO, S., LA ROSA, P., FIORENZA, M. T. & CANTERINI, S. 2022. Pleiotropic effects of BDNF on the cerebellum and hippocampus: Implications for neurodevelopmental disorders. *Neurobiol Dis,* 163**,** 105606.

CANETTA, S., BOLKAN, S., PADILLA-COREANO, N., SONG, L. J., SAHN, R., HARRISON, N. L., GORDON, J. A., BROWN, A. & KELLENDONK, C. 2016. Maternal immune activation leads to selective functional deficits in offspring parvalbumin interneurons. *Mol Psychiatry,* 21**,** 956-68.

CANKAYA, S., CANKAYA, B., KILIC, U., KILIC, E. & YULUG, B. 2019. The therapeutic role of minocycline in Parkinson's disease. *Drugs Context,* 8**,** 212553.

CANNON, M., JONES, P. B. & MURRAY, R. M. 2002. Obstetric complications and schizophrenia: historical and meta-analytic review. *Am J Psychiatry,* 159**,** 1080-92.

CARDIN, J. A., CARLEN, M., MELETIS, K., KNOBLICH, U., ZHANG, F., DEISSEROTH, K., TSAI, L. H. & MOORE, C. I. 2009. Driving fast-spiking cells induces gamma rhythm and controls sensory responses. *Nature,* 459**,** 663-7.

CARDIS, R., CABUNGCAL, J. H., DWIR, D., DO, K. Q. & STEULLET, P. 2018. A lack of GluN2A-containing NMDA receptors confers a vulnerability to redox dysregulation: Consequences on parvalbumin interneurons, and their perineuronal nets. *Neurobiol Dis,* 109**,** 64-75.

CARHART-HARRIS, R. L., BRUGGER, S., NUTT, D. J. & STONE, J. M. 2013. Psychiatry's next top model: cause for a re-think on drug models of psychosis and other psychiatric disorders. *J Psychopharmacol,* 27**,** 771-8.

CARLÉN, M., MELETIS, K., SIEGLE, J. H., CARDIN, J. A., FUTAI, K., VIERLING-CLAASSEN, D., RÜHLMANN, C., JONES, S. R., DEISSEROTH, K., SHENG, M., MOORE, C. I. & TSAI, L. H. 2012. A critical role for NMDA receptors in parvalbumin interneurons for gamma rhythm induction and behavior. *Mol Psychiatry,* 17**,** 537-48.

CARSTENS, K. E., PHILLIPS, M. L., POZZO-MILLER, L., WEINBERG, R. J. & DUDEK, S. M. 2016. Perineuronal Nets Suppress Plasticity of Excitatory Synapses on CA2 Pyramidal Neurons. *J Neurosci,* 36**,** 6312-20.

CARTÁGENES, S. C., DA SILVEIRA, C. C. S. M., PINHEIRO, B. G., FERNANDES, L. M. P., FARIAS, S. V., KOBAYASHI, N. H. C., DE SOUZA, P. H. F. S., PRADO, A. F. D., FERREIRA, M. K. M., LIMA, R. R., DE OLIVEIRA, E. H. C., DE LUNA, F. C. F., BURBANO, R. M. R., FONTES-JÚNIOR, E. A. & MAIA, C. D. S. F. 2022. "K-Powder" Exposure during Adolescence Elicits Psychiatric Disturbances Associated with Oxidative Stress in Female Rats. *Pharmaceuticals (Basel),* 15.

CARULLI, D., PIZZORUSSO, T., KWOK, J. C., PUTIGNANO, E., POLI, A., FOROSTYAK, S., ANDREWS, M. R., DEEPA, S. S., GLANT, T. T. & FAWCETT, J. W. 2010. Animals lacking link protein have attenuated perineuronal nets and persistent plasticity. *Brain,* 133**,** 2331-47.

CARULLI, D., RHODES, K. E., BROWN, D. J., BONNERT, T. P., POLLACK, S. J., OLIVER, K., STRATA, P. & FAWCETT, J. W. 2006. Composition of perineuronal nets in the adult rat cerebellum and the cellular origin of their components. *J Comp Neurol,* 494**,** 559-77.

CASQUERO-VEIGA, M., LAMANNA-RAMA, N., ROMERO-MIGUEL, D., ROJAS-MARQUEZ, H., ALCAIDE, J., BELTRAN, M., NACHER, J., DESCO, M. & SOTO-MONTENEGRO, M. L. 2022. The Poly I:C maternal immune stimulation model shows unique patterns of brain metabolism, morphometry, and plasticity in female rats. *Front Behav Neurosci,* 16**,** 1022622.

CASSELLA, S. N., HEMMERLE, A. M., LUNDGREN, K. H., KYSER, T. L., AHLBRAND, R., BRONSON, S. L., RICHTAND, N. M. & SEROOGY, K. B. 2016. Maternal immune activation alters glutamic acid decarboxylase-67 expression in the brains of adult rat offspring. *Schizophr Res,* 171**,** 195-9.

CASTAÑÉ, A., SANTANA, N. & ARTIGAS, F. 2015. PCP-based mice models of schizophrenia: differential behavioral, neurochemical and cellular effects of acute and subchronic treatments. *Psychopharmacology (Berl),* 232**,** 4085-97.

CATTS, V. S., DERMINIO, D. S., HAHN, C. G. & WEICKERT, C. S. 2015. Postsynaptic density levels of the NMDA receptor NR1 subunit and PSD-95 protein in prefrontal cortex from people with schizophrenia. *NPJ Schizophr,* 1**,** 15037.

CATTS, V. S., LAI, Y. L., WEICKERT, C. S., WEICKERT, T. W. & CATTS, S. V. 2016. A quantitative review of the postmortem evidence for decreased cortical N-methyl-D-aspartate receptor expression levels in schizophrenia: How can we link molecular abnormalities to mismatch negativity deficits? *Biol Psychol,* 116**,** 57-67.

CEA-DEL RIO, C. A. & HUNTSMAN, M. M. 2014. The contribution of inhibitory interneurons to circuit dysfunction in Fragile X Syndrome. *Front Cell Neurosci,* 8**,** 245.

CELIO, M. R. 1990. Calbindin D-28k and parvalbumin in the rat nervous system. *Neuroscience,* 35**,** 375-475.

CHAMERA, K., KOTARSKA, K., SZUSTER-GŁUSZCZAK, M., TROJAN, E., SKÓRKOWSKA, A., POMIERNY, B., KRZYŻANOWSKA, W., BRYNIARSKA, N. & BASTA-KAIM, A. 2020. The prenatal challenge with lipopolysaccharide and polyinosinic:polycytidylic acid disrupts CX3CL1-CX3CR1 and CD200-CD200R signalling in the brains of male rat offspring: a link to schizophrenia-like behaviours. *J Neuroinflammation,* 17**,** 247.

CHANCEY, J. H., ADLAF, E. W., SAPP, M. C., PUGH, P. C., WADICHE, J. I. & OVERSTREET-WADICHE, L. S. 2013. GABA depolarization is required for experience-dependent synapse unsilencing in adult-born neurons. *J Neurosci,* 33**,** 6614-22.

CHANG, S. H., CHIANG, S. Y., CHIU, C. C., TSAI, C. C., TSAI, H. H., HUANG, C. Y., HSU, T. C. & TZANG, B. S. 2011. Expression of anti-cardiolipin antibodies and inflammatory associated factors in patients with schizophrenia. *Psychiatry Res,* 187**,** 341-6.

CHANG, Y. K., CHU, C. H., WANG, C. C., WANG, Y. C., SONG, T. F., TSAI, C. L. & ETNIER, J. L. 2015. Dose-response relation between exercise duration and cognition. *Med Sci Sports Exerc,* 47**,** 159-65.

CHARLSON, F. J., FERRARI, A. J., SANTOMAURO, D. F., DIMINIC, S., STOCKINGS, E., SCOTT, J. G., MCGRATH, J. J. & WHITEFORD, H. A. 2018. Global Epidemiology and Burden of Schizophrenia: Findings From the Global Burden of Disease Study 2016. *Schizophr Bull,* 44**,** 1195-1203.

CHAUDHRY, I. B., HALLAK, J., HUSAIN, N., MINHAS, F., STIRLING, J., RICHARDSON, P., DURSUN, S., DUNN, G. & DEAKIN, B. 2012. Minocycline benefits negative symptoms in early schizophrenia: a randomised double-blind placebo-controlled clinical trial in patients on standard treatment. *J Psychopharmacol,* 26**,** 1185-93.

CHAZOT, P. L. 2004. The NMDA receptor NR2B subunit: a valid therapeutic target for multiple CNS pathologies. *Curr Med Chem,* 11**,** 389-96.

CHEN, H. R., CHEN, C. W., MANDHANI, N., SHORT-MILLER, J. C., SMUCKER, M. R., SUN, Y. Y. & KUAN, C. Y. 2020. Monocytic Infiltrates Contribute to Autistic-like Behaviors in a Two-Hit Model of Neurodevelopmental Defects. *J Neurosci,* 40**,** 9386-9400.

CHEN, M., JIANG, Q. & ZHANG, L. 2022. CACNA1C Gene rs1006737 Polymorphism Affects Cognitive Performance in Chinese Han Schizophrenia. *Neuropsychiatr Dis Treat,* 18**,** 1697-1704.

CHEN, V. S., MORRISON, J. P., SOUTHWELL, M. F., FOLEY, J. F., BOLON, B. & ELMORE, S. A. 2017. Histology Atlas of the Developing Prenatal and Postnatal Mouse Central Nervous System, with Emphasis on Prenatal Days E7.5 to E18.5. *Toxicol Pathol,* 45**,** 705-744.

CHEN, X., LEVY, J. M., HOU, A., WINTERS, C., AZZAM, R., SOUSA, A. A., LEAPMAN, R. D., NICOLL, R. A. & REESE, T. S. 2015. PSD-95 family MAGUKs are essential for anchoring AMPA and NMDA receptor complexes at the postsynaptic density. *Proc Natl Acad Sci U S A,* 112**,** E6983-92.

CHENG, D., HOOGENRAAD, C. C., RUSH, J., RAMM, E., SCHLAGER, M. A., DUONG, D. M., XU, P., WIJAYAWARDANA, S. R., HANFELT, J., NAKAGAWA, T., SHENG, M. & PENG, J. 2006. Relative and absolute quantification of postsynaptic density proteome isolated from rat forebrain and cerebellum. *Mol Cell Proteomics,* 5**,** 1158-70.

CHENG, L., WANG, S. H., JIA, N., XIE, M. & LIAO, X. M. 2014. Environmental stimulation influence the cognition of developing mice by inducing changes in oxidative and apoptosis status. *Brain Dev,* 36**,** 51-6.

CHENGAPPA, K. N., TURKIN, S. R., DESANTI, S., BOWIE, C. R., BRAR, J. S., SCHLICHT, P. J., MURPHY, S. L., HETRICK, M. L., BILDER, R. & FLEET, D. 2012. A preliminary, randomized, double-blind, placebo-controlled trial of L-carnosine to improve cognition in schizophrenia. *Schizophr Res,* 142**,** 145-52.

CHO, R. Y., KONECKY, R. O. & CARTER, C. S. 2006. Impairments in frontal cortical gamma synchrony and cognitive control in schizophrenia. *Proc Natl Acad Sci U S A,* 103**,** 19878-83.

CHO, S. Y., CHUNG, Y. S., YOON, H. K. & ROH, H. T. 2022. Impact of Exercise Intensity on Systemic Oxidative Stress, Inflammatory Responses, and Sirtuin Levels in Healthy Male Volunteers. *Int J Environ Res Public Health,* 19.

CHOI, G. B., YIM, Y. S., WONG, H., KIM, S., KIM, H., KIM, S. V., HOEFFER, C. A., LITTMAN, D. R. & HUH, J. R. 2016. The maternal interleukin-17a pathway in mice promotes autism-like phenotypes in offspring. *Science,* 351**,** 933-9.

CHOI, S. H., AID, S., KIM, H. W., JACKSON, S. H. & BOSETTI, F. 2012. Inhibition of NADPH oxidase promotes alternative and anti-inflammatory microglial activation during neuroinflammation. *J Neurochem,* 120**,** 292-301.

CHOURBAJI, S., HELLWEG, R., BRANDIS, D., ZÖRNER, B., ZACHER, C., LANG, U. E., HENN, F. A., HÖRTNAGL, H. & GASS, P. 2004. Mice with reduced brain-derived neurotrophic factor expression show decreased choline acetyltransferase activity, but regular brain monoamine levels and unaltered emotional behavior. *Brain Res Mol Brain Res,* 121**,** 28-36.

CHUNG, D. W., FISH, K. N. & LEWIS, D. A. 2016. Pathological Basis for Deficient Excitatory Drive to Cortical Parvalbumin Interneurons in Schizophrenia. *Am J Psychiatry,* 173**,** 1131-1139.

CIEŚLIK, M., GĄSSOWSKA-DOBROWOLSKA, M., JĘŚKO, H., CZAPSKI, G. A., WILKANIEC, A., ZAWADZKA, A., DOMINIAK, A., POLOWY, R., FILIPKOWSKI, R. K., BOGUSZEWSKI, P. M., GEWARTOWSKA, M., FRONTCZAK-BANIEWICZ, M., SUN, G. Y., BEVERSDORF, D. Q. & ADAMCZYK, A. 2020. Maternal Immune Activation Induces Neuroinflammation and Cortical Synaptic Deficits in the Adolescent Rat Offspring. *Int J Mol Sci,* 21.

CLINESCHMIDT, B. V. 1982. Effect of the benzodiazepine receptor antagonist Ro 15-1788 on the anticonvulsant and anticonflict actions of MK-801. *Eur J Pharmacol,* 84**,** 119-21.

COLLIN, T., CHAT, M., LUCAS, M. G., MORENO, H., RACAY, P., SCHWALLER, B., MARTY, A. & LLANO, I. 2005. Developmental changes in parvalbumin regulate presynaptic Ca2+ signaling. *J Neurosci,* 25**,** 96-107.

COLOVIC, M. & CACCIA, S. 2003. Liquid chromatographic determination of minocycline in brain-to-plasma distribution studies in the rat. *J Chromatogr B Analyt Technol Biomed Life Sci,* 791**,** 337-43.

CONUS, P., SEIDMAN, L. J., FOURNIER, M., XIN, L., CLEUSIX, M., BAUMANN, P. S., FERRARI, C., COUSINS, A., ALAMEDA, L., GHOLAM-REZAEE, M., GOLAY, P., JENNI, R., WOO, T. W., KESHAVAN, M. S., EAP, C. B., WOJCIK, J., CUENOD, M., BUCLIN, T., GRUETTER, R. & DO, K. Q. 2018. N-acetylcysteine in a Double-Blind Randomized Placebo-Controlled Trial: Toward Biomarker-Guided Treatment in Early Psychosis. *Schizophr Bull,* 44**,** 317-327.

CORRELL, C. U. & SCHOOLER, N. R. 2020. Negative Symptoms in Schizophrenia: A Review and Clinical Guide for Recognition, Assessment, and Treatment. *Neuropsychiatr Dis Treat,* 16**,** 519-534.

COTEL, M. C., LENARTOWICZ, E. M., NATESAN, S., MODO, M. M., COOPER, J. D., WILLIAMS, S. C., KAPUR, S. & VERNON, A. C. 2015. Microglial activation in the rat brain following chronic antipsychotic treatment at clinically relevant doses. *Eur Neuropsychopharmacol,* 25**,** 2098-107.

CRAPSER, J. D., SPANGENBERG, E. E., BARAHONA, R. A., ARREOLA, M. A., HOHSFIELD, L. A. & GREEN, K. N. 2020. Microglia facilitate loss of perineuronal nets in the Alzheimer's disease brain. *EBioMedicine,* 58**,** 102919.

CRAWFORD, L. & LOPRINZI, P. D. 2020. Effects of Exercise on Memory Interference in Neuropsychiatric Disorders. *Adv Exp Med Biol,* 1228**,** 425-438.

CRUZ-ÁLVAREZ, S., SANTANA-MARTÍNEZ, R., AVILA-CHÁVEZ, E., BARRERA-OVIEDO, D., HERNÁNDEZ-PANDO, R., PEDRAZA-CHAVERRI, J. & MALDONADO, P. D. 2017. Apocynin protects against neurological damage induced by quinolinic acid by an increase in glutathione synthesis and Nrf2 levels. *Neuroscience,* 350**,** 65-74.

CUENOD, M., STEULLET, P., CABUNGCAL, J. H., DWIR, D., KHADIMALLAH, I., KLAUSER, P., CONUS, P. & DO, K. Q. 2022. Caught in vicious circles: a perspective on dynamic feed-forward loops driving oxidative stress in schizophrenia. *Mol Psychiatry,* 27**,** 1886-1897.

CUI, K., ASHDOWN, H., LUHESHI, G. N. & BOKSA, P. 2009. Effects of prenatal immune activation on hippocampal neurogenesis in the rat. *Schizophr Res,* 113**,** 288-97.

DA SILVA ARAÚJO, T., MAIA CHAVES FILHO, A. J., MONTE, A. S., ISABELLE DE GÓIS QUEIROZ, A., CORDEIRO, R. C., DE JESUS SOUZA MACHADO, M., DE FREITAS LIMA, R., FREITAS DE LUCENA, D., MAES, M. & MACÊDO, D. 2017. Reversal of schizophrenia-like symptoms and immune alterations in mice by immunomodulatory drugs. *J Psychiatr Res,* 84**,** 49-58.

DAHLIN, E., ANDERSSON, M., THORÉN, A., HANSE, E. & SETH, H. 2019. Effects of physical exercise and stress on hippocampal CA1 and dentate gyrus synaptic transmission and long-term potentiation in adolescent and adult Wistar rats. *Neuroscience,* 408**,** 22-30.

DALTON, V. S., VERDURAND, M., WALKER, A., HODGSON, D. M. & ZAVITSANOU, K. 2012. Synergistic Effect between Maternal Infection and Adolescent Cannabinoid Exposure on Serotonin 5HT1A Receptor Binding in the Hippocampus: Testing the "Two Hit" Hypothesis for the Development of Schizophrenia. *ISRN Psychiatry,* 2012**,** 451865.

DAS, T. K., JAVADZADEH, A., DEY, A., SABESAN, P., THÉBERGE, J., RADUA, J. & PALANIYAPPAN, L. 2019. Antioxidant defense in schizophrenia and bipolar disorder: A meta-analysis of MRS studies of anterior cingulate glutathione. *Prog Neuropsychopharmacol Biol Psychiatry,* 91**,** 94-102.

DAVIS, K. L., KAHN, R. S., KO, G. & DAVIDSON, M. 1991. Dopamine in schizophrenia: a review and reconceptualization. *Am J Psychiatry,* 148**,** 1474-86.

DE ALMEIDA, L., IDIART, M. & LISMAN, J. E. 2009. A second function of gamma frequency oscillations: an E%-max winner-take-all mechanism selects which cells fire. *J Neurosci,* 29**,** 7497-503.

DE ARAÚJO, F. Y. R., CHAVES FILHO, A. J. M., NUNES, A. M., DE OLIVEIRA, G. V., GOMES, P. X. L., VASCONCELOS, G. S., CARLETTI, J., DE MORAES, M. O., DE MORAES, M. E., VASCONCELOS, S. M. M., DE SOUSA, F. C. F., DE LUCENA, D. F. & MACEDO, D. S. 2021. Involvement of anti-inflammatory, antioxidant, and BDNF up-regulating properties in the antipsychotic-like effect of the essential oil of Alpinia zerumbet in mice: a comparative study with olanzapine. *Metab Brain Dis,* 36**,** 2283-2297.

DE MIRANDA, J., YADDANAPUDI, K., HORNIG, M., VILLAR, G., SERGE, R. & LIPKIN, W. I. 2010. Induction of Toll-like receptor 3-mediated immunity during gestation inhibits cortical neurogenesis and causes behavioral disturbances. *mBio,* 1.

DE OLIVEIRA, L., SPIAZZI, C. M., BORTOLIN, T., CANEVER, L., PETRONILHO, F., MINA, F. G., DAL-PIZZOL, F., QUEVEDO, J. & ZUGNO, A. I. 2009. Different sub-anesthetic doses of ketamine increase oxidative stress in the brain of rats. *Prog Neuropsychopharmacol Biol Psychiatry,* 33**,** 1003-8.

DE PASQUALE, R., BECKHAUSER, T. F., HERNANDES, M. S. & GIORGETTI BRITTO, L. R. 2014. LTP and LTD in the visual cortex require the activation of NOX2. *J Neurosci,* 34**,** 12778-87.

DEAKIN, B., SUCKLING, J., DAZZAN, P., JOYCE, E., LAWRIE, S. M., UPTHEGROVE, R., HUSAIN, N., CHAUDHRY, I. B., DUNN, G., JONES, P. B., LISIECKA-FORD, D., LEWIS, S., BARNES, T. R. E., WILLIAMS, S. C. R., PARIANTE, C. M., KNOX, E., DRAKE, R. J., SMALLMAN, R. & BARNES,

N. M. 2019. Minocycline for negative symptoms of schizophrenia and possible mechanistic actions: the BeneMin RCT.

DEL GIUDICE, M. & GANGESTAD, S. W. 2018. Rethinking IL-6 and CRP: Why they are more than inflammatory biomarkers, and why it matters. *Brain Behav Immun,* 70**,** 61-75.

DEPCIUCH, J., JAKUBCZYK, P., PAJA, W., SARZYŃSKI, J., PANCERZ, K., AÇIKEL ELMAS, M., KESKINÖZ, E., BINGÖL ÖZAKPINAR, Ö., ARBAK, S., ÖZGÜN, G., ALTUNTAŞ, S. & GULEKEN, Z. 2022. Apocynin reduces cytotoxic effects of monosodium glutamate in the brain: A spectroscopic, oxidative load, and machine learning study. *Spectrochim Acta A Mol Biomol Spectrosc,* 279**,** 121495.

DESLAURIERS, J., LAROUCHE, A., SARRET, P. & GRIGNON, S. 2013. Combination of prenatal immune challenge and restraint stress affects prepulse inhibition and dopaminergic/GABAergic markers. *Prog Neuropsychopharmacol Biol Psychiatry,* 45**,** 156-64.

DEVANARAYANAN, S., NANDEESHA, H., KATTIMANI, S. & SARKAR, S. 2016. Relationship between matrix metalloproteinase-9 and oxidative stress in drug-free male schizophrenia: a case control study. *Clin Chem Lab Med,* 54**,** 447-52.

DEVIENNE, G., PICAUD, S., COHEN, I., PIQUET, J., TRICOIRE, L., TESTA, D., DI NARDO, A. A., ROSSIER, J., CAULI, B. & LAMBOLEZ, B. 2021. Regulation of perineuronal nets in the adult cortex by the activity of the cortical network. *J Neurosci,* 41**,** 5779-90.

DI CARLO, P., PUNZI, G. & URSINI, G. 2019. Brain-derived neurotrophic factor and schizophrenia. *Psychiatr Genet,* 29**,** 200-210.

DICKERSON, D. D., OVEREEM, K. A., WOLFF, A. R., WILLIAMS, J. M., ABRAHAM, W. C. & BILKEY, D. K. 2014. Association of aberrant neural synchrony and altered GAD67 expression following exposure to maternal immune activation, a risk factor for schizophrenia. *Transl Psychiatry,* 4**,** e418.

DICKSON, H., LAURENS, K. R., CULLEN, A. E. & HODGINS, S. 2012. Meta-analyses of cognitive and motor function in youth aged 16 years and younger who subsequently develop schizophrenia. *Psychol Med,* 42**,** 743-55.

DIENEL, S. J. & LEWIS, D. A. 2019. Alterations in cortical interneurons and cognitive function in schizophrenia. *Neurobiol Dis,* 131**,** 104208.

DING, J., ZHANG, C., ZHANG, Y. W., MA, Q. R., LIU, Y. M., SUN, T. & LIU, J. 2019. N-methyl-D-aspartate receptor subunit 1 regulates neurogenesis in the hippocampal dentate gyrus of schizophrenia-like mice. *Neural Regen Res,* 14**,** 2112-2117.

DITYATEV, A., BRUCKNER, G., DITYATEVA, G., GROSCHE, J., KLEENE, R. & SCHACHNER, M. 2007. Activity-dependent formation and functions of chondroitin sulfate-rich extracellular matrix of perineuronal nets. *Dev Neurobiol,* 67**,** 570-88.

DIXON, L. 2017. What It Will Take to Make Coordinated Specialty Care Available to Anyone Experiencing Early Schizophrenia: Getting Over the Hump. *JAMA Psychiatry,* 74**,** 7-8.

DO, K. Q. 2023. Bridging the gaps towards precision psychiatry: Mechanistic biomarkers for early detection and intervention. *Psychiatry Res,* 321**,** 115064.

DOCHERTY, A. R., BAKIAN, A. V., DIBLASI, E., SHABALIN, A. A., CHEN, D., KEESHIN, B., MONSON, E., CHRISTENSEN, E. D., LI, Q., GRAY, D. & COON, H. 2022. Suicide and Psychosis: Results From a Population-Based Cohort of Suicide Death (N = 4380). *Schizophr Bull,* 48**,** 457-462.

DOGRA, S., PUTNAM, J. & CONN, P. J. 2022. Metabotropic glutamate receptor 3 as a potential therapeutic target for psychiatric and neurological disorders. *Pharmacol Biochem Behav,* 221**,** 173493.

DOMENICI, E., WILLÉ, D. R., TOZZI, F., PROKOPENKO, I., MILLER, S., MCKEOWN, A., BRITTAIN, C., RUJESCU, D., GIEGLING, I., TURCK, C. W., HOLSBOER, F., BULLMORE, E. T., MIDDLETON, L., MERLO-PICH, E., ALEXANDER, R. C. & MUGLIA, P. 2010. Plasma protein biomarkers for depression and schizophrenia by multi analyte profiling of case-control collections. *PLoS One,* 5**,** e9166.

DOMINICZAK, M. H., NAISH, J. & SYNDERCOMBE COURT, D. 2019. *Biochemistry and cell biology - Medical Sciences*.

DOMINO, E. F., CHODOFF, P. & CORSSEN, G. 1965. PHARMACOLOGIC EFFECTS OF CI-581, A NEW DISSOCIATIVE ANESTHETIC, IN MAN. *Clin Pharmacol Ther,* 6**,** 279-91.

DONATO, F., CHOWDHURY, A., LAHR, M. & CARONI, P. 2015. Early- and late-born parvalbumin basket cell subpopulations exhibiting distinct regulation and roles in learning. *Neuron,* 85**,** 770-86.

DOREULEE, N., ALANIA, M., MITAISHVILI, E., CHIKOVANI, M. & CHKHARTISHVILI, B. 2009. The role of the mGluR allosteric modulation in the NMDA-hypofunction model of schizophrenia. *Georgian Med News***,** 59-65.

DOURS-ZIMMERMANN, M. T., MAURER, K., RAUCH, U., STOFFEL, W., FÄSSLER, R. & ZIMMERMANN, D. R. 2009. Versican V2 assembles the extracellular matrix surrounding the nodes of ranvier in the CNS. *J Neurosci,* 29**,** 7731-42.

DU, X., LI, J., LI, M., YANG, X., QI, Z., XU, B., LIU, W., XU, Z. & DENG, Y. 2020. Research progress on the role of type I vesicular glutamate transporter (VGLUT1) in nervous system diseases. *Cell Biosci,* 10**,** 26.

DUCHARME, G., LOWE, G. C., GOUTAGNY, R. & WILLIAMS, S. 2012. Early alterations in hippocampal circuitry and theta rhythm generation in a mouse model of prenatal infection: implications for schizophrenia. *PLoS One,* 7**,** e29754.

DUCHATEL, R. J., HARMS, L. R., MEEHAN, C. L., MICHIE, P. T., BIGLAND, M. J., SMITH, D. W., JOBLING, P., HODGSON, D. M. & TOONEY, P. A. 2019. Reduced cortical somatostatin gene expression in a rat model of maternal immune activation. *Psychiatry Res,* 282**,** 112621.

DUMAS, T. C. 2005. Developmental regulation of cognitive abilities: modified composition of a molecular switch turns on associative learning. *Prog Neurobiol,* 76**,** 189-211.

DUNCAN, G. E., MOY, S. S., PEREZ, A., EDDY, D. M., ZINZOW, W. M., LIEBERMAN, J. A., SNOUWAERT, J. N. & KOLLER, B. H. 2004. Deficits in sensorimotor gating and tests of social behavior in a genetic model of reduced NMDA receptor function. *Behav Brain Res,* 153**,** 507-19.

DUPUIS, J. P., LADÉPÊCHE, L., SETH, H., BARD, L., VARELA, J., MIKASOVA, L., BOUCHET, D., ROGEMOND, V., HONNORAT, J., HANSE, E. & GROC, L. 2014. Surface dynamics of GluN2B-NMDA receptors controls plasticity of maturing glutamate synapses. *EMBO J,* 33**,** 842-61.

DWIR, D., CABUNGCAL, J. H., XIN, L., GIANGRECO, B., PARIETTI, E., CLEUSIX, M., JENNI, R., KLAUSER, P., CONUS, P., CUÉNOD, M., STEULLET, P. & DO, K. Q. 2021. Timely N-Acetyl-Cysteine and Environmental Enrichment Rescue Oxidative Stress-Induced Parvalbumin Interneuron Impairments via MMP9/RAGE Pathway: A Translational Approach for Early Intervention in Psychosis. *Schizophr Bull,* 47**,** 1782-1794.

DWIR, D., GIANGRECO, B., XIN, L., TENENBAUM, L., CABUNGCAL, J. H., STEULLET, P., GOUPIL, A., CLEUSIX, M., JENNI, R., BAUMANN, P. S., KLAUSER, P., CONUS, P., TIROUVANZIAM, R., CUENOD, M. & DO, K. Q. 2019. MMP9/RAGE pathway overactivation mediates redox dysregulation and neuroinflammation, leading to inhibitory/excitatory imbalance: a reverse translation study in schizophrenia patients. *Mol Psychiatry*.

DWIR, D., GIANGRECO, B., XIN, L., TENENBAUM, L., CABUNGCAL, J. H., STEULLET, P., GOUPIL, A., CLEUSIX, M., JENNI, R., CHTARTO, A., BAUMANN, P. S., KLAUSER, P., CONUS, P., TIROUVANZIAM, R., CUENOD, M. & DO, K. Q. 2020. MMP9/RAGE pathway overactivation mediates redox dysregulation and neuroinflammation, leading to inhibitory/excitatory imbalance: a reverse translation study in schizophrenia patients. *Mol Psychiatry,* 25**,** 2889-2904.

EASTWOOD, S. L. & HARRISON, P. J. 2005. Decreased expression of vesicular glutamate transporter 1 and complexin II mRNAs in schizophrenia: further evidence for a synaptic pathology affecting glutamate neurons. *Schizophr Res,* 73**,** 159-72.

EGGERMANN, E. & JONAS, P. 2011. How the 'slow' Ca(2+) buffer parvalbumin affects transmitter release in nanodomain-coupling regimes. *Nat Neurosci,* 15**,** 20-2.

EHRLICH, I., KLEIN, M., RUMPEL, S. & MALINOW, R. 2007. PSD-95 is required for activity-driven synapse stabilization. *Proc Natl Acad Sci U S A,* 104**,** 4176-81.

ELIAS, G. M., ELIAS, L. A., APOSTOLIDES, P. F., KRIEGSTEIN, A. R. & NICOLL, R. A. 2008. Differential trafficking of AMPA and NMDA receptors by SAP102 and PSD-95 underlies synapse development. *Proc Natl Acad Sci U S A,* 105**,** 20953-8.

ELIAS, G. M. & NICOLL, R. A. 2007. Synaptic trafficking of glutamate receptors by MAGUK scaffolding proteins. *Trends Cell Biol,* 17**,** 343-52.

ELLEGREN, H. & PARSCH, J. 2007. The evolution of sex-biased genes and sex-biased gene expression. *Nat Rev Genet,* 8**,** 689-98.

EMSLEY, R., CHILIZA, B., ASMAL, L. & HARVEY, B. H. 2013. The nature of relapse in schizophrenia. *BMC Psychiatry,* 13**,** 50.

ENENI, A. O., BEN-AZU, B., AJAYI, A. M. & ADERIBIGBE, A. O. 2023. Lipopolysaccharide Exacerbates Ketamine-Induced Psychotic-Like Behavior, Oxidative Stress, and Neuroinflammation in Mice: Ameliorative Effect of Diosmin. *J Mol Neurosci*.

ENGEMANN, K., PEDERSEN, C. B., ARGE, L., TSIROGIANNIS, C., MORTENSEN, P. B. & SVENNING, J. C. 2018. Childhood exposure to green space - A novel risk-decreasing mechanism for schizophrenia? *Schizophr Res,* 199**,** 142-148.

ENWRIGHT, J. F., SANAPALA, S., FOGLIO, A., BERRY, R., FISH, K. N. & LEWIS, D. A. 2016. Reduced Labeling of Parvalbumin Neurons and Perineuronal Nets in the Dorsolateral Prefrontal Cortex of Subjects with Schizophrenia. *Neuropsychopharmacology,* 41**,** 2206-14.

ERMAKOV, E. A., DMITRIEVA, E. M., PARSHUKOVA, D. A., KAZANTSEVA, D. V., VASILIEVA, A. R. & SMIRNOVA, L. P. 2021. Oxidative Stress-Related Mechanisms in Schizophrenia Pathogenesis and New Treatment Perspectives. *Oxid Med Cell Longev,* 2021**,** 8881770.

ERTA, M., QUINTANA, A. & HIDALGO, J. 2012. Interleukin-6, a major cytokine in the central nervous system. *Int J Biol Sci,* 8**,** 1254-66.

ESPÓSITO, M. S., PIATTI, V. C., LAPLAGNE, D. A., MORGENSTERN, N. A., FERRARI, C. C., PITOSSI, F. J. & SCHINDER, A. F. 2005. Neuronal differentiation in the adult hippocampus recapitulates embryonic development. *J Neurosci,* 25**,** 10074-86.

ESTES, M. L. & MCALLISTER, A. K. 2016. Maternal immune activation: Implications for neuropsychiatric disorders. *Science,* 353**,** 772-7.

ETHELL, I. M. & ETHELL, D. W. 2007. Matrix metalloproteinases in brain development and remodeling: synaptic functions and targets. *J Neurosci Res,* 85**,** 2813-23.

ETNIER, J., LABBAN, J. D., PIEPMEIER, A., DAVIS, M. E. & HENNING, D. A. 2014. Effects of an acute bout of exercise on memory in 6th grade children. *Pediatr Exerc Sci,* 26**,** 250-8.

ETNIER, J. L., SPRICK, P. M., LABBAN, J. D., SHIH, C. H., GLASS, S. M. & VANCE, J. C. 2020. Effects of an aerobic fitness test on short- and long-term memory in elementary-aged children. *J Sports Sci,* 38**,** 2264-2272.

EVERS, M. R., SALMEN, B., BUKALO, O., ROLLENHAGEN, A., BÖSL, M. R., MORELLINI, F., BARTSCH, U., DITYATEV, A. & SCHACHNER, M. 2002. Impairment of L-type Ca2+ channel-dependent forms of hippocampal synaptic plasticity in mice deficient in the extracellular matrix glycoprotein tenascin-C. *J Neurosci,* 22**,** 7177-94.

FABRAZZO, M., CIPOLLA, S., CAMERLENGO, A., PERRIS, F. & CATAPANO, F. 2022. Second-Generation Antipsychotics' Effectiveness and Tolerability: A Review of Real-World Studies in Patients with Schizophrenia and Related Disorders. *J Clin Med,* 11.

FAHIMI, A., BAKTIR, M. A., MOGHADAM, S., MOJABI, F. S., SUMANTH, K., MCNERNEY, M. W., PONNUSAMY, R. & SALEHI, A. 2017. Physical exercise induces structural alterations in the hippocampal astrocytes: exploring the role of BDNF-TrkB signaling. *Brain Struct Funct,* 222**,** 1797-1808.

FALKAI, P., MALCHOW, B. & SCHMITT, A. 2017. Aerobic exercise and its effects on cognition in schizophrenia. *Curr Opin Psychiatry,* 30**,** 171-175.

FAN, N., LUO, Y., XU, K., ZHANG, M., KE, X., HUANG, X., DING, Y., WANG, D., NING, Y., DENG, X. & HE, H. 2015. Relationship of serum levels of TNF-α, IL-6 and IL-18 and schizophrenia-like symptoms in chronic ketamine abusers. *Schizophr Res,* 169**,** 10-15.

FANOUS, A. H., ZHAO, Z., VAN DEN OORD, E., MAHER, B. S., THISELTON, D. L., BERGEN, S. E., WORMLEY, B., BIGDELI, T., AMDUR, R. L., O'NEILL, F. A., WALSH, D., KENDLER, K. S. & RILEY, B. P. 2010. Association study of SNAP25 and schizophrenia in Irish family and case-control samples. *Am J Med Genet B Neuropsychiatr Genet,* 153b**,** 663-674.

FANSELOW, M. S. & DONG, H. W. 2010. Are the dorsal and ventral hippocampus functionally distinct structures? *Neuron,* 65**,** 7-19.

FARES, J., BOU DIAB, Z., NABHA, S. & FARES, Y. 2019. Neurogenesis in the adult hippocampus: history, regulation, and prospective roles. *Int J Neurosci,* 129**,** 598-611.

FARMER, J., ZHAO, X., VAN PRAAG, H., WODTKE, K., GAGE, F. H. & CHRISTIE, B. R. 2004. Effects of voluntary exercise on synaptic plasticity and gene expression in the dentate gyrus of adult male Sprague-Dawley rats in vivo. *Neuroscience,* 124**,** 71-9.

FATEMI, S. H., ARAGHI-NIKNAM, M., LAURENCE, J. A., STARY, J. M., SIDWELL, R. W. & LEE, S. 2004. Glial fibrillary acidic protein and glutamic acid decarboxylase 65 and 67 kDa proteins are increased in brains of neonatal BALB/c mice following viral infection in utero. *Schizophr Res,* 69**,** 121-3.

FAUMAN, B., ALDINGER, G., FAUMAN, M. & ROSEN, P. 1976. Psychiatric sequelae of phencyclidine abuse. *Clin Toxicol,* 9**,** 529-38.

FAVUZZI, E., MARQUES-SMITH, A., DEOGRACIAS, R., WINTERFLOOD, C. M., SANCHEZ-AGUILERA, A., MANTOAN, L., MAESO, P., FERNANDES, C., EWERS, H. & RICO, B. 2017. Activity-Dependent Gating of Parvalbumin Interneuron Function by the Perineuronal Net Protein Brevican. *Neuron,* 95**,** 639-655.e10.

FAZELZADEH, M., AFZALPOUR, M. E., FALLAH MOHAMMADI, Z. & FALAH MOHAMMADI, H. 2021. The effects of voluntary complex and regular wheel running exercises on the levels of 8-oxoguanine DNA glycosylase, semaphorin 3B, H2O2, and apoptosis in the hippocampus of diabetic rats. *Brain Behav,* 11**,** e01988.

FENG, Y., CUI, C., LIU, X., WU, Q., HU, F., ZHANG, H., MA, Z. & WANG, L. 2017. Protective Role of Apocynin via Suppression of Neuronal Autophagy and TLR4/NF-κB Signaling Pathway in a Rat Model of Traumatic Brain Injury. *Neurochem Res,* 42**,** 3296-3309.

FENNER, B. M. 2012. Truncated TrkB: beyond a dominant negative receptor. *Cytokine Growth Factor Rev,* 23**,** 15-24.

FERRARIS, M., CASSEL, J. C., PEREIRA DE VASCONCELOS, A., STEPHAN, A. & QUILICHINI, P. P. 2021. The nucleus reuniens, a thalamic relay for cortico-hippocampal interaction in recent and remote memory consolidation. *Neurosci Biobehav Rev,* 125**,** 339-354.

FETER, N., SPANEVELLO, R. M., SOARES, M. S. P., SPOHR, L., PEDRA, N. S., BONA, N. P., FREITAS, M. P., GONZALES, N. G., ITO, L., STEFANELLO, F. M. & ROMBALDI, A. J. 2019. How does physical activity and different models of exercise training affect oxidative parameters and memory? *Physiol Behav,* 201**,** 42-52.

FILICE, F., VÖRCKEL, K. J., SUNGUR, A., WÖHR, M. & SCHWALLER, B. 2016. Reduction in parvalbumin expression not loss of the parvalbumin-expressing GABA interneuron subpopulation in genetic parvalbumin and shank mouse models of autism. *Mol Brain,* 9**,** 10.

FILLMAN, S. G., WEICKERT, T. W., LENROOT, R. K., CATTS, S. V., BRUGGEMANN, J. M., CATTS, V. S. & WEICKERT, C. S. 2016. Elevated peripheral cytokines characterize a subgroup of people with schizophrenia displaying poor verbal fluency and reduced Broca's area volume. *Mol Psychiatry,* 21**,** 1090-8.

FIRTH, J., COTTER, J., ELLIOTT, R., FRENCH, P. & YUNG, A. R. 2015. A systematic review and meta-analysis of exercise interventions in schizophrenia patients. *Psychol Med,* 45**,** 1343-61.

FIRTH, J., STUBBS, B., ROSENBAUM, S., VANCAMPFORT, D., MALCHOW, B., SCHUCH, F., ELLIOTT, R., NUECHTERLEIN, K. H. & YUNG, A. R. 2017. Aerobic Exercise Improves Cognitive

Functioning in People With Schizophrenia: A Systematic Review and Meta-Analysis. *Schizophr Bull,* 43**,** 546-556.

FLATOW, J., BUCKLEY, P. & MILLER, B. J. 2013. Meta-analysis of oxidative stress in schizophrenia. *Biol Psychiatry,* 74**,** 400-9.

FORREST, C. M., KHALIL, O. S., PISAR, M., SMITH, R. A., DARLINGTON, L. G. & STONE, T. W. 2012. Prenatal activation of Toll-like receptors-3 by administration of the viral mimetic poly(I:C) changes synaptic proteins, N-methyl-D-aspartate receptors and neurogenesis markers in offspring. *Mol Brain,* 5**,** 22.

FOSSATI, G., MORINI, R., CORRADINI, I., ANTONUCCI, F., TREPTE, P., EDRY, E., SHARMA, V., PAPALE, A., POZZI, D., DEFILIPPI, P., MEIER, J. C., BRAMBILLA, R., TURCO, E., ROSENBLUM, K., WANKER, E. E., ZIV, N. E., MENNA, E. & MATTEOLI, M. 2015. Reduced SNAP-25 increases PSD-95 mobility and impairs spine morphogenesis. *Cell Death Differ,* 22**,** 1425-36.

FRAGUAS, D., DÍAZ-CANEJA, C. M., AYORA, M., HERNÁNDEZ-ÁLVAREZ, F., RODRÍGUEZ-QUIROGA, A., RECIO, S., LEZA, J. C. & ARANGO, C. 2019. Oxidative Stress and Inflammation in First-Episode Psychosis: A Systematic Review and Meta-analysis. *Schizophr Bull,* 45**,** 742-751.

FRAGUAS, D., DÍAZ-CANEJA, C. M., RODRÍGUEZ-QUIROGA, A. & ARANGO, C. 2017. Oxidative Stress and Inflammation in Early Onset First Episode Psychosis: A Systematic Review and Meta-Analysis. *Int J Neuropsychopharmacol,* 20**,** 435-444.

FRANK, R. A., KOMIYAMA, N. H., RYAN, T. J., ZHU, F., O'DELL, T. J. & GRANT, S. G. 2016. NMDA receptors are selectively partitioned into complexes and supercomplexes during synapse maturation. *Nat Commun,* 7**,** 11264.

FRIEDMAN, N. P. & ROBBINS, T. W. 2022. The role of prefrontal cortex in cognitive control and executive function. *Neuropsychopharmacology,* 47**,** 72-89.

FRISCHKNECHT, R., HEINE, M., PERRAIS, D., SEIDENBECHER, C. I., CHOQUET, D. & GUNDELFINGER, E. D. 2009. Brain extracellular matrix affects AMPA receptor lateral mobility and short-term synaptic plasticity. *Nature Neuroscience,* 12**,** 897-904.

FUJIHARA, K., MIWA, H., KAKIZAKI, T., KANEKO, R., MIKUNI, M., TANAHIRA, C., TAMAMAKI, N. & YANAGAWA, Y. 2015. Glutamate Decarboxylase 67 Deficiency in a Subset of GABAergic Neurons Induces Schizophrenia-Related Phenotypes. *Neuropsychopharmacology,* 40**,** 2475-86.

FUJIKAWA, R., YAMADA, J. & JINNO, S. 2021. Subclass imbalance of parvalbumin-expressing GABAergic neurons in the hippocampus of a mouse ketamine model for schizophrenia, with reference to perineuronal nets. *Schizophr Res,* 229**,** 80-93.

FUJITA, Y., ISHIMA, T., KUNITACHI, S., HAGIWARA, H., ZHANG, L., IYO, M. & HASHIMOTO, K. 2008. Phencyclidine-induced cognitive deficits in mice are improved by subsequent subchronic administration of the antibiotic drug minocycline. *Prog Neuropsychopharmacol Biol Psychiatry,* 32**,** 336-9.

FUNG, S. J., WEBSTER, M. J., SIVAGNANASUNDARAM, S., DUNCAN, C., ELASHOFF, M. & WEICKERT, C. S. 2010. Expression of interneuron markers in the dorsolateral prefrontal cortex of the developing human and in schizophrenia. *Am J Psychiatry,* 167**,** 1479-88.

FUNK, A. J., MIELNIK, C. A., KOENE, R., NEWBURN, E., RAMSEY, A. J., LIPSKA, B. K. & MCCULLUMSMITH, R. E. 2017. Postsynaptic Density-95 Isoform Abnormalities in Schizophrenia. *Schizophr Bull,* 43**,** 891-899.

GALDERISI, S., MUCCI, A., BUCHANAN, R. W. & ARANGO, C. 2018. Negative symptoms of schizophrenia: new developments and unanswered research questions. *Lancet Psychiatry,* 5**,** 664-677.

GALTREY, C. M., KWOK, J. C., CARULLI, D., RHODES, K. E. & FAWCETT, J. W. 2008. Distribution and synthesis of extracellular matrix proteoglycans, hyaluronan, link proteins and tenascin-R in the rat spinal cord. *Eur J Neurosci,* 27**,** 1373-90.

GANDAL, M. J., SISTI, J., KLOOK, K., ORTINSKI, P. I., LEITMAN, V., LIANG, Y., THIEU, T., ANDERSON, R., PIERCE, R. C., JONAK, G., GUR, R. E., CARLSON, G. & SIEGEL, S. J. 2012. GABAB-mediated rescue of altered excitatory-inhibitory balance, gamma synchrony and

behavioral deficits following constitutive NMDAR-hypofunction. *Transl Psychiatry,* 2**,** e142.

GAO, J., TANG, X., KANG, J., XIE, C., YU, M., SHA, W., WANG, X., ZHANG, X. & YI, H. 2019. Correlation between neurocognitive impairment and DNA methylation of MMP-9 gene in patients with deficit schizophrenia. *Schizophr Res,* 204**,** 455-457.

GAO, J., YI, H., TANG, X., FENG, X., YU, M., SHA, W., WANG, X. & ZHANG, X. 2018. DNA Methylation and Gene Expression of Matrix Metalloproteinase 9 Gene in Deficit and Non-deficit Schizophrenia. *Front Genet,* 9**,** 646.

GAO, R., JI, M. H., GAO, D. P., YANG, R. H., ZHANG, S. G., YANG, J. J. & SHEN, J. C. 2017. Neuroinflammation-Induced Downregulation of Hippocampacal Neuregulin 1-ErbB4 Signaling in the Parvalbumin Interneurons Might Contribute to Cognitive Impairment in a Mouse Model of Sepsis-Associated Encephalopathy. *Inflammation,* 40**,** 387-400.

GAO, R. & PENZES, P. 2015. Common mechanisms of excitatory and inhibitory imbalance in schizophrenia and autism spectrum disorders. *Curr Mol Med,* 15**,** 146-67.

GAO, X. M., SAKAI, K., ROBERTS, R. C., CONLEY, R. R., DEAN, B. & TAMMINGA, C. A. 2000. Ionotropic glutamate receptors and expression of N-methyl-D-aspartate receptor subunits in subregions of human hippocampus: effects of schizophrenia. *Am J Psychiatry,* 157**,** 1141-9.

GAO, X. M., SHIRAKAWA, O., DU, F. & TAMMINGA, C. A. 1993. Delayed regional metabolic actions of phencyclidine. *Eur J Pharmacol,* 241**,** 7-15.

GARAY, P. A., HSIAO, E. Y., PATTERSON, P. H. & MCALLISTER, A. K. 2013. Maternal immune activation causes age- and region-specific changes in brain cytokines in offspring throughout development. *Brain Behav Immun,* 31**,** 54-68.

GARBETT, K. A., HSIAO, E. Y., KÁLMÁN, S., PATTERSON, P. H. & MIRNICS, K. 2012. Effects of maternal immune activation on gene expression patterns in the fetal brain. *Transl Psychiatry,* 2**,** e98.

GARCÍA-MESA, Y., COLIE, S., CORPAS, R., CRISTÒFOL, R., COMELLAS, F., NEBREDA, A. R., GIMÉNEZ-LLORT, L. & SANFELIU, C. 2016. Oxidative Stress Is a Central Target for Physical Exercise Neuroprotection Against Pathological Brain Aging. *J Gerontol A Biol Sci Med Sci,* 71**,** 40-9.

GARCIA-VALTANEN, P., VAN DIERMEN, B. A., LAKHAN, N., LOUSBERG, E. L., ROBERTSON, S. A., HAYBALL, J. D. & DIENER, K. R. 2020. Maternal host responses to poly(I:C) during pregnancy leads to both dysfunctional immune profiles and altered behaviour in the offspring. *Am J Reprod Immunol,* 84**,** e13260.

GARRIDO-MESA, N., ZARZUELO, A. & GÁLVEZ, J. 2013. Minocycline: far beyond an antibiotic. *Br J Pharmacol,* 169**,** 337-52.

GARVER, D. L., TAMAS, R. L. & HOLCOMB, J. A. 2003. Elevated interleukin-6 in the cerebrospinal fluid of a previously delineated schizophrenia subtype. *Neuropsychopharmacology,* 28**,** 1515-20.

GAWRYLUK, J. W., WANG, J. F., ANDREAZZA, A. C., SHAO, L. & YOUNG, L. T. 2011. Decreased levels of glutathione, the major brain antioxidant, in post-mortem prefrontal cortex from patients with psychiatric disorders. *Int J Neuropsychopharmacol,* 14**,** 123-30.

GE, S., YANG, C. H., HSU, K. S., MING, G. L. & SONG, H. 2007. A critical period for enhanced synaptic plasticity in newly generated neurons of the adult brain. *Neuron,* 54**,** 559-66.

GEBREEGZIABHERE, Y., HABATMU, K., MIHRETU, A., CELLA, M. & ALEM, A. 2022. Cognitive impairment in people with schizophrenia: an umbrella review. *Eur Arch Psychiatry Clin Neurosci,* 272**,** 1139-1155.

GEIGER, J. R., LÜBKE, J., ROTH, A., FROTSCHER, M. & JONAS, P. 1997. Submillisecond AMPA receptor-mediated signaling at a principal neuron-interneuron synapse. *Neuron,* 18**,** 1009-23.

GENSINI, G. F., CONTI, A. A. & LIPPI, D. 2007. The contributions of Paul Ehrlich to infectious disease. *J Infect,* 54**,** 221-4.

GEOFFROY, C., PAOLETTI, P. & MONY, L. 2022. Positive allosteric modulation of NMDA receptors: mechanisms, physiological impact and therapeutic potential. *J Physiol,* 600**,** 233-259.

GEORGIEV, D., ARION, D., ENWRIGHT, J. F., KIKUCHI, M., MINABE, Y., CORRADI, J. P., LEWIS, D. A. & HASHIMOTO, T. 2014. Lower gene expression for KCNS3 potassium channel subunit in parvalbumin-containing neurons in the prefrontal cortex in schizophrenia. *Am J Psychiatry,* 171**,** 62-71.

GHASEMI, A., JEDDI, S. & KASHFI, K. 2021. The laboratory rat: Age and body weight matter. *EXCLI J,* 20**,** 1431-1445.

GHAVIMI, H., BAYANI ERSHADI, A. S., DASTVAR, S. & HOSSEINI, M. J. 2022. The effects of minocycline in improving of methamphetamine withdrawal syndrome in male mice. *Drug Chem Toxicol,* 45**,** 2319-2327.

GHIANI, C. A., MATTAN, N. S., NOBUTA, H., MALVAR, J. S., BOLES, J., ROSS, M. G., WASCHEK, J. A., CARPENTER, E. M., FISHER, R. S. & DE VELLIS, J. 2011. Early effects of lipopolysaccharide-induced inflammation on foetal brain development in rat. *ASN Neuro,* 3.

GHOLAMI MAHMOUDIAN, Z., KOMAKI, A., RASHIDI, I., AMIRI, I. & GHANBARI, A. 2022. The effect of minocycline on beta-amyloid-induced memory and learning deficit in male rats: A behavioral, biochemical, and histological study. *J Chem Neuroanat,* 125**,** 102158.

GIANNINI, A. J., EIGHAN, M. S., LOISELLE, R. H. & GIANNINI, M. C. 1984. Comparison of haloperidol and chlorpromazine in the treatment of phencyclidine psychosis. *J Clin Pharmacol,* 24**,** 202-4.

GIANNINI, A. J., LOISELLE, R. H., DIMARZIO, L. R. & GIANNINI, M. C. 1987. Augmentation of haloperidol by ascorbic acid in phencyclidine intoxication. *Am J Psychiatry,* 144**,** 1207-9.

GIGG, J., MCEWAN, F., SMAUSZ, R., NEILL, J. & HARTE, M. K. 2020. Synaptic biomarker reduction and impaired cognition in the sub-chronic PCP mouse model for schizophrenia. *J Psychopharmacol,* 34**,** 115-124.

GILFARB, R. A. & LEUNER, B. 2022. GABA System Modifications During Periods of Hormonal Flux Across the Female Lifespan. *Front Behav Neurosci,* 16**,** 802530.

GILMORE, J. H., JARSKOG, L. F. & VADLAMUDI, S. 2005. Maternal poly I:C exposure during pregnancy regulates TNF alpha, BDNF, and NGF expression in neonatal brain and the maternal-fetal unit of the rat. *J Neuroimmunol,* 159**,** 106-12.

GINSBERG, Y., KHATIB, N., SAADI, N., ROSS, M. G., WEINER, Z. & BELOOSESKY, R. 2018. Maternal pomegranate juice attenuates maternal inflammation-induced fetal brain injury by inhibition of apoptosis, neuronal nitric oxide synthase, and NF-κB in a rat model. *Am J Obstet Gynecol,* 219**,** 113.e1-113.e9.

GIOVANOLI, S., ENGLER, H., ENGLER, A., RICHETTO, J., VOGET, M., WILLI, R., WINTER, C., RIVA, M. A., MORTENSEN, P. B., FELDON, J., SCHEDLOWSKI, M. & MEYER, U. 2013. Stress in puberty unmasks latent neuropathological consequences of prenatal immune activation in mice. *Science,* 339**,** 1095-9.

GIOVANOLI, S., NOTTER, T., RICHETTO, J., LABOUESSE, M. A., VUILLERMOT, S., RIVA, M. A. & MEYER, U. 2015. Late prenatal immune activation causes hippocampal deficits in the absence of persistent inflammation across aging. *J Neuroinflammation,* 12**,** 221.

GIOVANOLI, S., WEBER-STADLBAUER, U., SCHEDLOWSKI, M., MEYER, U. & ENGLER, H. 2016. Prenatal immune activation causes hippocampal synaptic deficits in the absence of overt microglia anomalies. *Brain Behav Immun,* 55**,** 25-38.

GIOVANOLI, S., WEBER, L. & MEYER, U. 2014. Single and combined effects of prenatal immune activation and peripubertal stress on parvalbumin and reelin expression in the hippocampal formation. *Brain Behav Immun,* 40**,** 48-54.

GIRARD, T. A., WILKINS, L. K., LYONS, K. M., YANG, L. & CHRISTENSEN, B. K. 2018. Traditional test administration and proactive interference undermine visual-spatial working memory performance in schizophrenia-spectrum disorders. *Cogn Neuropsychiatry,* 23**,** 242-253.

GIRDLER, S. J., CONFINO, J. E. & WOESNER, M. E. 2019. Exercise as a Treatment for Schizophrenia: A Review. *Psychopharmacol Bull,* 49**,** 56-69.

GIROUARD, H., WANG, G., GALLO, E. F., ANRATHER, J., ZHOU, P., PICKEL, V. M. & IADECOLA, C. 2009. NMDA receptor activation increases free radical production through nitric oxide and NOX2. *J Neurosci,* 29**,** 2545-52.

GOEDEN, N., VELASQUEZ, J., ARNOLD, K. A., CHAN, Y., LUND, B. T., ANDERSON, G. M. & BONNIN, A. 2016. Maternal Inflammation Disrupts Fetal Neurodevelopment via Increased Placental Output of Serotonin to the Fetal Brain. *J Neurosci,* 36**,** 6041-9.

GOGOLLA, N., CARONI, P., LÜTHI, A. & HERRY, C. 2009a. Perineuronal nets protect fear memories from erasure. *Science,* 325**,** 1258-61.

GOGOLLA, N., LEBLANC, J. J., QUAST, K. B., SÜDHOF, T. C., FAGIOLINI, M. & HENSCH, T. K. 2009b. Common circuit defect of excitatory-inhibitory balance in mouse models of autism. *J Neurodev Disord,* 1**,** 172-81.

GOGOS, A., SBISA, A., WITKAMP, D. & VAN DEN BUUSE, M. 2020. Sex differences in the effect of maternal immune activation on cognitive and psychosis-like behaviour in Long Evans rats. *Eur J Neurosci,* 52**,** 2614-2626.

GOH, J. Y., O'SULLIVAN, S. E., SHORTALL, S. E., ZORDAN, N., PICCININI, A. M., POTTER, H. G., FONE, K. C. F. & KING, M. V. 2020. Gestational poly(I:C) attenuates, not exacerbates, the behavioral, cytokine and mTOR changes caused by isolation rearing in a rat 'dual-hit' model for neurodevelopmental disorders. *Brain Behav Immun,* 89**,** 100-117.

GOLD, J. M. 2004. Cognitive deficits as treatment targets in schizophrenia. *Schizophr Res,* 72**,** 21-8.

GOLDBERG, J. H., YUSTE, R. & TAMAS, G. 2003. Ca2+ imaging of mouse neocortical interneurone dendrites: contribution of Ca2+-permeable AMPA and NMDA receptors to subthreshold Ca2+dynamics. *J Physiol,* 551**,** 67-78.

GOLUB, D., YANAI, A., DARZI, K., PAPADOPOULOS, J. & KAUFMAN, B. 2018. Potential consequences of high-dose infusion of ketamine for refractory status epilepticus: case reports and systematic literature review. *Anaesth Intensive Care,* 46**,** 516-528.

GOMES DA SILVA, S., DONÁ, F., DA SILVA FERNANDES, M. J., SCORZA, F. A., CAVALHEIRO, E. A. & ARIDA, R. M. 2010. Physical exercise during the adolescent period of life increases hippocampal parvalbumin expression. *Brain Dev,* 32**,** 137-42.

GOMES, F. V., LLORENTE, R., DEL BEL, E. A., VIVEROS, M. P., LÓPEZ-GALLARDO, M. & GUIMARÃES, F. S. 2015. Decreased glial reactivity could be involved in the antipsychotic-like effect of cannabidiol. *Schizophr Res,* 164**,** 155-63.

GÓMEZ-PINILLA, F., YING, Z., ROY, R. R., MOLTENI, R. & EDGERTON, V. R. 2002. Voluntary exercise induces a BDNF-mediated mechanism that promotes neuroplasticity. *J Neurophysiol,* 88**,** 2187-95.

GONÇALVES, J. T., SCHAFER, S. T. & GAGE, F. H. 2016. Adult Neurogenesis in the Hippocampus: From Stem Cells to Behavior. *Cell,* 167**,** 897-914.

GONZALEZ-BURGOS, G. & LEWIS, D. A. 2008. GABA neurons and the mechanisms of network oscillations: implications for understanding cortical dysfunction in schizophrenia. *Schizophr Bull,* 34**,** 944-61.

GONZALEZ, A., HEANEY, L., PODDA, G., OLADIPO, J., GRAYSON, B., HARTE, M., LARGE, C. & NEILL, J. 2017. Brain-Derived Neurotrophic Factor and Exercise-Induced Reversal of Cognitive Deficit Symptoms of Relevance to Schizophrenia. *British Pharmacological Society.*

GORSKI, J. A., BALOGH, S. A., WEHNER, J. M. & JONES, K. R. 2003. Learning deficits in forebrain-restricted brain-derived neurotrophic factor mutant mice. *Neuroscience,* 121**,** 341-54.

GOTTSCHALL, P. E. & HOWELL, M. D. 2015. ADAMTS expression and function in central nervous system injury and disorders. *Matrix Biol,* 44-46**,** 70-6.

GRACIARENA, M., DEPINO, A. M. & PITOSSI, F. J. 2010. Prenatal inflammation impairs adult neurogenesis and memory related behavior through persistent hippocampal TGFβ1 downregulation. *Brain Behav Immun,* 24**,** 1301-9.

GRAYSON, B., ADAMSON, L., HARTE, M., LEGER, M., MARSH, S., PIERCY, C. & NEILL, J. C. 2014. The involvement of distraction in memory deficits induced by NMDAR antagonism: relevance to cognitive deficits in schizophrenia. *Behav Brain Res,* 266**,** 188-92.

GRAYSON, B., IDRIS, N. F. & NEILL, J. C. 2007. Atypical antipsychotics attenuate a sub-chronic PCP-induced cognitive deficit in the novel object recognition task in the rat. *Behav Brain Res,* 184**,** 31-8.

GRAYSON, B., LEGER, M., PIERCY, C., ADAMSON, L., HARTE, M. & NEILL, J. C. 2015. Assessment of disease-related cognitive impairments using the novel object recognition (NOR) task in rodents. *Behav Brain Res,* 285**,** 176-93.

GREIFENSTEIN, F. E., DEVAULT, M., YOSHITAKE, J. & GAJEWSKI, J. E. 1958. A study of a 1-aryl cyclo hexyl amine for anesthesia. *Anesth Analg,* 37**,** 283-94.

GRIESBACH, G. S., HOVDA, D. A. & GOMEZ-PINILLA, F. 2009. Exercise-induced improvement in cognitive performance after traumatic brain injury in rats is dependent on BDNF activation. *Brain Res,* 1288**,** 105-15.

GROC, L., HEINE, M., COUSINS, S. L., STEPHENSON, F. A., LOUNIS, B., COGNET, L. & CHOQUET, D. 2006. NMDA receptor surface mobility depends on NR2A-2B subunits. *Proc Natl Acad Sci U S A,* 103**,** 18769-74.

GRUSKIN, E. A., IACI, J. F., TSENG, J. L. & CAGGIANO, A. O. 2003. Chondroitinase ABC I impacts diffusion rates in CNS tissue. *LA: Society for Neuroscience.* New Orleans.

GUAN, F., ZHANG, T., HAN, W., ZHU, L., NI, T., LIN, H., LIU, D., CHEN, G., XIAO, J. & LI, T. 2020. Relationship of SNAP25 variants with schizophrenia and antipsychotic-induced weight change in large-scale schizophrenia patients. *Schizophr Res,* 215**,** 250-255.

GUARDIOLA-RIPOLL, M., ALMODÓVAR-PAYÁ, C., LUBEIRO, A., SALVADOR, R., SALGADO-PINEDA, P., GOMAR, J. J., GUERRERO-PEDRAZA, A., SARRÓ, S., MARISTANY, T., FERNÁNDEZ-LINSENBARTH, I., HERNÁNDEZ-GARCÍA, M., PAPIOL, S., MOLINA, V., POMAROL-CLOTET, E. & FATJÓ-VILAS, M. 2022. New insights of the role of the KCNH2 gene in schizophrenia: An fMRI case-control study. *Eur Neuropsychopharmacol,* 60**,** 38-47.

GUERRIERO, R. M., GIZA, C. C. & ROTENBERG, A. 2015. Glutamate and GABA imbalance following traumatic brain injury. *Curr Neurol Neurosci Rep,* 15**,** 27.

GUERRIN, C. G. J., SHOJI, A., DOORDUIN, J. & DE VRIES, E. F. J. 2022. Immune Activation in Pregnant Rats Affects Brain Glucose Consumption, Anxiety-like Behaviour and Recognition Memory in their Male Offspring. *Mol Imaging Biol,* 24**,** 740-749.

GUIDOTTI, A., AUTA, J., DAVIS, J. M., DI-GIORGI-GEREVINI, V., DWIVEDI, Y., GRAYSON, D. R., IMPAGNATIELLO, F., PANDEY, G., PESOLD, C., SHARMA, R., UZUNOV, D., COSTA, E. & DIGIORGI GEREVINI, V. 2000. Decrease in reelin and glutamic acid decarboxylase67 (GAD67) expression in schizophrenia and bipolar disorder: a postmortem brain study. *Arch Gen Psychiatry,* 57**,** 1061-9.

GUMUSOGLU, S. B., FINE, R. S., MURRAY, S. J., BITTLE, J. L. & STEVENS, H. E. 2017. The role of IL-6 in neurodevelopment after prenatal stress. *Brain Behav Immun,* 65**,** 274-283.

HAJISOLTANI, R., RASHIDY-POUR, A., VAFAEI, A. A., GHADERDOOST, B., BANDEGI, A. R. & MOTAMEDI, F. 2011. The glucocorticoid system is required for the voluntary exercise-induced enhancement of learning and memory in rats. *Behav Brain Res,* 219**,** 75-81.

HAMEETE, B. C., FERNÁNDEZ-CALLEJA, J. M. S., DE GROOT, M. W. G. D., OPPEWAL, T. R., TIEMESSEN, M. M., HOGENKAMP, A., DE VRIES, R. B. M. & GROENINK, L. 2021. The poly(I:C)-induced maternal immune activation model; a systematic review and meta-analysis of cytokine levels in the offspring. *Brain Behav Immun Health,* 11**,** 100192.

HAN, M., ZHANG, J. C., YAO, W., YANG, C., ISHIMA, T., REN, Q., MA, M., DONG, C., HUANG, X. F. & HASHIMOTO, K. 2016. Intake of 7,8-Dihydroxyflavone During Juvenile and Adolescent Stages Prevents Onset of Psychosis in Adult Offspring After Maternal Immune Activation. *Sci Rep,* 6**,** 36087.

HAN, Q. Q., SHEN, S. Y., CHEN, X. R., PILOT, A., LIANG, L. F., ZHANG, J. R., LI, W. H., FU, Y., LE, J. M., CHEN, P. Q. & YU, J. 2022a. Minocycline alleviates abnormal microglial phagocytosis of synapses in a mouse model of depression. *Neuropharmacology,* 220**,** 109249.

HAN, Y., LI, X., YANG, L., ZHANG, D., LI, L., DONG, X., LI, Y., QUN, S. & LI, W. 2022b. Ginsenoside Rg1 attenuates cerebral ischemia-reperfusion injury due to inhibition of NOX2-mediated calcium homeostasis dysregulation in mice. *J Ginseng Res,* 46**,** 515-525.

HAO, K., SU, X., LUO, B., CAI, Y., CHEN, T., YANG, Y., SHAO, M., SONG, M., ZHANG, L., ZHONG, Z., LI, W. & LV, L. 2019. Prenatal immune activation induces age-related alterations in rat offspring: Effects upon NMDA receptors and behaviors. *Behav Brain Res,* 370**,** 111946.

HAO, L. Y., HAO, X. Q., LI, S. H. & LI, X. H. 2010. Prenatal exposure to lipopolysaccharide results in cognitive deficits in age-increasing offspring rats. *Neuroscience,* 166**,** 763-70.

HARB, M., JAGUSCH, J., DURAIRAJA, A., ENDRES, T., LEßMANN, V. & FENDT, M. 2021. BDNF haploinsufficiency induces behavioral endophenotypes of schizophrenia in male mice that are rescued by enriched environment. *Transl Psychiatry,* 11**,** 233.

HARKNESS, J. H., GONZALEZ, A. E., BUSHANA, P. N., JORGENSEN, E. T., HEGARTY, D. M., DI NARDO, A. A., PROCHIANTZ, A., WISOR, J. P., AICHER, S. A., BROWN, T. E. & SORG, B. A. 2021. Diurnal changes in perineuronal nets and parvalbumin neurons in the rat medial prefrontal cortex. *Brain Struct Funct,* 226**,** 1135-1153.

HARRIS, V. M. 2015. Protein detection by Simple Western™ analysis. *Methods Mol Biol,* 1312**,** 465-8.

HARRISON, P. J., HUSAIN, S. M., LEE, H., LOS ANGELES, A., COLBOURNE, L., MOULD, A., HALL, N. A. L., HAERTY, W. & TUNBRIDGE, E. M. 2022. CACNA1C (CaV1.2) and other L-type calcium channels in the pathophysiology and treatment of psychiatric disorders: Advances from functional genomics and pharmacoepidemiology. *Neuropharmacology,* 220**,** 109262.

HÄRTIG, W., BRAUER, K. & BRUCKNER, G. 1992. Wisteria floribunda agglutinin-labelled nets surround parvalbumin-containing neurons. *Neuroreport,* 3**,** 869-72.

HARVEY, L. & BOKSA, P. 2012. A stereological comparison of GAD67 and reelin expression in the hippocampal stratum oriens of offspring from two mouse models of maternal inflammation during pregnancy. *Neuropharmacology,* 62**,** 1767-76.

HASCALL, V. & LAURENT, T. 1997. *Hyaluronan: Structure and Physical Properties* [Online]. Available: https://www.glycoforum.gr.jp/article/01A2.html [Accessed 05/06/2019].

HASHIMOTO, T., BERGEN, S. E., NGUYEN, Q. L., XU, B., MONTEGGIA, L. M., PIERRI, J. N., SUN, Z., SAMPSON, A. R. & LEWIS, D. A. 2005. Relationship of brain-derived neurotrophic factor and its receptor TrkB to altered inhibitory prefrontal circuitry in schizophrenia. *J Neurosci,* 25**,** 372-83.

HASHIMOTO, T., VOLK, D. W., EGGAN, S. M., MIRNICS, K., PIERRI, J. N., SUN, Z., SAMPSON, A. R. & LEWIS, D. A. 2003. Gene expression deficits in a subclass of GABA neurons in the prefrontal cortex of subjects with schizophrenia. *J Neurosci,* 23**,** 6315-26.

HAWKINS, C. L. & DAVIES, M. J. 2019. Detection, identification, and quantification of oxidative protein modifications. *J Biol Chem,* 294**,** 19683-19708.

HAYASHI, Y. 2022. Molecular mechanism of hippocampal long-term potentiation - Towards multiscale understanding of learning and memory. *Neurosci Res,* 175**,** 3-15.

HE, J., LIU, F., ZU, Q., XU, Z., ZHENG, H., LI, X. & WANG, W. 2018. Chronic administration of quetiapine attenuates the phencyclidine-induced recognition memory impairment and hippocampal oxidative stress in rats. *Neuroreport,* 29**,** 1099-1103.

HEANEY, L. 2020. Exercise in the subchronic phencyclidine rat model for schizophrenia: mechanisms and effects on cognitive deficits.

HEMMERLE, A. M., AHLBRAND, R., BRONSON, S. L., LUNDGREN, K. H., RICHTAND, N. M. & SEROOGY, K. B. 2015. Modulation of schizophrenia-related genes in the forebrain of adolescent and adult rats exposed to maternal immune activation. *Schizophr Res,* 168**,** 411-20.

HENRÍQUEZ-OLGUÍN, C., DÍAZ-VEGAS, A., UTRERAS-MENDOZA, Y., CAMPOS, C., ARIAS-CALDERÓN, M., LLANOS, P., CONTRERAS-FERRAT, A., ESPINOSA, A., ALTAMIRANO, F., JAIMOVICH, E. & VALLADARES, D. M. 2016. NOX2 Inhibition Impairs Early Muscle Gene Expression Induced by a Single Exercise Bout. *Front Physiol,* 7**,** 282.

HENSCH, T. K. 2005. Critical period plasticity in local cortical circuits. *Nat Rev Neurosci,* 6**,** 877-88.

HILL, M. A. 2023. *Embryology Animal Development.* [Online]. Retrieved from https://embryology.med.unsw.edu.au/embryology/index.php/Animal_Development. Available: https://embryology.med.unsw.edu.au/embryology/index.php/Animal_Development [Accessed].

HILL, S. K., BEERS, S. R., KMIEC, J. A., KESHAVAN, M. S. & SWEENEY, J. A. 2004. Impairment of verbal memory and learning in antipsychotic-naïve patients with first-episode schizophrenia. *Schizophr Res,* 68**,** 127-36.

HISKENS, M. I., VELLA, R. K., SCHNEIDERS, A. G. & FENNING, A. S. 2021. Minocycline improves cognition and molecular measures of inflammation and neurodegeneration following repetitive mTBI. *Brain Inj,* 35**,** 831-841.

HJORTHØJ, C., STÜRUP, A. E., MCGRATH, J. J. & NORDENTOFT, M. 2017. Years of potential life lost and life expectancy in schizophrenia: a systematic review and meta-analysis. *Lancet Psychiatry,* 4**,** 295-301.

HO, N. F., LEE, B. J. H., TNG, J. X. J., LAM, M. Z. Y., CHEN, G., WANG, M., ZHOU, J., KEEFE, R. S. E. & SIM, K. 2020. Corticolimbic brain anomalies are associated with cognitive subtypes in psychosis: A longitudinal study. *Eur Psychiatry,* 63**,** e40.

HOFFMAN-GOETZ, L., PERVAIZ, N. & GUAN, J. 2009. Voluntary exercise training in mice increases the expression of antioxidant enzymes and decreases the expression of TNF-alpha in intestinal lymphocytes. *Brain Behav Immun,* 23**,** 498-506.

HOFTMAN, G. D., VOLK, D. W., BAZMI, H. H., LI, S., SAMPSON, A. R. & LEWIS, D. A. 2015. Altered cortical expression of GABA-related genes in schizophrenia: illness progression vs developmental disturbance. *Schizophr Bull,* 41**,** 180-91.

HOLMES, M. M., GALEA, L. A., MISTLBERGER, R. E. & KEMPERMANN, G. 2004. Adult hippocampal neurogenesis and voluntary running activity: circadian and dose-dependent effects. *J Neurosci Res,* 76**,** 216-22.

HOMAYOUN, H. & MOGHADDAM, B. 2007. NMDA receptor hypofunction produces opposite effects on prefrontal cortex interneurons and pyramidal neurons. *J Neurosci,* 27**,** 11496-500.

HOPKINS, M. E. & BUCCI, D. J. 2010. BDNF expression in perirhinal cortex is associated with exercise-induced improvement in object recognition memory. *Neurobiol Learn Mem,* 94**,** 278-84.

HOPKINS, M. E., NITECKI, R. & BUCCI, D. J. 2011. Physical exercise during adolescence versus adulthood: differential effects on object recognition memory and brain-derived neurotrophic factor levels. *Neuroscience,* 194**,** 84-94.

HOU, Y., ZHANG, H., XIE, G., CAO, X., ZHAO, Y., LIU, Y., MAO, Z., YANG, J. & WU, C. 2013. Neuronal injury, but not microglia activation, is associated with ketamine-induced experimental schizophrenic model in mice. *Prog Neuropsychopharmacol Biol Psychiatry,* 45**,** 107-16.

HOUENOU, J., BOISGONTIER, J., HENRION, A., D'ALBIS, M. A., DUMAINE, A., LINKE, J., WESSA, M., DABAN, C., HAMDANI, N., DELAVEST, M., LLORCA, P. M., LANÇON, C., SCHÜRHOFF, F., SZÖKE, A., LE CORVOISIER, P., BARAU, C., POUPON, C., ETAIN, B., LEBOYER, M. & JAMAIN, S. 2017. A Multilevel Functional Study of a SNAP25 At-Risk Variant for Bipolar Disorder and Schizophrenia. *J Neurosci,* 37**,** 10389-10397.

HOWARD, M. W., RIZZUTO, D. S., CAPLAN, J. B., MADSEN, J. R., LISMAN, J., ASCHENBRENNER-SCHEIBE, R., SCHULZE-BONHAGE, A. & KAHANA, M. J. 2003. Gamma oscillations correlate with working memory load in humans. *Cereb Cortex,* 13**,** 1369-74.

HOWELL, M. D., TORRES-COLLADO, A. X., IRUELA-ARISPE, M. L. & GOTTSCHALL, P. E. 2012. Selective decline of synaptic protein levels in the frontal cortex of female mice deficient in the extracellular metalloproteinase ADAMTS1. *PLoS One,* 7**,** e47226.

HOWES, O. D. & KAPUR, S. 2009. The dopamine hypothesis of schizophrenia: version III--the final common pathway. *Schizophr Bull,* 35**,** 549-62.

HU, C., CHEN, W., MYERS, S. J., YUAN, H. & TRAYNELIS, S. F. 2016. Human GRIN2B variants in neurodevelopmental disorders. *J Pharmacol Sci,* 132**,** 115-121.

HU, H., GAN, J. & JONAS, P. 2014. Interneurons. Fast-spiking, parvalbumin^{+} GABAergic interneurons: from cellular design to microcircuit function. *Science,* 345**,** 1255263.

HU, T. M., WU, C. L., HSU, S. H., TSAI, H. Y., CHENG, F. Y. & CHENG, M. C. 2022. Ultrarare Loss-of-Function Mutations in the Genes Encoding the Ionotropic Glutamate Receptors of Kainate Subtypes Associated with Schizophrenia Disrupt the Interaction with PSD95. *J Pers Med,* 12.

HU, W., MACDONALD, M. L., ELSWICK, D. E. & SWEET, R. A. 2015. The glutamate hypothesis of schizophrenia: evidence from human brain tissue studies. *Ann N Y Acad Sci,* 1338**,** 38-57.

HUANG, D. X., YU, X., YU, W. J., ZHANG, X. M., LIU, C., LIU, H. P., SUN, Y. & JIANG, Z. P. 2022. Calcium Signaling Regulated by Cellular Membrane Systems and Calcium Homeostasis Perturbed in Alzheimer's Disease. *Front Cell Dev Biol,* 10**,** 834962.

HUANG, W. T., NIU, K. C., CHANG, C. K., LIN, M. T. & CHANG, C. P. 2008. Curcumin inhibits the increase of glutamate, hydroxyl radicals and PGE2 in the hypothalamus and reduces fever during LPS-induced systemic inflammation in rabbits. *Eur J Pharmacol,* 593**,** 105-11.

HUANG, Y., JIANG, H., ZHENG, Q., FOK, A. H. K., LI, X., LAU, C. G. & LAI, C. S. W. 2021a. Environmental enrichment or selective activation of parvalbumin-expressing interneurons ameliorates synaptic and behavioral deficits in animal models with schizophrenia-like behaviors during adolescence. *Mol Psychiatry,* 26**,** 2533-2552.

HUANG, Z., CHEN, B., LIU, X., LI, H., XIE, L., GAO, Y., DUAN, R., LI, Z., ZHANG, J., ZHENG, Y. & SU, W. 2021b. Effects of sex and aging on the immune cell landscape as assessed by single-cell transcriptomic analysis. *Proc Natl Acad Sci U S A,* 118.

HUCKER, H. B., HUTT, J. E., WHITE, S. D., ARISON, B. H. & ZACCHEI, A. G. 1983. Disposition and metabolism of (+)-5-methyl-10,11-dihydro-5H-dibenzo[a,d] cyclohepten-5,10-imine in rats, dogs, and monkeys. *Drug Metab Dispos,* 11**,** 54-8.

HUI-GUO, L., KUI, L., YAN-NING, Z. & YONG-JIAN, X. 2010. Apocynin attenuate spatial learning deficits and oxidative responses to intermittent hypoxia. *Sleep Med,* 11**,** 205-12.

HUNTER, C. A. & JONES, S. A. 2015. IL-6 as a keystone cytokine in health and disease. *Nat Immunol,* 16**,** 448-57.

HUNYADI, A. 2019. The mechanism(s) of action of antioxidants: From scavenging reactive oxygen/nitrogen species to redox signaling and the generation of bioactive secondary metabolites. *Med Res Rev,* 39**,** 2505-2533.

HWANG, D. S., KWAK, H. B., KO, I. G., KIM, S. E., JIN, J. J., JI, E. S., CHOI, H. H. & KWON, O. Y. 2016. Treadmill Exercise Improves Memory Function Depending on Circadian Rhythm Changes in Mice. *Int Neurourol J,* 20**,** S141-149.

IBI, D., NAKASAI, G., KOIDE, N., SAWAHATA, M., KOHNO, T., TAKABA, R., NAGAI, T., HATTORI, M., NABESHIMA, T., YAMADA, K. & HIRAMATSU, M. 2020. Reelin Supplementation Into the Hippocampus Rescues Abnormal Behavior in a Mouse Model of Neurodevelopmental Disorders. *Front Cell Neurosci,* 14**,** 285.

INAN, M., ZHAO, M., MANUSZAK, M., KARAKAYA, C., RAJADHYAKSHA, A. M., PICKEL, V. M., SCHWARTZ, T. H., GOLDSTEIN, P. A. & MANFREDI, G. 2016. Energy deficit in parvalbumin neurons leads to circuit dysfunction, impaired sensory gating and social disability. *Neurobiol Dis,* 93**,** 35-46.

IRITANI, S., NIIZATO, K., NAWA, H., IKEDA, K. & EMSON, P. C. 2003. Immunohistochemical study of brain-derived neurotrophic factor and its receptor, TrkB, in the hippocampal formation of schizophrenic brains. *Prog Neuropsychopharmacol Biol Psychiatry,* 27**,** 801-7.

ISSA, G., WILSON, C., TERRY, A. V., JR. & PILLAI, A. 2010. An inverse relationship between cortisol and BDNF levels in schizophrenia: data from human postmortem and animal studies. *Neurobiol Dis,* 39**,** 327-33.

ITO, W., CHEHAB, M., THAKUR, S., LI, J. & MOROZOV, A. 2011. BDNF-restricted knockout mice as an animal model for aggression. *Genes Brain Behav,* 10**,** 365-74.

IWAYAMA-SHIGENO, Y., YAMADA, K., ITOKAWA, M., TOYOTA, T., MEERABUX, J. M., MINABE, Y., MORI, N., INADA, T. & YOSHIKAWA, T. 2005. Extended analyses support the association of a functional (GT)n polymorphism in the GRIN2A promoter with Japanese schizophrenia. *Neurosci Lett,* 378**,** 102-5.

JANSEN, K. L. R. 2004. *Ketamine: Dreams and Realities*, MAPS.

JARDRI, R., HUGDAHL, K., HUGHES, M., BRUNELIN, J., WATERS, F., ALDERSON-DAY, B., SMAILES, D., STERZER, P., CORLETT, P. R., LEPTOURGOS, P., DEBBANÉ, M., CACHIA, A. & DENÈVE, S. 2016. Are Hallucinations Due to an Imbalance Between Excitatory and Inhibitory Influences on the Brain? *Schizophr Bull,* 42**,** 1124-34.

JENKINS, T. A., HARTE, M. K., MCKIBBEN, C. E., ELLIOTT, J. J. & REYNOLDS, G. P. 2008. Disturbances in social interaction occur along with pathophysiological deficits following sub-chronic phencyclidine administration in the rat. *Behav Brain Res,* 194**,** 230-5.

JENKINS, T. A., HARTE, M. K. & REYNOLDS, G. P. 2010. Effect of subchronic phencyclidine administration on sucrose preference and hippocampal parvalbumin immunoreactivity in the rat. *Neurosci Lett,* 471**,** 144-7.

JENTSCH, J. D. & ROTH, R. H. 1999. The neuropsychopharmacology of phencyclidine: from NMDA receptor hypofunction to the dopamine hypothesis of schizophrenia. *Neuropsychopharmacology,* 20**,** 201-25.

JI, M. H., LEI, L., GAO, D. P., TONG, J. H., WANG, Y. & YANG, J. J. 2020. Neural network disturbance in the medial prefrontal cortex might contribute to cognitive impairments induced by neuroinflammation. *Brain Behav Immun,* 89**,** 133-144.

JI, M. H., QIU, L. L., TANG, H., JU, L. S., SUN, X. R., ZHANG, H., JIA, M., ZUO, Z. Y., SHEN, J. C. & YANG, J. J. 2015. Sepsis-induced selective parvalbumin interneuron phenotype loss and cognitive impairments may be mediated by NADPH oxidase 2 activation in mice. *J Neuroinflammation,* 12**,** 182.

JIANG, Z., ROMPALA, G. R., ZHANG, S., COWELL, R. M. & NAKAZAWA, K. 2013. Social isolation exacerbates schizophrenia-like phenotypes via oxidative stress in cortical interneurons. *Biol Psychiatry,* 73**,** 1024-34.

JIN, J. J., KO, I. G., KIM, S. E., HWANG, L., LEE, M. G., KIM, D. Y. & JUNG, S. Y. 2017. Age-dependent differences of treadmill exercise on spatial learning ability between young- and adult-age rats. *J Exerc Rehabil,* 13**,** 381-386.

JOHNSON, L., CRAWFORD, L., ZOU, L. & LOPRINZI, P. D. 2019. Experimental Effects of Acute Exercise in Attenuating Memory Interference: Considerations by Biological Sex. *Medicina (Kaunas),* 55.

JONAS, K., LIAN, W., CALLAHAN, J., RUGGERO, C. J., CLOUSTON, S., REICHENBERG, A., CARLSON, G. A., BROMET, E. J. & KOTOV, R. 2022. The Course of General Cognitive Ability in Individuals With Psychotic Disorders. *JAMA Psychiatry,* 79**,** 659-666.

JURADO, C. 2013. Blood. *In:* SIEGEL, J. A., SAUKKO, P. J. & HOUCK, M. M. (eds.) *Encyclopedia of Forensic Sciences (Second Edition).* Waltham: Academic Press.

KALLER, C. P., LOOSLI, S. V., RAHM, B., GÖSSEL, A., SCHIETING, S., HORNIG, T., HENNIG, J., TEBARTZ VAN ELST, L., WEILLER, C. & KATZEV, M. 2014. Working memory in schizophrenia: behavioral and neural evidence for reduced susceptibility to item-specific proactive interference. *Biol Psychiatry,* 76**,** 486-94.

KANN, O., HUCHZERMEYER, C., KOVACS, R., WIRTZ, S. & SCHUELKE, M. 2011. Gamma oscillations in the hippocampus require high complex I gene expression and strong functional performance of mitochondria. *Brain,* 134**,** 345-58.

KANN, O., PAPAGEORGIOU, I. E. & DRAGUHN, A. 2014. Highly energized inhibitory interneurons are a central element for information processing in cortical networks. *J Cereb Blood Flow Metab,* 34**,** 1270-82.

KANTERS, S. 2022. Fixed- and Random-Effects Models. *Methods Mol Biol,* 2345**,** 41-65.

KARSTEN, E., BREEN, E. & HERBERT, B. R. 2018. Red blood cells are dynamic reservoirs of cytokines. *Sci Rep,* 8**,** 3101.

KARUBE, F., KUBOTA, Y. & KAWAGUCHI, Y. 2004. Axon branching and synaptic bouton phenotypes in GABAergic nonpyramidal cell subtypes. *J Neurosci,* 24**,** 2853-65.

KAUSHIK, R., LIPACHEV, N., MATUSZKO, G., KOCHNEVA, A., DVOEGLAZOVA, A., BECKER, A., PAVELIEV, M. & DITYATEV, A. 2021. Fine structure analysis of perineuronal nets in the ketamine model of schizophrenia. *Eur J Neurosci,* 53**,** 3988-4004.

KAWAGUCHI, Y. & KUBOTA, Y. 1997. GABAergic cell subtypes and their synaptic connections in rat frontal cortex. *Cereb Cortex,* 7**,** 476-86.

KAWAI, T., ADACHI, O., OGAWA, T., TAKEDA, K. & AKIRA, S. 1999. Unresponsiveness of MyD88-deficient mice to endotoxin. *Immunity,* 11**,** 115-22.

KEILHOFF, G., BERNSTEIN, H. G., BECKER, A., GRECKSCH, G. & WOLF, G. 2004. Increased neurogenesis in a rat ketamine model of schizophrenia. *Biol Psychiatry,* 56**,** 317-22.

KEITH, D. & EL-HUSSEINI, A. 2008. Excitation Control: Balancing PSD-95 Function at the Synapse. *Front Mol Neurosci,* 1**,** 4.

KELLY, D. L., SULLIVAN, K. M., MCEVOY, J. P., MCMAHON, R. P., WEHRING, H. J., GOLD, J. M., LIU, F., WARFEL, D., VYAS, G., RICHARDSON, C. M., FISCHER, B. A., KELLER, W. R., KOOLA, M. M., FELDMAN, S. M., RUSS, J. C., KEEFE, R. S., OSING, J., HUBZIN, L., AUGUST, S., WALKER, T. M. & BUCHANAN, R. W. 2015. Adjunctive Minocycline in Clozapine-Treated Schizophrenia Patients With Persistent Symptoms. *J Clin Psychopharmacol,* 35**,** 374-81.

KENTNER, A. C., KHOURY, A., LIMA QUEIROZ, E. & MACRAE, M. 2016. Environmental enrichment rescues the effects of early life inflammation on markers of synaptic transmission and plasticity. *Brain Behav Immun,* 57**,** 151-160.

KEPECS, A. & FISHELL, G. 2014. Interneuron cell types are fit to function. *Nature,* 505**,** 318-26.

KETTENMANN, H., KIRCHHOFF, F. & VERKHRATSKY, A. 2013. Microglia: new roles for the synaptic stripper. *Neuron,* 77**,** 10-8.

KHALIL, O. S., FORREST, C. M., PISAR, M., SMITH, R. A., DARLINGTON, L. G. & STONE, T. W. 2013. Prenatal activation of maternal TLR3 receptors by viral-mimetic poly(I:C) modifies GluN2B expression in embryos and sonic hedgehog in offspring in the absence of kynurenine pathway activation. *Immunopharmacol Immunotoxicol,* 35**,** 581-93.

KHANDAKER, G. M., ZIMBRON, J., LEWIS, G. & JONES, P. B. 2013. Prenatal maternal infection, neurodevelopment and adult schizophrenia: a systematic review of population-based studies. *Psychol Med,* 43**,** 239-57.

KIERDORF, K. & PRINZ, M. 2013. Factors regulating microglia activation. *Front Cell Neurosci,* 7**,** 44.

KIM, J. E. & KANG, T. C. 2017a. p47Phox/CDK5/DRP1-Mediated Mitochondrial Fission Evokes PV Cell Degeneration in the Rat Dentate Gyrus Following Status Epilepticus. *Front Cell Neurosci,* 11**,** 267.

KIM, J. H. 2019. Multicollinearity and misleading statistical results. *Korean J Anesthesiol,* 72**,** 558-569.

KIM, S. H., KO, Y. J. & BAEK, S. S. 2021. Resistance exercise improves short-term memory through inactivation of NF-κB pathway in mice with Parkinson disease. *J Exerc Rehabil,* 17**,** 81-87.

KIM, S. Y., COHEN, B. M., CHEN, X., LUKAS, S. E., SHINN, A. K., YUKSEL, A. C., LI, T., DU, F. & ÖNGÜR, D. 2017b. Redox Dysregulation in Schizophrenia Revealed by in vivo NAD+/NADH Measurement. *Schizophr Bull,* 43**,** 197-204.

KIM, T. W., KANG, H. S., PARK, J. K., LEE, S. J., BAEK, S. B. & KIM, C. J. 2014. Voluntary wheel running ameliorates symptoms of MK-801-induced schizophrenia in mice. *Mol Med Rep,* 10**,** 2924-30.

KIM, Y. M., JI, E. S., YOON, S. J. & YOON, J. H. 2013. Sudden detraining deteriorates swimming training-induced enhancement of short-term and spatial learning memories in mice. *J Exerc Rehabil,* 9**,** 243-9.

KING, M. V., KURIAN, N., QIN, S., PAPADOPOULOU, N., WESTERINK, B. H., CREMERS, T. I., EPPING-JORDAN, M. P., LE POUL, E., RAY, D. E., FONE, K. C., KENDALL, D. A., MARSDEN, C. A. & SHARP, T. V. 2014. Lentiviral delivery of a vesicular glutamate transporter 1

(VGLUT1)-targeting short hairpin RNA vector into the mouse hippocampus impairs cognition. *Neuropsychopharmacology,* 39**,** 464-76.

KINNEY, J. W., DAVIS, C. N., TABAREAN, I., CONTI, B., BARTFAI, T. & BEHRENS, M. M. 2006. A specific role for NR2A-containing NMDA receptors in the maintenance of parvalbumin and GAD67 immunoreactivity in cultured interneurons. *J Neurosci,* 26**,** 1604-15.

KIRKBRIDE, J. B., ERRAZURIZ, A., CROUDACE, T. J., MORGAN, C., JACKSON, D., BOYDELL, J., MURRAY, R. M. & JONES, P. B. 2012. Incidence of schizophrenia and other psychoses in England, 1950-2009: a systematic review and meta-analyses. *PLoS One,* 7**,** e31660.

KITCHEN, H., ROFAIL, D., HERON, L. & SACCO, P. 2012. Cognitive impairment associated with schizophrenia: a review of the humanistic burden. *Adv Ther,* 29**,** 148-62.

KLAUSBERGER, T. & SOMOGYI, P. 2008. Neuronal diversity and temporal dynamics: the unity of hippocampal circuit operations. *Science,* 321**,** 53-7.

KO, Y. J. & KO, I. G. 2020. Voluntary Wheel Running Improves Spatial Learning Memory by Suppressing Inflammation and Apoptosis via Inactivation of Nuclear Factor Kappa B in Brain Inflammation Rats. *Int Neurourol J,* 24**,** 96-103.

KOBAYASHI, K., IMAGAMA, S., OHGOMORI, T., HIRANO, K., UCHIMURA, K., SAKAMOTO, K., HIRAKAWA, A., TAKEUCHI, H., SUZUMURA, A., ISHIGURO, N. & KADOMATSU, K. 2013. Minocycline selectively inhibits M1 polarization of microglia. *Cell Death Dis,* 4**,** e525.

KOIZUMI, H., HIRAGA, T., OHAROMARI, L. K., HATA, T., SHIMA, T., YOOK, J. S., OKAMOTO, M., MOURI, A., NABESHIMA, T. & SOYA, H. 2021. Preventive role of regular low-intensity exercise during adolescence in schizophrenia model mice with abnormal behaviors. *Biochem Biophys Res Commun,* 534**,** 610-616.

KOLB, B., HARKER, A. & GIBB, R. 2017. Principles of plasticity in the developing brain. *Dev Med Child Neurol,* 59**,** 1218-1223.

KOMAL, A., NOREEN, M. & EL-KOTT, A. F. 2021. TLR3 agonists: RGC100, ARNAX, and poly-IC: a comparative review. *Immunol Res,* 69**,** 312-322.

KONDO, M., SUMINO, R. & OKADO, H. 1997. Combinations of AMPA receptor subunit expression in individual cortical neurons correlate with expression of specific calcium-binding proteins. *J Neurosci,* 17**,** 1570-81.

KOROTKOVA, T., FUCHS, E. C., PONOMARENKO, A., VON ENGELHARDT, J. & MONYER, H. 2010. NMDA receptor ablation on parvalbumin-positive interneurons impairs hippocampal synchrony, spatial representations, and working memory. *Neuron,* 68**,** 557-69.

KOSEKI, T., MOURI, A., MAMIYA, T., AOYAMA, Y., TORIUMI, K., SUZUKI, S., NAKAJIMA, A., YAMADA, T., NAGAI, T. & NABESHIMA, T. 2012. Exposure to enriched environments during adolescence prevents abnormal behaviours associated with histone deacetylation in phencyclidine-treated mice. *Int J Neuropsychopharmacol,* 15**,** 1489-501.

KOTERMANSKI, S. E. & JOHNSON, J. W. 2009. Mg2+ imparts NMDA receptor subtype selectivity to the Alzheimer's drug memantine. *J Neurosci,* 29**,** 2774-9.

KOTLICKA-ANTCZAK, M., PAWEŁCZYK, A., RABE-JABŁOŃSKA, J., SMIGIELSKI, J. & PAWEŁCZYK, T. 2014. Obstetrical complications and Apgar score in subjects at risk of psychosis. *J Psychiatr Res,* 48**,** 79-85.

KOWASH, H. M., POTTER, H. G., EDYE, M. E., PRINSSEN, E. P., BANDINELLI, S., NEILL, J. C., HAGER, R. & GLAZIER, J. D. 2019. Poly(I:C) source, molecular weight and endotoxin contamination affect dam and prenatal outcomes, implications for models of maternal immune activation. *Brain Behav Immun,* 82**,** 160-166.

KOWASH, H. M., POTTER, H. G., WOODS, R. M., ASHTON, N., HAGER, R., NEILL, J. C. & GLAZIER, J. D. 2022. Maternal immune activation in rats induces dysfunction of placental leucine transport and alters fetal brain growth. *Clin Sci (Lond),* 136**,** 1117-1137.

KOWIAŃSKI, P., LIETZAU, G., CZUBA, E., WAŚKOW, M., STELIGA, A. & MORYŚ, J. 2018. BDNF: A Key Factor with Multipotent Impact on Brain Signaling and Synaptic Plasticity. *Cell Mol Neurobiol,* 38**,** 579-593.

KRAFTS, K., HEMPELMANN, E. & SKÓRSKA-STANIA, A. 2012. From methylene blue to chloroquine: a brief review of the development of an antimalarial therapy. *Parasitol Res,* 111**,** 1-6.

KRAWCZYK, M., RAMANI, M., DIAN, J., FLOREZ, C. M., MYLVAGANAM, S., BRIEN, J., REYNOLDS, J., KAPUR, B., ZOIDL, G., POULTER, M. O. & CARLEN, P. L. 2016. Hippocampal hyperexcitability in fetal alcohol spectrum disorder: Pathological sharp waves and excitatory/inhibitory synaptic imbalance. *Exp Neurol,* 280**,** 70-9.

KRETSINGER, R. H. & MONCRIEF, N. D. 1989. Evolution of calcium modulated proteins. *Va Explor,* 5**,** 7-9.

KRISTÓF, Z., BARANYI, M., TOD, P., MUT-ARBONA, P., DEMETER, K., BITTER, I. & SPERLÁGH, B. 2022. Elevated Serum Purine Levels in Schizophrenia: A Reverse Translational Study to Identify Novel Inflammatory Biomarkers. *Int J Neuropsychopharmacol,* 25**,** 645-659.

KUMAR, S. P. & BABU, P. P. 2022. NADPH Oxidase: a Possible Therapeutic Target for Cognitive Impairment in Experimental Cerebral Malaria. *Mol Neurobiol,* 59**,** 800-820.

KUMAR, V., SINGH, B. K., CHAUHAN, A. K., SINGH, D., PATEL, D. K. & SINGH, C. 2016. Minocycline Rescues from Zinc-Induced Nigrostriatal Dopaminergic Neurodegeneration: Biochemical and Molecular Interventions. *Mol Neurobiol,* 53**,** 2761-2777.

KUMARASINGHE, N., BEVERIDGE, N. J., GARDINER, E., SCOTT, R. J., YASAWARDENE, S., PERERA, A., MENDIS, J., SURIYAKUMARA, K., SCHALL, U. & TOONEY, P. A. 2013. Gene expression profiling in treatment-naive schizophrenia patients identifies abnormalities in biological pathways involving AKT1 that are corrected by antipsychotic medication. *Int J Neuropsychopharmacol,* 16**,** 1483-503.

KWOK, J. C., CARULLI, D. & FAWCETT, J. W. 2010. In vitro modeling of perineuronal nets: hyaluronan synthase and link protein are necessary for their formation and integrity. *J Neurochem,* 114**,** 1447-59.

KWON, J. S., O'DONNELL, B. F., WALLENSTEIN, G. V., GREENE, R. W., HIRAYASU, Y., NESTOR, P. G., HASSELMO, M. E., POTTS, G. F., SHENTON, M. E. & MCCARLEY, R. W. 1999. Gamma frequency-range abnormalities to auditory stimulation in schizophrenia. *Arch Gen Psychiatry,* 56**,** 1001-5.

LABOUESSE, M. A., DONG, E., GRAYSON, D. R., GUIDOTTI, A. & MEYER, U. 2015. Maternal immune activation induces GAD1 and GAD2 promoter remodeling in the offspring prefrontal cortex. *Epigenetics,* 10**,** 1143-55.

LAN, L., WANG, H., ZHANG, X., SHEN, Q., LI, X., HE, L., RONG, X., PENG, J., MO, J. & PENG, Y. 2022. Chronic exposure of alcohol triggers microglia-mediated synaptic elimination inducing cognitive impairment. *Exp Neurol,* 353**,** 114061.

LANDRETH, K., SIMANAVICIUTE, U., FLETCHER, J., GRAYSON, B., GRANT, R. A., HARTE, M. H. & GIGG, J. 2020. Dissociating the effects of distraction and proactive interference on object memory through tests of novelty preference. *bioRxiv***,** 2020.08.16.253179.

LANGE, T., DIMITROV, S. & BORN, J. 2010. Effects of sleep and circadian rhythm on the human immune system. *Ann N Y Acad Sci,* 1193**,** 48-59.

LANZ, T. A., REINHART, V., SHEEHAN, M. J., RIZZO, S. J. S., BOVE, S. E., JAMES, L. C., VOLFSON, D., LEWIS, D. A. & KLEIMAN, R. J. 2019. Postmortem transcriptional profiling reveals widespread increase in inflammation in schizophrenia: a comparison of prefrontal cortex, striatum, and hippocampus among matched tetrads of controls with subjects diagnosed with schizophrenia, bipolar or major depressive disorder. *Transl Psychiatry,* 9**,** 151.

LAU, C. G. & MURTHY, V. N. 2012. Activity-dependent regulation of inhibition via GAD67. *J Neurosci,* 32**,** 8521-31.

LAU, C. G., ZHANG, H. & MURTHY, V. N. 2022. Deletion of TrkB in parvalbumin interneurons alters cortical neural dynamics. *J Cell Physiol,* 237**,** 949-964.

LAUNDERS, N., KIRSH, L., OSBORN, D. P. J. & HAYES, J. F. 2022. The temporal relationship between severe mental illness diagnosis and chronic physical comorbidity: a UK primary care cohort study of disease burden over 10 years. *Lancet Psychiatry,* 9**,** 725-735.

LAW, A. J. & DEAKIN, J. F. 2001. Asymmetrical reductions of hippocampal NMDAR1 glutamate receptor mRNA in the psychoses. *Neuroreport,* 12**,** 2971-4.

LE ROUX, N., CABEZAS, C., BÖHM, U. L. & PONCER, J. C. 2013. Input-specific learning rules at excitatory synapses onto hippocampal parvalbumin-expressing interneurons. *J Physiol,* 591**,** 1809-22.

LEAL, G., COMPRIDO, D. & DUARTE, C. B. 2014. BDNF-induced local protein synthesis and synaptic plasticity. *Neuropharmacology,* 76 Pt C**,** 639-56.

LEE, M. C., OKAMOTO, M., LIU, Y. F., INOUE, K., MATSUI, T., NOGAMI, H. & SOYA, H. 2012. Voluntary resistance running with short distance enhances spatial memory related to hippocampal BDNF signaling. *J Appl Physiol (1985),* 113**,** 1260-6.

LEE, S. E., LEE, Y. & LEE, G. H. 2019. The regulation of glutamic acid decarboxylases in GABA neurotransmission in the brain. *Arch Pharm Res,* 42**,** 1031-1039.

LEPETA, K., PURZYCKA, K. J., PACHULSKA-WIECZOREK, K., MITJANS, M., BEGEMANN, M., VAFADARI, B., BIJATA, K., ADAMIAK, R. W., EHRENREICH, H., DZIEMBOWSKA, M. & KACZMAREK, L. 2017. A normal genetic variation modulates synaptic MMP-9 protein levels and the severity of schizophrenia symptoms. *EMBO Mol Med,* 9**,** 1100-1116.

LEUNG, W. W., BOWIE, C. R. & HARVEY, P. D. 2008. Functional implications of neuropsychological normality and symptom remission in older outpatients diagnosed with schizophrenia: A cross-sectional study. *J Int Neuropsychol Soc,* 14**,** 479-88.

LEVKOVITZ, Y., LEVI, U., BRAW, Y. & COHEN, H. 2007. Minocycline, a second-generation tetracycline, as a neuroprotective agent in an animal model of schizophrenia. *Brain Res,* 1154**,** 154-62.

LEVKOVITZ, Y., MENDLOVICH, S., RIWKES, S., BRAW, Y., LEVKOVITCH-VERBIN, H., GAL, G., FENNIG, S., TREVES, I. & KRON, S. 2010. A double-blind, randomized study of minocycline for the treatment of negative and cognitive symptoms in early-phase schizophrenia. *J Clin Psychiatry,* 71**,** 138-49.

LEWIS, D. A. 2009. Neuroplasticity of excitatory and inhibitory cortical circuits in schizophrenia. *Dialogues Clin Neurosci,* 11**,** 269-80.

LEWIS, D. A., CRUZ, D. A., MELCHITZKY, D. S. & PIERRI, J. N. 2001. Lamina-specific deficits in parvalbumin-immunoreactive varicosities in the prefrontal cortex of subjects with schizophrenia: evidence for fewer projections from the thalamus. *Am J Psychiatry,* 158**,** 1411-22.

LEWIS, D. A., HASHIMOTO, T. & VOLK, D. W. 2005. Cortical inhibitory neurons and schizophrenia. *Nat Rev Neurosci,* 6**,** 312-24.

LI, D. & HE, L. 2007. Association study between the NMDA receptor 2B subunit gene (GRIN2B) and schizophrenia: a HuGE review and meta-analysis. *Genet Med,* 9**,** 4-8.

LIAN, J., HAN, M., SU, Y., HODGSON, J. & DENG, C. 2022. The long-lasting effects of early antipsychotic exposure during juvenile period on adult behaviours - A study in a poly I:C rat model. *Pharmacol Biochem Behav,* 219**,** 173453.

LIANG, D., LI, G., LIAO, X., YU, D., WU, J. & ZHANG, M. 2016. Developmental loss of parvalbumin-positive cells in the prefrontal cortex and psychiatric anxiety after intermittent hypoxia exposures in neonatal rats might be mediated by NADPH oxidase-2. *Behav Brain Res,* 296**,** 134-140.

LIANG, J. Q., CHEN, X. & CHENG, Y. 2022. Paeoniflorin Rescued MK-801-Induced Schizophrenia-Like Behaviors in Mice via Oxidative Stress Pathway. *Front Nutr,* 9**,** 870032.

LIAO, B., ZHAO, W., BEERS, D. R., HENKEL, J. S. & APPEL, S. H. 2012. Transformation from a neuroprotective to a neurotoxic microglial phenotype in a mouse model of ALS. *Exp Neurol,* 237**,** 147-52.

LIEBERMAN, J. A., KANE, J. M. & ALVIR, J. 1987. Provocative tests with psychostimulant drugs in schizophrenia. *Psychopharmacology (Berl),* 91**,** 415-33.

LIGHT, G. A., HSU, J. L., HSIEH, M. H., MEYER-GOMES, K., SPROCK, J., SWERDLOW, N. R. & BRAFF, D. L. 2006. Gamma band oscillations reveal neural network cortical coherence dysfunction in schizophrenia patients. *Biol Psychiatry,* 60**,** 1231-40.

LIN, Y. L. & WANG, S. 2014. Prenatal lipopolysaccharide exposure increases depression-like behaviors and reduces hippocampal neurogenesis in adult rats. *Behav Brain Res,* 259**,** 24-34.

LINDAHL, J. S. & KEIFER, J. 2004. Glutamate receptor subunits are altered in forebrain and cerebellum in rats chronically exposed to the NMDA receptor antagonist phencyclidine. *Neuropsychopharmacology,* 29**,** 2065-73.

LINS, B. R., HURTUBISE, J. L., ROEBUCK, A. J., MARKS, W. N., ZABDER, N. K., SCOTT, G. A., GREBA, Q., DAWICKI, W., ZHANG, X., RUDULIER, C. D., GORDON, J. R. & HOWLAND, J. G. 2018. Prospective Analysis of the Effects of Maternal Immune Activation on Rat Cytokines during Pregnancy and Behavior of the Male Offspring Relevant to Schizophrenia. *eNeuro,* 5.

LIPTON, S. A., CHOI, Y. B., TAKAHASHI, H., ZHANG, D., LI, W., GODZIK, A. & BANKSTON, L. A. 2002. Cysteine regulation of protein function--as exemplified by NMDA-receptor modulation. *Trends Neurosci,* 25**,** 474-80.

LISMAN, J. E., COYLE, J. T., GREEN, R. W., JAVITT, D. C., BENES, F. M., HECKERS, S. & GRACE, A. A. 2008. Circuit-based framework for understanding neurotransmitter and risk gene interactions in schizophrenia. *Trends Neurosci,* 31**,** 234-42.

LIU, F., GUO, X., WU, R., OU, J., ZHENG, Y., ZHANG, B., XIE, L., ZHANG, L., YANG, L., YANG, S., YANG, J., RUAN, Y., ZENG, Y., XU, X. & ZHAO, J. 2014. Minocycline supplementation for treatment of negative symptoms in early-phase schizophrenia: a double blind, randomized, controlled trial. *Schizophr Res,* 153**,** 169-76.

LIU, F. F., YANG, L. D., SUN, X. R., ZHANG, H., PAN, W., WANG, X. M., YANG, J. J., JI, M. H. & YUAN, H. M. 2016. NOX2 Mediated-Parvalbumin Interneuron Loss Might Contribute to Anxiety-Like and Enhanced Fear Learning Behavior in a Rat Model of Post-Traumatic Stress Disorder. *Mol Neurobiol,* 53**,** 6680-6689.

LIU, J., SUZUKI, T., SEKI, T., NAMBA, T., TANIMURA, A. & ARAI, H. 2006. Effects of repeated phencyclidine administration on adult hippocampal neurogenesis in the rat. *Synapse,* 60**,** 56-68.

LIU, J., YEO, H. C., OVERVIK-DOUKI, E., HAGEN, T., DONIGER, S. J., CHYU, D. W., BROOKS, G. A. & AMES, B. N. 2000. Chronically and acutely exercised rats: biomarkers of oxidative stress and endogenous antioxidants. *J Appl Physiol (1985),* 89**,** 21-8.

LIU, L., WANG, E. Q., DU, C., CHEN, H. S. & LV, Y. 2021a. Minocycline alleviates Gulf War Illness rats via altering gut microbiome, attenuating neuroinflammation and enhancing hippocampal neurogenesis. *Behav Brain Res,* 410**,** 113366.

LIU, T., ZHANG, L., JOO, D. & SUN, S. C. 2017. NF-κB signaling in inflammation. *Signal Transduct Target Ther,* 2**,** 17023-.

LIU, X. B., MURRAY, K. D. & JONES, E. G. 2004. Switching of NMDA receptor 2A and 2B subunits at thalamic and cortical synapses during early postnatal development. *J Neurosci,* 24**,** 8885-95.

LIU, Y., OUYANG, P., ZHENG, Y., MI, L., ZHAO, J., NING, Y. & GUO, W. 2021b. A Selective Review of the Excitatory-Inhibitory Imbalance in Schizophrenia: Underlying Biology, Genetics, Microcircuits, and Symptoms. *Front Cell Dev Biol,* 9**,** 664535.

LIU, Z., FAN, Y., WON, S. J., NEUMANN, M., HU, D., ZHOU, L., WEINSTEIN, P. R. & LIU, J. 2007. Chronic treatment with minocycline preserves adult new neurons and reduces functional impairment after focal cerebral ischemia. *Stroke,* 38**,** 146-52.

LIU, Z., FANG, X. X., CHEN, Y. P., QIU, Y. H. & PENG, Y. P. 2013. Interleukin-6 prevents NMDA-induced neuronal Ca2+ overload via suppression of IP3 receptors. *Brain Inj,* 27**,** 1047-55.

LONCHAMP, E., DUPONT, J. L., DOUSSAU, F., SHIN, H. S., POULAIN, B. & BOSSU, J. L. 2009. Deletion of Cav2.1(alpha1(A)) subunit of Ca2+-channels impairs synaptic GABA and glutamate release in the mouse cerebellar cortex in cultured slices. *Eur J Neurosci,* 30**,** 2293-307.

LOPRINZI, P. D., FRITH, E. & CRAWFORD, L. 2020. The Effects of Acute Exercise on Retroactive Memory Interference. *Am J Health Promot,* 34**,** 25-31.

LORUSSO, J. M., WOODS, R. M., MCEWAN, F., GLAZIER, J. D., NEILL, J. C., HARTE, M. & HAGER, R. 2022. Clustering of cognitive phenotypes identifies susceptible and resilient offspring in a rat model of maternal immune activation and early-life stress. *Brain Behav Immun Health,* 25**,** 100514.

LOSI, G., PRYBYLOWSKI, K., FU, Z., LUO, J., WENTHOLD, R. J. & VICINI, S. 2003. PSD-95 regulates NMDA receptors in developing cerebellar granule neurons of the rat. *J Physiol,* 548**,** 21-9.

LOU, S. J., LIU, J. Y., CHANG, H. & CHEN, P. J. 2008. Hippocampal neurogenesis and gene expression depend on exercise intensity in juvenile rats. *Brain Res,* 1210**,** 48-55.

LOUREIRO, C. M., FACHIM, H. A., HARTE, M. K., DALTON, C. F. & REYNOLDS, G. P. 2022. Subchronic PCP effects on DNA methylation and protein expression of NMDA receptor subunit genes in the prefrontal cortex and hippocampus of female rats. *J Psychopharmacol,* 36**,** 238-244.

LU, X. Y., WANG, H. D., XU, J. G., DING, K. & LI, T. 2014. NADPH oxidase inhibition improves neurological outcome in experimental traumatic brain injury. *Neurochem Int,* 69**,** 14-9.

LU, Y. C., YEH, W. C. & OHASHI, P. S. 2008. LPS/TLR4 signal transduction pathway. *Cytokine,* 42**,** 145-151.

LUBY, E. D., COHEN, B. D., ROSENBAUM, G., GOTTLIEB, J. S. & KELLEY, R. 1959. Study of a new schizophrenomimetic drug; sernyl. *AMA Arch Neurol Psychiatry,* 81**,** 363-9.

LÜCK, C., HAITJEMA, C. & HEGER, C. 2021. Simple Western: Bringing the Western Blot into the Twenty-First Century. *Methods Mol Biol,* 2261**,** 481-488.

LUNDELL, A., OLIN, A. I., MÖRGELIN, M., AL-KARADAGHI, S., ASPBERG, A. & LOGAN, D. T. 2004. Structural basis for interactions between tenascins and lectican C-type lectin domains: evidence for a crosslinking role for tenascins. *Structure,* 12**,** 1495-506.

LUONI, A., RICHETTO, J., LONGO, L. & RIVA, M. A. 2017. Chronic lurasidone treatment normalizes GABAergic marker alterations in the dorsal hippocampus of mice exposed to prenatal immune activation. *Eur Neuropsychopharmacol,* 27**,** 170-179.

LÜSCHER, C. & MALENKA, R. C. 2012. NMDA receptor-dependent long-term potentiation and long-term depression (LTP/LTD). *Cold Spring Harb Perspect Biol,* 4.

MA, Y. N., SUN, Y. X., WANG, T., WANG, H., ZHANG, Y., SU, Y. A., LI, J. T. & SI, T. M. 2020. Subchronic MK-801 treatment during adolescence induces long-term, not permanent, excitatory-inhibitory imbalance in the rat hippocampus. *Eur J Pharmacol,* 867**,** 172807.

MACKINLEY, M., FORD, S. D., JEON, P., THÉBERGE, J. & PALANIYAPPAN, L. 2022. Central Oxidative Stress and Early Vocational Outcomes in First Episode Psychosis: A 7-Tesla Magnetic Resonance Spectroscopy Study of Glutathione. *Schizophr Bull,* 48**,** 921-930.

MAEDA, K., SUGINO, H., HIROSE, T., KITAGAWA, H., NAGAI, T., MIZOGUCHI, H., TAKUMA, K. & YAMADA, K. 2007. Clozapine prevents a decrease in neurogenesis in mice repeatedly treated with phencyclidine. *J Pharmacol Sci,* 103**,** 299-308.

MAINY, N., KAHANE, P., MINOTTI, L., HOFFMANN, D., BERTRAND, O. & LACHAUX, J. P. 2007. Neural correlates of consolidation in working memory. *Hum Brain Mapp,* 28**,** 183-93.

MAKSYMETZ, J., MORAN, S. P. & CONN, P. J. 2017. Targeting metabotropic glutamate receptors for novel treatments of schizophrenia. *Mol Brain,* 10**,** 15.

MALIK, A. S. & AMIN, H. U. 2017. Chapter 1 - Designing an EEG Experiment. *In:* MALIK, A. S. & AMIN, H. U. (eds.) *Designing EEG Experiments for Studying the Brain.* Academic Press.

MALLYA, A. P., WANG, H. D., LEE, H. N. R. & DEUTCH, A. Y. 2019. Microglial Pruning of Synapses in the Prefrontal Cortex During Adolescence. *Cereb Cortex,* 29**,** 1634-1643.

MANICONE, A. M. & MCGUIRE, J. K. 2008. Matrix metalloproteinases as modulators of inflammation. *Semin Cell Dev Biol,* 19**,** 34-41.

MAO, M., ZHOU, Z., SUN, M., WANG, C. & SUN, J. 2021. The dysfunction of parvalbumin interneurons mediated by microglia contributes to cognitive impairment induced by lipopolysaccharide challenge. *Neurosci Lett,* 762**,** 136133.

MARTINA, M., VIDA, I. & JONAS, P. 2000. Distal initiation and active propagation of action potentials in interneuron dendrites. *Science,* 287**,** 295-300.

MASSEY, J. M., HUBSCHER, C. H., WAGONER, M. R., DECKER, J. A., AMPS, J., SILVER, J. & ONIFER, S. M. 2006. Chondroitinase ABC digestion of the perineuronal net promotes functional collateral sprouting in the cuneate nucleus after cervical spinal cord injury. *J Neurosci,* 26**,** 4406-14.

MATHEWS, M. J., MEAD, R. N. & GALIZIO, M. 2018. Effects of N-Methyl-D-aspartate (NMDA) antagonists ketamine, methoxetamine, and phencyclidine on the odor span test of working memory in rats. *Exp Clin Psychopharmacol,* 26**,** 6-17.

MATSUURA, A., ISHIMA, T., FUJITA, Y., IWAYAMA, Y., HASEGAWA, S., KAWAHARA-MIKI, R., MAEKAWA, M., TOYOSHIMA, M., USHIDA, Y., SUGANUMA, H., KIDA, S., YOSHIKAWA, T., IYO, M. & HASHIMOTO, K. 2018. Dietary glucoraphanin prevents the onset of psychosis in the adult offspring after maternal immune activation. *Sci Rep,* 8**,** 2158.

MATUSZKO, G., CURRELI, S., KAUSHIK, R., BECKER, A. & DITYATEV, A. 2017. Extracellular matrix alterations in the ketamine model of schizophrenia. *Neuroscience,* 350**,** 13-22.

MAUNEY, S. A., ATHANAS, K. M., PANTAZOPOULOS, H., SHASKAN, N., PASSERI, E., BERRETTA, S. & WOO, T. U. 2013. Developmental pattern of perineuronal nets in the human prefrontal cortex and their deficit in schizophrenia. *Biol Psychiatry,* 74**,** 427-35.

MAYER, A. R., HANLON, F. M., DODD, A. B., YEO, R. A., HAALAND, K. Y., LING, J. M. & RYMAN, S. G. 2016. Proactive response inhibition abnormalities in the sensorimotor cortex of patients with schizophrenia. *J Psychiatry Neurosci,* 41**,** 312-21.

MCCOLL, E. R. & PIQUETTE-MILLER, M. 2019. Poly(I:C) alters placental and fetal brain amino acid transport in a rat model of maternal immune activation. *Am J Reprod Immunol,* 81**,** e13115.

MCDAID, J., MUSTALY-KALIMI, S. & STUTZMANN, G. E. 2020. Ca2+ Dyshomeostasis Disrupts Neuronal and Synaptic Function

in Alzheimer's Disease. *Cells,* 9.

MCGORRY, P. D., KILLACKEY, E. & YUNG, A. 2008. Early intervention in psychosis: concepts, evidence and future directions. *World Psychiatry,* 7**,** 148-56.

MCGRATH, J., SAHA, S., CHANT, D. & WELHAM, J. 2008. Schizophrenia: a concise overview of incidence, prevalence, and mortality. *Epidemiol Rev,* 30**,** 67-76.

MCINTYRE, R. S. 2009. Understanding needs, interactions, treatment, and expectations among individuals affected by bipolar disorder or schizophrenia: the UNITE global survey. *J Clin Psychiatry,* 70 Suppl 3**,** 5-11.

MCKIBBEN, C. E., JENKINS, T. A., ADAMS, H. N., HARTE, M. K. & REYNOLDS, G. P. 2010. Effect of pretreatment with risperidone on phencyclidine-induced disruptions in object recognition memory and prefrontal cortex parvalbumin immunoreactivity in the rat. *Behav Brain Res,* 208**,** 132-6.

MEDINA, J. H. 2018. Neural, Cellular and Molecular Mechanisms of Active Forgetting. *Front Syst Neurosci,* 12**,** 3.

MEEHL, P. E. 1962. Schizotaxia, schizotypy, schizophrenia. *The American psychologist,* 17**,** 827-838.

MELTZER, H. Y., MATSUBARA, S. & LEE, J. C. 1989. Classification of typical and atypical antipsychotic drugs on the basis of dopamine D-1, D-2 and serotonin2 pKi values. *J Pharmacol Exp Ther,* 251**,** 238-46.

MENDIOLA, A. S. & CARDONA, A. E. 2018. The IL-1β phenomena in neuroinflammatory diseases. *J Neural Transm (Vienna),* 125**,** 781-795.

MEYER, U. 2023. Sources and Translational Relevance of Heterogeneity in Maternal Immune Activation Models. *Curr Top Behav Neurosci,* 61**,** 71-91.

MEYER, U., FELDON, J., SCHEDLOWSKI, M. & YEE, B. K. 2006a. Immunological stress at the maternal-foetal interface: a link between neurodevelopment and adult psychopathology. *Brain Behav Immun,* 20**,** 378-88.

MEYER, U., NYFFELER, M., ENGLER, A., URWYLER, A., SCHEDLOWSKI, M., KNUESEL, I., YEE, B. K. & FELDON, J. 2006b. The time of prenatal immune challenge determines the specificity of inflammation-mediated brain and behavioral pathology. *J Neurosci,* 26**,** 4752-62.

MEYTHALER, J., FATH, J., FUERST, D., ZOKARY, H., FREESE, K., MARTIN, H. B., REINEKE, J., PEDUZZI-NELSON, J. & ROSKOS, P. T. 2019. Safety and feasibility of minocycline in treatment of acute traumatic brain injury. *Brain Inj,* 33**,** 679-689.

MICHALUK, P., MIKASOVA, L., GROC, L., FRISCHKNECHT, R., CHOQUET, D. & KACZMAREK, L. 2009. Matrix metalloproteinase-9 controls NMDA receptor surface diffusion through integrin beta1 signaling. *J Neurosci,* 29**,** 6007-12.

MICHEVA, K. D., CHANG, E. F., NANA, A. L., SEELEY, W. W., TING, J. T., COBBS, C., LEIN, E., SMITH, S. J., WEINBERG, R. J. & MADISON, D. V. 2018. Distinctive Structural and Molecular Features of Myelinated Inhibitory Axons in Human Neocortex. *eNeuro,* 5.

MICHEVA, K. D., WOLMAN, D., MENSH, B. D., PAX, E., BUCHANAN, J., SMITH, S. J. & BOCK, D. D. 2016. A large fraction of neocortical myelin ensheathes axons of local inhibitory neurons. *Elife,* 5.

MICÓ, J. A., ROJAS-CORRALES, M. O., GIBERT-RAHOLA, J., PARELLADA, M., MORENO, D., FRAGUAS, D., GRAELL, M., GIL, J., IRAZUSTA, J., CASTRO-FORNIELES, J., SOUTULLO, C., ARANGO, C., OTERO, S., NAVARRO, A., BAEZA, I., MARTÍNEZ-CENGOTITABENGOA, M. & GONZÁLEZ-PINTO, A. 2011. Reduced antioxidant defense in early onset first-episode psychosis: a case-control study. *BMC Psychiatry,* 11**,** 26.

MILEV, P., MAUREL, P., CHIBA, A., MEVISSEN, M., POPP, S., YAMAGUCHI, Y., MARGOLIS, R. K. & MARGOLIS, R. U. 1998. Differential regulation of expression of hyaluronan-binding proteoglycans in developing brain: aggrecan, versican, neurocan, and brevican. *Biochem Biophys Res Commun,* 247**,** 207-12.

MILLIER, A., SCHMIDT, U., ANGERMEYER, M. C., CHAUHAN, D., MURTHY, V., TOUMI, M. & CADI-SOUSSI, N. 2014. Humanistic burden in schizophrenia: a literature review. *J Psychiatr Res,* 54**,** 85-93.

MILOSEVIĆ, J., VESKOV, R., VASILEV, V., RAKIĆ, L. & RUZDIJIĆ, S. 2000. Apoptosis induction by phencyclidine in the brains of rats of different ages. *Addict Biol,* 5**,** 157-65.

MISHRA, A., REETA, K. H., SARANGI, S. C., MAITI, R. & SOOD, M. 2022. Effect of add-on alpha lipoic acid on psychopathology in patients with treatment-resistant schizophrenia: a pilot randomized double-blind placebo-controlled trial. *Psychopharmacology (Berl),* 239**,** 3525-3535.

MISSAULT, S., VAN DEN EYNDE, K., VANDEN BERGHE, W., FRANSEN, E., WEEREN, A., TIMMERMANS, J. P., KUMAR-SINGH, S. & DEDEURWAERDERE, S. 2014. The risk for behavioural deficits is determined by the maternal immune response to prenatal immune challenge in a neurodevelopmental model. *Brain Behav Immun,* 42**,** 138-46.

MITRA, S., NATARAJAN, R., ZIEDONIS, D. & FAN, X. 2017. Antioxidant and anti-inflammatory nutrient status, supplementation, and mechanisms in patients with schizophrenia. *Prog Neuropsychopharmacol Biol Psychiatry,* 78**,** 1-11.

MITSADALI, I., GRAYSON, B., IDRIS, N. F., WATSON, L., BURGESS, M. & NEILL, J. 2020. Aerobic exercise improves memory and prevents cognitive deficits of relevance to schizophrenia in an animal model. *J Psychopharmacol,* 34**,** 695-708.

MIYATA, S. & KITAGAWA, H. 2017. Formation and remodeling of the brain extracellular matrix in neural plasticity: Roles of chondroitin sulfate and hyaluronan. *Biochim Biophys Acta Gen Subj,* 1861**,** 2420-2434.

MIYOSHI, G., HJERLING-LEFFLER, J., KARAYANNIS, T., SOUSA, V. H., BUTT, S. J., BATTISTE, J., JOHNSON, J. E., MACHOLD, R. P. & FISHELL, G. 2010. Genetic fate mapping reveals that the caudal ganglionic eminence produces a large and diverse population of superficial cortical interneurons. *J Neurosci,* 30**,** 1582-94.

MIZUI, T., ISHIKAWA, Y., KUMANOGOH, H., LUME, M., MATSUMOTO, T., HARA, T., YAMAWAKI, S., TAKAHASHI, M., SHIOSAKA, S., ITAMI, C., UEGAKI, K., SAARMA, M. & KOJIMA, M. 2015. BDNF pro-peptide actions facilitate hippocampal LTD and are altered by the common BDNF polymorphism Val66Met. *Proc Natl Acad Sci U S A,* 112**,** E3067-74.

MODARRESI, F., PEDRAM FATEMI, R., RAZAVIPOUR, S. F., RICCIARDI, N., MAKHMUTOVA, M., KHOURY, N., MAGISTRI, M., VOLMAR, C. H., WAHLESTEDT, C. & FAGHIHI, M. A. 2021. A

novel knockout mouse model of the noncoding antisense Brain-Derived Neurotrophic Factor (Bdnf) gene displays increased endogenous (Bdnf) protein and improved memory function following exercise. *Heliyon,* 7**,** e07570.

MOECHARS, D., WESTON, M. C., LEO, S., CALLAERTS-VEGH, Z., GORIS, I., DANEELS, G., BUIST, A., CIK, M., VAN DER SPEK, P., KASS, S., MEERT, T., D'HOOGE, R., ROSENMUND, C. & HAMPSON, R. M. 2006. Vesicular glutamate transporter VGLUT2 expression levels control quantal size and neuropathic pain. *J Neurosci,* 26**,** 12055-66.

MOGHADDAM, B., ADAMS, B., VERMA, A. & DALY, D. 1997. Activation of glutamatergic neurotransmission by ketamine: a novel step in the pathway from NMDA receptor blockade to dopaminergic and cognitive disruptions associated with the prefrontal cortex. *J Neurosci,* 17**,** 2921-7.

MOHLER, E., DING, Z., RUETER, L., CHAPIN, D., YOUNG, D. & KOZAK, R. 2015. Cross-site strain comparison of pharmacological deficits in the touchscreen visual discrimination test. *Psychopharmacology,* 232.

MOLNÁR, Z. & CLOWRY, G. 2012. Cerebral cortical development in rodents and primates. *Prog Brain Res,* 195**,** 45-70.

MOLTENI, R., YING, Z. & GÓMEZ-PINILLA, F. 2002. Differential effects of acute and chronic exercise on plasticity-related genes in the rat hippocampus revealed by microarray. *Eur J Neurosci,* 16**,** 1107-16.

MOLYNEAUX, B. J., ARLOTTA, P., MENEZES, J. R. & MACKLIS, J. D. 2007. Neuronal subtype specification in the cerebral cortex. *Nat Rev Neurosci,* 8**,** 427-37.

MONTE, A. S., DE SOUZA, G. C., MCINTYRE, R. S., SOCZYNSKA, J. K., DOS SANTOS, J. V., CORDEIRO, R. C., RIBEIRO, B. M., DE LUCENA, D. F., VASCONCELOS, S. M., DE SOUSA, F. C., CARVALHO, A. F. & MACÊDO, D. S. 2013. Prevention and reversal of ketamine-induced schizophrenia related behavior by minocycline in mice: Possible involvement of antioxidant and nitrergic pathways. *J Psychopharmacol,* 27**,** 1032-43.

MONTE, A. S., MELLO, B. S. F., BORELLA, V. C. M., DA SILVA ARAUJO, T., DA SILVA, F. E. R., SOUSA, F. C. F., DE OLIVEIRA, A. C. P., GAMA, C. S., SEEMAN, M. V., VASCONCELOS, S. M. M., LUCENA, D. F. & MACÊDO, D. 2017. Two-hit model of schizophrenia induced by neonatal immune activation and peripubertal stress in rats: Study of sex differences and brain oxidative alterations. *Behav Brain Res,* 331**,** 30-37.

MORASKA, A., DEAK, T., SPENCER, R. L., ROTH, D. & FLESHNER, M. 2000. Treadmill running produces both positive and negative physiological adaptations in Sprague-Dawley rats. *Am J Physiol Regul Integr Comp Physiol,* 279**,** R1321-9.

MORELLINI, F., SIVUKHINA, E., STOENICA, L., OULIANOVA, E., BUKALO, O., JAKOVCEVSKI, I., DITYATEV, A., IRINTCHEV, A. & SCHACHNER, M. 2010. Improved reversal learning and working memory and enhanced reactivity to novelty in mice with enhanced GABAergic innervation in the dentate gyrus. *Cereb Cortex,* 20**,** 2712-27.

MORISHITA, H., CABUNGCAL, J. H., CHEN, Y., DO, K. Q. & HENSCH, T. K. 2015. Prolonged Period of Cortical Plasticity upon Redox Dysregulation in Fast-Spiking Interneurons. *Biol Psychiatry,* 78**,** 396-402.

MORRIS, H. & WALLACH, J. 2014. From PCP to MXE: a comprehensive review of the non-medical use of dissociative drugs. *Drug Test Anal,* 6**,** 614-32.

MORRIS, R. W., QUAIL, S., GRIFFITHS, K. R., GREEN, M. J. & BALLEINE, B. W. 2015. Corticostriatal control of goal-directed action is impaired in schizophrenia. *Biol Psychiatry,* 77**,** 187-95.

MORTENSEN, P. B., NØRGAARD-PEDERSEN, B., WALTOFT, B. L., SØRENSEN, T. L., HOUGAARD, D., TORREY, E. F. & YOLKEN, R. H. 2007. Toxoplasma gondii as a risk factor for early-onset schizophrenia: analysis of filter paper blood samples obtained at birth. *Biol Psychiatry,* 61**,** 688-93.

MOTAGHINEJAD, M., MASHAYEKH, R., MOTEVALIAN, M. & SAFARI, S. 2021. The possible role of CREB-BDNF signaling pathway in neuroprotective effects of minocycline against alcohol-induced neurodegeneration: molecular and behavioral evidences. *Fundam Clin Pharmacol,* 35**,** 113-130.

MOTAGHINEJAD, M. & MOTEVALIAN, M. 2022. Neuroprotective Properties of Minocycline Against Methylphenidate-Induced Neurodegeneration: Possible Role of CREB/BDNF and Akt/GSK3 Signaling Pathways in Rat Hippocampus. *Neurotox Res,* 40**,** 689-713.

MOU, H., FANG, Q., TIAN, S. & QIU, F. 2023. Effects of acute exercise with different modalities on working memory in men with high and low aerobic fitness. *Physiol Behav,* 258**,** 114012.

MUCHA, P., SKOCZYŃSKA, A., MAŁECKA, M., HIKISZ, P. & BUDZISZ, E. 2021. Overview of the Antioxidant and Anti-Inflammatory Activities of Selected Plant Compounds and Their Metal Ions Complexes. *Molecules,* 26.

MUELLER, F. S., RICHETTO, J., HAYES, L. N., ZAMBON, A., POLLAK, D. D., SAWA, A., MEYER, U. & WEBER-STADLBAUER, U. 2019. Influence of poly(I:C) variability on thermoregulation, immune responses and pregnancy outcomes in mouse models of maternal immune activation. *Brain Behav Immun,* 80**,** 406-418.

MUELLER, F. S., SCARBOROUGH, J., SCHALBETTER, S. M., RICHETTO, J., KIM, E., COUCH, A., YEE, Y., LERCH, J. P., VERNON, A. C., WEBER-STADLBAUER, U. & MEYER, U. 2021. Behavioral, neuroanatomical, and molecular correlates of resilience and susceptibility to maternal immune activation. *Mol Psychiatry,* 26**,** 396-410.

MUENCH, J. & HAMER, A. M. 2010. Adverse effects of antipsychotic medications. *Am Fam Physician,* 81**,** 617-22.

MUKERJEE, S., MAHADIK, S. P., SCHEFFER, R., CORRENTI, E. E. & KELKAR, H. 1996. Impaired antioxidant defense at the onset of psychosis. *Schizophr Res,* 19**,** 19-26.

MÜLLER-PUTZ, G. R. 2020. Electroencephalography. *Handb Clin Neurol,* 168**,** 249-262.

MURPHY, M. P., BAYIR, H., BELOUSOV, V., CHANG, C. J., DAVIES, K. J. A., DAVIES, M. J., DICK, T. P., FINKEL, T., FORMAN, H. J., JANSSEN-HEININGER, Y., GEMS, D., KAGAN, V. E., KALYANARAMAN, B., LARSSON, N. G., MILNE, G. L., NYSTRÖM, T., POULSEN, H. E., RADI, R., VAN REMMEN, H., SCHUMACKER, P. T., THORNALLEY, P. J., TOYOKUNI, S., WINTERBOURN, C. C., YIN, H. & HALLIWELL, B. 2022. Guidelines for measuring reactive oxygen species and oxidative damage in cells and in vivo. *Nat Metab,* 4**,** 651-662.

MURRAY, B. G., DAVIES, D. A., MOLDER, J. J. & HOWLAND, J. G. 2017. Maternal immune activation during pregnancy in rats impairs working memory capacity of the offspring. *Neurobiol Learn Mem,* 141**,** 150-156.

MURRAY, K. N., EDYE, M. E., MANCA, M., VERNON, A. C., OLADIPO, J. M., FASOLINO, V., HARTE, M. K., MASON, V., GRAYSON, B., MCHUGH, P. C., KNUESEL, I., PRINSSEN, E. P., HAGER, R. & NEILL, J. C. 2019. Evolution of a maternal immune activation (mIA) model in rats: Early developmental effects. *Brain Behav Immun,* 75**,** 48-59.

MURUETA-GOYENA, A., ORTUZAR, N., GARGIULO, P., LAFUENTE, J. & BENGOETXEA, H. 2018. Short-Term Exposure to Enriched Environment in Adult Rats Restores MK-801-Induced Cognitive Deficits and GABAergic Interneuron Immunoreactivity Loss. *Molecular neurobiology,* 55.

MYERS, S. J., YUAN, H., KANG, J. Q., TAN, F. C. K., TRAYNELIS, S. F. & LOW, C. M. 2019. Distinct roles of GRIN2A and GRIN2B variants in neurological conditions. *F1000Res,* 8.

NADERI, Y., SABETKASAEI, M., PARVARDEH, S. & ZANJANI, T. M. 2017. Neuroprotective effect of minocycline on cognitive impairments induced by transient cerebral ischemia/reperfusion through its anti-inflammatory and anti-oxidant properties in male rat. *Brain Res Bull,* 131**,** 207-213.

NAGY, V., BOZDAGI, O., MATYNIA, A., BALCERZYK, M., OKULSKI, P., DZWONEK, J., COSTA, R. M., SILVA, A. J., KACZMAREK, L. & HUNTLEY, G. W. 2006. Matrix metalloproteinase-9 is required for hippocampal late-phase long-term potentiation and memory. *J Neurosci,* 26**,** 1923-34.

NAKAHARA, T., TSUGAWA, S., NODA, Y., UENO, F., HONDA, S., KINJO, M., SEGAWA, H., HONDO, N., MORI, Y., WATANABE, H., NAKAHARA, K., YOSHIDA, K., WADA, M., TARUMI, R., IWATA, Y., PLITMAN, E., MORIGUCHI, S., DE LA FUENTE-SANDOVAL, C., UCHIDA, H., MIMURA, M., GRAFF-GUERRERO, A. & NAKAJIMA, S. 2022. Glutamatergic and

GABAergic metabolite levels in schizophrenia-spectrum disorders: a meta-analysis of (1)H-magnetic resonance spectroscopy studies. *Mol Psychiatry,* 27**,** 744-757.

NAKAMURA, J. P., GILLESPIE, B., GIBBONS, A., JAEHNE, E. J., DU, X., CHAN, A., SCHROEDER, A., VAN DEN BUUSE, M., SUNDRAM, S. & HILL, R. A. 2021. Maternal immune activation targeted to a window of parvalbumin interneuron development improves spatial working memory: Implications for autism. *Brain Behav Immun,* 91**,** 339-349.

NAKAMURA, J. P., SCHROEDER, A., GIBBONS, A., SUNDRAM, S. & HILL, R. A. 2022. Timing of maternal immune activation and sex influence schizophrenia-relevant cognitive constructs and neuregulin and GABAergic pathways. *Brain Behav Immun,* 100**,** 70-82.

NAKAO, K., SINGH, M., SAPKOTA, K., HAGLER, B. C., HUNTER, R. N., RAMAN, C., HABLITZ, J. J. & NAKAZAWA, K. 2020. GSK3beta inhibition restores cortical gamma oscillation and cognitive behavior in a mouse model of NMDA receptor hypofunction relevant to schizophrenia. *Neuropsychopharmacology,* 45**,** 2207-2218.

NAYERNIA, Z., JAQUET, V. & KRAUSE, K. H. 2014. New insights on NOX enzymes in the central nervous system. *Antioxid Redox Signal,* 20**,** 2815-37.

NEILL, E., ROSSELL, S. L., YOLLAND, C., MEYER, D., GALLETLY, C., HARRIS, A., SISKIND, D., BERK, M., BOZAOGLU, K., DARK, F., DEAN, O. M., FRANCIS, P. S., LIU, D., PHILLIPOU, A., SARRIS, J. & CASTLE, D. J. 2022. N-Acetylcysteine (NAC) in Schizophrenia Resistant to Clozapine: A Double-Blind, Randomized, Placebo-Controlled Trial Targeting Negative Symptoms. *Schizophr Bull,* 48**,** 1263-1272.

NEILL, J. C., BARNES, S., COOK, S., GRAYSON, B., IDRIS, N. F., MCLEAN, S. L., SNIGDHA, S., RAJAGOPAL, L. & HARTE, M. K. 2010. Animal models of cognitive dysfunction and negative symptoms of schizophrenia: focus on NMDA receptor antagonism. *Pharmacol Ther,* 128**,** 419-32.

NEUGEBAUER, N. M., MIYAUCHI, M., SATO, T., TADANO, J., AKAL, H., ARDEHALI, H. & MELTZER, H. Y. 2018. Hippocampal GABA. *Behav Brain Res,* 342**,** 11-18.

NGUYEN, J. C., KILLCROSS, A. S. & JENKINS, T. A. 2013. Effect of low-intensity treadmill exercise on behavioural measures and hippocampal parvalbumin immunoreactivity in the rat. *Behav Brain Res,* 256**,** 598-601.

NICHOLS, J., BJORKLUND, G. R., NEWBERN, J. & ANDERSON, T. 2018. Parvalbumin fast-spiking interneurons are selectively altered by paediatric traumatic brain injury. *J Physiol,* 596**,** 1277-1293.

NIKAM, S. S. & MELTZER, L. T. 2002. NR2B selective NMDA receptor antagonists. *Curr Pharm Des,* 8**,** 845-55.

NIMMERJAHN, A., KIRCHHOFF, F. & HELMCHEN, F. 2005. Resting microglial cells are highly dynamic surveillants of brain parenchyma in vivo. *Science,* 308**,** 1314-8.

NISHIZAWA, Y. 2001. Glutamate release and neuronal damage in ischemia. *Life Sci,* 69**,** 369-81.

NISWENDER, C. M. & CONN, P. J. 2010. Metabotropic glutamate receptors: physiology, pharmacology, and disease. *Annu Rev Pharmacol Toxicol,* 50**,** 295-322.

NOGUEIRA, J. E., DE DEUS, J. L., AMORIM, M. R., BATALHÃO, M. E., LEÃO, R. M., CARNIO, E. C. & BRANCO, L. G. S. 2020. Inhaled molecular hydrogen attenuates intense acute exercise-induced hippocampal inflammation in sedentary rats. *Neurosci Lett,* 715**,** 134577.

NOMURA, T. 2021. Interneuron Dysfunction and Inhibitory Deficits in Autism and Fragile X Syndrome. *Cells,* 10.

NOMURA, T., OYAMADA, Y., FERNANDES, H. B., REMMERS, C. L., XU, J., MELTZER, H. Y. & CONTRACTOR, A. 2016. Subchronic phencyclidine treatment in adult mice increases GABAergic transmission and LTP threshold in the hippocampus. *Neuropharmacology,* 100**,** 90-7.

NOTARAS, M. & VAN DEN BUUSE, M. 2019. Brain-Derived Neurotrophic Factor (BDNF): Novel Insights into Regulation and Genetic Variation. *Neuroscientist,* 25**,** 434-454.

NOTARAS, M. & VAN DEN BUUSE, M. 2020. Neurobiology of BDNF in fear memory, sensitivity to stress, and stress-related disorders. *Mol Psychiatry,* 25**,** 2251-2274.

NOUEL, D., BURT, M., ZHANG, Y., HARVEY, L. & BOKSA, P. 2012. Prenatal exposure to bacterial endotoxin reduces the number of GAD67- and reelin-immunoreactive neurons in the hippocampus of rat offspring. *Eur Neuropsychopharmacol,* 22**,** 300-7.

NOVAK, G. & SEEMAN, M. V. 2022. Dopamine, Psychosis, and Symptom Fluctuation: A Narrative Review. *Healthcare (Basel),* 10.

NUECHTERLEIN, K. H. & DAWSON, M. E. 1984. A heuristic vulnerability/stress model of schizophrenic episodes. *Schizophr Bull,* 10**,** 300-12.

O'CALLAGHAN, R. M., OHLE, R. & KELLY, A. M. 2007. The effects of forced exercise on hippocampal plasticity in the rat: A comparison of LTP, spatial- and non-spatial learning. *Behav Brain Res,* 176**,** 362-6.

O'CARROLL, R. E., MURRAY, C., AUSTIN, M. P., EBMEIER, K. P., GOODWIN, G. M. & DUNAN, J. 1993. Proactive interference and the neuropsychology of schizophrenia. *Br J Clin Psychol,* 32**,** 353-6.

OHNUMA, T., KATO, H., ARAI, H., FAULL, R. L., MCKENNA, P. J. & EMSON, P. C. 2000. Gene expression of PSD95 in prefrontal cortex and hippocampus in schizophrenia. *Neuroreport,* 11**,** 3133-7.

OHSAWA, K., IMAI, Y., KANAZAWA, H., SASAKI, Y. & KOHSAKA, S. 2000. Involvement of Iba1 in membrane ruffling and phagocytosis of macrophages/microglia. *J Cell Sci,* 113 (Pt 17)**,** 3073-84.

OKAMURA, T., OKADA, M., KIKUCHI, T., WAKIZAKA, H. & ZHANG, M. R. 2018. Kinetics and metabolism of apocynin in the mouse brain assessed with positron-emission tomography. *Phytomedicine,* 38**,** 84-89.

OKUBO ENENI, A. E., BEN-AZU, B., MAYOWA AJAYI, A. & OLADELE ADERIBIGBE, A. 2020. Diosmin attenuates schizophrenia-like behavior, oxidative stress, and acetylcholinesterase activity in mice. *Drug Metab Pers Ther*.

OLNEY, J. W., LABRUYERE, J. & PRICE, M. T. 1989. Pathological changes induced in cerebrocortical neurons by phencyclidine and related drugs. *Science,* 244**,** 1360-2.

OMEIZA, N. A., BAKRE, A., BEN-AZU, B., SOWUNMI, A. A., ABDULRAHIM, H. A., CHIMEZIE, J., LAWAL, S. O., ADEBAYO, O. G., ALAGBONSI, A. I., AKINOLA, O., ABOLAJI, A. O. & ADERIBIGBE, A. O. 2023. Mechanisms underpinning Carpolobia lutea G. Don ethanol extract's neurorestorative and antipsychotic-like activities in an NMDA receptor antagonist model of schizophrenia. *J Ethnopharmacol,* 301**,** 115767.

ONI-ORISAN, A., KRISTIANSEN, L. V., HAROUTUNIAN, V., MEADOR-WOODRUFF, J. H. & MCCULLUMSMITH, R. E. 2008. Altered vesicular glutamate transporter expression in the anterior cingulate cortex in schizophrenia. *Biol Psychiatry,* 63**,** 766-75.

OSBORNE, A. L., SOLOWIJ, N., BABIC, I., HUANG, X. F. & WESTON-GREEN, K. 2017. Improved Social Interaction, Recognition and Working Memory with Cannabidiol Treatment in a Prenatal Infection (poly I:C) Rat Model. *Neuropsychopharmacology,* 42**,** 1447-1457.

OSBORNE, A. L., SOLOWIJ, N., BABIC, I., LUM, J. S., HUANG, X. F., NEWELL, K. A. & WESTON-GREEN, K. 2019. Cannabidiol improves behavioural and neurochemical deficits in adult female offspring of the maternal immune activation (poly I:C) model of neurodevelopmental disorders. *Brain Behav Immun,* 81**,** 574-587.

OSHODI, T. O., BEN-AZU, B., ISHOLA, I. O., AJAYI, A. M., EMOKPAE, O. & UMUKORO, S. 2021. Molecular mechanisms involved in the prevention and reversal of ketamine-induced schizophrenia-like behavior by rutin: the role of glutamic acid decarboxylase isoform-67, cholinergic, Nox-2-oxidative stress pathways in mice. *Mol Biol Rep,* 48**,** 2335-2350.

OSKVIG, D. B., ELKAHLOUN, A. G., JOHNSON, K. R., PHILLIPS, T. M. & HERKENHAM, M. 2012. Maternal immune activation by LPS selectively alters specific gene expression profiles of interneuron migration and oxidative stress in the fetus without triggering a fetal immune response. *Brain Behav Immun,* 26**,** 623-34.

OVERSTREET, L. S. & WESTBROOK, G. L. 2003. Synapse density regulates independence at unitary inhibitory synapses. *J Neurosci,* 23**,** 2618-26.

OWCZAREK-JANUSZKIEWICZ, A., MAGIERA, A. & OLSZEWSKA, M. A. 2022. Enzymatically Modified Isoquercitrin: Production, Metabolism, Bioavailability, Toxicity, Pharmacology, and Related Molecular Mechanisms. *Int J Mol Sci,* 23.

PACKER, A. M. & YUSTE, R. 2011. Dense, unspecific connectivity of neocortical parvalbumin-positive interneurons: a canonical microcircuit for inhibition? *J Neurosci,* 31**,** 13260-71.

PAN, L., CAO, Z., CHEN, L., QIAN, M. & YAN, Y. 2022. Association of BDNF and MMP-9 single-nucleotide polymorphisms with the clinical phenotype of schizophrenia. *Front Psychiatry,* 13**,** 941973.

PANDEY, G. N., RIZAVI, H. S., ZHANG, H. & REN, X. 2018. Abnormal gene and protein expression of inflammatory cytokines in the postmortem brain of schizophrenia patients. *Schizophr Res,* 192**,** 247-254.

PANTAZOPOULOS, H., WOO, T. U., LIM, M. P., LANGE, N. & BERRETTA, S. 2010. Extracellular matrix-glial abnormalities in the amygdala and entorhinal cortex of subjects diagnosed with schizophrenia. *Arch Gen Psychiatry,* 67**,** 155-66.

PAOLICELLI, R. C., SIERRA, A., STEVENS, B., TREMBLAY, M. E., AGUZZI, A., AJAMI, B., AMIT, I., AUDINAT, E., BECHMANN, I., BENNETT, M., BENNETT, F., BESSIS, A., BIBER, K., BILBO, S., BLURTON-JONES, M., BODDEKE, E., BRITES, D., BRÔNE, B., BROWN, G. C., BUTOVSKY, O., CARSON, M. J., CASTELLANO, B., COLONNA, M., COWLEY, S. A., CUNNINGHAM, C., DAVALOS, D., DE JAGER, P. L., DE STROOPER, B., DENES, A., EGGEN, B. J. L., EYO, U., GALEA, E., GAREL, S., GINHOUX, F., GLASS, C. K., GOKCE, O., GOMEZ-NICOLA, D., GONZÁLEZ, B., GORDON, S., GRAEBER, M. B., GREENHALGH, A. D., GRESSENS, P., GRETER, M., GUTMANN, D. H., HAASS, C., HENEKA, M. T., HEPPNER, F. L., HONG, S., HUME, D. A., JUNG, S., KETTENMANN, H., KIPNIS, J., KOYAMA, R., LEMKE, G., LYNCH, M., MAJEWSKA, A., MALCANGIO, M., MALM, T., MANCUSO, R., MASUDA, T., MATTEOLI, M., MCCOLL, B. W., MIRON, V. E., MOLOFSKY, A. V., MONJE, M., MRACSKO, E., NADJAR, A., NEHER, J. J., NENISKYTE, U., NEUMANN, H., NODA, M., PENG, B., PERI, F., PERRY, V. H., POPOVICH, P. G., PRIDANS, C., PRILLER, J., PRINZ, M., RAGOZZINO, D., RANSOHOFF, R. M., SALTER, M. W., SCHAEFER, A., SCHAFER, D. P., SCHWARTZ, M., SIMONS, M., SMITH, C. J., STREIT, W. J., TAY, T. L., TSAI, L. H., VERKHRATSKY, A., VON BERNHARDI, R., WAKE, H., WITTAMER, V., WOLF, S. A., WU, L. J. & WYSS-CORAY, T. 2022. Microglia states and nomenclature: A field at its crossroads. *Neuron,* 110**,** 3458-3483.

PAPADIA, S., SORIANO, F. X., LÉVEILLÉ, F., MARTEL, M. A., DAKIN, K. A., HANSEN, H. H., KAINDL, A., SIFRINGER, M., FOWLER, J., STEFOVSKA, V., MCKENZIE, G., CRAIGON, M., CORRIVEAU, R., GHAZAL, P., HORSBURGH, K., YANKNER, B. A., WYLLIE, D. J., IKONOMIDOU, C. & HARDINGHAM, G. E. 2008. Synaptic NMDA receptor activity boosts intrinsic antioxidant defenses. *Nat Neurosci,* 11**,** 476-87.

PARACHIKOVA, A., NICHOL, K. E. & COTMAN, C. W. 2008. Short-term exercise in aged Tg2576 mice alters neuroinflammation and improves cognition. *Neurobiol Dis,* 30**,** 121-9.

PARK, D. J., KANG, J. B., SHAH, F. A. & KOH, P. O. 2021. Quercetin attenuates the reduction of parvalbumin in middle cerebral artery occlusion animal model. *Lab Anim Res,* 37**,** 9.

PARSEGIAN, A. & SEE, R. E. 2014. Dysregulation of dopamine and glutamate release in the prefrontal cortex and nucleus accumbens following methamphetamine self-administration and during reinstatement in rats. *Neuropsychopharmacology,* 39**,** 811-22.

PARVARDEH, S., SHEIKHOLESLAMI, M. A., GHAFGHAZI, S., POURIRAN, R. & MORTAZAVI, S. E. 2022. Minocycline Improves Memory by Enhancing Hippocampal Synaptic Plasticity and Restoring Antioxidant Enzyme Activity in a Rat Model of Cerebral Ischemia-Reperfusion. *Basic Clin Neurosci,* 13**,** 225-235.

PATEL, K. R., CHERIAN, J., GOHIL, K. & ATKINSON, D. 2014. Schizophrenia: overview and treatment options. *P T,* 39**,** 638-45.

PATTERSON, P. H. 2009. Immune involvement in schizophrenia and autism: etiology, pathology and animal models. *Behav Brain Res,* 204**,** 313-21.

PAXINOS, G. & WATSON, C. 2007. *The rat brain in stereotaxic coordinates*.

PAYLOR, J. W., LINS, B. R., GREBA, Q., MOEN, N., DE MORAES, R. S., HOWLAND, J. G. & WINSHIP, I. R. 2016. Developmental disruption of perineuronal nets in the medial prefrontal cortex after maternal immune activation. *Sci Rep,* 6**,** 37580.

PAYLOR, J. W., WENDLANDT, E., FREEMAN, T. S., GREBA, Q., MARKS, W. N., HOWLAND, J. G. & WINSHIP, I. R. 2018. Impaired Cognitive Function after Perineuronal Net Degradation in the Medial Prefrontal Cortex. *eNeuro,* 5.

PEARCE, B. D. 2001. Schizophrenia and viral infection during neurodevelopment: a focus on mechanisms. *Mol Psychiatry,* 6**,** 634-46.

PEARLSON, G. D. 1981. Psychiatric and medical syndromes associated with phencyclidine (PCP) abuse. *Johns Hopkins Med J,* 148**,** 25-33.

PEDERSEN, B. K., STEENSBERG, A., FISCHER, C., KELLER, C., KELLER, P., PLOMGAARD, P., FEBBRAIO, M. & SALTIN, B. 2003. Searching for the exercise factor: is IL-6 a candidate? *J Muscle Res Cell Motil,* 24**,** 113-9.

PENISSON, M., LADEWIG, J., BELVINDRAH, R. & FRANCIS, F. 2019. Genes and Mechanisms Involved in the Generation and Amplification of Basal Radial Glial Cells. *Front Cell Neurosci,* 13**,** 381.

PENNER, J. D. & BROWN, A. S. 2007. Prenatal infectious and nutritional factors and risk of adult schizophrenia. *Expert review of neurotherapeutics.,* 7**,** 797-805.

PETERSEN, A. M. & PEDERSEN, B. K. 2005. The anti-inflammatory effect of exercise. *J Appl Physiol (1985),* 98**,** 1154-62.

PETROWSKI, K., WICHMANN, S. & KIRSCHBAUM, C. 2018. Stress-induced pro- and anti-inflammatory cytokine concentrations in panic disorder patients. *Psychoneuroendocrinology,* 94**,** 31-37.

PEYROVIAN, B., MCINTYRE, R. S., PHAN, L., LUI, L. M. W., GILL, H., MAJEED, A., CHEN-LI, D., NASRI, F. & ROSENBLAT, J. D. 2020. Registered clinical trials investigating ketamine for psychiatric disorders. *J Psychiatr Res,* 127**,** 1-12.

PHILPOT, B. D., SEKHAR, A. K., SHOUVAL, H. Z. & BEAR, M. F. 2001. Visual experience and deprivation bidirectionally modify the composition and function of NMDA receptors in visual cortex. *Neuron,* 29**,** 157-69.

PICARD, N., TAKESIAN, A. E., FAGIOLINI, M. & HENSCH, T. K. 2019. NMDA 2A receptors in parvalbumin cells mediate sex-specific rapid ketamine response on cortical activity. *Mol Psychiatry,* 24**,** 828-838.

PICCINNI, M. P., RAGHUPATHY, R., SAITO, S. & SZEKERES-BARTHO, J. 2021. Cytokines, Hormones and Cellular Regulatory Mechanisms Favoring Successful Reproduction. *Front Immunol,* 12**,** 717808.

PICÓN-PAGÈS, P., GARCIA-BUENDIA, J. & MUÑOZ, F. J. 2019. Functions and dysfunctions of nitric oxide in brain. *Biochim Biophys Acta Mol Basis Dis,* 1865**,** 1949-1967.

PIETRELLI, A., LOPEZ-COSTA, J., GOÑI, R., BRUSCO, A. & BASSO, N. 2012. Aerobic exercise prevents age-dependent cognitive decline and reduces anxiety-related behaviors in middle-aged and old rats. *Neuroscience,* 202**,** 252-66.

PILOWSKY, L. S., BRESSAN, R. A., STONE, J. M., ERLANDSSON, K., MULLIGAN, R. S., KRYSTAL, J. H. & ELL, P. J. 2006. First in vivo evidence of an NMDA receptor deficit in medication-free schizophrenic patients. *Mol Psychiatry,* 11**,** 118-9.

PINGITORE, A., LIMA, G. P., MASTORCI, F., QUINONES, A., IERVASI, G. & VASSALLE, C. 2015. Exercise and oxidative stress: potential effects of antioxidant dietary strategies in sports. *Nutrition,* 31**,** 916-22.

PIONTKEWITZ, Y., BERNSTEIN, H. G., DOBROWOLNY, H., BOGERTS, B., WEINER, I. & KEILHOFF, G. 2012. Effects of risperidone treatment in adolescence on hippocampal neurogenesis, parvalbumin expression, and vascularization following prenatal immune activation in rats. *Brain Behav Immun,* 26**,** 353-63.

PIOTROWSKA, A., POPIOLEK-BARCZYK, K., PAVONE, F. & MIKA, J. 2017. Comparison of the Expression Changes after Botulinum Toxin Type A and Minocycline Administration in

Lipopolysaccharide-Stimulated Rat Microglial and Astroglial Cultures. *Front Cell Infect Microbiol,* 7**,** 141.

PIYABHAN, P., TINGPEJ, P. & DUANSAK, N. 2019. Effect of pre- and post-treatment with Bacopa monnieri (Brahmi) on phencyclidine-induced disruptions in object recognition memory and cerebral calbindin, parvalbumin, and calretinin immunoreactivity in rats. *Neuropsychiatr Dis Treat,* 15**,** 1103-1117.

PIYABHAN, P. & WETCHATENG, T. 2013. Cognitive enhancement effects of Bacopa monnieri (Brahmi) on novel object recognition and VGLUT1 density in the prefrontal cortex, striatum, and hippocampus of sub-chronic phencyclidine rat model of schizophrenia. *J Med Assoc Thai,* 96**,** 625-32.

PIYABHAN, P. & WETCHATENG, T. 2016. Bacopa monnieri (Brahmi) Prevents Cognitive Deficit by Maintaining CA2/3 VGLUT1 Density of Sub-Chronic Phencyclidine Rat Model of Schizophrenia in Normal Level. *J Med Assoc Thai,* 99 Suppl 4**,** S222-9.

PIZZORUSSO, T., MEDINI, P., BERARDI, N., CHIERZI, S., FAWCETT, J. W. & MAFFEI, L. 2002. Reactivation of ocular dominance plasticity in the adult visual cortex. *Science,* 298**,** 1248-51.

PLACENCIA, E. V. D., SERRA, F. T., HENRIQUE, J. S., ARIDA, R. M. & GOMES DA SILVA, S. 2019. Hippocampal distribution of parvalbumin neurons in female and male rats submitted to the same volume and intensity of aerobic exercise. *Neurosci Lett,* 690**,** 162-166.

POLLARD, M., VARIN, C., HRUPKA, B., PEMBERTON, D. J., STECKLER, T. & SHABAN, H. 2012. Synaptic transmission changes in fear memory circuits underlie key features of an animal model of schizophrenia. *Behav Brain Res,* 227**,** 184-93.

POPOVIC, N., SCHUBART, A., GOETZ, B. D., ZHANG, S. C., LININGTON, C. & DUNCAN, I. D. 2002. Inhibition of autoimmune encephalomyelitis by a tetracycline. *Ann Neurol,* 51**,** 215-23.

POTTER, H. G., KOWASH, H. M., WOODS, R. M., REVILL, G., GRIME, A., DEENEY, B., BURGESS, M. A., AARONS, T., GLAZIER, J. D., NEILL, J. C. & HAGER, R. 2023. Maternal behaviours and adult offspring behavioural deficits are predicted by maternal TNFα concentration in a rat model of neurodevelopmental disorders. *Brain Behav Immun,* 108**,** 162-175.

POUILLE, F. & SCANZIANI, M. 2001. Enforcement of temporal fidelity in pyramidal cells by somatic feed-forward inhibition. *Science,* 293**,** 1159-63.

POVYSHEVA, N. V., ZAITSEV, A. V., GONZALEZ-BURGOS, G. & LEWIS, D. A. 2013. Electrophysiological heterogeneity of fast-spiking interneurons: chandelier versus basket cells. *PLoS One,* 8**,** e70553.

POZZI, D., CONDLIFFE, S., BOZZI, Y., CHIKHLADZE, M., GRUMELLI, C., PROUX-GILLARDEAUX, V., TAKAHASHI, M., FRANCESCHETTI, S., VERDERIO, C. & MATTEOLI, M. 2008. Activity-dependent phosphorylation of Ser187 is required for SNAP-25-negative modulation of neuronal voltage-gated calcium channels. *Proc Natl Acad Sci U S A,* 105**,** 323-8.

PRADHAN, S. N. 1984. Phencyclidine (PCP): some human studies. *Neurosci Biobehav Rev,* 8**,** 493-501.

PRENZLER, P. D., RYAN, D. & ROBARDS, K. 2021. *Handbook of antioxidant methodology : approaches to activity determination*.

PRUESSNER, M., CULLEN, A. E., AAS, M. & WALKER, E. F. 2017. The neural diathesis-stress model of schizophrenia revisited: An update on recent findings considering illness stage and neurobiological and methodological complexities. *Neurosci Biobehav Rev,* 73**,** 191-218.

PYNDT JØRGENSEN, B., KRYCH, L., PEDERSEN, T. B., PLATH, N., REDROBE, J. P., HANSEN, A. K., NIELSEN, D. S., PEDERSEN, C. S., LARSEN, C. & SØRENSEN, D. B. 2015. Investigating the long-term effect of subchronic phencyclidine-treatment on novel object recognition and the association between the gut microbiota and behavior in the animal model of schizophrenia. *Physiol Behav,* 141**,** 32-9.

QAID, E. Y. A., ABDULLAH, Z., ZAKARIA, R. & LONG, I. 2022. Minocycline Protects Against Lipopolysaccharide-Induced Cognitive Impairment and Oxidative Stress: Possible Role of the CREB-BDNF Signaling Pathway. *Neurochem Res*.

QIN, C., BIAN, X. L., WU, H. Y., XIAN, J. Y., CAI, C. Y., LIN, Y. H., ZHOU, Y., KOU, X. L., CHANG, L., LUO, C. X. & ZHU, D. Y. 2021. Dorsal Hippocampus to Infralimbic Cortex Circuit is Essential for the Recall of Extinction Memory. *Cereb Cortex,* 31**,** 1707-1718.

QIN, S., ZHAO, X., PAN, Y., LIU, J., FENG, G., FU, J., BAO, J., ZHANG, Z. & HE, L. 2005. An association study of the N-methyl-D-aspartate receptor NR1 subunit gene (GRIN1) and NR2B subunit gene (GRIN2B) in schizophrenia with universal DNA microarray. *Eur J Hum Genet,* 13**,** 807-14.

QIU, L. L., LUO, D., ZHANG, H., SHI, Y. S., LI, Y. J., WU, D., CHEN, J., JI, M. H. & YANG, J. J. 2016. Nox-2-Mediated Phenotype Loss of Hippocampal Parvalbumin Interneurons Might Contribute to Postoperative Cognitive Decline in Aging Mice. *Front Aging Neurosci,* 8**,** 234.

QUEDNOW, B. B., GEYER, M. A. & HALBERSTADT, A. L. 2020. *Chapter 39 - Serotonin and schizophrenia*, Elsevier.

RADAK, Z., TOLDY, A., SZABO, Z., SIAMILIS, S., NYAKAS, C., SILYE, G., JAKUS, J. & GOTO, S. 2006. The effects of training and detraining on memory, neurotrophins and oxidative stress markers in rat brain. *Neurochem Int,* 49**,** 387-92.

RAHMAN, T., WEICKERT, C. S., HARMS, L., MEEHAN, C., SCHALL, U., TODD, J., HODGSON, D. M., MICHIE, P. T. & PURVES-TYSON, T. 2020. Effect of Immune Activation during Early Gestation or Late Gestation on Inhibitory Markers in Adult Male Rats. *Sci Rep,* 10**,** 1982.

RAINEY, J. M. & CROWDER, M. K. 1975. Prolonged psychosis attributed to phencyclidine: report of three cases. *Am J Psychiatry,* 132**,** 1076-8.

RAPADO-CASTRO, M., DODD, S., BUSH, A. I., MALHI, G. S., SKVARC, D. R., ON, Z. X., BERK, M. & DEAN, O. M. 2017. Cognitive effects of adjunctive N-acetyl cysteine in psychosis. *Psychol Med,* 47**,** 866-876.

RAPOPORT, J. L., GIEDD, J. N. & GOGTAY, N. 2012. Neurodevelopmental model of schizophrenia: update 2012. *Mol Psychiatry,* 17**,** 1228-38.

RASMUSSEN, P., BRASSARD, P., ADSER, H., PEDERSEN, M. V., LEICK, L., HART, E., SECHER, N. H., PEDERSEN, B. K. & PILEGAARD, H. 2009. Evidence for a release of brain-derived neurotrophic factor from the brain during exercise. *Exp Physiol,* 94**,** 1062-9.

RATNAYAKE, U., QUINN, T., LAROSA, D. A., DICKINSON, H. & WALKER, D. W. 2014. Prenatal exposure to the viral mimetic poly I:C alters fetal brain cytokine expression and postnatal behaviour. *Dev Neurosci,* 36**,** 83-94.

REDROBE, J. P., ELSTER, L., FREDERIKSEN, K., BUNDGAARD, C., DE JONG, I. E., SMITH, G. P., BRUUN, A. T., LARSEN, P. H. & DIDRIKSEN, M. 2012. Negative modulation of GABAA α5 receptors by RO4938581 attenuates discrete sub-chronic and early postnatal phencyclidine (PCP)-induced cognitive deficits in rats. *Psychopharmacology (Berl),* 221**,** 451-68.

REICHELT, A. C., HARE, D. J., BUSSEY, T. J. & SAKSIDA, L. M. 2019. Perineuronal Nets: Plasticity, Protection, and Therapeutic Potential. *Trends Neurosci,* 42**,** 458-470.

REIF, A., FRITZEN, S., FINGER, M., STROBEL, A., LAUER, M., SCHMITT, A. & LESCH, K. P. 2006. Neural stem cell proliferation is decreased in schizophrenia, but not in depression. *Mol Psychiatry,* 11**,** 514-22.

REMINGTON, G., HAHN, M. K., AGARWAL, S. M., CHINTOH, A. & AGID, O. 2021. Schizophrenia: Antipsychotics and drug development. *Behav Brain Res,* 414**,** 113507.

REYCRAFT, J. T., ISLAM, H., TOWNSEND, L. K., HAYWARD, G. C., HAZELL, T. J. & MACPHERSON, R. E. K. 2020. Exercise Intensity and Recovery on Circulating Brain-derived Neurotrophic Factor. *Med Sci Sports Exerc,* 52**,** 1210-1217.

RICHETTO, J., CALABRESE, F., MEYER, U. & RIVA, M. A. 2013. Prenatal versus postnatal maternal factors in the development of infection-induced working memory impairments in mice. *Brain Behav Immun,* 33**,** 190-200.

RICHETTO, J., CALABRESE, F., RIVA, M. A. & MEYER, U. 2014. Prenatal immune activation induces maturation-dependent alterations in the prefrontal GABAergic transcriptome. *Schizophr Bull,* 40**,** 351-61.

RICHTER-SCHMIDINGER, T., ALEXOPOULOS, P., HORN, M., MAUS, S., REICHEL, M., RHEIN, C., LEWCZUK, P., SIDIROPOULOS, C., KNEIB, T., PERNECZKY, R., DOERFLER, A. & KORNHUBER, J. 2011. Influence of brain-derived neurotrophic-factor and apolipoprotein E genetic variants on hippocampal volume and memory performance in healthy young adults. *J Neural Transm (Vienna),* 118**,** 249-57.

RIORDAN, A. J., SCHALER, A. W., FRIED, J., PAINE, T. A. & THORNTON, J. E. 2018. Estradiol and luteinizing hormone regulate recognition memory following subchronic phencyclidine: Evidence for hippocampal GABA action. *Psychoneuroendocrinology,* 91**,** 86-94.

RIVA, M. A., TASCEDDA, F., MOLTENI, R. & RACAGNI, G. 1994. Regulation of NMDA receptor subunit mRNA expression in the rat brain during postnatal development. *Brain Res Mol Brain Res,* 25**,** 209-16.

ROBISON, L. S., POPESCU, D. L., ANDERSON, M. E., FRANCIS, N., HATFIELD, J., SULLIVAN, J. K., BEIGELMAN, S. I., XU, F., ANDERSON, B. J., VAN NOSTRAND, W. E. & ROBINSON, J. K. 2019. Long-term voluntary wheel running does not alter vascular amyloid burden but reduces neuroinflammation in the Tg-SwDI mouse model of cerebral amyloid angiopathy. *J Neuroinflammation,* 16**,** 144.

ROBISON, R. A., TAGHVA, A., LIU, C. Y. & APUZZO, M. L. 2013. Surgery of the mind, mood, and conscious state: an idea in evolution. *World Neurosurg,* 80**,** S2-26.

ROCCO, B. R., LEWIS, D. A. & FISH, K. N. 2016. Markedly Lower Glutamic Acid Decarboxylase 67 Protein Levels in a Subset of Boutons in Schizophrenia. *Biol Psychiatry,* 79**,** 1006-15.

RODRIGUES, S. M., SCHAFE, G. E. & LEDOUX, J. E. 2001. Intra-amygdala blockade of the NR2B subunit of the NMDA receptor disrupts the acquisition but not the expression of fear conditioning. *J Neurosci,* 21**,** 6889-96.

ROENKER, N. L., GUDELSKY, G., AHLBRAND, R., BRONSON, S. L., KERN, J. R., WATERMAN, H. & RICHTAND, N. M. 2011. Effect of paliperidone and risperidone on extracellular glutamate in the prefrontal cortex of rats exposed to prenatal immune activation or MK-801. *Neurosci Lett,* 500**,** 167-71.

ROGAEVA, E. & SCHMITT-ULMS, G. 2016. Does BDNF Val66Met contribute to preclinical Alzheimer's disease? *Brain,* 139**,** 2586-2589.

ROGERS, S. L., RANKIN-GEE, E., RISBUD, R. M., PORTER, B. E. & MARSH, E. D. 2018. Normal Development of the Perineuronal Net in Humans; In Patients with and without Epilepsy. *Neuroscience,* 384**,** 350-360.

ROMBERG, C., YANG, S., MELANI, R., ANDREWS, M. R., HORNER, A. E., SPILLANTINI, M. G., BUSSEY, T. J., FAWCETT, J. W., PIZZORUSSO, T. & SAKSIDA, L. M. 2013. Depletion of perineuronal nets enhances recognition memory and long-term depression in the perirhinal cortex. *J Neurosci,* 33**,** 7057-65.

ROMERO-MIGUEL, D., CASQUERO-VEIGA, M., MACDOWELL, K. S., TORRES-SANCHEZ, S., GARCIA-PARTIDA, J. A., LAMANNA-RAMA, N., ROMERO-MIRANDA, A., BERROCOSO, E., LEZA, J. C., DESCO, M. & SOTO-MONTENEGRO, M. L. 2021. A Characterization of the Effects of Minocycline Treatment During Adolescence on Structural, Metabolic, and Oxidative Stress Parameters in a Maternal Immune Stimulation Model of Neurodevelopmental Brain Disorders. *Int J Neuropsychopharmacol,* 24**,** 734-748.

ROTHAUG, M., BECKER-PAULY, C. & ROSE-JOHN, S. 2016. The role of interleukin-6 signaling in nervous tissue. *Biochim Biophys Acta,* 1863**,** 1218-27.

ROUSSET, C. I., CHALON, S., CANTAGREL, S., BODARD, S., ANDRES, C., GRESSENS, P. & SALIBA, E. 2006. Maternal exposure to LPS induces hypomyelination in the internal capsule and programmed cell death in the deep gray matter in newborn rats. *Pediatr Res,* 59**,** 428-33.

ROWLANDS, D., LENSJØ, K. K., DINH, T., YANG, S., ANDREWS, M. R., HAFTING, T., FYHN, M., FAWCETT, J. W. & DICK, G. 2018. Aggrecan Directs Extracellular Matrix-Mediated Neuronal Plasticity. *J Neurosci,* 38**,** 10102-10113.

RUDY, B. & MCBAIN, C. J. 2001. Kv3 channels: voltage-gated K+ channels designed for high-frequency repetitive firing. *Trends Neurosci,* 24**,** 517-26.

SÆTHER, L. S., UELAND, T., HAATVEIT, B., MAGLANOC, L. A., SZABO, A., DJUROVIC, S., AUKRUST, P., ROELFS, D., MOHN, C., ORMEROD, M. B. E. G., LAGERBERG, T. V., STEEN, N. E., MELLE, I. & ANDREASSEN, O. A. 2023. Inflammation and cognition in severe mental illness: patterns of covariation and subgroups. *Mol Psychiatry,* 28**,** 1284-1292.

SAGHATELYAN, A. K., DITYATEV, A., SCHMIDT, S., SCHUSTER, T., BARTSCH, U. & SCHACHNER, M. 2001. Reduced perisomatic inhibition, increased excitatory transmission, and impaired long-term potentiation in mice deficient for the extracellular matrix glycoprotein tenascin-R. *Mol Cell Neurosci,* 17**,** 226-40.

SAHA, S., CHANT, D., WELHAM, J. & MCGRATH, J. 2005. A systematic review of the prevalence of schizophrenia. *PLoS Med,* 2**,** e141.

SAKAGUCHI, M. & HAYASHI, Y. 2012. Catching the engram: strategies to examine the memory trace. *Mol Brain,* 5**,** 32.

SAMUELSSON, A. M., JENNISCHE, E., HANSSON, H. A. & HOLMÄNG, A. 2006. Prenatal exposure to interleukin-6 results in inflammatory neurodegeneration in hippocampus with NMDA/GABA(A) dysregulation and impaired spatial learning. *Am J Physiol Regul Integr Comp Physiol,* 290**,** R1345-56.

SANCHEZ-MENDOZA, E. H., CAMBLOR-PERUJO, S., MARTINS NASCENTES-MELO, L., DZYUBENKO, E., FLEISCHER, M., SILVA DE CARVALHO, T., SCHMITT, L. I., LEO, M., HAGENACKER, T., HERRING, A., KEYVANI, K., BERA, S., KONONENKO, N., KLEINSCHNITZ, C. & HERMANN, D. M. 2020. Compromised Hippocampal Neuroplasticity in the Interferon-α and Toll-like Receptor-3 Activation-Induced Mouse Depression Model. *Mol Neurobiol,* 57**,** 3171-3182.

SARANDOL, A., SARANDOL, E., ACIKGOZ, H. E., EKER, S. S., AKKAYA, C. & DIRICAN, M. 2015. First-episode psychosis is associated with oxidative stress: Effects of short-term antipsychotic treatment. *Psychiatry Clin Neurosci,* 69**,** 699-707.

SASAYAMA, D., HATTORI, K., WAKABAYASHI, C., TERAISHI, T., HORI, H., OTA, M., YOSHIDA, S., ARIMA, K., HIGUCHI, T., AMANO, N. & KUNUGI, H. 2013. Increased cerebrospinal fluid interleukin-6 levels in patients with schizophrenia and those with major depressive disorder. *J Psychiatr Res,* 47**,** 401-6.

SAVLA, S. R., LADDHA, A. P. & KULKARNI, Y. A. 2021. Pharmacology of apocynin: a natural acetophenone. *Drug Metab Rev,* 53**,** 542-562.

SAVOLAINEN, K., IHALAINEN, J., JALKANEN, A. J. & FORSBERG, M. M. 2018. Selective adrenergic alpha2C receptor antagonist ameliorates acute phencyclidine-induced schizophrenia-like social interaction deficits in rats. *Psychopharmacology (Berl)*.

SAWADA, K., BARR, A. M., NAKAMURA, M., ARIMA, K., YOUNG, C. E., DWORK, A. J., FALKAI, P., PHILLIPS, A. G. & HONER, W. G. 2005. Hippocampal complexin proteins and cognitive dysfunction in schizophrenia. *Arch Gen Psychiatry,* 62**,** 263-72.

SCHIAVONE, S., JAQUET, V., SORCE, S., DUBOIS-DAUPHIN, M., HULTQVIST, M., BÄCKDAHL, L., HOLMDAHL, R., COLAIANNA, M., CUOMO, V., TRABACE, L. & KRAUSE, K. H. 2012. NADPH oxidase elevations in pyramidal neurons drive psychosocial stress-induced neuropathology. *Transl Psychiatry,* 2**,** e111.

SCHIAVONE, S., SORCE, S., DUBOIS-DAUPHIN, M., JAQUET, V., COLAIANNA, M., ZOTTI, M., CUOMO, V., TRABACE, L. & KRAUSE, K. H. 2009. Involvement of NOX2 in the development of behavioral and pathologic alterations in isolated rats. *Biol Psychiatry,* 66**,** 384-92.

SCHIELZETH, H., DINGEMANSE, N. J., NAKAGAWA, S., WESTNEAT, D. F., ALLEGUE, H., TEPLITSKY, C., RÉALE, D., DOCHTERMANN, N. A., GARAMSZEGI, L. Z. & ARAYA-AJOY, Y. G. 2020. Robustness of linear mixed-effects models to violations of distributional assumptions. *Methods in Ecology and Evolution,* 11**,** 1141-1152.

SCHIZOPHRENIA WORKING GROUP OF THE PSYCHIATRIC GENOMICS CONSORTIUM 2014. Biological insights from 108 schizophrenia-associated genetic loci. *Nature,* 511**,** 421-7.

SCHMIDT, S., ARENDT, T., MORAWSKI, M. & SONNTAG, M. 2020. Neurocan Contributes to Perineuronal Net Development. *Neuroscience,* 442**,** 69-86.

SCHMITT, A., MAURUS, I., ROSSNER, M. J., RÖH, A., LEMBECK, M., VON WILMSDORFF, M., TAKAHASHI, S., RAUCHMANN, B., KEESER, D., HASAN, A., MALCHOW, B. & FALKAI, P. 2018. Effects of Aerobic Exercise on Metabolic Syndrome, Cardiorespiratory Fitness, and Symptoms in Schizophrenia Include Decreased Mortality. *Front Psychiatry,* 9**,** 690.

SCHOENFELD, T. J. & CAMERON, H. A. 2015. Adult neurogenesis and mental illness. *Neuropsychopharmacology,* 40**,** 113-28.

SCHOGGINS, J. W. 2019. Interferon-Stimulated Genes: What Do They All Do? *Annu Rev Virol,* 6**,** 567-584.

SCHOLZ, R., SOBOTKA, M., CARAMOY, A., STEMPFL, T., MOEHLE, C. & LANGMANN, T. 2015. Minocycline counter-regulates pro-inflammatory microglia responses in the retina and protects from degeneration. *J Neuroinflammation,* 12**,** 209.

SCHWIELER, L., LARSSON, M. K., SKOGH, E., KEGEL, M. E., ORHAN, F., ABDELMOATY, S., FINN, A., BHAT, M., SAMUELSSON, M., LUNDBERG, K., DAHL, M. L., SELLGREN, C., SCHUPPE-KOISTINEN, I., SVENSSON, C., ERHARDT, S. & ENGBERG, G. 2015. Increased levels of IL-6 in the cerebrospinal fluid of patients with chronic schizophrenia--significance for activation of the kynurenine pathway. *J Psychiatry Neurosci,* 40**,** 126-33.

SEAL, R. P. & EDWARDS, R. H. 2006. The diverse roles of vesicular glutamate transporter 3. *Handb Exp Pharmacol***,** 137-50.

SEARS, S. M. & HEWETT, S. J. 2021. Influence of glutamate and GABA transport on brain excitatory/inhibitory balance. *Exp Biol Med (Maywood),* 246**,** 1069-1083.

SEEMAN, P. & LEE, T. 1975. Antipsychotic drugs: direct correlation between clinical potency and presynaptic action on dopamine neurons. *Science,* 188**,** 1217-9.

SELTEN, M., VAN BOKHOVEN, H. & NADIF KASRI, N. 2018. Inhibitory control of the excitatory/inhibitory balance in psychiatric disorders. *F1000Res,* 7**,** 23.

SEMBA, J., WAKUTA, M. & SUHARA, T. 2006. Different effects of chronic phencyclidine on brain-derived neurotrophic factor in neonatal and adult rat brains. *Addict Biol,* 11**,** 126-30.

SEMPLE, B. D., BLOMGREN, K., GIMLIN, K., FERRIERO, D. M. & NOBLE-HAEUSSLEIN, L. J. 2013. Brain development in rodents and humans: Identifying benchmarks of maturation and vulnerability to injury across species. *Prog Neurobiol,* 106-107**,** 1-16.

SEPASI TEHRANI, H. & MOOSAVI-MOVAHEDI, A. A. 2018. Catalase and its mysteries. *Prog Biophys Mol Biol,* 140**,** 5-12.

SEPEHRMANESH, Z., HEIDARY, M., AKASHEH, N. & AKBARI, H. 2018. Therapeutic effect of adjunctive N-acetyl cysteine (NAC) on symptoms of chronic schizophrenia: A double-blind, randomized clinical trial. *Prog Neuropsychopharmacol Biol Psychiatry,* 82**,** 289-296.

SERI, B., GARCÍA-VERDUGO, J. M., MCEWEN, B. S. & ALVAREZ-BUYLLA, A. 2001. Astrocytes give rise to new neurons in the adult mammalian hippocampus. *J Neurosci,* 21**,** 7153-60.

SHAH, F. A., LIU, G., AL KURY, L. T., ZEB, A., ABBAS, M., LI, T., YANG, X., LIU, F., JIANG, Y., LI, S. & KOH, P. O. 2019. Melatonin Protects MCAO-Induced Neuronal Loss via NR2A Mediated Prosurvival Pathways. *Front Pharmacol,* 10**,** 297.

SHARIFI, M. D., KARIMI, N., KARAMI, M., BORHANI HAGHIGHI, A., SHABANI, M. & BAYAT, M. 2021. The Minocycline Ameliorated the Synaptic Plasticity Impairment in Vascular Dementia. *Iran J Pharm Res,* 20**,** 435-449.

SHEN, W. W. 1999. A history of antipsychotic drug development. *Compr Psychiatry,* 40**,** 407-14.

SHEN, Y. C., LIAO, D. L., CHEN, J. Y., WANG, Y. C., LAI, I. C., LIOU, Y. J., CHEN, Y. J., LUU, S. U. & CHEN, C. H. 2009. Resequencing and association study of vesicular glutamate transporter 1 gene (VGLUT1) with schizophrenia. *Schizophr Res,* 115**,** 254-60.

SHI, L., ZHANG, Z. & SU, B. 2016. Sex Biased Gene Expression Profiling of Human Brains at Major Developmental Stages. *Sci Rep,* 6**,** 21181.

SHI, X. J., DU, Y., LEI-CHEN, LI, X. S., YAO, C. Q. & CHENG, Y. 2022. Effects of brain-derived neurotrophic factor (BDNF) on the Schizophrenia model of animals. *J Psychiatr Res,* 156**,** 538-546.

SHIMADA, T., ITO, S., MAKABE, A., YAMANUSHI, A., TAKENAKA, A., KAWANO, K. & KOBAYASHI, M. 2022. Aerobic exercise and cognitive functioning in schizophrenia: An updated systematic review and meta-analysis. *Psychiatry Res,* 314**,** 114656.

SHIN YIM, Y., PARK, A., BERRIOS, J., LAFOURCADE, M., PASCUAL, L. M., SOARES, N., YEON KIM, J., KIM, S., KIM, H., WAISMAN, A., LITTMAN, D. R., WICKERSHAM, I. R., HARNETT, M. T., HUH, J. R. & CHOI, G. B. 2017. Reversing behavioural abnormalities in mice exposed to maternal inflammation. *Nature,* 549**,** 482-487.

SHIRAI, Y., FUJITA, Y., HASHIMOTO, R., OHI, K., YAMAMORI, H., YASUDA, Y., ISHIMA, T., SUGANUMA, H., USHIDA, Y., TAKEDA, M. & HASHIMOTO, K. 2015. Dietary Intake of Sulforaphane-Rich Broccoli Sprout Extracts during Juvenile and Adolescence Can Prevent Phencyclidine-Induced Cognitive Deficits at Adulthood. *PLoS One,* 10**,** e0127244.

SIBILLE, E., MORRIS, H. M., KOTA, R. S. & LEWIS, D. A. 2011. GABA-related transcripts in the dorsolateral prefrontal cortex in mood disorders. *Int J Neuropsychopharmacol,* 14**,** 721-34.

SIK, A., PENTTONEN, M., YLINEN, A. & BUZSÁKI, G. 1995. Hippocampal CA1 interneurons: an in vivo intracellular labeling study. *J Neurosci,* 15**,** 6651-65.

SIMÕES, L. R., SANGIOGO, G., TASHIRO, M. H., GENEROSO, J. S., FALLER, C. J., DOMINGUINI, D., MASTELLA, G. A., SCAINI, G., GIRIDHARAN, V. V., MICHELS, M., FLORENTINO, D., PETRONILHO, F., RÉUS, G. Z., DAL-PIZZOL, F., ZUGNO, A. I. & BARICHELLO, T. 2018. Maternal immune activation induced by lipopolysaccharide triggers immune response in pregnant mother and fetus, and induces behavioral impairment in adult rats. *J Psychiatr Res,* 100**,** 71-83.

SIMPLICIO, J. A., DO VALE, G. T., GONZAGA, N. A., LEITE, L. N., HIPÓLITO, U. V., PEREIRA, C. A., TOSTES, R. C. & TIRAPELLI, C. R. 2017. Reactive oxygen species derived from NAD(P)H oxidase play a role on ethanol-induced hypertension and endothelial dysfunction in rat resistance arteries. *J Physiol Biochem,* 73**,** 5-16.

SINGH, A. K., TIWARI, M. N., DIXIT, A., UPADHYAY, G., PATEL, D. K., SINGH, D., PRAKASH, O. & SINGH, M. P. 2011. Nigrostriatal proteomics of cypermethrin-induced dopaminergic neurodegeneration: microglial activation-dependent and -independent regulations. *Toxicol Sci,* 122**,** 526-38.

SLAKER, M., BARNES, J., SORG, B. A. & GRIMM, J. W. 2016. Impact of Environmental Enrichment on Perineuronal Nets in the Prefrontal Cortex following Early and Late Abstinence from Sucrose Self-Administration in Rats. *PLoS One,* 11**,** e0168256.

SMITH, C. C., MAURICIO, R., NOBRE, L., MARSH, B., WUST, R. C., ROSSITER, H. B. & ICHIYAMA, R. M. 2015. Differential regulation of perineuronal nets in the brain and spinal cord with exercise training. *Brain Res Bull,* 111**,** 20-6.

SMITH, P. J., BLUMENTHAL, J. A., HOFFMAN, B. M., COOPER, H., STRAUMAN, T. A., WELSH-BOHMER, K., BROWNDYKE, J. N. & SHERWOOD, A. 2010. Aerobic exercise and neurocognitive performance: a meta-analytic review of randomized controlled trials. *Psychosom Med,* 72**,** 239-52.

SMITH, S. E., LI, J., GARBETT, K., MIRNICS, K. & PATTERSON, P. H. 2007. Maternal immune activation alters fetal brain development through interleukin-6. *J Neurosci,* 27**,** 10695-702.

SNAIDERO, N., VELTE, C., MYLLYKOSKI, M., RAASAKKA, A., IGNATEV, A., WERNER, H. B., ERWIG, M. S., MÖBIUS, W., KURSULA, P., NAVE, K. A. & SIMONS, M. 2017. Antagonistic Functions of MBP and CNP Establish Cytosolic Channels in CNS Myelin. *Cell Rep,* 18**,** 314-323.

SNELL, L. D., BHAVE, S. V., TABAKOFF, B. & HOFFMAN, P. L. 2001. Chronic ethanol exposure delays the 'developmental switch' of the NMDA receptor 2A and 2B subunits in cultured cerebellar granule neurons. *J Neurochem,* 78**,** 396-405.

SNG, E., FRITH, E. & LOPRINZI, P. D. 2018. Experimental effects of acute exercise on episodic memory acquisition: Decomposition of multi-trial gains and losses. *Physiol Behav,* 186**,** 82-84.

SOKOLOV, B. P. 1998. Expression of NMDAR1, GluR1, GluR7, and KA1 glutamate receptor mRNAs is decreased in frontal cortex of "neuroleptic-free" schizophrenics: evidence on reversible up-regulation by typical neuroleptics. *J Neurochem,* 71**,** 2454-64.

SOMANI, S. M., HUSAIN, K., DIAZ-PHILLIPS, L., LANZOTTI, D. J., KARETI, K. R. & TRAMMELL, G. L. 1996. Interaction of exercise and ethanol on antioxidant enzymes in brain regions of the rat. *Alcohol,* 13**,** 603-10.

SONG, I. & DITYATEV, A. 2018. Crosstalk between glia, extracellular matrix and neurons. *Brain Res Bull,* 136**,** 101-108.

SONG, J. C., SEO, M. K., PARK, S. W., LEE, J. G. & KIM, Y. H. 2016. Differential Effects of Olanzapine and Haloperidol on MK-801-induced Memory Impairment in Mice. *Clin Psychopharmacol Neurosci,* 14**,** 279-85.

SØRENSEN, H. J., MORTENSEN, E. L., REINISCH, J. M. & MEDNICK, S. A. 2009. Association between prenatal exposure to bacterial infection and risk of schizophrenia. *Schizophr Bull,* 35**,** 631-7.

SOUMIYA, H., FUKUMITSU, H. & FURUKAWA, S. 2011. Prenatal immune challenge compromises development of upper-layer but not deeper-layer neurons of the mouse cerebral cortex. *J Neurosci Res,* 89**,** 1342-50.

SPATAZZA, J., LEE, H. H., DI NARDO, A. A., TIBALDI, L., JOLIOT, A., HENSCH, T. K. & PROCHIANTZ, A. 2013. Choroid-plexus-derived Otx2 homeoprotein constrains adult cortical plasticity. *Cell Rep,* 3**,** 1815-23.

SQUARZONI, P., OLLER, G., HOEFFEL, G., PONT-LEZICA, L., ROSTAING, P., LOW, D., BESSIS, A., GINHOUX, F. & GAREL, S. 2014. Microglia modulate wiring of the embryonic forebrain. *Cell Rep,* 8**,** 1271-9.

ST CLAIR, D., XU, M., WANG, P., YU, Y., FANG, Y., ZHANG, F., ZHENG, X., GU, N., FENG, G., SHAM, P. & HE, L. 2005. Rates of adult schizophrenia following prenatal exposure to the Chinese famine of 1959-1961. *JAMA,* 294**,** 557-62.

STAMENKOVIC, V., STAMENKOVIC, S., JAWORSKI, T., GAWLAK, M., JOVANOVIC, M., JAKOVCEVSKI, I., WILCZYNSKI, G. M., KACZMAREK, L., SCHACHNER, M., RADENOVIC, L. & ANDJUS, P. R. 2017. The extracellular matrix glycoprotein tenascin-C and matrix metalloproteinases modify cerebellar structural plasticity by exposure to an enriched environment. *Brain Struct Funct,* 222**,** 393-415.

STEDEHOUDER, J., BRIZEE, D., SLOTMAN, J. A., PASCUAL-GARCIA, M., LEYRER, M. L., BOUWEN, B. L., DIRVEN, C. M., GAO, Z., BERSON, D. M., HOUTSMULLER, A. B. & KUSHNER, S. A. 2019. Local axonal morphology guides the topography of interneuron myelination in mouse and human neocortex. *Elife,* 8.

STEDEHOUDER, J., COUEY, J. J., BRIZEE, D., HOSSEINI, B., SLOTMAN, J. A., DIRVEN, C. M. F., SHPAK, G., HOUTSMULLER, A. B. & KUSHNER, S. A. 2017. Fast-spiking Parvalbumin Interneurons are Frequently Myelinated in the Cerebral Cortex of Mice and Humans. *Cereb Cortex,* 27**,** 5001-5013.

STEENSBERG, A., VAN HALL, G., OSADA, T., SACCHETTI, M., SALTIN, B. & KLARLUND PEDERSEN, B. 2000. Production of interleukin-6 in contracting human skeletal muscles can account for the exercise-induced increase in plasma interleukin-6. *J Physiol,* 529 Pt 1**,** 237-42.

STĘPNICKI, P., KONDEJ, M. & KACZOR, A. A. 2018. Current Concepts and Treatments of Schizophrenia. *Molecules,* 23.

STEULLET, P., CABUNGCAL, J. H., COYLE, J., DIDRIKSEN, M., GILL, K., GRACE, A. A., HENSCH, T. K., LAMANTIA, A. S., LINDEMANN, L., MAYNARD, T. M., MEYER, U., MORISHITA, H., O'DONNELL, P., PUHL, M., CUENOD, M. & DO, K. Q. 2017. Oxidative stress-driven parvalbumin interneuron impairment as a common mechanism in models of schizophrenia. *Mol Psychiatry,* 22**,** 936-943.

STEULLET, P., CABUNGCAL, J. H., MONIN, A., DWIR, D., O'DONNELL, P., CUENOD, M. & DO, K. Q. 2016. Redox dysregulation, neuroinflammation, and NMDA receptor hypofunction: A "central hub" in schizophrenia pathophysiology? *Schizophr Res,* 176**,** 41-51.

STEULLET, P., NEIJT, H. C., CUÉNOD, M. & DO, K. Q. 2006. Synaptic plasticity impairment and hypofunction of NMDA receptors induced by glutathione deficit: relevance to schizophrenia. *Neuroscience,* 137**,** 807-19.

STILO, S. A. & MURRAY, R. M. 2019. Non-Genetic Factors in Schizophrenia. *Curr Psychiatry Rep,* 21**,** 100.

STOLK, J., HILTERMANN, T. J., DIJKMAN, J. H. & VERHOEVEN, A. J. 1994. Characteristics of the inhibition of NADPH oxidase activation in neutrophils by apocynin, a methoxy-substituted catechol. *Am J Respir Cell Mol Biol,* 11**,** 95-102.

STOLP, H. B., TURNQUIST, C., DZIEGIELEWSKA, K. M., SAUNDERS, N. R., ANTHONY, D. C. & MOLNÁR, Z. 2011. Reduced ventricular proliferation in the foetal cortex following maternal inflammation in the mouse. *Brain,* 134**,** 3236-48.

SU, Y., LIAN, J., HODGSON, J., ZHANG, W. & DENG, C. 2022. Prenatal Poly I:C Challenge Affects Behaviors and Neurotransmission via Elevated Neuroinflammation Responses in Female Juvenile Rats. *Int J Neuropsychopharmacol,* 25**,** 160-171.

SUBRAMANIAM, S. R. & FEDEROFF, H. J. 2017. Targeting Microglial Activation States as a Therapeutic Avenue in Parkinson's Disease. *Front Aging Neurosci,* 9**,** 176.

SULTANA, R., BROOKS, C. B., SHRESTHA, A., OGUNDELE, O. M. & LEE, C. C. 2021. Perineuronal Nets in the Prefrontal Cortex of a Schizophrenia Mouse Model: Assessment of Neuroanatomical, Electrophysiological, and Behavioral Contributions. *Int J Mol Sci,* 22.

SUN, H. J., ZHOU, H., FENG, X. M., GAO, Q., DING, L., TANG, C. S., ZHU, G. Q. & ZHOU, Y. B. 2014. Superoxide anions in the paraventricular nucleus mediate cardiac sympathetic afferent reflex in insulin resistance rats. *Acta Physiol (Oxf),* 212**,** 267-82.

SUN, X. R., ZHANG, H., ZHAO, H. T., JI, M. H., LI, H. H., WU, J., LI, K. Y. & YANG, J. J. 2016. Amelioration of oxidative stress-induced phenotype loss of parvalbumin interneurons might contribute to the beneficial effects of environmental enrichment in a rat model of post-traumatic stress disorder. *Behav Brain Res,* 312**,** 84-92.

SUTTKUS, A., ROHN, S., WEIGEL, S., GLOCKNER, P., ARENDT, T. & MORAWSKI, M. 2014. Aggrecan, link protein and tenascin-R are essential components of the perineuronal net to protect neurons against iron-induced oxidative stress. *Cell Death Dis,* 5**,** e1119.

SUVISAARI, J., HAUKKA, J., TANSKANEN, A., HOVI, T. & LÖNNQVIST, J. 1999. Association between prenatal exposure to poliovirus infection and adult schizophrenia. *Am J Psychiatry,* 156**,** 1100-2.

SUZUKI, H., AHUJA, C. S., SALEWSKI, R. P., LI, L., SATKUNENDRARAJAH, K., NAGOSHI, N., SHIBATA, S. & FEHLINGS, M. G. 2017. Neural stem cell mediated recovery is enhanced by Chondroitinase ABC pretreatment in chronic cervical spinal cord injury. *PLoS One,* 12**,** e0182339.

TADMOR, H., GOLANI, I., DORON, R., KREMER, I. & SHAMIR, A. 2018. ErbB signaling antagonist ameliorates behavioral deficit induced by phencyclidine (PCP) in mice, without affecting metabolic syndrome markers. *Prog Neuropsychopharmacol Biol Psychiatry,* 82**,** 322-331.

TAFOYA, L. C., MAMELI, M., MIYASHITA, T., GUZOWSKI, J. F., VALENZUELA, C. F. & WILSON, M. C. 2006. Expression and function of SNAP-25 as a universal SNARE component in GABAergic neurons. *J Neurosci,* 26**,** 7826-38.

TAKAHASHI, M., SHIRAKAWA, O., TOYOOKA, K., KITAMURA, N., HASHIMOTO, T., MAEDA, K., KOIZUMI, S., WAKABAYASHI, K., TAKAHASHI, H., SOMEYA, T. & NAWA, H. 2000. Abnormal expression of brain-derived neurotrophic factor and its receptor in the corticolimbic system of schizophrenic patients. *Mol Psychiatry,* 5**,** 293-300.

TALUKDAR, P. M., ABDUL, F., MAES, M., BINU, V. S., VENKATASUBRAMANIAN, G., KUTTY, B. M. & DEBNATH, M. 2020. Maternal Immune Activation Causes Schizophrenia-like Behaviors in the Offspring through Activation of Immune-Inflammatory, Oxidative and Apoptotic Pathways, and Lowered Antioxidant Defenses and Neuroprotection. *Mol Neurobiol,* 57**,** 4345-4361.

TAN, Y., FUJITA, Y., QU, Y., CHANG, L., PU, Y., WANG, S., WANG, X. & HASHIMOTO, K. 2020. Phencyclidine-induced cognitive deficits in mice are ameliorated by subsequent

repeated intermittent administration of (R)-ketamine, but not (S)-ketamine: Role of BDNF-TrkB signaling. *Pharmacol Biochem Behav,* 188**,** 172839.

TANDON, R., GAEBEL, W., BARCH, D. M., BUSTILLO, J., GUR, R. E., HECKERS, S., MALASPINA, D., OWEN, M. J., SCHULTZ, S., TSUANG, M., VAN OS, J. & CARPENTER, W. 2013. Definition and description of schizophrenia in the DSM-5. *Schizophr Res,* 150**,** 3-10.

TANG, B., JIA, H., KAST, R. J. & THOMAS, E. A. 2013. Epigenetic changes at gene promoters in response to immune activation in utero. *Brain Behav Immun,* 30**,** 168-75.

TANG, Y. & LE, W. 2016. Differential Roles of M1 and M2 Microglia in Neurodegenerative Diseases. *Mol Neurobiol,* 53**,** 1181-1194.

TANG, Y. P., SHIMIZU, E., DUBE, G. R., RAMPON, C., KERCHNER, G. A., ZHUO, M., LIU, G. & TSIEN, J. Z. 1999. Genetic enhancement of learning and memory in mice. *Nature,* 401**,** 63-9.

TANQUEIRO, S. R., MOURO, F. M., FERREIRA, C. B., FREITAS, C. F., FONSECA-GOMES, J., SIMÕES DO COUTO, F., SEBASTIÃO, A. M., DAWSON, N. & DIÓGENES, M. J. 2021. Sustained NMDA receptor hypofunction impairs brain-derived neurotropic factor signalling in the PFC, but not in the hippocampus, and disturbs PFC-dependent cognition in mice. *J Psychopharmacol,* 35**,** 730-743.

TARABEUX, J., KEBIR, O., GAUTHIER, J., HAMDAN, F. F., XIONG, L., PITON, A., SPIEGELMAN, D., HENRION, É., MILLET, B., FATHALLI, F., JOOBER, R., RAPOPORT, J. L., DELISI, L. E., FOMBONNE, É., MOTTRON, L., FORGET-DUBOIS, N., BOIVIN, M., MICHAUD, J. L., DRAPEAU, P., LAFRENIÈRE, R. G., ROULEAU, G. A., KREBS, M. O. & TEAM, S. D. 2011. Rare mutations in N-methyl-D-aspartate glutamate receptors in autism spectrum disorders and schizophrenia. *Transl Psychiatry,* 1**,** e55.

TARAZI, Z., SABET, M., DUDLEY, M. N. & GRIFFITH, D. C. 2019. Pharmacodynamics of Minocycline against *Acinetobacter baumannii* in a Rat Pneumonia Model. *Antimicrob Agents Chemother,* 63.

TAU, G. Z. & PETERSON, B. S. 2010. Normal development of brain circuits. *Neuropsychopharmacology,* 35**,** 147-68.

TAY, T. L., SAVAGE, J. C., HUI, C. W., BISHT, K. & TREMBLAY, M. 2017. Microglia across the lifespan: from origin to function in brain development, plasticity and cognition. *J Physiol,* 595**,** 1929-1945.

TEFFER, K. & SEMENDEFERI, K. 2012. Human prefrontal cortex: evolution, development, and pathology. *Prog Brain Res,* 195**,** 191-218.

THION, M. S., MOSSER, C. A., FÉRÉZOU, I., GRISEL, P., BAPTISTA, S., LOW, D., GINHOUX, F., GAREL, S. & AUDINAT, E. 2019. Biphasic Impact of Prenatal Inflammation and Macrophage Depletion on the Wiring of Neocortical Inhibitory Circuits. *Cell Rep,* 28**,** 1119-1126.e4.

THOMPSON RAY, M., WEICKERT, C. S., WYATT, E. & WEBSTER, M. J. 2011. Decreased BDNF, trkB-TK+ and GAD67 mRNA expression in the hippocampus of individuals with schizophrenia and mood disorders. *J Psychiatry Neurosci,* 36**,** 195-203.

THOMSEN, M. S., HANSEN, H. H. & MIKKELSEN, J. D. 2010. α7 nicotinic receptor agonism mitigates phencyclidine-induced changes in synaptophysin and Arc gene expression in the mouse prefrontal cortex. *Neurochem Int,* 57**,** 756-61.

THUNE, J. J., UYLINGS, H. B. & PAKKENBERG, B. 2001. No deficit in total number of neurons in the prefrontal cortex in schizophrenics. *J Psychiatr Res,* 35**,** 15-21.

TIEGO, J., TESTA, R., BELLGROVE, M. A., PANTELIS, C. & WHITTLE, S. 2018. A Hierarchical Model of Inhibitory Control. *Front Psychol,* 9**,** 1339.

TIKKA, T. M. & KOISTINAHO, J. E. 2001. Minocycline provides neuroprotection against N-methyl-D-aspartate neurotoxicity by inhibiting microglia. *J Immunol,* 166**,** 7527-33.

TONG, L., SHEN, H., PERREAU, V. M., BALAZS, R. & COTMAN, C. W. 2001. Effects of exercise on gene-expression profile in the rat hippocampus. *Neurobiol Dis,* 8**,** 1046-56.

TORDERA, R. M., TOTTERDELL, S., WOJCIK, S. M., BROSE, N., ELIZALDE, N., LASHERAS, B. & DEL RIO, J. 2007. Enhanced anxiety, depressive-like behaviour and impaired recognition memory in mice with reduced expression of the vesicular glutamate transporter 1 (VGLUT1). *Eur J Neurosci,* 25**,** 281-90.

TORRES, I. J., FLASHMAN, L. A., O'LEARY, D. S. & ANDREASEN, N. C. 2001. Effects of retroactive and proactive interference on word list recall in schizophrenia. *J Int Neuropsychol Soc,* 7**,** 481-90.

TOVAR, K. R. & WESTBROOK, G. L. 2002. Mobile NMDA receptors at hippocampal synapses. *Neuron,* 34**,** 255-64.

TRAYNELIS, S. F., WOLLMUTH, L. P., MCBAIN, C. J., MENNITI, F. S., VANCE, K. M., OGDEN, K. K., HANSEN, K. B., YUAN, H., MYERS, S. J. & DINGLEDINE, R. 2010. Glutamate receptor ion channels: structure, regulation, and function. *Pharmacol Rev,* 62**,** 405-96.

TSAI, C. L., PAN, C. Y., TSENG, Y. T., CHEN, F. C., CHANG, Y. C. & WANG, T. C. 2021. Acute effects of high-intensity interval training and moderate-intensity continuous exercise on BDNF and irisin levels and neurocognitive performance in late middle-aged and older adults. *Behav Brain Res,* 413**,** 113472.

TSAI, J. & ROSENHECK, R. A. 2013. Psychiatric comorbidity among adults with schizophrenia: a latent class analysis. *Psychiatry Res,* 210**,** 16-20.

ULBRICH, P., KHOSHNEVISZADEH, M., JANDKE, S., SCHREIBER, S. & DITYATEV, A. 2021. Interplay between perivascular and perineuronal extracellular matrix remodelling in neurological and psychiatric diseases. *Eur J Neurosci,* 53**,** 3811-3830.

UPTHEGROVE, R. & KHANDAKER, G. M. 2020. Cytokines, Oxidative Stress and Cellular Markers of Inflammation in Schizophrenia. *Curr Top Behav Neurosci,* 44**,** 49-66.

URYASH, A., FLORES, V., ADAMS, J. A., ALLEN, P. D. & LOPEZ, J. R. 2020. Memory and Learning Deficits Are Associated With Ca. *Front Aging Neurosci,* 12**,** 224.

UTTL, L., PETRASEK, T., SENGUL, H., SVOJANOVSKA, M., LOBELLOVA, V., VALES, K., RADOSTOVA, D., TSENOV, G., KUBOVA, H., MIKULECKA, A., SVOBODA, J. & STUCHLIK, A. 2018. Chronic MK-801 Application in Adolescence and Early Adulthood: A Spatial Working Memory Deficit in Adult Long-Evans Rats But No Changes in the Hippocampal NMDA Receptor Subunits. *Frontiers in pharmacology,* 9.

UYSAL, N., KIRAY, M., SISMAN, A. R., CAMSARI, U. M., GENCOGLU, C., BAYKARA, B., CETINKAYA, C. & AKSU, I. 2015. Effects of voluntary and involuntary exercise on cognitive functions, and VEGF and BDNF levels in adolescent rats. *Biotech Histochem,* 90**,** 55-68.

VAFADARI, B., MITRA, S., STEFANIUK, M. & KACZMAREK, L. 2019. Psychosocial Stress Induces Schizophrenia-Like Behavior in Mice With Reduced MMP-9 Activity. *Front Behav Neurosci,* 13**,** 195.

VAFADARI, B., SALAMIAN, A. & KACZMAREK, L. 2016. MMP-9 in translation: from molecule to brain physiology, pathology, and therapy. *J Neurochem,* 139 Suppl 2**,** 91-114.

VALERIO, A., FERRARIO, M., DREANO, M., GAROTTA, G., SPANO, P. & PIZZI, M. 2002. Soluble interleukin-6 (IL-6) receptor/IL-6 fusion protein enhances in vitro differentiation of purified rat oligodendroglial lineage cells. *Mol Cell Neurosci,* 21**,** 602-15.

VALLIÈRES, L., CAMPBELL, I. L., GAGE, F. H. & SAWCHENKO, P. E. 2002. Reduced hippocampal neurogenesis in adult transgenic mice with chronic astrocytic production of interleukin-6. *J Neurosci,* 22**,** 486-92.

VALVASSORI, S. S., CARARO, J. H., MENEGAS, S., POSSAMAI-DELLA, T., AGUIAR-GERALDO, J. M., ARAUJO, S. L., MASTELLA, G. A., QUEVEDO, J. & ZUGNO, A. I. 2021. Haloperidol elicits oxidative damage in the brain of rats submitted to the ketamine-induced model of schizophrenia. *Brain Res Bull,* 170**,** 246-253.

VAN ERP, T. G., HIBAR, D. P., RASMUSSEN, J. M., GLAHN, D. C., PEARLSON, G. D., ANDREASSEN, O. A., AGARTZ, I., WESTLYE, L. T., HAUKVIK, U. K., DALE, A. M., MELLE, I., HARTBERG, C. B., GRUBER, O., KRAEMER, B., ZILLES, D., DONOHOE, G., KELLY, S., MCDONALD, C., MORRIS, D. W., CANNON, D. M., CORVIN, A., MACHIELSEN, M. W., KOENDERS, L., DE HAAN, L., VELTMAN, D. J., SATTERTHWAITE, T. D., WOLF, D. H., GUR, R. C., GUR, R. E., POTKIN, S. G., MATHALON, D. H., MUELLER, B. A., PREDA, A., MACCIARDI, F., EHRLICH, S., WALTON, E., HASS, J., CALHOUN, V. D., BOCKHOLT, H. J., SPONHEIM, S. R., SHOEMAKER, J. M., VAN HAREN, N. E., HULSHOFF POL, H. E., OPHOFF, R. A., KAHN, R. S., ROIZ-SANTIAÑEZ, R., CRESPO-FACORRO, B., WANG, L., ALPERT, K. I., JÖNSSON, E. G.,

DIMITROVA, R., BOIS, C., WHALLEY, H. C., MCINTOSH, A. M., LAWRIE, S. M., HASHIMOTO, R., THOMPSON, P. M. & TURNER, J. A. 2016. Subcortical brain volume abnormalities in 2028 individuals with schizophrenia and 2540 healthy controls via the ENIGMA consortium. *Mol Psychiatry,* 21**,** 585.

VAN ERP, T. G. M., WALTON, E., HIBAR, D. P., SCHMAAL, L., JIANG, W., GLAHN, D. C., PEARLSON, G. D., YAO, N., FUKUNAGA, M., HASHIMOTO, R., OKADA, N., YAMAMORI, H., BUSTILLO, J. R., CLARK, V. P., AGARTZ, I., MUELLER, B. A., CAHN, W., DE ZWARTE, S. M. C., HULSHOFF POL, H. E., KAHN, R. S., OPHOFF, R. A., VAN HAREN, N. E. M., ANDREASSEN, O. A., DALE, A. M., DOAN, N. T., GURHOLT, T. P., HARTBERG, C. B., HAUKVIK, U. K., JØRGENSEN, K. N., LAGERBERG, T. V., MELLE, I., WESTLYE, L. T., GRUBER, O., KRAEMER, B., RICHTER, A., ZILLES, D., CALHOUN, V. D., CRESPO-FACORRO, B., ROIZ-SANTIAÑEZ, R., TORDESILLAS-GUTIÉRREZ, D., LOUGHLAND, C., CARR, V. J., CATTS, S., CROPLEY, V. L., FULLERTON, J. M., GREEN, M. J., HENSKENS, F. A., JABLENSKY, A., LENROOT, R. K., MOWRY, B. J., MICHIE, P. T., PANTELIS, C., QUIDÉ, Y., SCHALL, U., SCOTT, R. J., CAIRNS, M. J., SEAL, M., TOONEY, P. A., RASSER, P. E., COOPER, G., SHANNON WEICKERT, C., WEICKERT, T. W., MORRIS, D. W., HONG, E., KOCHUNOV, P., BEARD, L. M., GUR, R. E., GUR, R. C., SATTERTHWAITE, T. D., WOLF, D. H., BELGER, A., BROWN, G. G., FORD, J. M., MACCIARDI, F., MATHALON, D. H., O'LEARY, D. S., POTKIN, S. G., PREDA, A., VOYVODIC, J., LIM, K. O., MCEWEN, S., YANG, F., TAN, Y., TAN, S., WANG, Z., FAN, F., CHEN, J., XIANG, H., TANG, S., GUO, H., WAN, P., WEI, D., BOCKHOLT, H. J., EHRLICH, S., WOLTHUSEN, R. P. F., KING, M. D., SHOEMAKER, J. M., SPONHEIM, S. R., DE HAAN, L., KOENDERS, L., et al. 2018. Cortical Brain Abnormalities in 4474 Individuals With Schizophrenia and 5098 Control Subjects via the Enhancing Neuro Imaging Genetics Through Meta Analysis (ENIGMA) Consortium. *Biol Psychiatry,* 84**,** 644-654.

VAN KAMMEN DP, MCALLISTER-SISTILLI, C. G., KELLEY, M. E., GURKLIS, J. A. & YAO, J. K. 1999. Elevated interleukin-6 in schizophrenia. *Psychiatry Res,* 87**,** 129-36.

VAN PRAAG, H., CHRISTIE, B. R., SEJNOWSKI, T. J. & GAGE, F. H. 1999. Running enhances neurogenesis, learning, and long-term potentiation in mice. *Proc Natl Acad Sci U S A,* 96**,** 13427-31.

VARESE, F., SMEETS, F., DRUKKER, M., LIEVERSE, R., LATASTER, T., VIECHTBAUER, W., READ, J., VAN OS, J. & BENTALL, R. P. 2012. Childhood adversities increase the risk of psychosis: a meta-analysis of patient-control, prospective- and cross-sectional cohort studies. *Schizophr Bull,* 38**,** 661-71.

VASISTHA, N. A., PARDO-NAVARRO, M., GASTHAUS, J., WEIJERS, D., MÜLLER, M. K., GARCÍA-GONZÁLEZ, D., MALWADE, S., KORSHUNOVA, I., PFISTERER, U., VON ENGELHARDT, J., HOUGAARD, K. S. & KHODOSEVICH, K. 2020. Maternal inflammation has a profound effect on cortical interneuron development in a stage and subtype-specific manner. *Mol Psychiatry,* 25**,** 2313-2329.

VAYNMAN, S., YING, Z. & GOMEZ-PINILLA, F. 2004. Hippocampal BDNF mediates the efficacy of exercise on synaptic plasticity and cognition. *Eur J Neurosci,* 20**,** 2580-90.

VEERASAKUL, S., THANOI, S., REYNOLDS, G. P. & NUDMAMUD-THANOI, S. 2016. Effect of Methamphetamine Exposure on Expression of Calcium Binding Proteins in Rat Frontal Cortex and Hippocampus. *Neurotox Res,* 30**,** 427-33.

VENABLES, N. C., BERNAT, E. M. & SPONHEIM, S. R. 2009. Genetic and disorder-specific aspects of resting state EEG abnormalities in schizophrenia. *Schizophr Bull,* 35**,** 826-39.

VIEIRA, M., YONG, X. L. H., ROCHE, K. W. & ANGGONO, V. 2020. Regulation of NMDA glutamate receptor functions by the GluN2 subunits. *J Neurochem,* 154**,** 121-143.

VOLK, D. W., AUSTIN, M. C., PIERRI, J. N., SAMPSON, A. R. & LEWIS, D. A. 2000. Decreased glutamic acid decarboxylase67 messenger RNA expression in a subset of prefrontal cortical gamma-aminobutyric acid neurons in subjects with schizophrenia. *Arch Gen Psychiatry,* 57**,** 237-45.

VOLK, D. W., MOROCO, A. E., ROMAN, K. M., EDELSON, J. R. & LEWIS, D. A. 2019. The Role of the Nuclear Factor-κB Transcriptional Complex in Cortical Immune Activation in Schizophrenia. *Biol Psychiatry,* 85**,** 25-34.

VOLK, D. W., SAMPSON, A. R., ZHANG, Y., EDELSON, J. R. & LEWIS, D. A. 2016. Cortical GABA markers identify a molecular subtype of psychotic and bipolar disorders. *Psychol Med,* 46**,** 2501-12.

VON AHLFEN, S. & SCHLUMPBERGER, M. 2010. Effects of low A260/A230 ratios in RNA preparations on downstream applications. *In:* QIAGEN (ed.) 15 ed. https://www.qiagen.com/~/media/1ea8aec3bfa24543a28fcaea25986514.ashx: Qiagen.

VREUGDENHIL, M., JEFFERYS, J. G., CELIO, M. R. & SCHWALLER, B. 2003. Parvalbumin-deficiency facilitates repetitive IPSCs and gamma oscillations in the hippocampus. *J Neurophysiol,* 89**,** 1414-22.

VUILLERMOT, S., JOODMARDI, E., PERLMANN, T., ÖGREN, S. O., FELDON, J. & MEYER, U. 2012. Prenatal immune activation interacts with genetic Nurr1 deficiency in the development of attentional impairments. *J Neurosci,* 32**,** 436-51.

VYKLICKY, V., KORINEK, M., SMEJKALOVA, T., BALIK, A., KRAUSOVA, B., KANIAKOVA, M., LICHNEROVA, K., CERNY, J., KRUSEK, J., DITTERT, I., HORAK, M. & VYKLICKY, L. 2014. Structure, function, and pharmacology of NMDA receptor channels. *Physiol Res,* 63**,** S191-203.

WAGNER, E., SIAFIS, S., FERNANDO, P., FALKAI, P., HONER, W. G., RÖH, A., SISKIND, D., LEUCHT, S. & HASAN, A. 2021. Efficacy and safety of clozapine in psychotic disorders-a systematic quantitative meta-review. *Transl Psychiatry,* 11**,** 487.

WALSH, J. J. 2018. A multifaceted investigation into the effects of acute exercise on indices of brain function. *Appl Physiol Nutr Metab,* 43**,** 411.

WALTON, N. M., ZHOU, Y., KOGAN, J. H., SHIN, R., WEBSTER, M., GROSS, A. K., HEUSNER, C. L., CHEN, Q., MIYAKE, S., TAJINDA, K., TAMURA, K., MIYAKAWA, T. & MATSUMOTO, M. 2012. Detection of an immature dentate gyrus feature in human schizophrenia/bipolar patients. *Transl Psychiatry,* 2**,** e135.

WANG, C. X. & SHUAIB, A. 2005. NMDA/NR2B selective antagonists in the treatment of ischemic brain injury. *Curr Drug Targets CNS Neurol Disord,* 4**,** 143-51.

WANG, D. & FAWCETT, J. 2012. The perineuronal net and the control of CNS plasticity. *Cell Tissue Res,* 349**,** 147-60.

WANG, K., LI, L., SONG, Y., YE, X., FU, S., JIANG, J. & LI, S. 2013a. Improvement of pharmacokinetics behavior of apocynin by nitrone derivatization: comparative pharmacokinetics of nitrone-apocynin and its parent apocynin in rats. *PLoS One,* 8**,** e70189.

WANG, L., CAO, M., PU, T., HUANG, H., MARSHALL, C. & XIAO, M. 2018a. Enriched Physical Environment Attenuates Spatial and Social Memory Impairments of Aged Socially Isolated Mice. *Int J Neuropsychopharmacol,* 21**,** 1114-1127.

WANG, M., XIE, Y. & QIN, D. 2021. Proteolytic cleavage of proBDNF to mBDNF in neuropsychiatric and neurodegenerative diseases. *Brain Res Bull,* 166**,** 172-184.

WANG, Q., WANG, Y., JI, W., ZHOU, G., HE, K., LI, Z., CHEN, J., LI, W., WEN, Z., SHEN, J., QIANG, Y., JI, J., SHI, Y. & YI, Q. 2015. SNAP25 is associated with schizophrenia and major depressive disorder in the Han Chinese population. *J Clin Psychiatry,* 76**,** e76-82.

WANG, X., PINTO-DUARTE, A., SEJNOWSKI, T. J. & BEHRENS, M. M. 2013b. How Nox2-containing NADPH oxidase affects cortical circuits in the NMDA receptor antagonist model of schizophrenia. *Antioxid Redox Signal,* 18**,** 1444-62.

WANG, Y., BRANICKY, R., NOË, A. & HEKIMI, S. 2018b. Superoxide dismutases: Dual roles in controlling ROS damage and regulating ROS signaling. *J Cell Biol,* 217**,** 1915-1928.

WANG, Z., BRUMBACK, B. A., ALRWISAN, A. A. & WINTERSTEIN, A. G. 2019. Model-based standardization using an outcome model with random effects. *Stat Med,* 38**,** 3378-3394.

WASHBOURNE, P., THOMPSON, P. M., CARTA, M., COSTA, E. T., MATHEWS, J. R., LOPEZ-BENDITÓ, G., MOLNÁR, Z., BECHER, M. W., VALENZUELA, C. F., PARTRIDGE, L. D. & WILSON, M. C. 2002. Genetic ablation of the t-SNARE SNAP-25 distinguishes mechanisms of neuroexocytosis. *Nat Neurosci,* 5**,** 19-26.

WEBER, P., BARTSCH, U., RASBAND, M. N., CZANIERA, R., LANG, Y., BLUETHMANN, H., MARGOLIS, R. U., LEVINSON, S. R., SHRAGER, P., MONTAG, D. & SCHACHNER, M. 1999. Mice deficient for tenascin-R display alterations of the extracellular matrix and decreased axonal conduction velocities in the CNS. *J Neurosci,* 19**,** 4245-62.

WEGRZYN, D., JUCKEL, G. & FAISSNER, A. 2022. Structural and Functional Deviations of the Hippocampus in Schizophrenia and Schizophrenia Animal Models. *Int J Mol Sci,* 23.

WEGRZYN, D., MANITZ, M. P., KOSTKA, M., FREUND, N., JUCKEL, G. & FAISSNER, A. 2021. Poly I:C-induced maternal immune challenge reduces perineuronal net area and raises spontaneous network activity of hippocampal neurons in vitro. *Eur J Neurosci,* 53**,** 3920-3941.

WEI, H., CHADMAN, K. K., MCCLOSKEY, D. P., SHEIKH, A. M., MALIK, M., BROWN, W. T. & LI, X. 2012. Brain IL-6 elevation causes neuronal circuitry imbalances and mediates autism-like behaviors. *Biochim Biophys Acta,* 1822**,** 831-42.

WEI, Y., XIAO, L., FAN, W., ZOU, J., YANG, H., LIU, B., YE, Y., WEN, D. & LIAO, L. 2022. Astrocyte Activation, but not Microglia, Is Associated with the Experimental Mouse Model of Schizophrenia Induced by Chronic Ketamine. *J Mol Neurosci,* 72**,** 1902-1915.

WEICKERT, C. S., FUNG, S. J., CATTS, V. S., SCHOFIELD, P. R., ALLEN, K. M., MOORE, L. T., NEWELL, K. A., PELLEN, D., HUANG, X. F., CATTS, S. V. & WEICKERT, T. W. 2013. Molecular evidence of N-methyl-D-aspartate receptor hypofunction in schizophrenia. *Mol Psychiatry,* 18**,** 1185-92.

WEICKERT, C. S., HYDE, T. M., LIPSKA, B. K., HERMAN, M. M., WEINBERGER, D. R. & KLEINMAN, J. E. 2003. Reduced brain-derived neurotrophic factor in prefrontal cortex of patients with schizophrenia. *Mol Psychiatry,* 8**,** 592-610.

WEISER, M., GERSHON, A. A., RUBINSTEIN, K., PETCU, C., LADEA, M., SIMA, D., PODEA, D., KEEFE, R. S. & DAVIS, J. M. 2012. A randomized controlled trial of allopurinol vs. placebo added on to antipsychotics in patients with schizophrenia or schizoaffective disorder. *Schizophr Res,* 138**,** 35-8.

WEISER, M., LEVI, L., BURSHTEIN, S., CHIRIȚĂ, R., CIRJALIU, D., GONEN, I., YOLKEN, R., DAVIDSON, M., ZAMORA, D. & DAVIS, J. M. 2019. The effect of minocycline on symptoms in schizophrenia: Results from a randomized controlled trial. *Schizophr Res,* 206**,** 325-332.

WEN, T. H., AFROZ, S., REINHARD, S. M., PALACIOS, A. R., TAPIA, K., BINDER, D. K., RAZAK, K. A. & ETHELL, I. M. 2018a. Genetic Reduction of Matrix Metalloproteinase-9 Promotes Formation of Perineuronal Nets Around Parvalbumin-Expressing Interneurons and Normalizes Auditory Cortex Responses in Developing Fmr1 Knock-Out Mice. *Cereb Cortex,* 28**,** 3951-3964.

WEN, T. H., BINDER, D. K., ETHELL, I. M. & RAZAK, K. A. 2018b. The Perineuronal 'Safety' Net? Perineuronal Net Abnormalities in Neurological Disorders. *Front Mol Neurosci,* 11**,** 270.

WESSELING, H., WANT, E. J., GUEST, P. C., RAHMOUNE, H., HOLMES, E. & BAHN, S. 2015. Hippocampal Proteomic and Metabonomic Abnormalities in Neurotransmission, Oxidative Stress, and Apoptotic Pathways in a Chronic Phencyclidine Rat Model. *J Proteome Res,* 14**,** 3174-87.

WHITTAKER, R. G., TURNBULL, D. M., WHITTINGTON, M. A. & CUNNINGHAM, M. O. 2011. Impaired mitochondrial function abolishes gamma oscillations in the hippocampus through an effect on fast-spiking interneurons. *Brain,* 134**,** e180; author reply e181.

WIĘDŁOCHA, M., ZBOROWSKA, N., MARCINOWICZ, P., DĘBOWSKA, W., DĘBOWSKA, M., ZALEWSKA, A., MACIEJCZYK, M., WASZKIEWICZ, N. & SZULC, A. 2023. Oxidative Stress Biomarkers among Schizophrenia Inpatients. *Brain Sci,* 13.

WIERA, G., NOWAK, D., VAN HOVE, I., DZIEGIEL, P., MOONS, L. & MOZRZYMAS, J. W. 2017. Mechanisms of NMDA Receptor- and Voltage-Gated L-Type Calcium Channel-

Dependent Hippocampal LTP Critically Rely on Proteolysis That Is Mediated by Distinct Metalloproteinases. *J Neurosci,* 37**,** 1240-1256.

WIESEL, T. N. & HUBEL, D. H. 1963. SINGLE-CELL RESPONSES IN STRIATE CORTEX OF KITTENS DEPRIVED OF VISION IN ONE EYE. *Journal of Neurophysiology,* 26**,** 1003-1017.

WILKINS, A., NIKODEMOVA, M., COMPSTON, A. & DUNCAN, I. 2004. Minocycline attenuates nitric oxide-mediated neuronal and axonal destruction in vitro. *Neuron Glia Biol,* 1**,** 297-305.

WINGATE, S., CRAWFORD, L., FRITH, E. & LOPRINZI, P. D. 2018. Experimental investigation of the effects of acute exercise on memory interference. *Health Promot Perspect,* 8**,** 208-214.

WISCHHOF, L., IRRSACK, E., OSORIO, C. & KOCH, M. 2015. Prenatal LPS-exposure--a neurodevelopmental rat model of schizophrenia--differentially affects cognitive functions, myelination and parvalbumin expression in male and female offspring. *Prog Neuropsychopharmacol Biol Psychiatry,* 57**,** 17-30.

WITKIN, J. M., CERNE, R., NEWMAN, A. H., IZENWASSER, S., SMITH, J. L. & TORTELLA, F. C. 2021. N-Substituted-3-alkoxy-derivatives of dextromethorphan are functional NMDA receptor antagonists in vivo: Evidence from an NMDA-induced seizure model in rats. *Pharmacol Biochem Behav,* 203**,** 173154.

WOLF, S. A., MELNIK, A. & KEMPERMANN, G. 2011. Physical exercise increases adult neurogenesis and telomerase activity, and improves behavioral deficits in a mouse model of schizophrenia. *Brain Behav Immun,* 25**,** 971-80.

WONG, E. H., KEMP, J. A., PRIESTLEY, T., KNIGHT, A. R., WOODRUFF, G. N. & IVERSEN, L. L. 1986. The anticonvulsant MK-801 is a potent N-methyl-D-aspartate antagonist. *Proc Natl Acad Sci U S A,* 83**,** 7104-8.

WONG, J., ROTHMOND, D. A., WEBSTER, M. J. & WEICKERT, C. S. 2013. Increases in two truncated TrkB isoforms in the prefrontal cortex of people with schizophrenia. *Schizophr Bull,* 39**,** 130-40.

WOO, T. U., WHITEHEAD, R. E., MELCHITZKY, D. S. & LEWIS, D. A. 1998. A subclass of prefrontal gamma-aminobutyric acid axon terminals are selectively altered in schizophrenia. *Proc Natl Acad Sci U S A,* 95**,** 5341-6.

WOODWARD, E. M. & COUTELLIER, L. 2021. Age- and sex-specific effects of stress on parvalbumin interneurons in preclinical models: Relevance to sex differences in clinical neuropsychiatric and neurodevelopmental disorders. *Neurosci Biobehav Rev,* 131**,** 1228-1242.

WOŹNIAK, M., CIEŚLIK, P., MARCINIAK, M., LENDA, T., PILC, A. & WIERONSKA, J. M. 2018. Neurochemical changes underlying schizophrenia-related behavior in a modified forced swim test in mice. *Pharmacol Biochem Behav,* 172**,** 50-58.

WU, D., LV, P., LI, F., ZHANG, W., FU, G., DAI, J., HU, N., LIU, J., XIAO, Y., LI, S., SHAH, C., TAO, B., ZHAO, Y., GONG, Q. & LUI, S. 2019. Association of peripheral cytokine levels with cerebral structural abnormalities in schizophrenia. *Brain Res,* 1724**,** 146463.

WU, Y., DENG, F., WANG, J., LIU, Y., ZHOU, W., QU, L. & CHENG, M. 2020. Intensity-dependent effects of consecutive treadmill exercise on spatial learning and memory through the p-CREB/BDNF/NMDAR signaling in hippocampus. *Behav Brain Res,* 386**,** 112599.

WU, Y. C., DU, X., VAN DEN BUUSE, M. & HILL, R. A. 2014. Sex differences in the adolescent developmental trajectory of parvalbumin interneurons in the hippocampus: a role for estradiol. *Psychoneuroendocrinology,* 45**,** 167-78.

XIA, Y., ZHANG, Z., LIN, W., YAN, J., ZHU, C., YIN, D., HE, S., SU, Y., XU, N., CALDWELL, R. W., YAO, L. & CHEN, Y. 2020. Modulating microglia activation prevents maternal immune activation induced schizophrenia-relevant behavior phenotypes via arginase 1 in the dentate gyrus. *Neuropsychopharmacology,* 45**,** 1896-1908.

XIANCHU, L., KANG, L., BEIWAN, D., HUAN, P. & MING, L. 2021. Apocynin ameliorates cognitive deficits in streptozotocin-induced diabetic rats. *Bratisl Lek Listy,* 122**,** 78-84.

XIAO, X., XU, X., LI, F., XIE, G. & ZHANG, T. 2019. Anti-inflammatory treatment with β-asarone improves impairments in social interaction and cognition in MK-801 treated mice. *Brain Res Bull,* 150**,** 150-159.

XIE, Y., HUANG, D., WEI, L. & LUO, X. J. 2018. Further evidence for the genetic association between CACNA1I and schizophrenia. *Hereditas,* 155**,** 16.

XUE, M., ATALLAH, B. V. & SCANZIANI, M. 2014. Equalizing excitation-inhibition ratios across visual cortical neurons. *Nature,* 511**,** 596-600.

YAMADA, J. & JINNO, S. 2015a. Subclass-specific formation of perineuronal nets around parvalbumin-expressing GABAergic neurons in Ammon's horn of the mouse hippocampus. *J Comp Neurol,* 523**,** 790-804.

YAMADA, J., OHGOMORI, T. & JINNO, S. 2015b. Perineuronal nets affect parvalbumin expression in GABAergic neurons of the mouse hippocampus. *Eur J Neurosci,* 41**,** 368-78.

YAMADA, J., OHGOMORI, T. & JINNO, S. 2017. Alterations in expression of Cat-315 epitope of perineuronal nets during normal ageing, and its modulation by an open-channel NMDA receptor blocker, memantine. *J Comp Neurol,* 525**,** 2035-2049.

YAMADA, M., IWASE, M., SASAKI, B. & SUZUKI, N. 2022. The molecular regulation of oligodendrocyte development and CNS myelination by ECM proteins. *Front Cell Dev Biol,* 10**,** 952135.

YAMAMORI, H., HASHIMOTO, R., ISHIMA, T., KISHI, F., YASUDA, Y., OHI, K., FUJIMOTO, M., UMEDA-YANO, S., ITO, A., HASHIMOTO, K. & TAKEDA, M. 2013. Plasma levels of mature brain-derived neurotrophic factor (BDNF) and matrix metalloproteinase-9 (MMP-9) in treatment-resistant schizophrenia treated with clozapine. *Neurosci Lett,* 556**,** 37-41.

YAMAZAKI, Y., SATO, D., YAMASHIRO, K., TSUBAKI, A., TAKEHARA, N., UETAKE, Y., NAKANO, S. & MARUYAMA, A. 2018. Inter-individual differences in working memory improvement after acute mild and moderate aerobic exercise. *PLoS One,* 13**,** e0210053.

YANAGI, M., JOHO, R. H., SOUTHCOTT, S. A., SHUKLA, A. A., GHOSE, S. & TAMMINGA, C. A. 2014. Kv3.1-containing K(+) channels are reduced in untreated schizophrenia and normalized with antipsychotic drugs. *Mol Psychiatry,* 19**,** 573-9.

YANG, Y. S., DAVIS, M. C., WYNN, J. K., HELLEMANN, G., GREEN, M. F. & MARDER, S. R. 2019. N-acetylcysteine improves EEG measures of auditory deviance detection and neural synchronization in schizophrenia: A randomized, controlled pilot study. *Schizophr Res,* 208**,** 479-480.

YAO, J. K. & KESHAVAN, M. S. 2011. Antioxidants, redox signaling, and pathophysiology in schizophrenia: an integrative view. *Antioxid Redox Signal,* 15**,** 2011-35.

YASHIRO, K. & PHILPOT, B. D. 2008. Regulation of NMDA receptor subunit expression and its implications for LTD, LTP, and metaplasticity. *Neuropharmacology,* 55**,** 1081-94.

YAU, S. Y., BETTIO, L., VETRICI, M., TRUESDELL, A., CHIU, C., CHIU, J., TRUESDELL, E. & CHRISTIE, B. R. 2018. Chronic minocycline treatment improves hippocampal neuronal structure, NMDA receptor function, and memory processing in Fmr1 knockout mice. *Neurobiol Dis,* 113**,** 11-22.

YAU, S. Y., LI, A., ZHANG, E. D., CHRISTIE, B. R., XU, A., LEE, T. M. & SO, K. F. 2014. Sustained running in rats administered corticosterone prevents the development of depressive behaviors and enhances hippocampal neurogenesis and synaptic plasticity without increasing neurotrophic factor levels. *Cell Transplant,* 23**,** 481-92.

YE, Q. & MIAO, Q. L. 2013. Experience-dependent development of perineuronal nets and chondroitin sulfate proteoglycan receptors in mouse visual cortex. *Matrix Biol,* 32**,** 352-63.

YEE, N., RIBIC, A., DE ROO, C. C. & FUCHS, E. 2011. Differential effects of maternal immune activation and juvenile stress on anxiety-like behaviour and physiology in adult rats: no evidence for the "double-hit hypothesis". *Behav Brain Res,* 224**,** 180-8.

YEE, N., SCHWARTING, R. K., FUCHS, E. & WÖHR, M. 2012. Increased affective ultrasonic communication during fear learning in adult male rats exposed to maternal immune activation. *J Psychiatr Res,* 46**,** 1199-205.

YERKES, R. M. & DODSON, J. D. 1908. The relation of strength of stimulus to rapidity of habit-formation.

YI, Y., SONG, Y. & LU, Y. 2020. Parvalbumin Interneuron Activation-Dependent Adult Hippocampal Neurogenesis Is Required for Treadmill Running to Reverse Schizophrenia-Like Phenotypes. *Front Cell Dev Biol,* 8**,** 24.

YU, X., QI, X., WEI, L., ZHAO, L., DENG, W., GUO, W., WANG, Q., MA, X., HU, X., NI, P. & LI, T. 2023. Fingolimod ameliorates schizophrenia-like cognitive impairments induced by phencyclidine in male rats. *Br J Pharmacol,* 180**,** 161-173.

YUAN, L., WU, J., LIU, J., LI, G. & LIANG, D. 2015. Intermittent Hypoxia-Induced Parvalbumin-Immunoreactive Interneurons Loss and Neurobehavioral Impairment is Mediated by NADPH-Oxidase-2. *Neurochem Res,* 40**,** 1232-42.

YUNG, A. R., MCGORRY, P. D., MCFARLANE, C. A., JACKSON, H. J., PATTON, G. C. & RAKKAR, A. 1996. Monitoring and care of young people at incipient risk of psychosis. *Schizophr Bull,* 22**,** 283-303.

YUNG, A. R. & NELSON, B. 2011. Young people at ultra high risk for psychosis: a research update. *Early Interv Psychiatry,* 5 Suppl 1**,** 52-7.

ZAHIRUDDIN, S., KHAN, W., NEHRA, R., ALAM, M. J., MALLICK, M. N., PARVEEN, R. & AHMAD, S. 2017. Pharmacokinetics and comparative metabolic profiling of iridoid enriched fraction of Picrorhiza kurroa - An Ayurvedic Herb. *J Ethnopharmacol,* 197**,** 157-164.

ZAITSEV, A. V., POVYSHEVA, N. V., LEWIS, D. A. & KRIMER, L. S. 2007. P/Q-type, but not N-type, calcium channels mediate GABA release from fast-spiking interneurons to pyramidal cells in rat prefrontal cortex. *J Neurophysiol,* 97**,** 3567-73.

ZENI-GRAIFF, M., RIOS, A. C., MAURYA, P. K., RIZZO, L. B., SETHI, S., YAMAGATA, A. S., MANSUR, R. B., PAN, P. M., ASEVEDO, E., CUNHA, G. R., ZUGMAN, A., BRESSAN, R. A., GADELHA, A. & BRIETZKE, E. 2019. Peripheral levels of superoxide dismutase and glutathione peroxidase in youths in ultra-high risk for psychosis: a pilot study. *CNS Spectr,* 24**,** 333-337.

ZERON, M. M., HANSSON, O., CHEN, N., WELLINGTON, C. L., LEAVITT, B. R., BRUNDIN, P., HAYDEN, M. R. & RAYMOND, L. A. 2002. Increased sensitivity to N-methyl-D-aspartate receptor-mediated excitotoxicity in a mouse model of Huntington's disease. *Neuron,* 33**,** 849-60.

ZHANG, D., MA, X., WU, H., HONG, J., ZHANG, C., WU, L., LIU, J., ZHU, Y., YANG, L., WEI, K. & YAN, H. 2018a. Efficacy of herb-partitioned moxibustion at Qihai (CV 6) and bilateral Tianshu (ST 25) on colonic damage and the TLR4/NF-ÎºB signaling pathway in rats with Crohn's disease. *J Tradit Chin Med,* 38**,** 218-226.

ZHANG, H., SUN, X. R., WANG, J., ZHANG, Z. Z., ZHAO, H. T., LI, H. H., JI, M. H., LI, K. Y. & YANG, J. J. 2016a. Reactive Oxygen Species-mediated Loss of Phenotype of Parvalbumin Interneurons Contributes to Long-term Cognitive Impairments After Repeated Neonatal Ketamine Exposures. *Neurotox Res,* 30**,** 593-605.

ZHANG, L., ZHENG, H., WU, R., KOSTEN, T. R., ZHANG, X. Y. & ZHAO, J. 2019. The effect of minocycline on amelioration of cognitive deficits and pro-inflammatory cytokines levels in patients with schizophrenia. *Schizophr Res,* 212**,** 92-98.

ZHANG, M., WU, J., HUO, L., LUO, L., SONG, X., FAN, F., LU, Y. & LIANG, D. 2016b. Environmental Enrichment Prevent the Juvenile Hypoxia-Induced Developmental Loss of Parvalbumin-Immunoreactive Cells in the Prefrontal Cortex and Neurobehavioral Alterations Through Inhibition of NADPH Oxidase-2-Derived Oxidative Stress. *Mol Neurobiol,* 53**,** 7341-7350.

ZHANG, P. L., IZRAEL, M., AINBINDER, E., BEN-SIMCHON, L., CHEBATH, J. & REVEL, M. 2006. Increased myelinating capacity of embryonic stem cell derived oligodendrocyte precursors after treatment by interleukin-6/soluble interleukin-6 receptor fusion protein. *Mol Cell Neurosci,* 31**,** 387-98.

ZHANG, W. F., TAN, Y. L., ZHANG, X. Y., CHAN, R. C., WU, H. R. & ZHOU, D. F. 2011. Extract of Ginkgo biloba treatment for tardive dyskinesia in schizophrenia: a randomized, double-blind, placebo-controlled trial. *J Clin Psychiatry,* 72**,** 615-21.

ZHANG, X., SHEN, F., XU, D. & ZHAO, X. 2016c. A lasting effect of postnatal sevoflurane anesthesia on the composition of NMDA receptor subunits in rat prefrontal cortex. *Int J Dev Neurosci,* 54**,** 62-69.

ZHANG, X. Y., ZHOU, D. F., CAO, L. Y., ZHANG, P. Y. & WU, G. Y. 2003. Elevated blood superoxide dismutase in neuroleptic-free schizophrenia: association with positive symptoms. *Psychiatry Res,* 117**,** 85-8.

ZHANG, Y., CATTS, V. S. & SHANNON WEICKERT, C. 2018b. Lower antioxidant capacity in the prefrontal cortex of individuals with schizophrenia. *Aust N Z J Psychiatry,* 52**,** 690-698.

ZHANG, Y., CAZAKOFF, B. N., THAI, C. A. & HOWLAND, J. G. 2012. Prenatal exposure to a viral mimetic alters behavioural flexibility in male, but not female, rats. *Neuropharmacology,* 62**,** 1299-307.

ZHANG, Z. & VAN PRAAG, H. 2015. Maternal immune activation differentially impacts mature and adult-born hippocampal neurons in male mice. *Brain Behav Immun,* 45**,** 60-70.

ZHANG, Z. J. & REYNOLDS, G. P. 2002. A selective decrease in the relative density of parvalbumin-immunoreactive neurons in the hippocampus in schizophrenia. *Schizophr Res,* 55**,** 1-10.

ZHAO, Q., WANG, Q., WANG, J., TANG, M., HUANG, S., PENG, K., HAN, Y., ZHANG, J., LIU, G., FANG, Q. & YOU, Z. 2019. Maternal immune activation-induced PPARγ-dependent dysfunction of microglia associated with neurogenic impairment and aberrant postnatal behaviors in offspring. *Neurobiol Dis,* 125**,** 1-13.

ZHAO, X., QIN, S., SHI, Y., ZHANG, A., ZHANG, J., BIAN, L., WAN, C., FENG, G., GU, N., ZHANG, G., HE, G. & HE, L. 2007. Systematic study of association of four GABAergic genes: glutamic acid decarboxylase 1 gene, glutamic acid decarboxylase 2 gene, GABA(B) receptor 1 gene and GABA(A) receptor subunit beta2 gene, with schizophrenia using a universal DNA microarray. *Schizophr Res,* 93**,** 374-84.

ZHAO, X., TRAN, H., DEROSA, H., RODERICK, R. C. & KENTNER, A. C. 2021. Hidden talents: Poly (I:C)-induced maternal immune activation improves mouse visual discrimination performance and reversal learning in a sex-dependent manner. *Genes Brain Behav,* 20**,** e12755.

ZHOU, X. H., BRAKEBUSCH, C., MATTHIES, H., OOHASHI, T., HIRSCH, E., MOSER, M., KRUG, M., SEIDENBECHER, C. I., BOECKERS, T. M., RAUCH, U., BUETTNER, R., GUNDELFINGER, E. D. & FASSLER, R. 2001. Neurocan is dispensable for brain development. *Mol Cell Biol,* 21**,** 5970-8.

ZHOU, Y., GUO, M., WANG, X., LI, J., WANG, Y., YE, L., DAI, M., ZHOU, L., PERSIDSKY, Y. & HO, W. 2013. TLR3 activation efficiency by high or low molecular mass poly I:C. *Innate Immun,* 19**,** 184-92.

ZHOU, Y. Q., LIU, D. Q., CHEN, S. P., SUN, J., WANG, X. M., TIAN, Y. K., WU, W. & YE, D. W. 2018. Minocycline as a promising therapeutic strategy for chronic pain. *Pharmacol Res,* 134**,** 305-310.

ZHOU, Z., ZHANG, G., LI, X., LIU, X., WANG, N., QIU, L., LIU, W., ZUO, Z. & YANG, J. 2015. Loss of phenotype of parvalbumin interneurons in rat prefrontal cortex is involved in antidepressant- and propsychotic-like behaviors following acute and repeated ketamine administration. *Mol Neurobiol,* 51**,** 808-19.

ZHU, F., ZHENG, Y., DING, Y. Q., LIU, Y., ZHANG, X., WU, R., GUO, X. & ZHAO, J. 2014a. Minocycline and risperidone prevent microglia activation and rescue behavioral deficits induced by neonatal intrahippocampal injection of lipopolysaccharide in rats. *PLoS One,* 9**,** e93966.

ZHU, F., ZHENG, Y., LIU, Y., ZHANG, X. & ZHAO, J. 2014b. Minocycline alleviates behavioral deficits and inhibits microglial activation in the offspring of pregnant mice after administration of polyriboinosinic-polyribocytidilic acid. *Psychiatry Res,* 219**,** 680-6.

ZHU, S., STAVROVSKAYA, I. G., DROZDA, M., KIM, B. Y., ONA, V., LI, M., SARANG, S., LIU, A. S., HARTLEY, D. M., WU, D. C., GULLANS, S., FERRANTE, R. J., PRZEDBORSKI, S., KRISTAL, B. S. & FRIEDLANDER, R. M. 2002. Minocycline inhibits cytochrome c release and delays progression of amyotrophic lateral sclerosis in mice. *Nature,* 417**,** 74-8.

ZIMMERMANN, D. R. & DOURS-ZIMMERMANN, M. T. 2008. Extracellular matrix of the central nervous system: from neglect to challenge. *Histochem Cell Biol,* 130**,** 635-53.

ZMIGROD, L., GARRISON, J. R., CARR, J. & SIMONS, J. S. 2016. The neural mechanisms of hallucinations: A quantitative meta-analysis of neuroimaging studies. *Neurosci Biobehav Rev,* 69**,** 113-23.

ZONG, F. J., MIN, X., ZHANG, Y., LI, Y. K., ZHANG, X. T., LIU, Y. & HE, K. W. 2022. Circadian time- and sleep-dependent modulation of cortical parvalbumin-positive inhibitory neurons. *EMBO J***,** e111304.

ZUGNO, A. I., CANEVER, L., HEYLMANN, A. S., WESSLER, P. G., STECKERT, A., MASTELLA, G. A., DE OLIVEIRA, M. B., DAMÁZIO, L. S., PACHECO, F. D., CALIXTO, O. P., PEREIRA, F. P., MACAN, T. P., PEDRO, T. H., SCHUCK, P. F., QUEVEDO, J. & BUDNI, J. 2016. Effect of folic acid on oxidative stress and behavioral changes in the animal model of schizophrenia induced by ketamine. *J Psychiatr Res,* 81**,** 23-35.

ZUO, D. Y., ZHANG, Y. H., CAO, Y., WU, C. F., TANAKA, M. & WU, Y. L. 2006. Effect of acute and chronic MK-801 administration on extracellular glutamate and ascorbic acid release in the prefrontal cortex of freely moving mice on line with open-field behavior. *Life Sci,* 78**,** 2172-8.